

# University of Alberta

Improved ultraviolet induced fluorescence (UVIF)-standard cone penetration testing  
(CPT) system to detect petroleum hydrocarbon contaminants  
by

Moh'd Alostaz

A thesis submitted to the Faculty of Graduate Studies and Research  
in partial fulfillment of the requirements for the degree of

Doctor of Philosophy in Geotechnical Engineering

Civil and Environmental Engineering

Edmonton, Alberta  
Spring 2008



Library and  
Archives Canada

Bibliothèque et  
Archives Canada

Published Heritage  
Branch

Direction du  
Patrimoine de l'édition

395 Wellington Street  
Ottawa ON K1A 0N4  
Canada

395, rue Wellington  
Ottawa ON K1A 0N4  
Canada

*Your file* *Votre référence*  
*ISBN: 978-0-494-45392-6*  
*Our file* *Notre référence*  
*ISBN: 978-0-494-45392-6*

**NOTICE:**

The author has granted a non-exclusive license allowing Library and Archives Canada to reproduce, publish, archive, preserve, conserve, communicate to the public by telecommunication or on the Internet, loan, distribute and sell theses worldwide, for commercial or non-commercial purposes, in microform, paper, electronic and/or any other formats.

The author retains copyright ownership and moral rights in this thesis. Neither the thesis nor substantial extracts from it may be printed or otherwise reproduced without the author's permission.

**AVIS:**

L'auteur a accordé une licence non exclusive permettant à la Bibliothèque et Archives Canada de reproduire, publier, archiver, sauvegarder, conserver, transmettre au public par télécommunication ou par l'Internet, prêter, distribuer et vendre des thèses partout dans le monde, à des fins commerciales ou autres, sur support microforme, papier, électronique et/ou autres formats.

L'auteur conserve la propriété du droit d'auteur et des droits moraux qui protègent cette thèse. Ni la thèse ni des extraits substantiels de celle-ci ne doivent être imprimés ou autrement reproduits sans son autorisation.

---

In compliance with the Canadian Privacy Act some supporting forms may have been removed from this thesis.

Conformément à la loi canadienne sur la protection de la vie privée, quelques formulaires secondaires ont été enlevés de cette thèse.

While these forms may be included in the document page count, their removal does not represent any loss of content from the thesis.

Bien que ces formulaires aient inclus dans la pagination, il n'y aura aucun contenu manquant.

  
**Canada**

## **ABSTRACT**

This thesis describes the development of a miniature excitation-emission matrix (EEM) fluorescence sensor to become an integral part of an ultraviolet induced fluorescence (UVIF)-standard cone penetration testing (CPT) system. The UVIF-CPT can be used to detect petroleum hydrocarbon contaminants in subsurface soils using their fluorescing nature when excited by UV light. The thesis also introduces an analytical framework to characterize petroleum contaminants in the laboratory and in situ.

Chapter 2 synthesizes information to provide a background of the quantum physics associated with the fluorescence phenomenon, reviewing fluorescence measurement instrumentation, and describing various fluorescence measurement techniques including conventional, synchronous and time resolved spectroscopy. Chapters 3 and 4 introduce a novel approach to identify and semi-quantify common petroleum contaminants (natural gas condensate, gasoline, diesel, flare pit residue and heavy crude oil) and their underlying aromatic hydrocarbon components in solutions (chapter 3) and soil (chapter 4) based on their fluorescence spectral signatures. The method uses fluorescence EEMs combined with multivariate statistical procedures: parallel factor analysis (PARAFAC) and soft independent method of class analogy (SIMCA) to identify the petroleum products. Different soil matrices were used to examine the impact of soil type, grain size, porosity and mineralogy on fluorescence EEMs. Quantitatively, fluorescence intensities of EEMs of analyzed petroleum products at different concentrations were used to establish calibration curves that can

be employed to estimate unknown concentrations of similar petroleum products in solutions and soils.

Chapter 5 describes the design and testing of the new miniature UVIF sensor that employs a multi-wavelength light emitting diode (LED) as the excitation source and a lightweight, compact, linear variable filter (LVF) coupled with a photomultiplier tube (PMT) as the detection system. The performance of the instrument was verified and characterized in the laboratory using the tested petroleum contaminants. The verified capabilities of the UVIF sensor system suggest that this instrument provides an efficient, low-cost alternative that can be efficiently used to characterize and semi-quantify petroleum contaminants in soils.

# TABLE OF CONTENT

---

Chapter 1: <i>Introduction</i>	Page 1
Chapter 2: <i>Principles and Application of Ultraviolet Induced Fluorescence in Detecting Petroleum Hydrocarbon Contamination</i>	Page 15
2.1. Introduction	Page 15
2.2. Fluorescence Principles	Page 16
2.2.1. Aromatic Hydrocarbon Bonds	Page 17
2.2.2. Molecular Energy States	Page 21
2.2.3. Excitation and De-excitation Processes	Page 24
2.2.4. Non-Radiative De-Excitation Processes	Page 25
2.2.5. Radiative De-excitation Processes	Page 26
2.2.6. Characteristics of Fluorescence	Page 28
2.2.6.1. Emission and Excitation Spectra	Page 28
2.2.7. Quantitative Aspects of Fluorescence	Page 30
2.2.7.1. Excited-state lifetimes	Page 30
2.2.7.2. Quantum yield ( $\Phi$ )	Page 31
2.2.7.3. Stockes Shifts	Page 32
2.2.7.4. Quantitative Fluorescence Intensity	Page 33
2.2.8. Alternative Fluorescence Measurements	Page 35
2.2.8.1. Synchronous Fluorescence Spectroscopy	Page 35
2.2.8.2. Time Resolved Fluorescence Spectroscopy	Page 38
2.3. Fluorescence Measurements Instrumentation	Page 40

2.3.1. Excitation Sources	Page 40
2.3.2. Wavelength Selectors	Page 45
2.3.3. Detectors	Page 48
2.4. Site Investigation Fluorescence Sensors	Page 51
2.4.1. Site Characterization and Analysis Penetrometer System (SCAPS)	Page 53
2.4.2. Rapid Optical Screening Tool (ROST) System	Page 55
2.4.3. Tufts System Multi-channel LIF Sensor	Page 57
2.4.4. Ultraviolet induced fluorescence-cone penetration testing (UVIF-CPT) system	Page 58
2.4.5. Fluorescence Sensor Selection	Page 60
2.5. Summary	Page 62
2.6. References	Page 82
Chapter 3: <i>Petroleum Contamination Characterization and Quantification Using Fluorescence Emission-excitation Matrices (EEMs) and Parallel Factor Analysis (PARAFAC)</i>	Page 93
3.1. Introduction	Page 93
3.2. Fluorescence Spectroscopy	Page 95
3.2.1. Fluorescence Emission-Excitation Matrices (EEMs)	Page 96
3.2.2. Multivariate statistical techniques	Page 97
3.2.2.1. Parallel Factor Analysis (PARAFAC)	Page 98
3.2.2.2. Soft Independent Method of Class Analogy (SIMCA)	Page 99

3.3. Experimental Work	Page 100
3.4. Results and Discussion	Page 103
3.4.1. Qualitative Analysis	Page 103
3.4.1.1. Fluorescence EEMs	Page 104
3.4.1.2. PARAFAC and SIMCA Analysis	Page 106
3.4.2. Quantitative Analysis	Page 112
3.4.2.1. Concentration Calibration Curves	Page 112
3.4.2.2. PAH Components Concentration Estimation	Page 116
3.5. Summary and Conclusions	Page 123
3.6. References	Page 152
Chapter 4: <i>Soil Type Effects on Petroleum Contamination</i>	Page 157
<i>Characterization Using Ultra Violet Induced Fluorescence</i>	
<i>Emission-Excitation Matrices (EEMs) and Parallel Factor</i>	
<i>Analysis (PARAFAC)</i>	
4.1. Introduction	Page 157
4.2. Fluorescence Spectroscopy	Page 159
4.2.1. Multivariate statistical techniques	Page 161
4.2.2. Fluorescence and soil fabric	Page 162
4.3. Materials and Methods	Page 165
4.3.1. Soils	Page 165
4.3.2. Petroleum Products	Page 168
4.4. Results and Discussion	Page 171
4.4.1. Fluorescence EEMs	Page 171

4.4.2. PARAFAC Analysis	Page 177
4.4.3. SIMCA Analysis	Page 179
4.4.4. Fluorescence measurements calibration	Page 180
4.5. Summary and Conclusions	Page 183
4.6. References	Page 220
Chapter 5: <i>Light Emitting Diode Operated Ultraviolet Induced Fluorescence (UVIF)-Standard Cone Penetration Testing (CPT) System</i>	Page 225
5.1. Introduction	Page 225
5.2. Fluorescence EEMs	Page 227
5.3. UVIF Sensor Design	Page 229
5.3.1. Multi-Wavelength LED	Page 230
5.3.2. Linear Variable Filter (LVF)	Page 233
5.3.3. LVF Calibration	Page 234
5.4. Experimental Work	Page 235
5.4.1. Material	Page 235
5.4.2. Data Pre-processing	Page 238
5.4.2.1. Correction for Variation in LED Intensity	Page 238
5.4.2.2. Correction for LVF Opaque Band	Page 240
5.4.2.3. Correction for Scattered Light	Page 241
5.5. Results and Discussion	Page 242
5.5.1. Quantitative Fluorescence Measurements	Page 242
5.5.2. Fluorescence Measurement Calibration	Page 248



5.5. Summary and Conclusions	Page 250
5.6. References	Page 298
Chapter 6: <i>Conclusions</i>	Page 300
Appendix A: <i>Fluorescence EEMs (Using Varian Eclipse Spectrometer)</i>	Page 311
Appendix B: <i>Fluorescence EEMs (Using Newly Developed UVIF sensor)</i>	Page 337
Appendix C: <i>Fluorescence calibration curves (Using Varian Eclipse Spectrometer)</i>	Page 358
Appendix D: <i>Fluorescence and Porosity Relationship (Using Varian Eclipse Spectrometer)</i>	Page 369
Appendix E: <i>Fluorescence calibration curves (Using newly developed UVIF sensor)</i>	Page 382
Appendix F: <i>Fluorescence and Porosity Relationship (Using newly developed UVIF sensor)</i>	Page 392
Appendix G: <i>PARAFAC and SIMCA Modeling</i>	Page 398
Appendix H: <i>Standard Aromatic Hydrocarbon Fluorescence Calibration Curves and Estimation Procedure (Using Varian Eclipse Spectrometer)</i>	Page 440

## LIST OF FIGURES

---

Figure 2-1.	Examples of aromatic hydrocarbons (after McMurry 2004)	Page 64
Figure 2-2.	Atomic orbitals (after Griffiths 2004)	Page 65
Figure 2-3.	Graphic representation of s and p orbitals combination to form $\sigma$ and $\Pi$ bonds (after Brady and Humiston 1986)	Page 66
Figure 2-4.	The benzene ring structure with delocalized $\Pi$ electrons clouds around the plan of joined nuclei (after Morrison and Boyd 1989))	Page 67
Figure 2-5.	Morse potential energy functions for ground and excited states (after Morse 1929)	Page 68
Figure 2-6.	Singlet and triplet states (after Schulman 1977)	Page 69
Figure 2-7.	Jablonski diagram (after Atkins 2002)	Page 70
Figure 2-8.	Emission and excitation spectra (after Schulman 1977)	Page 71
Figure 2-9.	Radiative and non-radiative rate constants (after Valeur 2002)	Page 72
Figure 2-10.	Stokes Shift (after Lakowicz 1999)	Page 73
Figure 2-11.	Fluorescence synchronous spectrum (after Vo-Dinh, 1978)	Page 74
Figure 2-12.	3-dimensional (3D) and 2-dimensional contour map (2D) representations of emission-excitation matrix (EEM) (after Rho and Stuart 1978)	Page 75

- Figure 2-13. Time Resolved Fluorescence Spectrum (after O'Connor and Phillips 1984) Page 76
- Figure 2-14. Typical spectrometer arrangement (after Sharma and Schulman 1999) Page 77
- Figure 2-15. Monochromator arrangement showing separation of light wavelengths by reflection grating and mirror (after Skoog and West 1971) Page 78
- Figure 2-16. Typical fiber optic based fluorescence sensor Page 79
- Figure 2-17. General Scheme of LIF System (after Lieberman, 1998) Page 80
- Figure 2-18. ROST system schematic diagram including typical fluorescence profile and wavelength-time matrix (WTM) generated by the system (WTM) generated by the system (after Nielsen 1995) Page 81
- Figure 3-1. 3-dimensional (3D) and 2-dimensional contour map (2D) representations of emission-excitation matrix (EEM) (after Rho and Stuart 1978). Page 129
- Figure 3-2. Graphic representation of PARAFAC analysis of EEM data including generated concentration, emission and excitation spectra matrices of modeled underlying components (Adapted from PLS-Toolbox manual 2006) Page 130
- Figure 3-3. Reference fluorescence spectra of Rohdamine (Ex relates to the excitation wavelength associated with the plotted response) Page 131

Figure 3-4.	a. Gas condensate EEM (neat)	Page 132
	b. Gasoline EEM (neat)	Page 133
	c. Diesel EEM (neat)	Page 134
	d. Flare pit residue EEM (neat)	Page 135
	e. Heavy Crude oil EEM (40 mL/L )	Page 136
Figure 3-5.	Highest fluorescence intensity EEM peak locations of tested neat petroleum products and crude oil (40 mL/L)	Page 137
Figure 3-6.	a. Diesel EEM at solution concentration of 10 mL/L	Page 138
	b. Diesel EEM at solution concentration of 200 mL/L	Page 139
Figure 3-7.	Changes in fluorescence intensity of different emission peaks of diesel in relationship with increasing solution concentrations	Page 140
Figure 3-8.	a. PARAFAC model of gas condensate underlying component emission spectra	Page 141
	b. PARAFAC model of gasoline underlying component emission spectra	Page 142
	c. PARAFAC model of diesel underlying component emission spectra	Page 143
	d. PARAFAC model of flare pit residue underlying component emission spectra	Page 144
	e. PARAFAC model of crude oil underlying component emission spectra	Page 145
	f. Fluorescence emission spectra of standard PAH	Page 146

collected at laboratory

- Figure 3-9. Sample plot of SIMCA model normalized diesel and gas condensate scores Page 147
- Figure 3-10. Total fluorescence intensity versus solution concentration of tested petroleum products Page 148
- Figure 3-11. a. Relationship between total fluorescence intensity and total CCME hydrocarbon fraction concentrations of tested petroleum products (diesel not included) Page 149
- b. Relationship between total fluorescence intensity and total CCME hydrocarbon fraction concentrations of tested petroleum products (diesel included) Page 150
- Figure 3-12. P-Xylene relative concentration in standard calibration and diesel samples Page 151
- Figure 4-1. 3-dimensional (3D) and 2-dimensional contour map (2D) representations of emission-excitation matrix (EEM) (after Rho and Stuart 1978). Page 188
- Figure 4-2. Effect of soil sorting on voids structure (Blue circles represent coarse grained soil, black dots represent fine grained soil, white represents voids) Page 189
- Figure 4-3. a. Ottawa sand grain size distribution Page 190
- b. Well graded sand grain size distribution Page 191

	c. Well graded sand and Devon silt grain size distribution	Page 192
	d. Devon silt grain size distribution (after Arenson et al. 2005)	Page 193
Figure 4-4.	Schematics of soil and solvent in sample container	Page 194
Figure 4-5.	a. Gas condensate in Ottawa sand EEM (neat)	Page 195
	b. Gasoline in Ottawa sand EEM (neat)	Page 196
	c. Diesel in Ottawa sand EEM (neat)	Page 197
	d. Flare pit residue in Ottawa sand EEM (neat)	Page 198
	e. Crude Oil in Ottawa sand EEM (40 mL/L)	Page 199
Figure 4-6.	Highest fluorescence intensity EEM peak locations of tested neat petroleum products and crude oil (40 mL/L) in solution and soil samples	Page 200
Figure 4-7.	a. Flare pit residue in Ottawa sand EEM (neat)	Page 201
	b. Flare pit residue in Devon silt EEM (neat)	Page 202
Figure 4-8.	a. Flare pit residue in Ottawa sand EEM at solution concentration of 50 mL/L	Page 203
	b. Flare pit residue in Ottawa sand EEM at solution concentration of 200 mL/L	Page 204
Figure 4-8.	Effect of soil matrix on diesel total fluorescence intensity	Page 205
Figure 4-10.	Effect of soil matrix on flare pit residue total fluorescence intensity	Page 206
Figure 4-11.	a. Change in diesel total fluorescence intensity	Page 207

	versus soil porosity	Page 208
	b. Change in flare pit residue total fluorescence intensity versus soil porosity	
Figure 4-12.	a. PARAFAC model of gas condensate underlying component emission spectra in soil	Page 209
	b. PARAFAC model of gasoline underlying component emission spectra in soil	Page 210
	c. PARAFAC model of diesel underlying component emission spectra in soil	Page 211
	d. PARAFAC model of flare pit residue underlying component emission spectra in soil	Page 212
	e. PARAFAC model of crude oil underlying component emission spectra in soil	Page 213
Figure 4-13.	Fluorescence emission spectra of standard PAH collected at laboratory	Page 214
Figure 4-14.	Sample plot of SIMCA model normalized diesel and crude oil scores	Page 215
Figure 4-15.	a. Tested petroleum products calibration curves in Ottawa sand	Page 216
	b. Tested petroleum products calibration curves in well graded sand	Page 217
	c. Tested petroleum products calibration curves in well graded sand and Devon silt mixtures	Page 218

d. Tested petroleum products calibration curves in Devon silt.	Page 219
Figure 5-1. Typical LIF system setup (after Lieberman 1998)	Page 255
Figure 5-2. 3-dimensional (3D) and 2-dimensional contour map (2D) representations of emission-excitation matrix (EEM) (after Rho and Stuart 1978)	Page 256
Figure 5-3. Improved UVIF sensor schematics	Page 257
Figure 5-4. Multi-wavelength LED emission spectra	Page 258
Figure 5-5. LVF calibration procedure involved correlating observed peak locations in mercury lamp emission spectra generated by the improved UVIF sensor to wavelengths of similar peaks in standard mercury lamp emission spectrum	Page 259
Figure 5-6. Grain size distribution of tested soils	Page 261
Figure 5-7. Samples testing setup where sample container was mounted in direct contact with the sapphire window in the cone penetrometer to resemble site fluorescence measurements	Page 261
Figure 5-8.     a. Rohdamine fluorescence spectra (collected by Varian Eclipse Spectrometer)	Page 262
b. Rohdamine fluorescence spectra (collected by UVIF sensor)	
Figure 5-9. Opaque band in diesel fluorescence spectra	Page 263



Figure 5-10.	a. Methanol fluorescence spectra in presence of scattered light	Page 264
	b. Diesel fluorescence spectra in presence of scattered light	
Figure 5-11.	a. Gasoline fluorescence spectra - neat (using Varian Eclipse spectrometer)	Page 265
	b. Gasoline fluorescence spectra - neat (using UVIF sensor)	Page 266
	c. Diesel fluorescence spectra - neat (using Varian Eclipse spectrometer)	Page 267
	d. Diesel fluorescence spectra - neat (using UVIF sensor)	Page 268
	e. Flare pit residue fluorescence spectra - neat (using Varian Eclipse spectrometer)	Page 269
	f. Flare pit residue fluorescence spectra - neat (using UVIF sensor)	Page 270
	g. Crude oil fluorescence spectra – 40 mL/L (using Varian Eclipse spectrometer)	Page 271
	h. Crude oil fluorescence spectra – 40 mL/L (using UVIF sensor)	Page 272
Figure 5-12.	a. Gasoline EEM – neat (using Varian Eclipse spectrometer)	Page 273
	b. Gasoline EEM – neat (using UVIF sensor)	Page 274

	c. Diesel EEM – neat (using Varian Eclipse spectrometer)	Page 275
	d. Diesel EEM – neat (using UVIF sensor)	Page 276
	e. Flare pit residue EEM - neat (using Varian Eclipse spectrometer)	Page 277
	f. Flare pit residue EEM – neat (using UVIF sensor)	Page 278
	g. Crude oil EEM – 40 mL/L (using Varian Eclipse spectrometer)	Page 279
	h. Crude oil EEM – 40 mL/L (using UVIF sensor)	Page 280
Figure 5-13.	a. Gasoline EEM at solution concentration of 50 mL/L	Page 281
	b. Neat gasoline EEM	Page 282
Figure 5-14.	a. Gasoline EEM in solvent solution	Page 283
	b. Gasoline EEM in Ottawa sand	Page 284
Figure 5-15.	a. Effect of soil matrix on gasoline total fluorescence intensity	Page 285
	b. Effect of soil matrix on diesel total fluorescence intensity	Page 286
Figure 5-16.	a. Effect of soil matrix on flare pit residue total fluorescence intensity	Page 287
	b. Effect of soil matrix on crude oil total fluorescence intensity	Page 288
Figure 5-17.	a. Total fluorescence intensity of gasoline versus	Page 289

	tested soil porosities	
	b. Total fluorescence intensity of diesel versus tested soil porosities	Page 290
	c. Total fluorescence intensity of flare pit residue versus tested soil porosities	Page 291
	d. Total fluorescence intensity of crude oil versus tested soil porosities	Page 292
Figure 5-18.	a. Fluorescence intensity calibration curves of tested petroleum products in solution	Page 293
	b. Fluorescence intensity calibration curves of tested petroleum products in Ottawa sand	Page 294
	c. Fluorescence intensity calibration curves of tested petroleum products in well graded sand	Page 295
	d. Fluorescence intensity calibration curves of tested petroleum products in well graded sand and Devon silt mixture	Page 296
	e. Fluorescence intensity calibration curves of tested petroleum products in Devon silt	Page 297
Figure A-1.	f. Gas condensate in hexane EEM (1 mL/L)	Page 312
	g. Gas condensate in hexane EEM (10 mL/L)	
	h. Gas condensate in hexane EEM (50 mL/L)	
	i. Gas condensate in hexane EEM (200 mL/L)	
	j. Gas condensate in hexane EEM (600 mL/L)	

k. Gas condensate in hexane EEM (neat)

Figure A-2. a. Gas condensate in Ottawa sand EEM (1 mL/L) Page 313

b. Gas condensate in Ottawa sand EEM (10 mL/L)

c. Gas condensate in Ottawa sand EEM (50 mL/L)

d. Gas condensate in Ottawa sand EEM (200 mL/L)

e. Gas condensate in Ottawa sand EEM (600 mL/L)

f. Gas condensate in Ottawa sand EEM (neat)

Figure A-3. e. Gas condensate in well graded sand EEM (1 Page 314

mL/L)

f. Gas condensate in well graded sand EEM (10

mL/L)

g. Gas condensate in well graded sand EEM (50

mL/L)

h. Gas condensate in well graded sand EEM (200

mL/L)

i. Gas condensate in well graded sand EEM (600

mL/L)

j. Gas condensate in well graded sand EEM (neat)

Figure A-4. a. Gas condensate in well graded sand and Devon Page 315

Silt mixture EEM (1 mL/L)

b. Gas condensate in well graded sand and Devon

Silt mixture EEM (10 mL/L)

c. Gas condensate in well graded sand and Devon

Silt mixture EEM (50 mL/L)

d. Gas condensate in well graded sand and Devon

Silt mixture EEM (200 mL/L)

e. Gas condensate in well graded sand and Devon

Silt mixture EEM (600 mL/L)

f. Gas condensate in well graded sand and Devon

Silt mixture EEM (neat)

Figure A-5. a. Gas condensate in Devon silt EEM (1 mL/L) Page 316

b. Gas condensate in Devon silt EEM (10 mL/L)

c. Gas condensate in Devon silt EEM (50 mL/L)

d. Gas condensate in Devon silt EEM (200 mL/L)

e. Gas condensate in Devon silt EEM (600 mL/L)

f. Gas condensate in Devon silt EEM (neat)

Figure A-6. c. Gasoline in hexane EEM (1 mL/L) Page 317

d. Gasoline in hexane EEM (10 mL/L)

e. Gasoline in hexane EEM (50 mL/L)

f. Gasoline in hexane EEM (200 mL/L)

g. Gasoline in hexane EEM (600 mL/L)

h. Gasoline in hexane EEM (neat)

Figure A-7. c. Gasoline in Ottawa sand EEM (1 mL/L) Page 318

d. Gasoline in Ottawa sand EEM (10 mL/L)

e. Gasoline in Ottawa sand EEM (50 mL/L)

f. Gasoline in Ottawa sand EEM (200 mL/L)

- g. Gasoline in Ottawa sand EEM (600 mL/L)
- h. Gasoline in Ottawa sand EEM (neat)

Figure A-8.

- a. Gasoline in well graded sand EEM (1 mL/L)
- b. Gasoline in well graded sand EEM (10 mL/L)
- c. Gasoline in well graded sand EEM (50 mL/L)
- d. Gasoline in well graded sand EEM (200 mL/L)
- e. Gasoline in well graded sand EEM (600 mL/L)
- f. Gasoline in well graded sand EEM (neat)

Page 319

Figure A-9.

- a. Gasoline in well graded sand and Devon silt mixture EEM (1 mL/L)
- b. Gasoline in well graded sand and Devon silt mixture EEM (10 mL/L)
- c. Gasoline in well graded sand and Devon silt mixture EEM (50 mL/L)
- d. Gasoline in well graded sand and Devon silt mixture EEM (200 mL/L)
- e. Gasoline in well graded sand and Devon silt mixture EEM (600 mL/L)
- f. Gasoline in well graded sand and Devon silt mixture EEM (neat)

Page 320

Figure A-10.

- a. Gasoline in Devon silt mixture EEM (1 mL/L)
- b. Gasoline in Devon silt mixture EEM (10 mL/L)
- c. Gasoline in Devon silt mixture EEM (50 mL/L)

Page 321

- d. Gasoline in Devon silt mixture EEM (200 mL/L)
- e. Gasoline in Devon silt mixture EEM (600 mL/L)
- c. Gasoline in Devon silt mixture EEM (neat)

Figure A-11.

- a. Diesel in Hexane EEM (1 mL/L)
- b. Diesel in Hexane EEM (10 mL/L)
- c. Diesel in Hexane EEM (50 mL/L)
- d. Diesel in Hexane EEM (200 mL/L)
- e. Diesel in Hexane EEM (800 mL/L)
- f. Diesel in Hexane EEM (neat)

Page 322

Figure A-12.

- a. Diesel in Ottawa sand EEM (1 mL/L)
- b. Diesel in Ottawa sand EEM (10 mL/L)
- c. Diesel in Ottawa sand EEM (50 mL/L)
- d. Diesel in Ottawa sand EEM (200 mL/L)
- e. Diesel in Ottawa sand EEM (800 mL/L)
- f. Diesel in Ottawa sand EEM (neat)

Page 323

Figure A-13.

- a. Diesel in well graded sand EEM (1 mL/L)
- b. Diesel in well graded sand EEM (10 mL/L)
- c. Diesel in well graded sand EEM (50 mL/L)
- d. Diesel in well graded sand EEM (200 mL/L)
- e. Diesel in well graded sand EEM (800 mL/L)
- f. Diesel in well graded sand EEM (neat)

Page 324

Figure A-14.

- a. Diesel in well graded sand and Devon silt mixture  
EEM (1 mL/L)

Page 325

- b. Diesel in well graded sand and Devon silt mixture  
EEM (10 mL/L)
- c. Diesel in well graded sand and Devon silt mixture  
EEM (50 mL/L)
- d. Diesel in well graded sand and Devon silt mixture  
EEM (200 mL/L)
- e. Diesel in well graded sand and Devon silt mixture  
EEM (800 mL/L)
- f. Diesel in well graded sand and Devon silt mixture  
EEM (neat)

Figure A-15.

- a. Diesel and Devon silt EEM (1 mL/L)
- b. Diesel and Devon silt EEM (10 mL/L)
- c. Diesel and Devon silt EEM (50 mL/L)
- d. Diesel and Devon silt EEM (200 mL/L)
- e. Diesel and Devon silt EEM (800 mL/L)
- f. Diesel and Devon silt EEM (neat)

Page 326

Figure A-16.

- a. Flare pit residue in chloroform EEM (1 mL/L)
- b. Flare pit residue in chloroform EEM (10 mL/L)
- c. Flare pit residue in chloroform EEM (50 mL/L)
- d. Flare pit residue in chloroform EEM (200 mL/L)
- e. Flare pit residue in chloroform EEM (600 mL/L)
- f. Flare pit residue in chloroform EEM (neat)

Page 327

Figure A-17.

- a. Flare pit residue in Ottawa sand EEM (1 mL/L)

Page 328



- b. Flare pit residue in Ottawa sand EEM (10 mL/L)
- c. Flare pit residue in Ottawa sand EEM (50 mL/L)
- d. Flare pit residue in Ottawa sand EEM (200 mL/L)
- e. Flare pit residue in Ottawa sand EEM (600 mL/L)
- f. Flare pit residue in Ottawa sand EEM (neat)

Figure A-18.

- a. Flare pit residue in well graded sand EEM (1 mL/L)
- b. Flare pit residue in well graded sand EEM (10 mL/L)
- c. Flare pit residue in well graded sand EEM (50 mL/L)
- d. Flare pit residue in well graded sand EEM (200 mL/L)
- e. Flare pit residue in well graded sand EEM (600 mL/L)
- f. Flare pit residue in well graded sand EEM (neat)

Figure A-19.

- a. Flare pit residue in well graded sand and Devon silt mixture EEM (1 mL/L)
- b. Flare pit residue in well graded sand and Devon silt mixture EEM (10 mL/L)
- c. Flare pit residue in well graded sand and Devon silt mixture EEM (50 mL/L)
- d. Flare pit residue in well graded sand and Devon

silt mixture EEM (200 mL/L)

e. Flare pit residue in well graded sand and Devon

silt mixture EEM (800 mL/L)

f. Flare pit residue in well graded sand and Devon

silt mixture EEM (neat)

Figure A-20.

e. Flare pit residue in Devon silt EEM (1 mL/L)

Page 331

f. Flare pit residue in Devon silt EEM (10 mL/L)

g. Flare pit residue in Devon silt EEM (50 mL/L)

h. Flare pit residue in Devon silt EEM (200 mL/L)

i. Flare pit residue in Devon silt EEM (600 mL/L)

j. Flare pit residue in Devon silt EEM (neat)

Figure A-21.

a. Crude oil in chloroform EEM (1 mL/L)

Page 332

b. Crude oil in chloroform EEM (10 mL/L)

c. Crude oil in chloroform EEM (40 mL/L)

d. Crude oil in chloroform EEM (200 mL/L)

e. Crude oil in chloroform EEM (640 mL/L)

Figure A-22.

a. Crude oil in Ottawa sand EEM (1 mL/L)

Page 333

b. Crude oil in Ottawa sand EEM (10 mL/L)

c. Crude oil in Ottawa sand EEM (40 mL/L)

d. Crude oil in Ottawa sand EEM (200 mL/L)

e. Crude oil in Ottawa sand EEM (640 mL/L)

Figure A-23.

a. Crude oil in well graded sand EEM (1 mL/L)

Page 334

b. Crude oil in well graded sand EEM (10 mL/L)

- c. Crude oil in well graded sand EEM (40 mL/L)
- d. Crude oil in well graded sand EEM (200 mL/L)
- e. Crude oil in well graded sand EEM (640 mL/L)

Figure A-24.

- a. Crude oil in well graded sand and Devon silt mixture EEM (1 mL/L)
- b. Crude oil in well graded sand and Devon silt mixture EEM (10 mL/L)
- c. Crude oil in well graded sand and Devon silt mixture EEM (40 mL/L)
- d. Crude oil in well graded sand and Devon silt mixture EEM (200 mL/L)
- e. Crude oil in well graded sand and Devon silt mixture EEM (640 mL/L)

Page 335

Figure A-25.

- a. Crude oil in Devon silt EEM (1 mL/L)
- b. Crude oil in Devon silt EEM (10 mL/L)
- c. Crude oil in Devon silt EEM (40 mL/L)
- d. Crude oil in Devon silt EEM (200 mL/L)
- e. Crude oil in Devon silt EEM (640 mL/L)

Page 336

Figure B-1.

- i. Gasoline in hexane EEM (1 mL/L)
- j. Gasoline in hexane EEM (10 mL/L)
- k. Gasoline in hexane EEM (50 mL/L)
- l. Gasoline in hexane EEM (200 mL/L)
- m. Gasoline in hexane EEM (600 mL/L)

Page 338

- n. Gasoline in hexane EEM (neat)
- Figure B-2. i. Gasoline in Ottawa sand EEM (1 mL/L) Page 339
- j. Gasoline in Ottawa sand EEM (10 mL/L)
- k. Gasoline in Ottawa sand EEM (50 mL/L)
- l. Gasoline in Ottawa sand EEM (200 mL/L)
- m. Gasoline in Ottawa sand EEM (600 mL/L)
- n. Gasoline in Ottawa sand EEM (neat)
- Figure B-3. g. Gasoline in well graded sand EEM (1 mL/L) Page 340
- h. Gasoline in well graded sand EEM (10 mL/L)
- i. Gasoline in well graded sand EEM (50 mL/L)
- j. Gasoline in well graded sand EEM (200 mL/L)
- k. Gasoline in well graded sand EEM (600 mL/L)
- l. Gasoline in well graded sand EEM (neat)
- Figure B-4. g. Gasoline in well graded sand and Devon silt Page 341  
mixture EEM (1 mL/L)
- h. Gasoline in well graded sand and Devon silt  
mixture EEM (10 mL/L)
- i. Gasoline in well graded sand and Devon silt  
mixture EEM (50 mL/L)
- j. Gasoline in well graded sand and Devon silt  
mixture EEM (200 mL/L)
- k. Gasoline in well graded sand and Devon silt  
mixture EEM (600 mL/L)

l. Gasoline in well graded sand and Devon silt mixture EEM (neat)

Figure B-5.

- f. Gasoline in Devon silt mixture EEM (1 mL/L)
- g. Gasoline in Devon silt mixture EEM (10 mL/L)
- h. Gasoline in Devon silt mixture EEM (50 mL/L)
- i. Gasoline in Devon silt mixture EEM (200 mL/L)
- j. Gasoline in Devon silt mixture EEM (600 mL/L)
- d. Gasoline in Devon silt mixture EEM (neat)

Page 342

Figure B-6.

- g. Diesel in Hexane EEM (1 mL/L)
- h. Diesel in Hexane EEM (10 mL/L)
- i. Diesel in Hexane EEM (50 mL/L)
- j. Diesel in Hexane EEM (200 mL/L)
- k. Diesel in Hexane EEM (800 mL/L)
- l. Diesel in Hexane EEM (neat)

Page 343

Figure B-7.

- g. Diesel in Ottawa sand EEM (1 mL/L)
- h. Diesel in Ottawa sand EEM (10 mL/L)
- i. Diesel in Ottawa sand EEM (50 mL/L)
- j. Diesel in Ottawa sand EEM (200 mL/L)
- k. Diesel in Ottawa sand EEM (800 mL/L)
- l. Diesel in Ottawa sand EEM (neat)

Page 344

Figure B-8.

- g. Diesel in well graded sand EEM (1 mL/L)
- h. Diesel in well graded sand EEM (10 mL/L)
- i. Diesel in well graded sand EEM (50 mL/L)

Page 345

j. Diesel in well graded sand EEM (200 mL/L)

k. Diesel in well graded sand EEM (800 mL/L)

l. Diesel in well graded sand EEM (neat)

Figure B-9.

g. Diesel in well graded sand and Devon silt mixture  
EEM (1 mL/L) Page 346

h. Diesel in well graded sand and Devon silt mixture  
EEM (10 mL/L)

i. Diesel in well graded sand and Devon silt mixture  
EEM (50 mL/L)

j. Diesel in well graded sand and Devon silt mixture  
EEM (200 mL/L)

k. Diesel in well graded sand and Devon silt mixture  
EEM (800 mL/L)

l. Diesel in well graded sand and Devon silt mixture  
EEM (neat)

Figure B-10.

g. Diesel and Devon silt EEM (1 mL/L) Page 347

h. Diesel and Devon silt EEM (10 mL/L)

i. Diesel and Devon silt EEM (50 mL/L)

j. Diesel and Devon silt EEM (200 mL/L)

k. Diesel and Devon silt EEM (800 mL/L)

l. Diesel and Devon silt EEM (neat)

Figure B-11.

g. Flare pit residue in chloroform EEM (1 mL/L) Page 348

h. Flare pit residue in chloroform EEM (10 mL/L)

- i. Flare pit residue in chloroform EEM (50 mL/L)
- j. Flare pit residue in chloroform EEM (200 mL/L)
- k. Flare pit residue in chloroform EEM (600 mL/L)
- l. Flare pit residue in chloroform EEM (neat)

Figure B-12.

- g. Flare pit residue in Ottawa sand EEM (1 mL/L)
- h. Flare pit residue in Ottawa sand EEM (10 mL/L)
- i. Flare pit residue in Ottawa sand EEM (50 mL/L)
- j. Flare pit residue in Ottawa sand EEM (200 mL/L)
- k. Flare pit residue in Ottawa sand EEM (600 mL/L)
- l. Flare pit residue in Ottawa sand EEM (neat)

Page 349

Figure B-13.

- g. Flare pit residue in well graded sand EEM (1 mL/L)
- h. Flare pit residue in well graded sand EEM (10 mL/L)
- i. Flare pit residue in well graded sand EEM (50 mL/L)
- j. Flare pit residue in well graded sand EEM (200 mL/L)
- k. Flare pit residue in well graded sand EEM (600 mL/L)
- l. Flare pit residue in well graded sand EEM (neat)

Page 350

Figure B-14.

- g. Flare pit residue in well graded sand and Devon silt mixture EEM (1 mL/L)

Page 351

- h. Flare pit residue in well graded sand and Devon silt mixture EEM (10 mL/L)
- i. Flare pit residue in well graded sand and Devon silt mixture EEM (50 mL/L)
- j. Flare pit residue in well graded sand and Devon silt mixture EEM (200 mL/L)
- k. Flare pit residue in well graded sand and Devon silt mixture EEM (800 mL/L)
- l. Flare pit residue in well graded sand and Devon silt mixture EEM (neat)

Figure B-15.

- k. Flare pit residue in Devon silt EEM (1 mL/L)
- l. Flare pit residue in Devon silt EEM (10 mL/L)
- m. Flare pit residue in Devon silt EEM (50 mL/L)
- n. Flare pit residue in Devon silt EEM (200 mL/L)
- o. Flare pit residue in Devon silt EEM (600 mL/L)
- p. Flare pit residue in Devon silt EEM (neat)

Page 352

Figure B-16.

- f. Crude oil in chloroform EEM (1 mL/L)
- g. Crude oil in chloroform EEM (10 mL/L)
- h. Crude oil in chloroform EEM (40 mL/L)
- i. Crude oil in chloroform EEM (200 mL/L)
- j. Crude oil in chloroform EEM (640 mL/L)

Page 353

Figure B-17.

- f. Crude oil in Ottawa sand EEM (1 mL/L)
- g. Crude oil in Ottawa sand EEM (10 mL/L)

Page 354



- h. Crude oil in Ottawa sand EEM (40 mL/L)
- i. Crude oil in Ottawa sand EEM (200 mL/L)
- j. Crude oil in Ottawa sand EEM (640 mL/L)

Figure B-18.

- f. Crude oil in well graded sand EEM (1 mL/L)
- g. Crude oil in well graded sand EEM (10 mL/L)
- h. Crude oil in well graded sand EEM (40 mL/L)
- i. Crude oil in well graded sand EEM (200 mL/L)
- j. Crude oil in well graded sand EEM (640 mL/L)

Page 355

Figure B-19.

- f. Crude oil in well graded sand and Devon silt mixture EEM (1 mL/L)
- g. Crude oil in well graded sand and Devon silt mixture EEM (10 mL/L)
- h. Crude oil in well graded sand and Devon silt mixture EEM (40 mL/L)
- i. Crude oil in well graded sand and Devon silt mixture EEM (200 mL/L)
- j. Crude oil in well graded sand and Devon silt mixture EEM (640 mL/L)

Page 356

Figure B-20.

- f. Crude oil in Devon silt EEM (1 mL/L)
- g. Crude oil in Devon silt EEM (10 mL/L)
- h. Crude oil in Devon silt EEM (40 mL/L)
- i. Crude oil in Devon silt EEM (200 mL/L)
- j. Crude oil in Devon silt EEM (640 mL/L)

Page 357

Figure C-1.	Gas condensate fluorescence calibration curves in solvent solution and soil	Page 359
Figure C-2.	Gasoline fluorescence calibration curves in solvent solution and soil	Page 360
Figure C-3.	Diesel fluorescence calibration curves in solvent solution and soil	Page 361
Figure C-4.	Flare pit residue fluorescence calibration curves in solvent solution and soil	Page 362
Figure C-5.	Crude oil fluorescence calibration curves in solvent solution and soil	Page 363
Figure C-6.	Tested petroleum products fluorescence calibration curves in solvent solutions	Page 364
Figure C-7.	Tested petroleum products fluorescence calibration curves in Ottawa sand	Page 365
Figure C-8.	Tested petroleum products fluorescence calibration curves in well graded sand	Page 366
Figure C-9.	Tested petroleum products fluorescence calibration curves in well graded sand and Devon silt mixture	Page 367
Figure C-10.	Tested petroleum products fluorescence calibration curves in Devon silt	Page 368
Figure D-1.	Gas condensate fluorescence intensity versus soil porosity at different concentrations	Page 377
Figure D-2.	Gasoline fluorescence intensity versus soil porosity at	Page 378

	different concentrations	
Figure D-3.	Diesel fluorescence intensity versus soil porosity at different concentrations	Page 379
Figure D-4.	Flare pit residue fluorescence intensity versus soil porosity at different concentrations	Page 380
Figure D-5.	Crude oil fluorescence intensity versus soil porosity at different concentrations	Page 381
Figure E-1.	Gasoline fluorescence calibration curves in solvent solution and soil	Page 383
Figure E-2.	Diesel fluorescence calibration curves in solvent solution and soil	Page 384
Figure E-3.	Flare pit residue fluorescence calibration curves in solvent solution and soil	Page 385
Figure E-4.	Crude oil fluorescence calibration curves in solvent solution and soil	Page 386
Figure E-5.	Tested petroleum products fluorescence calibration curves in solvent solutions	Page 387
Figure E-6.	Tested petroleum products fluorescence calibration curves in Ottawa sand	Page 388
Figure E-7.	Tested petroleum products fluorescence calibration curves in well graded sand	Page 389
Figure E-8.	Tested petroleum products fluorescence calibration curves in well graded sand and Devon silt mixture	Page 390

Figure E-9. Tested petroleum products fluorescence calibration curves in Devon silt	Page 391
Figure F-1. Gasoline fluorescence intensity versus soil porosity at different concentrations	Page 394
Figure F-2. Diesel fluorescence intensity versus soil porosity at different concentrations	Page 395
Figure F-3. Flare pit residue fluorescence intensity versus soil porosity at different concentrations	Page 396
Figure F-4. Crude oil fluorescence intensity versus soil porosity at different concentrations	Page 397
Figure G-1. Core consistency plot	Page 404
Figure G-2. Residual fluorescence data plot	Page 405
Figure G-3. Core consistency plot of gas condensate PARAFAC model	Page 407
Figure G-4. Fluorescence data residual plot of gas condensate PARAFAC model	Page 407
Figure G-5. Core consistency plot of gasoline PARAFAC model	Page 408
Figure G-6. Fluorescence data residual plot of gasoline PARAFAC model	Page 408
Figure G-7. Core consistency plot of diesel PARAFAC model	Page 409
Figure G-8. Fluorescence data residual plot of diesel PARAFAC model	Page 409
Figure G-9. Core consistency plot of flare pit residue PARAFAC	Page 410

	model	
Figure G-10.	Fluorescence data residual plot of flare pit residue PARAFAC model	Page 410
Figure G-11.	Core consistency plot of crude oil PARAFAC model	Page 411
Figure G-12.	Fluorescence data residual plot of crude oil PARAFAC model	Page 411
Figure G-13.	Core consistency plot of gas condensate PARAFAC model (in soil)*	Page 413
Figure G-14.	Fluorescence data residual plot of gas condensate PARAFAC model (in soil)*	Page 413
Figure G-15.	Core consistency plot of gasoline PARAFAC model (in soil)*	Page 414
Figure G-16.	Fluorescence data residual plot of gasoline PARAFAC model (in soil)*	Page 414
Figure G-17.	Core consistency plot of diesel PARAFAC model (in soil)*	Page 415
Figure G-18.	Fluorescence data residual plot of diesel PARAFAC model (in soil)*	Page 415
Figure G-19.	Core consistency plot of flare pit residue PARAFAC model (in soil)*	Page 416
Figure G-20.	Fluorescence data residual plot of flare pit residue PARAFAC model (in soil)*	Page 416
Figure G-21.	Core consistency plot of crude oil PARAFAC model (in	Page 417

	soil)*	
Figure G-22.	Fluorescence data residual plot of crude oil PARAFAC model (in soil)*	Page 417
Figure G-23.	Classes of analyzed petroleum	Page 422
Figure G-24.	Classes of analyzed petroleum products in soil samples	Page 428
Figure H-1.	Fluorescence intensity versus concentration (aromatic compounds with 1 benzene ring)	Page 444
Figure H-2.	Fluorescence intensity versus concentration (aromatic compounds with 2 benzene rings)	Page 445
Figure H-3.	Fluorescence intensity versus concentration (aromatic compounds with 3 benzene rings)	Page 446
Figure H-4.	Fluorescence intensity versus concentration (aromatic compounds with 4 benzene rings)	Page 447
Figure H-5.	Gas condensate -PARAFAC score and calibration curve of p-xylene	Page 450
Figure H-6.	Gasoline -PARAFAC score and calibration curve of p-xylene	Page 452
Figure H-7.	Gasoline -PARAFAC score and calibration curve of methyl-naphthalene	Page 454
Figure H-8.	Diesel -PARAFAC score and calibration curve of p-xylene	Page 456
Figure H-9.	Diesel -PARAFAC score and calibration curve of methyl-naphthalene	Page 458

- Figure H-10. Diesel -PARAFAC score and calibration curve of phenanthrene Page 460
- Figure H-11. Flare pit residue -PARAFAC score and calibration curve of methyl-naphthalene Page 462
- Figure H-12. Flare pit residue -PARAFAC score and calibration curve of phenanthrene Page 464
- Figure H-13. Crude oil -PARAFAC score and calibration curve of methyl-naphthalene Page 465
- Figure H-14. Crude oil -PARAFAC score and calibration curve of phenanthrene Page 466

*\* In soil – Refers to all tested soils. Fluorescence EEMs of each of the tested petroleum products in all used soils were stacked together in one data set for PARAFAC analysis.*

## LIST OF TABLES

---

Table 3-1.	Minimum petroleum products concentration at which fluorescence signal was detected with Varian Eclipse spectrometer	Page 125
Table 3-2.	Results of laboratory chemical analysis for aromatic compounds in the analyzed petroleum compounds	Page 126
Table 3-3.	Quantitative values for aromatic compounds in the analyzed petroleum compounds	Page 127
Table 3-4.	Measured and estimated equivalent aromatic compound concentrations	Page 128
Table 4-1.	Minimum petroleum product concentration at which fluorescence signal was detected with Varian Eclipse spectrometer in various media	Page 185
Table 4-2.	Equations of linear relationship between total fluorescence values of tested petroleum products (where F is total fluorescence, m is the slope, n the porosity and b the intercept)	Page 186
Table 4-3.	Maximum concentrations of linear range for total fluorescence measurement in tested soils	Page 187
Table 5-1.	Minimum petroleum products concentration at which fluorescence signal was detected with UVIF sensor in various media	Page 253



Table 5-2. Maximum concentrations of linear range for total fluorescence measurement in tested soils Page 254

Table F-1. Equations of linear relationship between total fluorescence values of tested petroleum products (where F is total fluorescence, m is the slope, n the porosity and b the intercept) Page 393

# Chapter 1

## **Introduction**

Crude oil and refined petroleum products play an important role in our daily life. Petroleum products are used as fuels for transportation and industrial machinery, for heating and electricity generation, for the production of chemicals and plastics, and as a part of construction materials for roads and buildings. Petroleum products are complex mixtures of hundreds of hydrocarbon compounds ranging from light, volatile, short-chained organic compounds to heavy, long-chained, branched compounds. The exact composition of petroleum products varies depending upon the source of the crude oil and the refining practices used to produce the product. Petroleum hydrocarbons (PHCs) can typically be divided into aromatic, saturated and unsaturated hydrocarbon based compounds that are made up entirely of hydrogen and carbon atoms.

Saturated hydrocarbons (alkanes) are the simplest hydrocarbon compounds and the predominant class of hydrocarbons in most crude oils. They are made of straight and branched chains of single bonded carbon atoms saturated with hydrogen. Unsaturated hydrocarbons have one or more double or triple bonds between carbon atoms. Aromatic hydrocarbons account for a small percentage of PHCs and have at least one aromatic ring, which is a planar set of six carbon atoms connected by alternating single and double covalent bonds that resemble benzene in electronic configuration and chemical behaviour. The aromatics in most PHCs of interest at oil and gas

contaminated sites are mainly comprised of BTEX (benzene, toluene, ethylbenzene, and xylene isomers), other benzene compounds and polycyclic aromatic hydrocarbons (PAHs) (McMurry 2004).

The exploration, production, transportation and daily use of crude oil and petroleum products results in intentional and accidental releases into the environment. Oil spills could occur in rivers, lakes, coastal waterways, and soils (from which contaminants seep into groundwater). The spills range from continuous leakage from land sources, such as underground oil tanks to larger spill accidents that could spill thousands of barrels of oil into land or marine environments. BTEX and PAHs have been strongly associated with lung and skin cancer observed in human subjects exposed to these compounds via inhalation or dermal contact (Hsieh et al. 2006; McCormick et al. 1981). Accordingly, the US Environmental Protection Agency (<http://www.epa.gov>) has classified 16 individual PAHs as priority pollutants.

A wide range of chemical analytical techniques have been developed for the analysis of petroleum hydrocarbons in environmental samples including: thin layer chromatography, high performance liquid chromatography (HP-LC), gas chromatography with flame ionisation detection (GC-FID) (Wang et al. 1999), gas chromatography with mass spectroscopy GC-MS (Daling et al. 2002), two-dimensional gas chromatography (GC-GC) (Frysiner and Gaines 2001), and gas chromatography-isotope ratio mass spectrometry (GC-IRMS) (Rogers and Savard 1999). However most of the existing petroleum contaminants characterization and

identification methods involves initial screening in the field, then carefully obtaining samples in the field and having them analyzed in a distant laboratory, which is a time-consuming process. Therefore, having reliable analytical methods for detecting and characterizing aromatic compounds in environmental solution or soil in the field are of great interest (Bjorseth and Ramdahl 1985).

Fluorescence spectroscopy is an efficient analytical method that utilizes the fluorescing nature of PHCs when illuminated with ultraviolet (UV) light that can be used directly on various types of environmental samples without any pre-separation or other preparation steps. In fluorescence measurement, samples are not affected or destroyed in the process, and no hazardous by-products are generated. Therefore, fluorescence based techniques are gaining preference for detecting and characterizing petroleum contaminants in environmental samples. Several researchers have used fluorescence techniques for detection and classification of naturally occurring organic materials and aromatic hydrocarbons in the environment (Aiken and Leenheer 1993; Babichenko et al. 1995; Marhaba 2000), as well as crude oil petroleum product spills and other petroleum products including diesel, kerosene and gasoline (Eastwood 1981; Patra and Mishra 2002; Brown and Fingas 2003).

The fluorescing nature of PHCs is largely related to the electron structure and chemical bonds in their aromatic constituents. When aromatic hydrocarbon molecules are excited with UV light, electrons get promoted to higher energy levels. This movement of electrons between energy levels is common in aromatic hydrocarbon

compounds due to the nature of electron bonding in the conjugated structure of these molecules. After excitation, electrons return to the ground state from the higher energy levels through various non-radiative and radiative mechanisms, one of which is fluorescence that is termed ultraviolet induced fluorescence (UVIF) (Schulman 1977). For a particular petroleum product, the wavelength of the emitted fluorescence signal is unique. It is considered characteristic of the compound and can be used effectively to identify fluorescent compounds for analytical purposes (Lakowicz 1999).

Coupling fluorescence-based spectroscopic methods with a probe that can be pushed into the ground, allows the recording of profiles of in situ, real-time measurements of petroleum contaminants in subsurface environments. With this technology it is possible to take measurements continuously as the probe is pushed into the ground. This ability to generate real-time, high-spatial-resolution chemical measurement in the subsurface represents a significant improvement over traditional methods that have been used to delineate subsurface contamination. In the early 90's, this idea was first tested by detecting an artificial fluorophore that had been injected into the ground, and was found to be efficient (Lurk et al. 1990).

A variety of sensors that use fluorescence spectroscopy and coupled to cone penetration testing (CPT) technology to detect petroleum hydrocarbons in subsurface soils have been developed since then. One of the early devices used a laser-induced fluorescence (LIF) fibre-optic-based sensor, called the Site Characterization and

Analysis Penetrometer System (SCAPS). It was developed by the U.S. Department of Defense (DoD) and Tri-Service (Army, Navy, and Air Force) (Lieberman et al. 1991) to detect subsurface petroleum hydrocarbon contaminants. After that, the Rapid Optical Screening Tool (ROST) was developed by another grant from The U.S. DoD at North Dakota State University (NDSU) in consortium with U.S. Air Force Armstrong Laboratory, Loral Defense Systems and Dakota Technologies Inc. (St. Germain et al. 1993). The Advanced Applied Technology Demonstration Facility (AATDF) for Environmental Technology Program at Rice University, Houston, Texas, funded by the US DoD, developed a new technology that utilizes a multi-channel LIF screening system at Tufts University (Kenny et al. 1995). In Canada, a similar technology that combines ultraviolet induced fluorescence-with-cone penetration testing system (UVIF-CPT) has been developed and utilized by Conetec Investigation Ltd. (Vancouver, B.C.) (Biggar et al. 2003).

All fluorescence based sensor systems use a similar design where UV light from a laser or other light source is transmitted through a sapphire window on a probe installed behind a cone penetrometer. Fluorescence emitted by the aromatic components of petroleum hydrocarbons passes back through the window to a detector system located in the probe or via fibre-optic cables to a detector at the surface. A profile of fluorescence intensity versus depth can then be generated in combination with lithological data from the CPT system to provide a real time display of the location of petroleum hydrocarbon contamination. However these sensors could have many configuration variations that range from a simple configuration that uses a

single UV light emitting diode (LED) excitation source and a single photo-multiplier tube (PMT) detector, to complex systems that simultaneously excite at different wavelengths and collect the complete fluorescence signal using multi-channel charge-coupled devices (CCDs).

Despite the advantage of using fluorescence based measurements in site characterization applications, currently only limited field screening capabilities of the method are utilized in situ. Operational and price complexities, weight, size and lack of an appropriate calibration procedure of fluorescence for in situ measurements are believed to be the reasons why the fluorescence detection industry has shied away from employing fluorescence based sensors in environmental site investigation. This study introduces a fluorescence measurement instrument and analysis framework that strives to overcome some of the operational and price limitations associated with in situ fluorescence measurements. The presented instrument is an improved version of an existing UVIF-CPT system that offers an inexpensive, robust and compact fluorescence sensor that eliminates the use of bulky, expensive light sources, fiber optic cables and complex detection systems.

The instrument can generate fluorescence excitation-emission matrices (EEMs) of detected petroleum contaminants that have an inherent wealth of spectral information that can help better characterize and quantify petroleum products in environmental samples. The introduced analytical framework utilized multivariate statistical techniques to analyze three-dimensional fluorescence data generated from collected

fluorescence EEMs of solution and soil samples prepared with a range of petroleum products. The framework also provides fluorescence measurement calibration curves obtained using prepared petroleum product samples that can be utilized to estimate concentrations of similar contaminants in environmental samples from the field. This thesis is based on the following papers manuscripts:

Chapter 2 (paper I) - Alostaz, M., Biggar, K., Segó, D., Donhue, R. and Woeller, D. 2007. Principles and Application of Ultraviolet Induced Fluorescence in Detecting Petroleum Hydrocarbon Contamination. Under review by the Journal of Environmental Reviews.

Chapter 3 (paper II) - Alostaz, M., Biggar, K., Donhue, R. and Hall, G. 2007. Petroleum Contamination Characterization and Quantification Using Fluorescence Emission-Excitation Matrices (EEMs) and Parallel Factor Analysis (PARAFAC). Accepted by the Journal of Environmental Engineering and Science and forwarded to printing.

Chapter 4 (paper III) - Alostaz, M., Biggar, K., Donhue, R. and Hall, G. 2007. Soil Type Effects on Petroleum Contamination Characterization Using Ultra Violet Induced Fluorescence Emission-Excitation Matrices (EEMs) and Parallel Factor Analysis (PARAFAC). Journal of Environmental Engineering and Science. Under review by the Journal of Environmental Engineering and Science.

Chapter 5 (paper IV) - Alostaz, M., Biggar, K., Donhue, R. and Dolling, R. 2007. Light emitting diode operated ultraviolet induced fluorescence (UVIF)-



standard cone penetration testing (CPT) system.

Chapter 2 - *Principles and Application of Ultraviolet Induced Fluorescence in Detecting Petroleum Hydrocarbon Contamination* - discusses the PHCs fluorescence phenomenon based on amalgamated information from multi-disciplinary sources to provide a background of the quantum physics associated with the fluorescence phenomenon and understand how and why the fluorescence occurs. The chapter, also, reviews fluorescence measurement instrumentation and describes various fluorescence measurement techniques including conventional, synchronous as well as time resolved spectroscopy. Finally, the chapter describes how the fluorescence phenomenon was utilized in cone penetration testing to delineate petroleum presence and distribution in the subsurface. The information presented in this chapter, along with knowledge of commercially available fluorescence spectroscopy instrumentation, optimized the use of conventional and alternative fluorescence measuring techniques in the design of the improved UVIF-CPT module.

Chapter 3 - *Petroleum Contamination Characterization and Quantification Using Fluorescence Emission-Excitation Matrices (EEMs) and Parallel Factor Analysis (PARAFAC)* - presents an integrated framework for characterizing and semi-quantifying crude oil and petroleum products (natural gas condensate, gasoline, diesel, flare pit residue) and their underlying aromatic hydrocarbon components in solution samples based on their fluorescence spectral signatures. The presented procedure uses EEMs combined with multivariate statistical procedures (PARAFAC)

and soft independent method of class analogy (SIMCA) to identify the analyzed petroleum product samples. It also introduces standard calibration curves that allow estimating unknown concentrations of petroleum products similar to the tested products in solutions samples, based on fluorescence intensities of their EEMs. Also, the proposed framework estimates aromatic hydrocarbon content of tested petroleum products by performing customized PARAFAC analysis. This chapter provides a methodology to obtain fingerprints for different petroleum products along with estimates of their concentrations in non-fluorescing solvents that can be applied to potential fluorescence measurements obtained by the improved UVIF-CPT.

Chapter 4 - *Soil Type Effects on Petroleum Contamination Characterization Using Ultra Violet Induced Fluorescence Emission-Excitation Matrices (EEMs) and Parallel Factor Analysis (PARAFAC)* - extends the utility of using fluorescence measurements to detect petroleum contaminants in soils, and evaluates the impact of soil type, grain size, porosity and mineralogy on the spectral features of petroleum hydrocarbon fluorescence EEMs. The chapter uses the same analysis framework introduced in Chapter 3 (PARAFAC and SIMCA) to identify the petroleum products and their underlying aromatic hydrocarbon components. For quantitative analysis, total fluorescence values obtained from fluorescence EEMs of analyzed petroleum products are used to estimate their concentrations in different soil matrices. This approach provides fingerprinting capability and reasonable estimates of tested petroleum product concentrations in different soil matrices that can be extended to in situ fluorescence measurements by the improved UVIF-CPT.

Chapter 5 - *Light emitting diode operated ultraviolet induced fluorescence (UVIF)-standard cone penetration testing (CPT) system* - presents the design of the new UVIF sensor, which can be an integral part of the existing UVIF-CPT. The sensor employs a multi-wavelength light emitting diode (LED) as the excitation source, and a lightweight compact linear variable filter (LVF) coupled with photomultiplier tube (PMT) as the detection system, which allow collecting in situ fluorescence EEMs of petroleum products in subsurface soils. The excitation wavelengths provided by the multi-wavelength LED extend from the deep UV through the upper UV spectrum (265–360 nm) which is a suitable range to excite most petroleum contaminants encountered in the field. The performance of the instrument was tested and characterized in the laboratory utilizing the same petroleum products used in previous parts of the study (gas condensate, gasoline, diesel, flare pit residue and crude oil). Correct identification of tested petroleum products in solvent solutions and soil was verified against reference fluorescence spectral data for the same petroleum products collected using a Varian Eclipse fluorescence spectrometer. Similar to the calibration curves presented in Chapters 3 and 4, the fluorescence calibration curves were generated to estimate petroleum product concentration in solvent solutions and soils. The verified capabilities of the UVIF sensor suggest that this instrument may provide a portable, low-cost alternative that can be efficiently used to characterize and semi-quantify petroleum contaminants in situ.

## **ACKNOWLEDGMENTS**

This project was funded The University of Alberta - NSERC – ConeTec – EnCana – Worley Parsons Komex Improved Site Characterization Research Project. The author acknowledges the technical assistance of Mr. Steve Gamble and Jela Burkas at the University of Alberta Geotechnical Center, Mr. Ron dolling and Mr. Rishi Oppal from Conetec and Dr. Jonathon Kenny at Tufts University and LCDR Gregory Hall at U.S. Coast Guard Academy for their extended assistance with PARAFAC analysis.

## **REFERENCES**

- Aiken, G. and Leenheer, J. 1993. Isolation and chemical characterization of dissolved and colloidal organic matter. *Chemistry and Ecology*, 8, pp. 135–151.
- Babichenko, S., Lapimma, J., Poryvkina, L., and Varlamov, V. 1995. On-line fluorescence techniques for diagnostics of water environment. *Society of Photo-Optical Instrumentation Engineers Journal*, 2503, pp. 157-161.
- Biggar, K., Woeller, D., Murphy, S., and Armstrong, J. 2003. CPT-UVIF characterization at upstream oil and gas facilities. In *Proceedings of the 17<sup>th</sup> Annual Vancouver Geotechnical Society Symposium: Geotechnical Engineering for Geoenvironmental Applications*, Vancouver, BC. pp 31-37.
- Bjorseth, A. and Ramdahl, T. 1985. *Handbook of Polycyclic Aromatic Hydrocarbons, Vol. 2: Emission Sources and Recent Progress in Analytical Chemistry*, Marcel Dekker, New York.
- Brown. C. and Fingas, M. 2003. Review of the development of laser fluorosensors for

oil spill application. *Marine Pollution Bulletin*, 47, pp. 477–484.

Daling, P., Faksness, L., Hansen, A., and Stout, S. 2002. Improved and Standardized Methodology for Oil Spill Fingerprinting. *Environmental Forensics*, 3, pp. 263-278.

Eastwood, D. (in E. Wehry, E. Editor). 1981. *Modern Fluorescence Spectroscopy* (Vol. 4). Plenum Press, New York, N.Y.

Frysjer, G. and Gaines, B. 2001. Separation and Identification of Petroleum Biomarkers by Comprehensive Two-Dimensional Gas Chromatography. *Journal of Separation Science*, 24, pp. 87-96

Hsieh, L., Yang, H. and Chen, H. 2006. Ambient BTEX and MTBE in the neighbourhoods of different industrial parks in Southern Taiwan. *Journal of Hazardous Materials*, 128, pp. 106-115

Kenny, J., Lin, J., Hart, S., Wang, W. and Namytkine, D. 1995. Subsurface Contaminant Monitoring by Laser Fluorescence Excitation-Emission Spectroscopy in a Cone Penetrometer Probe. *SPIE*, Vol. 2504, pp. 59-67.

Lakowicz, J. 1999. *Principles of Fluorescence Spectroscopy* (2<sup>nd</sup> Edition). Kluwer Academic/Plenum Publisher, New York, N.Y.

Lieberman, S., Theriault, G., Cooper, S., Malone, P., Olsen, R. and Lurk, P. 1991. Rapid subsurface in situ field screening of petroleum hydrocarbon contamination using laser induced fluorescence over optical fibers, In *Proceedings of the 2<sup>nd</sup> International Symposium on Field Screening Methods for Hazardous Waste Site Investigations*, Las Vegas, Nevada. Air and Waste Management Association, Pittsburgh, P.A. pp. 57–63.

- Lurk, P., Cooper, S., Malone P. and Lieberman, S. 1990. Development of innovative penetrometer systems for the detection and delineation of contaminated groundwater and soil, Superfund '90. In Proceedings of the 11th National Superfund Conference, Washington, DC. Hazardous Materials Control Research Institute, pp. 297–299.
- Marhaba, T. 2000. Fluorescence techniques for rapid identification of DOM fractions. *Journal of Environmental Engineering*, February 2000, pp.145–152.
- McCormick, D., Burns, F and Alberg, R. 1981. Inhibition of benzo-[alpha]pyrene-induced mammary carcinogenesis. *Journal of National Cancer Institute*, 66, pp. 559–564
- McMurry, J. 2004. *Organic Chemistry* (6<sup>th</sup> edition). Brooks/Cole: Thomson Learning, Belmont, CA.
- Patra, D. and Mishra, A. 2002. Total synchronous fluorescence scan spectra of petroleum products. *Analytical and Bioanalytical Chemistry*, 373, pp. 304-309.
- Rogers, K. and Savard, M. 1999. Detection of petroleum contamination in river sediments from Quebeq City region using GC-IRMS. *Organic Geochemistry*, 30, pp. 1559-1569
- Schulman, S. 1977. *Fluorescence and Phosphorescence Spectroscopy: Physicochemical Principles and Practice*. Pergamon Press, New York, N.Y.
- St. Germain, R., Gillispie, G. and Klingfus, J. 1993. Variable Wavelength Laser System for Field Fluorescence Measurements. In Proceedings of Field

Screening Methods for Hazardous Wastes and Toxic Chemicals, Las Vegas, NV. Air & Waste Management Association, Pittsburgh, P.A. pp.1113–1122.

U.S. Environmental protection agency web site. 2007. <http://www.epa.gov>. Accessed on June 15, 2007.

Wang, Z., Fingas, M. and Page, D. 1999. Oil spill identification (review). Journal of Chromatography A, 843, pp. 369-411

## **Chapter 2**

# **Principles and Application of Ultraviolet Induced Fluorescence in Detecting Petroleum Hydrocarbon Contamination**

### **2.1. INTRODUCTION**

Petroleum hydrocarbons (PHCs) have a fluorescing nature when illuminated with UV light that is largely related to the electron structure and chemical bonds in their aromatic constituents. This highly fluorescent nature has made molecular fluorescence spectrometry a popular technique for PHCs analysis. In fluorescence measurement, samples are not affected or destroyed in the process, and no hazardous by-products are generated. Therefore, fluorescence based techniques are gaining preference for detecting and characterizing PHC contaminants in environmental samples. In addition to the high sensitivity and simplicity of fluorescence based measurements, they provide a wealth of information such as emission wavelength, excitation wavelength, intensity, polarization, and fluorescence lifetime, to better characterize targeted fluorophores. Coupling fluorescence-based spectroscopic methods with a probe that can be pushed into the ground, allows recording in situ realtime measurements of petroleum contaminants in subsurface environments. With this technology it is possible to take measurements continuously as the probe is pushed into the ground. This ability to generate real-time, high-spatial-resolution chemical measurement in the subsurface represents a significant improvement over



traditional methods that have been used to delineate subsurface contamination. This chapter discusses fluorescence principles to fully understand how the fluorescence phenomenon is related to the chemical nature of petroleum hydrocarbons and physiochemical changes that occur during and after excitation with UV light. This knowledge, coupled with an understanding of the electronic instrumentation, would optimize the use of conventional and alternative fluorescence measuring techniques in various geo-environmental site investigation applications.

## **2.2. FLUORESCENCE PRINCIPLES**

PHCs are made up of a complex mixture of aromatic, saturated (alkanes) and unsaturated (alkenes and alkynes) hydrocarbon based compounds that are composed entirely of hydrogen and carbon. Saturated hydrocarbons (alkanes) are the most simple of the hydrocarbon species. They are comprised entirely of single bonded carbon atoms and are saturated with hydrogen. Alkanes can exist in a form of one or more carbon rings to which hydrogen atoms are attached. In such a case, they are called Cycloalkanes. The general formula for saturated hydrocarbons is  $C_nH_{2n+2}$ . Unsaturated hydrocarbons (alkenes and alkynes) have one or more double or triple bonds between carbon atoms with the general formula  $C_nH_{2n}$  or  $C_nH_{2n-2}$ , respectively. Those with one double bond are called alkenes, while those containing triple bonds are called alkynes. Aromatic hydrocarbons have at least one aromatic ring, which is a planar set of six carbon atoms connected by alternating single and double covalent bonds and known as a benzene ring. Aromatic hydrocarbons can be monocyclic or polycyclic. A few examples of environmentally important aromatic hydrocarbons are

given in Figure 2-1 (McMurry 2004). PAHs share a chemical property known as aromaticity, in which a conjugated ring of unsaturated bonds show stabilization stronger than would be expected by the stabilization of conjugation alone. Aromaticity is manifested in the unique fluorescing nature of aromatic compounds when exposed to sufficient energy from UV light (Schleyer 2001; Balaban et al. 2005).

### **2.2.1. Aromatic Hydrocarbon Bonds**

Fluorescence is an optical phenomenon in which the molecular absorption of a photon triggers the emission of another photon usually with a longer wavelength. Thus, to realize the fluorescence characteristics of aromatic hydrocarbons, it is essential to understand the nature of the electronic structure, energy levels and chemical bonds in these compounds. The position of electrons in aromatic hydrocarbons is described by a probability distribution around the nucleus that is often visualized as an electron cloud. The thickness of the cloud is proportional to electron density that reflects the probability of an electron being present at a specific location around the atom and its bonds. Electrons belonging to an atom are observed more frequently in certain areas around the nucleus called orbitals. The electron cloud can transition between orbital states, where each state has a characteristic shape and energy.

Atomic orbitals can be described by  $n$ ,  $l$ ,  $m$  and  $s$  (principal, angular, magnetic and spin respectively) quantum numbers of the electron. The principal quantum number ( $n = 1, 2, 3, 4 \dots$ ) depends on the distance between the electron and the nucleus. Orbitals

with different principal quantum numbers are said to belong to different shells. Electron shells are made up of one or more electron sub-shells (sublevels) that have two or more orbitals corresponding to the angular momentum quantum number  $l$ . The angular quantum number ( $l = 0, 1 \dots n-1$ ) specifies the shape of an atomic orbital and strongly influences chemical bonds.  $l=0$  is called an s-orbital,  $l=1$  is a p-orbital,  $l=2$  a d-orbital and  $l=3$ , an f-orbital (Figure 2-2). The magnetic quantum number ( $m_l = -l, -l+1 \dots 0 \dots l-1, l$ ) is the third set of quantum numbers that describes the energy levels available within a sub-shell. Finally, the spin quantum number ( $s$ ) depicts the projection of the electron spin ( $s=1/2$ ) along the specified axis. It can have a value of  $-1/2$  or  $+1/2$ . (Griffiths 2004). Because electrons have only two possible spin states, an atomic orbital cannot contain more than two electrons according to the Pauli Exclusion Principle; that states no two electrons with identical half-integer spin may occupy the same quantum state. If this principle did not hold, all of the electrons in an atom would pile up in the lowest energy state. The Pauli Exclusion Principle holds not just for electrons, but for any fermions (half-integer spin particles like protons and neutrons) (Massimi 2005).

Molecules can be defined as electrically stable neutral groups of at least two atoms in a specific arrangement held together by chemical bonds that are responsible for the attractive interactions between atoms. Molecules tend to be most stable when the outermost electron shells of their constituent atoms contain eight electrons giving them the same electronic configuration as a noble gas, as suggested by the octet rule. Carbon atoms in the benzene ring have four electrons in their valence shell that can

hold eight electrons; hence, carbon always tends to form four covalent bonds with other atoms to obtain a full outermost electron (valence) shell (Daintith 2004). Chemical bonds can be explained in quantum mechanics by commonly accepted and related valence bond and molecular orbital theories. Valence bond theory argues that a chemical bond forms when two valence electrons, in their respective atomic orbitals, try to hold two nuclei together by virtue of system energy lowering effects. On the other hand, Molecular orbital theory uses a linear combination of atomic orbitals to form molecular orbitals that cover the whole molecule. Hence, electrons are not assigned to individual bonds between atoms, but are treated as moving under the influence of the nuclei in the whole molecule (Laidler 1993).

Chemical bonds by carbon atoms in aromatic hydrocarbons are the result of  $\sigma$  and  $\Pi$  bonds.  $\sigma$  bonds occur when the orbitals of the two shared electrons overlap head-to-head so the charge distribution is localized between the two bonded atoms along the line joining the nuclei.  $\sigma$  bonds are symmetrical with respect to rotation about the bond axis and commonly involve s-s orbitals. Alternatively,  $\Pi$  bonds occur when two orbitals of the two shared electrons overlap when they are parallel with charge concentration around the joined nuclei due to the overlap of two atomic orbitals at right angles to the line joining the nuclei (Figure 2-3). P-orbitals usually engage in  $\Pi$  bonding. In bond order, single bonds are usually  $\sigma$  bonds, double bonds consist of one  $\sigma$  bond and one  $\Pi$  bond, and triple bonds contain one  $\sigma$  bond and two  $\Pi$  bonds (Brady and Humiston 1986; Murrel et al. 1985)

The benzene ring system is a chemically conjugated system in which carbon atoms are covalently bonded with alternating single and double bonds and electrons are delocalized across all of the adjacent parallel aligned p-orbitals of the atoms. The electron delocalisation creates a region where electrons do not belong to a single bond or carbon atom, but rather are shared by all six atoms along the conjugation path of the benzene ring above and below the planar ring. This conjugation in cyclic structures enhances chemical stability of aromatic molecules compared to similar non-aromatic molecules as dictated by aromaticity, because even though there are not enough electrons to form double bonds on all the carbon atoms in benzene ring, the circulating  $\Pi$  electrons strengthen all of the bonds on the ring equally. The existence of delocalization is implicit in molecular orbital theory that considers the bonding electrons are not assigned to individual bonds between atoms but rather shared by all atoms.

Alternatively, valence bond theory represents delocalization in benzene ring by resonance structures, which is a tool used to model certain types of non-classical molecular structures. Carbon atoms in benzene ring can be connected by one or two covalent bonds, but the observed bond lengths in benzene rings are all equivalent (longer than double bonds yet shorter than single bonds) suggesting that benzene ring has equally contributing or resonating structures and the real molecule is considered to be their average. The average structure is called a resonance hybrid and it is more stable than any of the resonating structures would be if they existed. The conjugation or delocalization of six  $\Pi$  electrons over the benzene ring can be graphically indicated

by a circle inside a hexagon to show the de-localized nature of the compound (Figure 2-4) (Morrison and Boyd 1989).

A great amount of energy is required to promote  $\sigma$  electrons to higher energy levels because electrons involved in the  $\sigma$  bonds are held very tightly and reside in a low energy level. Accordingly, the molecular electronic spectra involving  $\sigma$  bonds occur in the vacuum ultraviolet region and are not very useful in conventional luminescence spectroscopy. In contrast, electrons involved in  $\Pi$  bonding have weaker binding forces and the required energy is in an experimentally convenient range to promote these electrons to higher energy levels. Therefore, most applications of fluorescence spectroscopy are based on electrons from  $\Pi$  orbital(s). Aromatic Hydrocarbons are good candidates for fluorescence based measurements because of their conjugated chemical structures that have delocalized  $\Pi$  electrons distributed over the entire molecule. Typically, conjugated systems of less than eight conjugated double bonds absorb light only in the ultraviolet region and are colorless to the human eye. The absorption of light in the ultraviolet to visible spectrum can be quantified using UV/VIS spectroscopy. With every double bond added, the system absorbs photons of longer wavelength (lower energy) and the compound color ranges from yellow to red (Atkins 2002).

### **2.2.2. Molecular Energy States**

The ground state of a quantum mechanical system such as atoms is its lowest-energy state. When an atom is in its ground state, its electrons fill the lowest energy orbitals

completely before they begin to occupy higher energy orbitals. At the ground state, atoms are not rigidly fixed in space but have periodic motions with respect to one another and with respect to the centre of mass of a molecule(s) due to the tendency of positively charged nuclei to repel each other and the affinity of bonding electrons to hold them together. These periodic relative motions are known as normal vibrations. Each of the molecular ground and excited states has unique vibrational energy sublevels ( $v=1,2,3,\dots$ ) (Schulman 1977). The Morse potential, named after physicist Philip M. Morse, is a convenient model for the potential energy of a diatomic molecule that approximates the vibrational structure of the molecule (Figure 2-5) (Morse 1929).

When sufficient energy is transferred to electrons in the ground state, they can be promoted from their ground state to higher energy orbitals resulting in an *electronically excited state* of the molecule. Simultaneous changes in electronic and vibrational energy levels of a molecule due to the absorption or emission of a photon of the appropriate energy can be described by the Franck-Condon principle. The principle suggests that an electronic transition is most likely to occur without changes in the positions of the nuclei in the molecular entity and its environment. The resulting state is called a Franck-Condon state, and the transition involved is a vertical transition. Figure 2-5 shows Morse potential energy curves for the vibration of the atoms in the ground and first excited state of the electron cloud, as functions of a vibration coordinate. However, exciting the electronic cloud of a molecule could induce changes in the  $\pi$ -electron density and slightly alter the molecule geometry, in

particular the distances between the carbon atoms (Bernath 1995).

In the ground state, electrons exist in pairs with opposite spins, which satisfies the Pauli Exclusion Principle. However, when an electron is promoted to a higher energy orbital one of the electrons may change spin. When an electron is promoted to a molecular orbital of higher energy without changing spin, the molecule is said to have a singlet (S) electronic excited state. On the other hand, when the promoted electron changes spin and both electrons have a parallel spin, the molecule is said to have a triplet (T) electronic excited state (Figure 2-6). The ground state of a large majority of fluorescent molecules is a singlet state and is called  $S_0$ . There are several excited states with specific energies, the first excited singlet and triplet states are called  $S_1$  and  $T_1$ .  $T_1$  is lower energy than  $S_1$  because of the exchange interaction effect that decreases the energy of  $T_1$  due to wave functions overlap (Schulman 1977).

The names of singlet and triplet excited states come from their spin multiplicity, which is the number of possible orientations. Spin multiplicity can be calculated as  $2S + 1$  of the spin angular momentum corresponding to a given total spin quantum number (S). A state of singlet multiplicity has  $S = 0$  and  $2S + 1 = 1$  On the other hand, a triple state has  $S = 1$ ,  $2S + 1 = 3$  (IUPAC 1997). Allowed electron transitions among ground and excited states are governed by selection rule that constrains the physical properties that are necessary for a process to occur considering angular momentum conservation. Selection rule required spin multiplicity must not change during electron transitions, which makes electron transitions between singlet and triplet



energy states typically forbidden. However, single-triplet electron transitions still occur but with low probability (Chiu 1971).

### 2.2.3. Excitation and De-excitation Processes

At low temperature, the molecule starts out in the  $v = 0$  vibrational level of the  $S_0$  and upon absorbing a photon of the necessary energy, makes a transition to a vibrational level excited electronic state  $S_1$  (or  $S_2$ ). This process is very fast and happens within  $10^{-15}$  second. The probability that the molecule can end up in any particular vibrational level is proportional to the square of the overlap of the vibrational wave functions of the original and final state (Atkins 1999; Coolidge 1936). As well, absorbed photon energy ( $E$ ) decides which vibrational level of  $S_1$  (or  $S_2$ ) becomes populated and can be described by Planck's quantum theory:

$$E = h \cdot \nu \quad [2-1]$$

Where:  $h$  = Planck's constant and  $\nu$  = frequency of light. The Planck constant has dimensions of energy multiplied by time and is expressed in joule-seconds. Also, it is expressed in eV·s because of the small energies that are usually encountered in quantum physics. The value of the Planck constant is:  $h = 6.626\ 068\ 96(33) \times 10^{-34}$  J.s. or  $4.135\ 667\ 33(10) \times 10^{-15}$  eV.s. It is essential that light energy ( $E$ ) has a value that matches the energy gap between the ground state and excited state to which excitation will occur, otherwise light will not be absorbed and the molecule is said to be transparent to light (Harris 1991).

The promotion of electrons to vibrational levels in excited states is usually represented by the Jablonski diagram, which is named after Polish physicist Aleksander Jablonski (Figure 2-7). The diagram illustrates the electronic states of a molecule and the transitions between them. The states are arranged vertically by energy and grouped horizontally by spin multiplicity. A molecule in its excited state can relax by various pathways: non-radiative and radiative de-excitation. Non-radiative de-excitation processes result in electrons moving to lower energy states and losing the excess energy without emission of radiative energy (light). In radiative de-excitation processes, the excess electronic energy is released in photons as waves of visible or ultraviolet light. In the Jablonski diagram, radiative transitions are indicated by straight arrows and non-radiative transitions by squiggly arrows. The favoured de-excitation route is the one that minimizes the life of the excited state and preserves angular momentum (Atkins 2002).

#### **2.2.4. Non-Radiative De-Excitation Processes**

After an excited electron arrives at a vibrational level higher than the lowest vibration level of the  $S_1$ , it starts to give up stepwise its excess vibrational energy with intra and intermolecular energy transfer, in which the excess energy of the excited vibrational mode is transferred to the kinetic modes in the surrounding molecules of excited species and solvent through collision, until it reaches the lowest vibrational level in  $S_1$ . This de-excitation process is called *vibrational relaxation* and has a lifetime of  $10^{-13} - 10^{-10}$  sec (Valeur 2002). When the electron arrives at the lowest vibrational level of the first excited state, it can lose excess energy and return back to the ground state

by *internal conversion* (Figure 2-7). Internal conversion is a mechanism that allows electron transition from electronic vibrational level in a higher singlet excited state to another vibrational level in lower singlet excited state of the same spin multiplicity. Internal conversion occurs when the higher vibrational levels of the lower singlet excited states overlap the lower vibrational levels of the higher singlet excited states. The internal conversion process is very efficient because it occurs between molecular electronic excited levels with the same spin multiplicity, which preserves angular momentum of the molecule. Internal conversion occurs in the order of  $10^{-12}$  sec (Harris 1991). Another non-radiative de-excitation process is *intersystem crossing* (Figure 2-7). Intersystem crossing is a non-radiative transition between two vibrational levels in electronic excited states having different multiplicities (i.e. singlet or triplet states). Intersystem crossing involves change in spin angular momentum and is classically forbidden by the Pauli Exclusion Principle and selection rule, which makes it less probable to happen. Thus, intersystem crossing transition rates are rather low to compete with internal conversion or vibrational relaxation, however still fall within a reasonable time scale to compete with radiative de-excitation processes. The lifetime of intersystem crossing is about  $10^{-8}$  sec (Schulman 1977).

#### **2.2.5. Radiative De-Excitation Processes**

Non-radiative transitions are much reduced for planar and rigid molecules such as benzene rings because the energy gap between vibrational levels in the  $S_1$  and  $S_0$  is relatively large, so that direct vibrational relaxation and internal conversion have quite

low probability of occurring and excess electronic energy is more likely released in photons of ultraviolet or visible light. Thus, radiative de-excitation processes prevail in chemically stable conjugated structures of benzene ring. A radiative transition is known as fluorescence, if the transition starts from  $S_1$  (Figure 2-7). Fluorescence emission is typically slower than vibrational relaxation and happens after  $10^{-9}$  second. Therefore, the molecule will be fully relaxed to the lowest vibrational level of  $S_1$  at the time of emission. Fluorescence response is based on the difference in energy between the lowest vibrational of  $S_1$  and the vibrational levels in  $S_0$  to which the excited electrons are transferred. Because emission always occurs from the lowest vibrational level of  $S_1$ , the fluorescence spectrum is generally independent of the excitation energy (wavelength) that could promote electrons to higher excited states. The electron may remain in the lowest vibrational level of the lowest excited state for  $10^{-8}$  second before it emits visible or ultraviolet fluorescence. After the fluorescence occurs, vibrational relaxation occurs in  $10^{-12}$  second, so the molecule will eventually arrive at the lowest vibrational level of the ground state (Skoog and West 1971).

If excited electrons change spin and get transferred by intersystem crossing to a triplet excited state, radiative de-excitation could then occur from the lowest vibrational level of  $T_1$  after vibrational relaxation process occurs, so electrons return to a vibrational level in  $S_0$ . This radiative transition is known as *phosphorescence* (Figure 2-7). Phosphorescence is more likely to occur in rigid medium or at low temperatures and its lifetime can range from  $10^{-4}$  second to as long as several seconds because of the low probability of single-triplet transition that involves forbidden spin change.

The Phosphorescence spectrum is located at a higher wavelength than the fluorescence spectrum because the energy gap is smaller between the lowest vibrational level of  $T_1$  and  $S_0$  (Valeur 2002).

## 2.2.6. Characteristics of Fluorescence

### 2.2.6.1. Emission and Excitation Spectra

There are two basic ways by which fluorescence spectra of a compound can be scanned: *emission* and *excitation* fluorescence spectra. In emission spectrum, the wavelength of the exciting radiation is held constant and the spectral distribution of the radiation emitted from the compound is measured. Alternatively, in excitation spectrum, the observation fluorescence wavelength is held constant while the fluorescence intensity is measured as a function of the excitation wavelength. Emission fluorescence spectrum represents graphically the distribution of transitions from the lowest vibrational level in  $S_1$  to the various vibrational levels in  $S_0$ . Hence, emission spectrum reflects the vibrational structure of  $S_0$ . In contrast, excitation spectrum represents graphically the intensities of absorbed light to promote electrons from  $S_0$  to various excited states. Because a molecule can fluoresce only after it has absorbed radiation, the excitation spectrum identifies the wavelengths of light that the fluorophore is able to absorb. Therefore, the corrected excitation spectrum is identical in shape to the absorption spectrum, provided that there is only a single species in the  $S_0$  (Valeur 2002).

The strengths of the electronic transitions in emission and excitation spectra are represented by very sharp lines at low temperatures that broaden to form smooth contours at room temperatures. Bands in emission and excitation fluorescence spectra that correspond to transitions between the lowest vibrational levels of  $S_0$  and  $S_1$  are known as *0-0 bands* (Figure 2-8). The 0-0 bands are identical in energy and correspond to the longest wavelength in the excitation spectrum and shortest wavelength in the emission spectrum. There often exist mirror image symmetry between the emission spectrum and the  $S_0 \rightarrow S_1$  excitation (absorption) spectrum (not the  $S_0 \rightarrow S_2$ ). The symmetry is explained by the Franck-Condon principle that suggests transition from the ground state to the excited state occurs in  $10^{-15}$  second, which is much faster than the  $10^{-10}$ - $10^{-12}$  second necessary for nuclear coordinates to change. Thus, the vibrational structure and geometry of the molecule after absorption is almost identical to its vibrational structure and geometry before absorption. However, this mirror symmetry is not observed in all fluorescing molecules due to intermolecular charge transfer mechanisms (Jaffe and Orchin 1962).

Because of the unique nature of emission and excitation spectra, they are considered characteristic of a given compound and can be used effectively to identify fluorescent compounds for analytical purposes (Lakowicz 1999). The use of fluorescence spectroscopy as a detection technique to determine PAHs in marine sediments was applied to detect freshly spilled crude oil in marine environment (Vandermeulen et al. 1979). Also, several researchers have used fluorescence techniques for detection and classification of naturally occurring organic materials and related aromatic

hydrocarbons in the environment (Aiken and Leenheer 1993; Babichenko et al. 1995; Kershaw and Fetzer 1995; Marhaba 2000), as well as oil spill applications (Brown and Fingas 2003). Fluorescence measurements were applied to detect and aromatic hydrocarbons in gases at room and high temperatures (Song et al. 2003; Cullum et al. 2000). Fluorescence based measurements were efficiently utilized in direct push probes allowing real time detecting and monitoring of PHC contaminants in subsurface soils (Lieberman 1998). This application of fluorescence based measurements will be discussed in more details later in this chapter.

## **2.2.7. Quantitative Aspects of Fluorescence**

### **2.2.7.1. Excited-State Lifetimes**

The fluorescence lifetime refers to the time a molecule stays in its excited state undergoing radiative and non-radiative de-excitation processes. The fluorescence lifetime is an important parameter for practical applications of fluorescence, such as time resolved spectroscopy. Fluorescence lifetime typically follows first-order kinetics and describes the decay of fluorescence intensity of uniform population of molecules excited by a brief pulse of light, as an exponential time function:

$$I(t) = I(t_0) e^{-t/\tau} \quad [2-2]$$

Where  $I(t)$  is the fluorescence intensity measured at time  $t$ ,  $I(t_0)$  is the initial intensity observed immediately after excitation and  $\tau$  is the lifetime of the excited state. Fluorescence lifetime ( $\tau$ ) is defined as the time in which the initial fluorescence intensity of a fluorophore decays to  $1/e$  (approximately 37%) of the initial intensity.

This quantity is the reciprocal of the depopulation rate of excited electrons to  $S_0$  through all de-excitation mechanisms (rate constant of fluorescence decay). The lifetime of the singlet excited state ( $\tau_s$ ) is linked to radiative and non-radiative de-excitation processes, thus  $\tau_s$  can be expressed as the inverse of the total rate constants (Figure 2-9):

$$\tau_s = 1 / (k_r^s + K_{nr}^s) \quad [2-3]$$

Where,  $K_r^s$  is the rate constant for radiative de-excitation from  $S_1$  to  $S_0$  (emission of fluorescence) and  $K_{nr}^s$  is the rate constant for non-radiative de-excitation from  $S_1$  to  $S_0$ .  $K_{nr}^s$  combines the rate constants for internal conversion ( $K_{ic}^s$ ) and intersystem crossing ( $K_{isc}^s$ ). The non-radiative rate constant usually ignores any contribution from vibrational relaxation because of the rapid speeds (picoseconds) of these conversions. If the only way of relaxation from  $S_1$  to  $S_0$  were fluorescence emission, the lifetime would be  $1/k_r^s$ . This is called radiative or intrinsic lifetime and is denoted by  $\tau_r$ . As in fluorescence emission, the lifetime of homogenous single fluorophore is independent of the excitation wavelength because the fluorescence emission occurs from lowest vibrational level in  $S_1$  (Valeur 2002).

#### 2.2.7.2. Quantum Yield ( $\Phi$ )

Quantum yield is a measure of fluorescence emission efficiency relative to all of the possible pathways for relaxation. It is generally expressed as the dimensionless ratio of photons emitted to the number of photons absorbed. The quantum yield reflects the probability that a given excited fluorophore will produce a photon (fluorescence);



therefore, the maximum possible value for the fluorescence quantum yield is 1. The number of molecules known to exhibit fluorescence quantum yields near the unity is very few. Benzene, which is the simplest polycyclic aromatic hydrocarbon compound with one aromatic ring, has fluorescence efficiency nearing 0.05. Higher quantum yield values are reported for larger polycyclic aromatic hydrocarbon molecules. The quantum yield of a given fluorophore varies with environmental factors such as pH, concentration, and solvent polarity.  $\Phi$  can be expressed as the rate of photons emitted divided by the total rate of depopulation of the excited state (Wehry 1990):

$$\Phi = k_r^s / (k_r^s + K_{nr}^s) \quad [2-4]$$

#### 2.2.7.3. Stokes Shifts

The peak of the emission band occurs at a longer wavelength than the peak of the absorption band in fluorescence spectrum of a compound. The energy difference between absorption and emission maxima is called Stokes shift, after Sir G. G. Stokes who first observed this phenomenon in 1852 (Figure 2-10). There are several mechanisms related to radiation absorption and intramolecular charge transfer that can result in Stokes shifts. Stokes shift is strongly affected by the secondary inner filter effect, the re-absorption of fluorescence photons by the fluorophores itself or other molecules. If Stokes shift is small, a relatively large part of the emitted photons are reabsorbed by sufficiently high fluorophore concentrations, which reduces apparent fluorescence efficiency. In contrast, when Stokes shift is large, the emitted photons are usually spectrally well separated from scattered excitation light and from impurity fluorescence that usually exhibit small Stokes shift properties. Other mechanisms that can induce Stokes shifts, such as the excimer/exciple formation and

excited-state intramolecular charge transfer mechanisms, have been well characterized. In an excimer/exciplex case, the formation of a complex of a ground-state with an excited-state molecule of the same (excimer) or of a different kind (exciplex) usually involves large intramolecular rearrangements, which induce changes to fluorescence emission wavelengths that are reflected by larger Stokes shifts. Conversely, excited state intramolecular charge transfer mechanism involves transfer of charge from one basic site to another in the same molecule (or molecular cluster) by means of charge tunnelling through large energy gaps that is classically forbidden, however, it can still have low probability to occur. This change in charge distribution has direct effect on fluorescence emission wavelengths and the value of Stokes shifts (Lakowicz 1999).

#### 2.2.7.4. Quantitative Fluorescence Intensity

Based on experimental work by Beer in 1852, an empirical relationship was developed to relate the absorption of light to the properties of the material and concentration of an absorbing species through which the light is travelling. The relationship is formally known as *Lambert-Beer law* or simply *Beer's law*:

$$A = \text{Log} (I_0/I) = \epsilon \cdot b \cdot c \quad [2-5]$$

Where,  $A$  is absorbance,  $I_0$  is the incident light intensity,  $I$  is the transmitted light intensity,  $b$  is the path length traveled by light in the sample in centimetres,  $c$  is the sample concentration in Mole/Liter and  $\epsilon$  is called *Molar Absorptivity*, which is a substance characteristic that indicates how much of light will be absorbed by the

sample at a certain wavelength and normally expressed in Liter/Mole.Centimetre. An unknown concentration of an analyte can be determined by measuring the amount of light that a sample absorbs and applying Beer's law.

Experimental measurements are usually made in terms of transmittance (T), which is defined as:

$$T = I / I_0 \quad [2-6]$$

The relation between A and T is:

$$A = -\log T = -\log (I / I_0) \quad [2-7]$$

Fluorescence intensity can be derived using Beer's law and fluorescence quantum yield ( $\Phi_F$ ) as in the following relationship:

$$I_F = K\Phi_F I_0 \epsilon b c \quad [2-8]$$

Where K is instrument constant. Equation 2-7 allows estimating the fluorescence intensity as a function of concentration (Lakowicz 1999). Lambert-Beer Law can only be applied when the sample fluorophore is at very low concentrations (< 0.01 M), as Beer-Lambert law deviates from linearity at high concentrations (>0.01M) due to electrostatic interactions between molecules in close proximity (Harris 1991). The decrease in fluorescence intensity at higher concentrations is related to inner filter effect and fluorescence quenching processes. As described earlier, inner filter effect describes the process of absorption of exciting and/or emitted radiation by dissolved species, including the fluorophore itself. Inner filter effect is more apparent in

mixtures of fluorophore molecules with overlapping excitation and emission fluorescence spectra. Alternatively, quenching is a process in which a fluorophore decreases the fluorescence intensity by direct interaction. There are two mechanisms that can describe fluorescence quenching: 1) dynamic quenching, resulting from enhanced collisional encounters between excited fluorophore molecules at higher concentrations, which causes a loss of excitation energy through non-radiative de-excitation which results in reduction of fluorescence intensity; and 2) static quenching, resulting from complex (excimer) formation between two fluorophore molecules in ground and excited states due to enhanced interaction between molecules at higher concentrations. The formed excimer typically fluoresces at longer wavelengths, which results in reduction of fluorophore fluorescence intensity at the original emission peak wavelength where it is expected to fluoresce (Schulman 1977).

## **2.2.8. Alternative Fluorescence Measurements**

### **2.2.8.1. Synchronous Fluorescence Spectroscopy**

In addition to conventional fluorescence scanning methods for emission or excitation fluorescence spectra, other approaches that provide more fluorescence spectral information to help characterize complex PAH mixtures are commonly used. One of these approaches is synchronous fluorescence scanning (SFS) that was first suggested by Lloyd (1971). In SFS, both excitation and the emission wavelengths are scanned simultaneously (synchronously) while keeping a constant wavelength difference ( $\Delta\lambda$ ) that often matches the Stokes shift of the analyzed components of interest. For an individual PAH, this results in no response over almost all wavelengths with exception to narrow band. The obtained synchronous spectrum will consist simply of

one single peak and decreased spectral bandwidth (Figure 2-11). Narrowing of spectral band is essentially a result of the multiplication of two simultaneously increasing and/or decreasing functions (excitation and emission) (Vo-Dinh 1978).

SFS enhances selectivity as it allows selecting one particular  $\Delta\lambda$  that matches one unique pair of excitation and emission bands of a particular compound, so the synchronous spectrum will show only one single peak related to that compound. For PAHs with a strong 0-0 band emission, such as anthracene and perylene, choosing a small  $\Delta\lambda$  is suitable to detect these compounds. In contrast, PAHs that do not have a strong 0-0 band, such as pyrene and coronene, are best scanned with larger  $\Delta\lambda$ . The use of a narrow  $\Delta\lambda$  usually results in maximum simplification of the fluorescence spectra, while wider settings lead to increased sensitivity for the target PAH but with greater chances for interferences. A compromise between simplification and sensitivity should be considered when  $\Delta\lambda$  is selected to detect particular PAH using SFS (Karcher 1988). In **multi-component analysis**, the synchronous spectrum is often a simplified spectrum that consists of a series of well-resolved peaks that correspond clearly to the synchronous signal of each individual component in the mixture (Vo-Dinh 1978).

In previous studies, *the* enhanced details in synchronous fluorescence spectra allowed firm conclusions to be drawn concerning the identity of various PAHs and crude oil samples (*Kershaw and Fetzer 1995; John and Soutor 1976*). Also, SFS has been described as a successful technique to characterize petroleum-derived products, such as diesel, petrol, kerosene and engine-lubricant oils (*Patra and Mishra 2002*).

Synchronous fluorescence spectra of oils found in ground water through seepage have been utilized to locate potential well drilling sites and to differentiate products from spills (Calhoun and Burrows 1992; Pharr et al. 1992). SFS can be used to quantify the concentrations of fluorescing hydrocarbon in contaminated samples because the linear relationship between the synchronous signal and the concentration of the fluorescence compound is preserved in the same way as with conventional spectrometry (Vo-Dinh 1978).

To enhance the capability of synchronous fluorescence spectrometry, it was suggested to combine information from both excitation and emission spectra into a single display by running many synchronous spectra for a particular compound, each at a different wavelength offset. All information present in the excitation and emission spectra of the compound can be captured and presented in the form of a three-dimensional matrix (Figure 2-12), known as an excitation–emission matrix (EEM) (Christian, et. al.1981; Vo-Dinh 1982). The three-dimensional EEM is usually displayed as a top-view fluorescence contour map, wherein points of equal intensity are connected. EEM presentation tends to separate different components of a multi-component system into isolated “peaks” (Figure 2-12). Rho and Stuart (1978) described another approach to obtain excitation–emission matrix in which the emission spectrum is scanned repeatedly at a series of fixed excitation wavelengths that cover the excitation region of interest in regular increments. Three-dimensional fluorescence EEM has been used to identify crude oil petroleum product spills and have been reported for petroleum products, such as diesel, kerosene and petrol (Patra and Mishra 2002; Eastwood 1981).

### 2.2.8.2. Time Resolved Fluorescence Spectroscopy

Fluorescent compounds with overlapping emission and excitation spectra often have very different fluorescent lifetimes, therefore, their intensity contributions can be resolved in time or frequency domains. The combination of fluorescence spectral and lifetime dimensions (Figure 2-13) is known as *time-resolved fluorescence spectroscopy*. These measurements can reveal more related spectral characteristics than conventional fluorescence measurements, and strengthen the ability of the fluorescence spectroscopy to analyze multi-component samples. There are two different approaches that can be used in such measurements: pulse fluorescence spectroscopy and phase resolved fluorescence spectroscopy (O'Connor and Phillips 1984).

Pulse fluorescence spectroscopy works in the time domain and uses a short excitation light pulse to produce fluorescence response that is recorded as a function of time. The fluorescence observed from the sample will then include decay characteristics of all fluorescing species whose decay times are longer than that of the pulsed source. Complex mixtures such as crude oils that have a blend of aromatic hydrocarbons are expected to have different decay functions as the nature and relative concentrations of their fluorescing constituents vary. Thus, a lifetime can be assigned to an individual aromatic hydrocarbon for identification. Unlike the conventional fluorescence measurements, fluorescence lifetime measurements do not depend on the concentration of the fluorophore. Also, fluorescence lifetime measurements could

discriminate against light scattering and short-lived fluorescence from scanned samples. These attributes make it possible to use time resolved fluorescence spectroscopy for the simultaneous analysis of aromatic hydrocarbon mixtures and characterize different types of crude oil, heavy refined oil and light refined oil based on their fluorescence decay function with time (Rayner and Szabo 1978; Millican and McGown 1988).

Phase-resolved fluorescence spectroscopy works in the frequency domain. In phase-resolved fluorescence spectroscopy, the sample is excited with sinusoidally modulated light at high frequency to produce a sinusoidal fluorescence response at the same frequency but partially demodulated and delayed in phase because of the time lag between absorption and emission. The phase shift and modulation factor are used to generate fluorescence decay times and time-resolved fluorescence spectra (McGown and Nithipatikom 1986a). Phase-resolved fluorescence spectroscopy can be utilized to selectively enhance or reduce the fluorescence contributions of sample components as a function of their fluorescence lifetimes. It can also suppress the scattered light that has a lifetime of zero by setting the detector phase at  $90^\circ$ . Suppression of scattered light should improve the analysis by allowing the direct observation of spectral peaks (McGown and Nithipatikom 1989). Phase-resolved fluorescence spectroscopy was used successfully to characterize a multi-component mixture of six aromatic hydrocarbon components with overlapping spectra using multidimensional data formats of phase resolved fluorescence intensity as a function of spectral and lifetime parameters (McGown and Nithipatikom 1986). Another study



demonstrated the ability of multi-frequency phase resolved fluorescence spectroscopy to selectively enhance fluorescence as a function of fluorescence lifetime to detect aromatic hydrocarbons in mixtures (Vo-Dinh et al 1990).

### **2.3. FLUORESCENCE MEASUREMENTS INSTRUMENTATION**

Fluorescence measurement instrumentation utilize the following scheme: 1) light source to electronically excite fluorescing molecules in the sample, 2) wavelength selector to isolate the desired excitation light wavelength, 3) a fluorophore sample at which some of the excitation light is absorbed, making some of the molecules in the sample fluoresce, 4) wavelength selector to separate the desired fluorescence wavelength emitted by sample, 5) a photo-detector to translate the fluorescent light into an electrical signal, and 6) a read out system (Figure 2-14). In addition to the optical components shown, most fluorescence spectrometers have dedicated computers, which control the instrumental operating parts and acquisition of spectral data (Sharma and Schulman 1999).

#### **2.3.1. Excitation Sources**

The ideal source of exciting light should have the following criteria: 1) generate intense light with sufficient power for ready detection and measurement, 2) provide continuous radiation that contains all wavelengths in the near ultraviolet-visible range that are required to excite the sample, 3) have independent intensity that is not affected by the wavelength and 4) be stable, so that intensity or spectral characteristics will not change during the time needed for measuring fluorescence.

(Skoog and West 1971) There are a variety of different excitation sources that could be used in fluorescence spectroscopy. Commonly used sources are listed herein detailing their advantages and limitations.

***Gas Discharge Lamps:*** Gas discharge lamps are a group of excitation sources that produce light by electrical breakdown of gas (electric arc). The lamp consists of two electrodes typically made of tungsten separated by a gas or metal vapour. When operated, the electrical field generated between the electrodes ionize the gas in the lamp and excite free electrons. When electrons fall back to their original state, they emit photons, resulting in visible light or ultraviolet radiation. The gas contained in the bulb can be neon, argon, xenon, krypton, sodium, metal halide or mercury. The wavelength distribution of emissions is determined by the nature of the gas filling the lamp and pressure. Spectral output of arc discharge lamps is usually composed of line and continuous emission components. The amount of each component depends on the gas (or metal vapour) pressure in the lamp. At low pressure, more sharp lines with little continuous background are emitted. As the pressure increases, the lines broaden and continuum background intensity increases. Commercial fluorescence spectrometers use high-pressure xenon, mercury or mercury-xenon arc lamps as excitation sources because they are stable and provide broad excitation wavelengths range and sufficient intensity for fluorescence spectroscopy purposes. Mercury vapour lamps have intense mercury line emissions between 254 and 579 nm, which make them an excellent light source for spectrometer calibration purposes. Xenon lamps are short-arc gas-discharge lamps that provide a good continuum spectrum from 250 to

800 nm, which is desirable for fluorescence scanning spectrometers. Gas discharge lamps require a high voltage pulse from well regulated direct current power source to start the lamp. Also, their efficiency is highly affected by voltage losses across the electrodes; nearly half the power delivered to the lamp is wasted heating up the electrodes. Therefore, gas discharge lamps require a sophisticated power supply and continuous maintenance to achieve stable, long-life operation, which make them expensive to produce and operate (Harry and Yuan 2000; Schulman 1977).

***Laser Excitation Sources:*** A laser (Light Amplification by Stimulated Emission of Radiation) is an inherently pure, intense source of light that emits monochromatic light with a very well defined wavelengths that ranges from ultraviolet to infrared, which makes the laser a very useful excitation source for fluorescence spectroscopy applications (Maiman, 1962). A laser consists of a gain medium inside an optical cavity that in its simplest form consists of two mirrors arranged such that coherent beam of light bounces between reflective surfaces in the gain medium. When passing back and forth, the light beam gains energy by stimulated emission before it is emitted from the output aperture. Stimulated emission is the process by which matter produces photon when perturbed by different photon. The perturbing photon is not destroyed in the process, and the second photon is created with the same phase, frequency, polarization, and direction of travel as the original. The gain medium can be gas, liquid, solid or free electrons and is typically energized by an external energy source such as a flash lamp or another laser (Andrews and Demidove 2002).

According to the nature of the gain medium, lasers can be grouped into different categories that include: Gas lasers, Dye lasers, Excimer lasers, Metal-vapor lasers, Solid-state lasers and Semiconductor lasers. The output of a laser may be continuous, constant amplitude output or a pulsed coherent beam of light at specific wavelength or range of tunable wavelengths. Gas lasers are one of the oldest types of laser and use different gases. Nitrogen laser is an inexpensive gas laser that produces UV Light at 337.1 nm and commonly used in fluorescence spectroscopy. Metal ion lasers are gas lasers that generate deep ultraviolet wavelengths. Helium-silver (HeAg) and neon-copper (NeCu) are two examples of metal ion lasers that produce UV light at 224 and 248 nm. Excimer lasers are powered by a chemical reaction involving an excited excimer. Commonly used excimer molecules include XeCl and XeF. They produce UV light at 308 and 351 nm respectively, and are frequently utilized in fluorescence spectroscopy. Solid state laser materials are made by doping a crystalline solid host with ions that provide the required energy states. Neodymium is a common dopant in various solid state laser crystals such as yttrium orthovanadate (Nd:YVO<sub>4</sub>), yttrium lithium fluoride (Nd:YLF) and yttrium aluminium garnet (Nd:YAG) that produce lasers at 532, 355 and 266 nm, which are common wavelengths used in fluorescence spectroscopy (Koechner, 1999; Svelto, 1998; Csele, 2004). Tunable lasers are gaining preference in fluorescence spectroscopy because they offer a wider range of excitation wavelengths that spans from deep UV to infrared light. Tunable lasers have gain medium with a broad gain profile that allow broadband laser emission and one can choose laser emission wavelength by using suitable intra-cavity aperture and dispersive elements. Lasers do not require a complex power source to start the lamp

and are relatively inexpensive to produce and operate. Also, lasers provide a wide range of different intensities, which makes them an attractive choice for excitation sources in fluorescence spectroscopy (Duarte 1995).

***Light Emitting Diodes (LEDs):*** LED is a semiconductor device that converts electrical energy into visible/UV incoherent monochromatic light when connected to voltage source in the forward direction (electrically biased). Semiconductor chips in LEDs are impregnated (doped) with impurities to create a distinctive structures known as p-n junction that can accommodate both electrons (negatively charged) and holes (positively charged electron vacancies) separated by a band-gap. When a forward voltage is applied, charge-carriers (electrons and electron holes) flow into the junction, so electrons move from the n layer toward the p layer, and holes move toward the n area voltages. When an electron meets a hole, it falls into a lower energy level, and releases energy in the form of a photon (Holonyak and Bevcqua 1962). The energy of the released photons, and accordingly their emission wavelength, is determined primarily by the energy band gap that is a characteristic of the semiconductor. Semiconductor materials typically used in LED have energy band gaps that correspond to emitted light wavelengths that range from ultraviolet to infrared. Conventional LEDs are made from a variety of inorganic minerals such as Aluminium gallium arsenide (AlGaAs), Aluminium gallium phosphide (AlGaP), Aluminium gallium indium phosphide (AlGaInP), Gallium arsenide phosphide (GaAsP), Diamond (C), Aluminium nitride (AlN), aluminium gallium nitride (AlGaN), aluminium gallium indium nitride (AlGaInN) and organic compound such

as polymers (Kovac et al. 2003). AlGaInN and AlGaInN are used to produce LEDs to emit light wavelengths in the UV range. Near-UV emitters at wavelengths around 375-395 nm are common, inexpensive and available in the market. Shorter wavelength diodes are also commercially available for wavelengths down to 247 nm but considerably more expensive (<http://www.s-et.com> 2007). LEDs can emit light of an intended wavelength without using filters that traditional lighting methods require. Because of that monochromatic nature, LEDs are suitable for applications of fluorescence spectroscopy that require specific operational excitation wavelengths. LEDs can be very small, inexpensive, produce more light per watt than most light sources and have an extremely long life span allowing considerable energy-saving. For that reason, LEDs are becoming a viable option for excitation sources for fluorescence spectroscopy applications (Kovac et al. 2003).

### **2.3.2. Wavelength Selectors**

There are two major types of wavelength selectors used in fluorescence spectroscopy measurements: filters and monochrometers. Filters allow a wider range of wavelengths to excite the sample and to pass through to the detection system. Monochromators allow the passage of a smaller range of wavelengths that is ultimately determined by the optical characteristics of the diffraction grating. Optical filter is an optically homogeneous material that can transmit selectively only a small part of the incident polychromatic radiation, namely a particular range of wavelengths, while blocking the remainder. Optical filters can be made of tinted glass, gelatin containing organic dyes or a liquid solution of absorbing substances.

Filters can be grouped into two main categories: *absorption* and *interference filters*.

Absorption filters selectively absorb the undesired portion of the incident light and transmit only the light of desired wavelengths. Alternatively, interference filters utilize the principle of constructive interference of radiation for their transmission characteristics. Interference filters can be divided into two categories: long-pass and short-pass filters. Long-pass filter is an optical interference filter that attenuates shorter wavelengths and transmits longer wavelengths over the active range of the target spectrum (ultraviolet, visible, or infrared region). In fluorescence microscopy, long-pass filters are frequently utilized in emission filters. A short-pass (SP) Filter is an optical interference filter that attenuates longer wavelengths and transmits shorter wavelengths over the active range of the target spectrum (usually the ultraviolet and visible region). Short-pass filters are frequently employed in excitation filters in fluorescence microscopy. If a long-pass filter and a short-pass filter are combined, they produce a band-pass filter. These filters have usually lower transmittance values than short-pass and long-pass filters. Also, they block all wavelengths outside of a selected interval that can be wide or narrow depending on the number of layers of the filter (Lakowicz 1999).

A monochromator is a device that separates radiation into its component wavelengths to allow selecting the desired wavelength from the remaining unwanted wavelengths. Monochromators are used extensively in laboratory environments to select excitation light and emitted fluorescence wavelengths. Monochromators are usually composed

of different arrangements of lenses, slits and dispersing elements (prisms or diffraction gratings) to spatially separate the wavelengths of light. In the prism case, when light enters through the hypotenuse face of reflective prism, it gets reflected back by the mirrored side through the prism allowing for total dispersion. A grating disperses light into its component wavelengths by utilizing the principle of destructive and constructive interference of light upon reflection by a triangular groove reflective surface.

When light enters the monochromator through the entrance slit, it gets refracted by the prism or diffracted from the grating and is then collected by a mirror that refocuses the dispersed light on the exit slit. At the exit slit, the light wavelengths will be spread out and each wavelength arrives at a separate point in the exit slit plane. Rotation of the dispersing element causes wavelength bands to move relative to the exit slit, so that the desired light wavelength is centered on the exit slit (Figure 2-15). The range of wavelengths leaving the exit slit is a function of the width of the entrance and exit slits, which usually can be adjusted as desired. Slits help to focus the light and control the range of wavelengths that can excite the sample or pass onto the detection system upon emission. Therefore, they are important components of the monochromator that can determine its quality (Skoog and West 1971; Schulman 1977; Lakowicz 1999).

### **2.3.3. Detectors**

Generally, an efficient fluorescence detector should have the following criteria: 1) respond rapidly to radiation over a wide range of wavelengths, 2) produce an



amplified electrical signal that is proportional to the fluorescence intensity, 3) be sensitive to low radiation levels and 4) have a low noise level. The primary radiation detector employed in the ultraviolet-visible fluorescence spectroscopy that satisfies these characteristics is the photomultiplier tube (PMT). PMT is an extremely sensitive detector of ultraviolet, visible and near infrared light that can detect weak optical signals in most fluorescing solutions. PMTs are constructed from a glass vacuum tube that accommodates a photocathode, several dynodes (a series of electrodes, at which each electrode is held at a more positive voltage than the previous one) and an anode.

When, incident photons move toward the first dynode after striking the photocathode material at the entry window of the device, they get accelerated by the electric field and arrive with much greater energy. On striking the first dynode, more electrons get emitted and accelerated toward the second dynode. The geometry of the dynode chain is such that a cascade occurs with an ever-increasing number of electrons being produced at each stage. Finally the anode is reached where the accumulation of charge results in a sharp current pulse indicating the arrival of a photon at the photocathode. PMTs are capable of amplifying primary photocurrent by as much as  $10^8$  times allowing measurable pulses to be obtained from a single photon. The combination of high gain, low noise and high frequency response make PMTs very effective in various applications of fluorescence spectrometry (Skoog and West 1971).

Because a PMT only provides a single channel of output in response to incoming

fluorescence, it must be combined with a monochromator to scan the output across the desired wavelength range in order to obtain a spectrum. To overcome this limitation, one and two-dimensional array detectors such as photodiodes and intensified photodiode arrays are being used in fluorescence spectroscopy. A photodiode is a semiconductor diode that functions as a photo detector and packaged with either a window or optical fiber connection, in order to let in the light to the sensitive part of the device. When a photon of sufficient energy strikes the p-n junction in the semiconductor material of diode, it excites an electron thereby creating a mobile electron and a positively charged electron hole, which produces detectable photocurrent. The material used to make a photodiode is critical to defining its properties, because only photons with sufficient energy to excite electrons across the material band gap will produce significant photocurrents. Materials commonly used to produce photodiodes include: silicon, germanium, indium gallium arsenide and lead sulfide. Photodiode arrays are typically assembled in a way that each photodiode responds to a different wavelength range, so the fluorescence intensity of different wavelengths are recorded simultaneously and then compiled to define the spectrum. These multi-channel detectors have proved advantageous over PMT based instrumentation because both quantitative and spectral information can be generated simultaneously. However, they are less sensitive than PMTs (Ryan et al. 1978; Jadamec et al. 1977). Generations of more sensitive photodiodes known as Avalanche photodiodes are now being used in fluorescence spectrometry, which can generate an internal gain making these detectors much more sensitive than regular photodiodes (Horowitz and Hill 1989).

Another promising electronic detection technology that is applied in fluorescence spectroscopy is the charge-coupled device (CCD). CCD is a silicon solid-state device capable of storing an electronic charge produced by incident photons in an integrated circuit containing an array of linked capacitors. Once the CCD has been exposed to the photons, a control circuit causes each capacitor to transfer its contents to its neighbour. The last capacitor in the array dumps its charge into an amplifier that converts the charge into a voltage. CCDs can be assembled as a two-dimensional array that is composed of channels, or rows along which charge is transferred to act as multi-channel detectors. Each channel is basically a one-dimensional CCD array. Charge is prevented from moving sideways by channel stops, which are the narrow barriers between the closely spaced channels of the CCD (Weisner 1992; Howes and Morgan 1979).

CCDs share the same multi-channel detectors advantages of simultaneous generation of quantitative and spectral information, but have a much lower detector noise levels (Lakowicz 1999). The use of CCD based spectrometers has grown fast over recent years because they proven to be sensitive, fast and cheap fluorescence measurements tools. CCD based spectrometers are now available miniature sized package with different configurations to allow detecting UV/VIS fluorescence with increased spectral range and minimal decrease in resolution. The technology is expected to gain more preference in future with continued developments in CCD sensitivities.

## 2.4. SITE INVESTIGATION FLUORESCENCE SENSORS

Conventionally, techniques for the analysis of aromatic hydrocarbons in environmental samples is performed in a laboratory using a separation and/or extraction procedures such as chromatography that can be time consuming and expensive. Recent developments in the use of fluorescence spectrometers and fibre optics have made it possible to develop fibre optic fluorescence sensors to analyse aromatic hydrocarbons in environmental samples in the laboratory and the field. In fibre optic sensors, light from a source travels along an optical fibre cable to sample and fluorescence is collected by another fibre that transmits the signal to the detector system (Figure 2-16).

The material of the optical fibre determines the wavelength that can be transmitted. Silica can be used for the ultraviolet range down to 220 nm, while glass is suitable for the use in the visible region and plastic fibres are of limited use above 450 nm (Narayanaswamy 1993; Arnold 1992). After fluorescence based fibre optic sensor systems were used for real-time monitoring of inorganic (metal ions) and organic (aromatic hydrocarbons) contaminants in seawater in the early 90's, the idea was introduced to combine fluorescence sensors with a cone penetrometer probe that maps soil type and changes in stratigraphy to detect aromatic in soils (Lieberman et al. 1990). The viability of the concept of incorporating fluorescence sensors in cone penetrometer probes was first tested by detecting an artificial fluorophore that had been injected into the ground, and found to be efficient (Lurk et al. 1990). Subsequently, a laser-induced fluorescence (LIF) fibre-optic-based sensor was

developed to detect subsurface petroleum hydrocarbons contaminants (Lieberman et al. 1991). Since these early efforts, a variety of sensor probes that use fluorescence spectroscopy to detect petroleum hydrocarbons have been developed. All fluorescence based sensor systems use a similar scheme where UV light from a laser or other light source is transmitted through a sapphire window on a probe installed behind a cone penetrometer. Sapphire is used for the window material because it does not fluoresce when exposed to UV light and has a high scratch resistance to abrasive soil particles. Fluorescence produced by the aromatic components of petroleum hydrocarbons passes back through the window to a detector system located in the probe or via fibre-optic cables to a detector at the surface. A profile of fluorescence intensity versus depth can then be generated in combination with lithological data from the CPT system to provide a real time display of the location of petroleum hydrocarbon contamination (Figure 2-17).

One of the early fluorescence sensors combined with standard cone penetrometers was Site Characterization and Analysis Penetrometer System (SCAPS), developed by the U.S. Department of Defense (DoD) Tri-Service (Army, Navy, and Air Force) (Lieberman et al. 1991). Then, the rapid optical screening tool (ROST) evolved from The U.S. DoD funded research performed at North Dakota State University (NDSU) in consortium with U.S. Air Force Armstrong Laboratory, Loral Defense Systems and Dakota Technologies Inc. (St. Germain et al. 1993 and Nielsen 1995). Advanced Applied Technology Demonstration Facility (AATDF) for Environmental Technology Program at Rice University, Houston, Texas, with Grant from the US

DoD funded a promising technology that utilizes a multi-channel LIF screening system that was developed at Tufts University (Kenny et al. 1995). In Canada, the National Science and Engineering Research Council (NSERC) of Canada in partnership with University of Alberta (U of A) and ConeTec Investigation Ltd, Vancouver, B.C., are working to improve an existing technology known as the ultraviolet induced fluorescence-cone penetration testing system (UVIF-CPT) (Bigger et al. 2003).

#### **2.4.1. Site Characterization and Analysis Penetrometer System (SCAPS)**

SCAPS uses a fibre optic based sensor coupled with a cone penetrometer in a standard 4.0- centimetre diameter probe that can be pushed into the soil to a maximum depth of 50 meters at a rate of 1 meter/minute by a 20-ton truck. SCAPS probe is modified with a 0.6-centimeter diameter sapphire window flush mounted 61 centimetres behind the probe tip. A Nitrogen laser at 337 nm is used as an excitation source. A laser is mounted in the truck coupled to a fibre-optic cable that carries the light down to the sapphire window. Another fibre collects the fluorescence signal emitted by the contaminants in the soil matrix and carries it back to detection system in the truck. At the surface, the fluorescence fibre is coupled to a grating, and a gated linear photodiode is used to record the emitted spectrum from 350 to 720 nm (Lieberman, et. al., 1991; Lieberman, 1998). Data acquisition is automated using software control that generates a spectral curve at each depth and extracts the maximum intensity along with associated peak wavelengths for real time depth display. The system provides a continuous, full spectral classification of the

fluorescence emission signal as the probe is pushed into the ground. SCAPS allows subsurface detection of petroleum, oil and lubricants with a vertical spatial resolution of approximately 6.0 centimetres (Inman et al. 1990; Theriault et al. 1992 and McGinnis 1995).

To improve the probe sensitivity to detect lighter fuels in the soil matrix, two new lasers were used in the SCAPS : 1) an XeCl Excimer laser that produces at 308-nm light and 2) a miniature Nd:YAG laser diode that produces light at 266 nm (Knowles and Kertesz 1996). SCAPS capabilities were tested at a number of different sites near leaking diesel fuel storage tanks. It was able to generate fluorescence intensity data that precisely described the vertical and lateral extent of the fuel spills (Knowles and Lieberman 1995). SCAPS was also used at an old oil refinery site to characterize present contaminants. The captured fluorescence signal profiles clearly identified the presence of heavy and light weight petroleum products (McGinnis 1995). SCAPS detection limit for a specific fuel product in soil (expressed on a weight/ weight basis) are on the order of 100 ppm. This detection limit is a function of the specific fuel product, soil type, soil moisture content and other variables (Apitz et al. 1992 and 1992a). The U.S. EPA verified the capability of SCAPS as qualitative or semi-quantitative field screening methods for petroleum hydrocarbons (Bujewski and Rutherford 1997).

#### **2.4.2. Rapid Optical Screening Tool (ROST) System**

Gillispie and co-workers at North Dakota State University (1993) developed a

fluorescence sensor that also utilizes laser spectroscopy to analyze contaminated soil and groundwater and map the distribution of many hazardous chemicals in the field. The system was called Rapid Optical Screening Tool (ROST) (St. Germain et al. 1993, Gillispie et al. 1993). ROST has a similar components setup to SCAPS, in which the laser source along with detection system are located in a cone penetrometer truck and fibre optic cables are used to transmit pulsed laser light to contaminated soils via sapphire window and fluorescence back to detection system on the truck. In contrast, the ROST has an Nd:YAG pumped dye laser system that produce tuneable multiple-wavelengths that vary over wavelength range of approximately 266–300 nm. The tuneable laser system is unique feature of the ROST system as it takes in consideration the fact that aromatic hydrocarbons require different excitation wavelengths to emit fluorescence based on the number of aromatic rings that compose their structure (Berlman 1971). Thus, the laser output may be tuned to select the optimum wavelength to stimulate fluorescence of particular class of aromatic hydrocarbon contaminants while minimizing potential interferences.

The ROST detector system consists of a monochromator, photomultiplier tube, and a gated optical multi-channel analyzer to digitize and display the fluorescence intensity as a function of time. The monochromator is incremented over a series of different emission wavelengths to generate a series of fluorescence intensity versus time waveforms to produce a wavelength–time matrix (WTM). The resultant fluorescence spectral emission and fluorescent lifetime are used as a fingerprint to characterize contaminants, while the fluorescent intensity indicates approximate contaminant



concentrations (St. Germain et al. 1995 and Gillispie et al. 1995). The ROST system is designed to collect data in two different modes: 1) push or 2) static. In the push mode, the laser excitation frequency is fixed and the fluorescence signal is monitored as the cone penetrometer probe is advanced at a rate of 2 cm/sec, acquiring fluorescence intensity-versus-depth (FVD) profile. Operation in the static mode (with the probe stopped) allows collection of fluorescence multidimensional data sets, typically the fluorescence emission wavelength, intensity, and time of decay matrices (WTMs) (Figure 2-18).

The ROST system has been used in several sites in Europe and the United Kingdom with light, medium, and heavy PHC contaminants (Germain et al. 1993; Gillispie et al. 1993). In London (UK), ROST was used successfully to investigate possible tank leakage at a retail petroleum distribution facility. Also, ROST was used to characterize BTEX contamination from a chemical manufacturing plant in Wales and a coal tar at gas facility in France. The technology demonstrated an ability to identify the presence and nature of different petroleum contaminants such as gasoline, diesel fuel, fuel oils, jet fuel, creosote and coal tars (Nielsen 1995). Exact detection limits of the ROST system might not be easy to determine as they vary between sites and petroleum products. Typically, ROST has shown an ability to detect petroleum products in the range of 100 ppm, however, it was able to detect diesel in sand matrix at a low concentration of 5 ppm in a particular site (Bujewski and Rutherford 1997a). The capability of the ROST has been verified as qualitative or semi-quantitative field screening methods for PHCs by several different programs. ROST participated in the

U.S. EPA-sponsored SITE Demo program (Hess Hamilton 1995) and its performance was endorsed by the U.S. EPA Consortium for Site Screening Technology (CSST) Program (Bujewski and Rutherford 1997a).

#### **2.4.3. Tufts System Multi-Channel LIF Sensor**

The multi-channel laser induced fluorescence (LIF) system developed at Tufts University uses similar components setup to the SCAPS and ROST system. However, it uses a hydrogen-methane Raman shifter, pumped by a pulsed Nd:YAG laser as an excitation source to produce a large number of output beams at different intensities and wavelengths ranging from 258 to 379 nm. In the early generations of this multi-channel LIF sensor, 10 of the resulting beams were coupled into separate fibers and transmitted down the penetrometer probe to separate sapphire windows. These windows were positioned along the length of the probe body and spaced approximately 3.8-centimeters apart. Fibre optical cables were used in the sensor to deliver light to each window, while fluorescence generated at each window was collected by a separate fiber and transmitted to the detection system in truck. At the surface, all 10 channels are arranged in a vertical array and coupled into an imaging spectrograph with a CCD that detected the dispersed fluorescence. The collected data was displayed as three-dimensional EEMs. In addition to the delineation of spatial distribution of contamination in subsurface, patterns observed in the three-dimensional EEMs provide fingerprints that can be utilized to discriminate between different contaminant sources and fuel types (Kenny et. al 1995; 1996). The probe has recently been redesigned so that fluorescence data resulting from all 10 excitation

wavelengths can be collected through a single window (Kenny et al. 2002). The performance of the probe was examined at different military sites contaminated with gasoline and jet fuel spills. The system was able to detect these contaminants and obtained contamination profiles quickly and with good depth resolution. The Generated EEMs were also used for identification and quantitation of fluorescent composition of detected contaminants and showed an acceptable agreement with laboratory tests (Kenny et al. 1996a; 2002). Tufts University multi-channel LIF system detection limits were examined in laboratory and in situ study. The system obtained a significant fluorescence signals for benzene and p-xylene in cyclohexane at concentrations of 500 and 200 ppm. Fluorescence signal was still detectable for p-xylene at 50 ppm. The system was also able to detect jet fuel in soil samples with detection limits of 330 ppm (Kenny et al. 2002).

#### **2.4.4. Ultraviolet Induced Fluorescence-Cone Penetration Testing (UVIF-CPT)**

##### **System**

Like other LIF systems, UVIF-CPT system couple a fluorescence based sensor with standard cone penetrometer that can be pushed into the soil at a rate of 2.5 cm/sec by a standard 20-ton truck. However, this system uses a slightly different component setup that eliminates the use of fibre optics. In UVIF-CPT, both the excitation source and radiation detector are mounted behind a sapphire window for direct illumination and detection. Because they are located down-hole in the probe, the system does not require any fibre optic cables to deliver excitation light to the sapphire window or

carry fluorescence signal back to detection system. This feature is an advantage compared to LIF systems that suffer signal attenuation and distortion while carried by fibre optics, particularly at lower radiation wavelength in the UV range. Additionally, fibre-optic cable quality deteriorates over time due wear and tear during use, which requires periodic replacement causing an increased operating cost (Biggar et al. 2003).

UVIF-CPT uses a high intensity ultraviolet light emitting diode (LED) as an excitation source and sensitive PMT for fluorescence detection. Both components are small and easily fitted within the fluorescence sensor. The LED used in the probe emits high intensity UV light at wavelength 375 nm and can be replaced with other LEDs that emit UV light at different wavelength if required. Even though UVIF-CPT has a somewhat different components setup, it still uses a similar operational concept to LIF sensors. In UVIF-CPT, fluorescence measurements are made during penetration by illuminating the soil with ultraviolet light through the sapphire window. The fluorescence emitted by the aromatic compounds in the soil is detected by the PMT and the signal from the PMT, measured in volts (V), is then transmitted through the electrical cable to a data processing computer in the truck. Depending on the site conditions and soil profile, an average of 20 holes could be pushed and investigated by the CPT-UVIF system in one day with an average depth of 5-7 meters/hole. The current system can identify the presence or absence of free phase PHC contaminants and was used successfully to delineate petroleum contaminants such as crude oil and flare pit residue in subsurface soils (Alostaz et al. 2005; Biggar

et al. 2003). The intensity of fluorescence recorded by the PMT provides a gross indication of relative concentration; however it cannot provide information about the type of contaminant, nor is it calibrated to provide semi-quantitative information about the contaminant concentration. To overcome these limitations, this research program was conducted at the University of Alberta (Edmonton, Alberta) in partnership with Conetec Investigation Ltd. (Vancouver, B.C.) to improve and calibrate the UVIF-CPT system so it can provide more detailed fluorescence spectral information about detected contaminants to allow better characterization and semi-quantification of these contaminants.

#### **2.4.5. Fluorescence Sensor Selection**

Rapid, reliable and cost effective field screening technologies are needed to assist in the complex task of characterizing and monitoring of petroleum contaminated sites. All direct-push fluorescence sensors provide continuous log of fluorescence intensity versus depth. However, these sensors could have many configuration variations that range from a simple configuration that uses a single UV LED excitation source and a single PMT detector, to complex systems that simultaneously excite different wavelengths and collect the complete fluorescence signal using multi-channel CCD. Remediation site engineers and managers have to decide which new site characterization technology will meet the investigation work requirements. Therefore, having some guidelines or judging criteria to facilitate selection of the most appropriate system configuration for a particular application is important.

System parameters that a user needs to consider in determining the applicability of a particular system configuration are wavelength of the excitation source and the system capability to identify fluorescence signature of target contaminants. Because not all aromatic hydrocarbons are induced to fluoresce at all excitation wavelengths, the choice of excitation wavelength can have important impact on the capability of the fluorescence sensor. In general, shorter excitation wavelengths are required to induce fluorescence in aromatics with lower number of benzene rings, while aromatics with higher number of benzene rings require longer wavelength excitation source. For example, a fluorescence sensor that has excitation source with wavelength of 270 nm or less will be sufficient to induce fluorescence in single-ring aromatics such as BTEX compounds (benzene, toluene, ethylbenzene, and xylene) (Brelman, 1971). The second criterion to be considered in choosing a fluorescence based sensor for a particular application is the ability of the detection scheme to extract information from the fluorescence emission signal. Detection schemes range from the simple systems that monitor fluorescence intensity in a single spectral band to advanced ones that fully characterize the properties of the fluorescence emission signal. Using simple inexpensive detection systems would be suitable to discriminate between different contaminants (for example light weight fuel product, such as, jet fuel and heavier product, such as, diesel fuel) using fluorescence intensity in a single spectral band, considering that heavier aromatic compounds fluoresce at longer wavelengths than lighter compounds. In contrast, the wealth of information inherent in fluorescence EEM and lifetime would be useful for discriminating between more complex contaminant types and multiple contaminant sources.

## 2.5. SUMMARY

PHCs have a fluorescing nature when illuminated with UV light due to the presence of  $\Pi$ -electrons in the conjugated structure of their aromatic compound constituents. The fluorescence signal produced by a particular aromatic compound is unique and reflects its electron structure; therefore, it can be used as a fingerprint to identify that compound. The fluorescence signal of a compound could be generated through conventional fluorescence scanning and presented as emission or excitation (absorption) fluorescence spectrum. In multi-component mixtures, the fluorescence signals could be complex due the significant overlap between the fluorescing compounds spectra. With such complexity, conventional fluorescence measurements do not allow proper identification of individual compounds. Therefore, alternative fluorescence measurement analysis techniques, such as synchronous (including fluorescence EEMs) and time resolved spectroscopy might be used to resolve complex fluorescence signals.

The phenomenon of petroleum hydrocarbons fluorescence has promoted the development of fluorescence-based sensor systems to delineate PHCs in subsurface environment. A number of rapid screening systems have been developed since the early 1990's where different fluorescence sensors have been coupled behind a standard geotechnical cone penetrometer. The coupled cone penetrometer and fluorescence sensor systems provide detailed soil stratigraphic data along with fluorescence profiles that describe vertical distribution of contamination in the cone

hole with high-resolution spatial scales in real-time. Data provided by fluorescence based sensors about soil and the lateral and vertical distribution of hydrocarbon contamination at investigated sites supply engineers and managers with a more complete picture of the contamination to assist them in cleanup and remediation activities selection and planning, such as, choosing proper the location of samples sent to the laboratory for more rigorous and efficient analyses. These are important advantages over conventional drilling and sampling technologies for the purpose of screening a site for the nature and extent of contamination. However, fluorescence based sensors are not expected to completely take the place of a conventional sampling program, but add significant benefits in terms of cost savings and more thorough characterization.



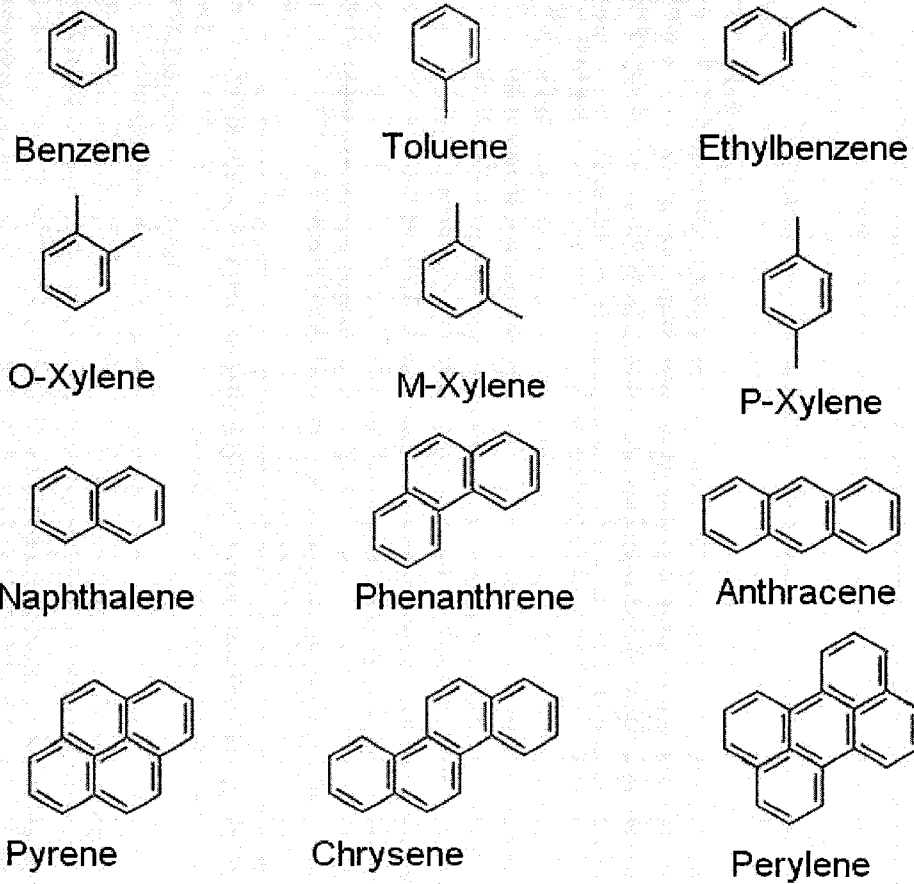


Figure 2-1. Examples of aromatic hydrocarbons (after McMurry 2004)

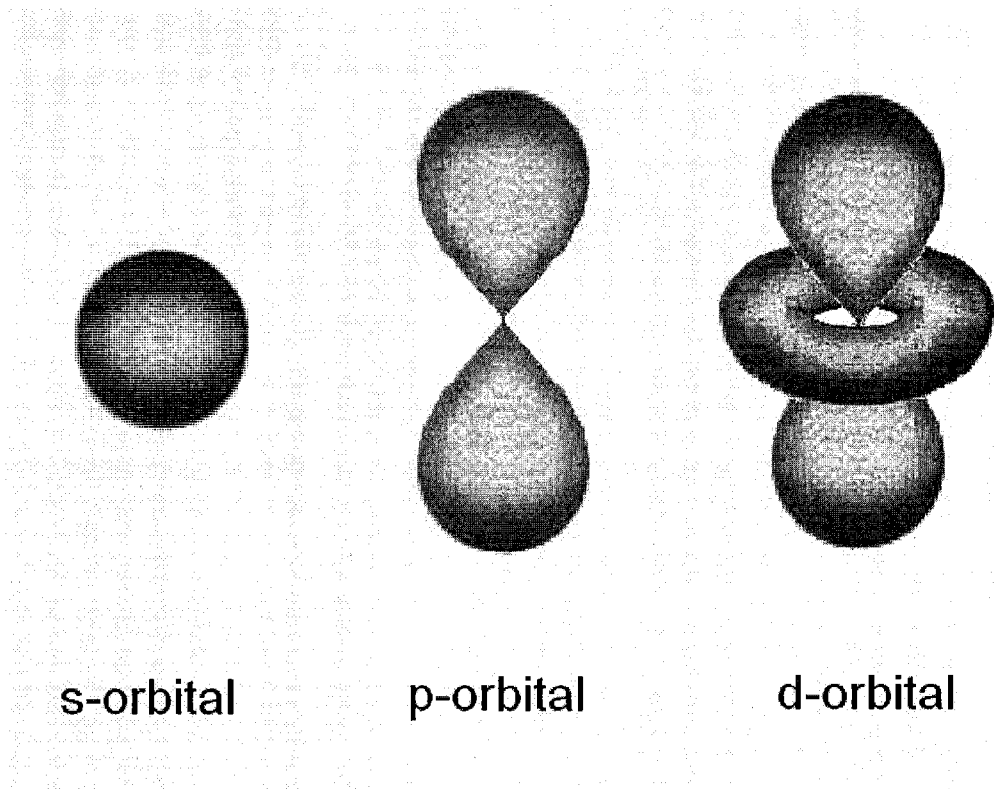


Figure 2-2. Atomic orbitals (after Griffiths 2004)

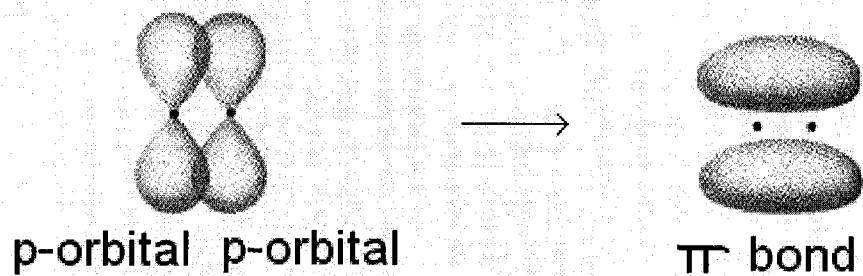
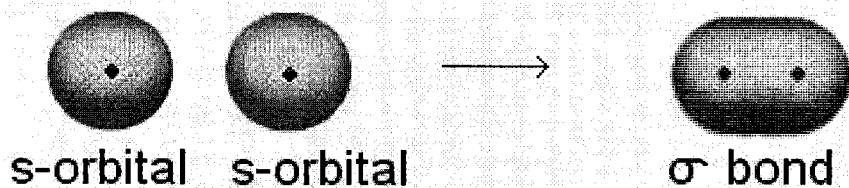


Figure 2-3. Graphic representation of s and p orbitals combination to form  $\sigma$  and  $\pi$  bonds (after Brady and Humiston 1986)

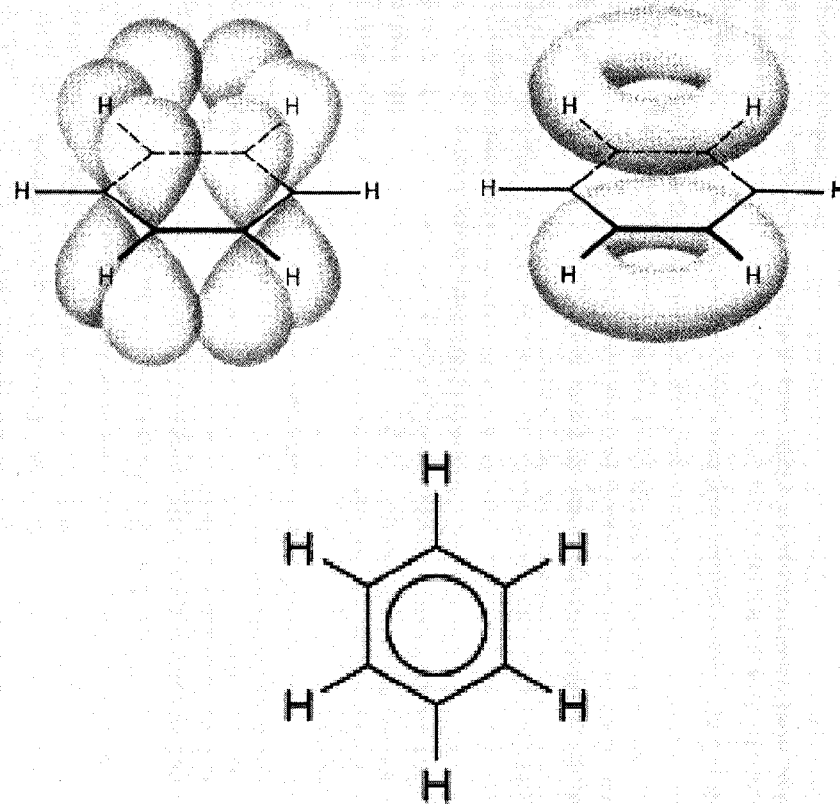


Figure 2-4. The benzene ring structure with delocalized  $\pi$  electrons clouds around the plan of joined nuclei (after Morrison and Boyd 1989)

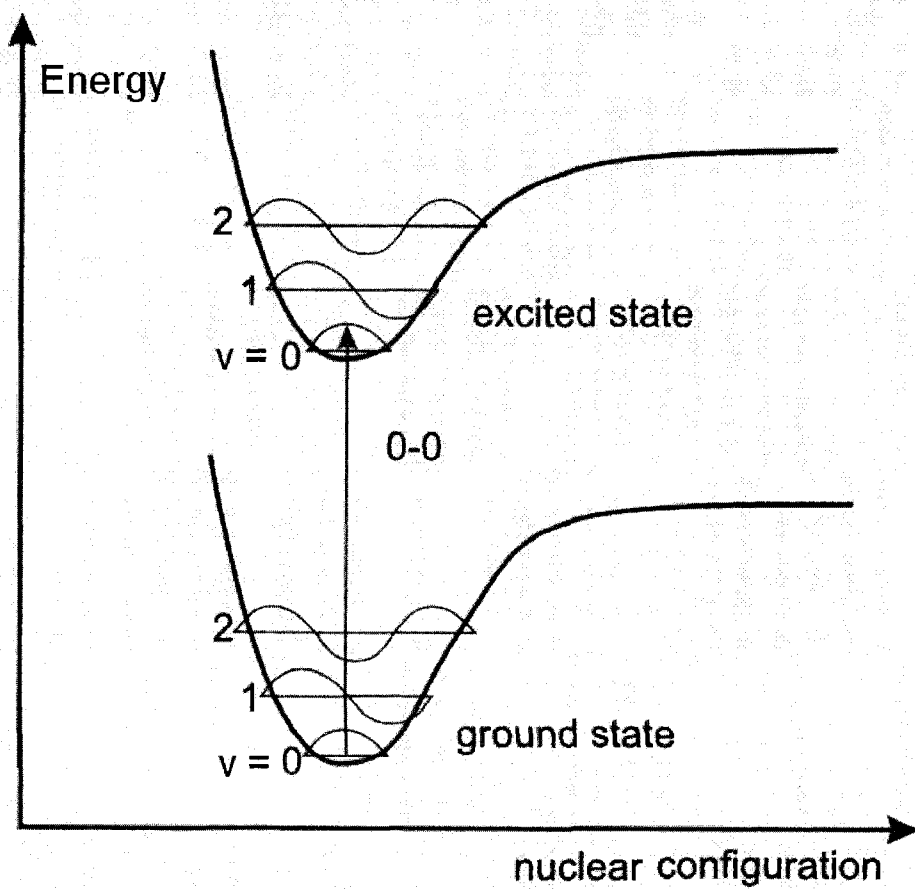


Figure 2-5. Morse potential energy functions for ground and excited states (after Morse 1929)

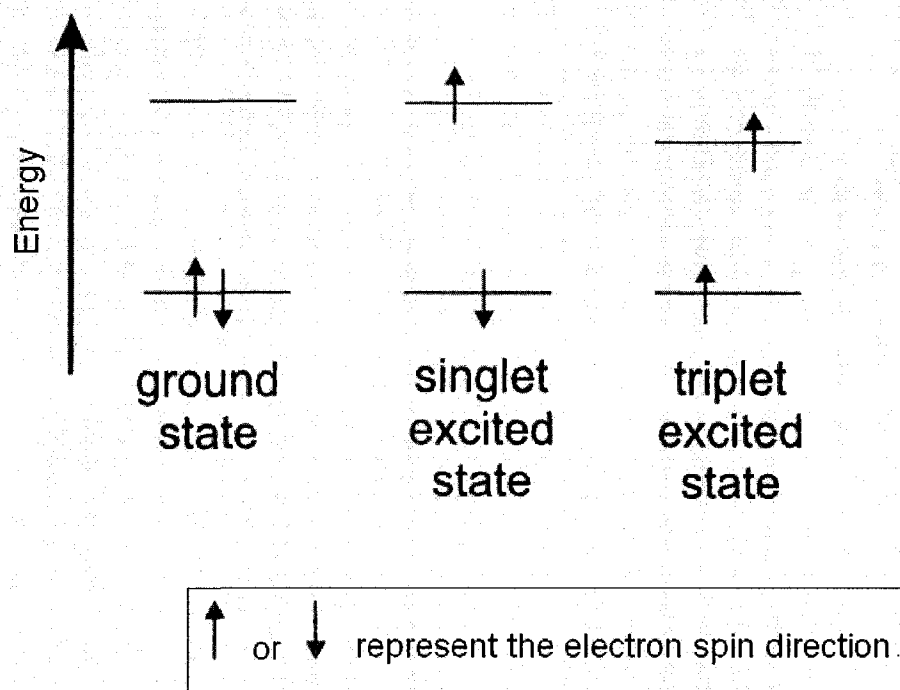


Figure 2-6. Singlet and triplet states (after Schulman 1977)

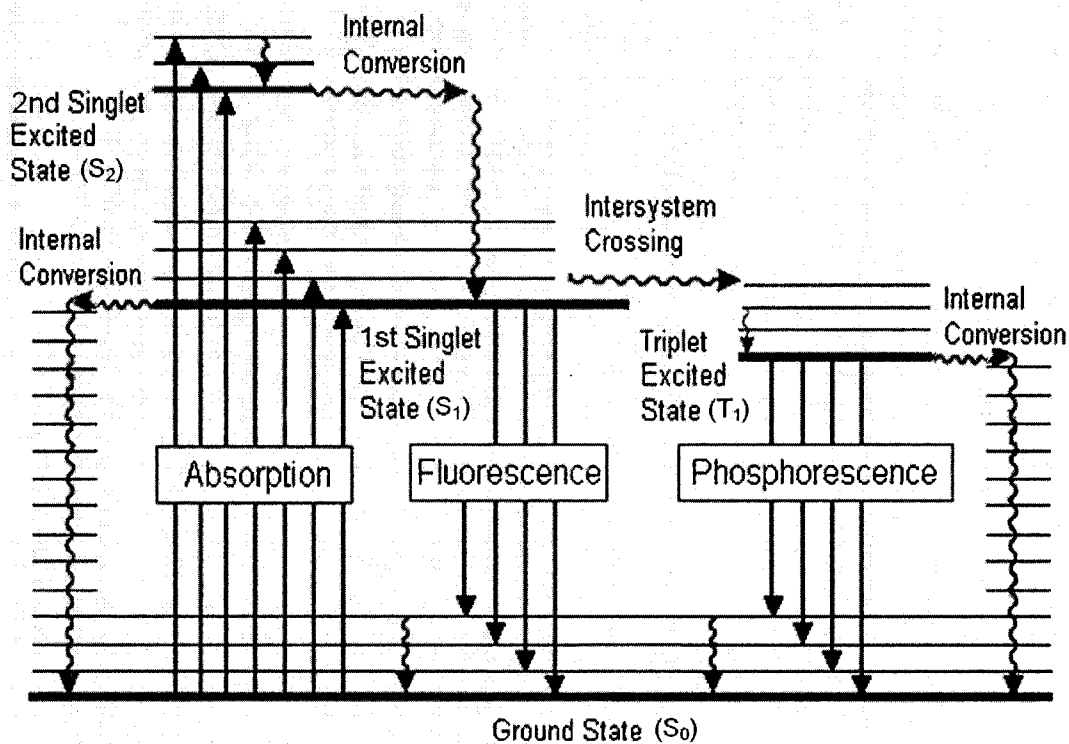


Figure 2-7. Jablonski diagram (after Atkins 2002)

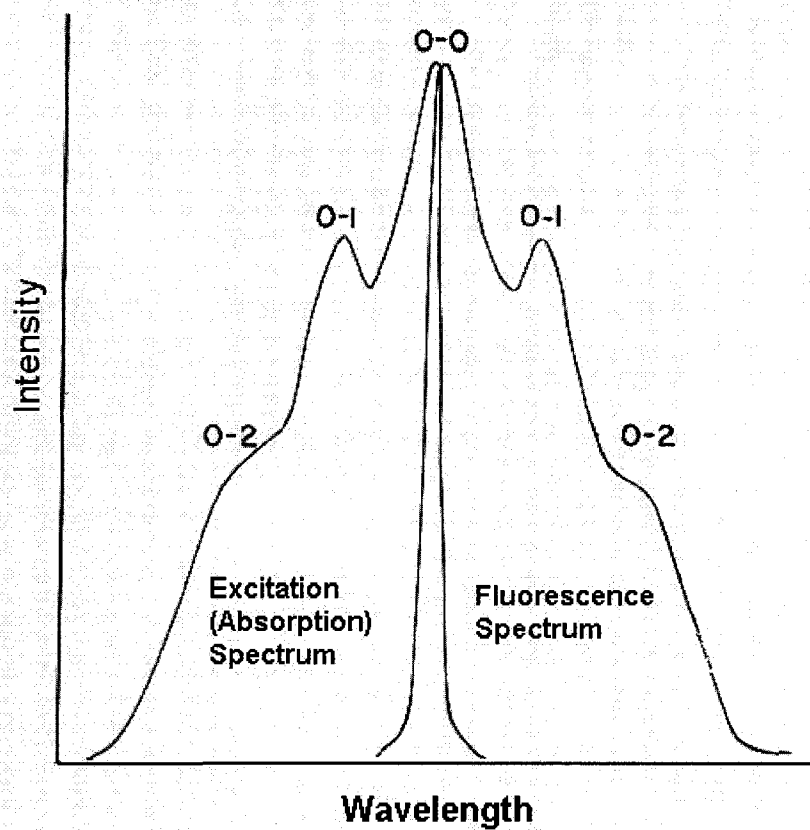


Figure 2-8. Emission and excitation spectra (after Schulman 1977)



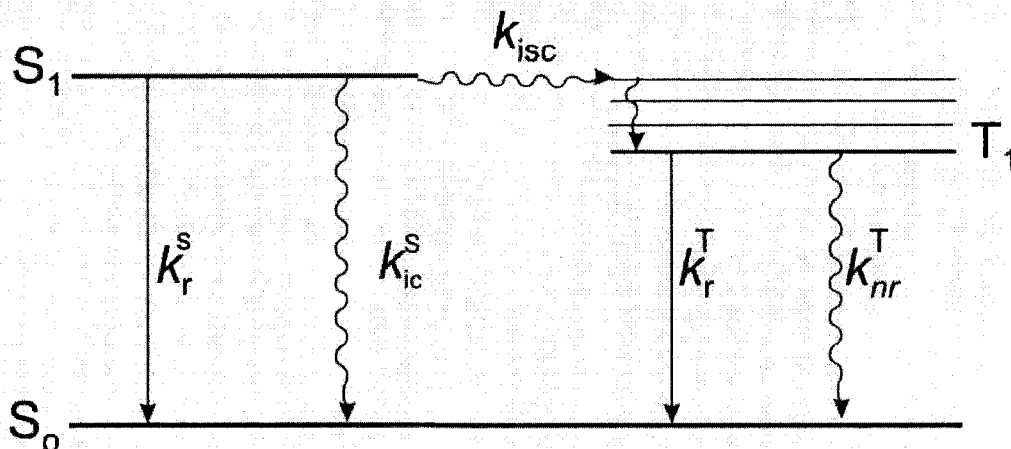


Figure 2-9. Radiative and non-radiative rate constants (after Valeur 2002)

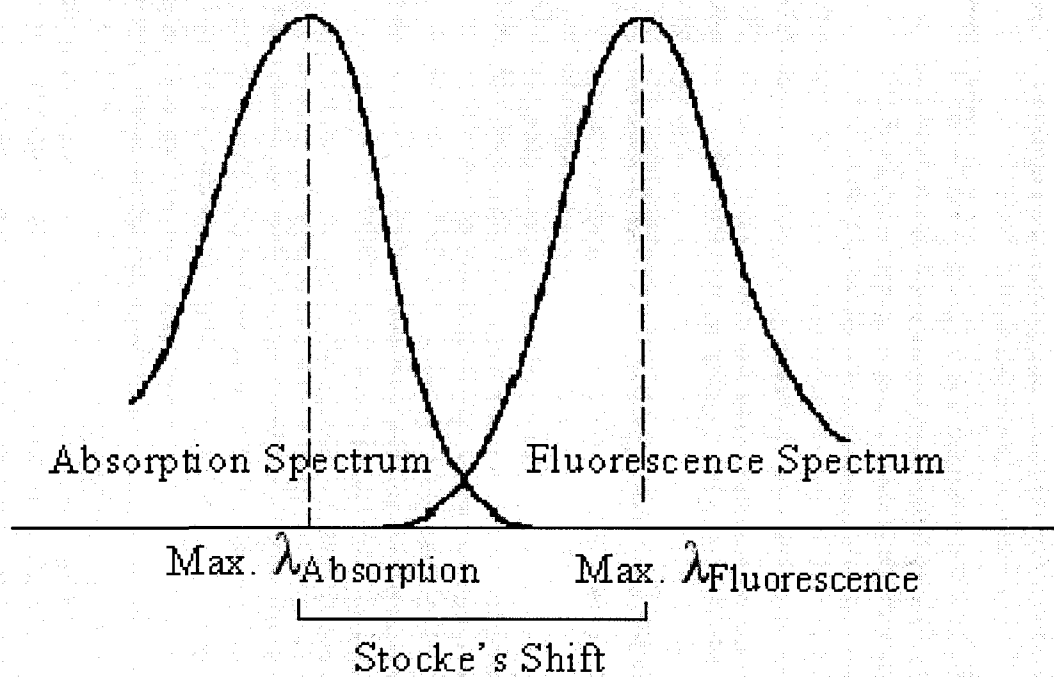


Figure 2-10. Stokes Shift (after Lakowicz 1999)

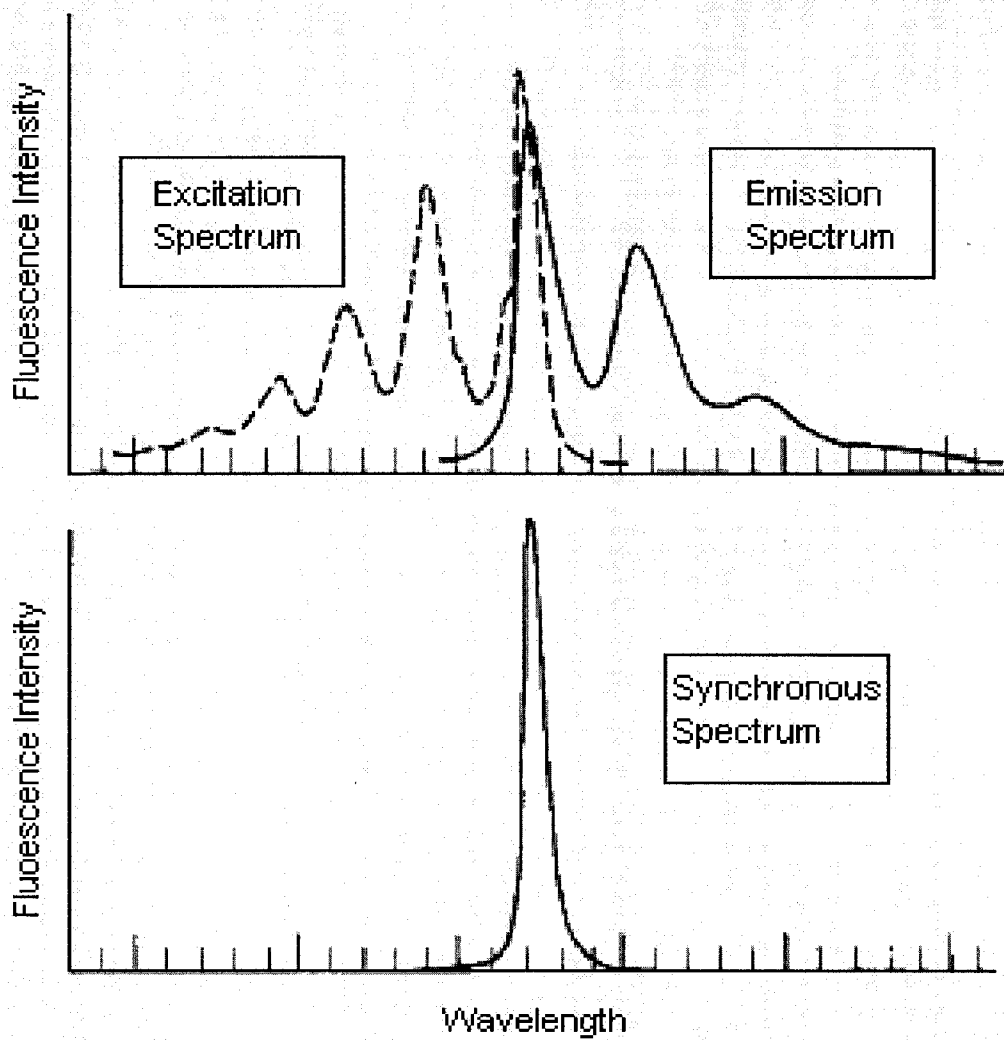


Figure 2-11. Fluorescence synchronous spectrum (after Vo-Dinh 1978)

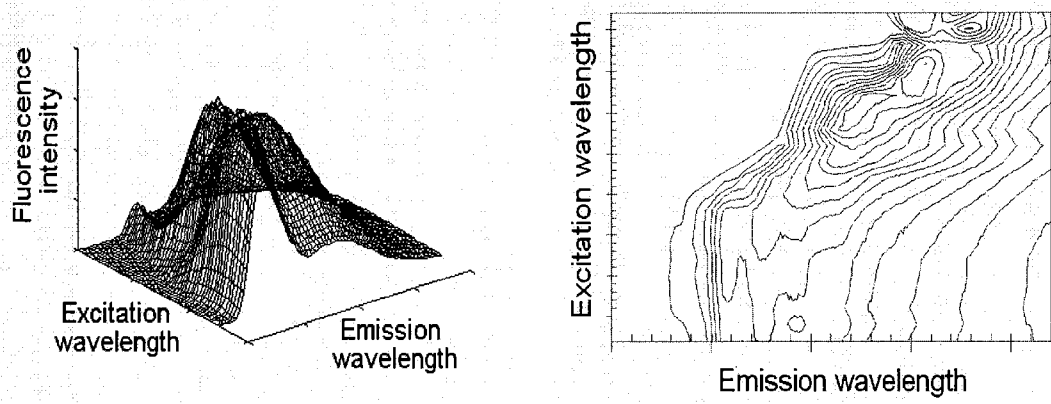


Figure 2-12. 3-dimensional (3D) and 2-dimensional contour map (2D) representations of emission-excitation matrix (EEM) (after Rho and Stuart 1978)

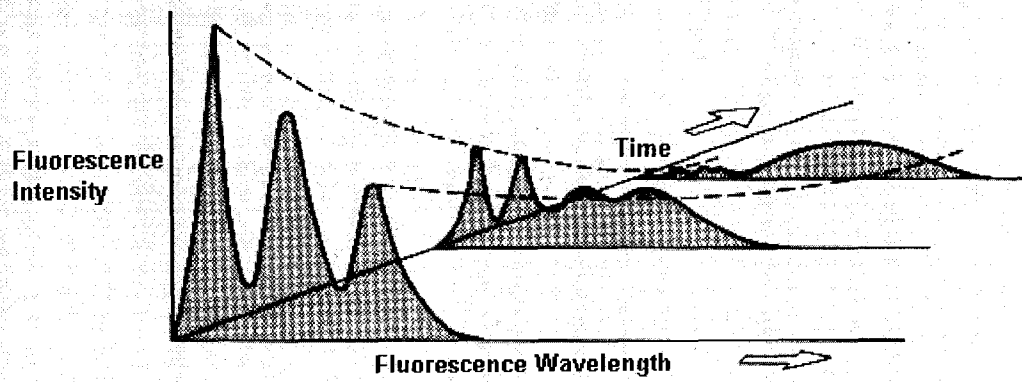


Figure 2-13. Time Resolved Fluorescence Spectrum (after O'Connor and Phillips

1984)

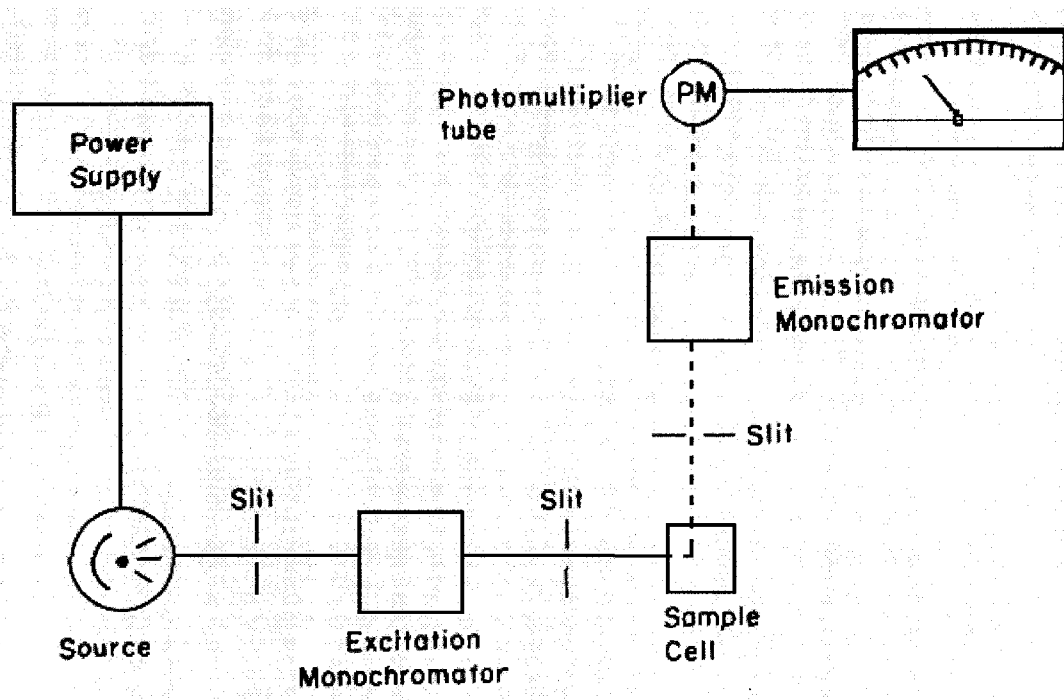


Figure 2-14. Typical spectrometer arrangement (after Sharma and Schulman 1999)

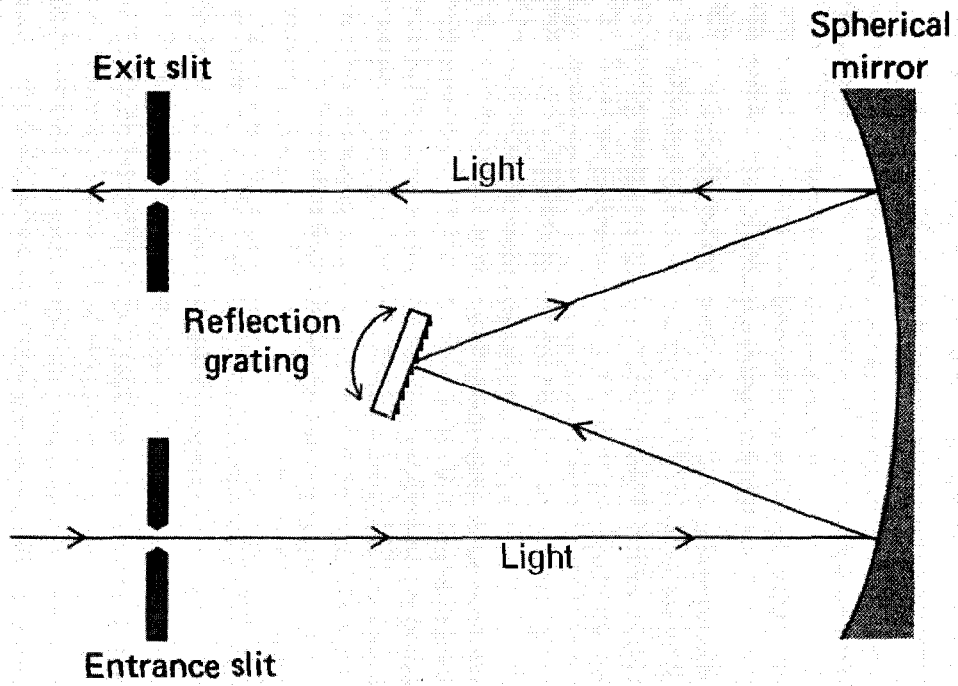


Figure 2-15. Monochromator arrangement showing separation of light wavelengths by reflection grating and mirror (after Skoog and West 1971)

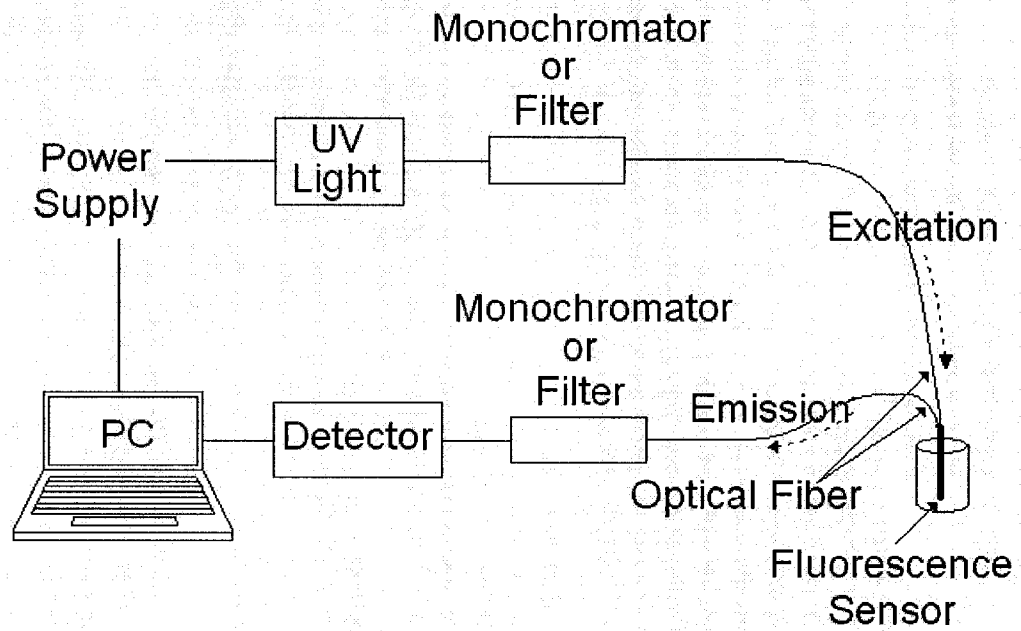


Figure 2-16. Typical fiber optic based fluorescence sensor



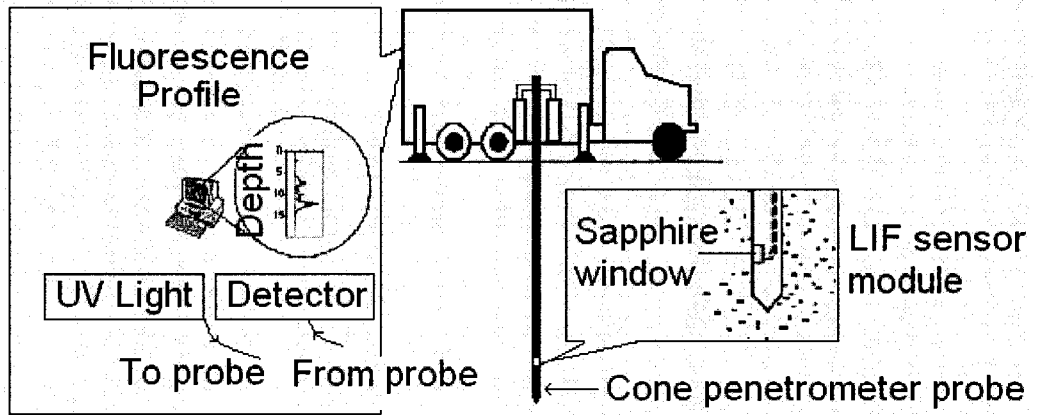


Figure 2-17. General Scheme of LIF System (after Lieberman, 1998)

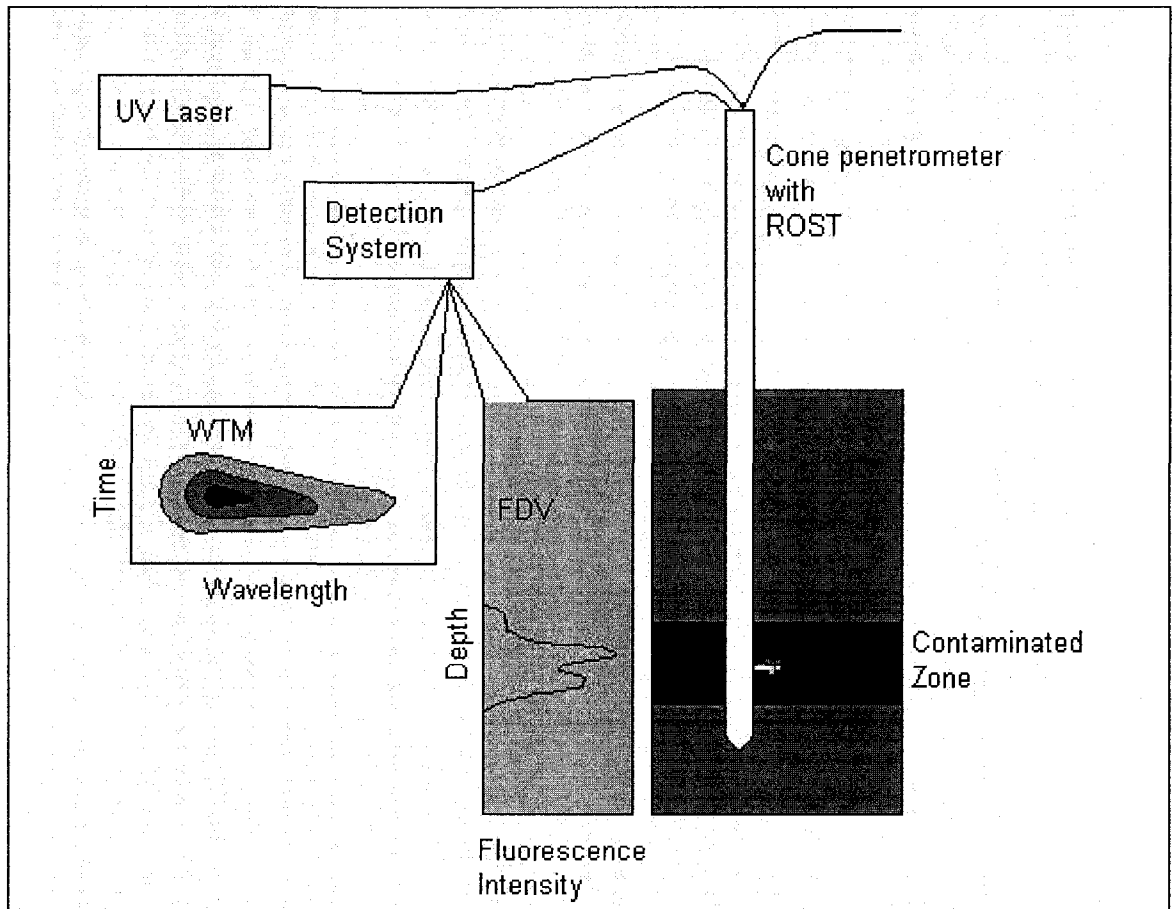


Figure 2-18. ROST system schematic diagram including typical fluorescence profile and wavelength-time matrix (WTM) generated by the system (after Nielsen 1995)

## 2.6. REFERENCES

- Aiken, G. and Leenheer, J. 1993. Isolation and Chemical Characterization Of Dissolved And Colloidal Organic Matter. *Chemistry and Ecology*, 8, pp. 135–151.
- Alostaz, M., Biggar, K., Robertson, P. Professor, Sego, D., Professor, Donhue, R. and Woeller, D. 2005. CPT-UVIF Evaluation of Subsurface Crude Oil Contamination at the Atlantic No. 3 Site. In *Proceedings of 58<sup>th</sup> Canadian Geotechnical Conference*, Saskatoon, SK. pp 778-785.
- Andrews, D. and Demidove, A. 2002. *An Introduction to Laser Spectroscopy*. Kluwer Academic/Plenum Publishers, New York, N.Y.
- Apitz, S., Theriault, G. and Lieberman, S. 1992. Optimization of the Optical Characteristics of a Fiber Optic Guided Fluorescence Technique for the In Situ evaluation of fuels in soils. *SPIE*, 1637, pp. 241–254.
- Apitz, S., Borbridge, L., Bracchi, K. and Lieberman, S. 1992a. The Fluorescent Response of Fuels In Soils: Insights Into Fuel-Soil Interactions. *SPIE*, 1716, pp.139-147.
- Arnold, M. 1992. Fiber-Optic Chemical Sensors. *Analytical. Chemistry*. 64, pp. 1015A-1025A.
- Atkins, P. and Frieman, R. 1999. *Molecular Quantum Mechanics*. Oxford University Press, Oxford, N.Y.
- Atkins, P. 2002. *Atkins Physical Chemistry (7<sup>th</sup> edition)*. Oxford University Press, Oxford, N.Y.
- Babichenko, S., Lapimma, J., Poryvkina, L., and Varlamov, V. 1995. On-Line

- Fluorescence Techniques for Diagnostics Of Water Environment. Society of Photo-Optical Instrumentation Engineers Journal, 2503, pp. 157-161.
- Berlman, I. 1971. Handbook of Fluorescence Spectra of Aromatic Molecules (2<sup>nd</sup> Edition). Academic Press, New York, N.Y.
- Bernath, P. 1995. Spectra of Atoms and Molecules (Topics in Physical Chemistry). Oxford University Press, Oxford, N.Y.
- Biggar, K., Woeller, D., Murphy, S., and Armstrong, J. 2003. CPT-UVIF Characterization at Upstream Oil and Gas Facilities. In Proceedings of the 17<sup>th</sup> Annual Vancouver Geotechnical Society Symposium: Geotechnical Engineering for Geoenvironmental Applications, Vancouver, BC. pp 31-37.
- Brady, J. and Humiston, G. 1986. General Chemistry: Principles & Structure (4<sup>th</sup> edition). John Wiley and Sons, New York, N.Y.
- Brown. C. and Fingas, M. 2003. Review of The Development Of Laser Fluorosensors For Oil Spill Application. Marine Pollution Bulletin, 47, pp. 477-484.
- Bujewski, G., Rutherford, B. 1997. Site Characterization and Analysis Penetrometer System (SCAPS) Laser-induced Fluorescence (LIF) Sensor and Support System. EPA/600/R-97/019. Las Vegas, NV: U.S. Environmental Protection Agency.
- Bujewski, G. and Rutherford, B. 1997a. Rapid Optical Screening Tool (ROST) Laser Induced Fluorescence (LIF) for Screening of Petroleum Hydrocarbons in Subsurface Soils. EPA Report, EPA/600/R-97/020, Las Vegas, NV: U.S. Environmental Protection Agency.

- Calhoun, G. and Burrows, R. 1992. Surface Fluorescence Method Can Identify Potential Oil Pay Zones in Permian Basin. *Oil and Gas Journal*, 90, pp. 96-101.
- Chiu, Y. 1971. On Singlet-Triplet Transitions Induced by Exchange with Paramagnetic Molecules and Intermolecular Coupling of Spin Angular Momenta. *The Journal of Chemical Physics*, 56, pp. 4882-4898.
- Cho, M. 2003. Correlation Between Electronic And Molecular Structure Distortions and Vibrational Properties. I. Adiabatic approximations. *The Journal of Chemical Physics*, 118, pp. 3480-3490.
- Christian, G., Callis, J. and Davidson, E. (Wehry, E. Editor). 1981. *Modern Fluorescence Spectroscopy (Vol. 4)*, Plenum, New York. N. Y.
- Coolidge, A., James, H. and Present, R. 1936. A study of the Franck-Condon Principle. *Journal of Chemical Physics*, 4, pp. 193-211.
- Csele, M. 2004. *Fundamentals of Light Sources and Lasers*. John Wiley and Sons, New York, N.Y.
- Cullum, B., Chi, Z. and Vo-Dinh, T. 2000. High-Temperature Fluorescence Measurements And Instrumentation For Polyaromatic Hydrocarbons (PAH): A Review. *Polycyclic Aromatic Compounds*, 18, pp. 25-47.
- Duarte, F. 1995. *Tunable Lasers Handbook Academic*, New York, N.Y.
- Eastwood, D. (in E. Wehry, E. Editor). 1981. *Modern Fluorescence Spectroscopy (Vol. 4)*. Plenum Press, New York, N.Y.
- Gillispie, G., St. Germain R. and Klingfus, J. 1993. Subsurface Optical Probes: Current Status and Future Prospects, In *Proceedings of Field Screening*

- Methods for Hazardous Wastes and Toxic Chemicals, Las Vegas, NV. Air & Waste Management Association, Pittsburgh, P.A. pp. 793– 805.
- Gillispie, G. and St. Germain, R. 1995. Performance Characterization of the Rapid Optical Screening Tool (ROST), In Proceedings of Field Screening Methods for Hazardous Wastes and Toxic Chemicals, Las Vegas, NV, 1995. Air & Waste Management Association, Pittsburgh, P.A. pp. 478–489.
- Harris, D. 1991. Quantitative Chemical Analysis (3<sup>rd</sup> Edition). W. H. Freeman and Company, New York, N.Y.
- Harry, J. and Yuan, Q. 2000. Distinguishing Discharge Modes Using Their Spectral Lines. International Journal of Electronics, 87, pp.1105-1112.
- Hess, E. and Hamilton, D. 1995. Rapid Optical Screen Tool (ROST). Innovative Technology Evaluation Report, EPA/540/R-95/519, Office of Research and Development, Environmental Protection Agency Washington, D.C.
- Holonyak, N. and Bevcqua, S. 1962. Coherent (Visible) Light Emission from Ga (As<sub>1-x</sub>P<sub>x</sub>) Junctions. Applied Physics Letters, 1, pp.82-83.
- Horowitz, P. and Hill, W. 1989. The Art of Electronics (2<sup>nd</sup> edition). Cambridge University Press, New York, N.Y.
- Howes, M. and Morgan, D. 1979. Charge-Coupled Devices and Systems. Wiley and Sons Inc., New York, N.Y.
- Inman, S., Thibado, P., Theriault, G. and Lieberman, S. 1990. Development of a Pulsed-Laser, Fiber Optic-Based Fluorometer for Time- Resolved Measurements of Polycyclic Aromatic Hydrocarbons in Seawater.

Analytical Chemistry Acta, 239, pp. 45–51.

International Union of Pure and Applied Chemistry Compendium of Chemical Terminology (IUPAC) (2<sup>nd</sup> edition). 1997. Compiled by Alan D. McNaught and Andrew Wilkinson (Royal Society of Chemistry, Cambridge, UK).

Jadamec, J., Saner, W. and Tall, Y. 1977. Optical Multichannel Analyzer for Characterization of Fluorescent Liquid Chromatographic Petroleum Fractions. Analytical Chemistry, 49, pp. 1316-1321.

Jaffe, H. and Orchin, M. 1962. Theory and Application of Ultraviolet Spectroscopy. John Wiley and Sons, Inc., New York, N.Y.

John, P. and Soutor, I. 1976. Identification of Crude Oils by Synchronous Excitation Spectrofluorimetry. Analytical Chemistry, 48, pp. 520-524.

Karcher, W. 1988. Spectral Atlas of Polyarlic Aromatic Compounds (Vol. 2). Kluwer Publishers, Dordrecht, MA.

Kenny, J., Lin, J., Hart, S., Wang, W. and Namytkine, D. 1995. Subsurface Contaminant Monitoring by Laser Fluorescence Excitation-Emission Spectroscopy in a Cone Penetrometer Probe. SPIE, 2504, pp. 59-67.

Kenny, J., Hart, S., Chen, Y. and Lien, B. 1996. A Fiber Optic Multichannel Spectrometer System for Remote Fluorescence Detection in Soils. SPIE, 2835, pp. 73–82.

Kenny, J., Pepper, J. and Wright, A. 2002. In Situ Measurements of Subsurface Contaminants with A Multi-Channel Laser-Induced Fluorescence System. Spectrochimica Acta-Part A, 58, pp. 317–331.

- Kershaw, J. and Fetzer, J. 1995. The Room Temperature Fluorescence Analysis of Polycyclic Compounds in Petroleum and Related Materials, Polycyclic Aromatic Compounds, 7, pp. 253-268.
- Koechner, W. 1999. Solid-State Laser Engineering (3<sup>rd</sup> edition). Springer-Verlag, New York, N.Y.
- Knorr, F. and Harris, J. 1981. Resolution of multicomponent fluorescence spectra by an emission wavelength-decay time data matrix. Analytical Chemistry, 53, pp. 272-276.
- Knowles, D. and Lieberman, S. 1995. Field Results From The SCAPS Laser-Induced Fluorescence (LIF) Sensor for In-Situ, Subsurface Detection of Petroleum Hydrocarbons. SPIE, 2504, pp. 297-307.
- Knowles, D. and Kertesz, J. 1996. Fluorescence Detection of Petroleum Contamination: Evaluation of Various Lasers for SCAPS Sensor. SPIE, 2835, pp. 228-233.
- Kovac, J., Peternai, L. and Lengyel, O. 2003. Advanced Light Emitting Diodes Structures for Optoelectronic Applications. Thins Solid Films, 433 (1-2): 22-26.
- Lakowicz, J. 1999. Principles of Fluorescence Spectroscopy (2<sup>nd</sup> Edition). Kluwer Academic/Plenum Publisher, New York, N.Y.
- Lieberman, S., Inman, S., Theriault, G., Cooper, S., Malone P. and Lurk, P. 1990. Fiber Optic-Based Chemical Sensors for In Situ Measurement of Metals and Aromatic Organic Compounds in Seawater and Soil Systems. SPIE, 1269, pp. 175-184.



- Lieberman, S., Theriault, G., Cooper, S., Malone, P., Olsen, R. and Lurk, P. 1991. Rapid Subsurface In-Situ Field Screening of Petroleum Hydrocarbon Contamination Using Laser Induced Fluorescence Over Optical Fibers, In Proceedings of the 2<sup>nd</sup> International Symposium on Field Screening Methods for Hazardous Waste Site Investigations, Las Vegas, Nevada. Air and Waste Management Association, Pittsburgh, P.A. pp. 57–63.
- Lieberman, S. 1998. Direct-Push, Fluorescence-Based Sensor Systems for In Situ Measurement of Petroleum Hydrocarbons in Soils. *Field Analytical Chemistry and Technology*, 2, pp. 63–73.
- Lloyd, J. 1971. Synchronized Excitation of Fluorescence Emission Spectra. *Nature-Physical Science*, 231, pp. 64-66.
- Lurk, P., Cooper, S., Malone P. and Lieberman, S. 1990. Development of Innovative Penetrometer Systems for The Detection And Delineation of Contaminated Groundwater And Soil, Superfund '90. In Proceedings of the 11th National Superfund Conference, Washington, DC. Hazardous Materials Control Research Institute, pp. 297–299.
- Maiman, T. 1962. Solid State Laser and Iraser Studies. *Solid-State Electronics*, 4, pp. 236-249.
- Marhaba, T. 2000. Fluorescence Techniques for Rapid Identification of DOM Fractions. *Journal of Environmental Engineering*, 126, pp.145–152.
- Massimi, M. 2005. Pauli's Exclusion Principle: The Origin and Validation of a Scientific Principle. Cambridge University Press, New York, NY.
- McGinnis, W., Davey, M., Wu, K. and Lieberman, S. 1995. Capabilities and

- Limitations of a Cone Penetrometer Deployed Fiber Optic Laser Induced Fluorescence (LW) Petroleum Oil and Lubricant (POL) Sensor. SPIE, 2367, pp. 2 – 16.
- McGown, L. and Nithipatikom, K. 1986a. Elimination of Scatter Background in Synchronous Excitation Spectrofluorometry By The Use Of Phase-Resolved Fluorescence Spectroscopy. *Analytical Chemistry*, 58, pp. 3145-3148.
- McGown, L. and Nithipatikom, K. 1986. Multidimensional Data Formats for Phase-Resolved Fluorometric Multicomponent Determinations Using Synchronous Excitation And Emission Spectra. *Analytical Chemistry*, 58, pp. 2469-2473.
- McGown, L. and Nithipatikom, K. (In Vo-Dinh, T. Editor). 1989. *Chemical Analysis of Polycyclic Compounds*. Wiley, New York, N.Y.
- McMurry, J. 2004. *Organic Chemistry* (6<sup>th</sup> edition). Brooks/Cole: Thomson Learning, Belmont, CA.
- Millican, D. and McGown, L. 1988. Fluorescence Lifetime Selectivity in Multi-Frequency Phase-Resolved Fluorescence Spectroscopy. *Applied Spectroscopy*, 42, pp. 1084-1089.
- Morse, P. 1929. Diatomic Molecules According to the Wave Mechanics. II. Vibrational levels. *Physical Reviews*, 34, pp. 57-64
- Morrison, R. and Boyd, R. 1989. *Organic Chemistry* (5<sup>th</sup> Edition), Prentice Hall of India, New Delhi, India.
- Narayanaswamy, R. 1993. *Optical Chemical Sensors: Transduction and Signal*

- Processing. *Analyst*, 118, pp. 317–322.
- Nielsen, B., Gillispie, G., Bohne, D. and Lindstrom, D. 1995. A New Site Characterization and Monitoring Technology. *SPIE*, 2504, pp. 278-290.
- O'Connor, D. and Phillips, D. 1984. *Time-Correlated Single Photon Counting*. Academic Press Inc, London. UK.
- Patra, D. and Mishra, A. 2002. Total Synchronous Fluorescence Scan Spectra of Petroleum Products. *Analytical and Bioanalytical Chemistry*, 373, pp. 304-309.
- Pharr, D., MacKenzie, J. and Hickman, A. 1992. Fingerprinting Petroleum Contamination Using Synchronous Scanning Fluorescence Spectroscopy. *Ground Water*, 30, pp. 484-489
- Rayner, D. and Szabo, A. 1978. Time-Resolved Laser Fluorosensors: A Laboratory Study of Their Potential In The Remote Characterization Of Oil. *Applied Optics*, 17, pp. 1624-1630.
- Rho, J. and Stuart, J. 1978. Automated Three-Dimensional Plotter for Fluorescence Measurements. *Analytical Chemistry*, 50, pp. 620-625.
- Schulman, S. 1977. *Fluorescence and Phosphorescence Spectroscopy: Physicochemical Principles and Practice*. Pergamon Press, New York, N.Y.
- Sharma, A. and Schulman, S. 1999. *Introduction to Fluorescence Spectroscopy*. Wiley-Interscience, New York, N. Y.
- Skoog, D. and West, D. 1971. *Principles of Instrumental Analysis*. Holt, Rinehart and Winston. INC., New York, N.Y.

- Song, J., Jagannathan, R., Stokes, D., Vo-Dinh, T. and Hajaligol, M. 2003. Real-Time Monitoring Of Polycyclic Aromatic Hydrocarbons in Cigarette Smoke Using Time-Resolved Laser-Induced Fluorescence. *Polycyclic Aromatic Compounds*, 23, pp. 429-439.
- St. Germain, R., Gillispie, G. and Klingfus, J. 1993. Variable Wavelength Laser System for Field Fluorescence Measurements. In *Proceedings of Field Screening Methods for Hazardous Wastes and Toxic Chemicals*, Las Vegas, NV. Air & Waste Management Association, Pittsburgh, P.A. pp.1113–1122.
- St. Germain, R. and Gillispie, G. 1995. Real-Time Continuous Measurement of Subsurface Petroleum Contamination With The Rapid Optical Screening Tool (ROST), In *Proceedings of Field Screening Methods for Hazardous Wastes and Toxic Chemicals*, Las Vegas, NV. Air & Waste Management Association, Pittsburgh, P.A. pp. 467–477.
- Svelto, O. 1998. *Principles of Lasers* (4<sup>th</sup> edition)-translated by Hanna, D. Plenum Publishing Corporation, New York, N.Y.
- Theriault, G., Newbery, R., Andrews, J., Apitz, S. and Lieberman, S. 1992. Fiber Optic Fluorometer System Based on a Dual-Wavelength Laser Excitation Source. *SPIE*, 1796, pp. 115–123.
- Valeur, B. 2002. *Molecular Fluorescence: principles and applications*. Wiley-Vec., New York, N.Y.
- Vandermeulen, J., Buckley, D., Levy, E., Long, B., McLaren, P., Wells, P., 1979. *Sediment Penetration Of Amoco Cadiz Oil, Potential For Future Release*,

- and Toxicity. *Marine Pollution Bulletin*, 10, 222-227.
- Vo-Dinh, T. 1978. Multicomponent Analysis by Synchronous Luminescence Spectrometry. *Analytical Chemistry*, 50. pp. 396-401.
- Vo-Dinh, T. 1982. Synchronous Luminescence Spectrometry: Methodology and Applicability. *Applied Spectroscopy*, 36, pp. 576-581.
- Vo-Dinh, T., Nolan, T., Cheng, Y., Sepaniak, M. and Alarie, J. 1990. Phase-Resolved Fiberoptics Fluoroimmunosensor. *Applied Spectroscopy*, 44, pp. 128-132.
- Wehry E. (In Guilbault, G. Ed.). 1990. *Practical Fluorescence* (2<sup>nd</sup> Edition). Marcel Dekker, New York, N.Y.
- Weisner, D. 1992. Charged-Coupled Devices-McGraw-Hill Encyclopaedia of Science and Technology (7<sup>th</sup> edition). McGraw Hill Inc., New York, N.Y.
- Winefordner, J., Schulman, S. and O'Haver, T. 1972. *Luminescence Spectroscopy in Analytical Chemistry*. Wiley and Sons, Inc., New York, N.Y.

## Chapter 3

# **Petroleum Contamination Characterization and Quantification Using Fluorescence Emission-Excitation Matrices (EEMs) and Parallel Factor Analysis (PARAFAC)**

### **3.1. INTRODUCTION**

Polycyclic aromatic hydrocarbons (PAHs) in petroleum products are considered as significant environmental pollutants; therefore, reliable analytical methods for detecting and characterizing these compounds in environmental solution or soil samples are of great interest (Bjorseth and Ramdahl 1985). Existing petroleum contaminants characterization and identification methods involve initial screening in the field, then carefully obtaining samples in the field and having them analyzed in a distant laboratory, which is an expensive and time-consuming procedure. Fluorescence spectroscopy is an efficient screening method that could complement current screening methods and may be used directly on various types of environmental samples because it does not require any pre-separation steps, and has been used successfully to detect petroleum products at contaminated sites. The use of fluorescence spectroscopy as a detection technique to determine PAHs in marine sediments was applied successfully to detect freshly spilled crude oil in marine environment (Vandermeulen et al. 1979). Also, PAHs fluorescence has been used to identify crude oil petroleum product spills and other petroleum products including diesel, kerosene and petrol (Eastwood 1981; Patra and Mishra 2002). Kram et al.

(2004) described fluorescence spectroscopic method combined with CPT to detect PAHs in non-aqueous phase liquid (NAPL) and dense non-aqueous phase liquid (DNAPL) in petroleum contaminants.

Feasibility of incorporating fluorescence sensors in cone penetrometer probes that can be pushed into the ground and allows recording in situ real-time measurements of petroleum contaminants in subsurface environments was tested in the early 90's (Lurk et al. 1990). Then, the first laser-induced fluorescence (LIF) fibre-optic-based sensor was developed to detect subsurface petroleum hydrocarbons contaminants and called Site Characterization and Analysis Penetrometer System (SCAPS) (Lieberman et al. 1991). After that, a number of fluorescence sensor probes to detect petroleum hydrocarbons have been developed including: the rapid optical screening tool (ROST) (St. Germain et al. 1993) and a multi-channel LIF screening system that was developed at Tufts University (Kenny et al. 1995) and ultraviolet induced fluorescence-cone penetration testing system (UVIF-CPT) (Biggar et al. 2003).

This study is part of a research project to improve the existing UVIF-CPT system that currently can generate soil stratigraphy and fluorescence profile data from contaminated sites, which allow mapping petroleum contaminants' spatial distribution in subsurface environments (Alostaz et al. 2005). The system has limited characterization capabilities that are mainly restricted to indicating "presence/absence" of petroleum contaminants. The research project aims to enhance the existing UVIF-CPT, so it could collect more fluorescence spectral data

(fluorescence excitation-emission matrices - EEMs) of detected petroleum contaminants, which can be utilized to better characterize and quantify these contaminants. Potentially generated fluorescence EEMs by the improved UVIF-CPT can be analyzed using the methodology described herein to rapidly discern different contaminant compounds during the contaminated site field investigation. Analysis methodology presented in this chapter deals with petroleum contaminants that are neat or diluted in solvent solutions. The same methodology could be extended to petroleum contaminants mixed in soils, however, the effect of soil matrix on fluorescence signal should be considered.

### **3.2. FLUORESCENCE SPECTROSCOPY**

The fluorescing nature of petroleum products is related to the electron structure and chemical bonds in their aromatic compounds constituents (i.e. compounds that have benzene ring ( $C_6H_6$ ) as a basic structure). The benzene ring has a hybrid chemical structure with bonds that are considered an average of equally contributing single and double bonds. In single bond, shared electron pair forms a  $\sigma$  bond, while in double bond, the first shared electron pair forms a  $\sigma$  bond and the second pair forms a  $\Pi$  bond. Electron pairs involved in  $\Pi$  bonding have weak binding forces, therefore, when illuminated with sufficient energy (UV light), electrons engaged in  $\Pi$  bond(s) can absorb the induced energy (light photons) and get promoted to higher energy levels, from which they return to the ground state through various radiative and non-radiative mechanisms including fluorescence. Due to the rigid structure of aromatic



rings, they do not allow for efficient non-radiative relaxation and favor radiative mechanisms, namely fluorescence (Morrison and Boyd 1989).

Despite the lack of fine spectral structure, fluorescence spectral signature produced by a particular aromatic compound is unique because it typically has peaks at specific emission wavelengths that can be used as a fingerprint to identify that compound. Emission fluorescence spectrum can be generated by scanning the spectral distribution of the emitted fluorescence radiation at a particular exciting radiation wavelength (typically in the UV range). In excitation fluorescence spectrum, the observation fluorescence wavelength is held constant while the fluorescence intensity is measured as a function of the excitation wavelength (Schulman 1977). In multi-component mixtures, the overlap of fluorescence signals can be significant. Thus, alternative fluorescence analysis techniques, such as synchronous spectroscopy (Vo-Dinh 1978), fluorescence emission-excitation matrices (EEMs) (Rho and Stuart 1978; and Vo-Dinh 1982), and time resolved fluorescence spectroscopy (O'Connor and Phillips 1984), may be used to resolve complex fluorescence signals.

### **3.2.1. Fluorescence Emission-Excitation Matrices (EEMs)**

EEMs of a particular aromatic compound are collected by scanning its fluorescence spectra at different excitation wavelengths. The information from both the excitation spectrum and the emission spectrum are combined into a single display (Figure 3-1). In this way all information present in the excitation and emission fluorescence spectral features of the compound can be captured and presented in the form of a

matrix. The data in an EEM may be visually presented in the form of a fluorescence contour plot that can separate different components of a multi-component system into isolated peaks (Figure 3-1), which helps to characterize these components (Rho and Stuart 1978; Vo-Dinh 1982).

Overlap in fluorescence signals of individual compounds in multi-component mixtures such as petroleum products that contain hundreds of individual PAHs can be severe, and produces complex EEMs that are difficult to interpret. Also quenching and energy-transfer processes can extensively affect fluorescence EEMs (Schulman 1977). While the effect of quenching and energy-transfer processes on fluorescence of multi-component mixtures can be reduced by sample dilution, the complexity of fluorescence EEMs due to significant fluorescence signal overlap can be resolved by implementing advanced multivariate statistical techniques in Chemometrics.

### **3.2.2. Multivariate Statistical Techniques**

Chemometrics represents an interesting alternative for discrimination in multi-component samples. Multivariate statistical analysis techniques such as Parallel Factor Analysis (PARAFAC) and Soft Independent Method of Class Analogy (SIMCA) have been shown to be reliable tools to resolve multi-component mixtures of polycyclic aromatic hydrocarbons (Christensen et al. 2005; Jiji et al. 2000; Pharr et al. 1992; Wold and Sjostrom 1977).

### 3.2.2.1. Parallel Factor Analysis (PARAFAC)

PARAFAC is a multi-way decomposition statistical technique that is suitable for decomposing three-dimensional fluorescence data generated from collecting fluorescence EEMs of a particular petroleum product at different concentrations into its underlying components (Figure 3-2). Fluorescence EEMs can be arranged in a three-way array ( $X$ ) of dimensions  $I \times J \times K$ , where  $I$  is the number of samples (at different concentrations),  $J$  the number of emission wavelengths, and  $K$  the number of excitation wavelengths. PARAFAC decomposes this array into three matrices:  $A$  (the score matrix),  $B$ , and  $C$  (loading matrices) with elements  $a_{if}$ ,  $b_{jf}$ , and  $c_{kf}$ . The scores in  $a_{if}$  reflect relative fluorescence intensity of analyte  $f$  in sample  $i$  and can be interpreted as the relative concentration of the analyte  $f$  in sample  $I$ , considering that fluorescence intensity is function of concentration (Valeur 2002). Thus, values in the score matrix could refer interchangeably to fluorescence intensity or the relative concentration. The vector  $b_f$  with elements  $b_{jf}$  is the estimated emission spectrum of that analyte and likewise  $c_f$  is the estimated excitation spectrum (Figure 3-2). Elements in the  $X$  array are modelled by PARAFAC as expressed in Equation 3-1, where  $F$  is the number of PARAFAC analytes and  $e_{ijk}$  represent the residual elements reflecting variability that can not be modelled:

$$x_{ijk} = \sum_{f=1}^F a_{if}b_{jf}c_{kf} + e_{ijk} \quad [3-1]$$

PARAFAC utilizes a least squares optimization technique, which, when given a series of measured data, attempts to find a function that closely approximates the data. It attempts to minimize the sum of the squares of the ordinate differences (residuals)

between points generated by the function and corresponding points in the data (BRO 1997; Bro and Andersen 2003).

### **3.2.2.2. Soft Independent Method of Class Analogy (SIMCA)**

SIMCA is a classification technique based on principal component analysis (PCA) models made for groups of samples (classes) in a data set. SIMCA constructs local PCA models for each class and retains a sufficient number of principal components to account for most of the variation within each class. New data to be classified is projected onto the PCA models and classified to one of the established class models on the basis of their best fit to the respective model. By comparing the residual variance of new data to the average residual variance of those samples that make up the class, it is possible to obtain a direct measure of the similarity of the new data to the class (Wold and Sjostrom 1977). SIMCA computes the distance of new data from the model with respect to the explanatory variable in order to compute the class membership probabilities. Sample distances from each class are based on the  $Q$  and  $T^2$  statistics. Simply,  $Q$  and  $T^2$  represent the variation of the sample outside and within the model, respectively. The 95% confidence intervals can be calculated for both  $Q$  and  $T^2$  (Hall and Kenny 2007). This comparison is also a measure of the goodness of fit of the sample to a particular principal component model. Samples of new data close to a class (low  $Q$  and  $T^2$ ) are considered belonging to that class. Large distances (high  $Q$  and  $T^2$ ) suggest that a sample does not belong to that class. Therefore, in SIMCA it is possible for a sample to belong to one, none, or more than one class (PLS\_ToolBox 2006).

SIMCA is a robust classification method with high discrimination power that assigns new data to a class to which it has a high belonging probability. If the residual variance of new data exceeds the upper limit for every modeled class in the data set, the sample would not be assigned to any of the classes because it is either an outlier or comes from a class that is not represented in the data set (Vogt and Sjoegren 1989). SIMCA can be used along with PARAFAC models to discriminate between different classes of petroleum products (i.e. gas condensate, gasoline, diesel, flare pit residue and crude oil) based on the variation of scores of their modeled factors. Scores are suitable to use to construct PCA models that describe classes of petroleum products because they provide high modeling and discriminatory power. The modeling power describes how well a variable helps the principal components to model variation, and discriminatory power describes how well the variable helps the principal components to classify the samples in the data set.

### **3.3. EXPERIMENTAL WORK**

Petroleum product samples used in this study were: 1) natural gas condensate, 2) gasoline, 3) diesel, 4) flare pit residue and 5) heavy crude oil. These samples were selected because they cover the typical range of petroleum contaminants that are usually encountered at upstream oil and gas sites. As well, they contain a variety of aromatic constituents with a wide range of aromatic ring sizes. Gasoline and diesel samples used in this study were purchased from the local market in Edmonton, AB. Gas condensate and flare pit residue samples were from two research sites in Alberta.

The crude oil sample came from Cold Lake, AB, and was supplied by the National Centre for Upgrading Technology (NCUT) laboratories, Devon, AB. All samples were stored in airtight containers that were clearly marked and kept in a cold environmental chamber at the Applied Environmental Geochemistry Research Facility at the University of Alberta.

Neat and diluted samples of each petroleum product were prepared before proceeding with fluorescence measurements. Diluted samples had concentrations that ranged from 0.5 to 800 mL/L. This wide range of concentrations was selected to provide an adequate number of fluorescence EEMs for subsequent PARAFAC analysis, and to monitor the effect of fluorescence quenching and energy-transfer processes on the measured EEMs. In total, 70 stock solution samples (including duplicates) of all petroleum products were prepared. Hexane was used as a solvent to dilute the gas condensate, gasoline and diesel samples. Chloroform was used to dilute flare pit residue and heavy crude oil due to presence of the larger PAHs in these samples that cannot be dissolved by hexane.

Individual standards of PAHs were prepared including: BTEX compounds (Benzene, Toluene, Ethyl-Benzene and Xylenes), Naphthalene and Methyl-Naphthalene, Phenanthrene, Fluorene, Pyrene, Dibenzothiophene, and Fluoranthene. These PAH compounds were selected because they most likely correspond to the major components of the analyzed petroleum products and their fluorescence signatures (EEMs) are needed to characterize the predicted components by PARAFAC analysis.

In total 120 stock solution samples (including duplicates) of standard PAH compounds were prepared with concentrations that ranged from 0.08 to 50 mL/L (or in equivalent g/L) using hexane as solvent. For validation purposes, samples of gas condensate, gasoline, diesel, flare pit residue and heavy crude oil were sent to a commercial laboratory to be analyzed for their constituent BTEX and PAH compounds concentrations.

Fluorescence EEMs were measured on a Varian Eclipse fluorescence spectrophotometer in the scan mode. Analyzed samples were prepared in solutions where 3 ml of each stock solution were transferred directly to the sample container to be analyzed. The sample container is made of black anodized aluminium to reduce light reflection, and is 33.28 mm in diameter and 30.14 mm high. A circular quartz glass with the same diameter is fitted at the top of the container to allow UV light illumination and fluorescence emission from the tested sample. The container was mounted in the spectrometer compartment on a solid sample holder that allows for front-face fluorescence detection. This set-up was selected to permit fluorescence detection from highly concentrated liquid samples that do not allow for right angle ( $90^\circ$ ) fluorescence detection, and it also simulates the way fluorescence measurement will be collected using the UVIF-CPT system. A collection of emission scans from 250 to 600 nm with 1 nm increments was obtained at varying excitation wavelengths ranging from 240 to 450 nm with 10 nm increments. The bandwidths (slit width) were 5 nm for both excitation and emission for most scans, but were reduced to 2.5 nm when fluorescence intensity was out of range. The scan rate was 600 nm/min, which

gave a scan time of about 20 minutes per sample. Blank samples of hexane and chloroform were analyzed each day, and a reference material (anthracene) was analyzed every day to monitor any variation in the spectrophotometer performance. A total of 180 fluorescence EEMs were collected for selected petroleum products in addition to the blanks and PAH standards.

### **3.4. RESULTS AND DISCUSSION**

#### **3.4.1. Qualitative Analysis**

One should consider when reviewing fluorescence EEMs of analyzed petroleum products presented in this chapter, that generated EEMs might have different appearance than similar fluorescence data reported in other studies. These differences are associated with several sources of variations including, differences of source region, processing method, aging and history of tested petroleum products, as well as, fluorescence measurement instrumentation. Investigating these sources of variation in details is beyond this study scope that intended to present a simple and structured approach to utilize fluorescence measurements in detecting petroleum contaminants. However, identifying changes in fluorescence EEMs due to differences of source region, processing procedure and aging of petroleum products can be accomplished by testing a large number of samples that reflect these conditions. On the other hand, to be able to compare fluorescence EEMs of a particular analyte generated using two different fluorescence measurement instruments, differences in excitation light intensity and instrumentation setup between the two instruments should be accounted for. To correct these differences, fluorescence intensities of peaks in reference



material (e.g. Rohdamine) emission spectra can be collected by both instruments and used to produce correction factors to normalize collected fluorescence intensities. The procedure is discussed in further details in chapter 5 (section 5.4.2.1). Rohdamine is a good reference analyte to use, as it has a quantum efficiency value that is almost 1 (Wehry 1990), which means intensities in the fluorescence spectra are a true reflection of excitation light intensities at different wavelengths. Rohdamine fluorescence spectra collected using a Varian Eclipse spectrometer at different excitation wavelengths is presented in Figure 3-3.

#### **3.4.1.1. Fluorescence EEMs**

Figure 3-4 illustrates the collected fluorescence EEMs for undiluted analyzed petroleum products, except for crude oil. The EEM of crude oil is for dilution in chloroform (40 mL/L) and it is included instead of the undiluted sample because it shows better peak fluorescence intensity. Undiluted crude oil fluorescence EEM is highly affected by fluorescence quenching that significantly attenuates fluorescence intensity. The presented EEMs show that each of the analyzed petroleum products has a unique fluorescence EEM with specific peak locations that can be utilized as a fingerprint for that particular product. Figure 3-5 maps the location of EEM peaks with highest fluorescence intensity of the tested petroleum products and crude oil. The variation in the emission peak locations in the fluorescence EEMs reflects the variation in the relative PAHs composition of the various petroleum products. For instance, peaks in gas condensate fluorescence EEMs are mostly located at lower wavelengths, around 290 nm; while peaks in heavy crude oil EEMs are located at

higher wavelengths, around 460 nm. These peak locations indicate that gas condensate is mostly composed of lighter aromatic compounds with 1 benzene ring that are known to fluoresce at 275-285 nm, while crude oil is mostly composed of heavier aromatic compounds with 3-4 benzene rings that are known to fluoresce at 360-480 and a number of lighter PAH compounds (Berlman 1971). The number and locations of fluorescence peaks in the presented EEMs can provide a general idea about the variation in PAH components in the analyzed petroleum products. Multiple peaks in gasoline and diesel fluorescence EEMs indicate that they contain a wider range of aromatic compounds with varied numbers of benzene rings.

Examining collected fluorescence EEMs of tested petroleum products at different concentrations indicated that EEMs tend to have more pronounced emission peaks at longer wavelengths at higher concentrations. As the concentration of the contaminant decreases, peaks start to shift slightly toward shorter wavelengths. An example of diesel peak shift with dilution is illustrated in Figure 3-6. This observation is in agreement with findings of previous study by Kram et al. (2004a). The observed peak shift is a manifestation of enhancement or attenuation of emission peaks intensities in fluorescence spectra at different concentrations due to energy transfer mechanism known as inner filter effect. In that mechanism, higher energy fluorescence emitted by compounds with small number of aromatic rings get re-absorbed by compounds with larger number of aromatic rings and utilized as excitation energy (Lakowicz 1999). Figure 3-7 presents the change in fluorescence intensity for different emission peaks in the diesel fluorescence signal as concentration changes. Energy transfer between

different constituents is well demonstrated in the figure by the increase of fluorescence intensities of emission peaks at longer wavelengths as fluorescence intensities of emission peaks at shorter wavelengths decrease. It is evident that larger aromatic constituents re-absorb fluorescence energy of lighter aromatic compounds as excitation energy. Fluorescence EEMs are still unique fingerprints of petroleum products despite the apparent shift of peak locations at different concentrations, because they capture the unique combinations of excitation and emission wavelengths' associated different peaks, which is an exclusive characteristic of the tested product.

In this study, fluorescence signals detection criterion was set to  $3\sigma_{\text{background}}$ , where  $\sigma_{\text{background}}$  represents the standard deviation of background signal obtained by scanning fluorescence EEM of blank solvent (Hart and JiJi 2002). Minimum concentration at which fluorescence was detected are listed in Table 3-1, which can be used as preliminary detection limits for tested petroleum products in solvent solutions. These detection limits values are based on the sample concentrations used in this study, however, they might be further refined by testing more samples with intermediate petroleum product concentration values between the lowest concentration at which the fluorescence signal was detected and next lower one at which the signal was not detected in this study.

#### **3.4.1.2. PARAFAC and SIMCA Analysis**

EEMs of each of the analyzed petroleum products at different concentrations were

analyzed using PARAFAC that modeled excitation and emission spectra and provided relative concentrations for underlying PAH components in all samples. These results were used subsequently by SIMCA analysis to distinguish different petroleum products. Before proceeding with PARAFAC analysis, data pre-processing was required because experimental EEMs often deviate from trilinearity and are affected by scatter effects, which could lead to inaccurate model estimates. Radiation scatter in fluorescence measurements, especially in the front face setup that was used in this study, can be problematic because it is unrelated to the sample chemical composition and cannot be modeled adequately into a few PARAFAC factors. Rayleigh and Raman scatter show up in three-way fluorescence data as diagonal lines across EEMs (denoted by light scatter in Figure 3-4). No Raman scatter was observed in blank solutions so was ignored. On the other hand, Rayleigh scatter was detected in all collected EEMs as illustrated in Figure 3-4. Several methods have been used to reduce detrimental effects due to scatter (Bro and Andersen 2003). In this study, scatter data within the diagonal lines across the EEMs were removed and set to NaN, or 'not a number' indicating missing data in the data set. These regions were then replaced by expectation values using the PARAFAC algorithm. Inserting missing values instead of zeros in the scatter region was based on previous work by Bro and Anderson (2003) who argued that arbitrarily inserting zeros in this region of the EEM may interfere with the trilinearity of data. To ensure proper model estimation and to enhance the modeling process, certain constraints are usually applied. In the case of modeling fluorescence EEMs, "non-negativity" constraints are often enforced to the estimates of A, B, and C loadings that represent relative concentration, emission and

excitation spectra. These constraints improve the stability of the modeling and are based on a priori knowledge that negative concentrations or fluorescence intensities are impossible (Bro 1997).

The PARAFAC models were fitted using the PLS\_toolbox 3.5 in MATLAB ver.7.1. The convergence criteria (Relative and Absolute change in fit) and maximum number of iterations used throughout the modeling were  $10^{-6}$ ,  $10^{-6}$  and 10,000, respectively. A large number of PARAFAC models were estimated for all analyzed samples in the solutions using an increasing number of factors (from 1 to 5). Determination of the appropriate number of factors was mainly based on the number of iterations, core consistency and analysis of residuals (see Appendix G for more details). Core consistency describes deviations in the modeled PARAFAC loadings and fluorescence data that can not be modeled. Appropriate numbers of factors in the appropriate PARAFAC model is achieved when a low number of iterations, low core consistency and minimum residuals are achieved (Andersen and Bro, 2003). Figure 3-8 illustrates the emission spectra produced by PARAFAC models for the underlying PAH components in the analyzed petroleum product samples (Figures 3-8a to 3-8e) along with the fluorescence spectra of the PAH standards that were collected during this study (Figure 3-8f). “Low and high concentration” tags are used in Figure 3-8f to identify pyrene fluorescence spectrum at concentrations less and higher than 0.2 g/L. Pyrene fluorescence spectrum is known to have two different emission peaks at lower and higher concentrations due to formation of excimers, which is discussed later (Berlman 1971).

Modelled fluorescence emission spectra by PARAFAC are not associated with specific excitation wavelength; they are generic illustration of the behaviour trends of fluorescence spectral data in all tested samples as a function of emission wavelengths. To obtain an actual representation of fluorescence intensities of modelled components in a particular sample, modelled emission spectra should be multiplied by the score value ( $a_{if}$ ) related to that sample from the scores matrix (A) that reflect the variation in fluorescence intensity of these components in analyzed samples. Interpretation of factors in PARAFAC models was based on fluorescence characteristics of modeled factors. Comparisons of the fluorescence characteristics, namely emission peak(s) wavelength(s), of the PARAFAC factors with the fluorescence signals collected for individual PAH standards indicated that each of the factors can be related to one of these compounds. PARAFAC modelled components agreed with laboratory chemical analysis results for the aromatic composition of the analyzed samples that are listed in Table 3-2, and showed that PAH's content of the analyzed petroleum products is mainly composed of BTEX compounds, naphthalene/methylnaphthalene, phenanthrene, and to lesser extent pyrene.

PARAFAC was not able to model BTEX compounds in flare pit residue and crude oil due to fluorescence quenching that cause the BTEX compounds' fluorescence signal to be diminished and be re-absorbed by larger aromatic compounds as a source of excitation energy. This concept of fluorescence quenching will be discussed in more details later in this chapter. On the other hand, it was observed that PARAFAC was

not be able to model separately individual compounds that have very similar fluorescence spectra in petroleum products with complex PAH composition so it would characterize them under one class of compounds, such as BTEX, Naphthalene or Methyl Naphthalene compounds. For example, PARAFAC was able to model more individual BTEX compounds in the gas condensate sample yet it was only able to model the BTEX compounds as a class of compounds in other analyzed samples because the gas condensate EEM had fewer peaks which made it easier for PARAFAC to detect fine variations within these peaks (Figure 3-8a).

Being able to analytically discriminate between the fluorescence signatures (EEMs) of the analyzed petroleum samples is of great interest as it allows rapid characterization of different petroleum contaminants in environmental samples using UVIF. The SIMCA function in the PLS\_toolbox 3.5 in MATLAB ver.7.1. was employed to characterize the analyzed petroleum product samples based on variations in scores of their modelled PARAFAC components that map the relationships between samples based on their chemical composition. This method could eliminate the necessity for visual comparison that is used in the standard methods for initial screening of petroleum samples. To prepare for SIMCA analysis, scores of modelled PARAFAC factors of all tested petroleum samples were assembled in one matrix and imported in the PLS\_toolbox as a data set. Scores from each factor were normalized as a fraction over the sum of scores from that factor. Scores were normalized to avoid one factor controlling the class definition. Each of the tested petroleum products was considered as a separate class and assigned a specific number. Gas condensate,

gasoline, diesel, flare pit residue and crude oil were assigned class identification numbers 1, 2, 3, 4 and 5, respectively. Once classes were assigned, SIMCA was run and PCA models of adequate number of principle components (3 in this case) that capture  $\geq 99\%$  of the variance were developed for each class. After constructing SIMCA models, scores from each of the analyzed petroleum samples were projected on the generated models to investigate SIMCA's ability to discriminate between various samples and assign a correct class for each sample.

SIMCA modelling results are usually presented as lists of analyzed samples with assigned classes or plots that illustrate similarities of normalized scores of analyzed samples based on constructed PCA model components by SIMCA. A list of analyzed samples with assigned classes was used herein to investigate the capability of SIMCA to discriminate between different classes (See Appendix G for more details). Figure 3-9 shows an example of plots that could be generated by SIMCA models, in which normalized diesel and gas condensate sample scores are plotted based on the constructed PCA model components: PCA1 and PCA2. Gas condensate samples can be easily distinguished from diesel samples in Figure 3-9 because they share almost the same location and show minimum overlap with diesel samples in the plot.

SIMCA was able to discriminate and assign a correct class for gas condensate, gasoline and diesel samples. SIMCA did not identify flare pit residue and crude oil samples to the same extent, due to the absence of distinguished variations in the spectral features of their EEMs and similarities in their modelled components as



illustrated in Figures 3-8d and 3-8e. The discrimination power of SIMCA is likely to be enhanced by modifying its classification criteria and using larger fluorescence datasets for flare pit residue and crude oil samples that might include more variations.

### **3.4.2. Quantitative Analysis**

#### **3.4.2.1. Concentration Calibration Curves**

To establish calibration functions to estimate petroleum products' concentration in the solutions, the relationship between total fluorescence intensity and standard concentrations of analyzed petroleum products solutions was utilized. A total fluorescence intensity value for a particular petroleum product at a specified concentration was generated by integrating areas under all fluorescence curves (signals) in the related fluorescence EEM. The integration limits were consistent in all EEMs: 250 nm and 450nm for excitation, and 260 nm and 600 nm for emission. Integrating fluorescence intensities at all excitation wavelengths was used to produce the calibration functions because it encompasses contributions of all underlying PAH components to the fluorescence signal of the analyzed petroleum product, whereas using fluorescence signal intensity at a specific excitation wavelength only accounts for input of specific classes of underlying PAH components. Total fluorescence intensity values are inclusive and more representative of the spectral features of the analyzed petroleum products.

Figure 3-10 presents the relationship between total fluorescence intensity (in arbitrary units, a. u.) and concentration (in mL/L) of all tested petroleum products. The

presented curves in Figure 3-10 can be used to estimate unknown concentrations of the same petroleum products in solutions in the laboratory or in situ using their fluorescence signal intensity. Figure 3-10 indicates that diesel produced the highest total fluorescence intensity at all concentrations, followed by flare pit residue, crude oil, gasoline then gas condensate. This behavior is related to the relative composition of aromatic compounds in each of the analyzed products. PAH concentration values obtained by laboratory chemical analysis in Table 3-2 show that diesel and flare pit residue have the higher contents of methyl-naphthalene and pyrene. Fluorescence signals collected for the PAH standards used in this test program indicated that methyl-naphthalene and pyrene also yield the higher fluorescence intensities. That explains why diesel and flare pit residue show higher fluorescence intensity. In contrast, PAHs in gas condensate and gasoline are mainly comprised of BTEX, and have low concentrations of methyl-naphthalene and pyrene. Fluorescence signals for BTEX compounds, with exception to p-xylene, gave lower fluorescence intensities. Detailed chemical analysis indicated that p-xylene only represents 7% and 15% of BTEX compounds in gas condensate and gasoline, respectively. With such low content of p-xylene, gas condensate and gasoline are expected to show lower fluorescence intensities at all concentration.

All examined petroleum products showed an almost linear relationship between the concentration of the analyte in the solution and the fluorescence intensity at lower concentrations. The extent of linearity in the relationship varied among the analyzed petroleum products. For petroleum products that yield higher fluorescence intensities

such as diesel, flare pit residue and heavy crude oil, the relationship is linear up to concentration of approximately 0.4 mL/L. On the other hand, the relationship is linear up to 0.6 mL/L for gasoline and 0.9 mL/L for gas condensate, which generally has lower fluorescence intensities (Figure 3-10). As tested petroleum product concentrations increase in solution, the relationship starts to divert from linearity. The deviation is a result of fluorescence quenching. At higher concentrations, interaction between the analyte molecules increases and energy transfer between molecules become more evident. Energy transfer involves passing fluorescence energy from one molecule (donor) during its excitation lifetime to a nearby molecule (acceptor) that absorbs the energy to yield fluorescence. Such loss of the excitation energy results in luminescence reduction or “quenching” of the donor as its concentration increases. This fluorescence quenching mechanism usually occurs in mixtures that are composed of different components with overlapping excitation and emission fluorescence spectra. Another mechanism that contributes to fluorescence quenching is due to interaction between analyte molecules at the ground and excited states, which produces an excited polymer or “excimer”. Due to the nature of coupling between molecules in the excited and ground states, excimers do luminesce at longer wavelengths. This results in a reduction of the fluorescence intensity at the original emission peak wavelength where the analyte is expected to fluoresce. This mechanism is usually observed in mixtures with fewer components (Schulman 1977).

For quantitative purposes, the relationship between total fluorescence intensity and concentrations of analyzed petroleum products is unique, even though more than one

concentration value could have the same fluorescence intensity due to fluorescence quenching at higher analyte concentration. When two samples with different concentration values are associated the same fluorescence value, they can still be differentiated from each other by examining their EEMs. The sample with the higher concentration value will have more pronounced emission peaks at longer wavelengths when compared with the EEM of the lower concentration sample as highlighted earlier in this chapter. To estimate the concentration of specific petroleum product in a solution, it is recommended to use the calibration curves presented in this study along with the related fluorescence EEM of the analyte.

The correlation between total fluorescence intensity and total The Canadian Council of Ministers of the Environment (CCME) hydrocarbon fraction concentrations (CCME 2001) of the analyzed petroleum products (undiluted) was examined. Total CCME hydrocarbon fraction concentration values were obtained by summing F1 (nC<sub>6</sub>-nC<sub>10</sub>), F2 (nC<sub>10</sub>-nC<sub>16</sub>), F3 (nC<sub>16</sub>-nC<sub>34</sub>) and F4 (nC<sub>34</sub>-nC<sub>50</sub>) hydrocarbon fractions from laboratory chemical analysis of hydrocarbons in petroleum compounds. Total CCME hydrocarbon fraction concentration values are presented as milligram of hydrocarbons per kilogram of petroleum product. Figure 3-11 (a-b) shows the relationship between total fluorescence intensity values obtained in this study for undiluted petroleum products (on the y-axis) and total CCME fraction concentrations of the same petroleum products (on the x-axis). The relationship shows good correlation with R<sup>2</sup> value of 0.963 that indicated a linear behavior for natural gas condensate, gasoline, flare pit residue and crude oil (Figure 3-11a). However, the

relationship diverts from linearity when diesel samples are included, which is reflected in a lower  $R^2$  value of 0.476 indicating a poor correlation between total fluorescence intensity and total CCME hydrocarbon fraction concentrations (Figure 3-11b). This divergence from linearity is expected because diesel yields the highest fluorescence intensity of all examined petroleum products. While fluorescence measurements reflect aromatic hydrocarbons in analyzed petroleum products, total CCME hydrocarbon fractions represent all hydrocarbons including aromatic and non-aromatic compounds. Therefore, total CCME hydrocarbons fractions might not be an accurate reflection of aromatic hydrocarbon compounds in analyzed petroleum samples, which introduces divergences in the correlation between total fluorescence intensity and total CCME hydrocarbon fraction concentrations that are more pronounced in highly fluorescing petroleum products. This observation of divergence from linearity in the relationship between total fluorescence intensity and total CCME hydrocarbon fraction concentrations agrees with findings of previous work by Kenny et al (2000).

#### **3.4.2.2. PAH Components Concentration Estimation**

Concentrations of the aromatic compounds in petroleum products can be estimated using information produced by PARAFAC analysis in the A matrix (the score matrix) that describe the relative concentration of underlying components derived from the variation of their fluorescence intensity in analyzed samples. When fluorescence EEMs of specific concentrations of standard PAH (calibration set) and EEMs of a petroleum product that contains the same PAH are combined in one PARAFAC

analysis, the generated score matrix by PARAFAC analysis will include relative concentrations of the PAH in all tested samples. Values in the score matrix related to the relative concentration of standard PAH calibration set can be used to predict unknown concentrations of the same PAH in petroleum samples.

Two issues are to be considered when calibration sets and score matrices are used to estimate concentrations of underlying components in unknown samples. The first issue to be considered is fluorescence quenching, which could lead PARAFAC analysis to predict a low relative concentration in the score matrix as a result of decreasing fluorescence at higher concentrations. To avoid that, EEMs for calibration and unknown samples should be arranged and entered into PARAFAC analysis in order of ascending concentrations so that fluorescence quenching effect can be detected in the score matrix easily as concentration increases. Arranging calibration samples in such way is not difficult because the concentration of the analyte of interest in these samples is known. It is harder to arrange petroleum product samples in an increasing concentrations order, solely based on their total EEM fluorescence values due to fluorescence quenching that could yield same total fluorescence intensity values for two samples with different concentrations or lower fluorescence intensities at higher concentrations. Therefore, fluorescence EEM peak locations should also be examined for all samples to distinguish higher concentrations from lower ones as explained earlier. Once PARAFAC analysis is performed on appropriately arranged EEMs, the concentration profile of the analyte of interest is examined in the calibration set and the unknown samples to determine which samples

are least effected by fluorescence quenching, so they can be used in subsequent prediction of the target analyte concentration. Fluorescence quenching can then be detected in score matrix values when they start to decrease or level off while the concentration of target analyte is actually increasing.

The second matter to be considered when fluorescence EEMs are used to estimate concentrations of aromatic compounds in petroleum products is the similarities in the fluorescence signals of some of the aromatic compounds that have comparable numbers of benzene rings in their structure. Concentrations of aromatic compounds with similar fluorescence signatures such as BTEX or naphthalene and methyl-naphthalene compounds cannot be determined separately. Therefore, the concentration of these compounds can be expressed as an "equivalent concentration" of one of the compounds that share the same fluorescence signal. BTEX compounds can be expressed in equivalent concentration of p-xylene, and naphthalene/methylnaphthalene compounds may be expressed in equivalent 1-methylnaphthalene concentrations. P-xylene and 1-methylnaphthalene are selected because they yield the highest fluorescence in comparison to other compounds in their groups, which should allow better detection of the BTEX and naphthalene / methylnaphthalene compounds fluorescence signals by PARAFAC analysis. To convert naphthalene to equivalent 1-methylnaphthalene concentration, the ratio between their fluorescence intensities can be used as a conversion factor, considering that fluorescence is a function of concentration. Laboratory work indicates that 1-methylnaphthalene fluorescence intensity is approximately 2.8 times higher than

naphthalene fluorescence intensity at various concentrations (see Figure H-4 in Appendix H). That means, almost 3 times the amount of naphthalene is required to yield an equivalent fluorescence intensity of the same amount of 1-methylnaphthalene, or less than half the amount of 1-methylnaphthalene is required to yield the same fluorescence of the same amount of naphthalene. These suggested conversion factors agree with values obtained in previous research (Kenny, et. al 2000). The following relationship can be used to calculate the total equivalent 1-methylnaphthalene concentration using conversion factors:

$$\text{Eq. } C_M = C_M + 0.4 C_N \quad [3-2]$$

Where,  $C_M$  and  $C_N$  are the concentration of 1-methylnaphthalene and naphthalene respectively. Similarly, the following relationship is used to calculate the total equivalent p-xylene concentration:

$$\text{Eq. } C_{PX} = C_{PX} + 0.1 C_B + 0.6 C_T + 0.4 C_E + 0.5 C_{MX} + 0.5 C_{OX} \quad [3-3]$$

Where,  $C_B$ ,  $C_T$ ,  $C_E$ ,  $C_{PX}$ ,  $C_{MX}$ , and  $C_{OX}$  are the concentration of benzene, toluene, ethylbenzene, p-xylene, m-xylene and o-xylene respectively. Equivalent p-xylene and 1-methylnaphthalene concentrations in all analyzed petroleum product samples based on analytical laboratory results are listed in Table 3-3. Aromatic compound concentration values were reported in gm of aromatic compound / kg of petroleum product. All concentration values were converted into gm of aromatic compound / L of petroleum product using related product densities to be consistent with estimated concentration values by PARAFAC analysis for prepared product samples.



To predict concentrations of different PAHs in analyzed petroleum products, fluorescence EEM related calibration sets of each PAH standard and petroleum product samples were appropriately arranged and loaded to perform PARAFAC analysis. The following aromatic compounds were used in PAH calibration sets in PARAFAC analysis: p-xylene (representing BTEX compounds), 1-methylnaphthalene (representing naphthalene compounds), phenanthrene and pyrene. PARAFAC models were fitted in the PLS\_toolbox 3.5.in MATLAB ver. 7.1. with convergence criteria (Relative and Absolute change in fit) and maximum number of iterations used throughout the modelling of  $10^{-6}$ ,  $10^{-6}$  and 10,000, respectively. The number of factors used to fit the PARAFAC models is the same as in previous models (Figure 3-8).

Once PARAFAC models were generated for all PAH standards and petroleum product samples, relative concentration profiles were examined to determine samples that were not affected by fluorescence quenching, which could be used in following steps. Figure 3-12 illustrates an example of generated relative concentration profiles for p-xylene in a standard calibration set (samples 1-4) and diesel samples (5-10). The generated profile of p-xylene is represented by the dashed line in all samples. Other concentration profiles that appear in the diesel samples (5-10) represent other underlying PAH components in the diesel (naphthalene/1-methyl naphthalene, phenanthrene and pyrene). Relative concentration values of p-xylene in the calibration set do not appear to be affected

by fluorescence quenching because they show increasing values that match the order that they were arranged in when entered into PARAFAC analysis. Relative concentration values in the calibration set can be used to estimate p-xylene equivalent concentrations in the diesel samples, however, the value in sample 1 will be used because it contains the lowest concentration of p-xylene and least likely to be affected by fluorescence quenching, if any. On the other hand, the values of relative p-xylene concentrations in the diesel samples appear to be noticeably affected by fluorescence quenching, because they show decreasing relative concentration values with increasing diesel concentration (from sample 6-10). Therefore, the value of p-xylene relative concentration in sample 5 will be used because it is the sample with lowest diesel concentration and expected to be least affected by fluorescence quenching, which should induce the least error in the estimate.

To estimate the equivalent p-xylene concentrations in the first diesel sample (sample 5), correlation between p-xylene relative concentration in samples 1 and 5 in score matrix was first determined. Figure 3-12 shows that samples 1 and 5 have relative concentration values of 2410 and 103 a.u., respectively. These values indicate that fluorescence intensity of p-xylene in sample 5 is approximately 4% of its intensity in sample 1, considering that values in the score matrix also represent relative fluorescence intensities of the analyte in different samples as mentioned earlier in this chapter.

Now that correlation is established between p-xylene in the standard calibration and diesel samples, actual fluorescence intensity and concentration values can be estimated using the p-xylene standard calibration curve. The p-xylene in calibration sample 1 had a concentration of 0.14 g/L and gave a total fluorescence intensity value of 420 a.u. using the ratio between fluorescence intensity of p-xylene in sample 5 and sample 1 of 4%, the total fluorescence intensity of p-xylene in sample 5 is calculated to be 18 a.u. By projecting this value on the p-xylene calibration curve, a total fluorescence intensity value of 18 can be related to p-xylene concentration of 0.005 g/L. The diesel in sample 5 was diluted 1000 times to a concentration of 1 mL/L; therefore the p-xylene concentration in undiluted diesel sample is expected to be approximately 5.00 g/L. This estimated value is approximately 23% higher than the concentration value of equivalent p-xylene in diesel listed in Table 3-2 that is based on analytical laboratory results. Details of estimation PAH compound concentrations in neat samples of analyzed petroleum products based on PARAFAC scores are discussed in Appendix-H.

PARAFAC estimated values of equivalent and actual concentrations of different aromatic compounds in analyzed petroleum products are listed in Table 3-4. Values in the table indicate that estimated PAH concentrations followed the same increasing or decreasing trends in concentration data reported in laboratory results for the same PAHs. The proposed procedure estimated concentrations of PAHs in all analyzed petroleum products samples with detection limits of approximately 0.50 g/l and accuracy that fell within 50% of values obtained by laboratory

chemical analysis. Such accuracy is likely acceptable for in situ contamination screening purposes to assist clean-up decisions. PARAFAC did not estimate pyrene concentration because pyrene concentrations in all analyzed petroleum products were below the detection limits. Also, pyrene does not have consistent fluorescence signal shape at all concentrations as mentioned earlier. This behavior doesn't allow PARAFAC to recognize pyrene fluorescence signal correctly in the calibration set and petroleum product samples to assign accurate relative concentration values.

### **3.5. SUMMARY AND CONCLUSIONS**

An innovative method that can be employed to characterize and quantify common petroleum contaminants (gas condensate, gasoline, diesel, flare pit residue and crude oil) and their underlying aromatic components in solutions is introduced in this study. Petroleum product characterization is based on multi-way decomposition of fluorescence EEMs of analyzed petroleum products by PARAFAC analysis and subsequent classification and matching of tested samples by SIMCA analysis. After PARAFAC modelling was completed, estimated emission spectra of underlying PAH components were correlated to fluorescence spectra of PAH standards to determine the chemical compound or group of compounds that is represented by each component. The study revealed that BTEX compounds, naphthalene/methylnaphthalene, phenanthrene, and to lesser extent pyrene were the major PAH components of the analyzed petroleum products, and laboratory chemical analysis results validated this finding. PARAFAC analysis also generated relative concentration profiles of PAH components in analyzed

petroleum products that was subsequently utilized by SIMCA to analytically differentiate between tested petroleum products. SIMCA demonstrated promising discrimination power to distinguish between petroleum products samples, which provide a more objective approach than conventional visual comparison in the standard method for initial screening of petroleum samples, and may be applied to various types of environmental samples without pre-separation steps.

Quantitatively, this study presented general detection limits and calibration curves for different petroleum contaminants that make use of the relationship between fluorescence intensity of different petroleum products and their concentrations in solutions. Once fluorescence EEMs of petroleum product under investigation are collected, total fluorescence intensity values can be obtained and used to estimate the concentration of the analyte in the solution using calibration curves. Also, this method allowed estimating concentrations of major PAH components in analyzed petroleum products in solutions with reasonable accuracy in the range of +/- 50% of values obtained by laboratory chemical analysis. The presented procedure provides quick and efficient framework for characterization and quantification of different petroleum contaminants in solutions that can be easily adapted to in-situ measurements, which is of great interest as it helps in planning further environmental site investigation activities and gives a preliminary idea about future screening and clean up decisions.

Table 3-1. Minimum petroleum products concentration at which fluorescence signal was detected with Varian Eclipse spectrometer

<b>Petroleum Products</b>	<b>Solvent Solution (mL/L)</b>
Gas Condensate	10.0
Gasoline	0.50
Diesel	0.50
Flare Pit Residue	1.00
Crude Oil	1.00

Table 3-2. Results of laboratory chemical analysis for aromatic compounds in the analyzed petroleum compounds

Sample	Total BTEX (mg/kg)	Naphthalene (mg/kg)	Benzo[e]pyrene (mg/kg)	Benzo(a)pyrene (mg/kg)
Gas				
Condensate	25,700	9.40	0.00	0.00
Flare Pit				
residue	2,580	461	18.5	1.80
Gasoline	15,1000	3,230	0.00	0.00
Diesel	7,340	1,100	0.00	0.00
Crude Oil	9,300	42.2	5.74	3.28

Sample	Perylene (mg/kg)	Methyl naphthalene (mg/kg)	Phenanthrene (mg/kg)	Pyrene (mg/kg)
Gas				
Condensate	0.00	5.60	0.00	0.00
Flare Pit				
residue	0.00	1,180	175	32.0
Gasoline	0.00	675	6.70	1.35
Diesel	0.00	5,910	1,250	82.1
Crude Oil	11.9	109	75.4	13.1

*Note:*

- *Laboratory method used is the Canada Wide Standards for Petroleum Hydrocarbons (CCME PHC)*
- *Quality control procedures and levels of uncertainty followed the O'Reg 153 Analytical Protocols.*

Table 3-3. Quantitative values for aromatic compounds in the analyzed petroleum compounds

Sample	Total BTEX (g/kg)	Eq. C <sub>PX</sub> (g/kg)	Eq. C <sub>PX</sub> (g/L)
Gas Condensate	25.7	11.3	7.76
Flare Pit Residue	2.58	1.38	1.23
Gasoline	151	92.0	69.0
Diesel	7.34	4.61	3.83
Crude Oil	9.30	4.86	4.71

Sample	Total Naphthalene compounds (g/kg)	Eq. C <sub>M</sub> (g/kg)	Eq. C <sub>M</sub> (g/L)
Gas Condensate	0.0150	0.0100	0.0100
Flare Pit residue	1.64	1.60	1.59
Gasoline	3.91	0.920	0.69
Diesel	7.01	8.02	6.66
Crude Oil	0.150	0.150	0.140

Sample	Phenanthrene (g/kg)	Phenanthrene (g/L)
Gas Condensate	0.00	0.00
Flare Pit residue	0.180	0.160
Gasoline	0.00	0.00
Diesel	1.25	1.04
Crude Oil	0.0800	0.0700

Sample	Pyrene (mg/kg)	Pyrene (g/L)
Gas Condensate	0.00	0.00
Flare Pit residue	32.0	0.0300
Gasoline	1.35	0.00
Diesel	82.1	0.0700
Crude Oil	13.1	0.0100



Table 3-4. Measured and estimated equivalent aromatic compound concentrations

Sample	Measured Eq. C <sub>PX</sub> (g/l)	Est. Eq. C <sub>PX</sub> (g/l)	Variation (%)
Gas Condensate	7.76	8.00	+3%
Flare Pit residue	1.23	Not Modeled	-
Gasoline	69.0	80.0	+14%
Diesel	3.83	5.00	+23%
Crude Oil	4.71	Not Modeled	-

Sample	Eq. C <sub>M</sub> (g/l)	Est. Eq. C <sub>M</sub> (g/l)	Variation (%)
Gas Condensate	0.01	Not detected	-
Flare Pit residue	1.59	2.50	+46%
Gasoline	0.69	1.50	+54%
Diesel	6.66	4.50	-32%
Crude Oil	0.14	Not detected	-

Sample	Phenanthrene (g/l)	Est. Phenanthrene (g/l)	Variation (%)
Gas Condensate	0.00	-	-
Flare Pit residue	0.16	Not detected	-
Gasoline	0.00	-	-
Diesel	1.04	1.60	+54%
Crude Oil	0.07	Not detected	-

Sample	Pyrene (g/L)	Est. Pyrene (g/L)	Variation (%)
Gas Condensate	0.00	-	-
Flare Pit residue	0.03	Not detected	-
Gasoline	0.00	-	-
Diesel	0.07	Not detected	-
Crude Oil	0.01	Not detected	-

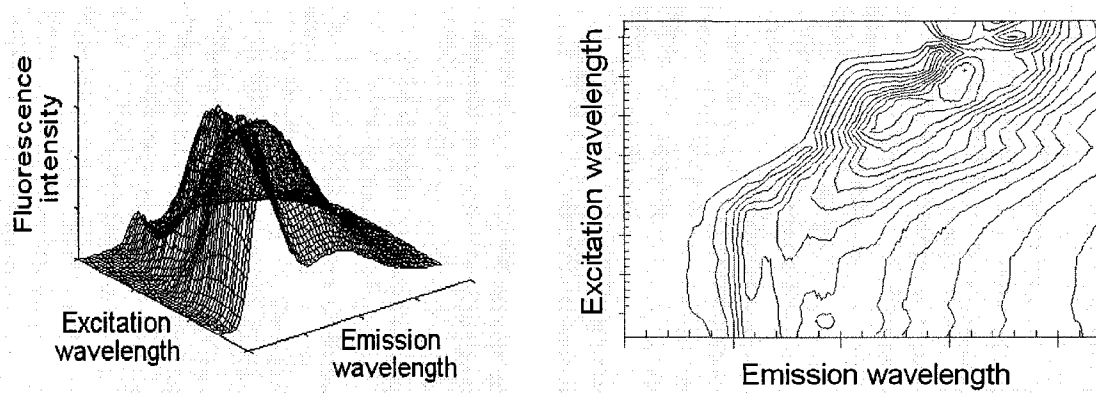


Figure 3-1. 3-dimensional (3D) and 2-dimensional contour map (2D) representations of emission-excitation matrix (EEM) (after Rho and Stuart 1978)

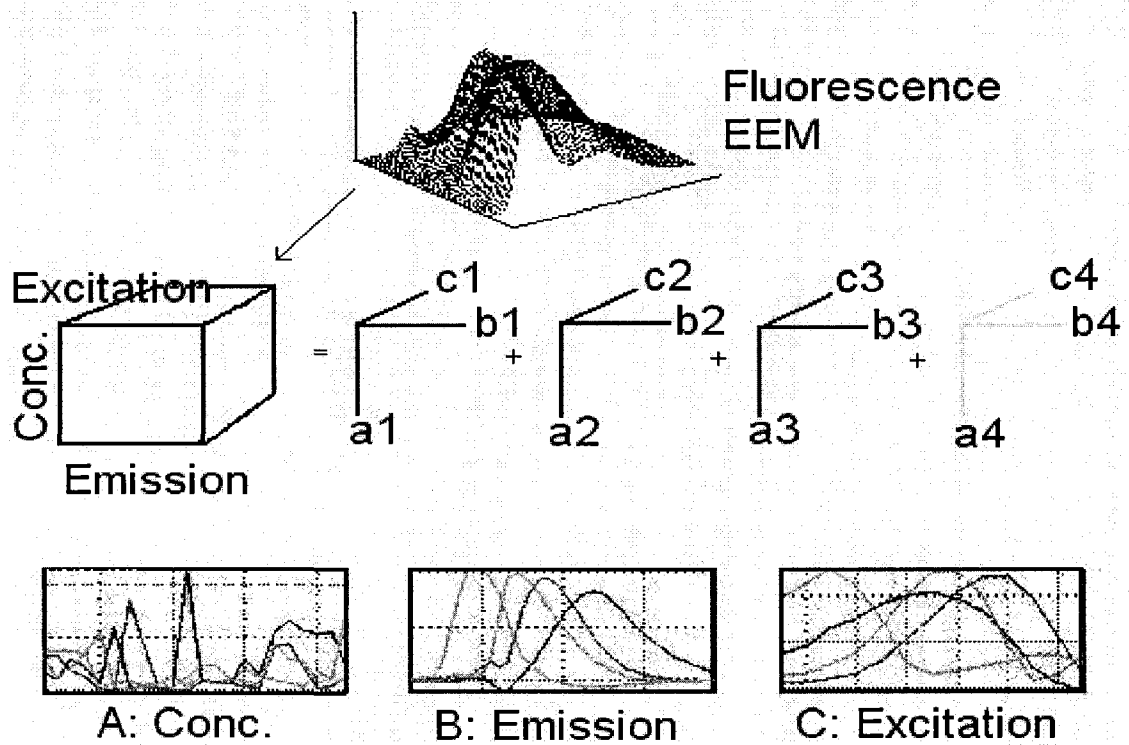


Figure 3-2. Graphic representation of PARAFAC analysis of EEM data including generated concentration, emission and excitation spectra matrices of modeled underlying components (Adapted from PLS-Toolbox manual 2006)

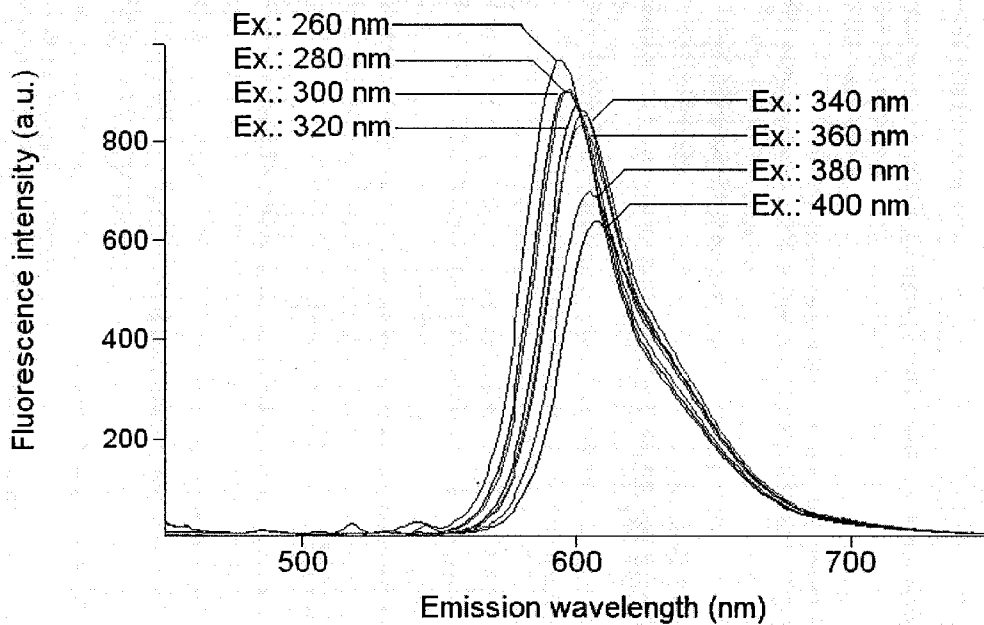


Figure 3-3. Reference fluorescence spectra of Rhodamine (Ex relates to the excitation wavelength associated with the plotted response)

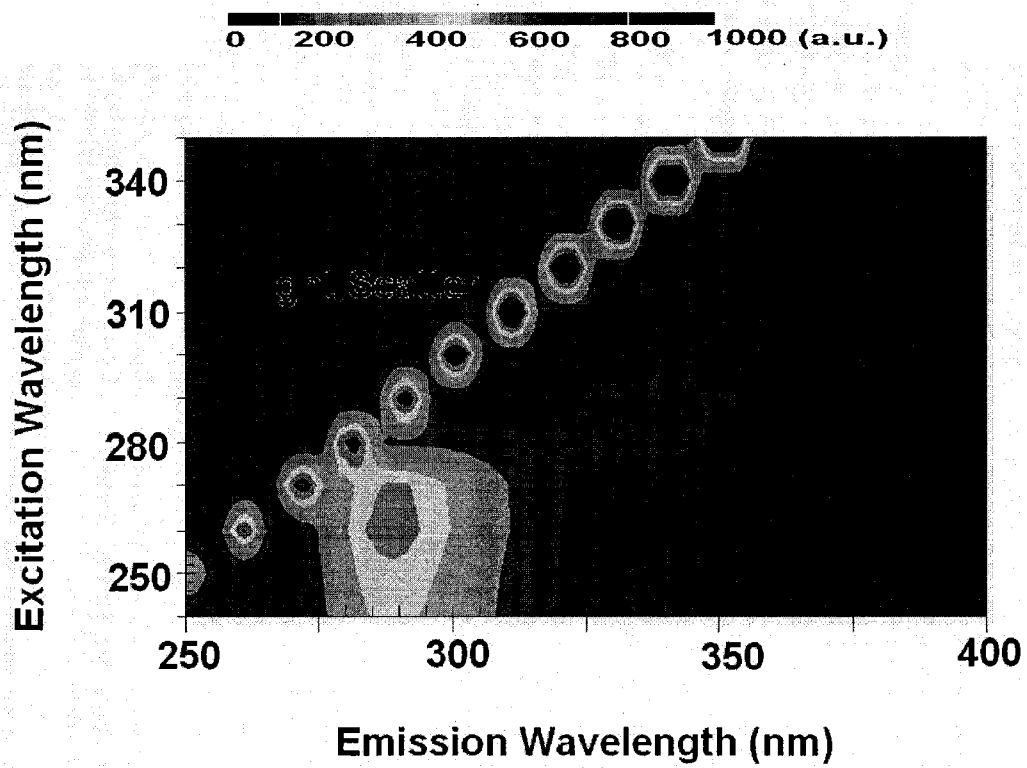


Figure 3-4a. Gas condensate EEM (neat)

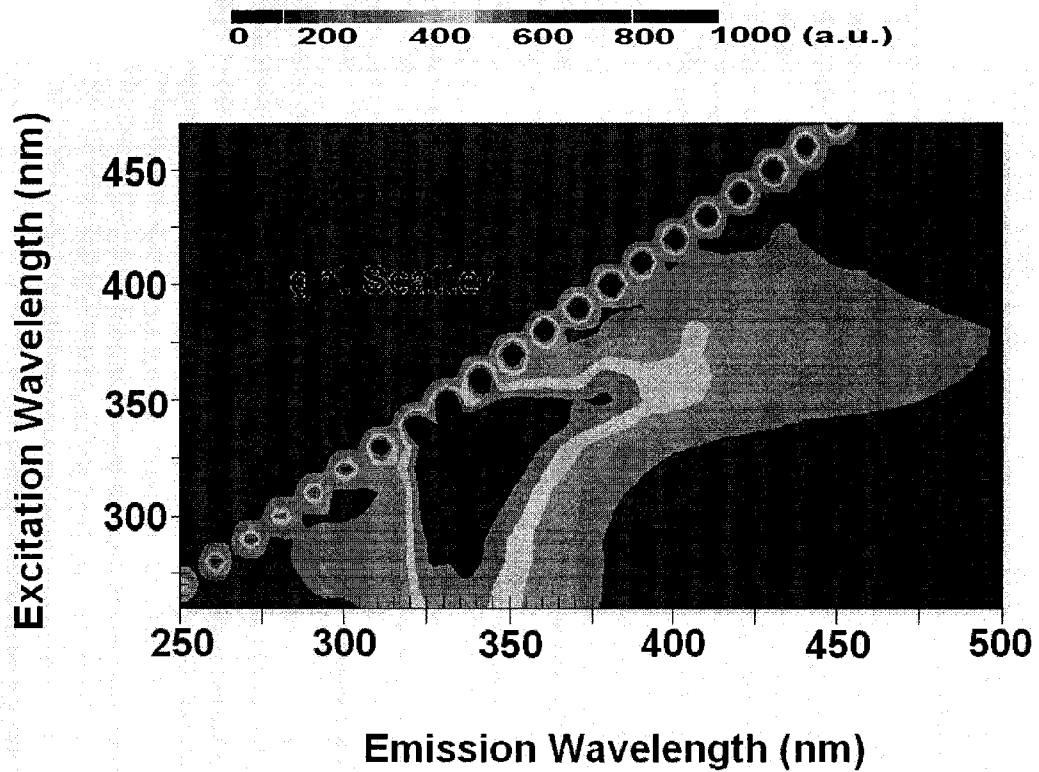


Figure 3-4b. Gasoline EEM (neat)

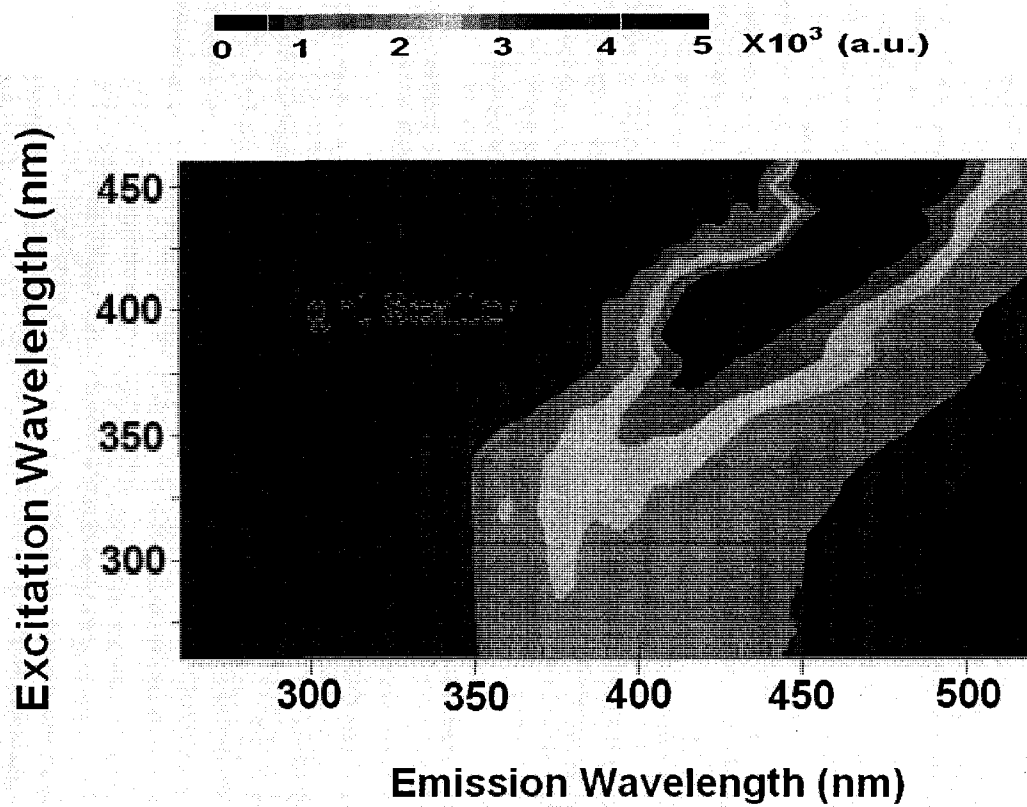


Figure 3-4c. Diesel EEM (neat)

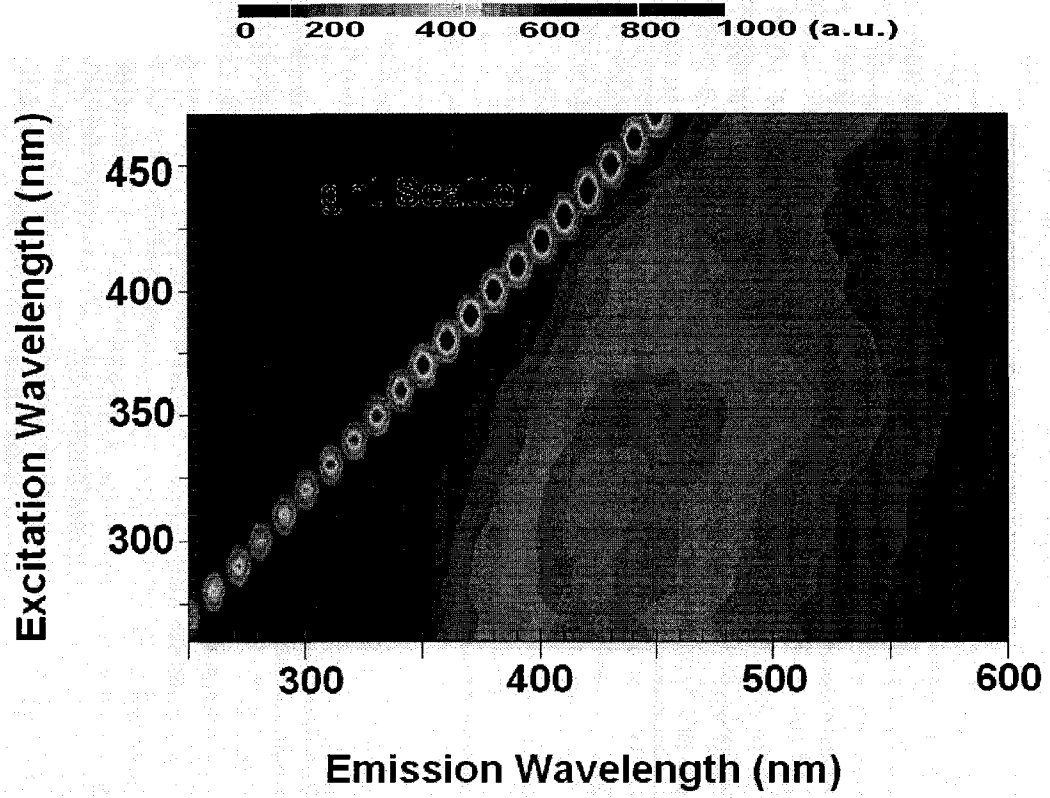


Figure 3-4d. Flare pit residue EEM (neat)



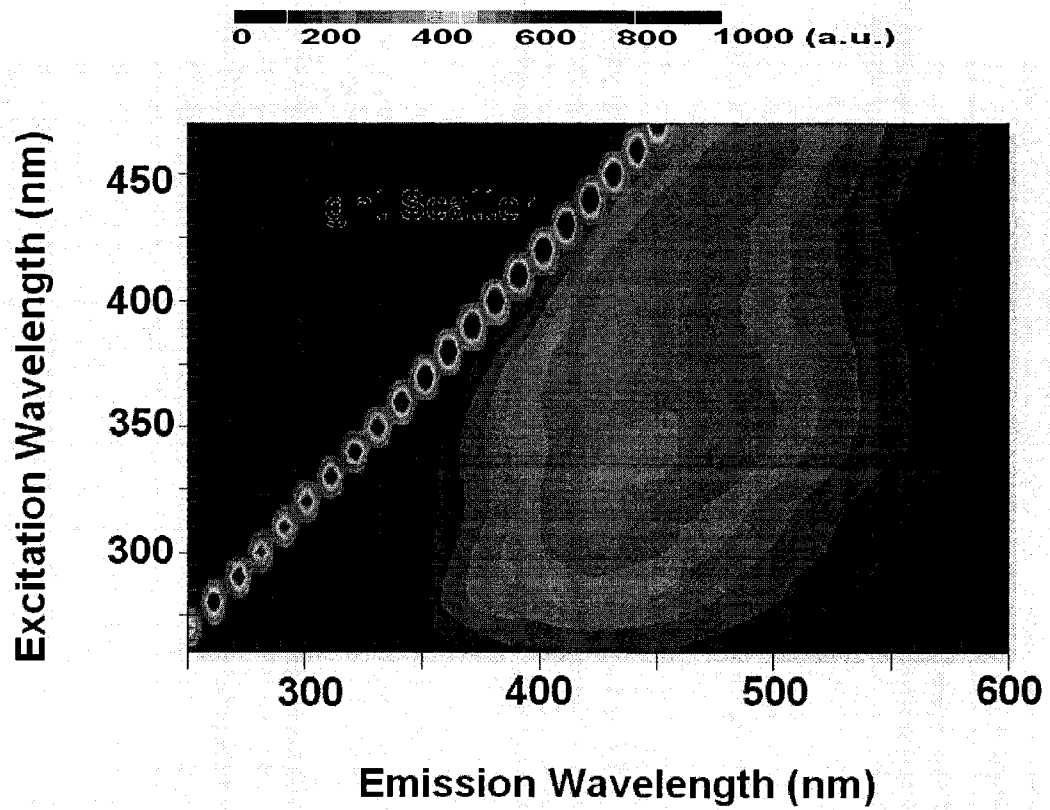


Figure 3-4e. Crude oil EEM (40 mL/L )

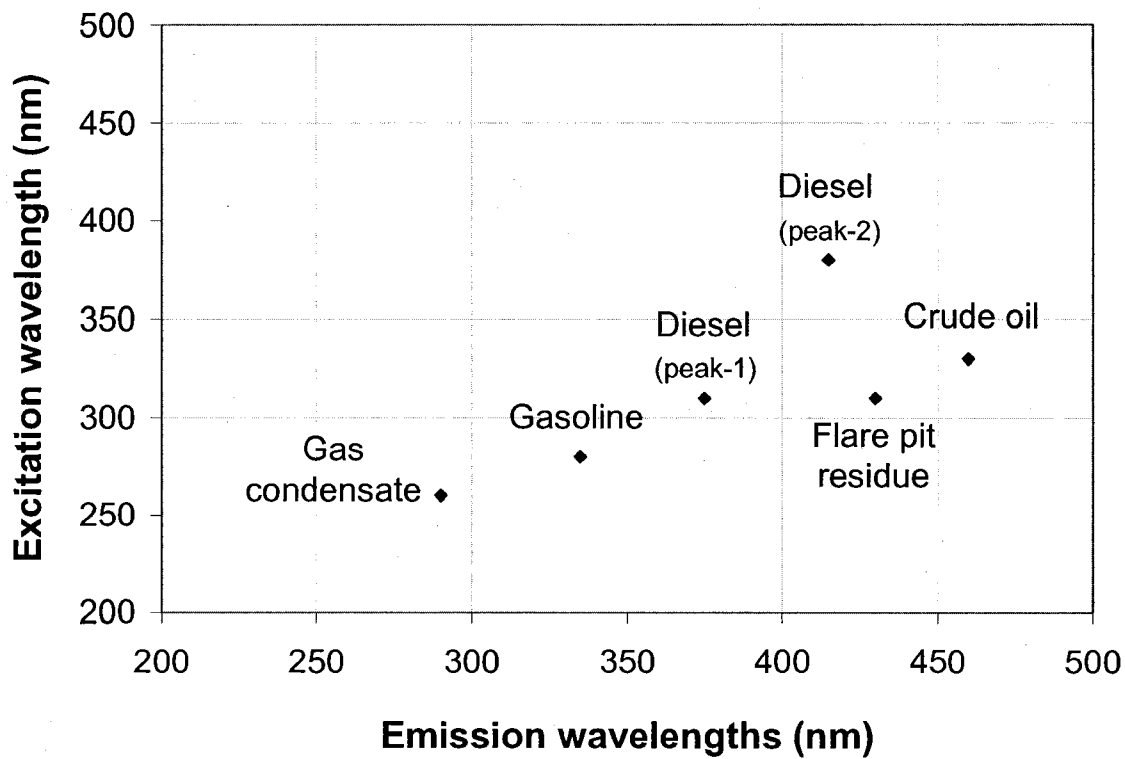


Figure 3-5. Highest fluorescence intensity EEM peak locations of the tested neat petroleum products and crude oil (40 mL/L)

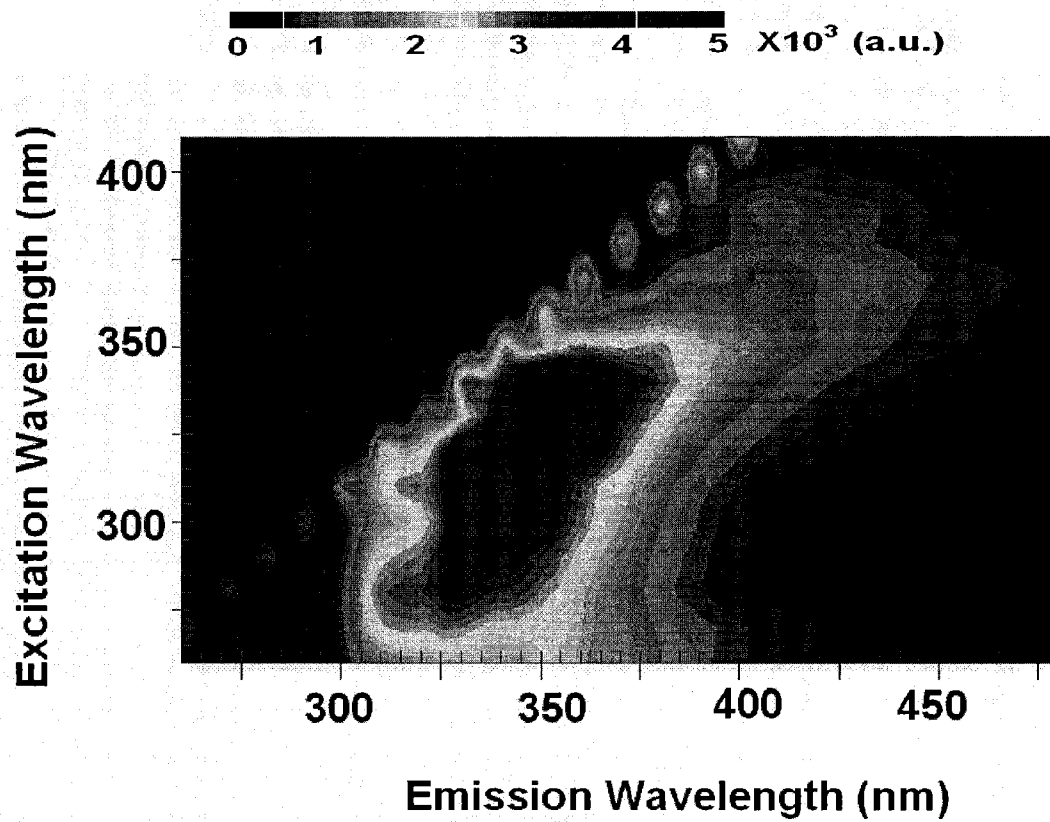


Figure 3-6a. Diesel EEM at solution concentration of 10 mL/L

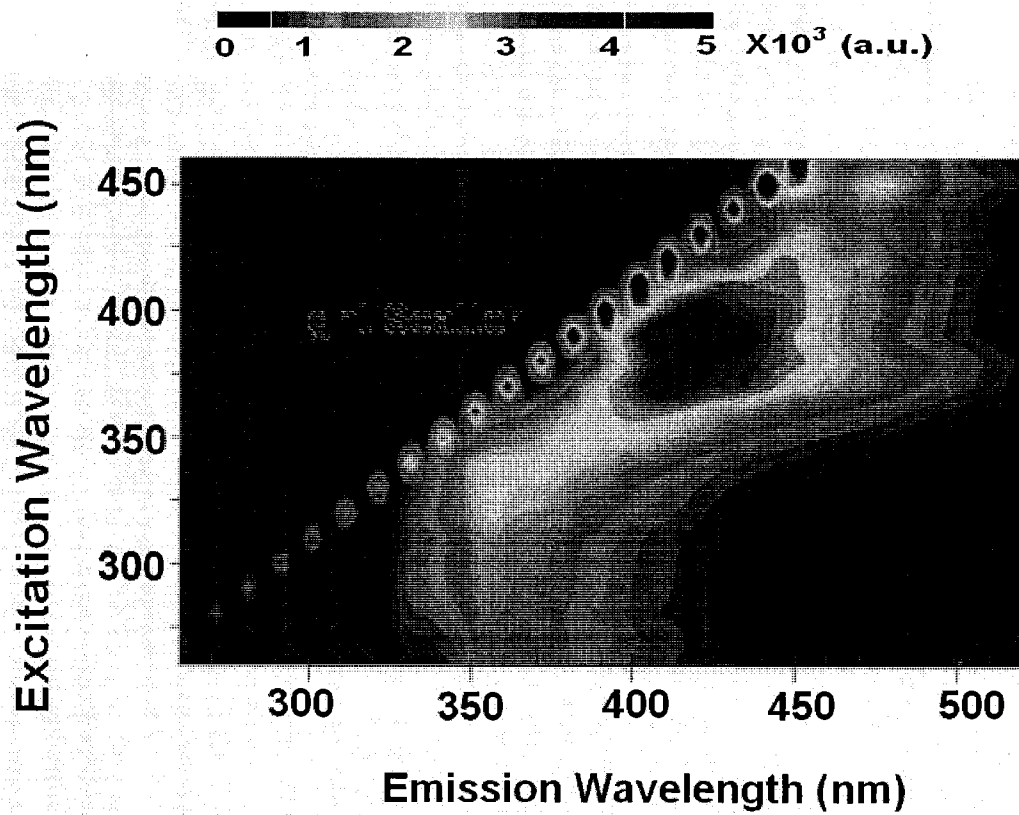


Figure 3-6b. Diesel EEM at solution concentration of 200 mL/L

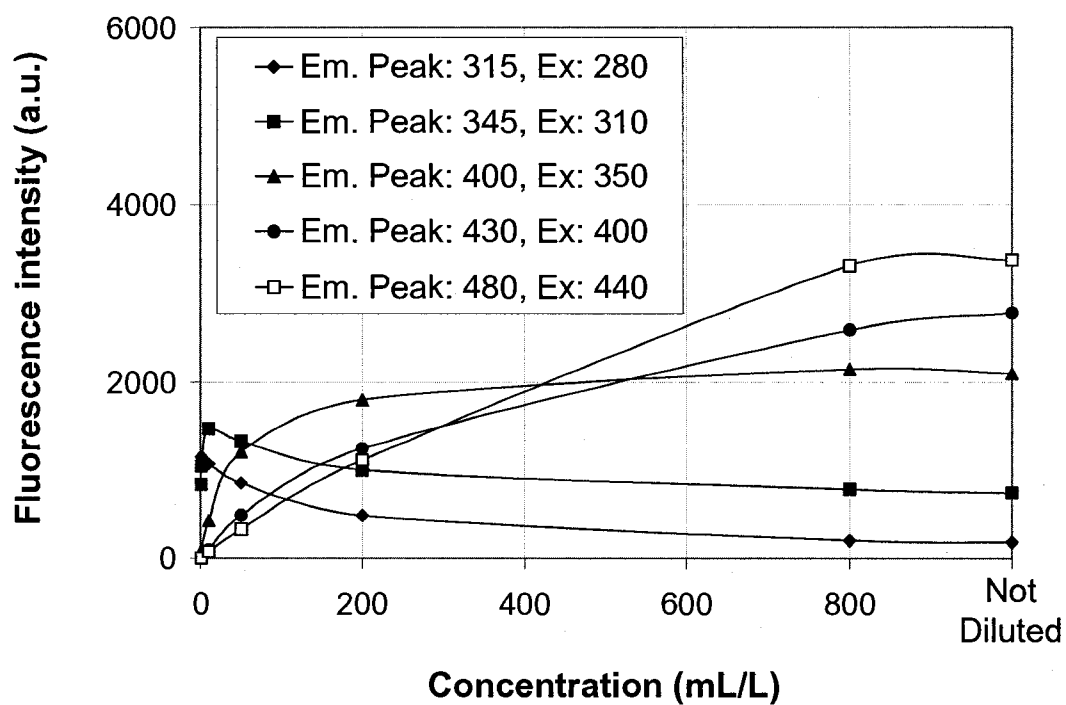


Figure 3-7. Changes in fluorescence intensity of different emission peaks for diesel in relationship with increasing solution concentrations

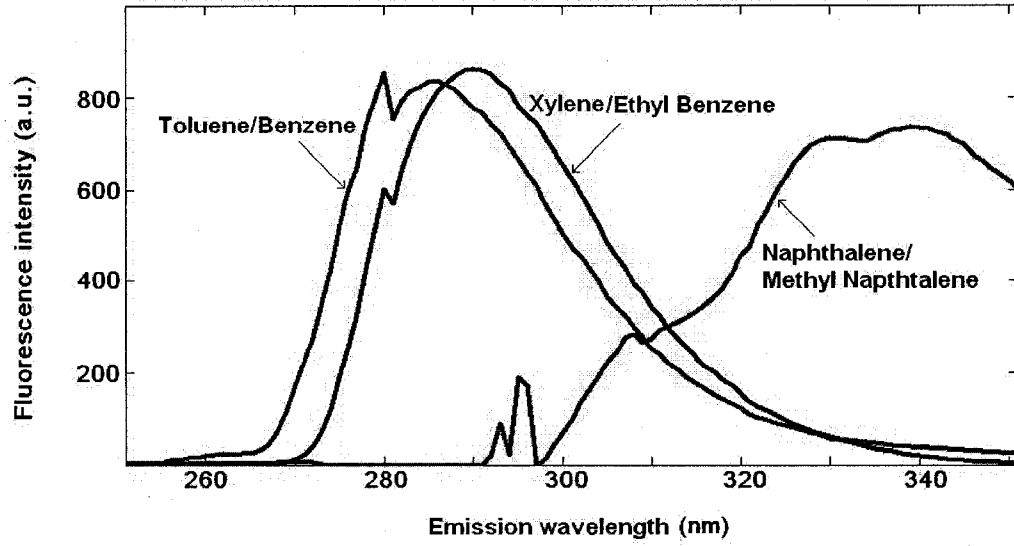


Figure 3-8a. PARAFAC model of gas condensate underlying component emission spectra

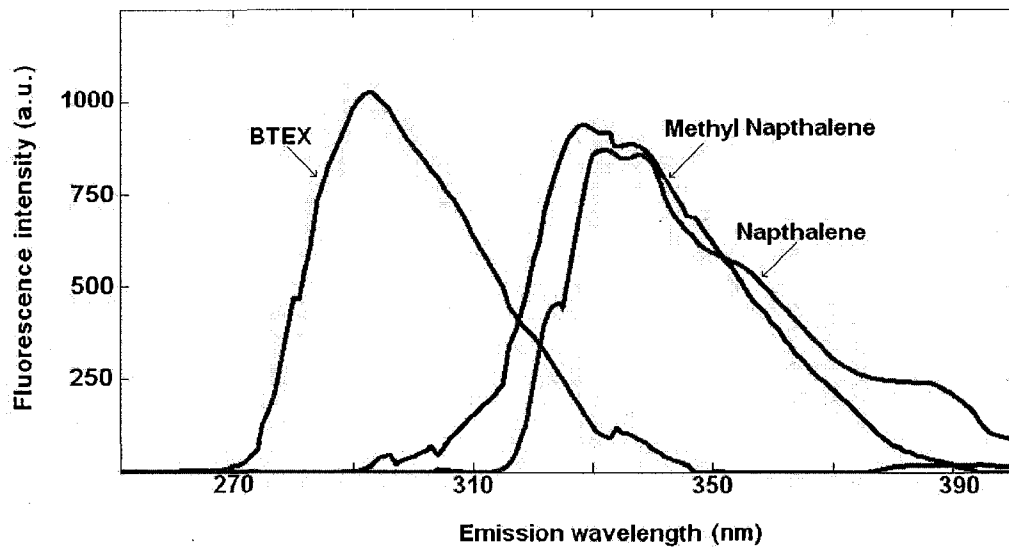


Figure 3-8b. PARAFAC model of gasoline underlying component emission spectra

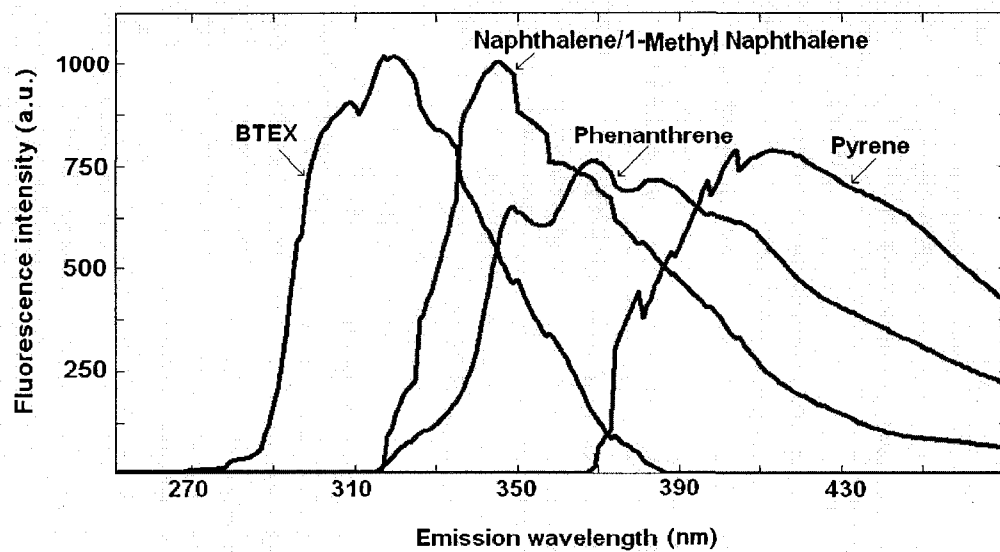


Figure 3-8c. PARAFAC model of diesel underlying component emission spectra



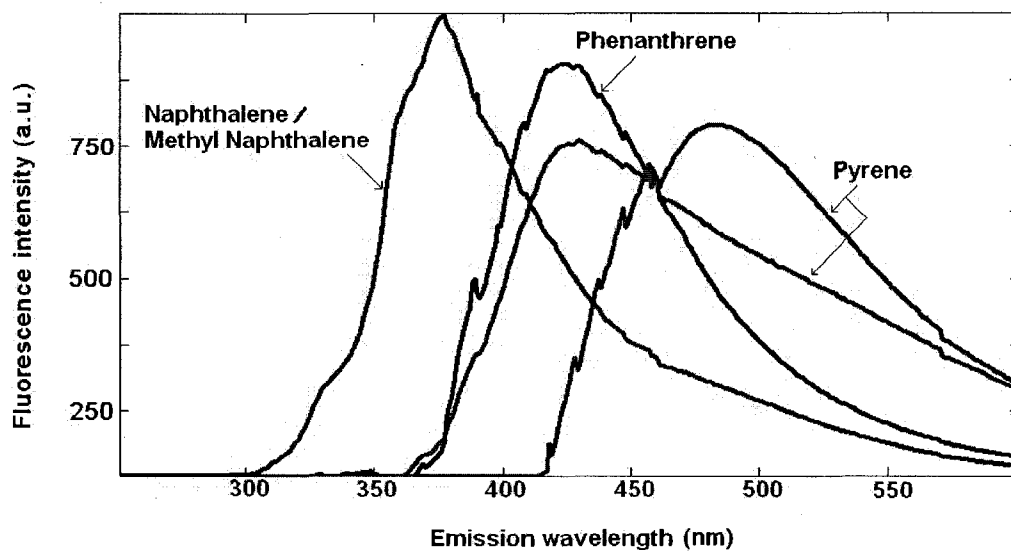


Figure 3-8d. PARAFAC model of flare pit residue underlying component emission spectra

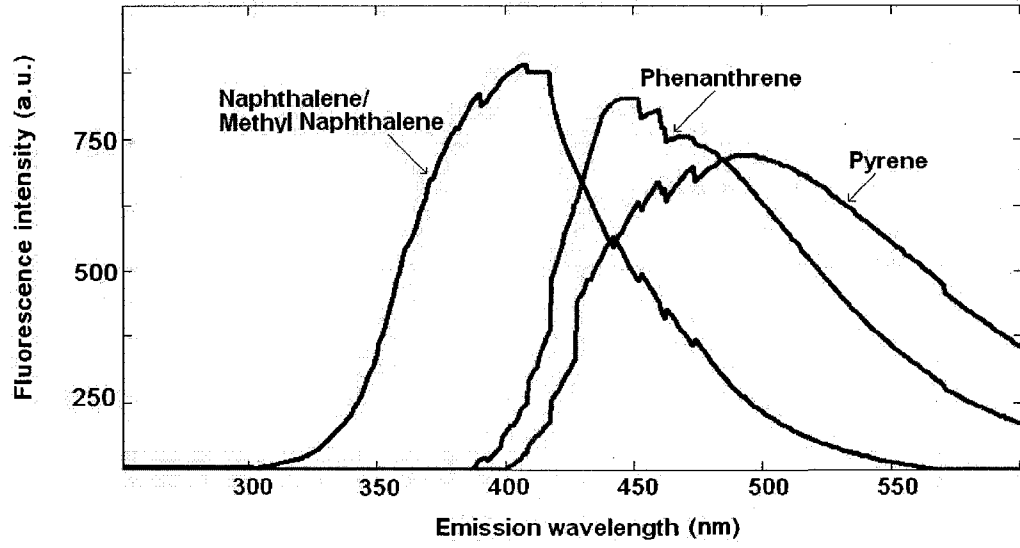


Figure 3-8e. PARAFAC model of crude oil underlying component emission spectra

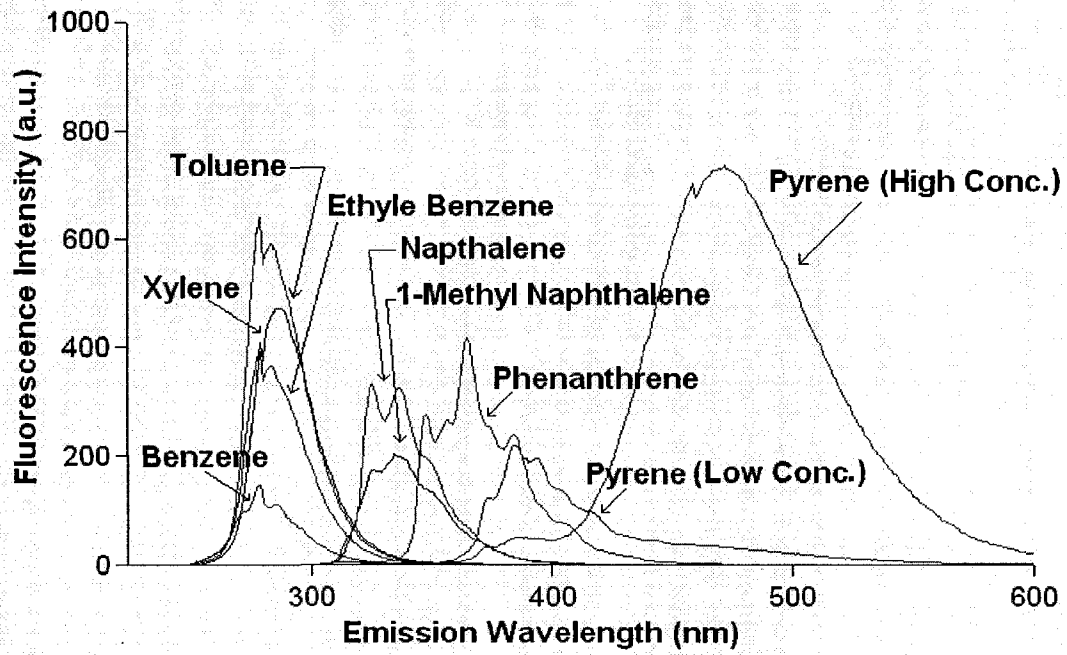


Figure 3-8f. Fluorescence emission spectra of standard PAH collected at laboratory

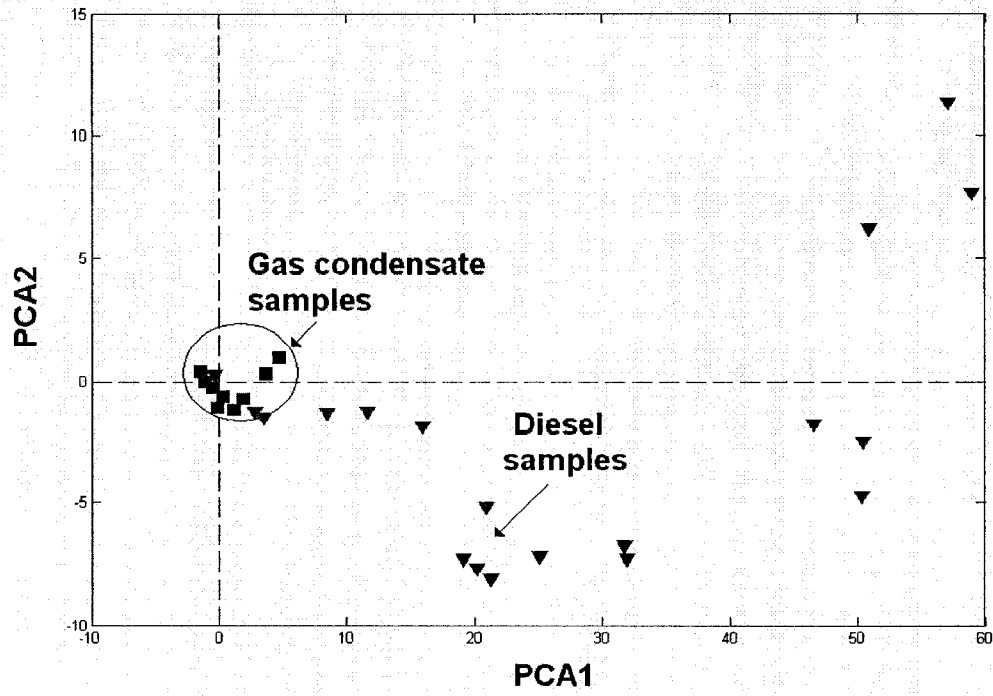


Figure 3-9. Sample plot of SIMCA modelled normalized diesel and gas condensate scores

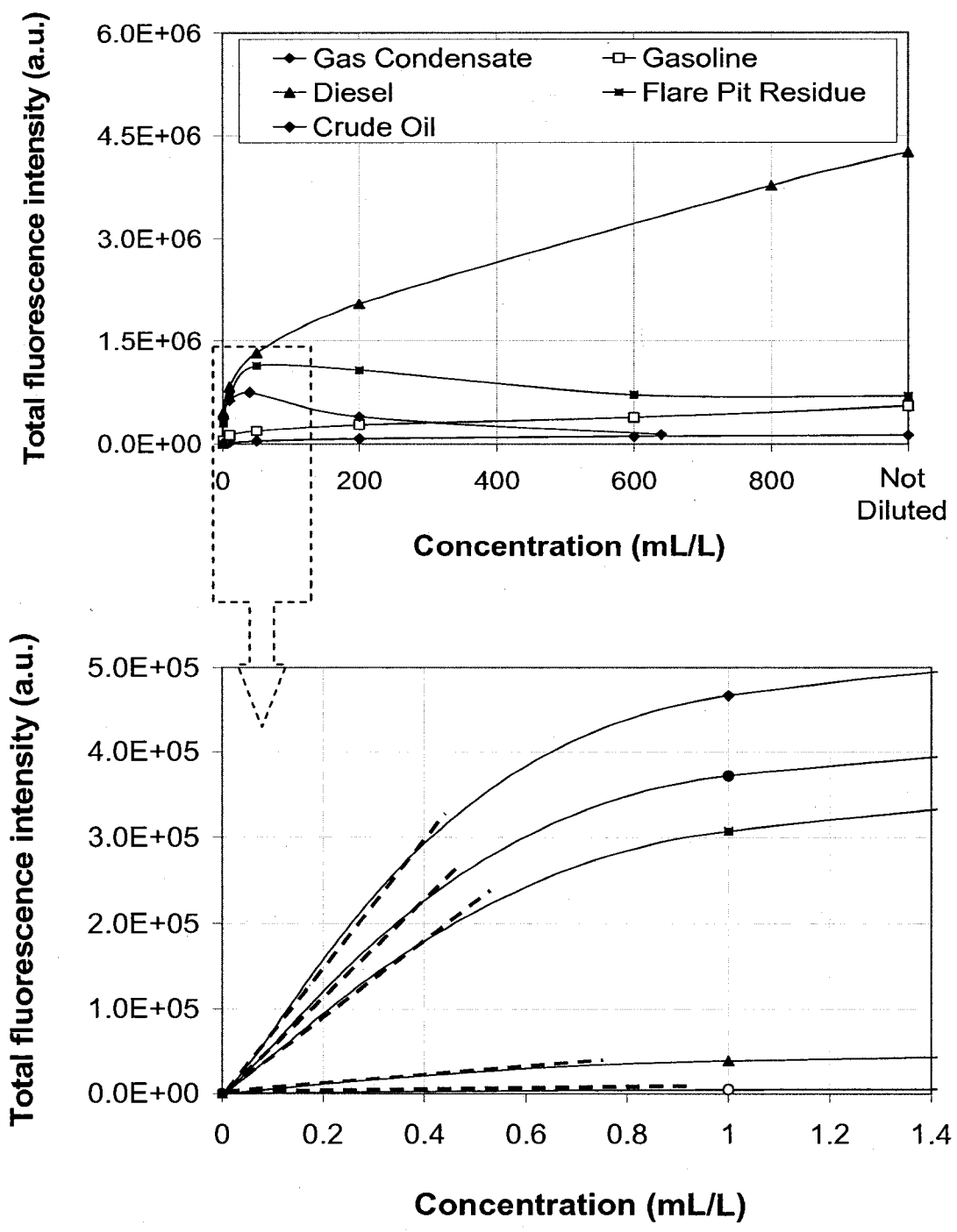


Figure 3-10. Total fluorescence intensity versus solution concentration of tested petroleum products

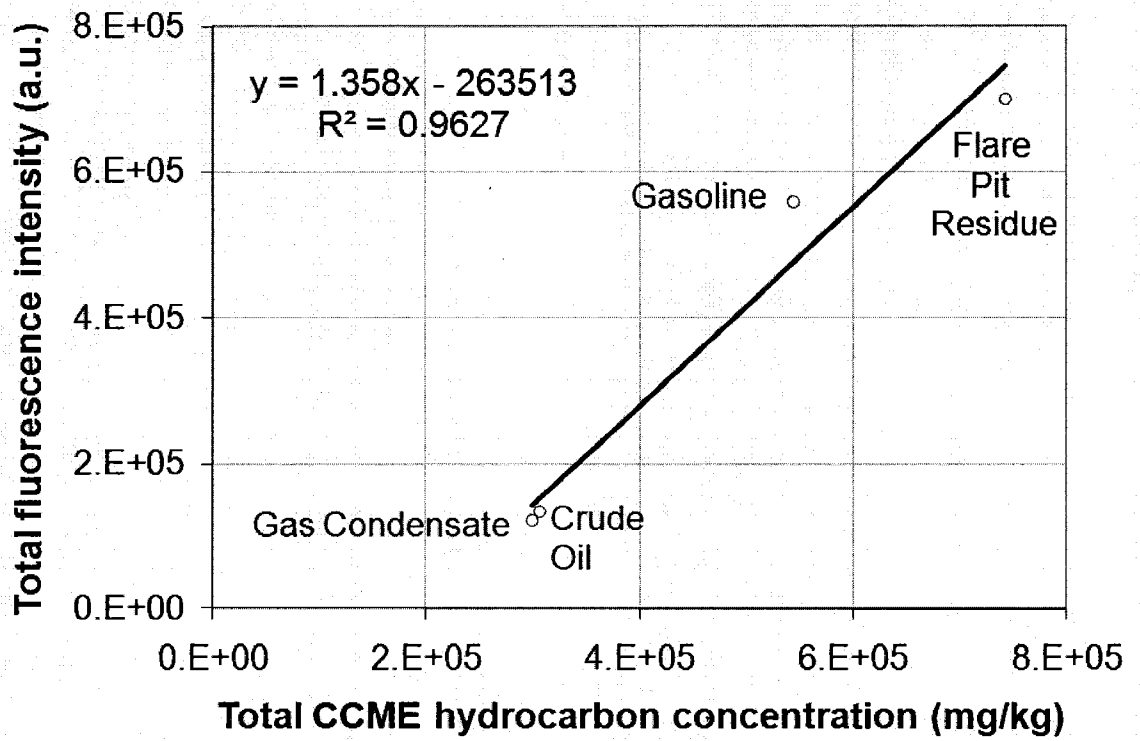


Figure 3-11a. Relationship between total fluorescence intensity and total CCME hydrocarbon fraction concentrations of tested petroleum products (diesel not included)

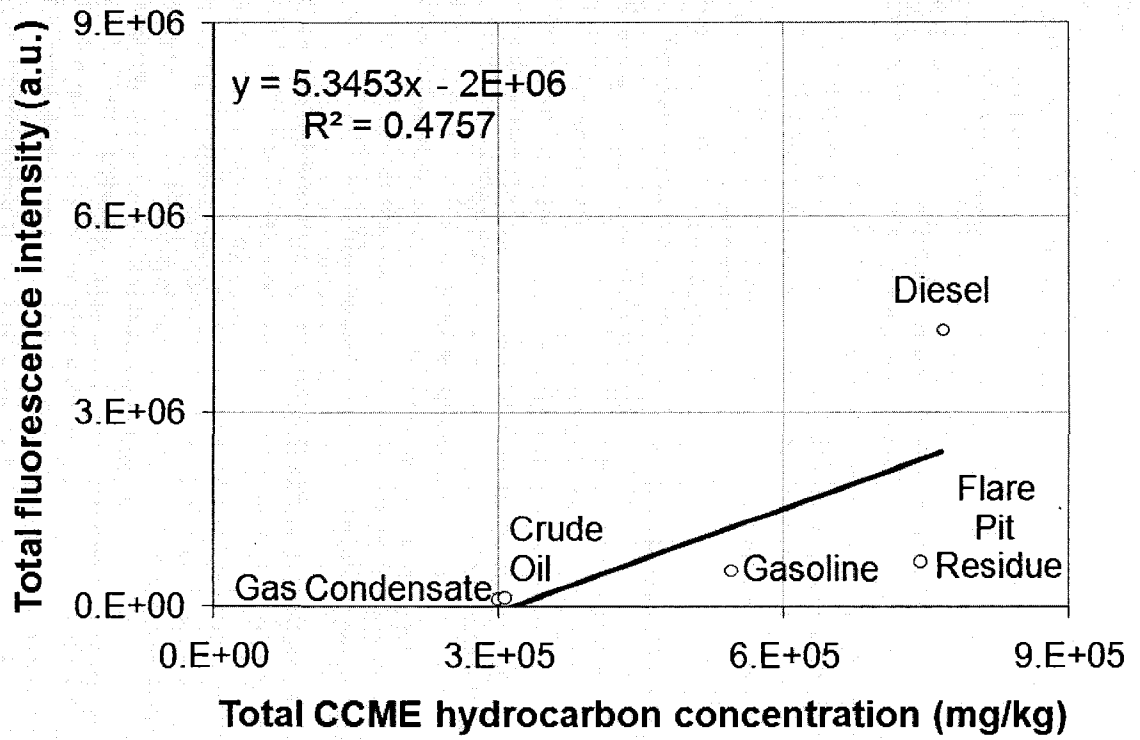
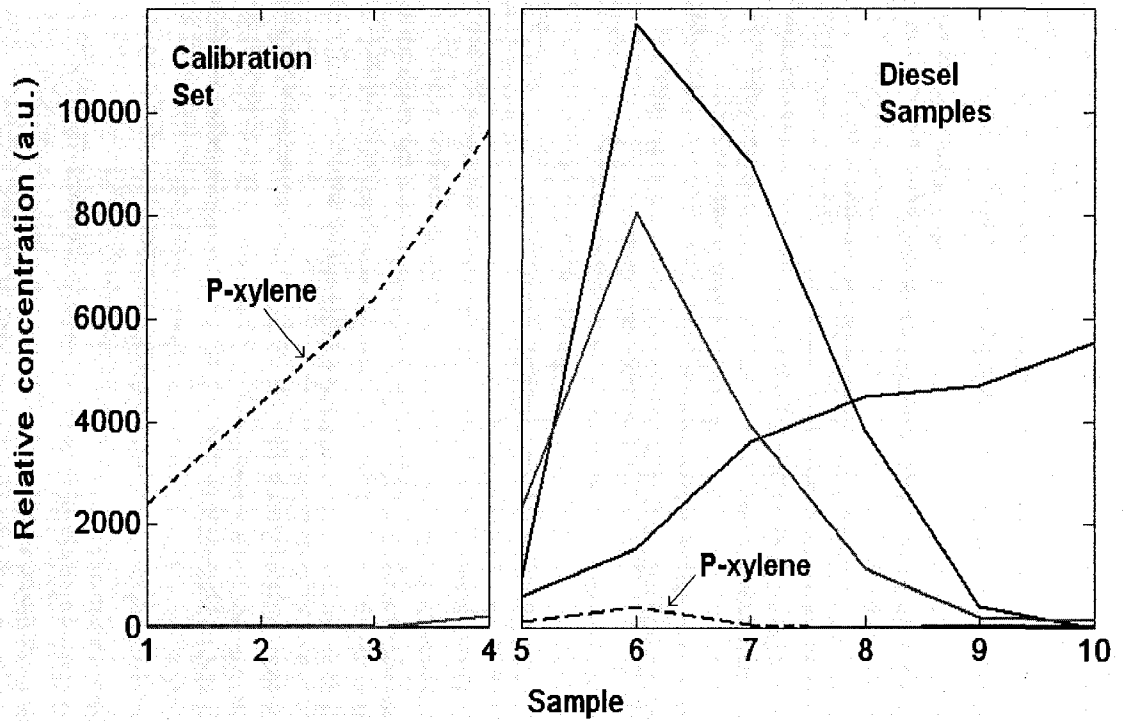


Figure 3-11b. Relationship between total fluorescence intensity and total CCME hydrocarbon fraction concentrations of tested petroleum products (diesel included)



### P-xylene calibration curve

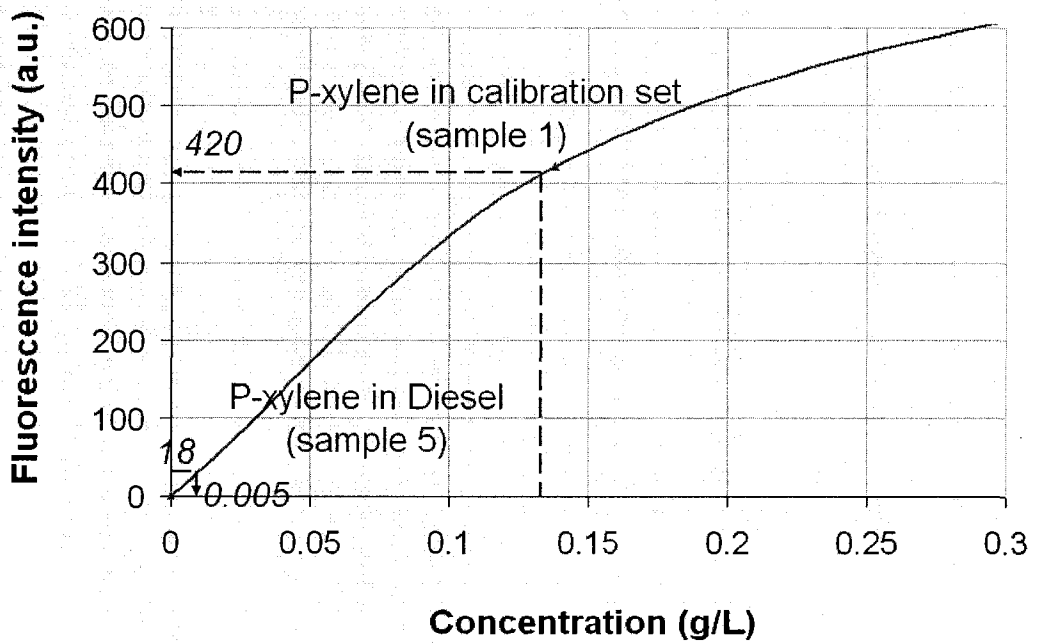


Figure 3-12. P-Xylene relative concentration in standard calibration and diesel samples



### 3.6. REFERENCES

- Alostaz, M., Biggar, K., Donhue, R., Segó, D., Robertson, P., Woeller, D. 2005. CPT-UVIF Evaluation of Subsurface Crude Oil Contamination At The Atlantic No3 Site. Proceedings of Annual Canadian Geotechnical Society Conference, Saskatoon, SK: 8p.
- Berlman, I. 1971. Handbook of Fluorescence Spectra of Aromatic Molecules. Academic Press Inc., New York.
- Biggar, K., Woeller, D., Murphy, S., and Armstrong, J. 2003. CPT-UVIF Characterization at Upstream Oil And Gas Facilities. In Proceedings of the 17th Annual Vancouver Geotechnical Society Symposium: Geotechnical Engineering for Geoenvironmental Applications, Vancouver, BC. pp 31-37.
- Bjorseth, A. and Ramdahl, T. 1985. Handbook of Polycyclic Aromatic Hydrocarbons, Vol. 2: Emission Sources and Recent Progress in Analytical Chemistry, Marcel Dekker, New York.
- Bro, R. 1997. PARAFAC: Tutorial and Applications. Journal of Chemometrics, 38, pp. 149-71.
- Bro, R. and Andersen, C. 2003. Practical Aspects of PARAFAC Modeling Of Fluorescence EEM Data. Journal of Chemometrics, 17, pp. 200 – 215.
- Canadian Council of Ministers of the Environment (CCME). 2001. Reference Method for the Canada-Wide Standard for Petroleum Hydrocarbons in Soil - Tier 1 Method, publication no. 1310.
- Christensen, J., Hansen, A., Mortensen, J. and Andersen, O. 2005. Characterization and Matching of Oil Samples Using Fluorescence Spectroscopy and Parallel

- Factor Analysis. *Analytical Chemistry*, 77, pp. 2210-2217.
- Eastwood, D. (in E. Wehry, E. Editor). 1981. *Modern Fluorescence Spectroscopy* (Vol. 4). Plenum Press, New York, N.Y.
- Hart, S. and JiJi, R. 2002. Light Emitting Diode Excitation Emission Matrix Fluorescence Spectroscopy. *Analyst*, 127, pp. 1693–1699.
- JiJi, R., Andersson, G. and Booksh, K. 2000. Application of PARAFAC For Calibration With Excitation–Emission Matrix Fluorescence Spectra of Three Classes of Environmental Pollutants. *Journal of Chemometrics*, 14, pp. 71–185.
- Kenny , J., Lin, J., Hart, S., Wang, W. and Namytkhine, D. 1995. Subsurface Contaminant Monitoring by Laser Fluorescence Excitation-Emission Spectroscopy in a Cone Penetrometer Probe. *SPIE*, 2504, pp. 59-67.
- Kenny, J., Pepper, J., Wright, A., Chen, Y., Schwartz, S., and Shelton, C. 2000. *Subsurface Contamination Monitoring Using Laser Fluorescence*. Lewis Publishers, Washington, D.C.
- Kenny, J. and Hall, G. 2007. Estuarine Water Classification Using EEM Spectroscopy and PARAFAC–SIMCA. *Analytica Chimica Acta*, 581, pp. 118–124.
- Kram, M., Keller, A., Massick, S. and Laverman, L. 2004. Complex NAPL Site Characterization Using Fluorescence (Part 1): selection of excitation wavelength Based on NAPL composition. *Soil and Sediment Contamination*, 13, pp. 103-118.
- Lakowicz, J. 1999. *Principles of Fluorescence Spectroscopy* (2nd Edition). Kluwer Academic/Plenum Publisher, New York, N.Y.
- Lieberman, S., Theriault, G., Cooper, S., Malone, P., Olsen, R. and Lurk, P. 1991. *Rapid Subsurface In Situ Field Screening Of Petroleum Hydrocarbon*

Contamination Using Laser Induced Fluorescence Over Optical Fibers, In Proceedings of the 2nd International Symposium on Field Screening Methods for Hazardous Waste Site Investigations, Las Vegas, Nevada. Air and Waste Management Association, Pittsburgh, P.A. pp. 57–63.

Lurk, P., Cooper, S., Malone P. and Lieberman, S. 1990. Development of Innovative Penetrometer Systems for the Detection And Delineation of Contaminated Groundwater And Soil, Superfund '90. In Proceedings of the 11th National Superfund Conference, Washington, DC. Hazardous Materials Control Research Institute, pp. 297–299.

Morrison, R. and Boyd, R. 1989. Organic Chemistry (5th Edition), Prentice Hall of India, New Delhi, India.

O'Connor, D. and Phillips, D. 1984. Time-Correlated Single Photon Counting. Academic Press Inc, London, UK.

Patra, D. and Mishra, A. 2002. Total Synchronous Fluorescence Scan Spectra of Petroleum Products. Analytical and Bioanalytical Chemistry, 373, pp. 304-309.

Pharr, D., McKenzie, J. and Hickman, A. 1992. Fingerprinting Petroleum Contamination Using Synchronous Scanning Fluorescence Spectroscopy. Ground Water, 30, pp. 484-489.

PLS-Toolbox manual. 2006. [http://software.eigenvector.com/toolbox/3\\_5](http://software.eigenvector.com/toolbox/3_5). Accessed on April 22, 2006.

Rho, J. and Stuart, J. 1978. Automated Three-Dimensional Plotter for Fluorescence Measurements. Analytical Chemistry, 50, p. 620-626.

- Schulman, S. 1977. Fluorescence and Phosphorescence Spectroscopy: Physicochemical Principles and Practice, Pergamon Press, New York, NY.
- St. Germain, R., Gillispie, G. and Klingfus, J. 1993. Variable Wavelength Laser System for Field Fluorescence Measurements. In Proceedings of Field Screening Methods for Hazardous Wastes and Toxic Chemicals, Las Vegas, NV. Air & Waste Management Association, Pittsburgh, P.A., pp.1113–1122.
- Valeur, B. 2002. Molecular Fluorescence: Principles and Applications. Wiley-Vec., New York, N.Y.
- Vandermeulen, J., Buckley, D., Levy, E., Long, B., McLaren, P., Wells, P., 1979. Sediment Penetration of Amoco Cadiz Oil, Potential for Future Release and Toxicity. Marine Pollution Bulletin, 10, pp. 222-227.
- Vo-Dinh, T. 1978. Multi-component Analysis by Synchronous Luminescence Spectrometry. Analytical Chemistry, 50, pp. 396-401.
- Vo-Dinh, T. 1982. Synchronous Luminescence Spectrometry: Methodology and Applicability. Applied Spectroscopy, 36, pp. 576-585.
- Vogt, N. and Sjoegren, C. 1989. Investigation of Chemical and Statistical Methods for Oil Spill Classification. Analytica Chimica Acta, 222, pp. 135-150.
- Wang, Z., Fingas, M., Page, D. 1999. Oil Spill Identification. Journal of Chromatography A, 843, pp. 369-411.
- Wehry E. (In Guilbault, G. Ed.). 1990. Practical Fluorescence (2nd Edition). Marcel Dekker, New York, N.Y.
- Wold, S. and Sjostrom, M. 1977. SIMCA: A Method for Analyzing Chemical Data In Terms Of Similarity and Analogy, In Kowalski, B.R., ed., Chemometrics Theory

and Application. American Chemical Society Symposium Series 52, Wash., D.C.,  
American Chemical Society, p. 243-282.

## **Chapter 4**

### **Soil Type Effects on Petroleum Contamination**

#### **Characterization Using Ultraviolet Induced Fluorescence**

#### **Emission-Excitation Matrices (EEMs) and Parallel Factor**

#### **Analysis (PARAFAC)**

### **4.1. INTRODUCTION**

Advances in optical and computational technology have encouraged the development of fluorescence sensors designed to detect petroleum contaminants using their optical properties. When aromatic hydrocarbon molecules, present in petroleum products, are excited with ultraviolet (UV) light, they emit fluorescence. This is termed ultraviolet induced fluorescence (UVIF). For a particular petroleum product, the emitted fluorescence wavelengths vary uniquely in intensity as a function of the excitation wavelengths and elapsed time after excitation (Schulman 1977; Vo-Dinh 1982; O'Connor and Phillips 1984). This fluorescing nature of petroleum hydrocarbons has been the focus of numerous research efforts, and reliable devices now exist to perform UVIF contaminant analyses in situ (Lieberman et al. 1991; St. Germain et al. 1993; Kenny et al. 1995; Biggar et al. 2003).

With recent advances in computational and optical technologies as well as electronics, fluorescence spectroscopy has become suited for in situ analysis of soil and water

contaminated with petroleum compounds. The major advantage of in situ UVIF analysis is that it does not require any preparation or sampling prior to analysis, which makes it attractive for field screening site characterization applications. However, only the “presence/absence” field screening capabilities of the method can generally be utilized, with a rough, semi-quantitative interpretation. This is mainly due to the lack of an appropriate calibration procedure to give quantitative results to the fluorescence analysis. It has been reported that fluorescence measurements can be employed to determine petroleum product concentrations in water or soil with limits of detection in a range relevant for the surveillance of regulatory limits or clean-up decisions (Kotzick et al. 1996; Knowles and Liberman 1995; Schade and Bublitz 1996), but this has been limited to more costly laser induced fluorescence (LIF) systems.

Chapter 3 showed that UVIF measurements in solvent solutions could characterize petroleum contaminants and detect their concentrations to levels around 400 mg/L (section 3.4.1.1.). Extending the utility of UVIF measurements to characterize and detect petroleum contaminants in soils is of great interest, as it will allow more efficient screening and analysis of petroleum contaminants in situ. Nevertheless, establishing a reliable calibration procedure to analyze petroleum product contamination in soils is challenging due to the varying properties of petroleum products and the impacts of soil matrices, which strongly influence the obtained fluorescence signal. For calibration purposes, well-characterized laboratory reference petroleum products and specific soils are required to model as closely as possible the

properties of the contamination and soil matrix. Furthermore, using standard reference petroleum products and soils will allow us to identify the influence of soil matrix on the measured fluorescence signal. Several researchers have shown that the intensity of fluorescence measurements can be significantly influenced by the presence of soil grains (Apitz et al. 1992; 1993; Moise et al. 1995; and Roch et al. 1995). This chapter presents a calibration procedure that employs fluorescence spectroscopy to detect petroleum products in soils, and investigate the effect of soil properties on observed fluorescence induced in petroleum products in the soil pore spaces using a bench-top fluorescence spectrometer. Primary attention is given to the effect of soil grain size distribution, porosity and mineralogy of the tested soils.

## **4.2. FLUORESCENCE SPECTROSCOPY**

The fluorescing nature of refined petroleum products and crude oil is related to the molecular electron structure of their aromatic compound constituents that allows electrons, when illuminated with sufficient energy (UV light), to absorb the induced energy (light photons) and be promoted to higher energy levels. The excited electrons could return to the ground state from the higher energy levels through various non-radiative and radiative mechanisms. One of the radiative mechanisms generates fluorescence. This movement of electrons between energy levels is most prevalent in aromatic hydrocarbons due to the nature of electron bonding in these molecules. The fluorescence signal or spectrum produced by a particular aromatic compound is unique and can be used as a fingerprint to identify that compound. An emission fluorescence spectrum can be generated by scanning the spectral distribution of the



emitted radiation at a particular exciting radiation wavelength. Alternatively, in an excitation fluorescence spectrum, the observation fluorescence wavelength is held constant with the fluorescence intensity measured as the excitation wavelength is varied (Schulman 1977).

The information from both the excitation spectrum and the emission spectrum can be combined into a single display known as a fluorescence emission-excitation matrix (EEM) that presents all the information of the excitation and emission fluorescence spectral features of the compound in one plot (Figure 4-1). The data in an EEM is often visually presented in the form of a contour plot that separates different aromatic components in the mixture into isolated peaks, which help to characterize these components (Rho and Stuart 1978; Vo-Dinh 1982). EEMs are effective in characterizing multi-component mixtures, where the overlap of fluorescence signals can be significant, making it difficult to identify individual compounds solely based on their conventional fluorescence signals. Even with the enhanced resolution of the spectral features of a particular compound in fluorescence EEMs, there can be considerable overlap in fluorescence signals of refined petroleum products and crude oil that contain large numbers of individual polycyclic aromatic hydrocarbons (PAHs). To further resolve the complexity of fluorescence EEMs due to significant fluorescence signal overlap, advanced multivariate statistical techniques in Chemometrics such as Parallel Factor Analysis (PARAFAC) and Soft Independent Method of Class Analogy (SIMCA) can be implemented.

#### 4.2.1. Multivariate Statistical Techniques

Multivariate statistical analysis techniques such as Parallel Factor Analysis (PARAFAC) and Soft Independent Method of Class Analogy (SIMCA) have shown an ability to resolve multi-component mixtures of PAHs (Christensen et al. 2005; Jiji, et. al. 2000; Phar et. al. 1992; Vogt and Sjoegren 1989).

PARAFAC is an advanced multivariate statistical technique that can decompose fluorescence EEM data of a particular petroleum product generated at different concentrations, into its underlying components. Fluorescence EEMs can be arranged in a three-way array ( $X$ ) of dimensions  $I \times J \times K$ , where  $I$  is the number of samples (different concentrations),  $J$  the number of emission wavelengths, and  $K$  the number of excitation wavelengths. PARAFAC decomposes this array into three matrices:  $A$  (the score matrix),  $B$ , and  $C$  (loading matrices) with elements  $a_{if}$ ,  $b_{jf}$ , and  $c_{kf}$ . The scores in  $a_{if}$  can be interpreted as the relative concentration of the analyte  $f$  in sample  $i$ , the vector  $b_f$  with elements  $b_{jf}$  is the estimated emission spectrum of that analyte, and  $c_f$  is the estimated excitation spectrum. Elements in  $X$  array can be modeled by PARAFAC as expressed in Equation 4-1, where  $f$  is the number of PARAFAC factors and  $e_{ijk}$  represent the residual elements that reflect variability can not be modeled:

$$x_{ijk} = a_{if}b_{jf}c_{kf} + e_{ijk} \quad [4-1]$$

PARAFAC utilizes a least squares optimization technique, which, when given a series of measured data, attempts to find a function that closely approximates the data. It attempts to minimize the sum of the squares of the ordinate differences (residuals)

between points generated by the function and corresponding points in the data (Bro and Andersen 2003).

SIMCA is a classification technique based on principal component analysis (PCA) models made for groups of samples (classes). SIMCA constructs PCA models for each class and then projects new data to be classified onto the PCA models. Sample distances from each class are determined based on the Q and  $T^2$  statistics. Samples close to a class (low Q and  $T^2$ ) are considered to belong to that class. Large distances (high Q and  $T^2$ ) suggest that a sample does not belong to that class. The SIMCA method is robust for non-normal distributions (Vogt and Sjoegren 1989). SIMCA can be used along with PARAFAC analysis to discriminate different types of refined petroleum products and crude oil based on the modeled factors obtained from their fluorescence EEMs.

#### **4.2.2. Fluorescence and Soil Fabric**

When released into soils, petroleum contaminants move into and through the voids (pores) within the soil matrix. The intensity of a fluorescence signal is a function of the amount of petroleum compounds that occupy the area illuminated with UV light. Therefore, volume and distribution of the petroleum filled voids within the soil will directly affect the intensity of the generated fluorescence EEMs. Volume and distribution of voids in the soil matrix is best described by soil porosity and sorting. Porosity of soil describes how densely the soil grains are packed and is defined as the ratio between voids volume to the total volume of the soil, represented by the

following relationship:

$$n = V_{\text{voids}} / V_{\text{soil}} \quad [4-2]$$

Where,  $n$  is the porosity,  $V_{\text{voids}}$  is the non-solid volume (pores) and  $V_{\text{soil}}$  is the total volume of material, including the solid and non-solid parts. Theoretically, porosity could range between 0 and 1 and is usually presented as a percentage. Typical values range between 20% and 45%. Sorting is a soil property that can be described by the grain size distribution. A well sorted soil is soil that has grains that are approximately all one size. Poorly sorted soil is soil that has grains with a wider range of sizes (Jumikis 1962).

Reported porosity of unconsolidated sands typically range from 39% to 49% (Terzaghi 1925 and Trask 1931). Tickell and Hiatt (1938) reported that porosity is closely related to the degree of sorting of soil particles, and is affected by the soil grain shape. Beard and Weyl (1973) studied sand samples with particle size ranging from 0.074mm to 0.840 mm, and indicated dependence of porosity on sorting for wet-packed material. Observed porosities ranged from 23% to 44% with higher porosity for better sorting and vice versa. Poorly sorted materials have lower porosity than similar well sorted materials because the smaller particles tend to fill the voids between larger particles. Studies reported that porosity of material assembled by mixing components with different particle sizes is less than the porosity of each of the separate components, suggesting that finer particles occupied the voids between the larger particles (Furnas 1931; Harr 1977).

Figure 4-2 shows how some smaller grains can fill the pores, considerably reducing porosity even when fine material represents a small fraction of the total volume of the material. It was indicated that a loose sand structure requires 32% by weight of clayey silt in order to fill the voids between the sand grains. A dense assemblage of sand requires only 20% of clayey silt to completely fill the pore space between the coarser particles (Konrad 1999; Mitchell 1993).

In general, clean soils, except carbonaceous or humic soils, don't emit fluorescence when illuminated with UV light. Carbonaceous soils fluorescence is related to fluorescence of carbonate minerals within the carbonate mineral matrix. Calcite doesn't fluoresce by itself; however, trace element substitution in the calcite crystal structure may induce a fluorescing nature. Calcite fluoresces in different colors due to various trace elements; it may fluoresce green due to uranyl ion traces or red and pink due to the presence of lead and manganese traces (Machel et al. 1991). In addition to carbonaceous soils, soils with high humic content are expected to fluoresce at different wavelengths due to presence of humic matter (Matthews et al. 1996). It is possible to isolate any background fluorescence due to carbonate minerals because it occurs at different wavelengths that would not interfere with petroleum product fluorescence signals. On the other hand, it might not be simple to isolate background fluorescence due to humic substances that can be convoluted with petroleum product fluorescence signals. Identifying petroleum product fluorescence characteristics in soil with high humic content was not included in this research scope to allow better characterization of simpler cases of soil-fluorescence interaction before pursuing

more complex ones. Therefore, with exception to soils with high humic content, mineralogy is expected to have no measurable effect on fluorescence signals of petroleum products in soils (Löhmannsröbena et al. 1997).

It is clear then that soil particle sizes and degree of sorting should have the most effect on the fluorescence intensity of petroleum contaminants, and these factors should be examined in more detail to assess their impact. It has been shown that fluorescence intensities in soils were considerably less than those in solvent solution for the same contaminant. As the grain size of the soil decreases, so did the maximum observed fluorescence signal (Sinfield et al. 1999). The same study found that in coarse grained soils with particle sizes between 0.07 to 2.00 mm, soil may reduce the fluorescence signal by as much as a factor of five, relative to those in solutions. Previous work by Aptiz et al. (1992a) showed that the fluorescence response of marine diesel fuel varied by an order of magnitude or more as a function of the soil type, which reflected the variable surface area of that substrate. It was observed that soils with smaller specific surface area (coarser grained soils) decrease the maximum observed fluorescence signal to a lesser extent than soils with larger specific surface area (finer grained soils).

### **4.3. MATERIALS AND METHODS**

#### **4.3.1. Soils**

To examine the effect of soil structure on petroleum product fluorescence, four different soils were used with a variety of particle sizes and distributions that

represent a reasonable range of expected soils at field sites. The soils used in the test were clean quartz sands and Devon silt (composed of quartz, feldspar and clay minerals). The grain size distributions of these soil types is shown in Figure 4-3, and included: 1) Ottawa sand (a uniform sand with a grain size of 0.42 mm), 2) a well graded sand that was assembled by mixing equal portions of coarse sand (sand with mean particle size ( $d_{50}$ ) of 0.72 mm), Ottawa sand (0.42 mm) and fine sand (a uniform sand with a grain size of 0.15 mm), 3) a mixture of well graded sand and Devon silt and 4) Devon silt. These soil samples represent well sorted, poorly sorted, poorly sorted sand with higher fines content and poorly sorted fine grained soils, respectively. Dry sieving was used to obtain the distribution of particle sizes larger than the No. 200 sieve (75  $\mu\text{m}$ ) for Ottawa sand, well graded sand and a mixture of well graded sand and Devon silt samples. Soil particles finer than No. 200 sieve were considered as fines and were not further analyzed (ASTM D422-63(2002)). Devon silt grain size distribution obtained in the laboratory study of Arenson et al. (2005) at the geotechnical centre of University of Alberta is used herein. The grain size distribution curves for the tested soils reflect clearly the degree of sorting of each of the tested soils.

The tested soil samples mixed with different petroleum products were placed in special sample container used in this study and tapped lightly to densify the soil prior to analysis. The sample container is made of black anodized aluminum, has a 33.28 mm outside diameter circular cross section and a height of 30.14 mm. A circular quartz glass top of the same diameter is fitted to one end of the container to allow UV

light illumination and fluorescence emission from the tested sample.

To obtain representative porosities for these soils, a sample preparation method was used as follows. A known weight of each soil was mixed with a known volume of the solvent used in the test program (hexane and chloroform) in the sample container. The samples were set aside for 30 minutes to allow the soil grains to settle and sample containers were tapped on the side until no further changes in soil volume was observed. The final height of soil and excess solvent on top of soil in the sample container were then measured through the glass top (Figure 4-4). Because the dimensions of the inner cross section and height of the sample container are known, the volume of soil and excess solvent were accurately obtained. The difference between the volume of the solvent that was originally in the sample container and the excess solvent equaled the volume of the voids in each soil matrix. The porosity was then obtained for each soil type using the relationship in equation 4-2. The porosities obtained were: Ottawa sand 44%, well graded sand 34%, well graded sand and Devon silt mixture 24% and Devon silt 19%. These values are within the expected range and in agreement with results from previous studies (Terzaghi 1925 and Trask 1931, Beard and Weyl 1973).

To verify the obtained soil porosity values, a known volume of each soil was mixed with a known volume of the solvent used in the test program in a graded volumetric beaker. These samples were set aside for a few hours to allow the soil grains to settle. Beakers were sealed to eliminate solvent evaporation and tapped on the side until no



further changes in soil volume was observed. The solvent was removed from above the soil surface and the solvent volume was measured. The difference between the volume of the solvent that was originally in the beaker and the solvent that was removed equaled the volume of the voids in each soil matrix. The porosity was then obtained for each soil type using the relationship in equation 4-2. The porosity values obtained using larger beakers were in agreement with earlier obtained values using sample containers.

#### **4.3.2. Petroleum Products**

The tested petroleum products included natural gas condensate, gasoline, diesel, flare pit residue and crude oil. These petroleum products represent petroleum contaminants that are often encountered at upstream oil and gas sites and contain a variety of aromatic constituents. Gasoline and diesel samples used in this study were purchased from the local market in Edmonton, AB. Gas condensate and flare pit residue samples were obtained from two research sites in Alberta. The crude oil sample came from Cold Lake, AB, and was supplied by National Centre for Upgrading Technology (NCUT) laboratories, Devon, AB. All samples were stored in airtight containers that were clearly marked and kept in a refrigerated storage room at the Applied Environmental Geochemistry Research Facility at the University of Alberta.

Along with samples containing pure product, a number of diluted samples of each petroleum product were prepared before proceeding with fluorescence measurements. Diluted sample had concentrations that ranged from 0.5 to 800 ml /L in solvent

solutions which corresponded to 140 to 190,000 mg/kg (ppm) in soil matrices. This wide range of concentrations was selected to provide a proper number of fluorescence EEMs for subsequent PARAFAC analysis and to monitor the effect of fluorescence quenching and energy-transfer processes at higher concentrations on the measured EEMs. In total, 70 stock solution samples (including duplicates) of all petroleum products were prepared. Hexane was used as the solvent to dilute gas condensate, gasoline and diesel samples. Chloroform was used to dilute flare pit residue and heavy crude oil due to the presence of higher molecular weight PAHs in these products that could not be dissolved by Hexane.

Individual standards of PAHs were prepared and mixed with soils including: BTEX compounds (Benzene, Toluene, Ethyl-Benzene and Xylenes), Naphthalene and Methyl-Naphthalene, Phenanthrene, Fluorene, Pyrene, Dibenzothiophene, and Fluoranthene. These PAH compounds were selected because they represent the major components of the analyzed petroleum products, and their fluorescence signatures (EEMs) are needed to characterize the predicted components by PARAFAC analysis. In total 120 stock solution samples (including duplicates) of individual PAH compounds were prepared to produce concentrations that ranged from 0.08 to 50 ml/L (or in equivalent g/L) in hexane as solvent representing 22 to 12,000 mg/kg (ppm) in soil matrices. For validation purposes, chemical analysis results indicating BTEX and PAH compound contents of tested petroleum products previously presented in chapter 3 were used.

Fluorescence EEMs were measured on a Varian Eclipse fluorescence spectrophotometer in the scan mode. Samples were prepared by mixing 3 ml of each stock solution with 5 gm of Ottawa Sand, well graded sand, well graded sand with silt and 3 gm of Devon Silt, and then transferred to the sample container. The sample container was mounted in the spectrophotometer compartment on a solid sample holder that allows for front-face fluorescence detection. This set-up was necessary to permit front-face fluorescence detection from soil and highly concentrated liquid samples that do not allow for regular right angle fluorescence detection.

A collection of emission scans from 250 to 600 nm with 1 nm increments was obtained at varying excitation wavelengths ranging from 240 to 450 nm with 10 nm increments. The bandwidths (slit width) were 5 nm for both excitation and emission for most scans, but were reduced to 2.5 nm when fluorescence intensity was out of range. The scan rate was 600 nm/min, which allowed a scan time of approximately 20 minutes per sample. Blank samples of soils were scanned to detect fluorescence background, and no fluorescence signal was observed in any of the tested soil samples. In addition, samples of hexane, chloroform, and a reference material (anthracene) were analyzed every day to monitor any variation in the spectrophotometer performance. Observed variation in emission peak locations and intensities of control samples throughout the experiment was very limited ( $\pm 2\%$ ). A total of 200 fluorescence EEMs were collected excluding blanks and PAH standards.

## **4.4. RESULTS AND DISCUSSION**

Presented fluorescence EEMs of analyzed petroleum products in this chapter might have different appearance than similar fluorescence data reported in other studies. The difference might be associated with several sources of variations including: differences of tested petroleum products source, processing procedure, aging, as well as, utilized fluorescence measurement instrumentation. Therefore, proper corrections should be considered when fluorescence spectral data comparison is attempted as explained in chapter 5 (section 5.4.2.1.).

### **4.4.1. Fluorescence EEMs**

Figure 4-5a-e illustrates the collected fluorescence EEMs for the analyzed pure petroleum products in Ottawa sand except the crude oil EEM which was diluted in chloroform (40 mL /L) because it shows better fluorescence intensity due to fluorescence quenching at higher concentrations of crude oil. The presented EEMs show that each of the analyzed petroleum products has an exclusive fluorescence signature with specific peak locations that can be used to identify that particular product. The location of the fluorescence EEM peaks in Figures 4-5a-e remained essentially unchanged from EEMs for the same petroleum products in solvent solutions that were collected in chapter 3 indicating that the fluorescence EEM peak locations are unaffected by the presence of the soils, as was anticipated (Figure 4-6). However, it was observed that fluorescence peaks in EEMs of petroleum products in solvent solutions might be diminished or enhanced for the same products in soils because of fluorescence attenuation or enhancement due to the presence of soil

particles (which will be discussed later in this chapter). Fluorescence EEMs of all the examined petroleum products maintained the locations of their peaks in all soil matrices tested (at the same concentration). Figure 4-7 shows an example of the similarities of collected fluorescence EEMs of flare pit residue (not diluted) in Ottawa sand and Devon silt. This observation is consistent with findings of previous research (Sinfield et al. 1999) and confirms that soil mineralogy has no effect on observed fluorescence signals of petroleum products. On the other hand, it was noticed that variation of soil fabrics induced attenuation or enhancement of fluorescence peaks intensities, similar to observed effects of including petroleum product in soil matrices.

The observed attenuation or enhancement of fluorescence peak intensities had an effect on the minimum concentrations of petroleum products at which fluorescence signals were detected in tested soil samples. A list of these concentrations that can be interpreted as general detection limits of different petroleum products in solvent solutions and different soils is in Table 4-1. Listed concentrations values in the “solvent solution” column are obtained from chapter 3. The fluorescence signals were detected if they exceeded a threshold set to  $3\sigma_{\text{background}}$ , where  $\sigma_{\text{background}}$  is the standard deviation of background signal obtained by scanning fluorescence EEM of blank soil and solvent samples (Hart and JiJi 2002). The listed detection limit values are based on selected concentrations in this study. For a particular petroleum product, listed detection limits might be further refined by preparing and testing more soil samples with petroleum product concentration values that fill the gap between the lowest concentration value at which the fluorescence signal was detected in this study and

next lower one at which fluorescence signal was not detected.

Monitoring peak locations of a particular petroleum contaminant in specific soil at different concentrations indicated that EEMs typically have more pronounced emission peaks at long wavelengths. As the concentration of the contaminant decreases, peaks start to shift slightly toward shorter wavelengths (Figure 4-8a-b). This behavior was, also, detected in solvent solutions in chapter 3 and a previous study (Kram et al. 2004). The apparent peak shifts is related to an inter-molecular mechanism, known as inner filter effect, by which emitted radiation of dissolved species get re-absorbed by the fluorophores mixture itself (Lakowicz 1999). At higher concentrations of petroleum products, compounds with a larger number of aromatic rings re-absorb fluorescence photons with sufficient excitation energy emitted by compounds with smaller number of aromatic rings. In our previous study, it was found that, despite the apparent shift of peak locations at different concentrations, fluorescence EEMs are still unique because they show the unique combinations of excitation and emission wavelengths associated different peaks which is an exclusive characteristic of the tested product.

Even though mixing petroleum products with different soils did not change the shape of fluorescence EEM, it did significantly affect the intensity of the EEM peaks in different ways based on the susceptibility of the products to fluorescence quenching. Mixing petroleum products that are less prone to fluorescence quenching such as gas condensate, gasoline and diesel with different soil types, attenuated the maximum

fluorescence values at different concentrations compared to the tests with no soil. The amount of attenuation is not the same for all soil types. Soil porosity and sorting degree appear to have a significant effect on fluorescence signal intensity. On the other hand, petroleum products where quenching was observed in solvent solution samples at high concentrations, did not show this consistent attenuation of fluorescence intensity in soils.

To examine the effect of different soil matrices on the fluorescence of the tested petroleum products, the relationship between total fluorescence intensity and petroleum product concentration in both solvent solutions and soil matrices was investigated. Total fluorescence values were obtained by integrating the areas under all fluorescence curves (signals) in the related fluorescence EEM. The integration limits were consistent in all EEMs, were and limited to excitation and emission wavelengths between 250 nm and 450nm, and 260 nm and 600 nm, respectively. For each analyzed petroleum product, total fluorescence values were plotted versus related concentrations in solvent solutions and different soil matrices. These same profiles are used for quantitative calibration purposes which will be discussed later.

In soils, the maximum fluorescence would be achieved when the largest amount of void space is exposed to the irradiated area on the fluorescence sensor window. Soils with more void space are expected to attenuate fluorescence the least. Figure 4-9 shows the attenuation of total fluorescence for diesel when mixed with different soils. Reduction in fluorescence was the least in Ottawa sand, where reductions of

approximately 30% were observed compared to that in solvent solution. The Ottawa sand has uniformly distributed large soil particles with the largest voids volume of the tested soils, (44%), for the other soils tested, the reduction in fluorescent intensity was directly related to the soil porosity; as porosity decreased, fluorescence intensity decreased. The largest fluorescence attenuation was observed in Devon silt that has more than 80% of its composition as fines and had a porosity of 19%, where the observed diesel fluorescence signal was 60% less than that in solvent solution.

The systematic attenuation of fluorescence signal in soil matrices discussed above, applies to petroleum products that don't show significant fluorescence quenching at higher concentrations. Earlier work in chapter 3 indicated that flare pit residue and crude oil are more susceptible to fluorescence quenching. Therefore, mixing these analytes with soils is expected to have different effects on their fluorescence signal intensity. Figure 4-10 shows that the flare pit residue total fluorescence values were attenuated in soils at lower concentrations with no significant attenuation at higher concentrations. In fact, fluorescence signal intensity was enhanced at higher concentrations in the well graded sand and Devon silt mixture, as well as, Devon silt. These soils have better sorting and less porosity. The presence of flare pit residue fluorescing molecules in separate small voids within the soil matrix reduces the chances of interaction between these excited molecules, which is essential for the energy transfer mechanism that contributes significantly to fluorescence quenching (Lackwicz 1999). As the void sizes decrease when smaller particles fill the voids between larger particles in better sorted soil, less fluorescence quenching is expected.



That is why well sorted soil with higher content of fines such as Devon silt resulted in the fluorescence intensity of flare pit residue exceeding the fluorescence intensity in solvent solution by almost 22% at the highest concentration tested.

There appears to be a relationship between fluorescence signal intensity attenuation or enhancement of a particular petroleum contaminant mixed with soil and the porosity of that soil. To investigate this relationship, total fluorescence values of the analyzed petroleum products in solvent solutions and in different soils (at different concentrations) were plotted against the porosity of the soils. A porosity value of 100% indicates that no soil is present, and was assigned for petroleum products in pure solution. The relationship is presented in Figure 4-11a for diesel (representing petroleum products that are less affected by fluorescence quenching) and in Figure 4-11b for flare pit residue (corresponding to petroleum products that are more susceptible to fluorescence quenching). High  $R^2$  values that range between 0.943 and 0.983 in Figure 4-11a indicate that total fluorescence intensity of diesel in soil at all concentrations is linearly related to soil porosity. In Figure 4-11b, high  $R^2$  values that range between 0.965 and 0.993 indicate that total fluorescence intensity of flare pit residue in soil at lower concentrations (up to 50 ml/L in solution) is linearly related to soil porosity. The relationship departs from linearity at higher concentrations because of the impact of fluorescence quenching on fluorescence signal intensity as discussed earlier. Table 4-2 provides a list of equations that describe the linear relationship between total fluorescence values of tested petroleum products at different concentrations and porosity. Equations are presented as:  $F = m*n + b$ , where F is total

fluorescence,  $m$  is the slope,  $n$  the porosity and  $b$  the intercept. Associated  $R^2$  values are also listed.

The above analysis revealed that the fluorescence intensity attenuation or enhancement of petroleum products due to presence of soil matrices is systematic and closely related to soil grain size distribution and porosity for all tested samples. Such consistency may permit expanding the generated total fluorescence profiles to other soils that are not addressed in this study. To estimate contaminant concentration, the total fluorescence must be calculated, and the grain size distribution and porosity of the new soil must be characterized and correlated to grain size distributions of standard soil matrices in this study that share most common characteristics. Once correlated, a total fluorescence profile can be fitted in relation to generated fluorescence profile(s) of the target petroleum product.

#### **4.4.2. PARAFAC Analysis**

Data pre-processing is usually required before proceeding with PARAFAC analysis because experimental EEMs can be affected by scatter effects and measurement variability. Radiation scatter can be Raleigh and/or Raman scatter that shows up in fluorescence EEMs as diagonal lines. In this study, no Raman scatter was observed in blank solutions so it was ignored. Raleigh scatter was detected in all collected EEMs as illustrated in Figure 4-5a-e. Scatter data within the diagonal lines across the EEMs were removed and set to NaN, or 'not a number' indicating missing data in the data set. These regions were then filled by expectation values by the PARAFAC

algorithm. Inserting missing values instead of zeros in the scatter region was based on previous work by Andersen and Bro (2003). To ensure proper statistical modeling, constraints are usually applied: “non-negativity” constraints are often enforced on the estimates of A, B, and C loadings. These constraints improve the stability of the modeling and are based on a prior knowledge that negative concentrations or fluorescence intensities are impossible (Bro 1997).

The PARAFAC models were fitted using MATLAB ver.7.1 with the PLS\_toolbox 3.5 for fluorescence EEMs of tested petroleum products in all soil samples together. The convergence criteria (Relative and Absolute change in fit) and maximum number of iterations used throughout the modeling were  $10^{-6}$ ,  $10^{-6}$  and 10,000, respectively. A large number of PARAFAC models were estimated for all analyzed samples in solvent solutions and soil matrices using an increasing number of factors (from 1 to 5). Determination of the appropriate number of factors was mainly based on the number of iterations, core consistency, analysis of residuals (Andersen and Bro, 2003) and comparison of PARAFAC factors with fluorescence spectra of individual PAHs (see Appendix G for more details). Figures 4-12a-f illustrates the emission loadings of the PARAFAC modeled components for the analyzed petroleum products

Interpretation of factors in PARAFAC models was based on fluorescence characteristics of modeled factors. Visual comparisons of the fluorescence characteristics, namely emission peak(s) wavelength(s), of the PARAFAC factors with fluorescence signals collected for individual PAH standards presented in Figure

4-13 indicated that each of the factors can be related to a specific PAH compound or class of compounds. PARAFAC modelled components of petroleum products in soil samples agreed with laboratory chemical analysis results for the aromatic composition of the analyzed samples that are listed in chapter 3 (Table 3-2) and showed that PAHs content of the analyzed petroleum products is mainly composed of BTEX compounds, naphthalene/methylnaphthalene, phenanthrene, and to lesser extent pyrene. These results closely matched components of the same petroleum products in solvent solution predicted in chapter 3.

#### **4.4.3. SIMCA Analysis**

Being able to discriminate between fluorescence signatures (EEMs) of the analyzed petroleum samples is of a great interest as it allows fast in situ characterization of different petroleum contaminants in environmental samples (aqueous solutions or soil matrices). SIMCA analysis utilizes these variations of relative composition of PAHs to discriminate between various petroleum samples. To characterize the tested samples, estimated scores from PARAFAC modeled factors of all tested petroleum products in soil samples were normalized as a fraction of the sum of scores from that factor for all samples. Scores were normalized to avoid one factor controlling the class definition. Classes were then assigned to each sample. Gas condensate, gasoline, diesel, flare pit residue and crude oil had class identification numbers 1, 2, 3, 4, and 5, respectively. Scores of all samples were assembled in one matrix that was imported into the PLS\_toolbox 3.5 in MATLAB as a data set. Then the SIMCA model was fitted and PCA models of adequate number of principle components (3 in this case)

that capture  $\geq 99\%$  of the variance were constructed for each class. After constructing a SIMCA model for each of the analyzed samples, scores of all samples were projected on the SIMCA model to discriminate between various samples and assign a correct class for each one of them.

Results can be presented as a list of analyzed samples with assigned classes or as plots that illustrate similarities of normalized scores of analyzed samples based on constructed PCA model components by SIMCA. The list of analyzed samples with assigned classes was used herein to investigate the capability of SIMCA to discriminate between different classes (See Appendix G for more details). Figure 4-14 plots normalized diesel and crude oil samples in soil. Scores are plotted based on the constructed PCA model components PC2 and PC3, which shows that crude oil samples can be easily distinguished from diesel samples. In general, the SIMCA model was able to discriminate and assign a correct class for gas condensate, gasoline and diesel in solvent solution and soil samples. SIMCA did not clearly identify flare pit residue and crude oil samples to the same extent, due to similarities of the spectral features of their EEMs. These findings agree with observations in chapter 3.

#### **4.4.4. Fluorescence Measurements Calibration**

The demonstrated capabilities of PARAFAC and SIMCA analysis to identify various petroleum products in different soil matrices are encouraging and could possibly be used to characterize petroleum contaminants in soil environmental samples without extracting the substances under investigation. Once the analytes are identified and the

soil matrix effect is characterized, further quantitative analysis may also be performed. The capability of quantitative analysis of petroleum contaminated soils is promising but does hold some experimental challenges and analytical difficulties because petroleum products are not well defined analytes and soils are complex matrices. Therefore, a calibration procedure will likely be needed for fluorescence investigation of contaminated soils to refine the correlation between the UVIF sensor response (fluorescence signal) and the concentration of the petroleum product(s) taking into consideration the effect of soil matrices on the generated fluorescence signals. This may be accomplished by measuring the fluorescence signal of a set of calibration standards of known concentration in solvent solutions and soil matrices. The analytes and soil matrices should be selected to best represent the petroleum contaminant and real soil in the field. The procedure to obtain these calibration functions of total fluorescence profiles was described previously in chapter 3. Total fluorescence profiles of a petroleum product in solvent solutions and soils allow estimation of unknown concentrations of that substance in relevant environmental samples based on the generated total fluorescence value. Figures 4-15a-d show the total fluorescence profiles of the petroleum products analyzed in this study in the test soils obtained under controlled laboratory conditions. A linear relationship was assumed between fluorescence intensity and concentration below the limit of detection and represented by a dashed line in Figures 4-15c and d. This assumption considers the fact that fluorescence quenching contributes more to the departure of the relationship between fluorescence intensity and concentration from linearity at higher concentrations.

The relationship between fluorescence intensity and petroleum product concentrations is almost linear at lower concentrations in solvent solutions and soil matrices for all analytes. As the concentration of the analytes increase in the solution and soil, the relationship starts to divert from the linear behavior due to fluorescence quenching that induces fluorescence reduction as the concentration of the analyte increases. Fluorescence quenching is discussed in more details in chapter 3. The linear range of concentrations varied among the analyzed petroleum products based on their susceptibility to fluorescence quenching. In solvent solutions of diesel, flare pit residue and heavy crude oil, the relationship is linear up to concentration of 0.3 mL/L, up to 0.6 mL/L for gasoline and 0.9 mL/L for gas condensate. The linear range in all fluorescence profiles appears to be extended when petroleum products are mixed with soils due to reduction of fluorescence quenching that causes the departure from linearity. The linear ranges for the different soils tested are listed in Table 4-3.

The extended linear range relationship between fluorescence intensity and concentrations expands the utility of the quantitative analysis and provides singular concentration estimates in that range. Despite the observed diversion from linearity at higher concentrations, the relationship is unique, even though more than one concentration value could occur for the same fluorescence intensity. When two samples with different concentrations share the same fluorescence intensity value, they can be differentiated from each other by examining their EEMs. As discussed earlier, the sample with the higher concentration value will have more pronounced

emission peaks at longer wavelengths when compared with the EEM of the lower concentration sample. Produced calibration profiles can be used to provide estimates for petroleum contaminant concentrations in situ based on their total fluorescence intensity values. These estimates can be compared to the relevant regulatory concentrations.

#### **4.5. SUMMARY AND CONCLUSIONS**

A laboratory testing program was conducted to identify and interpret the fundamental factors affecting ultraviolet induced fluorescence measurements in soils. The experimental program was designed to isolate the effects of soil properties such as grain size distribution, soil porosity, and mineralogy. No measurable effects of mineralogy were observed in the soils tested. The test results also indicated that soils tested had no measurable effect on the shape of fluorescence signal of the tested petroleum products. However, for a given contaminant concentration, the porosity of the soil had a significant effect on fluorescence signal intensity. The effect varied based on soil grain sizes and degree of sorting, as well as type of petroleum contaminant. In general, fluorescence signal intensity decreased as soil grain size and porosity decreased. Nevertheless, fluorescence intensity increased at higher concentrations of contaminants known to be highly affected by fluorescence quenching as soil grain size decreased. There appears to be a relationship between fluorescence signal intensity attenuation or enhancement of a particular petroleum contaminant mixed with soil and the porosity of that soil. The study also indicated that there is a linear relationship between total fluorescence values of the analyzed



petroleum products in solvent solutions and the porosity of the soils. Typically, fluorescence intensity decreased in soil samples as the porosity of tested soils decreased. However, the relationship departed from linearity at higher concentrations of petroleum products that are more susceptible to fluorescence quenching. This linear relationship may permit expanding the generated total fluorescence profiles in this study to other soils that are not tested.

PARAFAC and SIMCA demonstrated strong capabilities to characterize gas condensate, gasoline, diesel, flare pit residue and crude oil and their underlying aromatic components in soil samples using their fluorescence EEMs. The PARAFAC modeling results indicated that analyzed petroleum products are mainly composed of BTEX compounds, naphthalene / methylnaphthalene, phenanthrene, and to lesser extent pyrene, which agrees with chemical analysis results for the same analytes. SIMCA was able to distinguish between different analyzed petroleum products and crude oil samples in the soils tested, which could allow this approach be applied to various types of environmental samples without pre-separation steps.

This study presents a calibration procedure that takes into consideration the effect of soil matrix and allows estimation of the concentration of various petroleum products in soil matrices based on their total fluorescence intensity values generated from their relevant EEMs. This procedure will allow quick and efficient quantification of different petroleum contaminants in soil samples with minimum human intervention.

Table 4-1. Minimum petroleum product concentration at which fluorescence signal was detected with Varian Eclipse spectrometer in various media

<b>Petroleum Products</b>	<b>Solvent Solution (mL/L)</b>	<b>Ottawa Sand (mL/L in solution)</b>	<b>Well Graded Sand (mL/L in solution)</b>	<b>Well Graded Sand and Devon Silt (mL/L in solution)</b>	<b>Devon Silt (mL/L in solution)</b>
Gas Condensate	10.0	50.0	50.0	200	600
Gasoline	0.5	10.0	10.0	50	50
Diesel	0.5	0.50	1.00	1.0	10
Flare Pit Residue	1.00	10.0	10.0	50	50
Crude Oil	1.00	10.0	10.0	40	40

Table 4-2. Equations of linear relationship between total fluorescence values of tested petroleum products (where F is total fluorescence, m is the slope, n the porosity and b the intercept)

<b>Gas Condensate</b>		
<b>Concentration (mL/L)</b>	<b>F = m*n + b</b>	<b>R<sup>2</sup></b>
1	-	-
10	-	-
50	F = 434*n - 1.19*10 <sup>3</sup>	0.923
200	F = 729*n - 4.60*10 <sup>2</sup>	0.949
600	F = 1090*n - 1.49*10 <sup>3</sup>	0.951
Neat	F = 1206*n + 6.33*10 <sup>3</sup>	0.934
<b>Gasoline</b>		
<b>Concentration (mL/L)</b>	<b>F = m*n + b</b>	<b>R<sup>2</sup></b>
1	-	-
10	F = 450*n - 4.16*10 <sup>3</sup>	0.915
50	F = 2025*n - 3.84*10 <sup>3</sup>	0.928
200	F = 2763*n + 2.27*10 <sup>4</sup>	0.886
600	F = 3335*n + 6.64*10 <sup>4</sup>	0.968
Neat	F = 4653*n + 1.07*10 <sup>5</sup>	0.964
<b>Diesel</b>		
<b>Concentration (mL/L)</b>	<b>F = m*n + b</b>	<b>R<sup>2</sup></b>
1	F = 5502*n - 8.63*10 <sup>4</sup>	0.979
10	F = 8753*n - 1.94*10 <sup>4</sup>	0.943
50	F = 13765*n - 1.04*10 <sup>4</sup>	0.965
200	F = 19919*n + 1.08*10 <sup>5</sup>	0.973
800	F = 29361*n + 9.36*10 <sup>5</sup>	0.965
Neat	F = 30638*n + 1.00*10 <sup>6</sup>	0.967
<b>Flare Pit Residue</b>		
<b>Concentration (mL/L)</b>	<b>F = m*n + b</b>	<b>R<sup>2</sup></b>
1	-	-
10	F = 8828*n - 2.05*10 <sup>5</sup>	1
50	F = 12530*n - 1.27*10 <sup>5</sup>	0.992
200	N/A	N/A
600	N/A	N/A
Neat	N/A	N/A
<b>Crude Oil</b>		
<b>Concentration (mL/L)</b>	<b>F = m*n + b</b>	<b>R<sup>2</sup></b>
1	-	-
10	F = 7075*n - 7.15*10 <sup>4</sup>	0.968
40	F = 2528*n + 4.82*10 <sup>5</sup>	0.834
200	N/A	N/A
640	N/A	N/A

*Note: N/A is used to refer to concentration at which linear relationship between total fluorescence values and porosity doesn't exist.*

Table 4-3. Maximum concentrations of linear range for total fluorescence measurement in tested soils

<b>Petroleum product</b>	<b>Ottawa Sand (mg/kg)</b>	<b>Well Graded Sand (mg/kg)</b>	<b>Well Graded Sand and Devon Silt (mg/kg)</b>	<b>Devon Silt (mg/kg)</b>
Gas Condensate	2.0*10 <sup>4</sup>	2.4*10 <sup>4</sup>	3.2*10 <sup>4</sup>	-
Gasoline	3.0*10 <sup>3</sup>	4.0*10 <sup>3</sup>	7.0*10 <sup>3</sup>	1.8*10 <sup>4</sup>
Diesel	1.2*10 <sup>3</sup>	2.0*10 <sup>3</sup>	2.4*10 <sup>3</sup>	2.0*10 <sup>3</sup>
Flare Pit Residue	3.0*10 <sup>3</sup>	1.2*10 <sup>4</sup>	1.8*10 <sup>4</sup>	2.4*10 <sup>4</sup>
Crude Oil	3.0*10 <sup>3</sup>	9.5*10 <sup>3</sup>	5.2*10 <sup>3</sup>	5.0*10 <sup>3</sup>

*Note: Gas condensate didn't have enough detected fluorescence in Devon silt samples to establish concentration linearity range.*

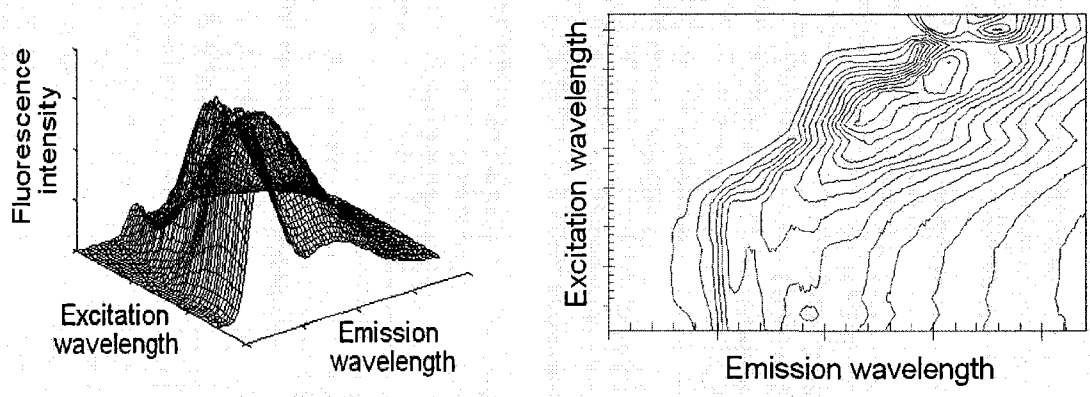


Figure 4-1. 3-dimensional (3D) and 2-dimensional contour map (2D) representations of emission-excitation matrix (EEM) (after Rho and Stuart 1978).

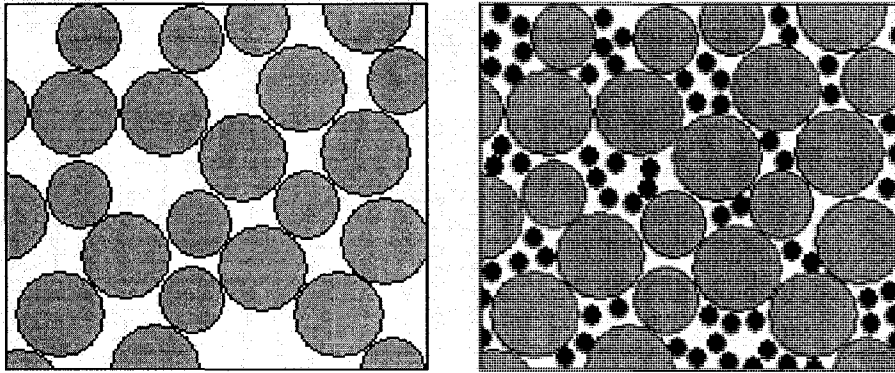


Figure 4-2. Effect of soil sorting on voids structure (Blue circles represent coarse grained soil, black dots represent fine grained soil, white represents voids)

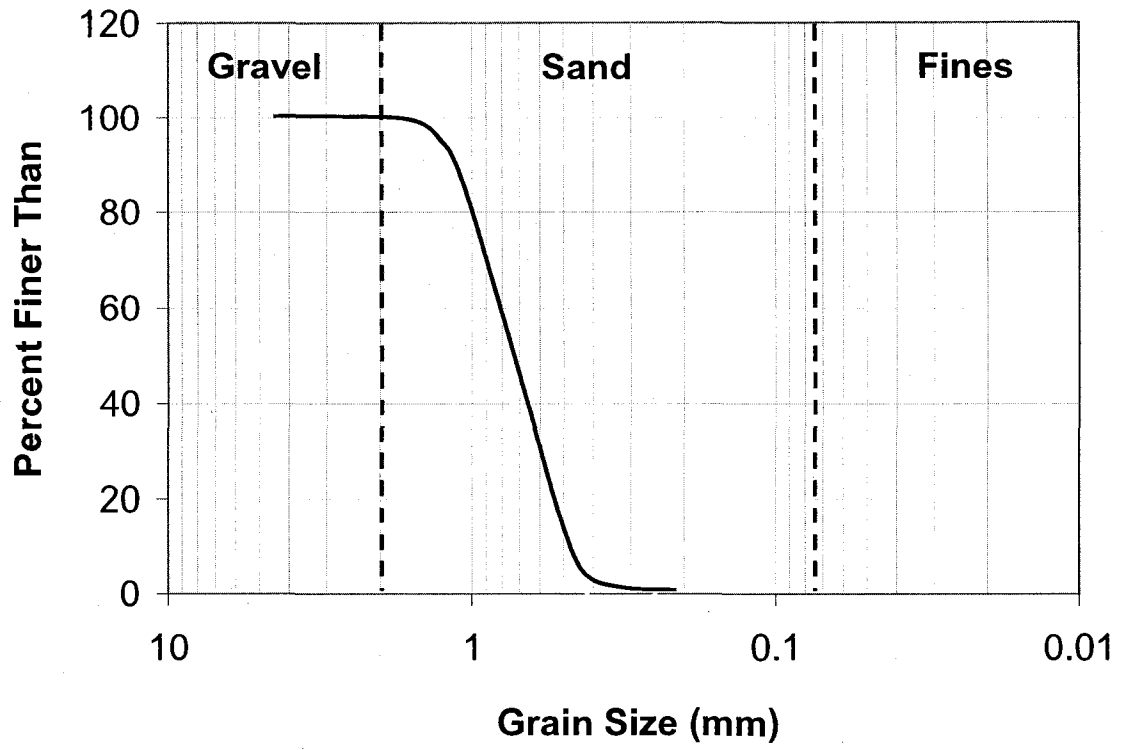


Figure 4-3a. Ottawa sand grain size distribution

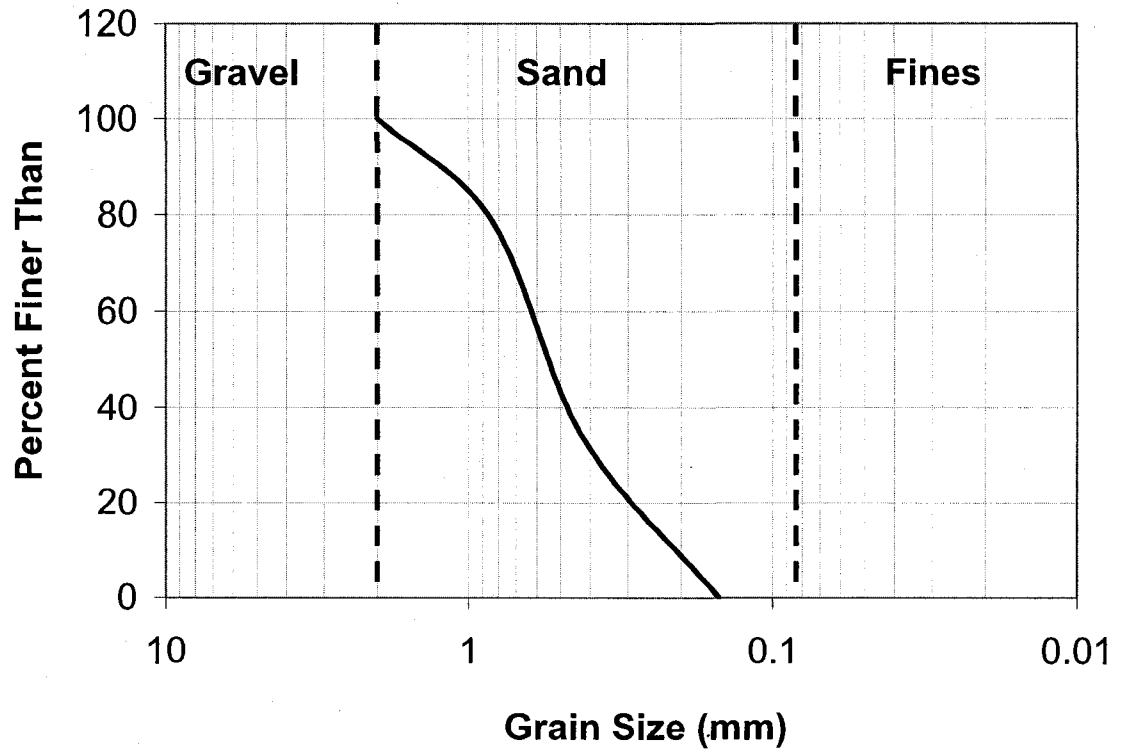


Figure 4-3b. Well graded sand grain size distribution



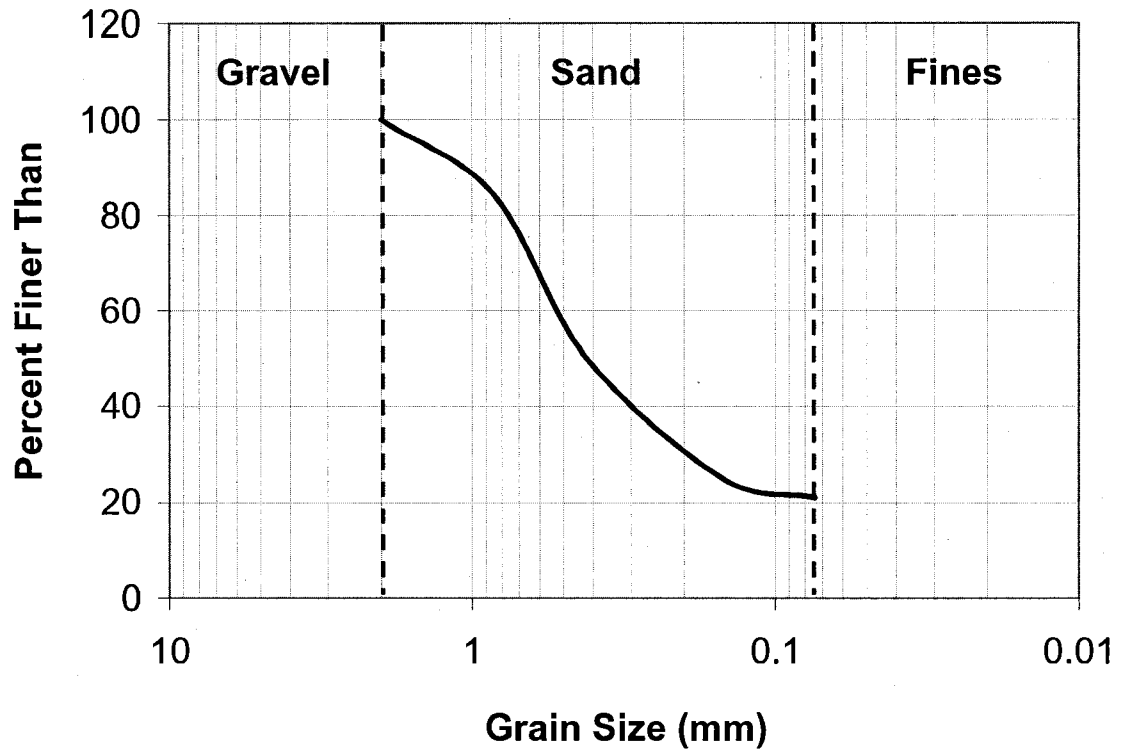


Figure 4-3c. Well graded sand and Devon silt grain size distribution

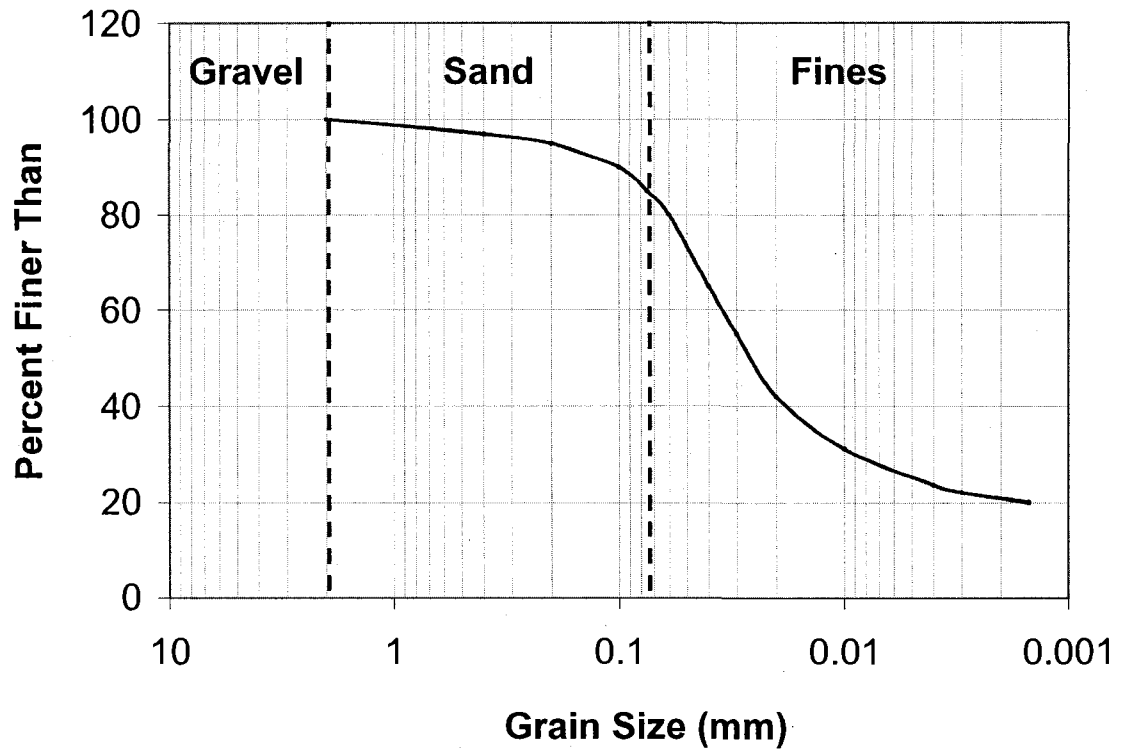


Figure 4-3d. Devon silt grain size distribution (after Arenson et al. 2005)

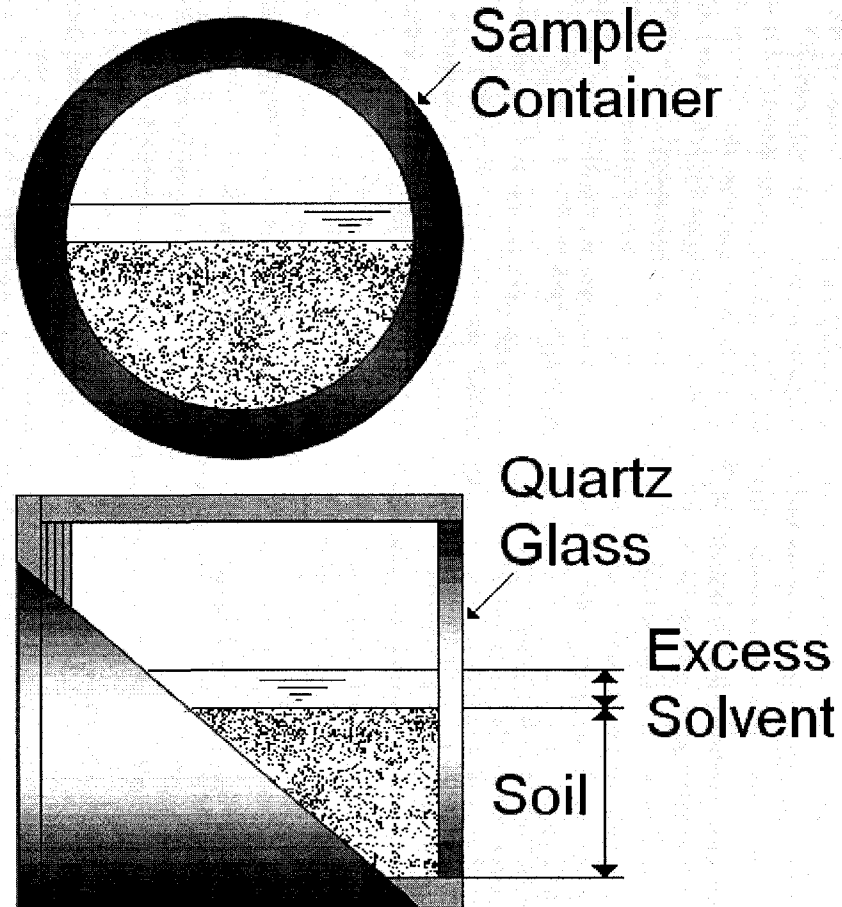


Figure 4-4. Schematics of soil and solvent in sample container

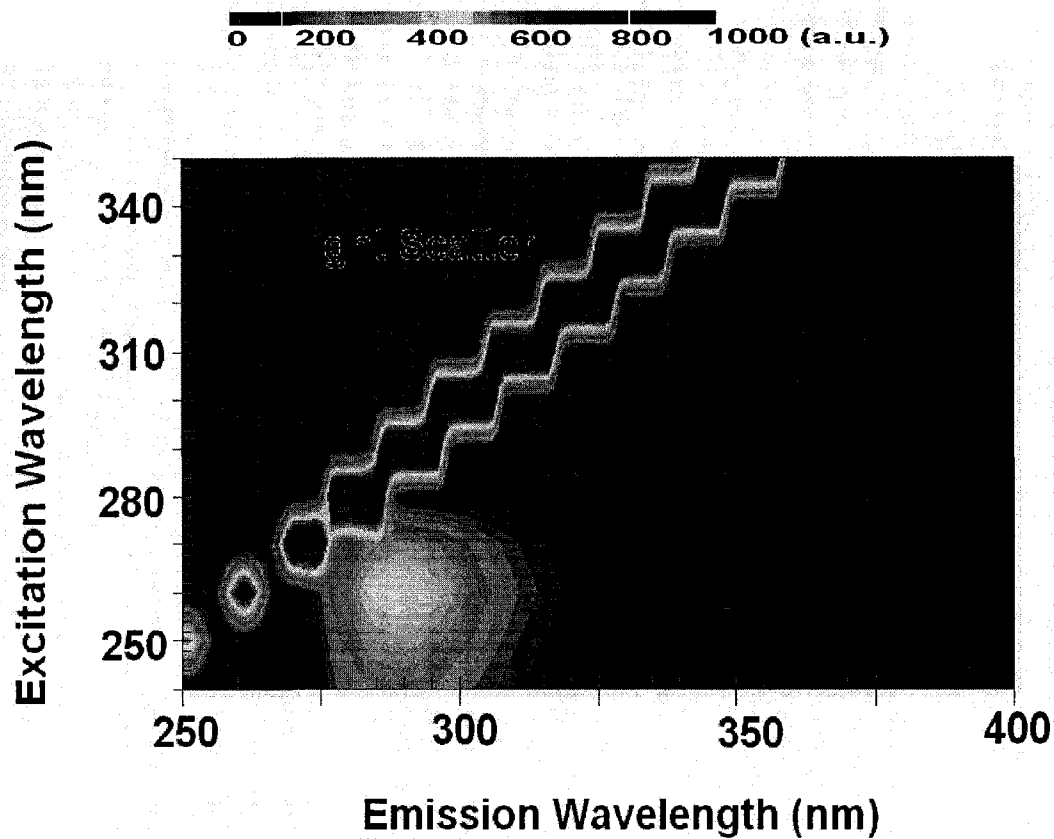


Figure 4-5a. Gas condensate in Ottawa sand EEM (neat)

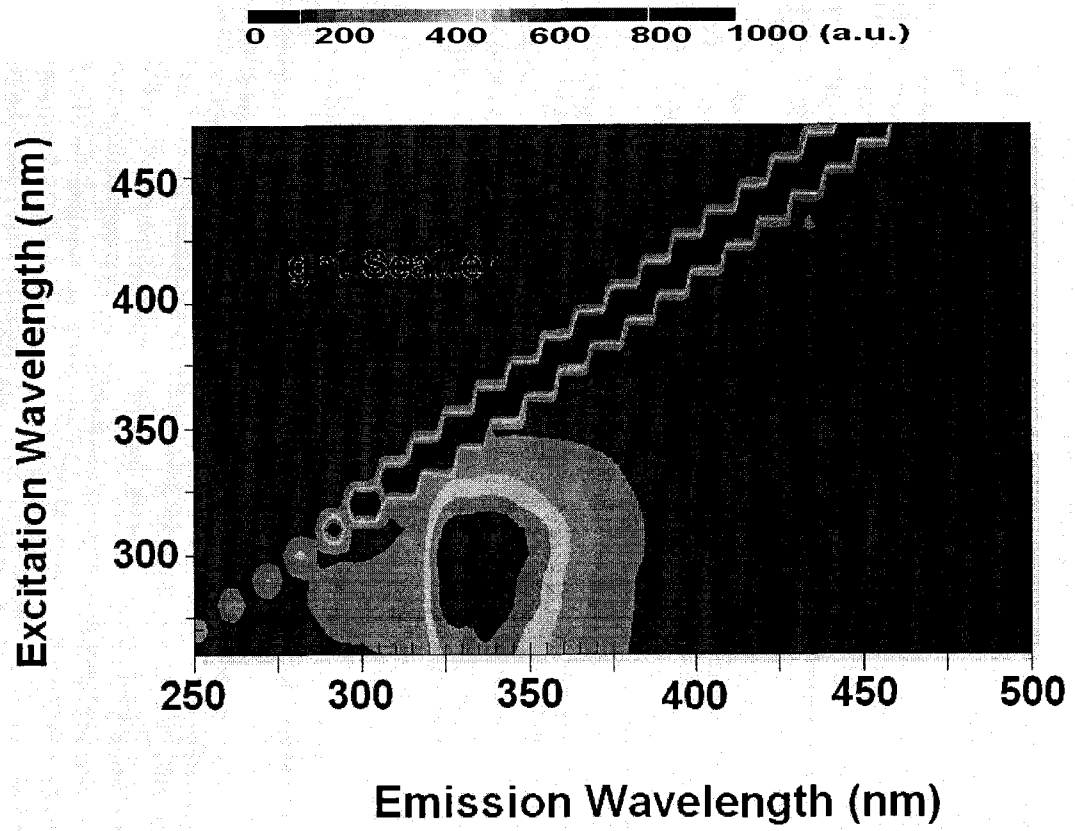


Figure 4-5b. Gasoline in Ottawa sand EEM (neat)

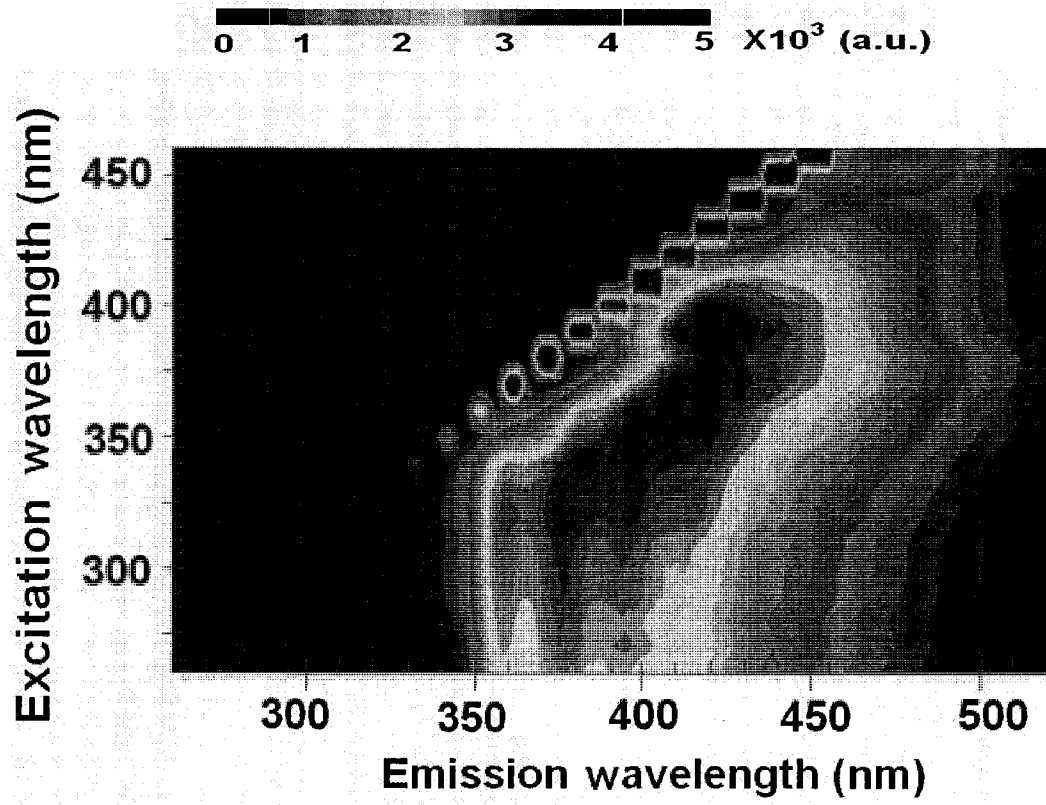


Figure 4-5c. Diesel in Ottawa sand EEM (neat)

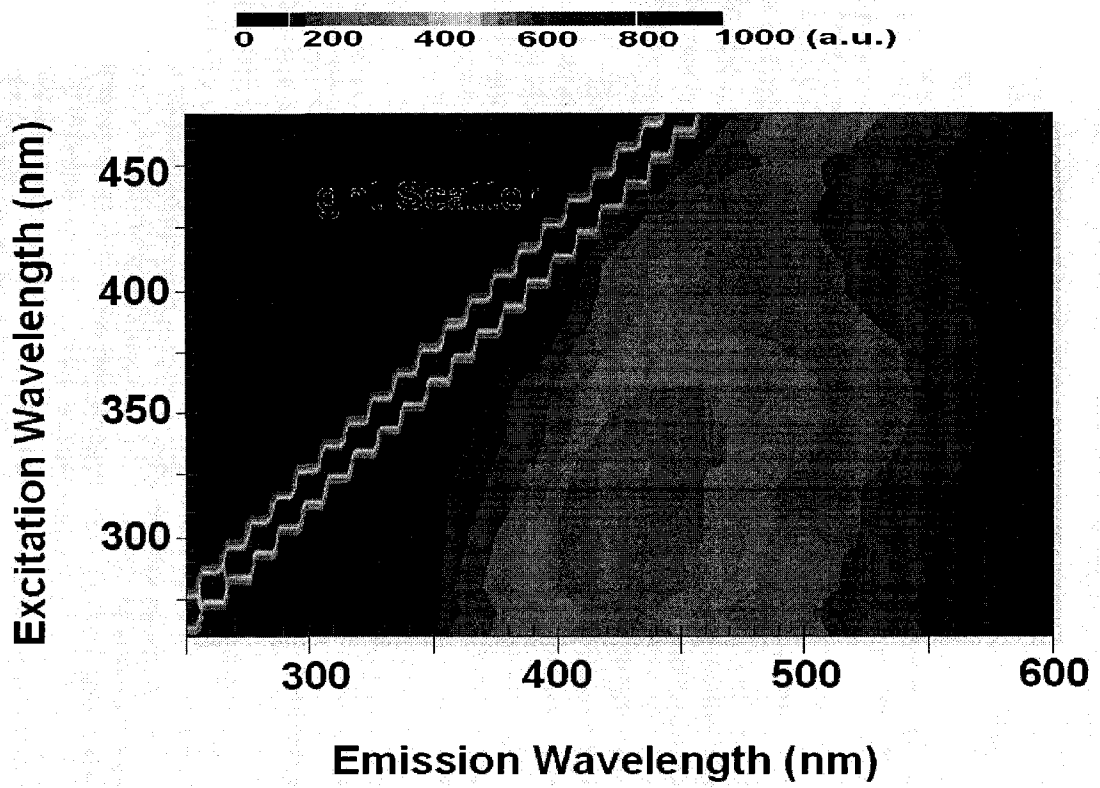


Figure 4-5d. Flare pit residue in Ottawa sand EEM (neat)

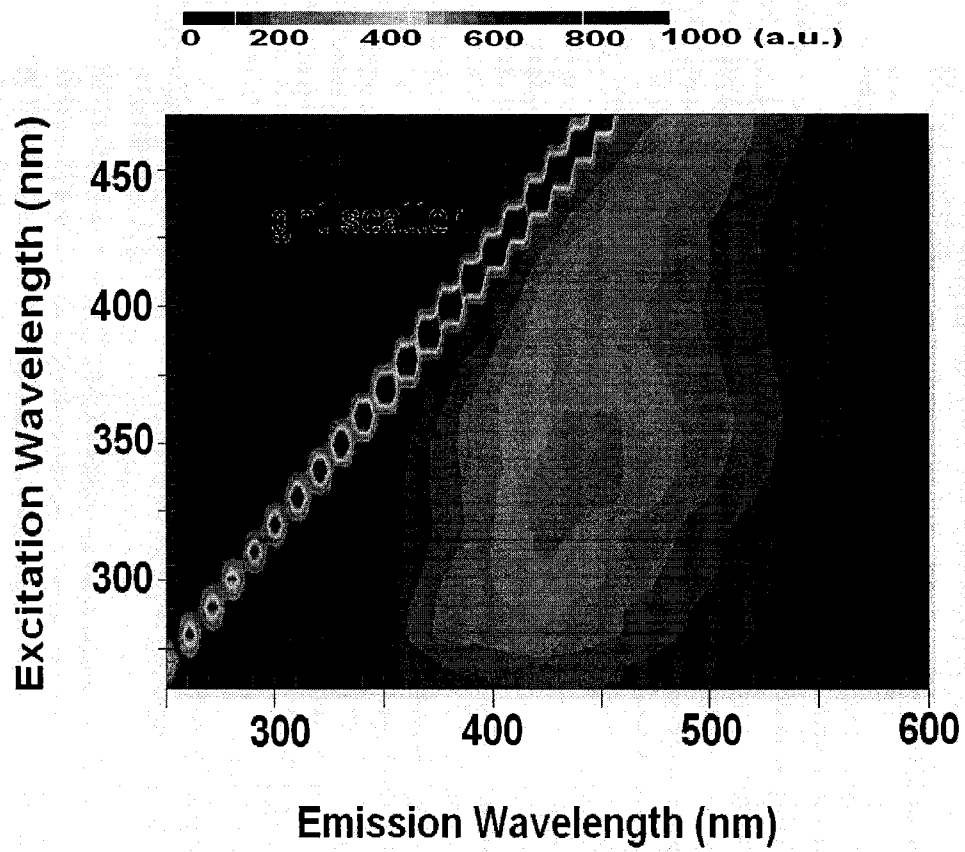


Figure 4-5e. Crude Oil in Ottawa sand EEM (40 mL/L)



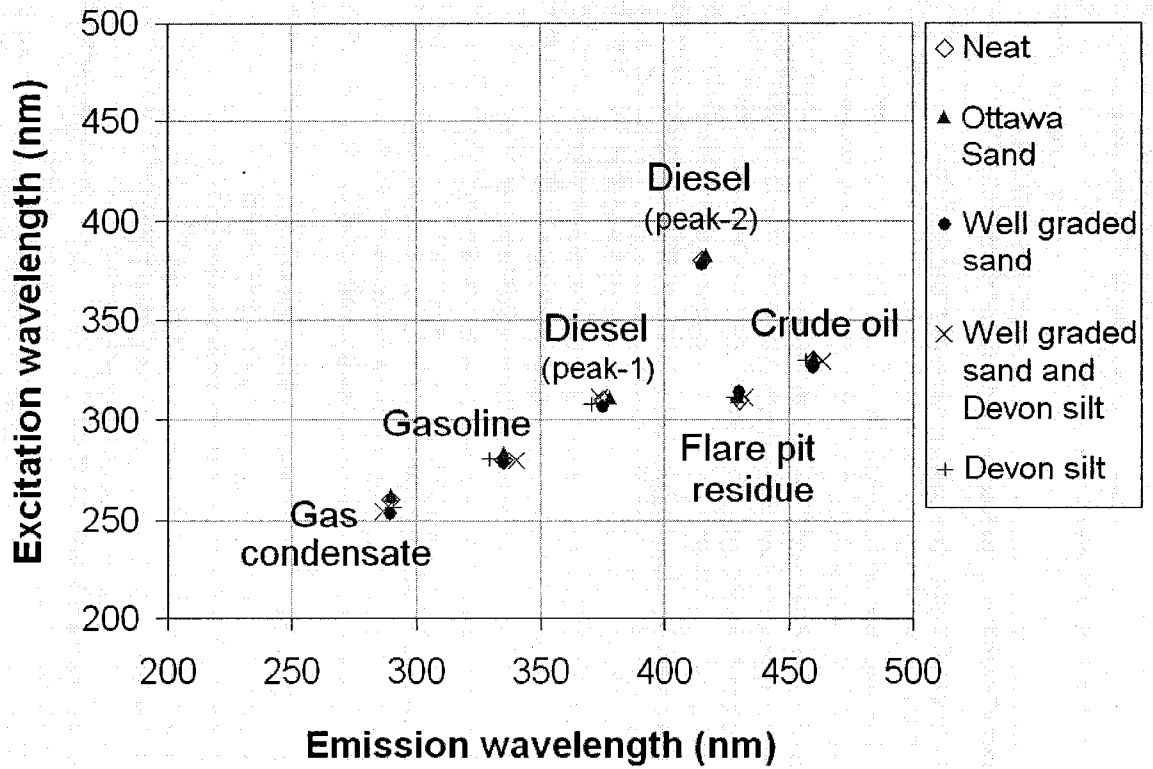


Figure 4-6. Highest fluorescence intensity EEM peak locations of tested neat petroleum products and crude oil (40 mL/L) in solution and soil samples

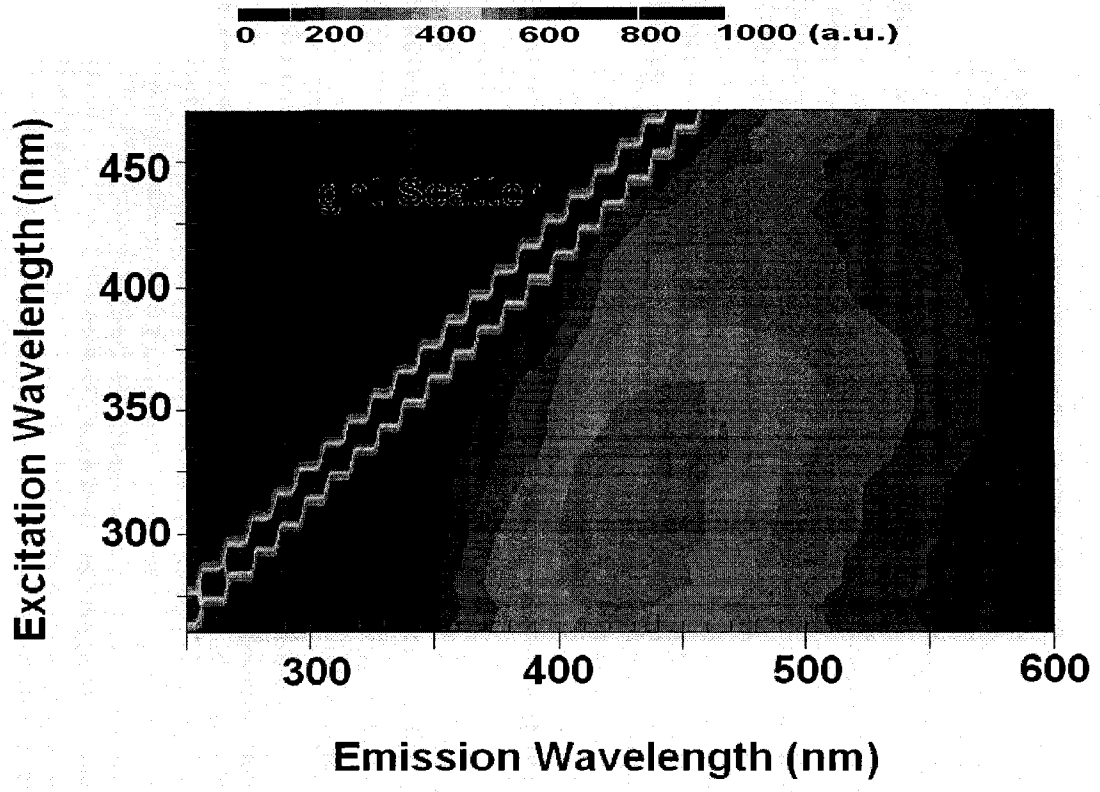


Figure 4-7a. Flare pit residue in Ottawa sand EEM (neat)

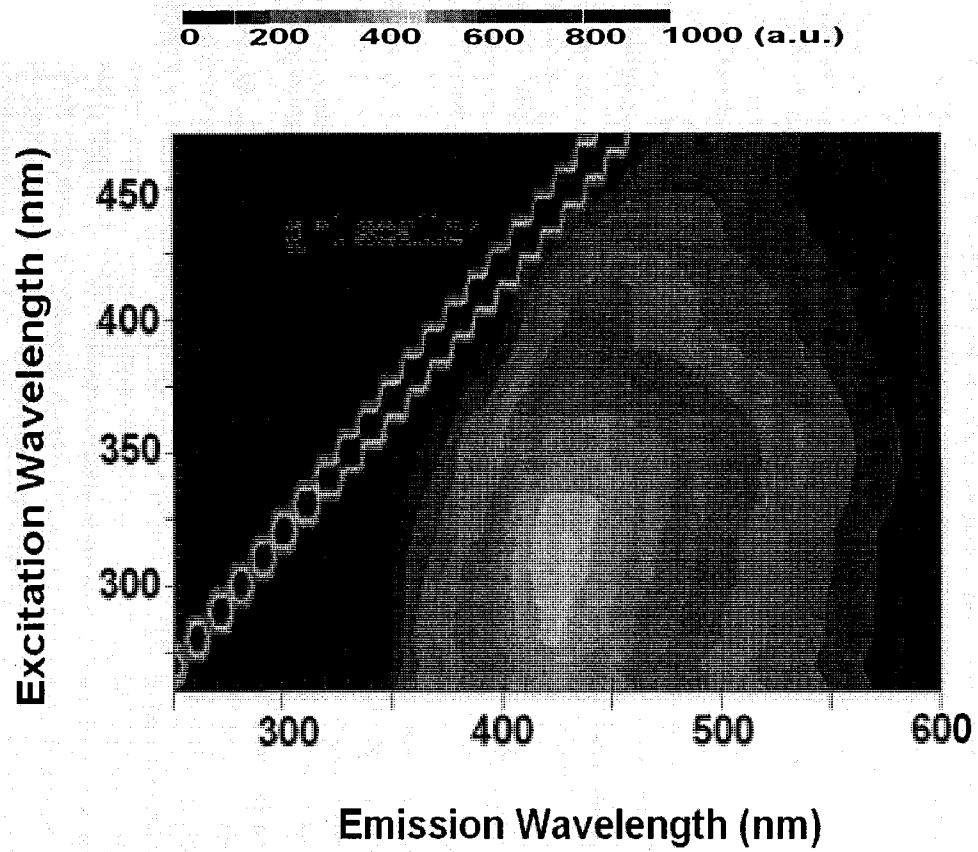


Figure 4-7b. Flare pit residue in Devon silt EEM (neat)

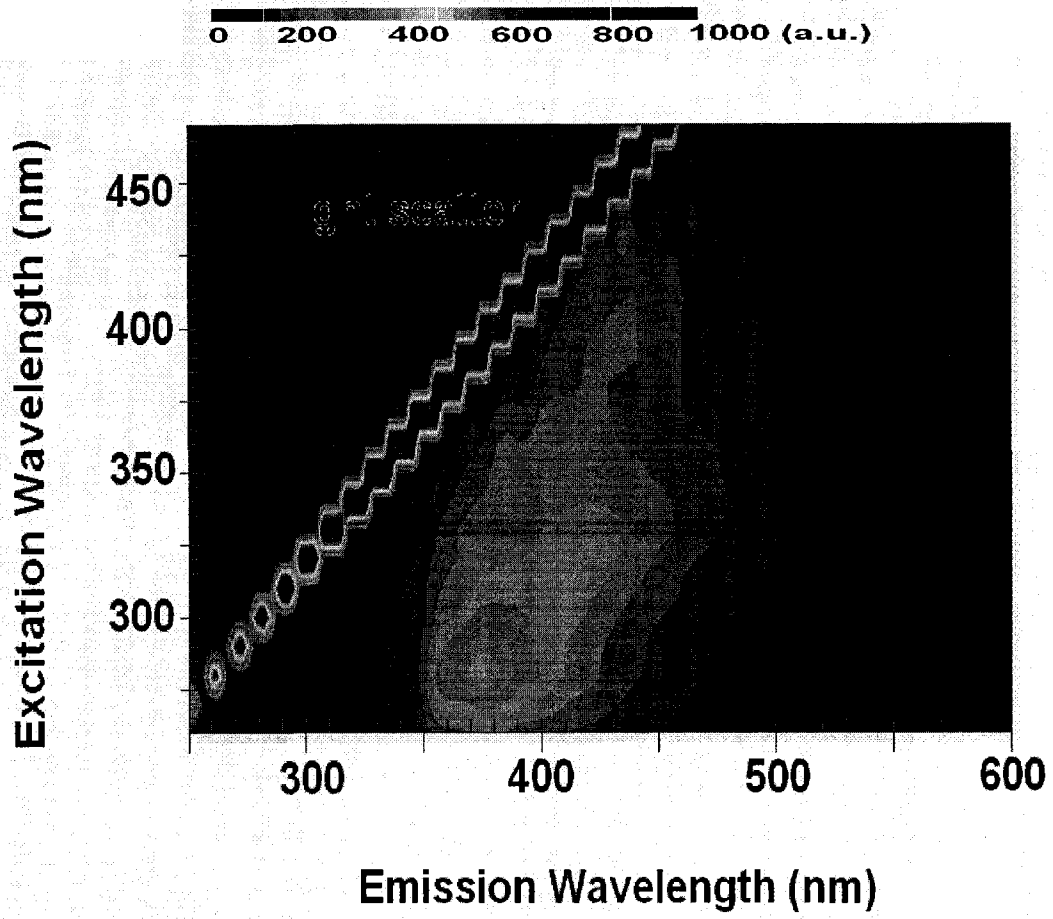


Figure 4-8a. Flare pit residue in Ottawa sand EEM at solution concentration of 50 mL/L

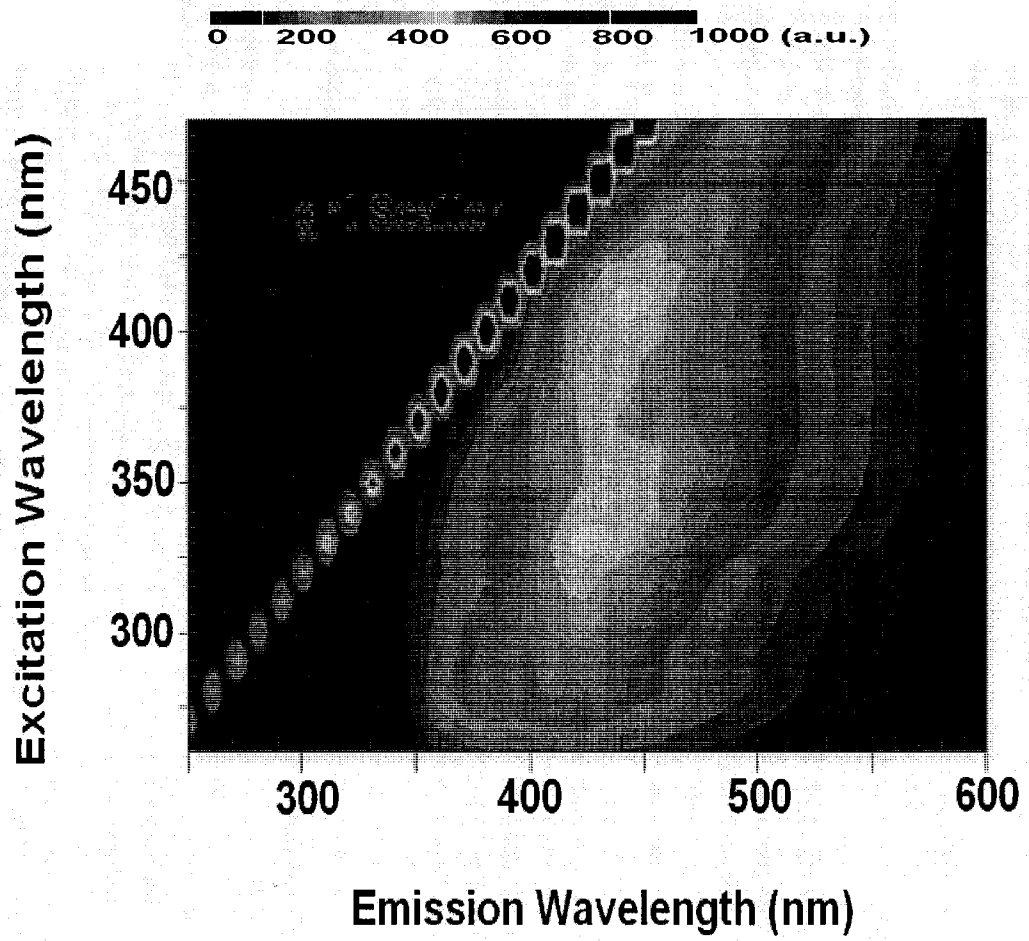


Figure 4-8b. Flare pit residue in Ottawa sand EEM at solution concentration of 200 mL/L

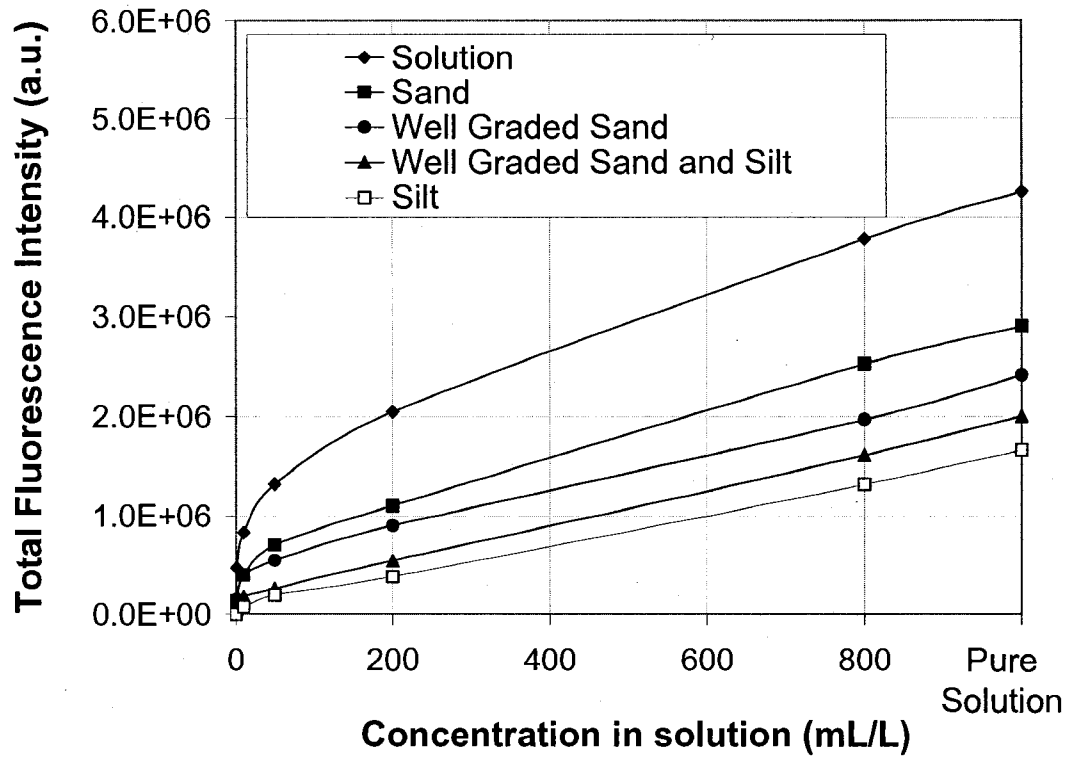


Figure 4-9. Effect of soil matrix on diesel total fluorescence intensity

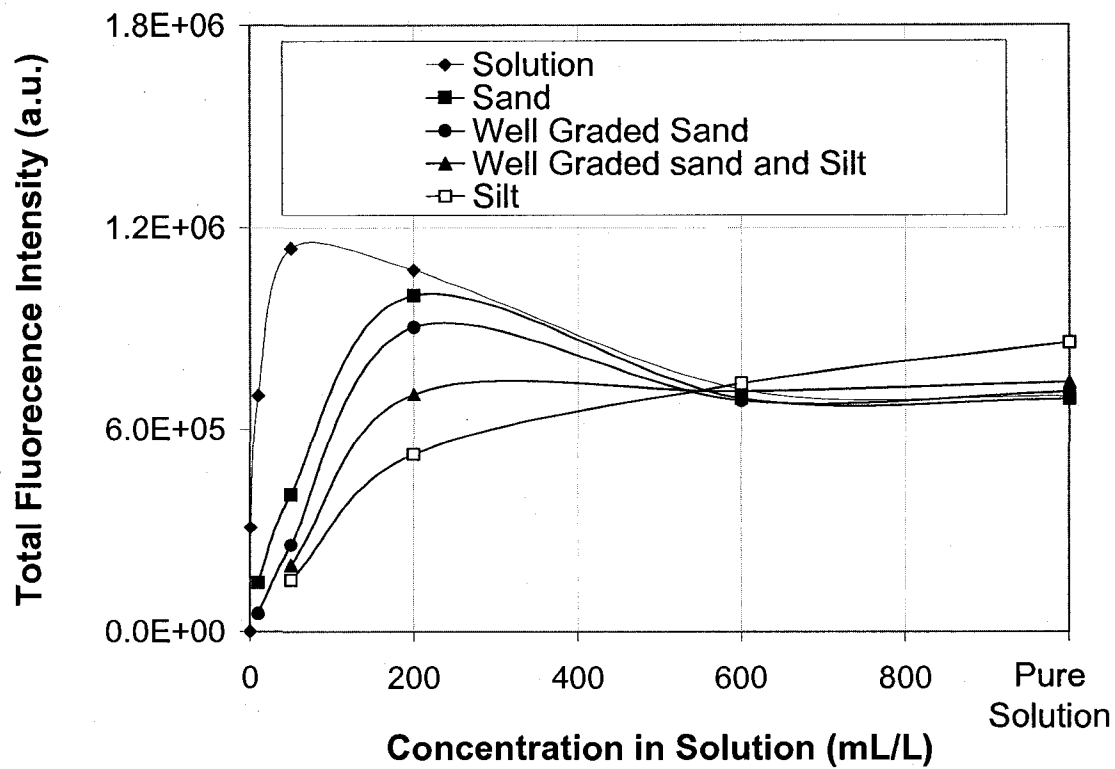


Figure 4-10. Effect of soil matrix on flare pit residue total fluorescence intensity

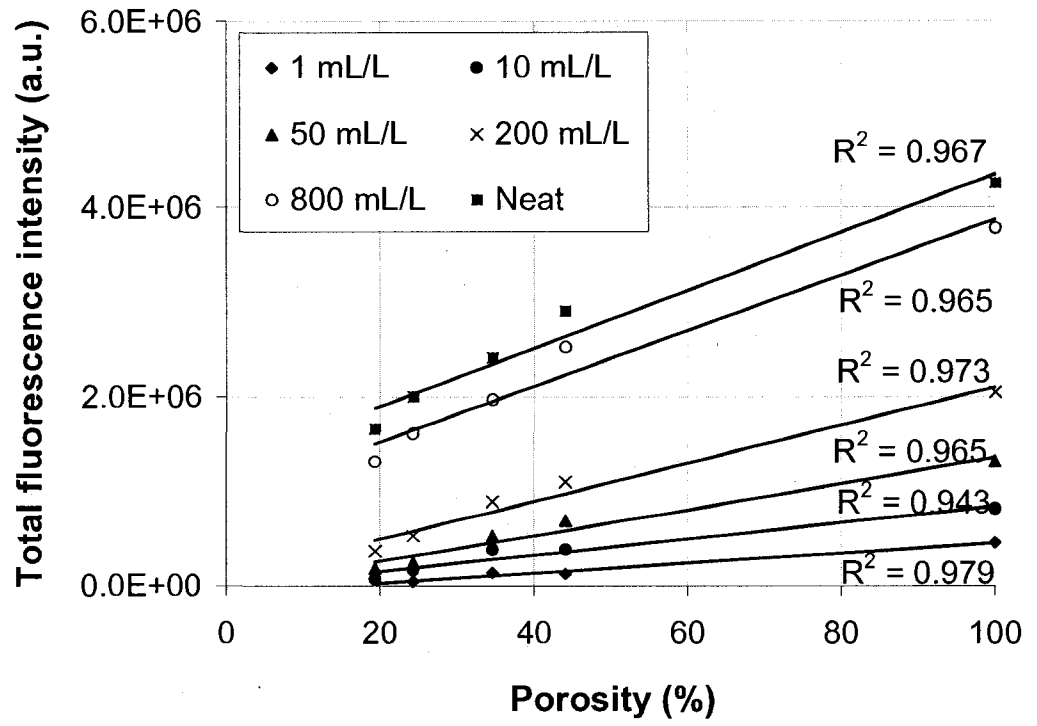


Figure 4-11a. Change in diesel total fluorescence intensity versus soil porosity



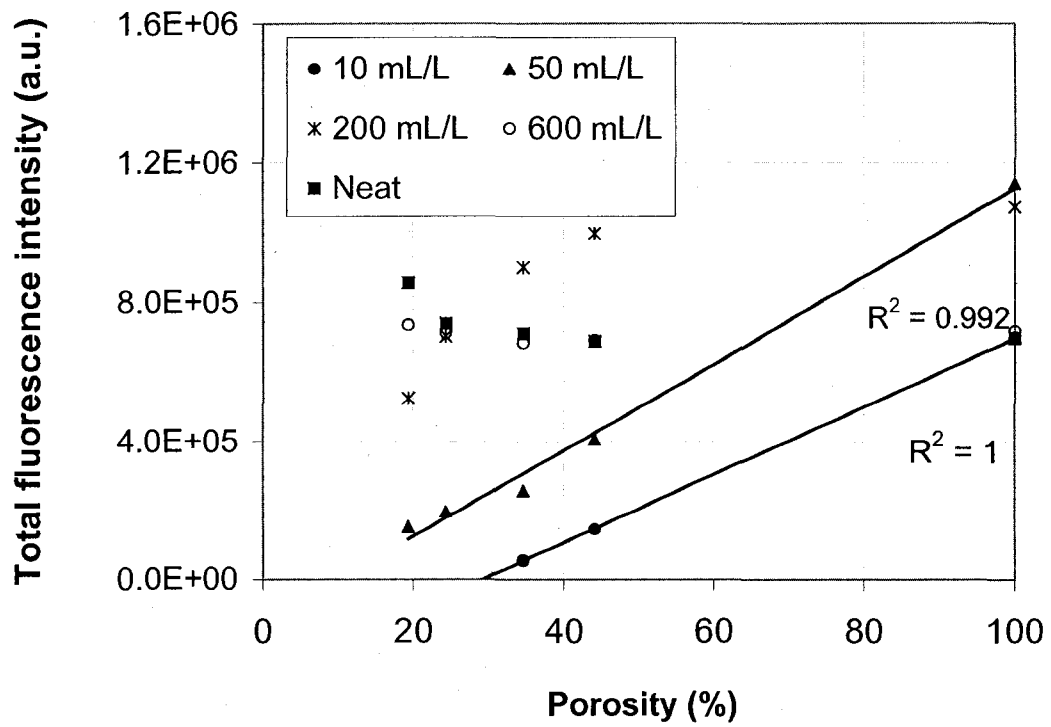


Figure 4-11b. Change in flare pit residue total fluorescence intensity versus soil porosity

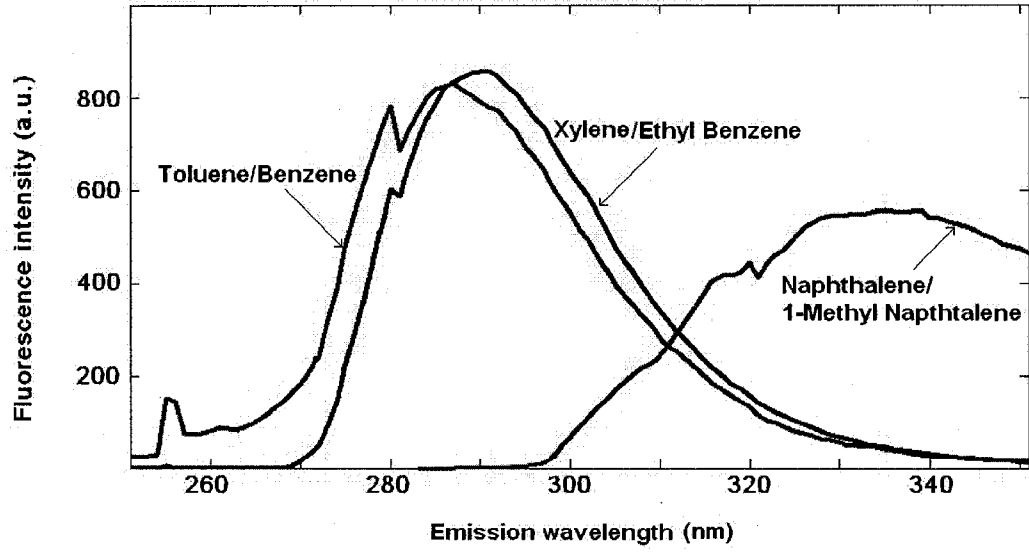


Figure 4-12a. PARAFAC model of gas condensate underlying component emission spectra in soil

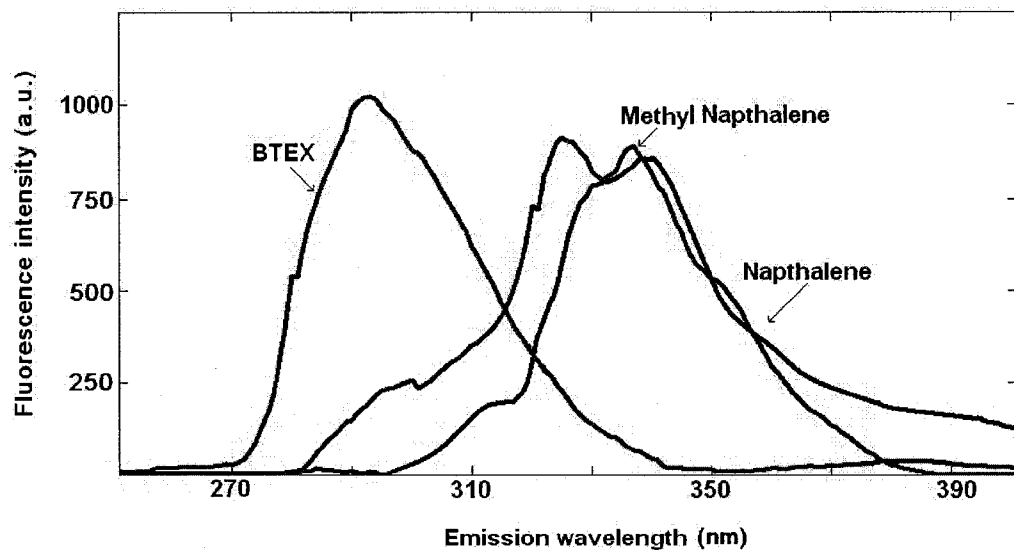


Figure 4-12b. PARAFAC model of gasoline underlying component emission spectra in soil

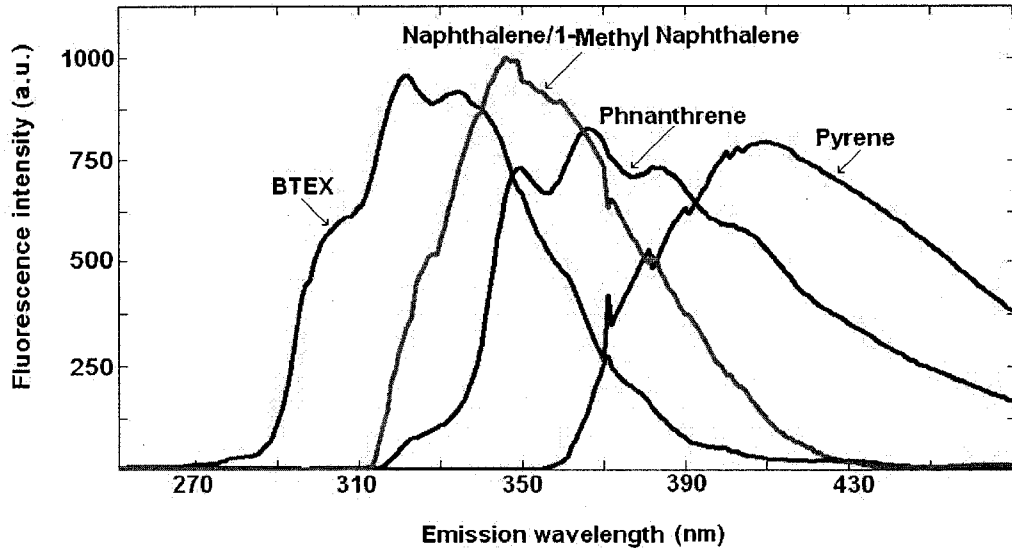


Figure 4-12c. PARAFAC model of diesel underlying component emission spectra in soil

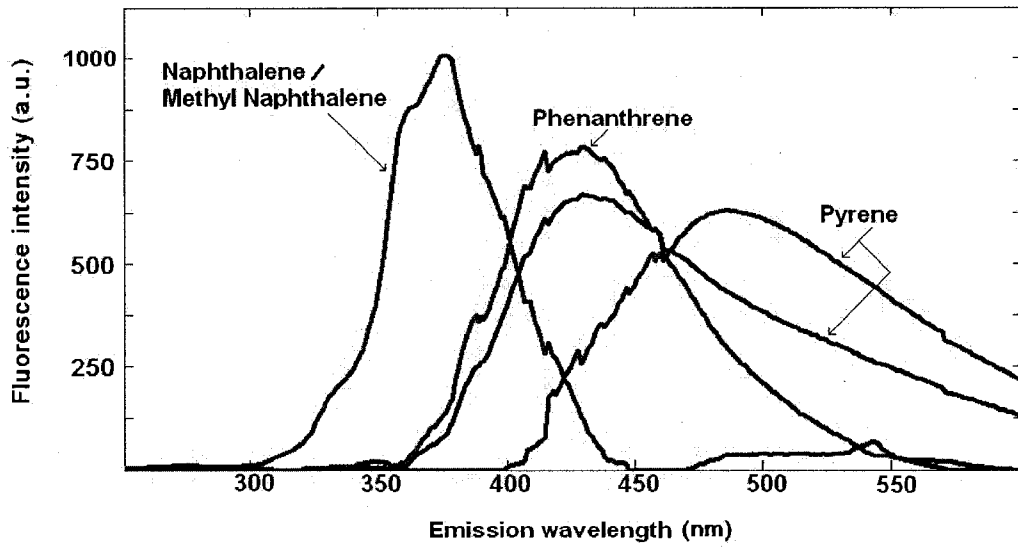


Figure 4-12d. PARAFAC model of flare pit underlying component emission spectra in soil

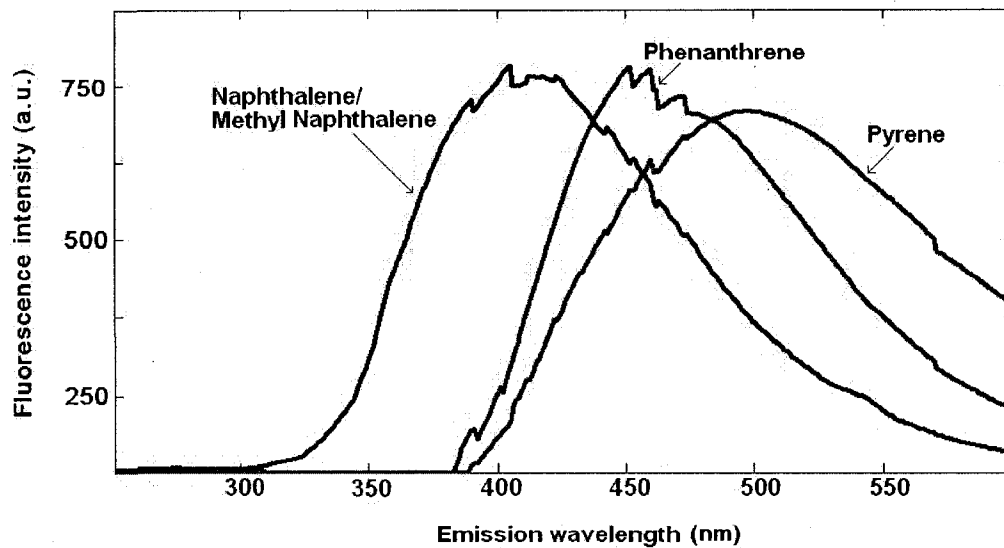


Figure 4-12e. PARAFAC model of crude oil underlying component emission spectra in soil

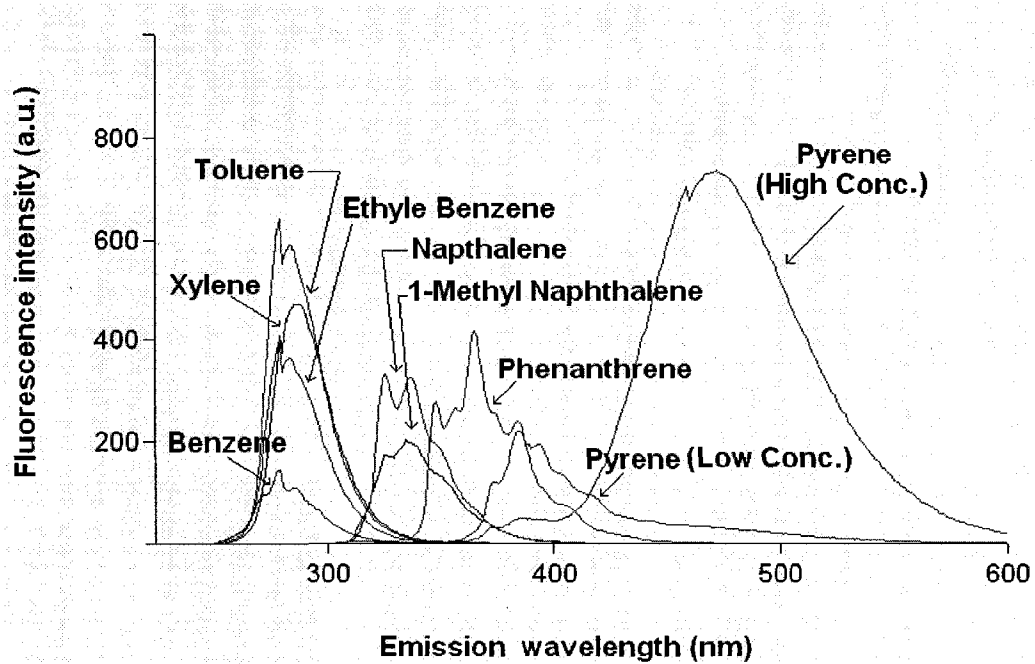


Figure 4-13. Fluorescence emission spectra of standard PAH collected at laboratory

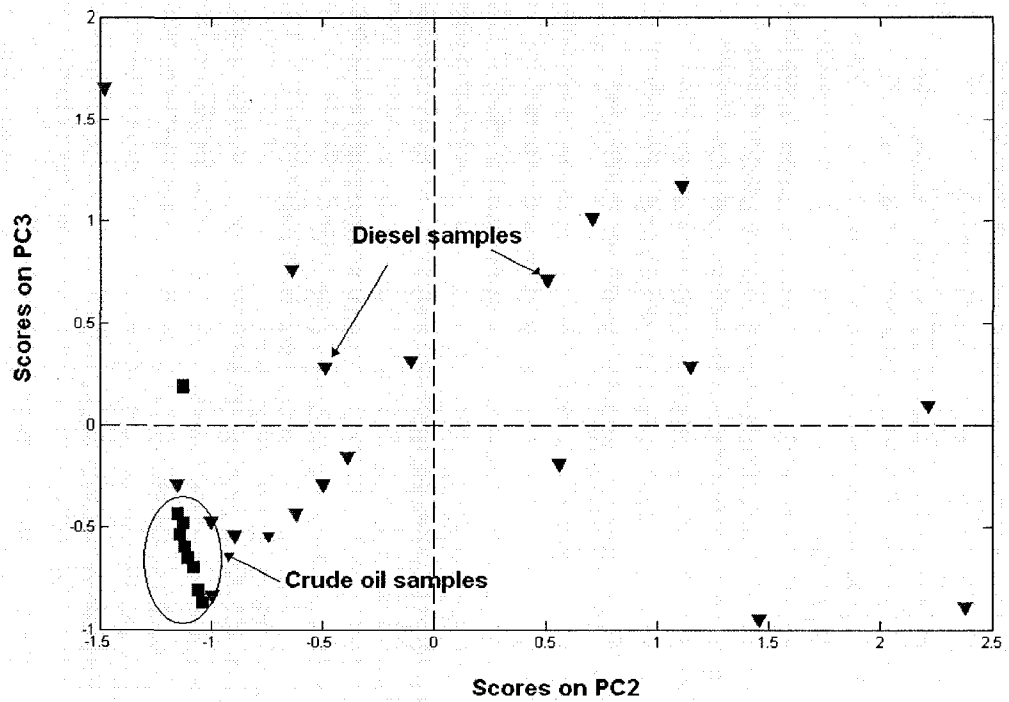


Figure 4-14. Sample plot of SIMCA model normalized diesel and crude oil scores



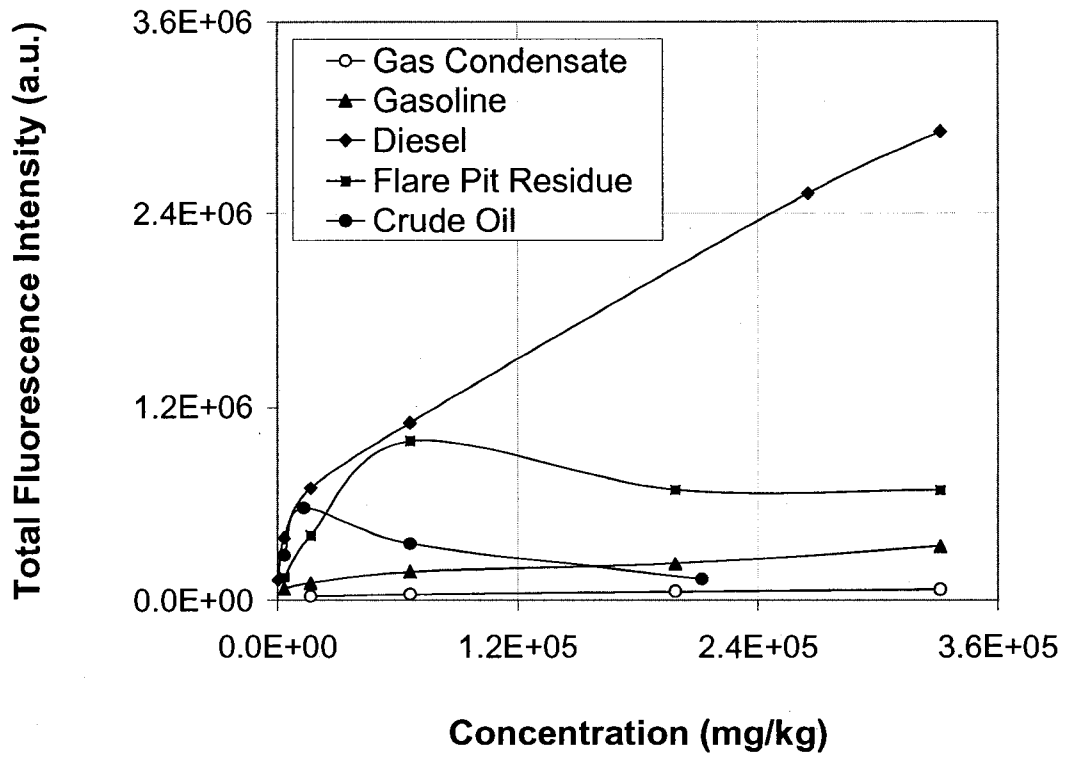


Figure 4-15a. Tested petroleum products calibration curves in Ottawa sand

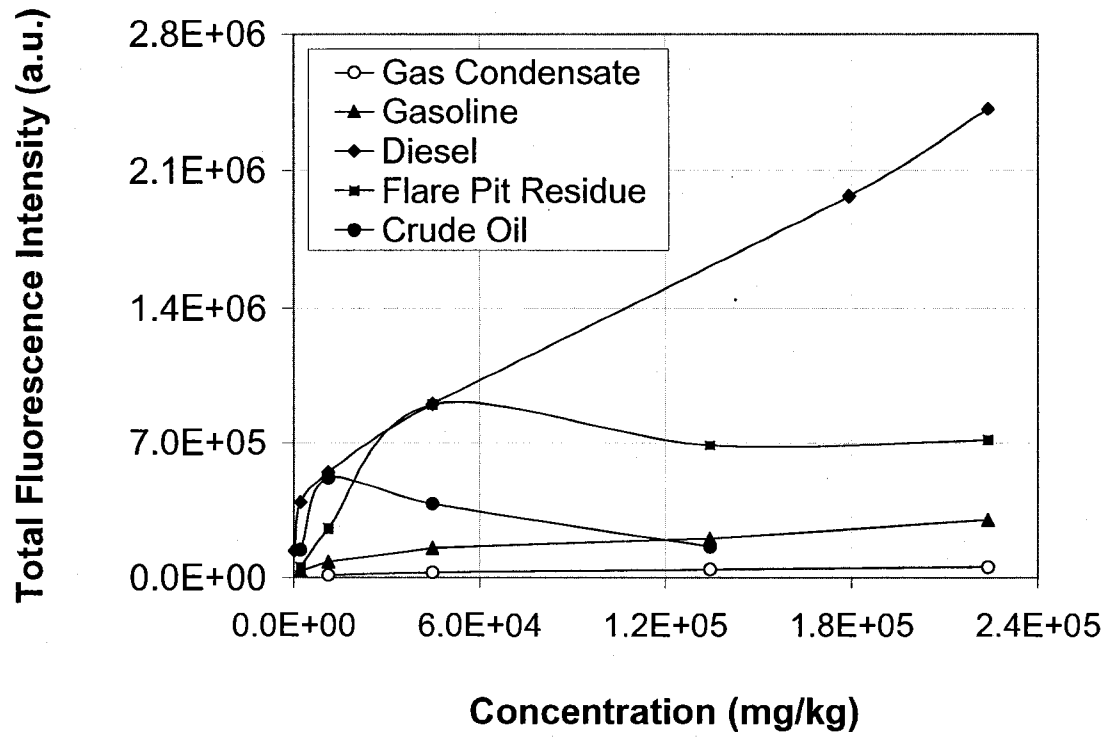


Figure 4-15b. Tested petroleum products calibration curves in well graded sand

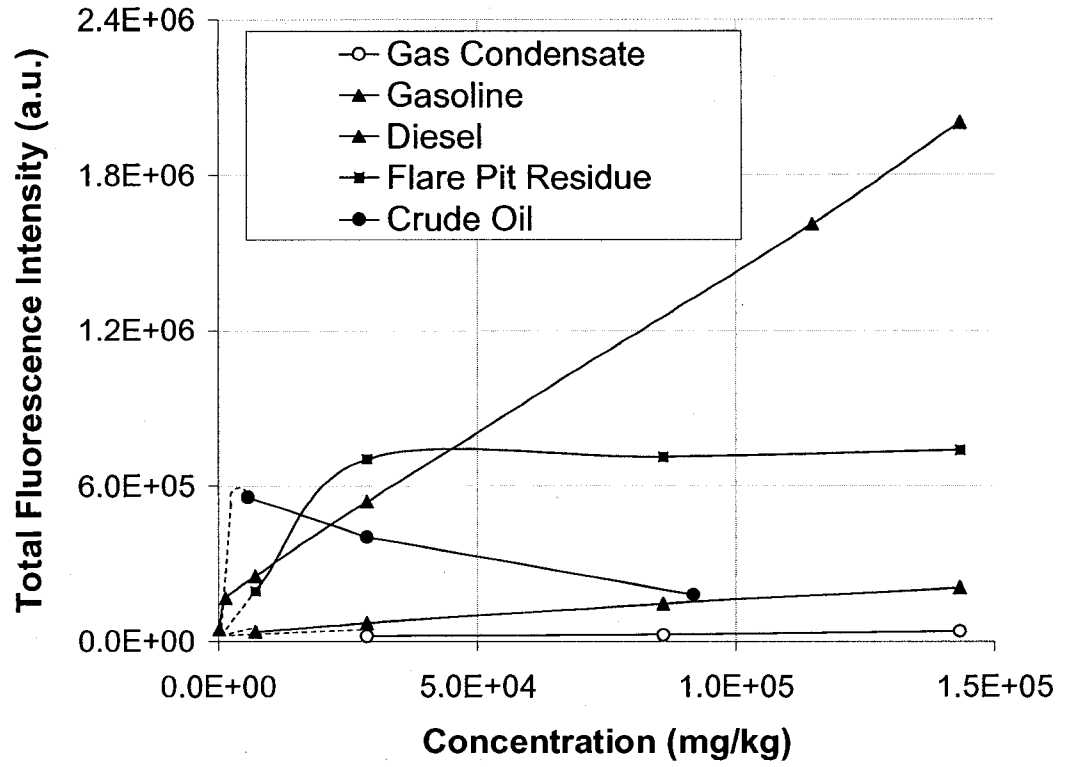


Figure 4-15c. Tested petroleum products calibration curves in well graded sand and Devon silt mixtures

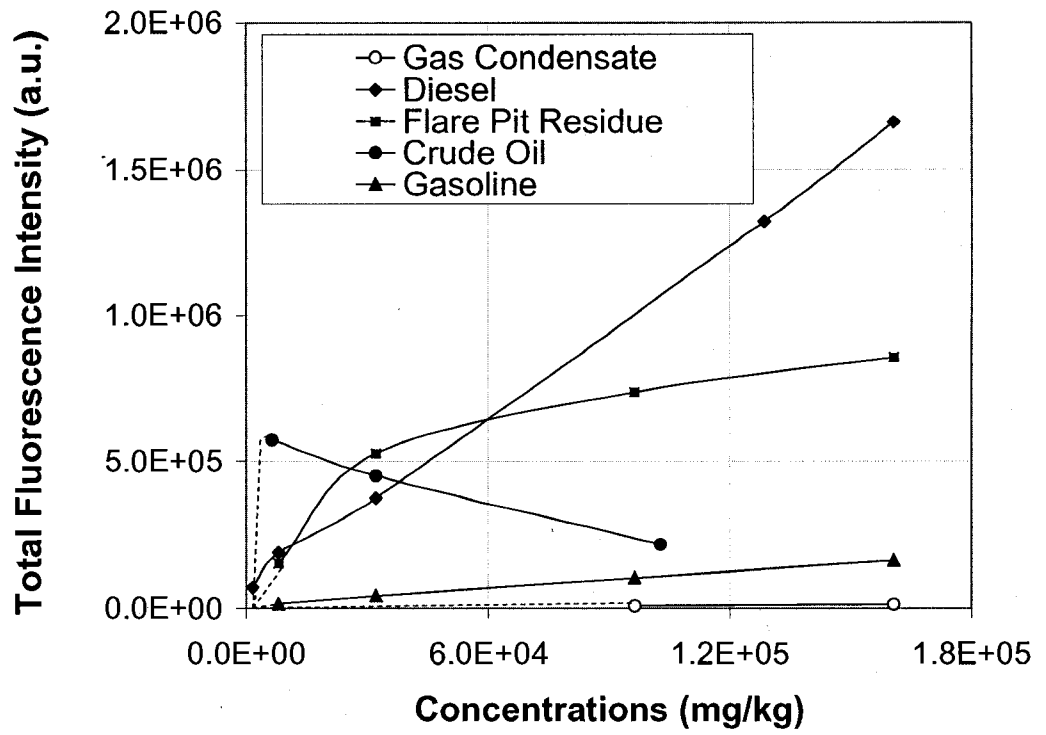


Figure 4-15d. Tested petroleum products calibration curves in Devon silt.

#### 4.6. REFERENCES

- Apitz, S., Theriault, G., and Lieberman, S. 1992. Optimization of The Optical Characteristics Of A Fiber-Optic Guided Laser Fluorescence Technique For The In Situ Evaluation Of Fuels In Soils. SPIE, 1637, pp. 241–254.
- Apitz, S., Borbridge, L., Theriault, G., and Lieberman, S. 1992a. Remote In-Situ Determination Of Fuel Products In Soils: Field Results and Laboratory Investigations. *Analysis*, 20, pp. 461-467.
- Apitz, S., Borbridge, L., Bracchi, K. and Lieberman. 1993. The Fluorescent Response of Fuels in Soil: Insights into Fuel-Soil Interactions. SPIE, 1716, pp.139-147.
- Arenson, L.U., Xia, D., Biggar, K.W., and Segó, D.C. 2005. Freezing Process in Devon Silt - Using Time Laps Photography. In Proceedings of the 58th Canadian Geotechnical Conference, Saskatoon, SK.
- ASTM D422-63. 2002. Standard Test Method for Particle-Size Analysis of Soils
- Beard, D. and Weyl, P. 1973. Influence of Texture on Porosity and Permeability Of Unconsolidated Sand. *American Association of Petroleum Geologists Bulletin*, 57, pp. 349-369.
- Biggar, K., Woeller, D., Murphy, S., and Armstrong, J. 2003. CPT-UVIF Characterization at Upstream Oil And Gas Facilities. In Proceedings of the 17<sup>th</sup> Annual Vancouver Geotechnical Society Symposium: Geotechnical Engineering for Geoenvironmental Applications, Vancouver, BC. pp 31-37.
- Bro, R. 1997. PARAFAC: Tutorial and Applications. *Journal of Chemometrics*, 38, pp. 149-71.

- Bro, R. and Andersen, C. 2003. Practical aspects of PARAFAC modeling of fluorescence EEM data. *Journal of Chemometrics*, 17, pp. 200 – 215.
- Christensen, J., Hansen, A., Mortensen, J. and Andersen, O. 2005. Characterization and Matching of Oil Samples Using Fluorescence Spectroscopy and Parallel Factor Analysis. *Analytical Chemistry*, 77, pp. 2210-2217.
- Furnas, C. 1931. Grading Aggregates. I. Mathematical Relations for Beds of Broken Solids Of Maximum Density. *Industrial and Engineering Chemistry*, 23, pp. 1052-1058.
- Harr, M.E. 1977. *Mechanics of Particulate Media: A Probabilistic Approach*. McGraw-Hill International Book Company, NewYork, NY.
- Hart, S. and JiJi, R. 2002. Light Emitting Diode Excitation Emission Matrix Fluorescence Spectroscopy. *Analyst*, 127, pp. 1693–1699.
- JiJi, R., Andersson, G. and Booksh, K. 2000. Application of PARAFAC for Calibration With Excitation–Emission Matrix Fluorescence Spectra of Three Classes of Environmental Pollutants. *Journal of Chemometrics*, 14, pp. 71–185.
- Jumikis, A. 1962, *Soil Mechanics*. D. Van Norstrand Company, Inc. Yew Yourk, NY.
- Kram, M., Keller, A., Massick, S. and Laverman, L. 2004. Complex NAPL Site Characterization Using Fluorescence Part 1: Selection of Excitation Wavelength Based on NAPL Composition. *Soil and Sediment Contamination*, 13, pp. 103-118.
- Kenny, J., Lin, J., Hart, S., Wang, W. and Namytkhine, D. 1995. Subsurface Contaminant Monitoring by Laser Fluorescence Excitation-Emission

- Spectroscopy in a Cone Penetrometer Probe. SPIE, 2504, pp. 59-67.
- Knowles, D. and Lieberman, S. 1995. Field Results From The SCAPS Laser-Induced Fluorescence (LIF) Sensor for In-Situ, Subsurface Detection Of Petroleum Hydrocarbons. SPIE, 2504, pp. 297-307.
- Konrad, J. 1999. Frost Susceptibility Related to Soil Index Properties. Canadian Geotechnical Journal, 36, pp. 403-417.
- Kotzick, R. and Niessner, R. 1996. Application of Time-Resolved, Laser-Induced and Fiber-Optically Guided Fluorescence for Monitoring of a PAH-Contaminated Remediation Site. Fresenius, Journal of Analytical Chemistry, 354, pp. 72-76.
- Lakowicz, J. 1999. Principles of Fluorescence Spectroscopy (2<sup>nd</sup> edition). Kluwer Academic/Plenum Publishers, New York, NY.
- Lieberman, S., Theriault, G., Cooper, S., Malone, P., Olsen, R. and Lurk, P. 1991. Rapid Subsurface In-Situ Field Screening of Petroleum Hydrocarbon Contamination Using Laser Induced Fluorescence Over Optical Fibers, In Proceedings of the 2<sup>nd</sup> International Symposium on Field Screening Methods for Hazardous Waste Site Investigations, Las Vegas, Nevada. Air and Waste Management Association, Pittsburgh, P.A. pp. 57-63.
- Löhmannsröbena, H., Rocha, T., Schaefer, R., Schultzea, R. and Vereecken, H. 1997. Laser-Induced Fluorescence (LIF) Spectroscopy for In-Situ Analysis of Fluorescence Tracers In Water And Soils. SPIE, 3107, pp. 207-216.
- Machel, H., Mason, R., Mariano, A. and Mucci, A. 1991. Causes and Emission of Luminescence in Calcite and Dolomite In Luminescence Microscopy:

- Quantitative And Qualitative Aspects. In: Luminescence Microscopy: Qualitative and Quantitative Aspects (SEPM-1991) (Edited by Barker, C. and Kopp, O.). pp. 37-57.
- Matthews, B., Jones, A., Theodorou, N. and Tudhope, A. 1996. Excitation-Emission-Matrix Fluorescence Spectroscopy Applied to Humic Bands In Coral Reefs. *Marine Chemistry*, 55, pp. 317-332.
- Mitchell, J. 1993. *Fundamentals of Soil Behaviour* (2<sup>nd</sup> Edition). JohnWiley and Sons, Inc., New York, NY.
- Moise, N., Vasile, A., and Pascu, M. 1995. Measuring of Water and Soil Contamination With Oil Components Using Laser Induced Fluorescence Transmitted Through Optical Fibers. *SPIE*, 2461, pp. 636–643.
- O'Connor, D. and Phillips, D. 1984. *Time-Correlated Single Photon Counting*. Academic Press Inc, London. UK.
- Schade, W. and Bublitz, J. 1996. On-Site Laser Probe For The Detection of Petroleum Products in Water And Soil. *Environmental Science and Technology*, 30, pp. 1451-1458.
- Schulman, S. 1977. *Fluorescence and Phosphorescence Spectroscopy: Physicochemical Principles and Practice*. Pergamon Press, New York, N.Y.
- Sinfield, V., Germaine, J. and Harold, F. 1999. Effect of Soils on Laser Induced Fluorescence of BTEX Pore Contaminated Waters. *Journal of Geotechnical and Geoenvironmental Engineering*, 125, pp.1072-1077
- St. Germain, R., Gillispie, G. and Klingfus, J. 1993. Variable Wavelength Laser System for Field Fluorescence Measurements. In *Proceedings of Field*



- Screening Methods for Hazardous Wastes and Toxic Chemicals, Las Vegas, NV. Air & Waste Management Association, Pittsburgh, P.A. pp.1113–1122.
- Pharr, D., McKenzie, J. and Hickman, A. 1992. Fingerprinting Petroleum Contamination Using Synchronous Scanning Fluorescence Spectroscopy. *Ground Water*, 30, pp. 484-489.
- Rho, J. and Stuart, J. 1978. Automated Three-Dimensional Plotter for Fluorescence Measurements. *Analytical Chemistry*, 50, pp. 620-625.
- Roch, T., Lohmannsroben, H. G., and Meyer, T. 1995. Laser-Induced Fluorescence Analysis of PAC-Doped Model Oils on Alumina, Sand, And Soil Surfaces. *SPIE*, 2504, SPIE, pp. 453–464.
- Tickell, F. G. and W. N. Hiatt. 1938. Effect of Angularity of Grain on Porosity and Permeability of Unconsolidated Sands. *American Association of Petroleum Geologists Bulletin*, 22, pp. 1272–1279.
- Terzaghi, C. 1925. Principles of Soil Mechanics: Physical Differences between Sand and Clay. *Engineering News Record*, 95, pp. 912–916.
- Trask, P. 1931. Compaction of Sediments. *American Association of Petroleum Geologists Bulletin*, 15, pp. 271–276.
- Vo-Dinh, T. 1982. Synchronous Luminescence Spectrometry: Methodology and Applicability. *Applied Spectroscopy*, 36, pp. 576-581
- Vogt and Sjoegren. 1989. Investigation of Chemical and Statistical Methods. *Analytica Chimica Acta*, 222, pp. 135-150.

## **CHAPTER 5**

# **LIGHT EMITTING DIODE OPERATED ULTRAVIOLET INDUCED FLUORESCENCE (UVIF)-STANDARD CONE PENETRATION TESTING (CPT) SYSTEM**

### **5.1. INTRODUCTION**

The fluorescing nature of refined petroleum products and crude oil is related to the excitation of electrons to higher energy levels when illuminated with sufficient energy (ultraviolet (UV) light). After excitation, electrons return to the ground state from the higher energy levels through various non-radiative and radiative mechanisms, one of which is fluorescence. This transition of electrons between energy levels is common in aromatic hydrocarbon compounds in petroleum products due to the nature of electron bonding in their conjugated structure. The fluorescence signal or spectrum produced by a particular aromatic compound typically contains peak(s) at specific location(s), which provides a unique signature and therefore can be used to identify that compound (Schulman 1977).

In the early 90's the idea of combining fluorescence sensors with a cone penetrometer probe that maps soil type and changes in stratigraphy and also detects petroleum contaminants in soils was introduced. Initially a variety of laser-induced fluorescence (LIF) fibre-optic-based sensors were developed to detect subsurface petroleum hydrocarbons contaminants. One of the early fluorescence sensors

combined with standard cone penetrometers was the Site Characterization and Analysis Penetrometer System (SCAPS), developed by the U.S. Department of Defence (DoD) (Lieberman et al. 1991). Subsequently the rapid optical screening tool (ROST) was developed by the U.S. DoD (St. Germain et al. 1993). Following that development, the Advanced Applied Technology Demonstration Facility (AATDF), part of the Environmental Technology Program at Rice University, Houston, Texas, developed a new technology that utilizes a multi-channel LIF screening system at Tufts University (Kenny et al. 1995). In Canada, similar technology known as ultraviolet induced fluorescence-cone penetration testing (UVIF-CPT) system was also developed. UVIF-CPT system utilizes intense single wavelength UV light emitting diode (LED) instead of laser and eliminates using fibre optics (Biggar et al. 2003). Typically, fluorescence based sensor systems use a similar design where UV light from a laser or other light source is transmitted directly or via fibre optic cables through a sapphire window on a probe installed in a module placed immediately behind a cone penetrometer. Fluorescence emitted by the aromatic components of petroleum hydrocarbons passes back through the window to either a detector system located in the module or via fibre-optic cables to a detector at the surface. A profile of fluorescence intensity versus depth can then be generated in combination with lithological data from the CPT system to provide a real time display of the location of petroleum hydrocarbon contamination (Figure 5-1).

The advantage of using fluorescence based measurements is that they do not require any preparation or sampling prior to analysis, which makes it attractive for field

screening site characterization applications. However, use of LIF based systems has been limited to date due to price constraints. Additionally, the fibre-optic system used to convey the UV light to the sensor and convey the fluorescence to the detector at the surface is sensitive and somewhat costly to maintain. This chapter describes the development of a new UVIF sensor to replace the existing sensor in the current UVIF-CPT system and includes details regarding its design, construction, calibration and testing. The improved UVIF-CPT system presented in this chapter addresses operational and price limitations associated with in situ fluorescence measurements by providing a less expensive, robust and compact fluorescence sensor that eliminates the use of expensive laser induced light sources, fiber optic systems and complex detection system. The UVIF-CPT system can generate fluorescence excitation-emission matrices (EEMs) of detected petroleum contaminants with a system contained in the down-hole probe, and send the data to the surface in electrical form. The generated fluorescence EEMs have an inherent wealth of spectral information that can help to better characterize and quantify petroleum products in environmental samples.

## **5.2. FLUORESCENCE EEMs**

Fluorescence EEM spectroscopy has long been known as a powerful method for petroleum product analysis (Patra and Mishra 2002; Eastwood 1981). Unlike conventional fluorescence spectra where fluorescence intensity of an analyte is plotted as a function of the emission wavelength when excited by the light of a fixed wavelength or presented as a plot of fluorescence intensity received within a fixed

spectral band as a function of the excitation wavelength, EEMs are three-dimensional representations of fluorescence intensity as a function of both the excitation and the emission wavelengths (Figure 5-2). This presentation captures all fluorescence spectral features of the tested analyte allowing much more effective characterization, especially for multi-component mixtures that are difficult to identify solely based on their conventional fluorescence signals. The data in an EEM is often visually presented in the form of a contour plot that separates different aromatic components in the mixture into isolated peaks. This representation of EEM data enables the extraction of the spectral features of specific petroleum products, even in the presence of unknown interferences (Rho and Stuart 1978; Vo-Dinh, 1982).

The ability to collect full fluorescence EEMs by scanning emission spectra for several excitation wavelengths generally requires expensive, complex, and large sized spectrometers, which prevents using them in applications where operating practicality and field portability are desired. Many researchers have developed alternative instrumentation to overcome these obstacles and stimulate a broader utilization of the EEM fluorescence technique for mainstream fluorescent detection. A variety of light sources are now used in developed instruments including gas discharge lamps or lasers coupled with monochromators for excitation light selection, a laser Raman shifter system, or a set of fixed wavelength LEDs. The fluorescence signal detection system in these instruments is mostly composed of a monochromator and a charge coupled device (CCD) to image the resulting EEM spectrum (Muroski et al. 1996; Jiji et. al. 1999; Lohmannsroben and schober1999; Sinfield et al. 1999; Hart and Jiji

2002; Gouzman et al. 2004). Despite efforts to simplify and miniaturize the instrumentation required for fluorescence EEM spectroscopy, most of the available systems didn't eliminate using costly, large light sources or monochromators that require specific geometrical spaces to disperse light. The UVIF-CPT system described in this chapter employs a small and inexpensive multi-wavelength LED as the excitation source, along with a detection system composed of a compact, light-weight linear variable filter (LVF), coupled with a photomultiplier tube (PMT) to generate fluorescence EEMs. Both the excitation and detection components of the UVIF-CPT system can be fitted inside a module coupled to a standard cone penetrometer allowing full down-hole fluorescence measurements. The UVIF-CPT doesn't require fiber optics to deliver excitation light or fluorescence signals, which is an advantage compared to LIF systems that suffer signal attenuation and distortion while carried by fibre optics, particularly at lower radiation wavelength in the UV range. Additionally, fibre-optic cable quality deteriorates over time due to wear and tear during use, requiring periodic replacement, which results in increased operating costs (Biggar et al. 2003).

### **5.3. UVIF SENSOR DESIGN**

A schematic diagram of the UVIF sensor module is shown in Figure 5-3. The dimensions of the module were selected so the module would fit entirely inside a standard 43.7 mm probe directly behind the sapphire window. The UVIF module has the following parts: 1) excitation source (multi-wavelength LED), 2) optical components (reflective mirrors and quartz glass tube) to direct fluorescence radiation

through the module to the detection system, 3) detection system (step motor-driven LVF coupled with sensitive PMT) and 4) data acquisition system. The LED was fitted in the module closely behind the sapphire window to allow direct excitation of the analyte through the sapphire window. The selected distance between the LED and the sapphire window, as well as, the angle at which the LED was aligned resulted in an appropriate reduction of scatter excitation light reflected back into the module. The LED was powered by a circuit that allows switching each of the excitation wavelengths on and off separately or all together as required and controlled by interactive computer program. Upon excitation, fluorescence radiation emitted by the tested analyte entered the module through the sapphire window and was directed into the entrance point of a quartz glass tube (used as a light pipe) and transmitted to a detection system using a 45° micro-rod mirror. At the exit point of the glass tube, the transmitted fluorescence radiation was redirected again, across the LVF plane using another 45° micro rod mirror. To obtain the fluorescence EEM, the fluorescence emission signal was scanned over a specific range of wavelengths at each (LED) excitation wavelength by moving the LVF across an emission slit, behind which the PMT was mounted to detect incident photons. The motion and positioning of LVF was regulated by a computer controlled, linear step motor. The data was collected using a 400 MHz Pentium PC.

#### **5.3.1. Multi-Wavelength LED**

There are many advantages to using LEDs in analytical fluorescence spectroscopy. LEDs require minimal voltage to produce a significant quantity of stable light, and

LEDs are also cost effective. The cost of traditional excitation sources (e.g. xenon lamps and lasers) in conventional spectrometers used in fluorescence EEM measurements is generally more than \$10,000, while the cost of a multi wavelength LED is typically less than \$1,000. Another advantage is that the LEDs are small, 1 to 10 mm in diameter or length, so they can be fixed directly to optical elements in compact fluorescence sensors where space is limited. Also, LEDs provide almost monochromatic excitation, which allows their use without the filters that traditional lighting methods require to select desired excitation wavelengths (Kovac et al. 2003). These advantages allow LEDs to be effectively integrated into compact fluorescence sensors.

The novel light source used in this UVIF sensor was a UVTOP® multi-wavelength LED assembled and supplied by Sensor Electronic Technology, Columbia, SC. The LED has an AlGaIn/GaN chip array mounted on a single header with peak emission wavelengths of 265, 280, 310, 340 and 360 nm. The LED comes in a small package that is 9.14 mm in diameter and 5 mm thick. The package is hermetically sealed with customized, proprietary reflector, heat sink, and UV-transparent optical window to optimize the output power from the LED. The LED is driven by a maximum forward current of 30 mA and voltage of 7.5 V. It can also be driven by a pulse forward current of 200 mA with duty factor of 1% and frequency of 1kHz as specified by the manufacturer. The LED can, on average, produce 0.5 mW of optical power with typical full width half maximum (FWHM) of 12 nm (Sensor electronic Technology 2007). While testing, the LED was driven at voltages below the optimum levels



recommended by the manufacturer at a constant current mode. Operating the LED on pulse mode was attempted to obtain higher excitation intensity, however it was problematic during the course of the experiment, and was therefore dismissed.

Figure 5-4 shows emission spectra of the multi-wavelength LED generated using the UVIF module. The LED light was reflected back into the module by a mirror mounted in front of the sapphire window. When examining the LED emission spectra presented in Figure 5-4, the following points need to be considered:

- The emission peak of wavelength 265 nm is not shown in the figure because it was below the detection range of LVF.
- The emission spectra for wavelengths 310, 340 and 360 nm didn't show sharp emission peaks as expected because emission intensity of these wavelengths exceeded the PMT gain limits and only the maximum allowed PMT intensity readings were recorded. The emission peaks of LED 310, 340 and 360 nm wavelengths were assumed to be at the middle of the emission maximum value ranges of each wavelength.
- The intensity of emission peak of wavelength 280 nm appears to be less than emission peak intensities of wavelengths 310, 340 and 360 nm because the LVF has a low light transmission coefficient (less than 20%) at the lower range of wavelengths.

Comparing the LED emission peak wavelength values in Figure 5-4 with peak wavelength values provided by the manufacture showed a small variation of +/- 5 nm. These wavelength variations are relatively minor, considering the large wavelength

range covered by the LED.

### **5.3.2. Linear Variable Filter (LVF)**

LVFs have been utilized successfully as wavelength-selection elements in fluorescence spectroscopy in an effort to provide compact, robust and inexpensive fluorescence spectrometers. The detection system in LVF based spectrometer is typically composed of a detector array (photo diode or CCD) which is either coated with an LVF or mounted behind a moving LVF that converts the spectral fluorescence information into a spatially dependent signal that is analyzed by the detector array (Gouzman et al. 2004; Wahl et al. 2005, Schmidt et al. 2007). LVFs are inexpensive: the cost of the LVF is typically around \$500 (Ocean optics 2007). These filters are small and light weight, and don't require specific geometrical space that might not be available in miniature sensors. These characteristics make LVFs an attractive choice suitable for compact fluorescence sensors.

The LVF used in the UVIF module is LVF-HL® manufactured and supplied by Ocean Optics (Dunedin, Florida). The filter allows radiation to pass through at specific adjustable wavelength bandwidths distributed throughout its length, which converts the spectral information of the incident light into a spatially dependent signal. The filter is assembled by fastening together a high-pass filter and a low-pass filter to create a variable band pass filter with 20 nm minimum transmission bandwidth. The filter allows for the adjustment of the center wavelength and the bandwidth by sliding the filters against one another, so one can move the transmission

or blocking band throughout the length of the filter. The LVF could allow up to 65% of the radiation to pass through in transmission bands and block up to 99.8% of radiation in the blocking bands. The spectral range extends from the UV to the visible region (just below 300 nm to 750 nm) with light transmission coefficient varying from 20% to 65%. The LVF is made of two 57 mm x 10 mm quartz substrates that are coated with interference coatings (Ocean Optics 2007).

### **5.3.3. LVF calibration**

Because fluorescence intensity data points were collected at specific rates as the LVF moved in front of the PMT at a constant speed by the linear step motor, the wavelength of each recorded emission reading could be correlated to a specific location along the length of the LVF. In order to convert fluorescence readings to actual wavelength values, the LVF had to be calibrated. Spectral calibration of the LVF was performed using a mercury lamp because it has distinct spectral lines at specific wavelengths that could be easily identified when the lamp emission spectrum is scanned by the UVIF module (Figure 5-5). Mercury spectral lines that have been found useful for calibrating spectral measuring equipment are: 253, 296, 313, 334, 365, 404, 435, 546 and 579 nm (Sansonetti et al. 1996). Plotting the known wavelength of emission lines in the mercury lamp spectrum versus the readings related to the same emission lines of the mercury lamp spectrum collected by the UVIF module, allowed for the generation of a calibration function to correlate fluorescence reading numbers to actual wavelength values. Data points in Figure 5-6 show a strong linear function ( $\text{Wavelength} = 4.85 * \text{Reading number} + 195.22$ ) with

high correlation represented by  $R^2$  value of 0.9969 that can be used to convert fluorescence readings to actual wavelengths values.

## **5.4. EXPERIMENTAL WORK**

### **5.4.1. Material**

The performance of the UVIF sensor was examined with a number of petroleum products in solvent solutions and soils. The tested petroleum products included natural gas condensate, gasoline, diesel, flare pit residue and crude oil. These petroleum products represent petroleum contaminants that are often encountered at upstream oil and gas sites and contain a variety of aromatic constituents. Gasoline and diesel samples used in this study were purchased from the local market in Edmonton, AB. Gas condensate and flare pit residue samples were obtained from two field research sites in Alberta. The crude oil sample came from Cold Lake, AB, and was supplied by the National Centre for Upgrading Technology (NCUT) laboratories, Devon, AB. All samples were stored in airtight containers that were clearly marked and kept in a refrigerated storage room at the Applied Environmental Geochemistry Research Facility at the University of Alberta.

The initial tests were performed on neat samples at varying concentrations. Also, to examine the changes of petroleum product fluorescence signals when included in soil matrices, petroleum products were mixed with four different soils with various particle size distributions that represent a reasonable range of expected soils at field sites. The soils used in the test were clean quartz sands and Devon silt (composed of

quartz, feldspar and clay minerals). They included: 1) Ottawa sand (a uniform quartz sand with a grain size of 0.42 mm), 2) a well graded sand that was assembled by mixing equal portions of coarse sand (sand with mean particle size ( $d_{50}$ ) of 0.72 mm), Ottawa sand (0.42 mm) and fine sand (a uniform sand with a grain size of 0.15 mm), 3) a mixture of well graded sand and Devon silt and 4) Devon silt. Grain size distribution of each of the tested soils is illustrated in Figure 5-6. These soil samples represent well sorted, poorly sorted, poorly sorted sand with higher fines content and poorly sorted fine grained soils, respectively, that have a wide range of porosities. Chapter 4 indicated that the porosity values of these soils were as follows: Ottawa sand 44%, well graded sand 34%, well graded sand and Devon silt mixture 24% and Devon silt 19%.

Along with samples of pure petroleum product, a number of diluted samples were prepared for each petroleum product analyzed. Diluted samples had concentrations that ranged from 1 to 800 mL /L in solvent solutions which corresponded to 280 to 190,000 mg/kg (ppm) in soil matrices. Hexane was used as the solvent to dilute gas condensate, gasoline and diesel samples. Chloroform was used to dilute flare pit residue and heavy crude oil due to the presence of higher molecular weight PAHs in these products that could not be dissolved by Hexane. This wide range of concentrations was selected to reflect concentrations encountered at the field, and also to monitor the effect of fluorescence quenching and energy-transfer processes on the measured EEMs. Fluorescence quenching is an intermolecular mechanism that lowers fluorescence intensity at higher concentrations through the loss of excitation energy

by enhanced collisional encounters between excited fluorophore molecules (Schulman 1977). In total, 70 stock solution samples (including duplicates) of all petroleum products were prepared.

Soil samples were prepared by mixing 3 mL of each stock solution with 5 gm of Ottawa Sand, well graded sand, well graded sand with silt and 3 gm of Devon Silt. All samples in solvent solutions and soils were tested in cylindrical sample containers made of black anodized aluminum, with a 33.28 mm outside diameter and a height of 30.14 mm. The top of the sample container was fitted with a circular quartz glass cover of the same diameter to allow UV light illumination and fluorescence emission from the tested sample. During testing, the sample container was mounted in direct contact with the sapphire window of the UVIF module to better simulate actual field conditions where contaminated soils typically press against the sapphire window while the cone penetrometer is pushed into the ground (Figure 5-7).

Emission scans from 280 to 700 nm with 5 nm increments were obtained at excitation wavelengths 265, 289, 310, 340 to 360 nm. The scan rate was approximately 300 nm/min., which allowed a scan time of less than 7 minutes per sample. Blank samples of solvents and soils were scanned to detect fluorescence background. No significant fluorescence signal was observed in any of the tested solvents or soil samples at any of the excitation wavelengths. In addition, samples of hexane, chloroform, and a reference material (Rohdamine-B) were analyzed every day to monitor any variation in the UVIF module performance. Observed variation in emission peak locations and

intensities of control samples throughout the experiment was very limited ( $\pm 5\%$ ).

A total of 200 fluorescence EEMs were collected excluding blanks and controls.

#### **5.4.2. Data Pre-Processing**

Due to the instrumental and geometrical setup, as well as the operational nature of the UVIF sensor, collected fluorescence data needed to be pre-processed to consider instrumentation and scattered light interferences. Instrumentation interference is associated with the variation of LED light intensity at different wavelengths and LVF transmittance. Scattered light interference is associated with reflected excitation light entering the module.

##### **5.4.2.1. Correction for Variation in LED Light Intensity**

For a particular analyte, fluorescence intensity is directly dependant on excitation light intensity, when fluorescence measurement conditions and instrumentation remain the same during the course of testing as suggested by Beer's Law (Lackwicz 1999). Therefore, fluorescence spectra of a particular analyte generated at different excitation wavelengths might have different appearances as excitation light intensity changes. To be able to compare fluorescence spectra of tested petroleum products generated by the UVIF sensor with similar ones collected using the Varian Eclipse spectrometer used in our previous chapters 3 and 4, differences in excitation light intensity between the two instruments must be considered. To quantify these differences, Rohdamine fluorescence spectra collected by the UVIF sensor and Varian Eclipse spectrometer were examined (Figures 5-8a-b). Rohdamine has a quantum

efficiency value that is almost 1. This means that in response to every photon in the excitation light, Rohdamine will emit a photon in fluorescence, which makes the intensities in the fluorescence spectra a true reflection of excitation light intensities at different wavelengths.

The Rohdamine fluorescence spectra in Figure 5-8 show the differences in light intensities of the light sources from the Varian Eclipse spectrometer (Fig 5-8a) and the UVIF sensor (Fig 5-8b). To obtain correction factors that account for these differences, the fluorescence intensity of Rohdamine generated by both instruments at the excitation wavelength of 265 nm was considered the datum and given a value of 1 (Wehry 1990). Relative fluorescence intensity values of other excitation wavelengths were then calculated according to the datum. Correction factors for excitation wavelengths of the UVIF sensor were then calculated as follows:

$$\text{Correction factor } (\lambda_{\text{excitation}}) = \frac{[\text{RRI } (\lambda_{\text{excitation}})]_{\text{Varian spectrometer}}}{[\text{RRI } (\lambda_{\text{excitation}})]_{\text{UVIF sensor}}}$$

[5-1]

Where,  $[\text{RRI } (\lambda_{\text{excitation}})]_{\text{Varian spectrometer}}$  is the relative intensity value of Rohdamine fluorescence spectra generated Varian Eclipse spectrometer at particular excitation wavelength and  $[\text{RRI } (\lambda_{\text{excitation}})]_{\text{UVIF sensor}}$  is the similar value generated using the UVIF module. Correction factors ranging from 0.28 to 1.17 could be then applied to intensities of fluorescence spectra of tested petroleum products generated by the UVIF sensor to obtain corrected fluorescence spectra that could be compared to the



corresponding fluorescence spectral data collected by the Varian Eclipse spectrometer. All fluorescence spectra and EEMs presented in this chapter have been corrected for comparison and validation reasons. The same correction procedure using Rohdamine fluorescence spectra collected by the UVIF sensor should be considered when fluorescence spectra are to be compared with similar fluorescence spectra collected using different instruments.

#### **5.4.2.2. Correction for LVF Opaque Band**

As mentioned earlier, the filter used in the UVIF module is assembled by coupling a high-pass filter and a low-pass filter to create a variable band pass filter that allows adjustment of the bandwidth by sliding the filters against one another. To obtain an optimum spectral resolution and light transmittance through the LVF, a high-pass filter and a low-pass filter were assembled in a way that created an opaque band on the filter resulting in light being totally blocked between wavelengths 419 and 450 nm. This resulted in a gap of fluorescence data in all generated fluorescence spectra between 419 and 450 nm (Figure 5-9). Linear interpolation was used to predict the values of missing fluorescence data to fill the gap in generated fluorescence spectra. Linear interpolation was selected because it is a simple approach that provided good estimates. Higher order polynomial or logarithmic interpolation functions might not necessarily provide better representation of petroleum products fluorescence intensity because fluorescence is strongly affected by various factors that might not be easily accounted for in regular interpolation functions. Factors that influence fluorescence intensity include: molecular structure, quantum efficiency and concentration of the

analyte, excitation light intensity and instrument constants (Valeur 2002).

#### **5.4.2.3. Correction for Scattered Light**

In the present UVIF module, the relatively wide spectral width of the excitation beam and geometrical setup create a well-known problem of scattered excitation light that interferes with the fluorescent signal. The scattered light is generated by reflection of part of the excitation light back into the UVIF module and the Rayleigh scattering of the excitation light on the solvent molecules in the sample, and the high concentration of the analyte. In practice, the scattered signal does not influence the measurements of the fluorescent spectrum except where the analyte excitation and emission wavelengths are close, which could obstruct the observation of these small Stokes shifted fluorescence bands. The effect is more noticeable at a low concentration of analytes, when the fluorescent light intensity becomes overwhelmed by the intensity of scattered light. Figures 5-10a and 5-10b show a sample of methanol (background) fluorescence spectra and diesel fluorescence spectra, respectively, collected by the UVIF module. It shows how scattered light can dominate the collected spectra of diesel and methanol. The presence of scattered light overwhelms the fluorescence spectra of diesel and masks some of the unique fluorescence spectral features of diesel. As a result, diesel might not appear to have significantly different spectral features from methanol for the most part, despite the fact that methanol does not fluoresce. This scattered light interference becomes even more pronounced at higher excitation wavelengths that are close to emission peaks of diesel fluorescence spectra.

This obstacle can be dealt with using pre-processing methods including background subtraction, which has been demonstrated as useful techniques for mitigating scattered light effects (Christensen et al. 2005). In this study, background signals of solvents or soils were subtracted from all generated fluorescence signals of petroleum products in solvent solution or soil samples, which helped fluorescence signals to appear clearly.

## **5.5. RESULTS AND DISCUSSION**

### **5.5.1. Quantitative Fluorescence Measurements**

Figures 5-11a-h and 5-12a-h illustrate the fluorescence spectra and EEMs, respectively, collected using the UVIF module and the Varian Eclipse spectrometer from chapter 3. (Presented fluorescence EEM were generated using the *contour* feature in MATLAB 7.1.) The plots show the results of the excitation wavelengths 265, 280, 310, 340 and 360 nm for the analyzed petroleum products. Note that no fluorescence signal was detected for the gas condensate by the UVIF module because the gas condensate has a low intensity fluorescence emission peak emission at 290 nm, as indicated in chapter 3, which falls within the wavelengths range at which the LVF has less than 20% transmission coefficient. This low transmission prevented detection of the signal. Accordingly, no spectra or EEM are presented herein for the gas condensate.

Despite the lack of fine spectral signature resolution, the generated fluorescence spectra and EEMs show that each of the analyzed petroleum products has a

significantly different fluorescence signature with specific emission peak locations, which can be used to identify that particular compound. The location of the fluorescence peaks in the fluorescence spectra and EEMs generated using the UVIF module remained almost unchanged from the fluorescence data for the same petroleum products that were collected using Varian Eclipse spectrometer. However a few of the emission peaks in fluorescence spectra and EEMs collected by the UVIF module seem to be shifted or diminished when compared to ones collected by the Varian Eclipse spectrometer. This is either because these peaks are located at a wavelength within the opaque band on the LVF so they were lost due to the linear interpolation over this range, or they were very close to the excitation signal, so they were removed when scatter light was subtracted. The absence of these peaks does not significantly influence the integrity of collected fluorescence spectra and EEMs so they still provide unique fingerprints of the tested petroleum products and have matching spectral features to similar fluorescence data collected using the Varian Eclipse fluorescence spectrometer.

Examining the collected fluorescence data indicates that EEMs of a particular petroleum contaminant in the solvent solution or the soil at different concentrations tend to have more pronounced emission peaks at longer wavelengths and at higher concentrations. As the contaminant concentration decreases, the peaks shift slightly toward shorter wavelengths. An example of the gasoline peak shift with dilution is illustrated in Figures 5-13a and b. This observation is in agreement with findings in chapter 3. In fact, not a real shift in emission peak, it is more accurately an

enhancement or attenuation of emission peak intensities at different wavelengths. This enhancement or attenuation is related to an inner filter effect that is commonly observed in petroleum products. The concept is explained in more details in chapter 3. Fluorescence EEMs can still be used to fingerprint petroleum products despite the apparent shift of peak locations at different concentration, because the combination of excitation and emission wavelengths at which peaks occur at different concentrations is unique and an inherent characteristic of the tested product.

Examining the fluorescence EEMs collected by the UVIF module for the tested petroleum products in soil samples indicated that the fluorescence EEM peak locations did not change from the EEMs for the same petroleum products in solvent solutions. An example of the similarities in gasoline fluorescence signal in solvent solution and soil is presented in Figure 5-14. Also, the fluorescence EEM peaks location did not change for the same petroleum product in different soils, indicating that soil mineralogy has no effect on fluorescence signal for the soils tested. However the EEM fluorescence peak intensities in solvent solutions were significantly affected when the same products were mixed with soil, causing the peaks to be diminished or enhanced. These observations match results in chapter 4 and previous study that indicated fluorescence EEM shapes are not likely to be affected by the presence of the soils, but their peak intensity values will be altered (Sinfield et al. 1999).

The detection limits of the tested petroleum products in solvent solution and soil samples using the UVIF module are listed in Table 5-1. The limits were assigned

based on observation of fluorescence signals exceeding a threshold of  $3\sigma_{\text{background}}$ , where  $\sigma_{\text{background}}$  is the standard deviation of background signal obtained from the fluorescence EEMs of the blank solvent and soil samples (Hart and JiJi 2002). The values could be further refined by testing more samples with petroleum product concentrations below those used in this study. The listed values in Table 5-1 are higher than similar detection limits obtained in chapter 4 for the same petroleum products and soils where the Varian Eclipse spectrometer was used. This is expected, because the xenon lamp used as an excitation source in the Varian Eclipse provides much higher excitation intensity than the LEDs used in the UVIF sensor, which allows detecting lower concentrations.

To examine the effect of different soil matrices on the fluorescence intensity of the tested petroleum products, the relationship between total fluorescence intensity and petroleum product concentration in both solvent solutions and soil matrices was investigated. Total fluorescence values were obtained by integrating the areas under all fluorescence curves (signals) in the related fluorescence EEMs. The integration extents in all EEMs were limited to emission wavelengths between 300 and 600 nm. For each analyzed petroleum product, total fluorescence values (arbitrary units, au) were plotted versus the related concentrations in solvent solutions and different soil matrices, taking in consideration the detection limit listed in Table 5-1. A linear relationship was assumed between fluorescence intensity and concentration below the limit of detection and is represented by a dashed line. This assumption considers that fluorescence is a linear function of concentration in diluted samples with limited

fluorescence emission, where fluorescence quenching is expected to have the least effect on the linearity of the relationship (Schulman 1977).

Figures 5-15a and 15b show the attenuation of gasoline and diesel total fluorescence when mixed with different soils. The reduction in fluorescence was the least in the Ottawa sand that has the highest porosity value (44%), where fluorescence in solution was reduced to approximately 40% for gasoline and 75% for diesel. The largest fluorescence attenuation was observed in Devon silt that has more than 80% of its composition as fines (<75  $\mu\text{m}$ ) and had the lowest porosity of 19%, where the observed gasoline and diesel fluorescence signals were reduced to approximately 20% and 40%, respectively, compared to the solvent solution. This behaviour is expected because the maximum fluorescence in soils is achieved when the largest amount of contaminant filled void space is exposed to the irradiated area on the fluorescence sensor window. Thus soils with more void space, such as Ottawa sand, are expected to attenuate fluorescence the least.

The observed attenuation of fluorescence signal in soil matrices typically applies to petroleum products that do not tend to be significantly affected by fluorescence quenching at higher concentrations. Chapter 3 indicated that flare pit residue and crude oil are more susceptible to fluorescence quenching; therefore, placing these analytes in a soil matrix may be expected to have different effects on their fluorescence signal intensity. Figures 5-16a and b show that the flare pit residue and crude oil total fluorescence values were slightly attenuated in soils at lower

concentrations, and had no significant attenuation at higher concentrations. In fact, the fluorescence signal intensity was enhanced at higher concentrations in the less porous soils. The presence of flare pit residue and crude oil fluorescing molecules in separate smaller voids within the soil matrix reduces the energy transfer through the collision mechanism, which in turn reduces fluorescence quenching at higher concentrations. Similar results were obtained using the Varian Eclipse spectrometer reported in chapter 4.

For petroleum contaminants mixed with soil, the relationship between fluorescence signal intensity attenuation and enhancement and the soil porosity was also investigated. Total fluorescence values of the analyzed petroleum products in solvent solutions and in the different soils (at different concentrations) were plotted against the porosity of the soils. A porosity value of 100% indicates that no soil is present, and was assigned for petroleum products in neat solution (Figures 5-17a and d). High  $R^2$  values ranging between 0.958 and 0.999 in Figures 5-17a and b indicated that total fluorescence intensity of gasoline and diesel in soil at all concentrations is linearly related to soil porosity. In Figures 5-17c and d, high  $R^2$  values that range between 0.960 and 0.978 indicated that total fluorescence intensity of flare pit residue and crude oil in soil at lower concentrations (approximately up to 50 mL/L in solution) is linearly related to soil porosity. The relationship did not maintain the linear behaviour at higher concentrations due to fluorescence quenching. Fluorescence intensity attenuation for gasoline and diesel, as well as low concentrations of flare pit residue and crude due to the presence of soil matrices, appears to be systematic. This



consistent behaviour is encouraging because it may permit expanding the generated total fluorescence profiles to other soils that are not addressed in this study but share similar grain size distribution and sorting.

Due to the presence of the opaque band on the LVF and correction for scattered light generated by reflection of part of the excitation light back into the UVIF module and the Rayleigh scattering, part of fluorescence spectral data related to analyzed petroleum products was lost. The missing fluorescence data from collected EEMs influenced the attempts to perform PARAFAC analysis and did not allow generating interpretable and stable models that satisfy set model selection criteria described in chapters 3 and 4, as well as Appendix G. For that reason, PARAFAC and, consequently, SIMCA analysis were not performed for fluorescence EEMs of tested petroleum products collected using the improved UVIF sensor.

### **5.5.2. Qualitative Fluorescence Measurement**

Fluorescence EEMs generated by the UVIF sensor have shown promising capabilities to efficiently identify various petroleum products in solvent solutions and different soil matrices. That encouraged extending these capabilities, so quantitative analysis may also be performed to estimate the concentration of analyzed petroleum products in solvent solution or soil. The already produced functions that describe the relationship between total fluorescence intensity and petroleum product concentration in both solvent solutions and soil matrices can be used as calibration functions to correlate the UVIF sensor response (fluorescence signal) and the concentration of the

petroleum product(s). Figures 5-18a through e show the total fluorescence profiles of the petroleum products analyzed in this study in the solvent solutions and in the different soils obtained under controlled laboratory conditions. The plots show clearly the induced changes to total fluorescence intensity values when the products are mixed with different soils, as well as at different concentrations. Also, these generated calibration curves match similar calibration curves that were produced for the same petroleum products using the Varian Eclipse reported in chapters 2 and 3. These generated total fluorescence profiles allow for the estimation of unknown concentrations of a particular product in a relevant environmental medium, based on the generated total fluorescence value. This is of a great interest because it could permit preliminary quantification of petroleum contaminants in situ in a timely manner without extracting soil samples.

The relationship between fluorescence intensity and petroleum product concentrations is expected to exhibit a linear behaviour at lower concentrations in solvent solutions and soil matrices for all analytes. As the concentration of the analytes increases, the relationship starts to divert from this linear behaviour due to fluorescence quenching that reduces fluorescence intensities at higher concentrations. The linear range of concentrations varied among the analyzed petroleum products based on their susceptibility to fluorescence quenching and the porosity of soil they are mixed with. In solvent solutions of diesel, flare pit residue and heavy crude oil, the relationship is linear up to a concentration of 1 mL/L for diesel, flare pit residue and crude oil, and 10 mL/L for gasoline. The linear range in all fluorescence profiles appears to be

extended when petroleum products are mixed with soils due to reduction of fluorescence quenching that causes the departure from linearity. The linear ranges for the different soils tested are listed in Table 4-2. Despite the observed diversion from linearity at higher concentrations, the relationship between fluorescence intensity and petroleum product concentrations in solvent solutions and soils is unique, even though more than one concentration value could be associated with the same fluorescence intensity. Even when two samples with different concentrations share the same fluorescence intensity value, they can still be discriminated from each other by examining their EEMs. Earlier discussion indicated that fluorescence peak locations will slightly shift to longer wavelengths as the concentration of petroleum products increases in solvent solution and soil. Therefore, the sample with the higher concentration value will have more pronounced emission peaks at longer wavelengths when compared with the EEM of the lower concentration sample that shares the same total fluorescence intensity value.

## **5.6. SUMMARY AND CONCLUSIONS**

An innovative, cost effective and compact UVIF sensor was developed for multi-way fluorescence measurement applications based on commercially available small sized multi-wavelength UV LED (as the excitation source) coupled with a PMT and an LVF (as the emission wavelength selection element). The sensor is part of a CPT system used in geo-environmental site investigations to detect subsurface petroleum contaminants, while acquiring soil profile stratigraphy data. The sensor was carefully designed and assembled to fit entirely inside a standard cone penetration

penetrometer, eliminating the use of fibre optics and allowing fluorescence measurements to be performed down-hole. The LVF was spectrally calibrated using a mercury lamp and, instrumentation interference and scattered light was accounted for. A laboratory testing program was conducted to test the performance of the new UVIF sensor with a number of petroleum products, which may be encountered in the field including: gas condensate, gasoline, diesel, flare pit residue and crude oil. Samples of each product were tested at different concentrations in both solvent solutions and in a variety of different soils. The soils used in this study include: Ottawa sand, well graded sand, well graded sand - Devon silt blend, and Devon silt, representing a wide range of grain size distributions and sorting degrees. The instrument was capable of detecting and generating fluorescence signals of all tested petroleum products, except gas condensate, in solvent solutions and soils at concentrations levels as low as 1 mL/L in certain cases.

The collected fluorescence signals of the tested petroleum products were presented as fluorescence spectra and EEMs that can be employed to characterize these petroleum contaminants in solvent solutions and soil either in field or laboratory settings. The UVIF sensor-generated fluorescence spectra and EEMs of the petroleum products in solvent solutions and soils were compared against ones collected by a Varian Eclipse spectrometer and found to be in reasonable agreement. Examining fluorescence spectral data of the tested petroleum products in solvent solution and soil samples indicated that no measurable effects of mineralogy were observed in the soils tested. The data also indicated that soils had no measurable effect on the shape of

fluorescence signal. However, for a given contaminant concentration, the fluorescence intensity in the soil samples decreased linearly as the porosity of the soils decreased. However, the relationship departed from linearity at higher concentrations for the petroleum products that are more susceptible to fluorescence quenching.

Quantitatively, this study generated calibration curves for the tested petroleum products that are based on the relationship between fluorescence intensity and the concentrations in solvent solutions and soils. These curves can be used to estimate the concentration of petroleum products based on their fluorescence intensity obtained by the improved UVIF-CPT system. The procedure developed in this chapter provides a quick and efficient approach to quantify concentrations of different petroleum contaminants that can be easily adapted to in situ measurements.

Table 5-1. Minimum petroleum products concentration at which fluorescence signal was detected with UVIF sensor in various media

<b>Petroleum Products</b>	<b>Solvent solution (mL/L)</b>	<b>Ottawa sand (mL/L in solution)</b>	<b>Well graded sand (mL/L in solution)</b>	<b>Well graded sand and Devon silt (mL/L in solution)</b>	<b>Devon silt (mL/L in solution)</b>
Gasoline	10	200	200	600	600
Diesel	1.00	1.00	1.00	1.00	10.0
Flare Pit Residue	1.00	10.0	50.0	50.0	50.0
Crude Oil	1.00	10.0	40.0	40.0	40.0

Table 5- 2. Maximum concentrations of linear range for total fluorescence measurement in tested soils

<b>Petroleum product</b>	<b>Ottawa sand (mg/kg)</b>	<b>Well graded sand (mg/kg)</b>	<b>Well graded sand and Devon silt (mg/kg)</b>	<b>Devon silt (mg/kg)</b>
Gasoline	$1.5 \times 10^5$	$1.6 \times 10^5$	-	-
Diesel	$4.0 \times 10^3$	$3.0 \times 10^3$	$1.5 \times 10^3$	$2.0 \times 10^3$
Flare Pit Residue	$6.0 \times 10^3$	$3.0 \times 10^4$	$1.5 \times 10^4$	$3.2 \times 10^4$
Crude Oil	$8.0 \times 10^3$	$9.0 \times 10^3$	$5.0 \times 10^3$	$6.0 \times 10^3$

*Note: Gas condensate was not detectable with the sensor system, and gasoline did not have enough samples at which fluorescence was detected in well graded sand and Devon silt mixture and Devon silt to establish the linear range.*

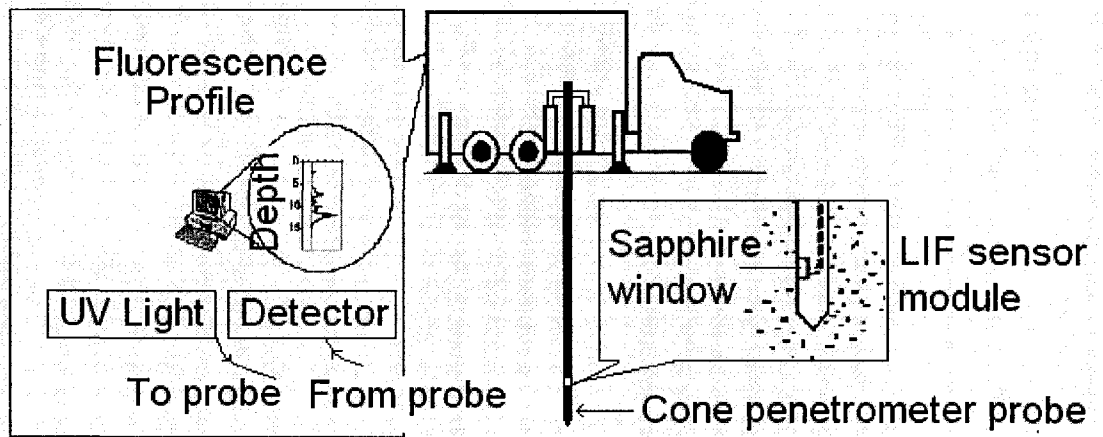


Figure 5-1. Typical LIF system setup (after Lieberman 1998)



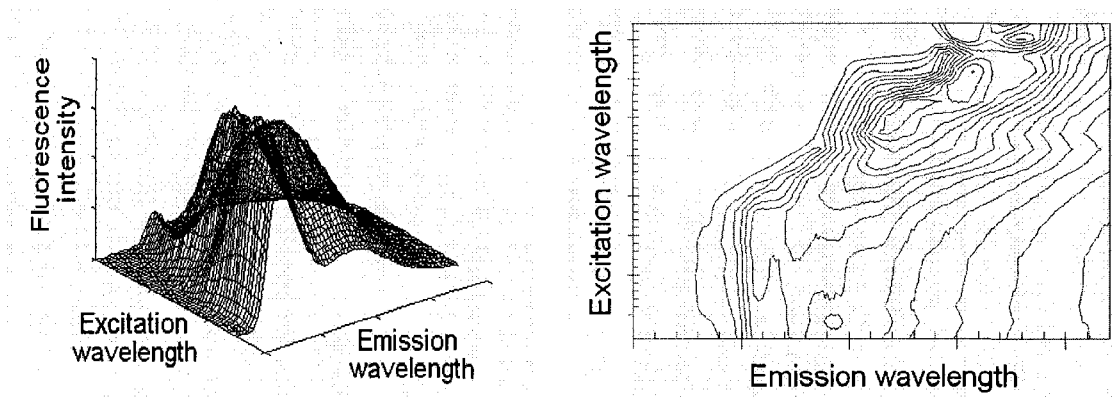


Figure 5-2. 3-dimensional (3D) and 2-dimensional contour map (2D) representations of emission-excitation matrix (EEM) (after Rho and Stuart 1978)

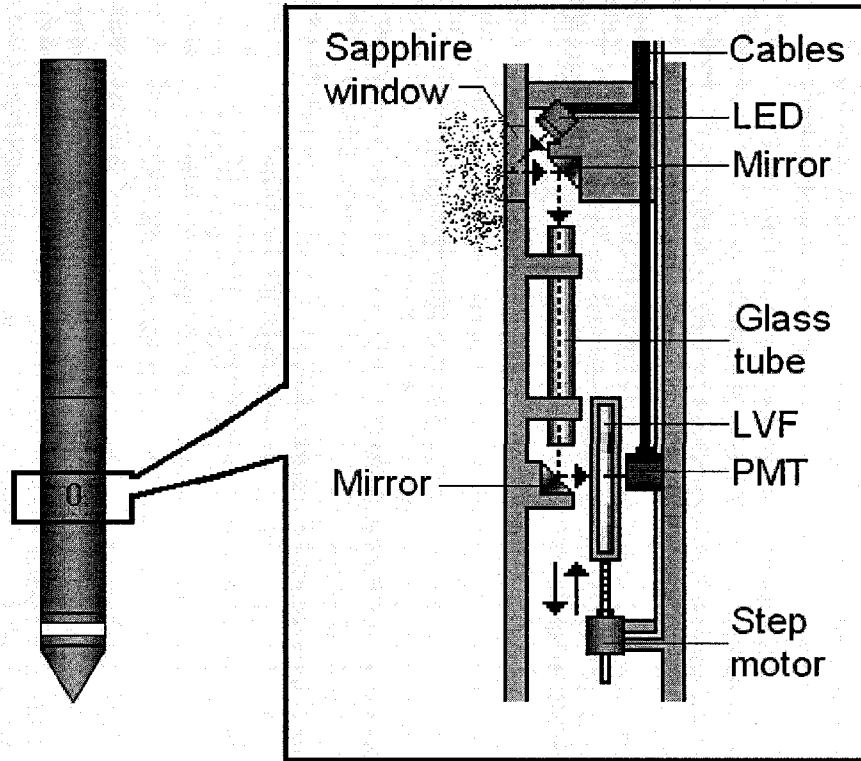


Figure 5-3. Improved UVIF sensor schematic

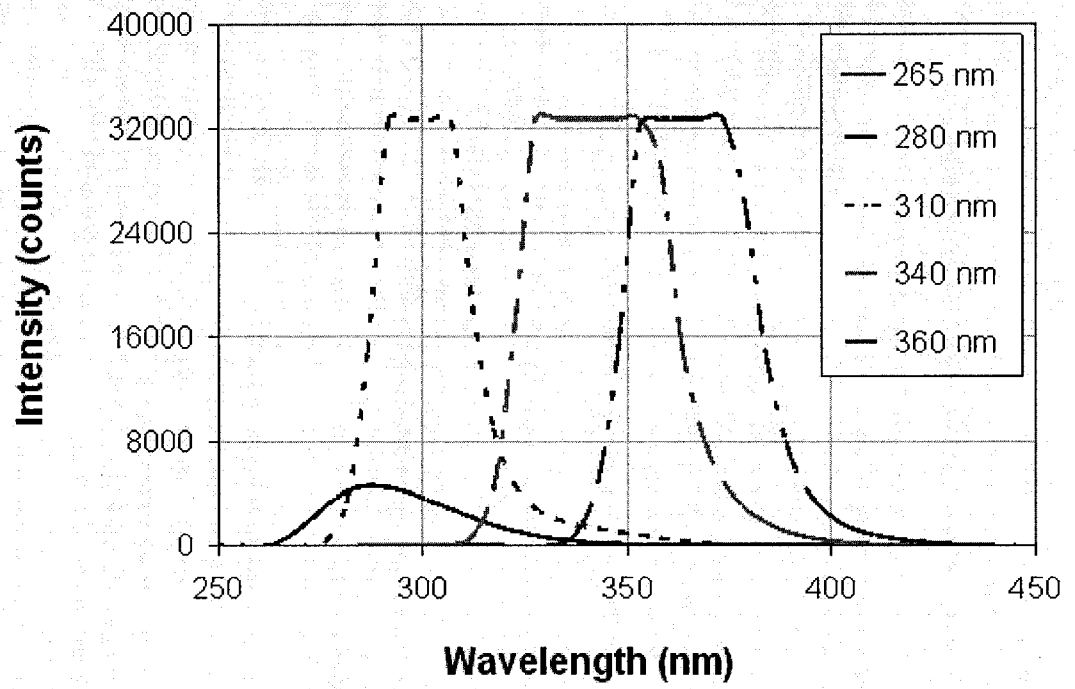


Figure 5-4. Multi-wavelength LED emission spectra

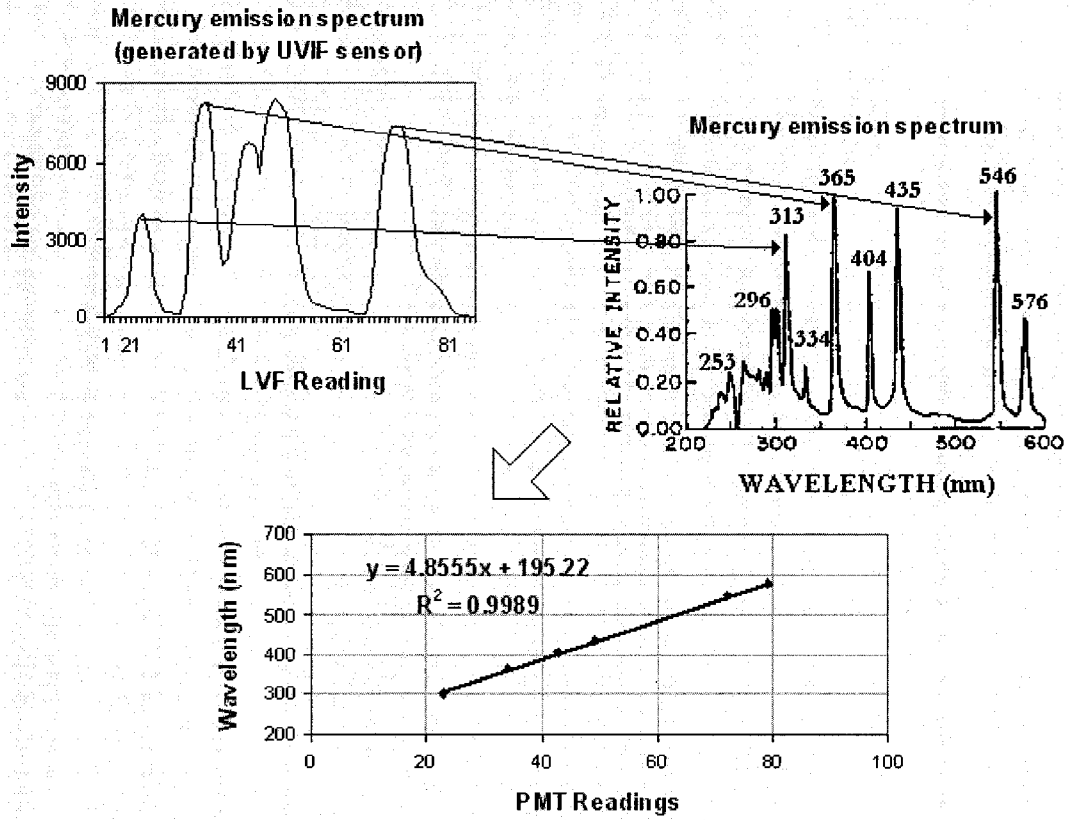
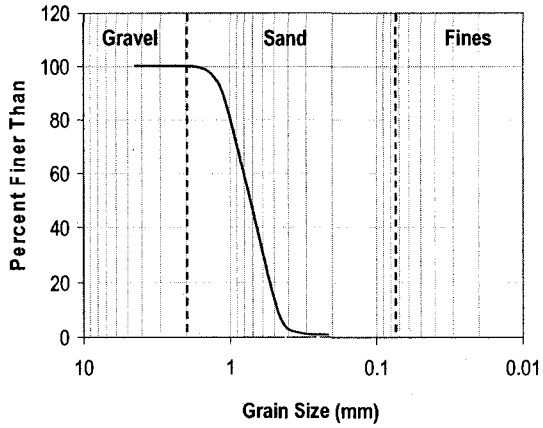
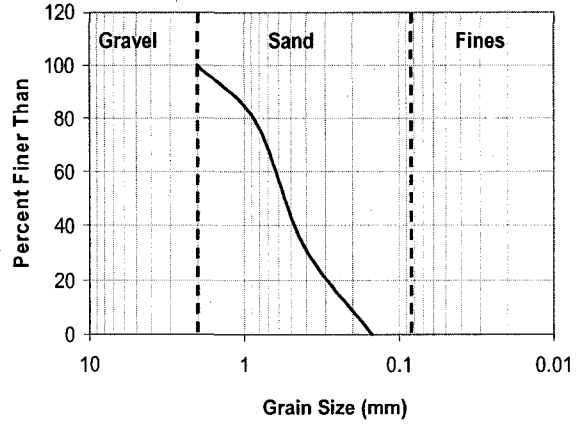


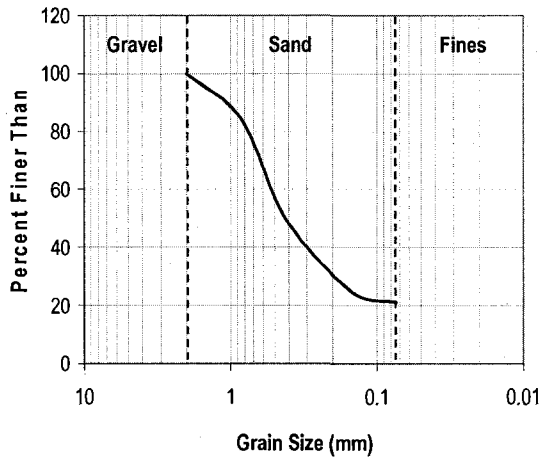
Figure 5-5. LVF calibration procedure involved correlating observed peak locations in mercury lamp emission spectra generated by the improved UVIF sensor to wavelengths of similar peaks in standard mercury lamp emission spectrum



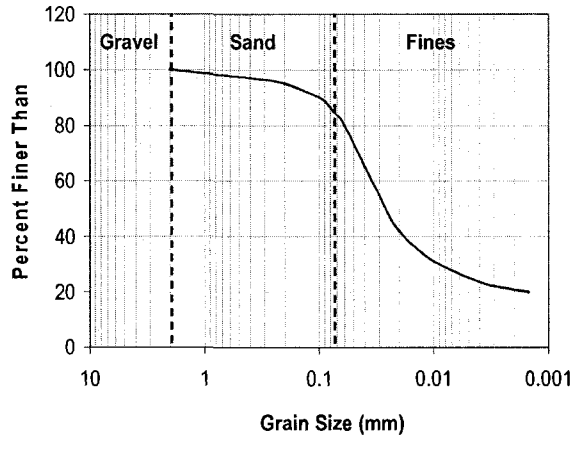
Ottawa sand grain size distribution



Well graded sand grain size distribution



Well graded sand and Devon silt grain size distribution



Devon silt grain size distribution (after Arenson et al. 2005)

Figure 5-6. Grain size distribution of tested soils

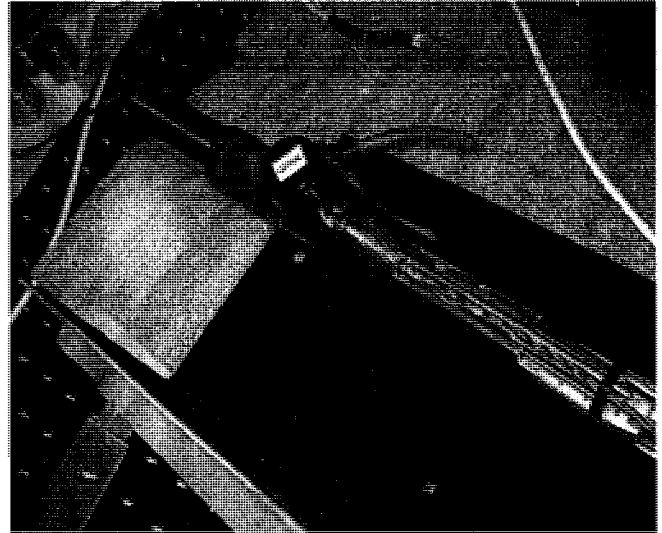
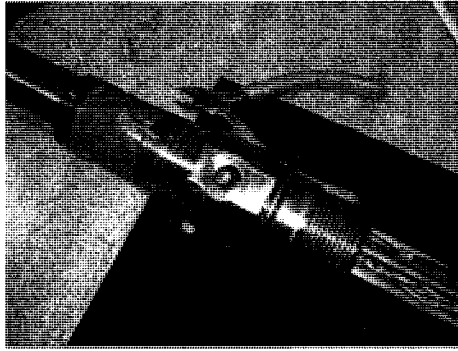


Figure 5-7. Samples testing setup where sample container was mounted in direct contact with the sapphire window in the cone penetrometer to resemble site fluorescence measurements

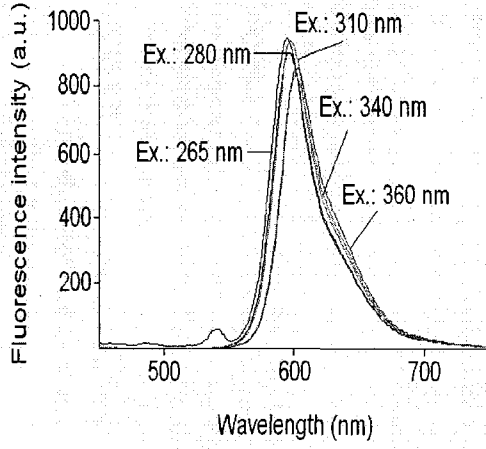


Figure 5-8a. Rohdamine fluorescence spectra (collected by Varian Eclipse Spectrometer)

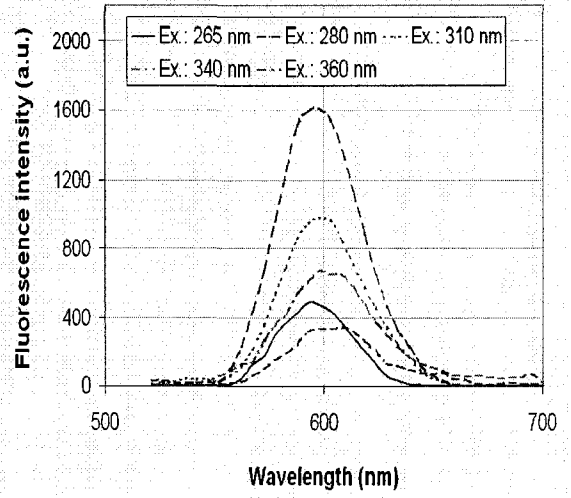


Figure 5-8b. Rohdamine fluorescence spectra (collected by UVIF sensor)

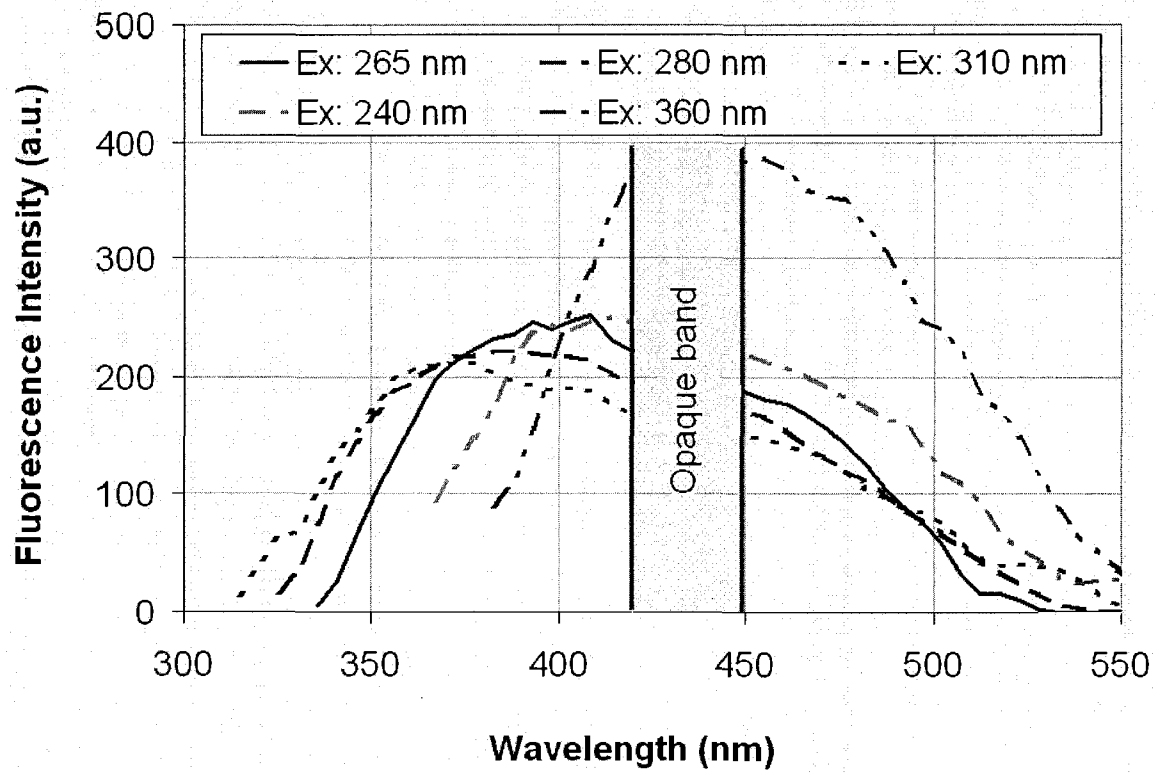


Figure 5-9. Opaque band in diesel fluorescence spectra



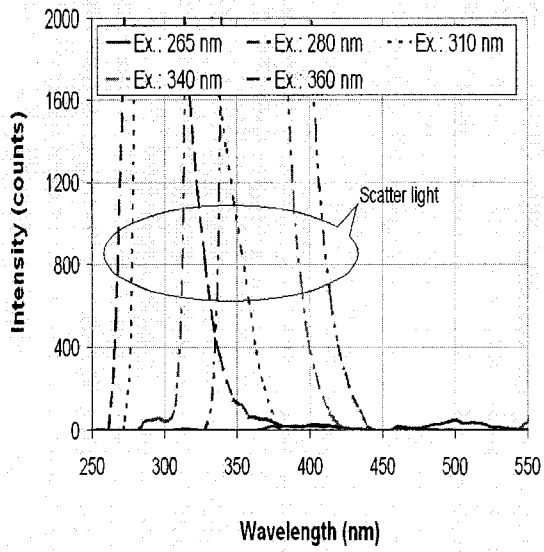


Figure 5-10a. Methanol fluorescence spectra in presence of scattered light

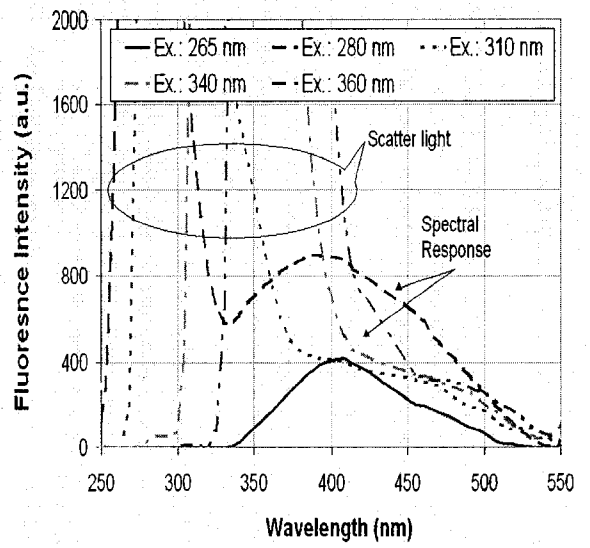


Figure 5-10b. Diesel fluorescence spectra in presence of scattered light

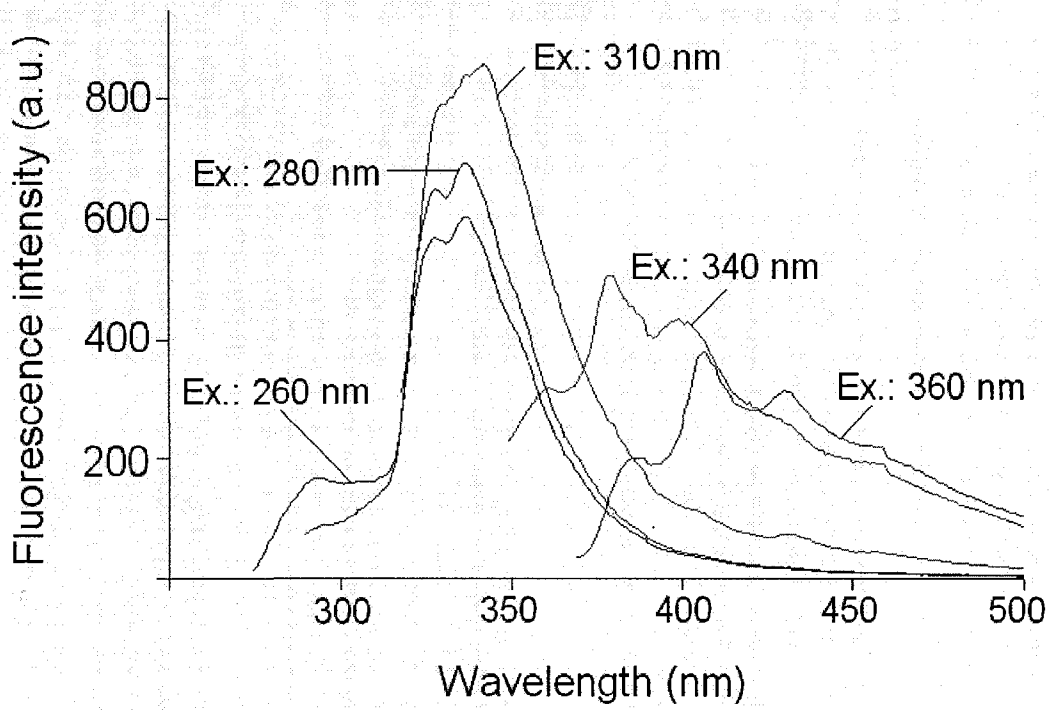


Figure 5-11 a. Gasoline fluorescence spectra – neat (using Varian Eclipse spectrometer)

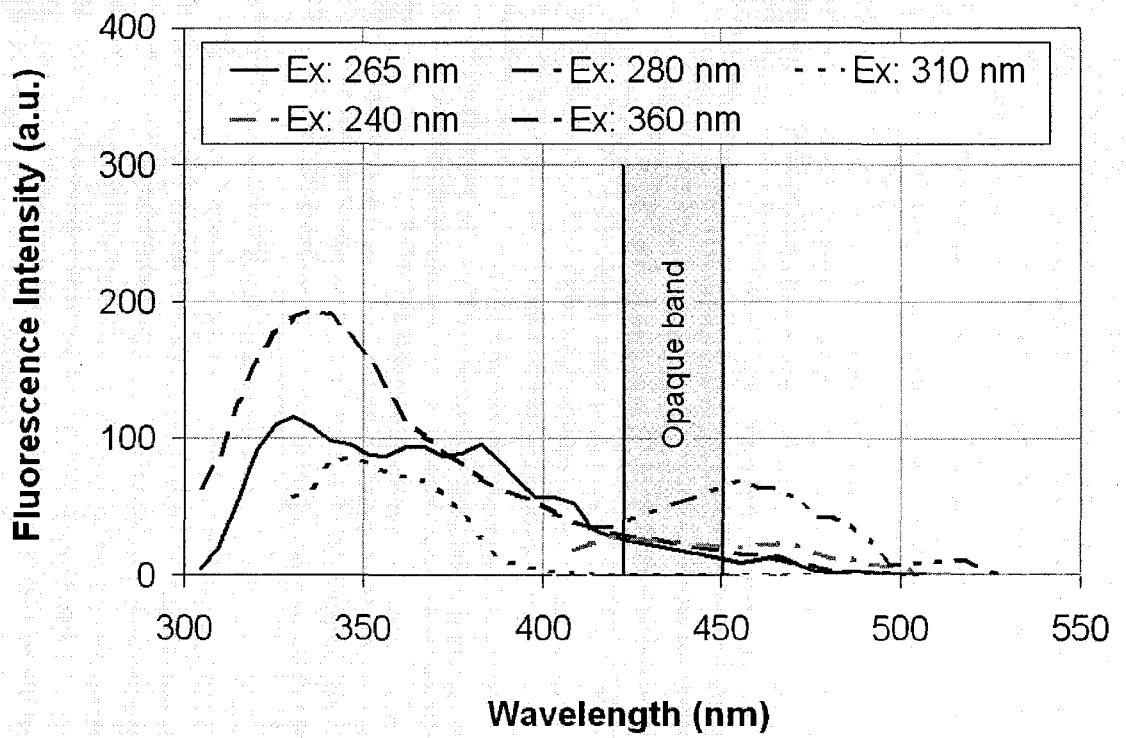


Figure 5-11b. Gasoline fluorescence spectra – neat (using UVIF sensor)

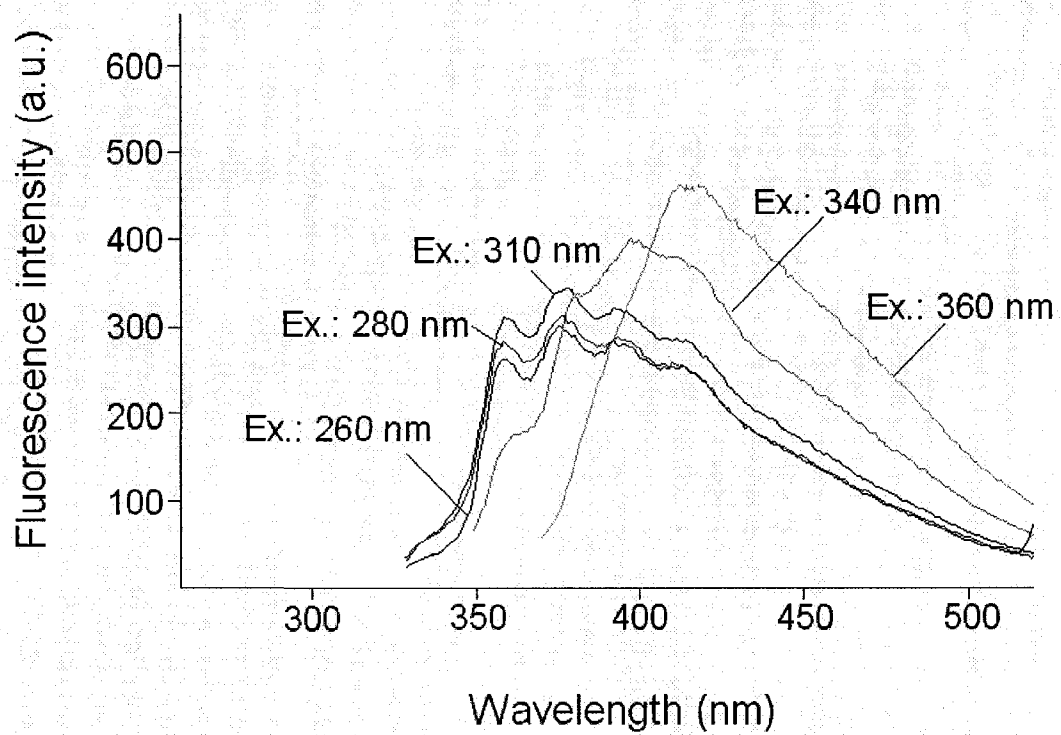


Figure 5-11c. Diesel fluorescence spectra – neat (using Varian Eclipse spectrometer)

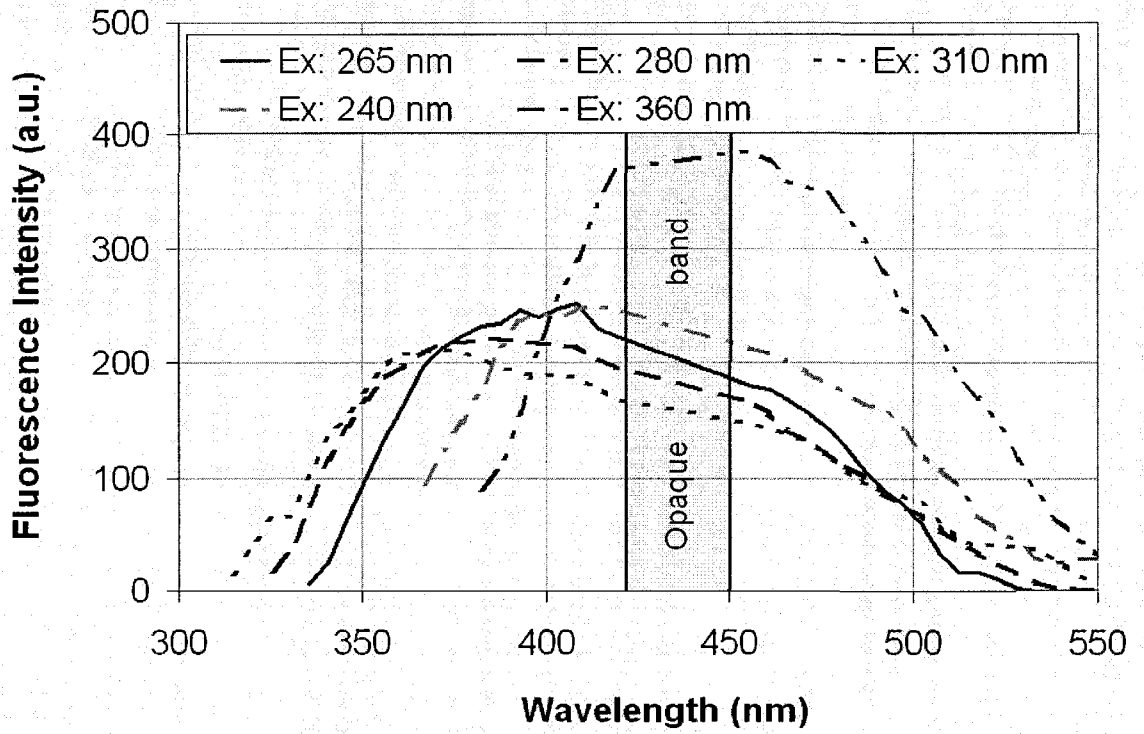


Figure 5-11d. Diesel fluorescence spectra – neat (using UVIF sensor)

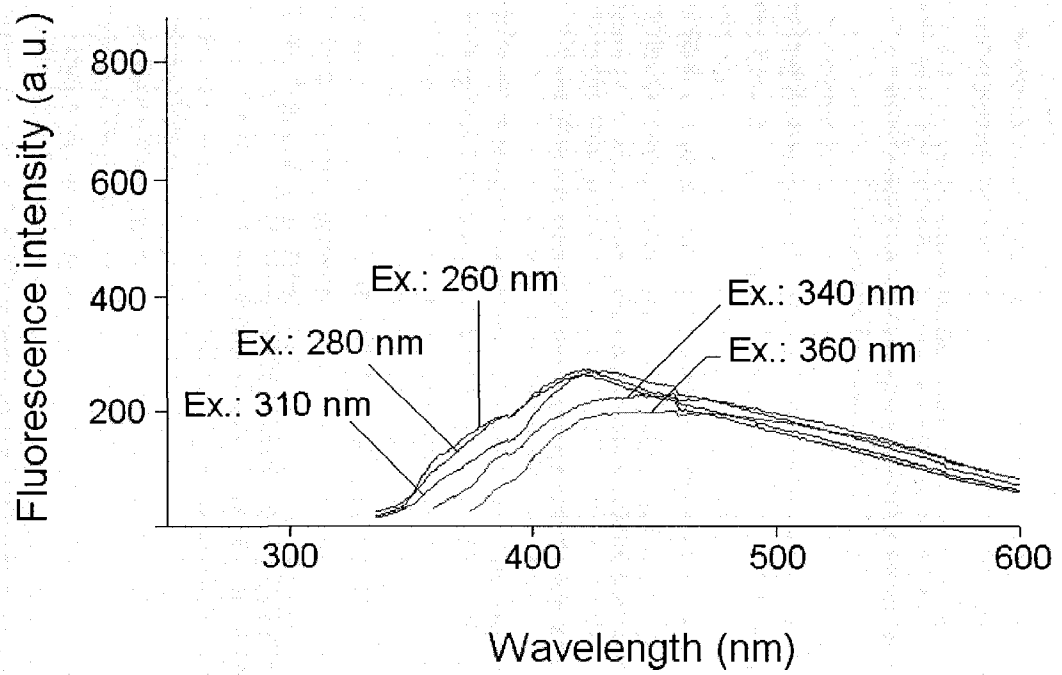


Figure 5-11e. Flare pit residue fluorescence spectra – neat (using Varian Eclipse spectrometer)

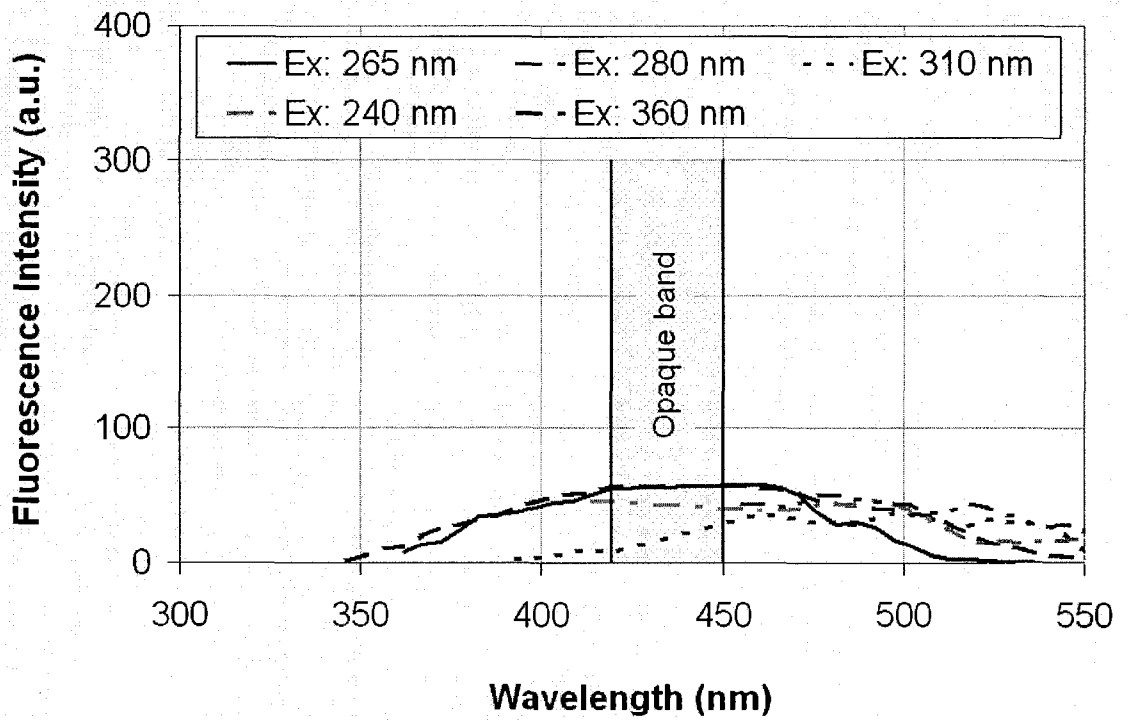


Figure 5-11f. Flare pit residue fluorescence spectra – neat (using UVIF sensor)

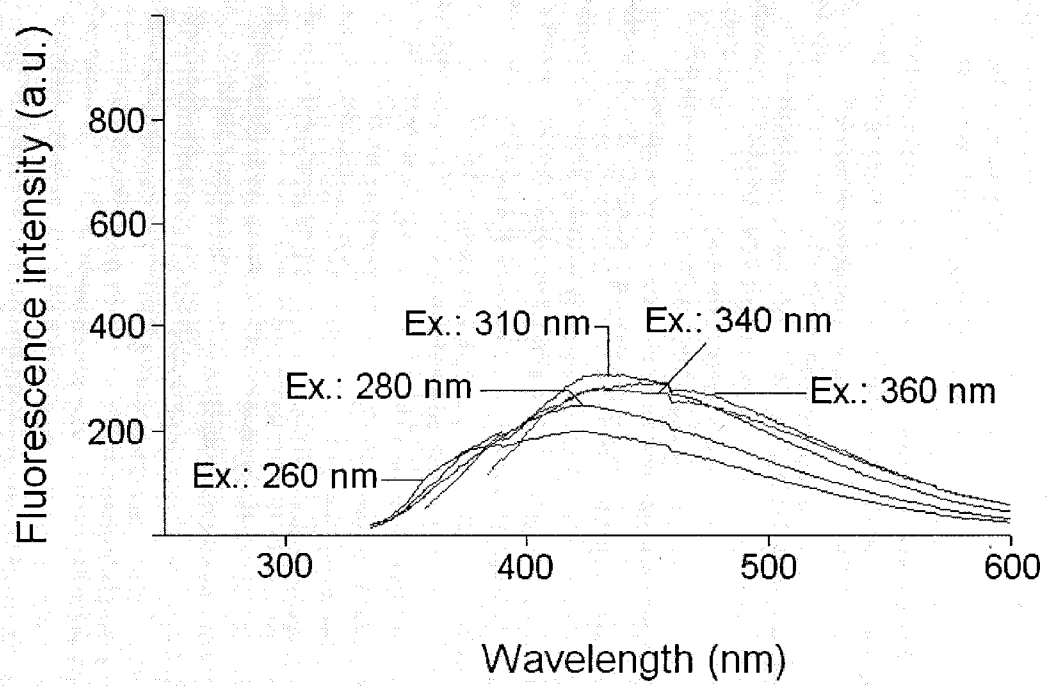


Figure 5-11g. Crude oil fluorescence spectra – 40 mL/L (using Varian Eclipse spectrometer)



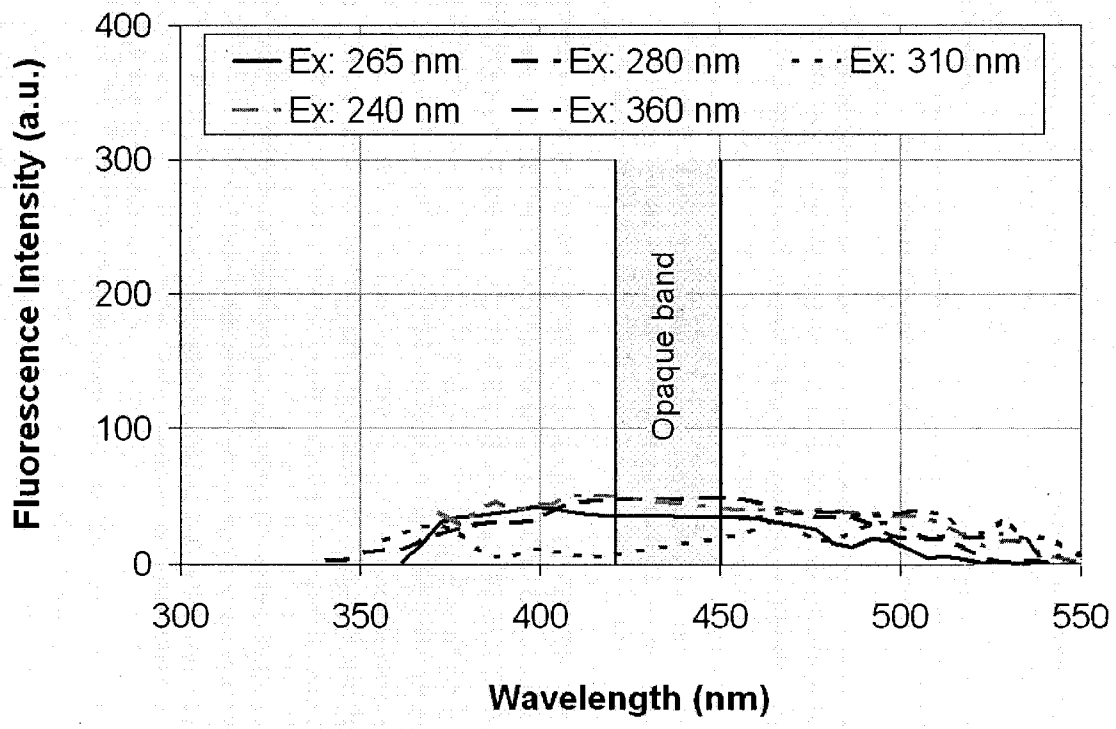


Figure 5-11h. Crude oil fluorescence spectra – 40 mL/L (using UVIF sensor)

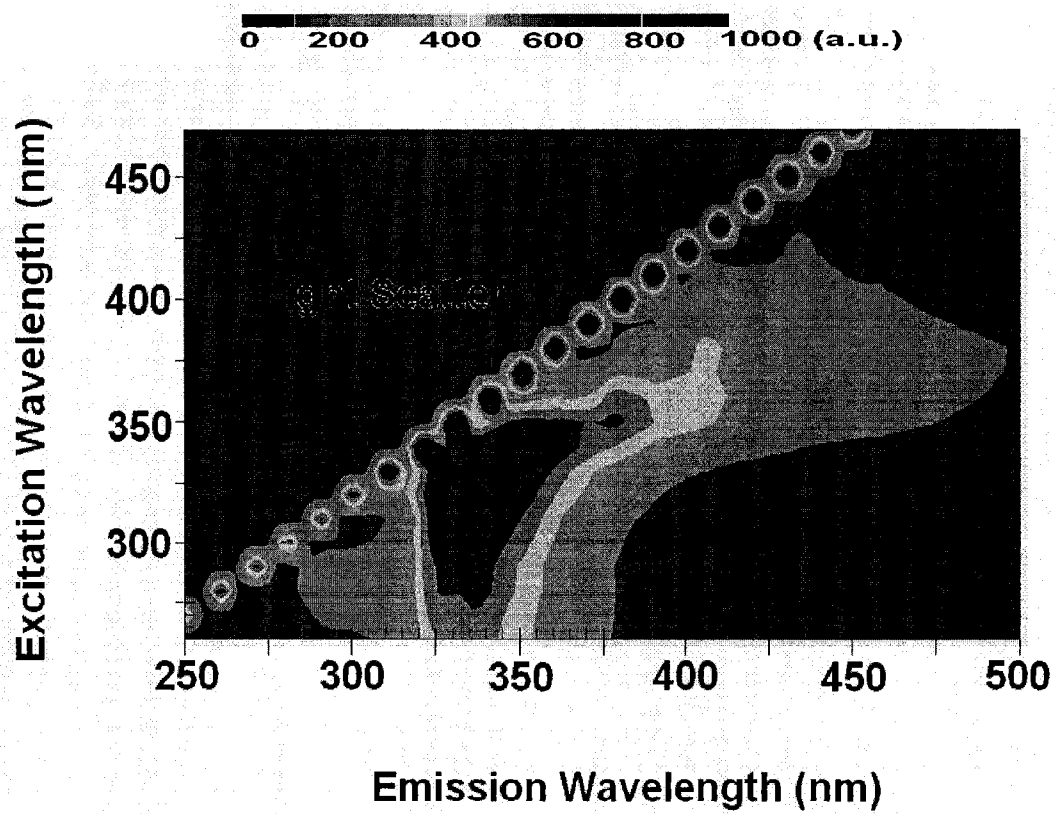


Figure 5-12a. Gasoline EEM – neat (using Varian Eclipse spectrometer)

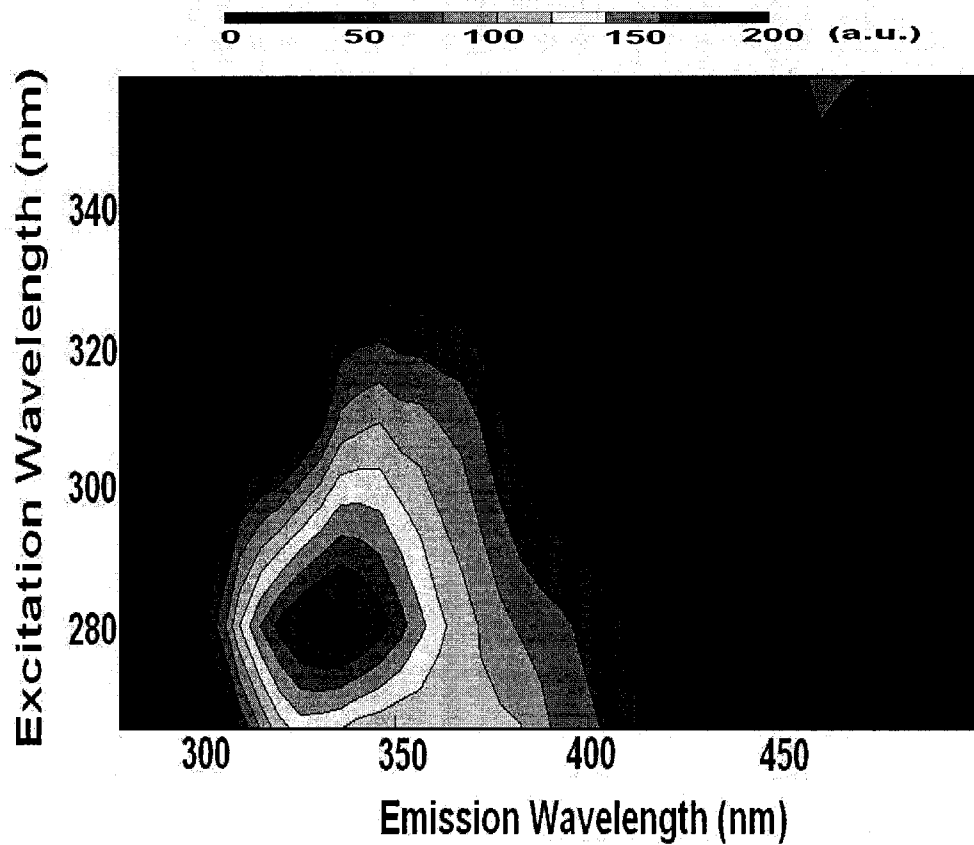


Figure 5-12b. Gasoline EEM – neat (using UVIF sensor)

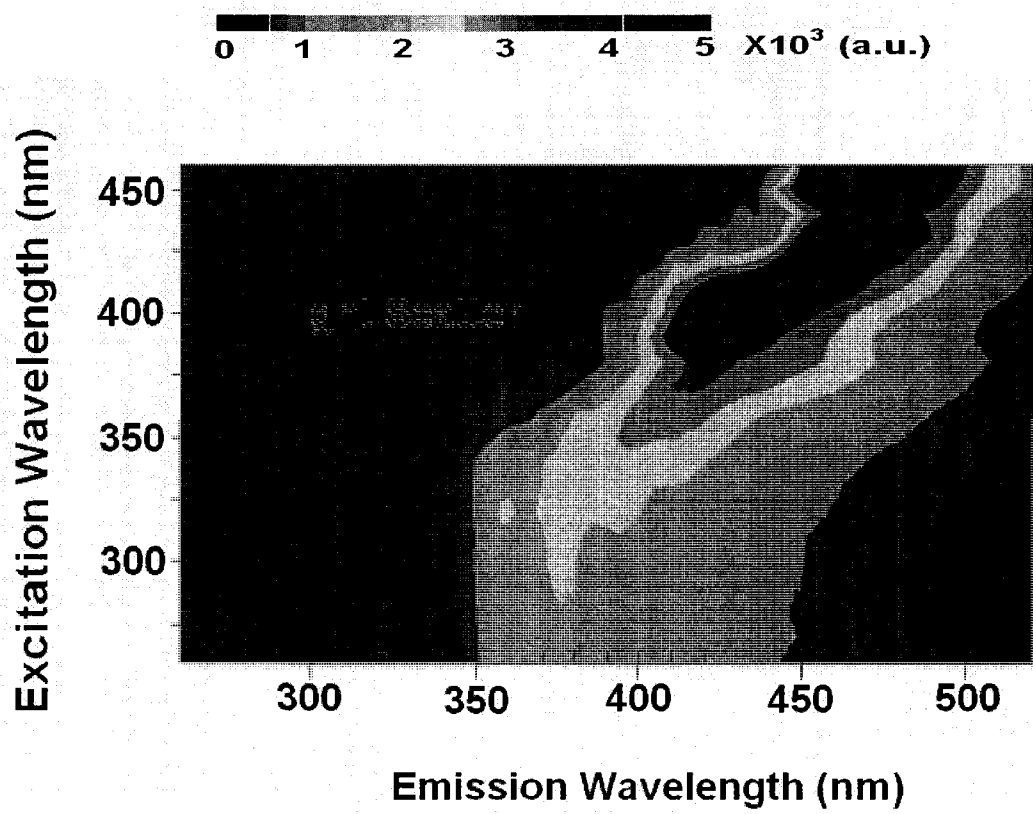


Figure 5-12c. Diesel EEM – neat (using Varian Eclipse spectrometer)

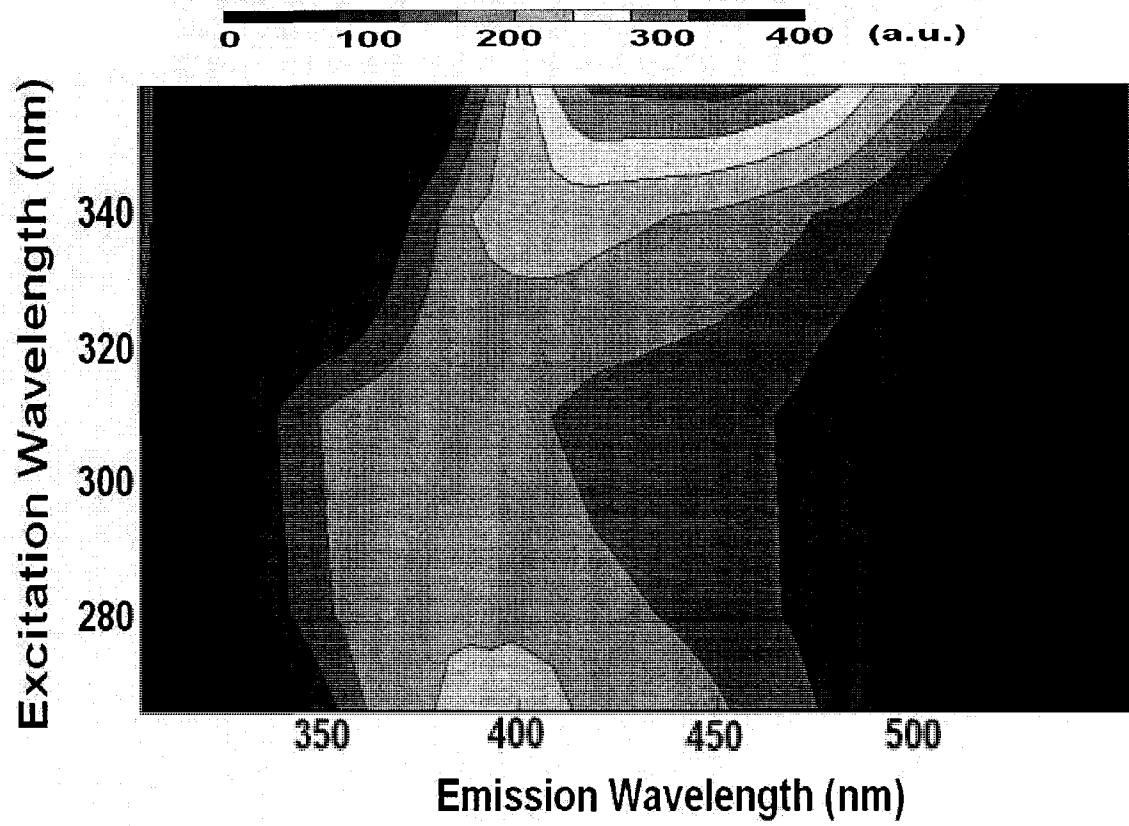


Figure 5-12d. Diesel EEM – neat (using UVIF sensor)

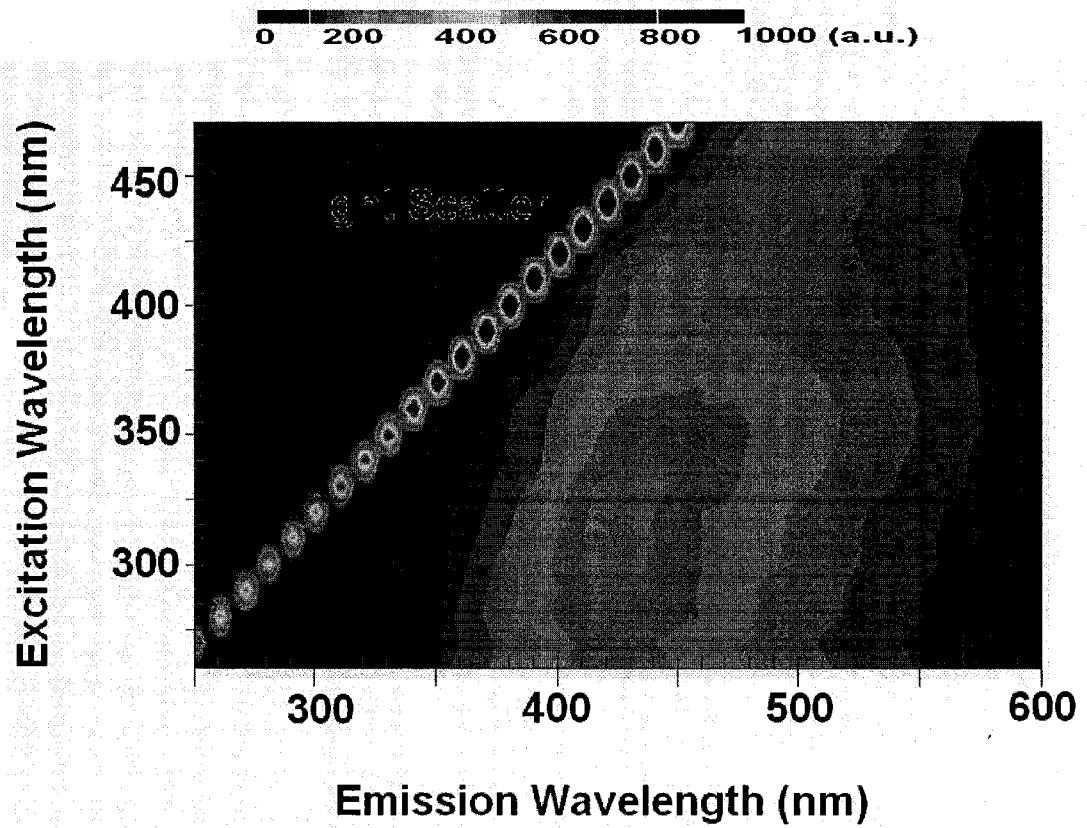


Figure 5-12c. Flare pit residue EEM – neat (using Varian Eclipse spectrometer)

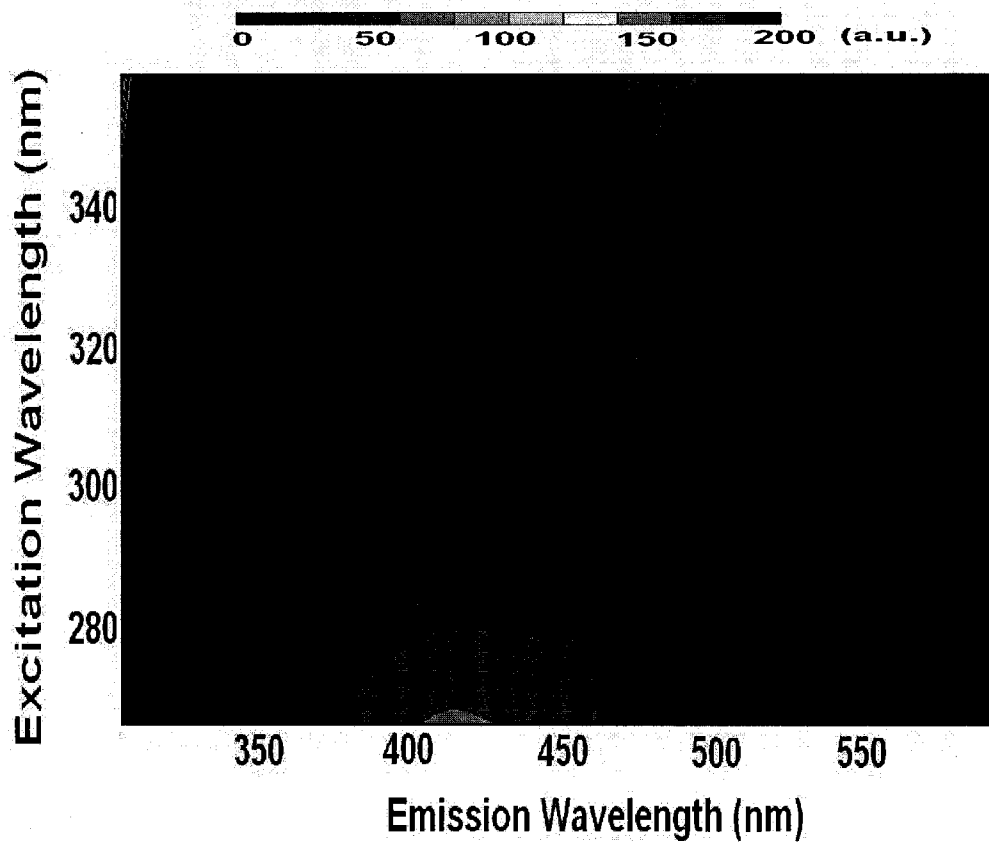


Figure 5-12f. Flare pit residue EEM – neat (using UVIF sensor)

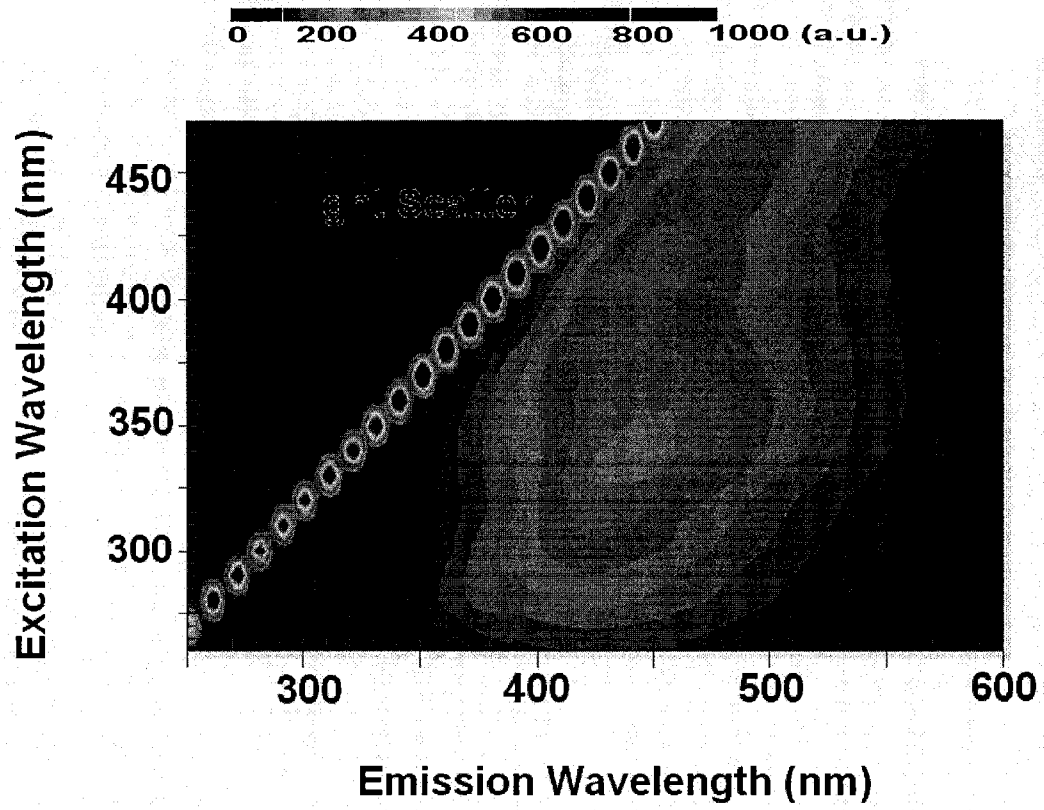


Figure 5-12g. Crude oil EEM – 40 mL/L (using Varian Eclipse spectrometer)



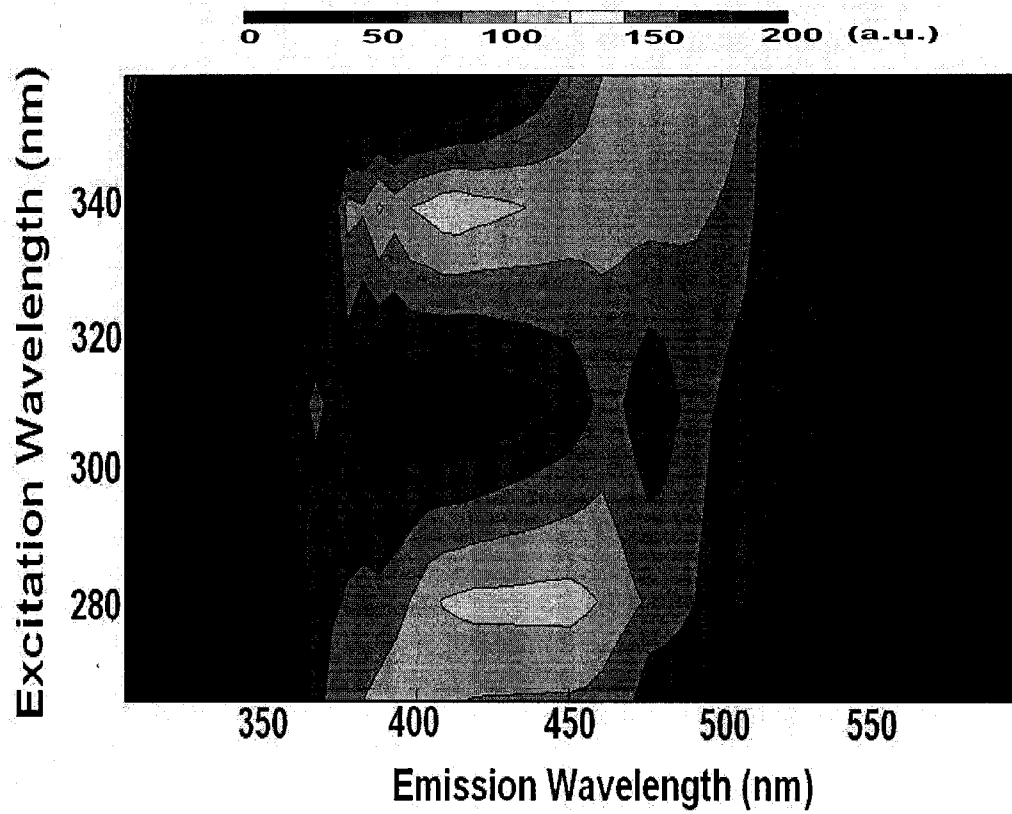


Figure 5-12h. Crude oil EEM – 40 mL/L (using UVIF sensor)

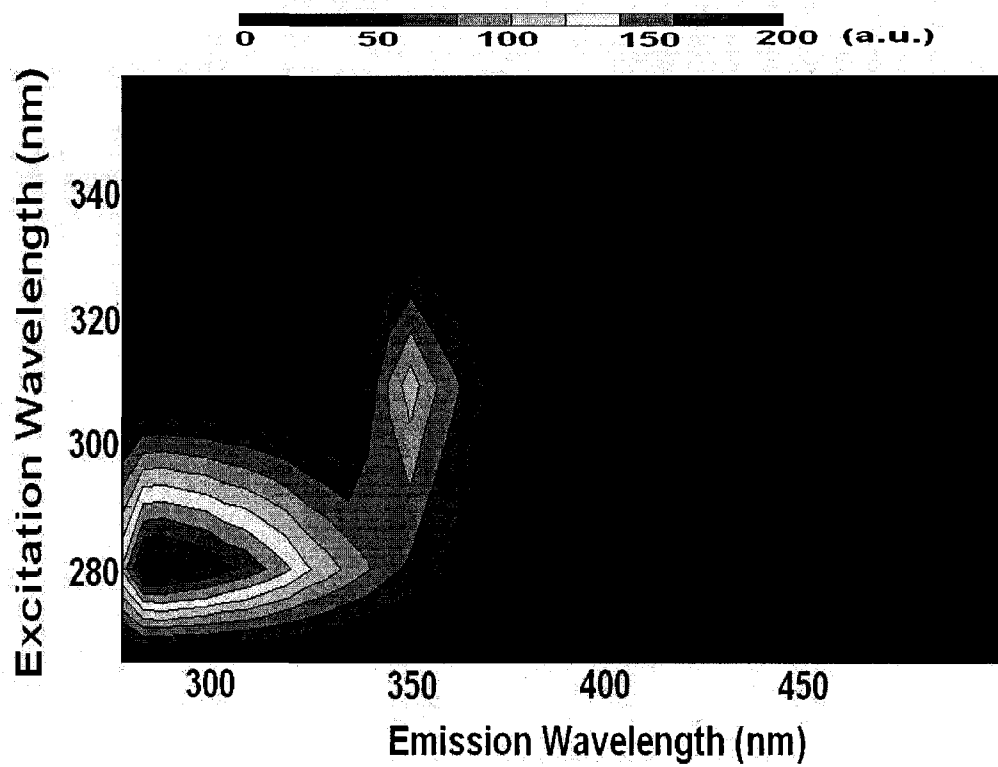


Figure 5-13a. Gasoline EEM at solution concentration of 50 mL/L

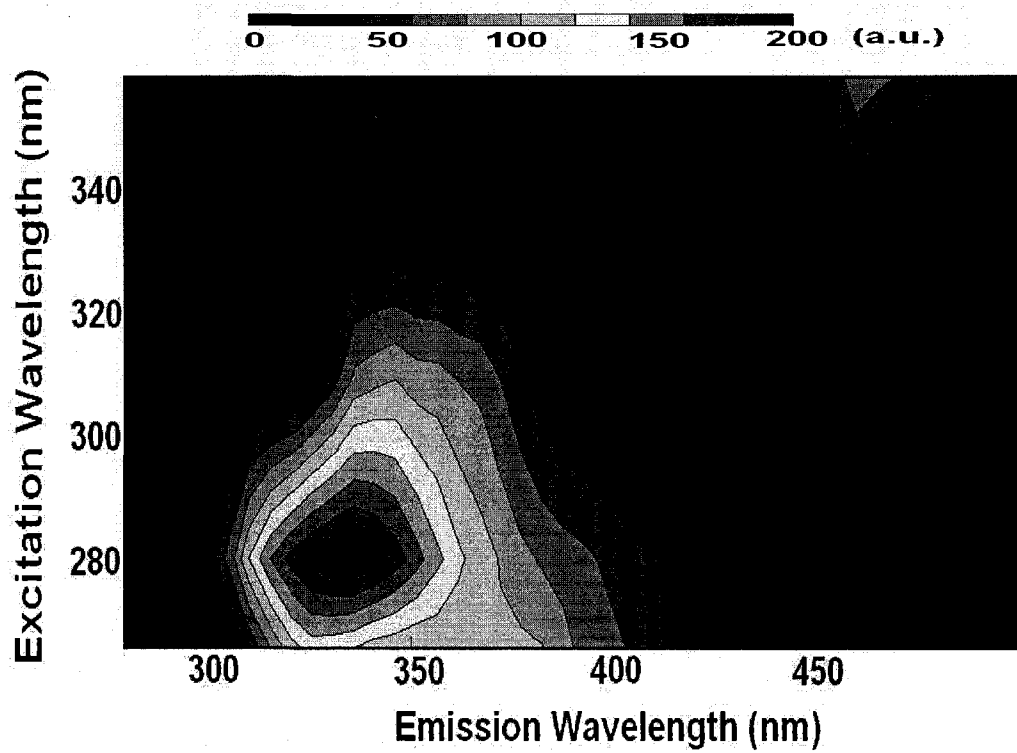


Figure 5-13b. Neat gasoline EEM

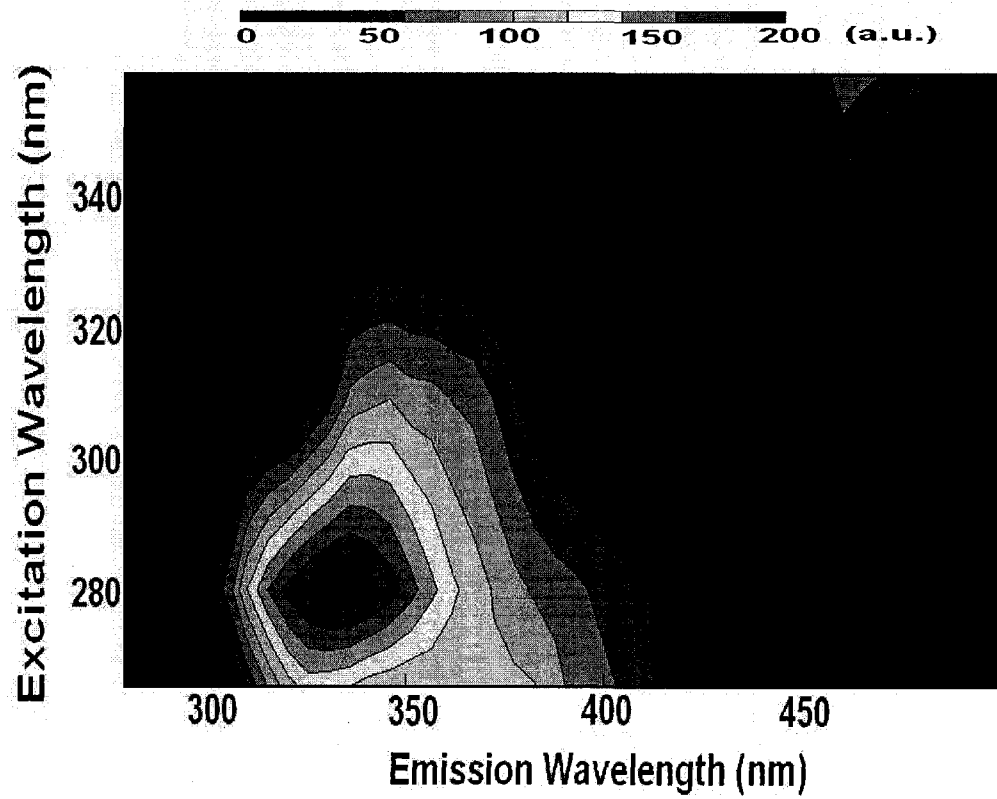


Figure 5-14a. Gasoline EEM in solvent solution

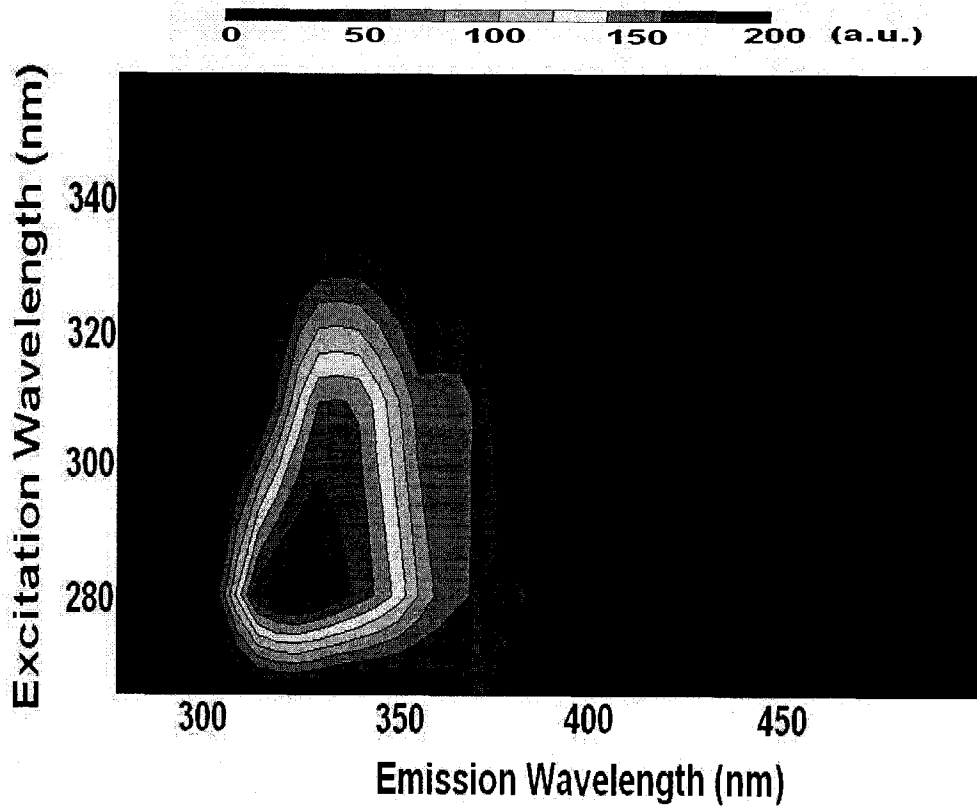


Figure 5-14b. Gasoline EEM in Ottawa sand

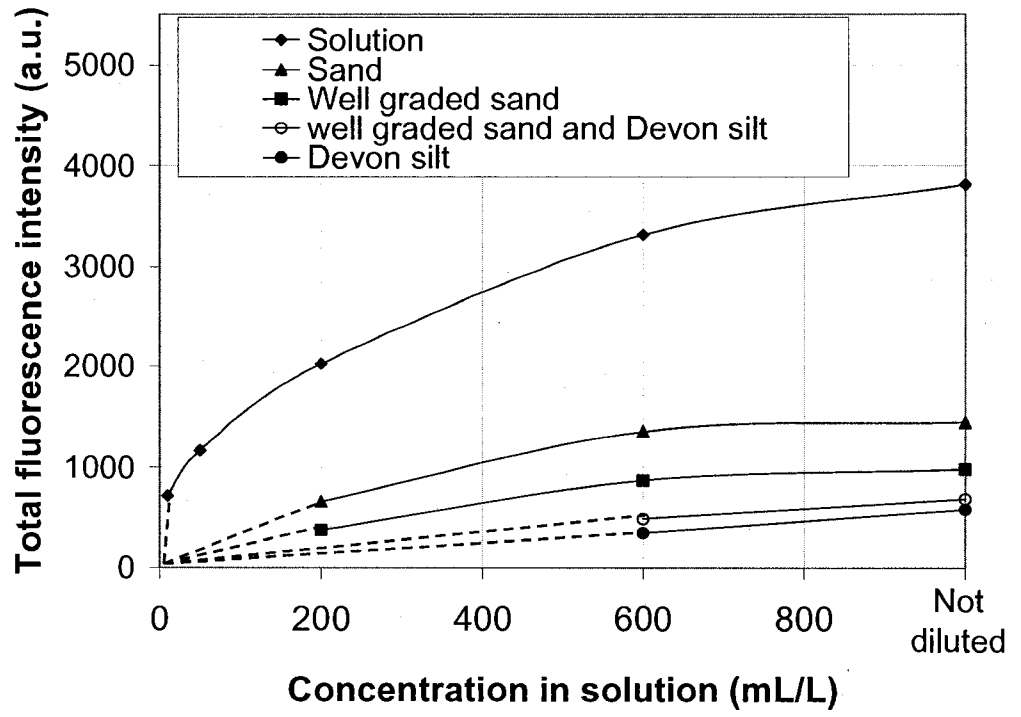


Figure 5-15a. Effect of soil matrix on gasoline total fluorescence intensity

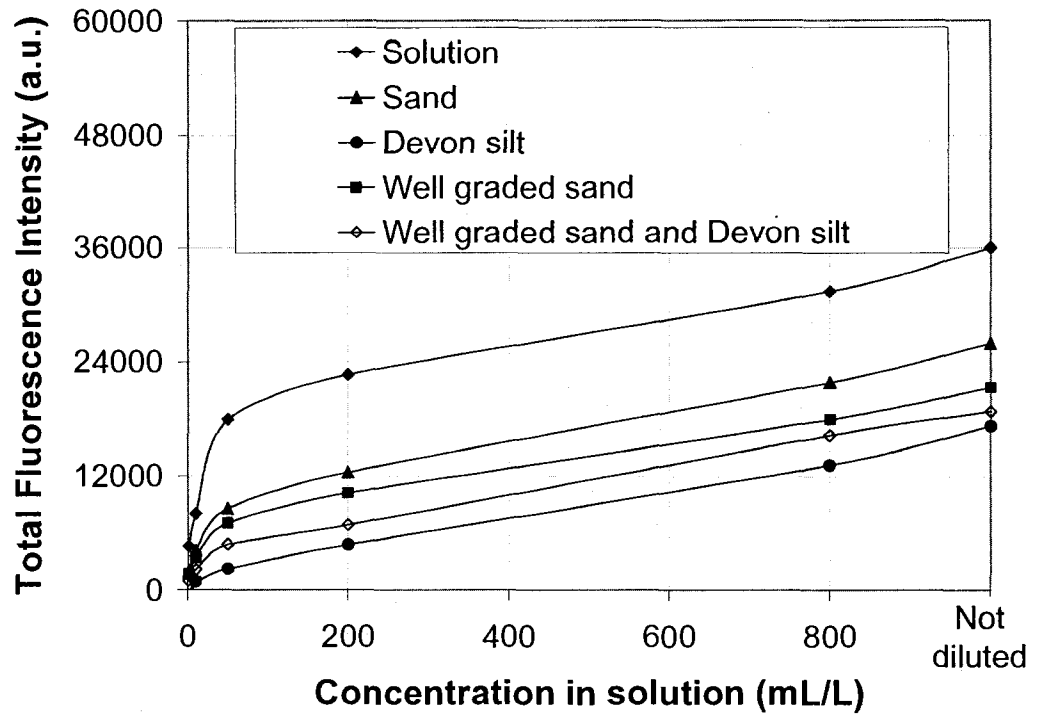


Figure 5-15b. Effect of soil matrix on diesel total fluorescence intensity

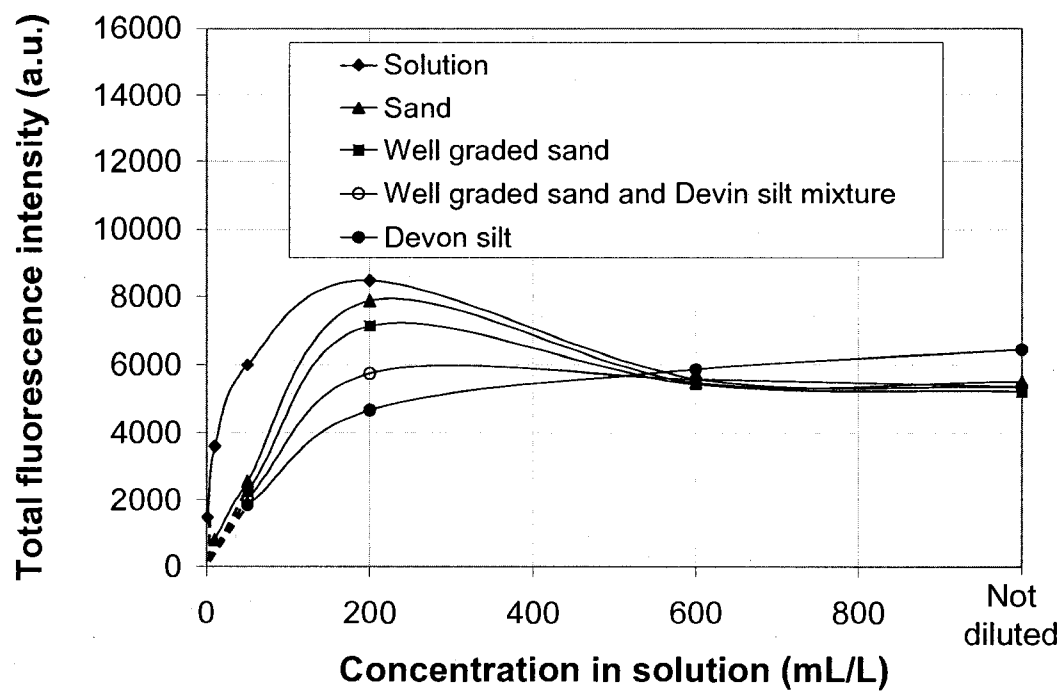


Figure 5-16a. Effect of soil matrix on flare pit residue total fluorescence intensity



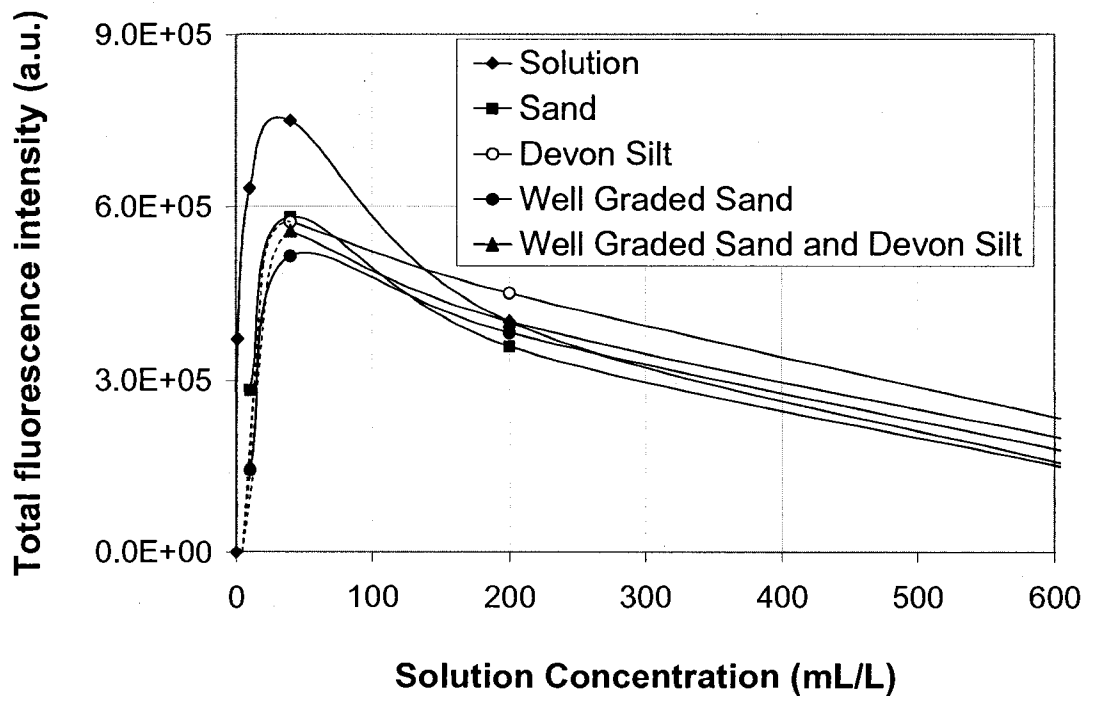


Figure 5-16b. Effect of soil matrix on crude oil total fluorescence intensity

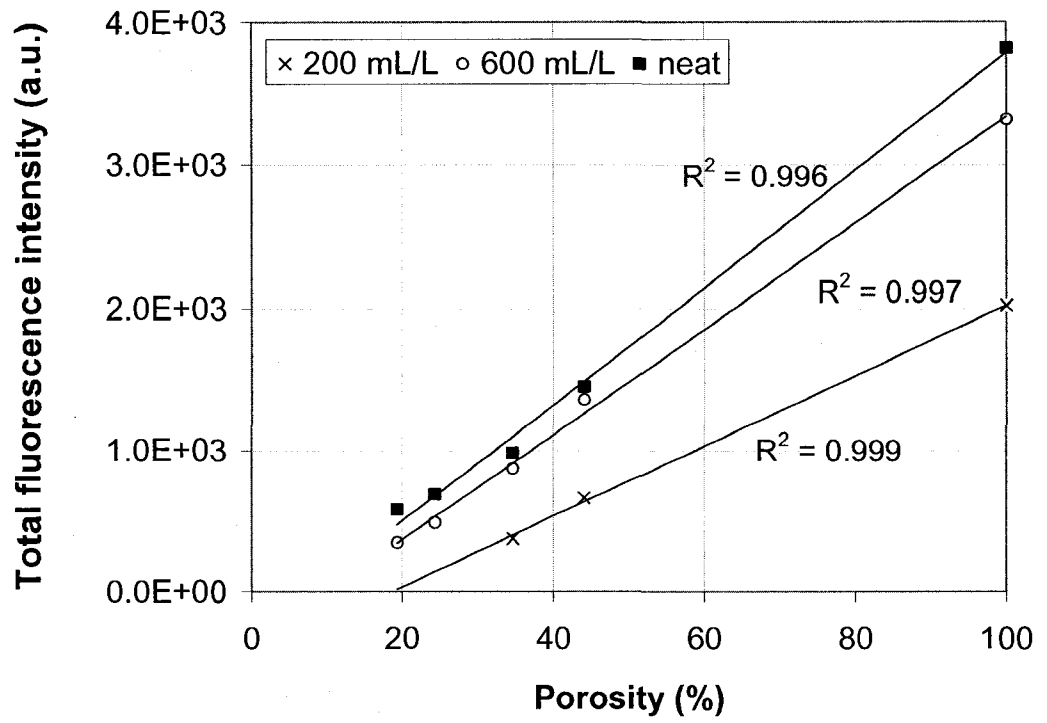


Figure 5-17a. Total fluorescence intensity of gasoline versus tested soil porosities

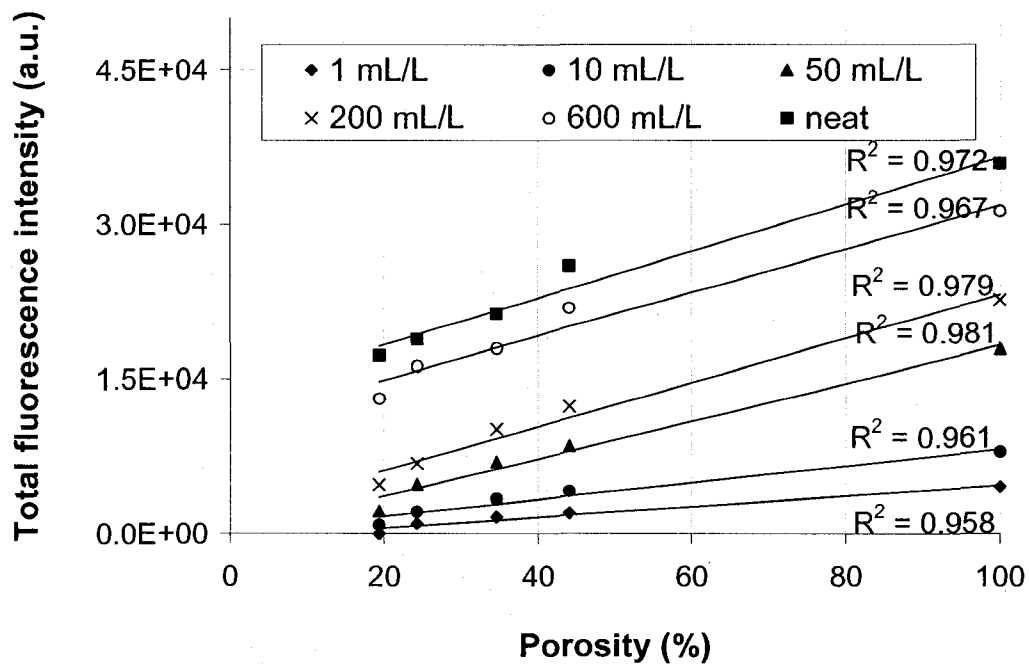


Figure 5-17b. Total fluorescence intensity of diesel versus tested soil porosities

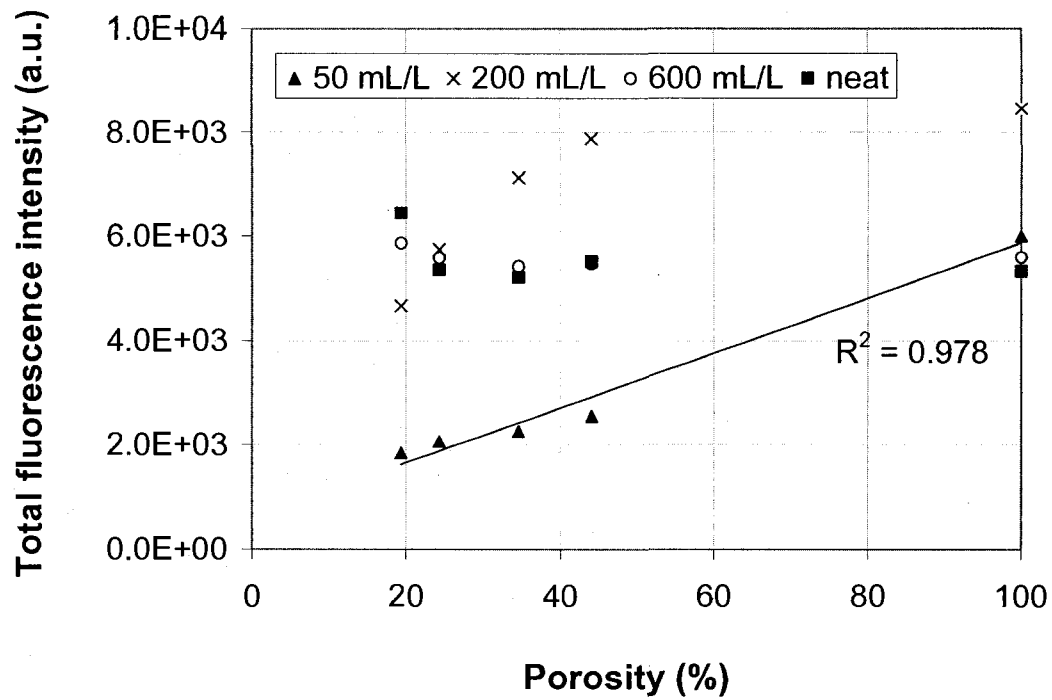


Figure 5-17c. Total fluorescence intensity of flare pit residue versus tested soil porosities

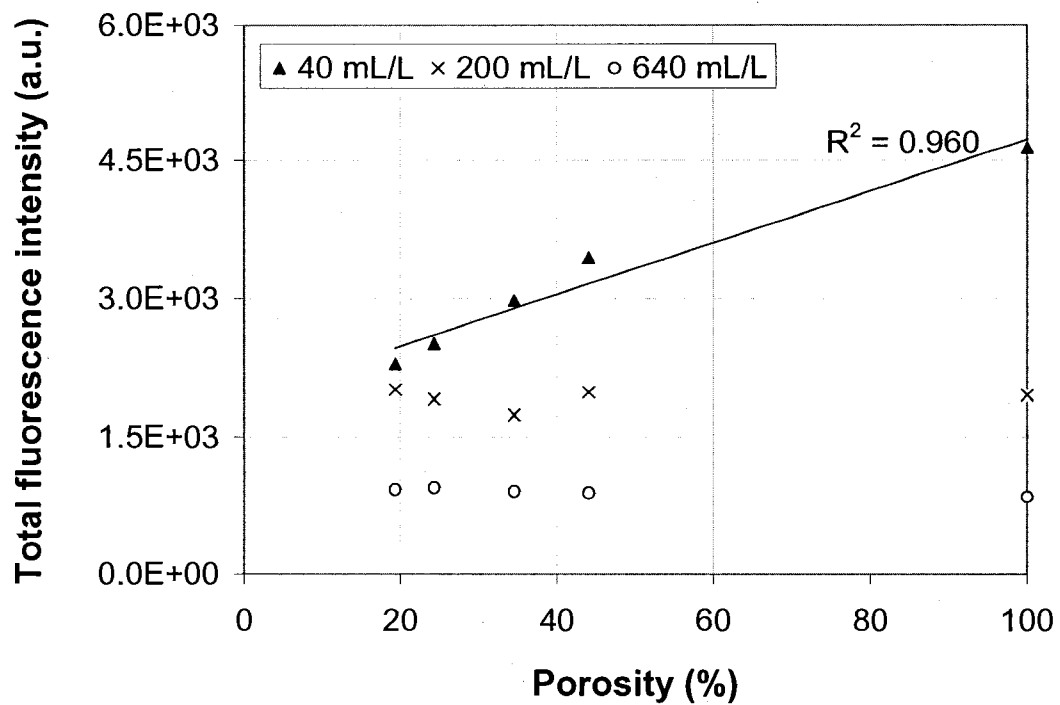


Figure 5-17d. Total fluorescence intensity of crude oil versus tested soil porosities

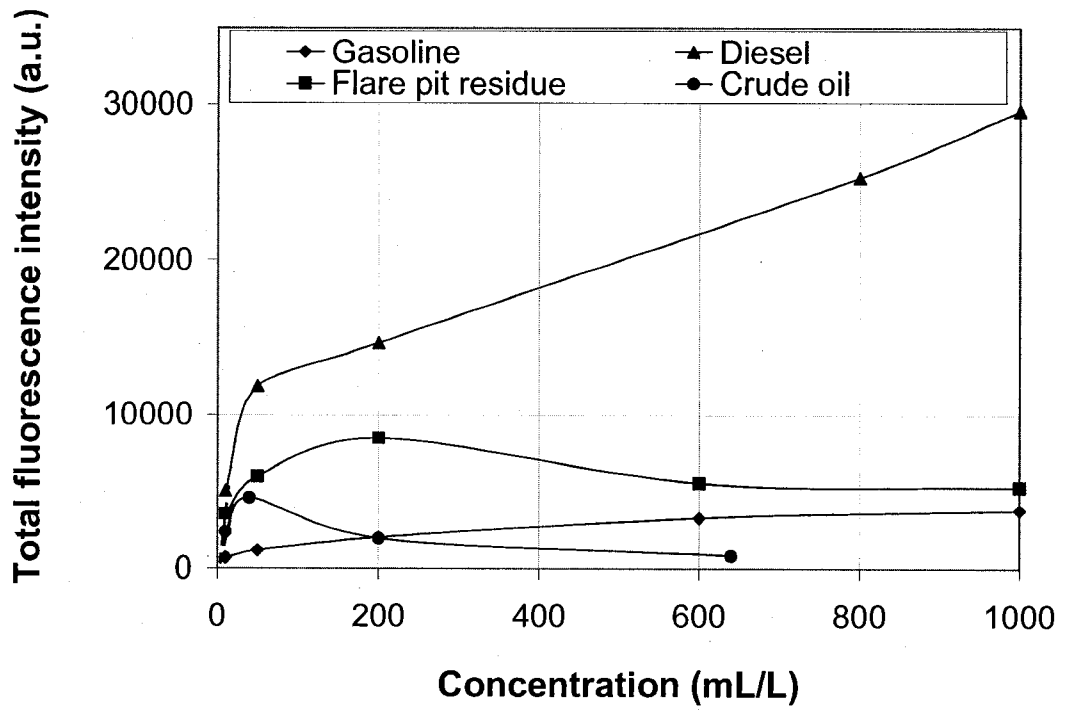


Figure 5-18a. Fluorescence intensity calibration curves of tested petroleum products in solution

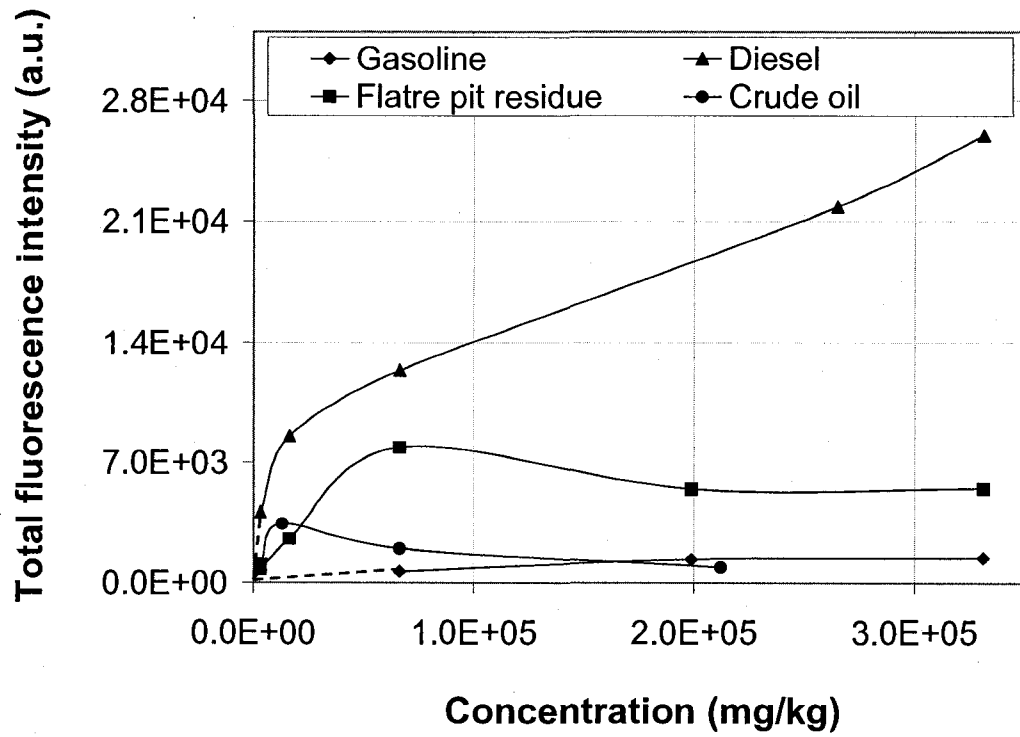


Figure 5-18b. Fluorescence intensity calibration curves of tested petroleum products in Ottawa sand

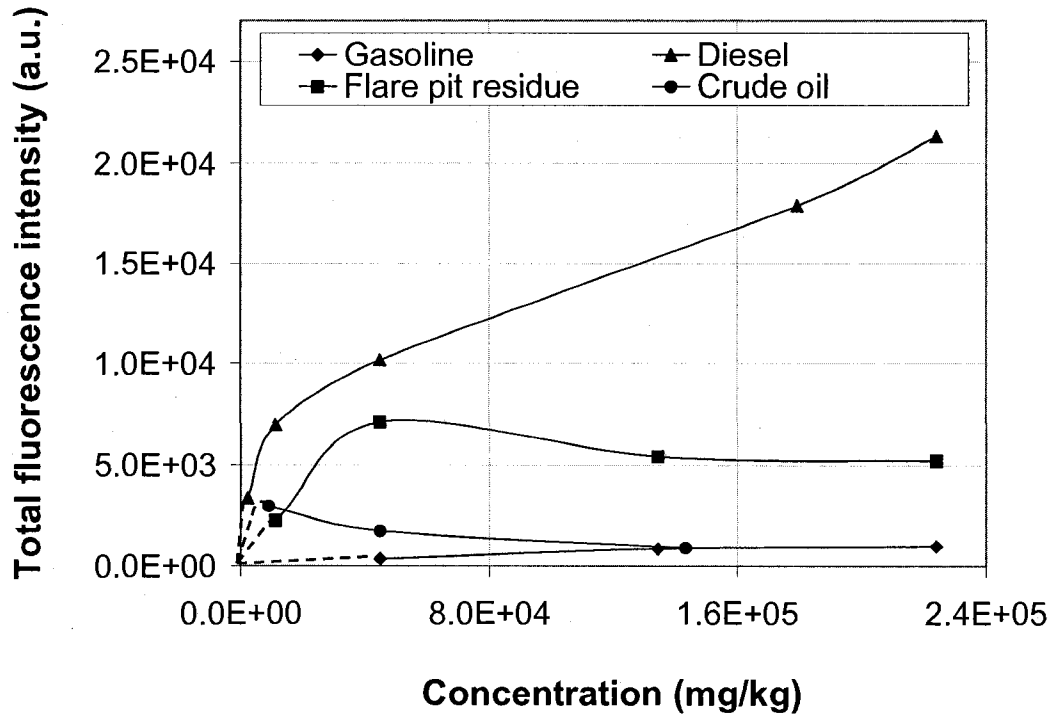


Figure 5-18c. Fluorescence intensity calibration curves of tested petroleum products in well graded sand



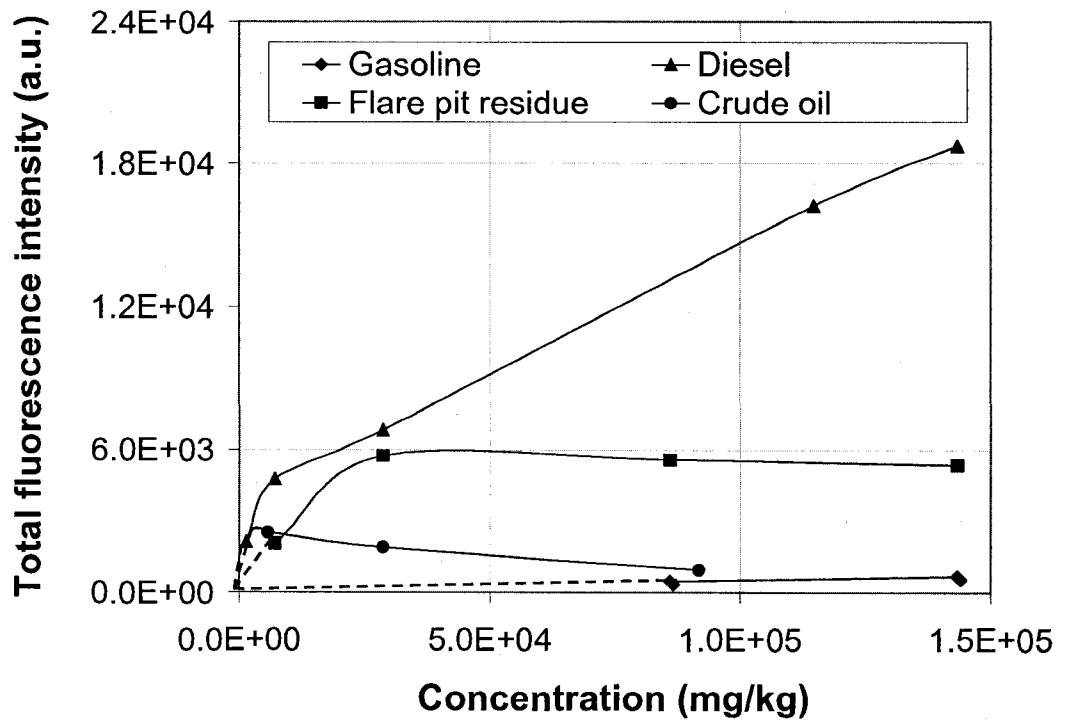


Figure 5-18d. Fluorescence intensity calibration curves of tested petroleum products in well graded sand and Devon silt

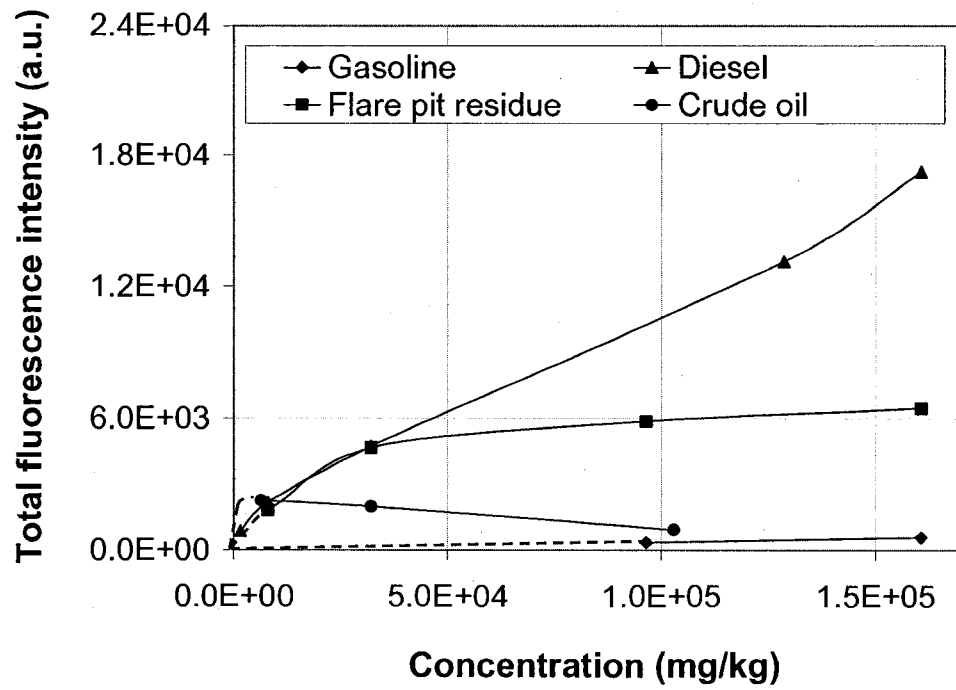


Figure 5-18e. Fluorescence intensity calibration curves of tested petroleum products in Devon silt

## 5.7. REFERENCES

- Arenson, L.U., Xia, D., Biggar, K.W., and Segó, D.C. 2005. Freezing Process in Devon Silt - Using Time Laps Photography. In Proceedings of the 58th Canadian Geotechnical Conference, Saskatoon, SK.
- Biggar, K., Woeller, D., Murphy, S., and Armstrong, J. 2003. CPT-UVIF Characterization at Upstream Oil and Gas Facilities. In Proceedings of the 17<sup>th</sup> Annual Vancouver Geotechnical Society Symposium: Geotechnical Engineering for Geoenvironmental Applications, Vancouver, BC. pp 31-37.
- Christensen, J., Hansen, A., Mortensen, J. and Andersen, O. 2005. Characterization and Matching of Oil Samples Using Fluorescence Spectroscopy and Parallel Factor Analysis. *Analytical Chemistry*, 77, pp. 2210-2217.
- Eastwood, D. (in E. Wehry, E. Editor). 1981. Modern Fluorescence Spectroscopy (Vol. 4). Plenum Press, New York, N.Y.
- Gouzman, M., Lifshitz, N., Luryi, S., Semyonov, O., Gavrilov, D. and Kuzminskiy, V. 2004. Excitation-Emission Fluorimeter Based on Linear Interference Filters. *Applied Optics*, 43, pp. 3066-3072.
- Hart, S. and Jiji, R. 2002. Light Emitting Diode Excitation Emission Matrix Fluorescence Spectroscopy. *Analyst*, 127, pp. 1693-1699.
- Jiji, R., Cooper, G. and Booksh, K. 1999. Excitation-Emission Matrix Fluorescence Based Determination of Carbamate Pesticides and Polycyclic and Aromatic Hydrocarbons. *Analytical Chimica Acta*, 397, pp. 61-72.
- Kenny, J., Lin, J., Hart, S., Wang, W. and Namytkhine, D. 1995. Subsurface Contaminant Monitoring by Laser Fluorescence Excitation-Emission

- Spectroscopy in a Cone Penetrometer Probe. SPIE, 2504, pp. 59-67.
- Kovac, J., Peternai, L. and Lengyel, O. 2003. Advanced Light Emitting Diodes Structures for Optoelectronic Applications. *Thin Solid Films*, 433 (1-2), pp. 22-26
- Lakowicz, J. 1999. *Principles of Fluorescence Spectroscopy* (2nd Edition). Kluwer Academic/Plenum Publisher, New York, N.Y.
- Lieberman, S., Theriault, G., Cooper, S., Malone, P., Olsen, R. and Lurk, P. 1991. Rapid Subsurface In-Situ Field Screening of Petroleum Hydrocarbon Contamination Using Laser Induced Fluorescence Over Optical Fibers, In *Proceedings of the 2nd International Symposium on Field Screening Methods for Hazardous Waste Site Investigations*, Las Vegas, Nevada. Air and Waste Management Association, Pittsburgh, P.A. pp. 57-63.
- Lieberman, S. 1998. Direct-Push, Fluorescence-Based Sensor Systems for In Situ Measurement of Petroleum Hydrocarbons in Soils. *Field Analytical Chemistry and Technology*, 2, pp. 63-73.
- Lohmannsro, H. and Schober, L. 1999. Combination of Laser-Induced Fluorescence and Diffuse-Reflectance Spectroscopy for the In-Situ Analysis Of Diesel-Fuel-Contaminated Soils. *Applied Optics*, 38, pp. 1404-1410.
- Muroski, A., Booksh, K. and Myrick, M. 1996. Single-Measurement Excitation/Emission Matrix Spectrofluorometer for Determination of Hydrocarbons in Ocean Water. 1. Instrumentation and Background Correction. *Analytical Chemistry*, 68, pp. 3534 - 3538.
- Ocean Optics. 2007. <http://www.oceanoptics.com>. Accessed on February 7, 2007.

- Patra, D. and Mishra, A. 2002. Total Synchronous Fluorescence Scan Spectra of Petroleum Products. *Analytical and Bioanalytical Chemistry*, 373, pp. 304-309.
- Rho, J. and Stuart, J. 1978. Automated Three-Dimensional Plotter for Fluorescence Measurements. *Analytical Chemistry*, 50, pp. 620-625.
- Sansonetti, C. Salit, M. and Reader, J. 1996. Wavelengths of Spectral Lines in Mercury Pencil Lamps. *Applied Optics*, 35, pp. 74-79.
- Schmidt, O., Bassler, M., Kiesel, P., Knollenberg, C. and Johnson, N. 2007. Fluorescence Spectrometer-On-A-Fluidic-Chip. *Lab Chip*, 7, 626-629.
- Schulman, S. 1977. *Fluorescence and Phosphorescence Spectroscopy: Physicochemical Principles and Practice*, Pergamon Press, New York, NY.
- Sensor electronic Technology. 2007. <http://www.s-et.com>. Accessed on February 19, 2007.
- Sinfield, V., Germaine, J. and Harold, F. 1999. Effect of Soils on Laser Induced Fluorescence of BTEX Pore Contaminated Waters. *Journal of Geotechnical and Geoenvironmental Engineering*, 125, pp.1072-1077.
- St. Germain, R., Gillispie, G. and Klingfus, J. 1993. Variable Wavelength Laser System for Field Fluorescence Measurements. In *Proceedings of Field Screening Methods for Hazardous Wastes and Toxic Chemicals*, Las Vegas, NV. Air & Waste Management Association, Pittsburgh, P.A. pp.1113-1122.
- Valeur, B. 2002. *Molecular Fluorescence: Principles and Applications*. Wiley-Vec., New York, N.Y.
- Vo-Dinh, T. 1982. Synchronous Luminescence Spectrometry: Methodology and Applicability. *Applied Spectroscopy*, 36, pp. 576-585.

Wahl, J., Van Delden, J. and Tiwari, S. 2005. Multiple-Fluorophore-Specie Detection with a Tapered Fabry–Perot Fluorescence Spectrometer. *Applied Optics*, 44, pp. 5190-5197.

## Chapter 6

### Conclusions

This thesis describes the development of an original, miniature UVIF sensor, to be incorporated in the existing CPT-UVIF module to allow for the collection of fluorescence EEMs of petroleum contaminants in solutions and soils. The existing system has a detection capability that is restricted to indicating presence or absence of contaminants and only provides rough semi-quantitative information. To compliment the new sensor system, an integrated fluorescence measurement analytical procedure is proposed that employs multivariate statistical techniques, namely PARAFAC and SIMCA, along with fluorescence calibration curves. The procedure allowed characterizing and a much more definitive quantification capability for a range of petroleum products in solutions and soils.

The literature review provided a detailed understanding of the quantum physics of the fluorescence phenomenon in order to optimize proposed design changes to improve the performance of the existing CPT-UVIF system. The review indicated that PHCs have a fluorescing nature when illuminated with UV light due to the presence of  $\pi$ -electrons in the conjugated structure of their aromatic compound constituents. The fluorescence signal produced by a particular aromatic compound is unique and reflects its electron structure and can therefore be used as a *fingerprint* to identify that compound. The fluorescence signal of a compound can be generated by scanning fluorescence intensity as a function of emission wavelength and be presented as

emission or excitation fluorescence spectrum. In multi-component mixtures, the fluorescence signals could be complex due the overlap between the fluorescing compounds spectra, hence, conventional fluorescence measurements might not allow proper identification of individual compounds. Alternative fluorescence measurement analytical techniques, such as synchronous, fluorescence EEMs and time resolved spectroscopy might be used to resolve complex fluorescence signals.

Before discussing the development of fluorescence-based sensor systems to delineate PHCs in subsurface environments, the review highlighted the standard spectrometric setup typically used to collect fluorescence data including all the required electronic and optical components. A number of rapid screening systems with different fluorescence sensors coupled behind a standard geotechnical cone penetrometer were discussed in the review. Knowledge gained from the review indicated that Fluorescence EEMs appear to be a good fluorescence measurement technique to be utilized in the improved UVIF sensor because they can be obtained with a relatively simple spectrometric setup that utilizes commercially available technologies and captures all spectral features of tested analytes in one 3 or 2-dimensional presentation. Therefore, fluorescence EEMs were adapted to the fluorescence measurement technique to be used in the improved CPT-UVIF system and design criteria were set accordingly.

At the same time, a novel method that can be employed to characterize and quantify common petroleum contaminants (gas condensate, gasoline, diesel, flare pit residue



and crude oil) and their underlying aromatic components in solutions based on their fluorescence EEMs was developed using samples of these petroleum products. The characterization process started with visual examination of fluorescence EEMs collected in the laboratory using a Varian Eclipse fluorescence spectrometer that indicated each of tested petroleum products has a unique fluorescence signature that can be used as an identification fingerprint. After that, fluorescence EEMs of analyzed petroleum products were decomposed by PARAFAC analysis and subsequently tested samples were classified by SIMCA analysis. PARAFAC modelled emission spectra of underlying PAH components were correlated to fluorescence spectra of PAH standards and it was found that BTEX compounds, naphthalene/methylnaphthalene, phenanthrene, and to lesser extent pyrene, were the major PAH components of the analyzed petroleum products. Laboratory chemical analysis results validated this finding. PARAFAC-generated relative concentration profiles of PAH components in analyzed petroleum products were subsequently utilized by SIMCA to analytically differentiate between tested petroleum products. SIMCA demonstrated promising discrimination power to distinguish between petroleum products samples that could allow identifying petroleum contaminants in environmental samples without pre-separation steps. General detection limits and calibration curves were presented for different petroleum contaminants based on the relationship between fluorescence intensity of different petroleum products and their concentrations in solutions. The generated calibration curves could allow estimating the concentration of petroleum products in solution based on total fluorescence intensity values of their EEMs. Furthermore, the proposed analysis method allowed

estimating concentrations of major PAH components in analyzed petroleum products in solutions using PARAFAC, estimating relative concentrations of these components with reasonable accuracy in the range of +/- 50% of values obtained by laboratory chemical analysis. The result of using the proposed fluorescence measurement analytical procedure indicated that the method provides a quick and efficient framework for characterization and quantification of different petroleum contaminants in solutions that can be easily adapted to in situ measurements.

The laboratory testing program was extended to include petroleum contamination in a variety of soil samples that may be encountered in the field, to characterize the factors affecting fluorescence measurements in soils. The experimental program used a range of soils that reflect various grain size distributions, porosity and mineralogy. The tested soil samples included: Ottawa sand, well graded sand, well graded sand and Devon silt mixture and Devon silt. No measurable effects of mineralogy were observed in the soils tested. The test results also indicated that soils tested had no measurable effect on the shape of fluorescence signal of the tested petroleum products. However, for a given contaminant concentration, the porosity of the soil had a significant effect on fluorescence signal intensity. The effect varied based on soil grain sizes and degree of sorting, as well as type of petroleum contaminant. In general, fluorescence signal intensity decreased linearly as soil porosity decreased. However, fluorescence intensity increased at higher concentrations of contaminants known to be highly affected by fluorescence quenching as soil porosity decreased. A fluorescence measurement analytical procedure similar to the one used with solution

samples was utilized with petroleum contaminated soil samples. Visual examination of fluorescence EEMs indicated that petroleum products maintained a unique fluorescence signature that can be utilized to identify them. PARAFAC and SIMCA demonstrated strong capabilities to characterize gas condensate, gasoline, diesel, flare pit residue and crude oil and their underlying aromatic components in soil samples using their fluorescence EEMs. The PARAFAC modeling results indicated that the analyzed petroleum products are mainly composed of BTEX compounds, naphthalene / methylnaphthalene, phenanthrene, and to lesser extent pyrene, which agrees with chemical analysis results for the same analytes. SIMCA was able to distinguish between different analyzed petroleum products and crude oil samples in the soils tested. Also, this study presents a calibration procedure that takes into consideration the effect of soil matrix and allows estimation of the concentration of various petroleum products in soil matrices based on their EEMs total fluorescence intensity values. The procedure has proven to be a quick and efficient quantification method of different petroleum contaminants in soil samples with minimum human intervention that can be utilized in field fluorescence measurements.

Upon the completion of the design improvements, the UVIF sensor was assembled by the technical team at Conetec (Vancouver, BC). The improved UVIF sensor was based on a commercially available small size multi-wavelength UV LED (as the excitation source) and an LVF (as the emission wavelength selection element). The sensor was carefully designed and assembled to fit entirely inside standard cone penetration penetrometer, eliminating the use of fibre optics and allowing

fluorescence measurements to be performed down-hole. The improvement allowed the UVIF-CPT to collect multi-way fluorescence spectral data, and fluorescence EEMs of detected petroleum contaminants in subsurface environments, which would help in assessing the identity and quantity, to some extent, of these petroleum products. Before proceeding with testing, The LVF in the sensor was spectrally calibrated using a mercury lamp. Also, corrections were applied to account for instrumentation interference and scattered light. Preliminary testing indicated that the LVF contained an opaque band that prevented detection of radiation occurring between wavelengths 419 and 450 nm. A laboratory testing program was conducted to test the performance of the UVIF with samples of similar petroleum products to the ones used in earlier parts of the study. The tested petroleum products included: gas condensate, gasoline, diesel, flare pit residue and crude oil. Samples of each product were tested at different concentrations in solvent solutions and soils simulating a variety of field conditions. Soil used in this study include: Ottawa sand, well graded sand, well graded sand and Devon silt, as well as Devon silt representing a wide range of grain size distributions and sorting degrees. The instrument was capable of detecting and generating fluorescence signals of tested petroleum products, except gas condensate, in solvent solutions and soils at concentration levels as low as 1 mL/L in certain cases. The gas condensate was not detected because it has a low intensity fluorescence emission peak at 290 nm that falls within a wavelengths range at which the LVF has very low transmission allowance. Given that a fluorescence signal was obtained with the Varian Eclipse but not the UVIF module for the gas condensate, if a different LVF with higher light transmission allowance at shorter wavelength and/or a

more intense excitation source is used, it may be possible to detect the gas condensate fluorescence signal with the UVIF module. Collected fluorescence signals of tested petroleum products were presented as fluorescence spectra and EEMs that can be employed to characterize these petroleum contaminants in solvent solutions and soils either at the field or in laboratory settings. The UVIF sensor-generated fluorescence spectra and EEMs were verified against ones collected using the Varian Eclipse spectrometer in earlier parts of the study and found to be in reasonable agreement. The presence of the opaque band on the LVF created a gap of missing fluorescence data that introduced minor changes to fluorescence spectra and EEMs generated by the UVIF sensor in comparison to the ones collected by Varian Eclipse spectrometer. The introduced changes did not significantly affect the integrity of the spectral features of the collected fluorescence data allowing efficient visual identification of tested petroleum products. However, these changes did not permit proper fluorescence data modelling using PARAFAC and SIMCA as demonstrated in earlier parts of the study; therefore, utilizing these multivariate statistical techniques was set aside. Examining fluorescence spectral data of tested petroleum products in solvent solution and soil samples indicated that soils had no measurable effect on the shape of fluorescence signal. For a given contaminant concentration, the soil had a significant effect on fluorescence signal intensity. Typically, fluorescence intensity of petroleum products in soils samples decreased linearly as the porosity of tested soils decreased. The relationship departed from linearity at higher concentrations of petroleum products that are more susceptible to fluorescence quenching. For quantitative purposes, calibration curves similar ones obtained earlier for tested petroleum

contaminants that are based on the relationship between fluorescence intensity and concentrations in solvent solutions and soils were obtained and showed good agreement with previous ones. As utilized before, the obtained calibration curves can be used to estimate laboratory and in situ concentration of petroleum products under investigation using their total fluorescence intensity values.

The research work presented in this thesis shows that the enhanced quality of fluorescence data collected by the improved UVIF for tested petroleum products along with the suggested fluorescence measurements analysis framework provide a rapid, reliable and objective tool and procedure that can be applied for petroleum contaminant characterization and semi-quantification in subsurface environments to help in planning further environmental site investigation and remediation activities, and provide a rough idea about future screening and clean up decisions. The robustness, efficiency and cost effectiveness of the improved CPT-UVIF system is expected to stimulate a wider spread of the technology applications in geo-environmental site investigation. The performance of the improved UVIF-CPT can be further refined in future research projects that might address the following issues:

- 1- Extend the range of tested petroleum products to include samples that reflect diversified sources origins, refinement procedures and aging processes. These factors are expected to have an effect on generated fluorescence signals, which could impact the characterizing and quantifying capabilities of the suggested

fluorescence measurement analysis procedure. Therefore, these factors should be investigated.

- 2- Examine more samples of the tested petroleum products in solutions and soil samples at lower concentrations than used in this study to refine the obtained detection limits of the suggested fluorescence measurement methodology.
- 3- Resolve the problem encountered with operating LED on higher pulsed current, so higher excitation intensities could be generated by the LED to allow obtaining stronger fluorescence intensities from more diluted petroleum product solution and soil samples.
- 4- Source an alternative LVF that does not contain an opaque band and one that allows higher radiation transmission at shorter wavelengths. This should allow collecting more complete fluorescence EEMs of analyzed petroleum contaminants that can be further analyzed using multivariate statistical techniques such as PARAFAC and SIMCA. Also, better radiation transmission allowance should permit detecting weaker fluorescing petroleum products such as natural gas condensate.

#### **ACKNOWLEDGMENTS**

This project was funded The University of Alberta - NSERC – ConeTec – EnCana – WorleyParsons Komex Improved Site Characterization Research Project. The author acknowledges the technical assistance of Mr. Steve Gamble and Jela Burkas at the University of Alberta Geotechnical Center, as well as, Dr. Jonathon Kenny at Tufts University and LCDR Gregory Hall at U.S. Coast Guard Academy.

Appendix A  
Fluorescence EEMs  
(*Using Varian Eclipse  
Spectrometer*)



0 200 400 600 800 1000 (a.u.)

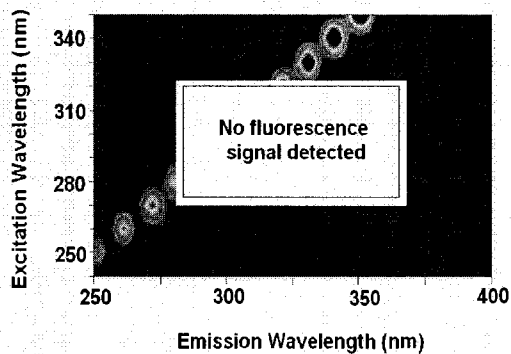


Figure A-1a. Gas condensate in hexane  
EEM (1 mL/L)

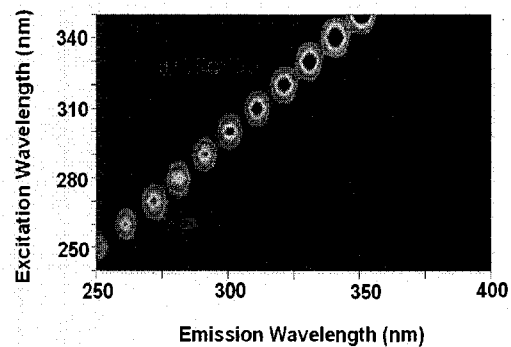


Figure A-1b. Gas condensate in hexane  
EEM (10 mL/L)

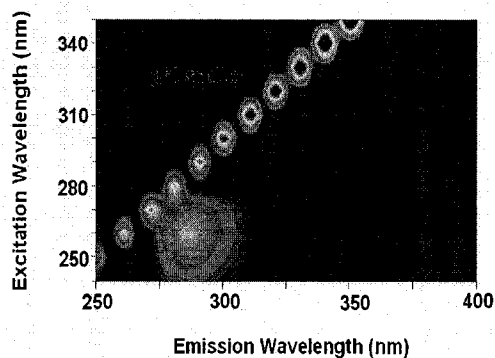


Figure A-1c. Gas condensate in hexane  
EEM (50 mL/L)

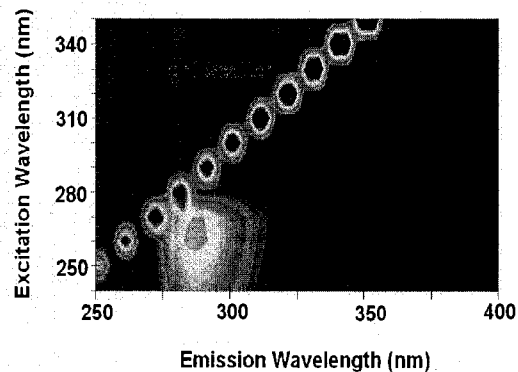


Figure A-1d. Gas condensate in hexane  
EEM (200 mL/L)

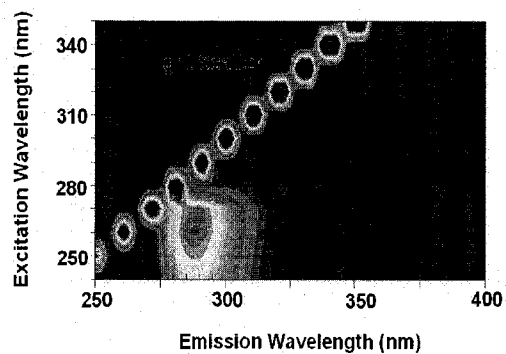


Figure A-1e. Gas condensate in hexane  
EEM (600 mL/L)

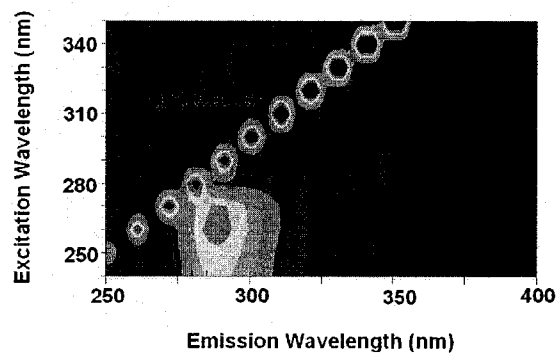


Figure A-1f. Gas condensate EEM (neat)

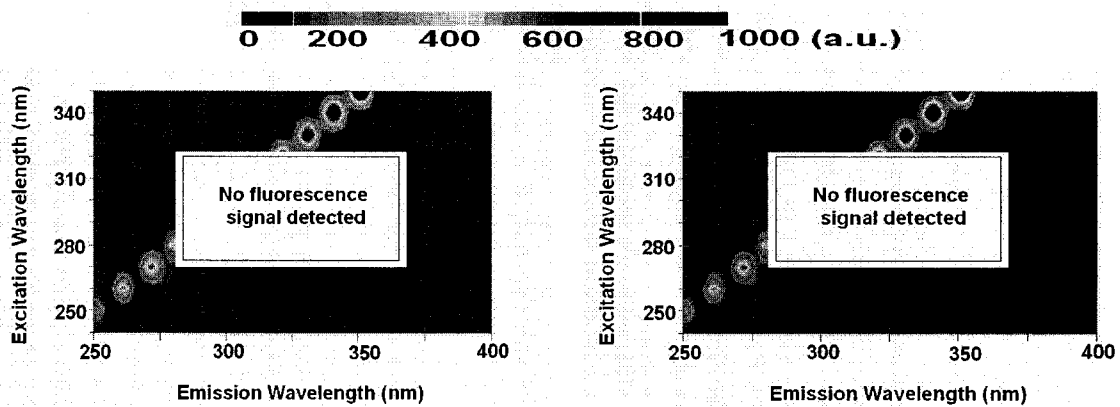


Figure A-2a. Gas condensate in Ottawa sand EEM (1 mL/L)

Figure A-2b. Gas condensate in Ottawa sand EEM (10 mL/L)

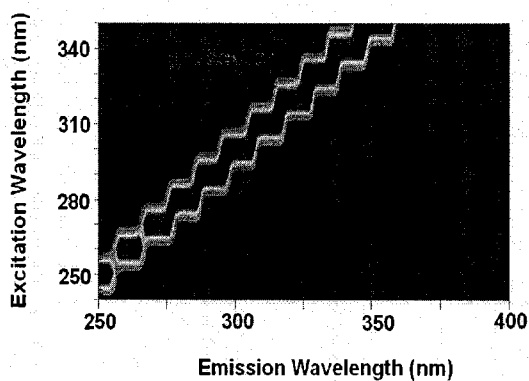


Figure A-2c. Gas condensate in Ottawa sand EEM (50 mL/L)

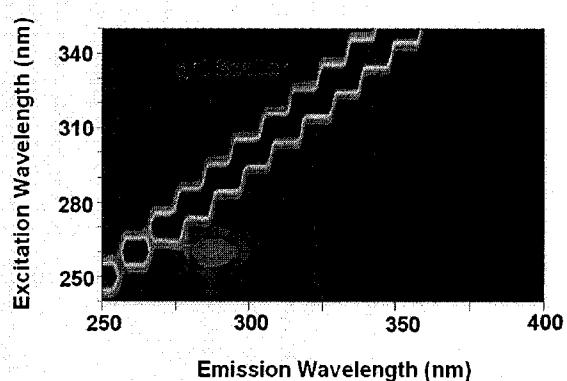


Figure A-2d. Gas condensate in Ottawa sand EEM (200 mL/L)

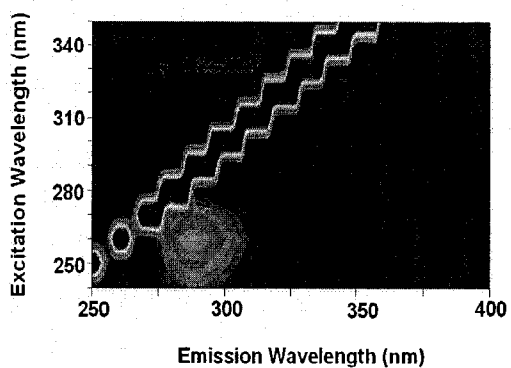


Figure A-2e. Gas condensate in Ottawa sand EEM (600 mL/L)

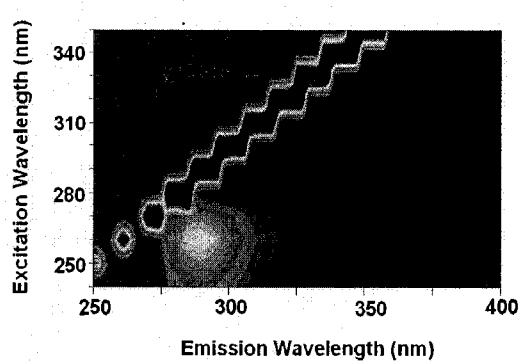


Figure A-2f. Gas condensate in Ottawa sand EEM (neat)

0 200 400 600 800 1000 (a.u.)

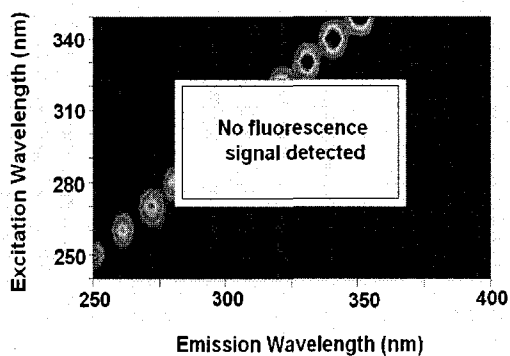


Figure A-3a. Gas condensate in well graded sand EEM (1 mL/L)

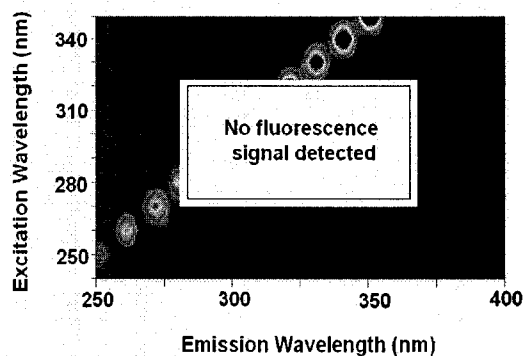


Figure A-3b. Gas condensate in well graded sand EEM (10 mL/L)

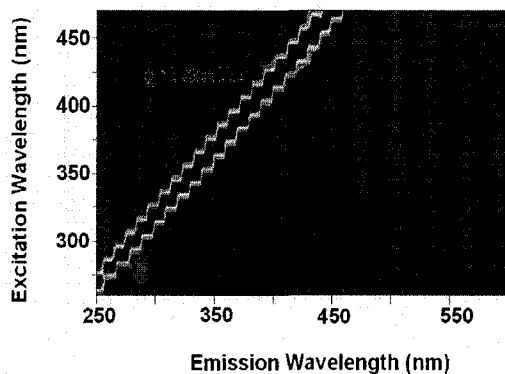


Figure A-3c. Gas condensate in well graded sand EEM (50 mL/L)

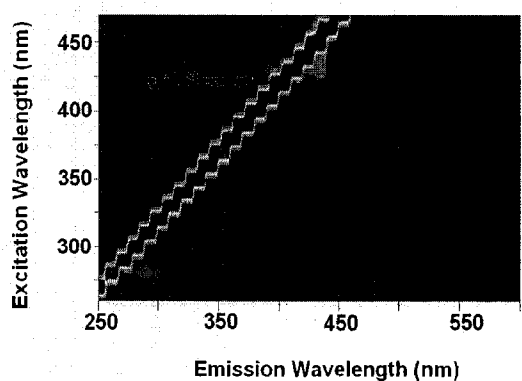


Figure A-3d. Gas condensate in well graded sand EEM (200 mL/L)

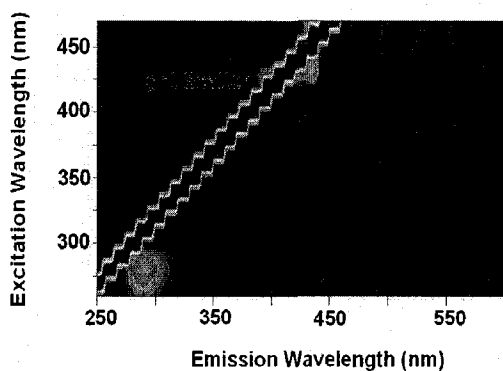


Figure A-3e. Gas condensate in well graded sand EEM (600 mL/L)

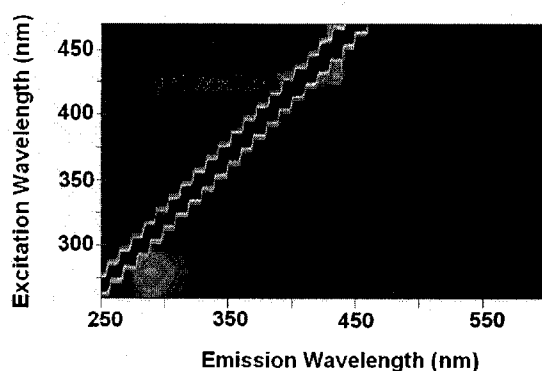


Figure A-3f. Gas condensate in well graded sand EEM (neat)

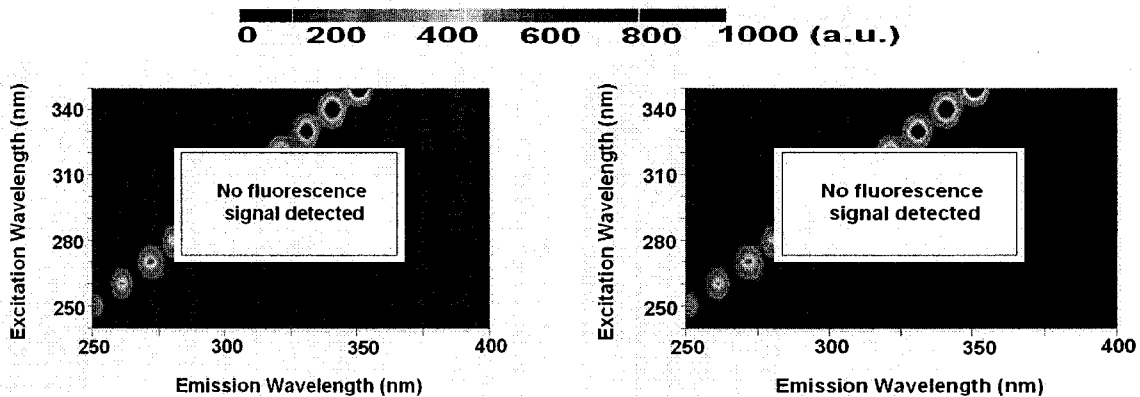


Figure A-4a. Gas condensate in well graded sand and Devon silt EEM (1 mL/L)

Figure A-4b. Gas condensate in well graded sand and Devon silt EEM (10 mL/L)

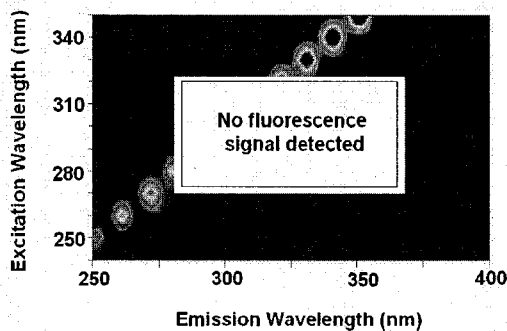


Figure A-4c. Gas condensate in well graded sand and Devon silt EEM (50 mL/L)

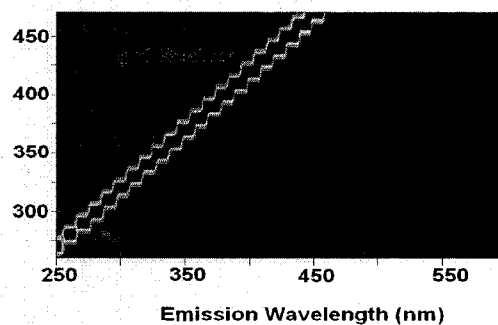


Figure A-4d. Gas condensate in well graded sand and Devon silt EEM (200 mL/L)

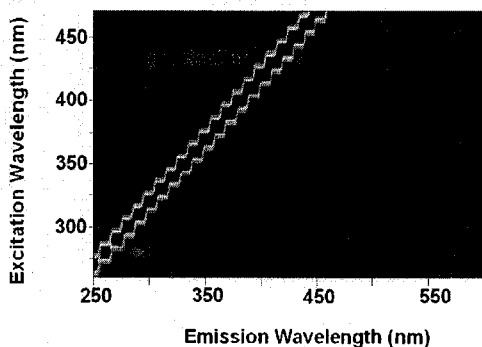


Figure A-4e. Gas condensate in well graded sand and Devon silt EEM (600 mL/L)

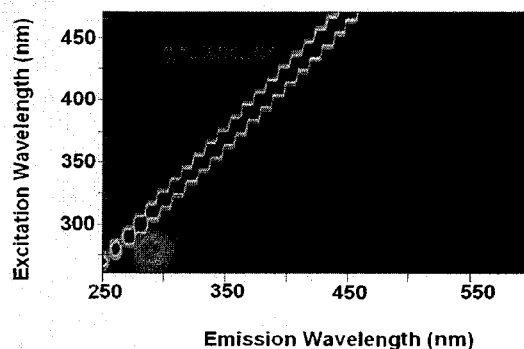


Figure A-4f. Gas condensate in well graded sand and Devon silt EEM (neat)

0 200 400 600 800 1000 (a.u.)

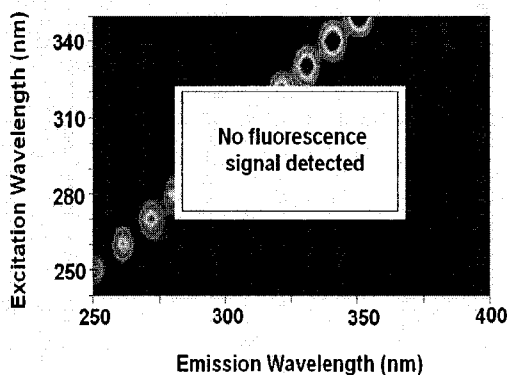


Figure A-5a. Gas condensate in Devon silt  
EEM (1 mL/L)

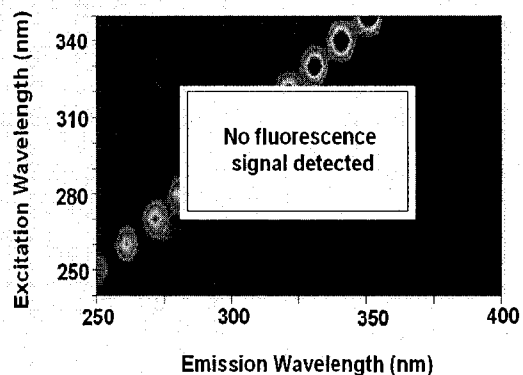


Figure A-5b. Gas condensate in Devon silt  
EEM (10 mL/L)

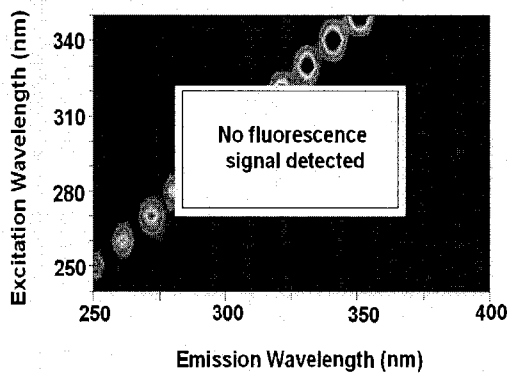


Figure A-5c. Gas condensate in Devon silt  
EEM (50 mL/L)

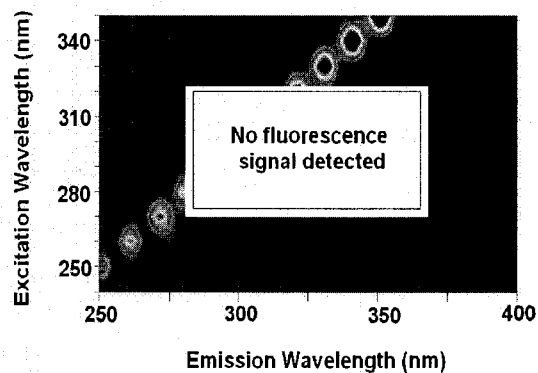


Figure A-5d. Gas condensate in Devon silt  
EEM (200 mL/L)

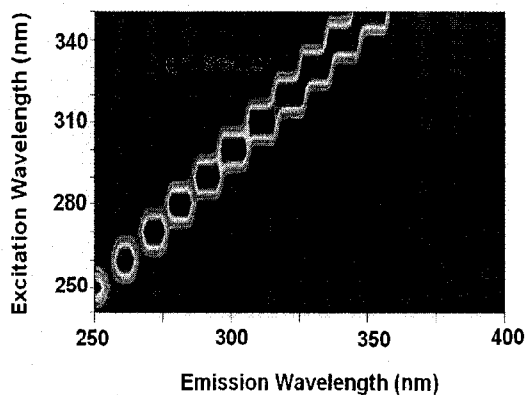


Figure A-5e. Gas condensate in Devon silt  
EEM (600 mL/L)

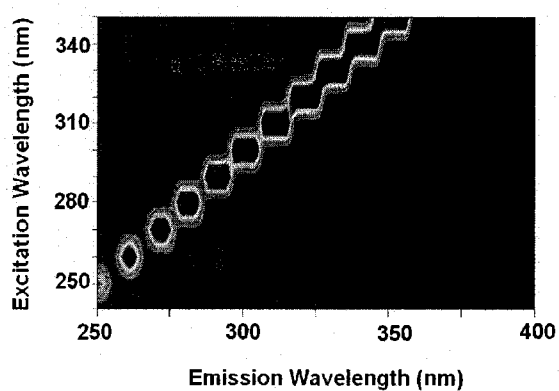


Figure A-5f. Gas condensate in Devon silt  
EEM (neat)

0 200 400 600 800 1000 (a.u.)

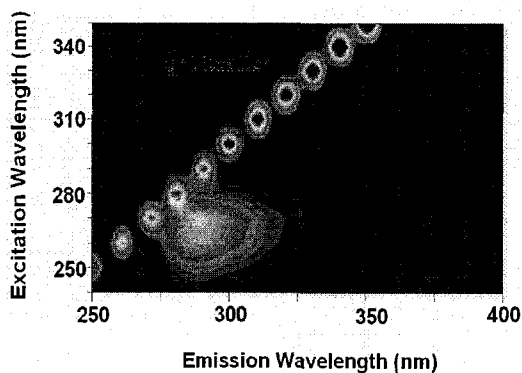


Figure A-6a. Gasoline in hexane EEM (1 mL/L)

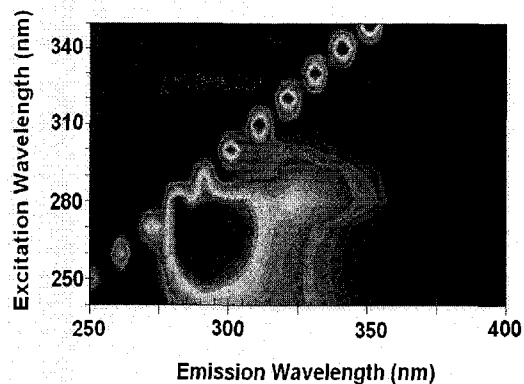


Figure A-6b. Gasoline in hexane EEM (10 mL/L)

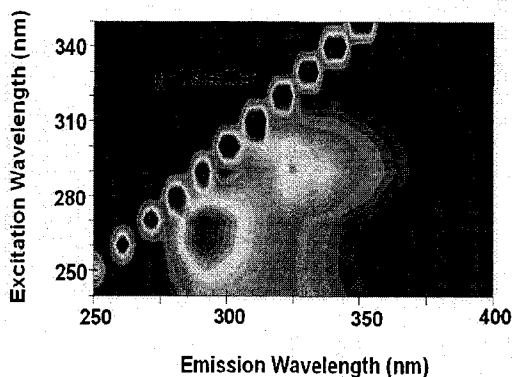


Figure A-6c. Gasoline in hexane EEM (50 mL/L)

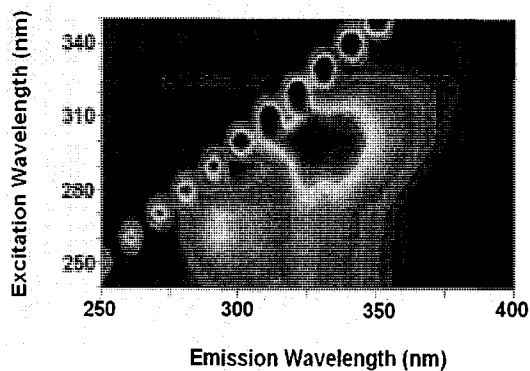


Figure A-6d. Gasoline in hexane EEM (200 mL/L)

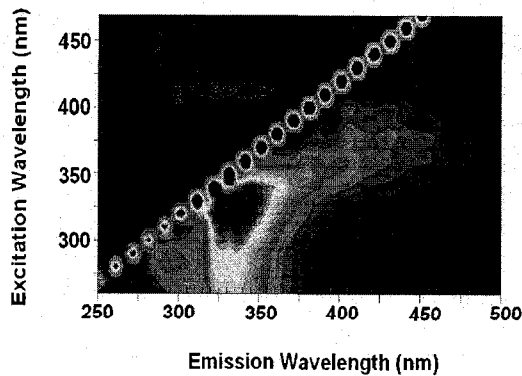


Figure A-6e. Gasoline in hexane EEM (600 mL/L)

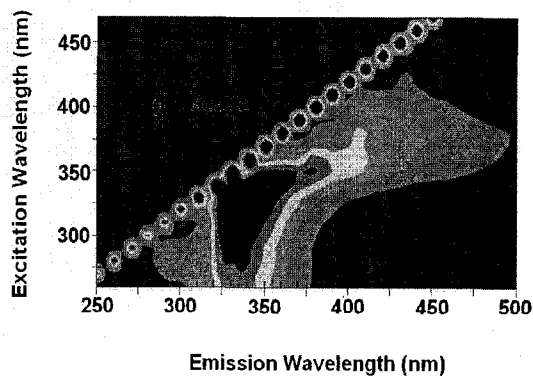


Figure A-6f. Gasoline EEM (neat)

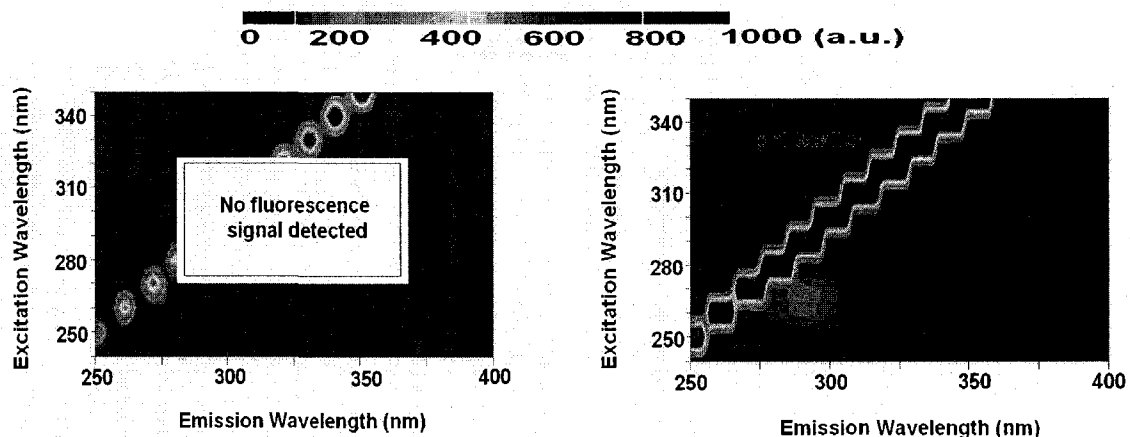


Figure A-7a. Gasoline in Ottawa sand EEM (1 mL/L)

Figure A-7b. Gasoline in Ottawa sand EEM (10 mL/L)

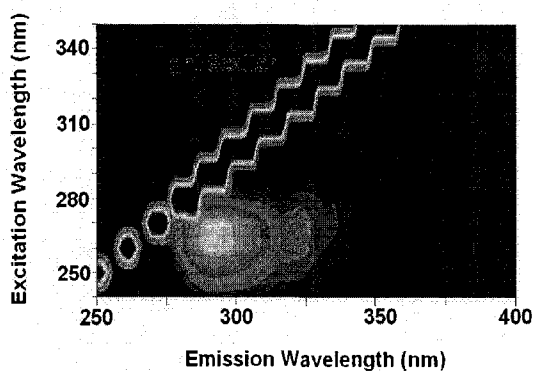


Figure A-7c. Gasoline in Ottawa sand EEM (50 mL/L)

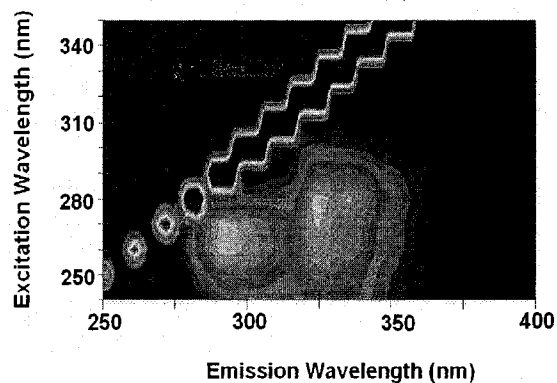


Figure A-7d. Gasoline in Ottawa sand EEM (200 mL/L)

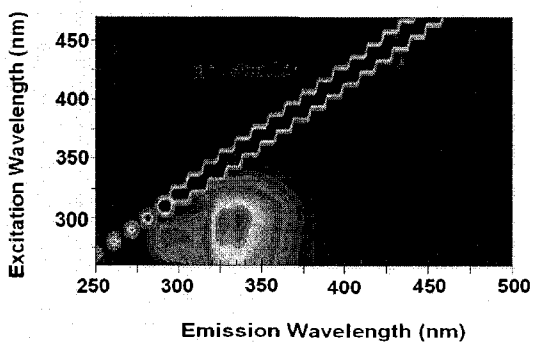


Figure A-7e. Gasoline in Ottawa sand EEM (600 mL/L)

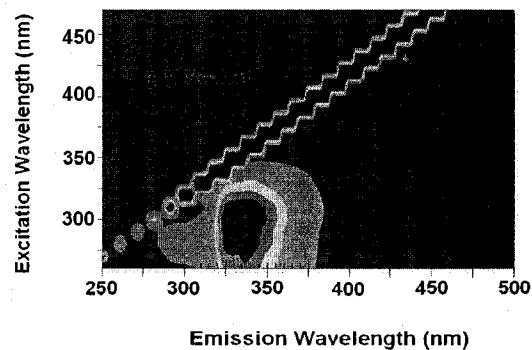


Figure A-7f. Gasoline in Ottawa sand EEM (neat)

0 200 400 600 800 1000 (a.u.)

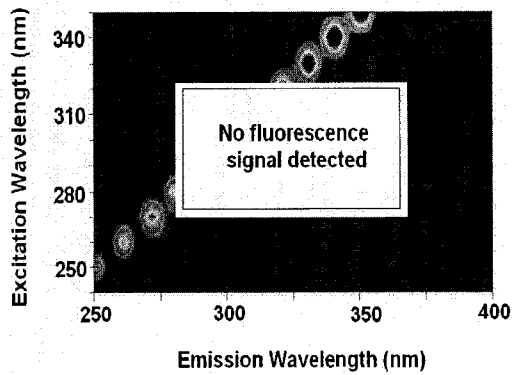


Figure A-8a. Gasoline in well graded sand  
EEM (1 mL/L)

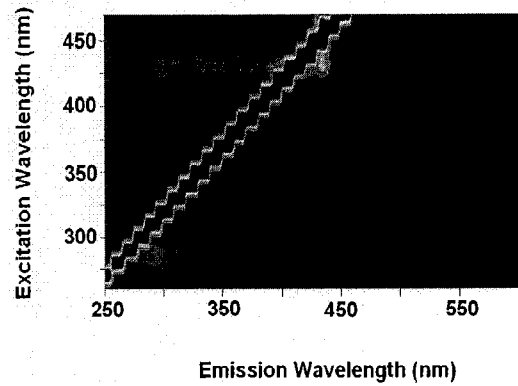


Figure A-8b. Gasoline in well graded sand  
EEM (10 mL/L)

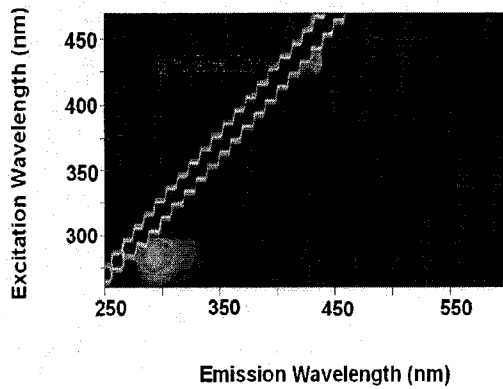


Figure A-8c. Gasoline in well graded sand  
EEM (50 mL/L)

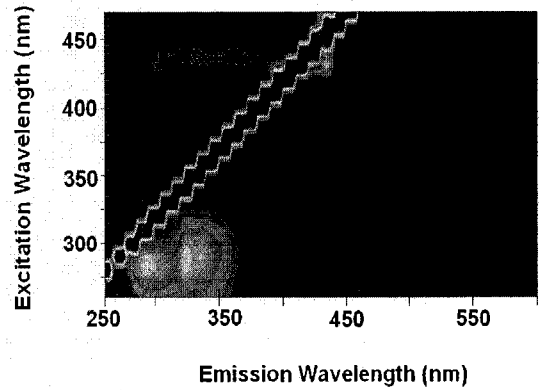


Figure A-8d. Gasoline in well graded sand  
EEM (200 mL/L)

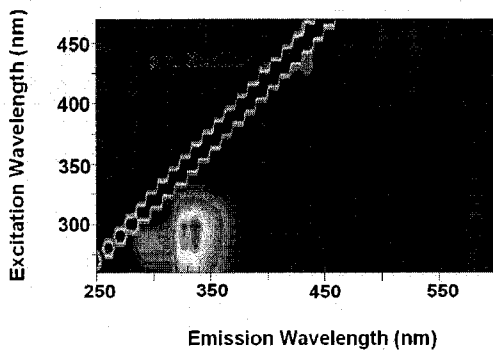


Figure A-8a. Gasoline in well graded sand  
EEM (600 mL/L)

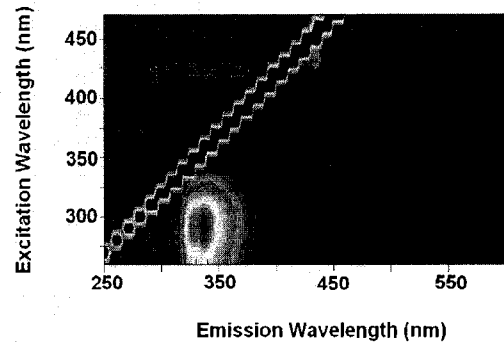


Figure A-8a. Gasoline in well graded sand  
EEM (neat)



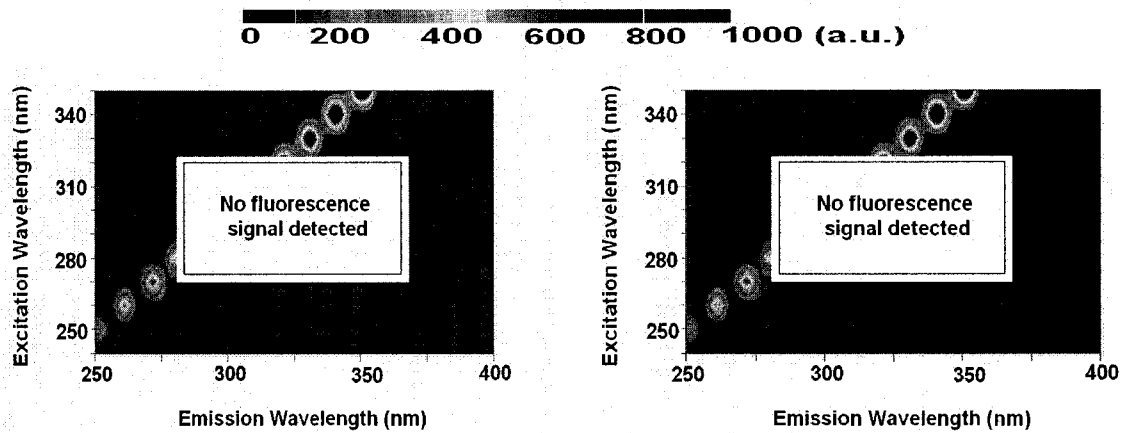


Figure A-9a. Gasoline in well graded sand and Devon silt EEM (1 mL/L)

Figure A-9b. Gasoline in well graded sand and Devon silt EEM (10 mL/L)

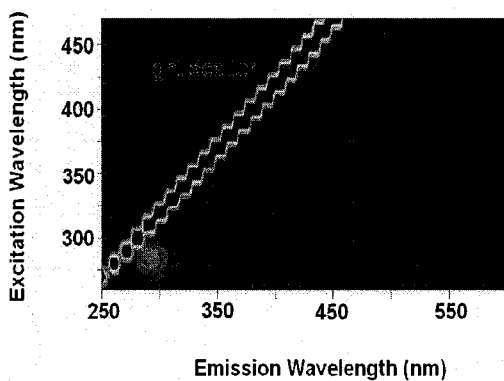


Figure A-9c. Gasoline in well graded sand and Devon silt EEM (50 mL/L)

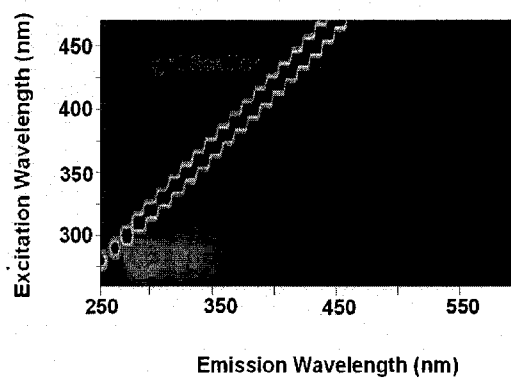


Figure A-9d. Gasoline in well graded sand and Devon silt EEM (200 mL/L)

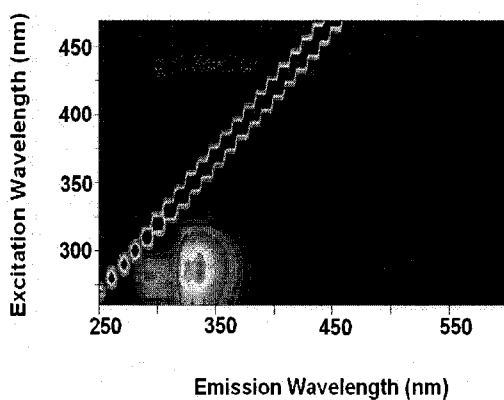


Figure A-9e. Gasoline in well graded sand and Devon silt EEM (600 mL/L)

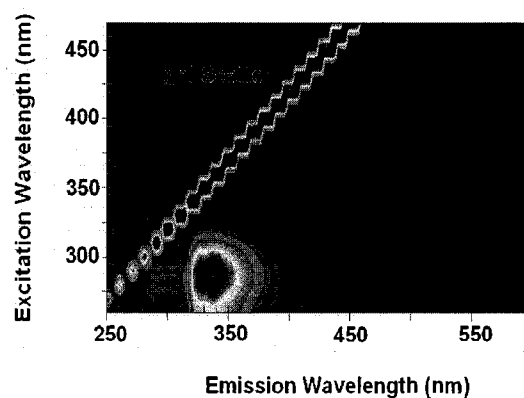


Figure A-9f. Gasoline in well graded sand and Devon silt EEM (neat)

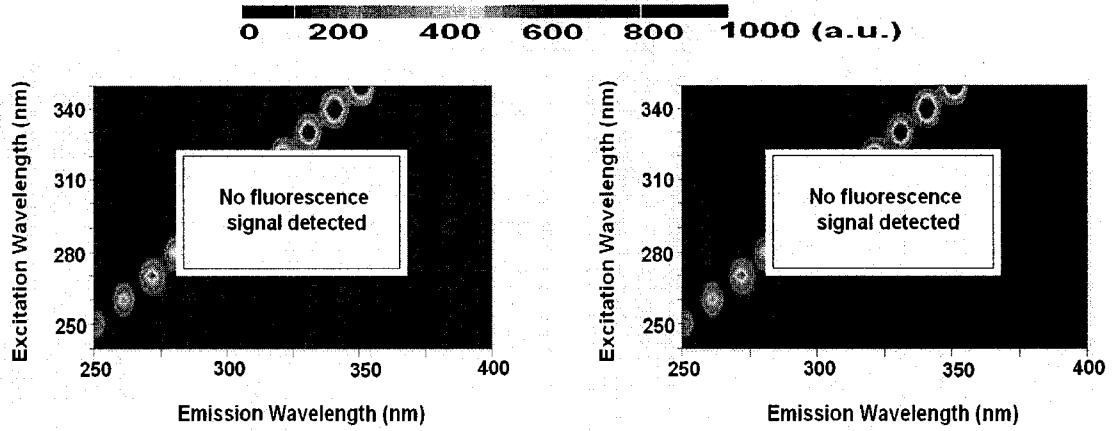


Figure A-10a. Gasoline in Devon silt EEM  
(1 mL/L)

Figure A-10b. Gasoline in Devon silt EEM  
(10 mL/L)

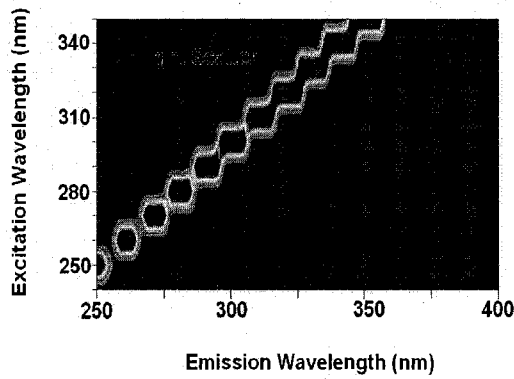


Figure A-10c. Gasoline in Devon silt EEM  
(50 mL/L)

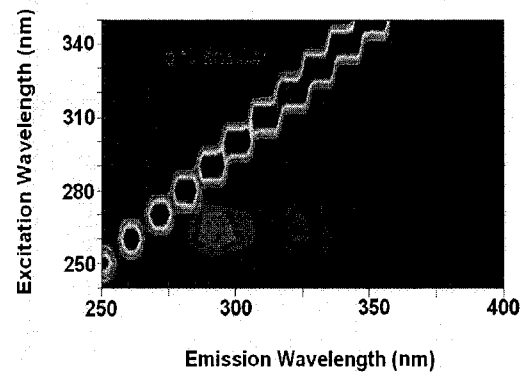


Figure A-10d. Gasoline in Devon silt EEM  
(200 mL/L)

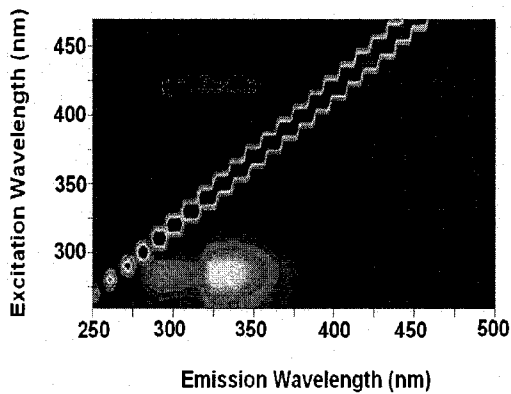


Figure A-10e. Gasoline in Devon silt EEM  
(600 mL/L)

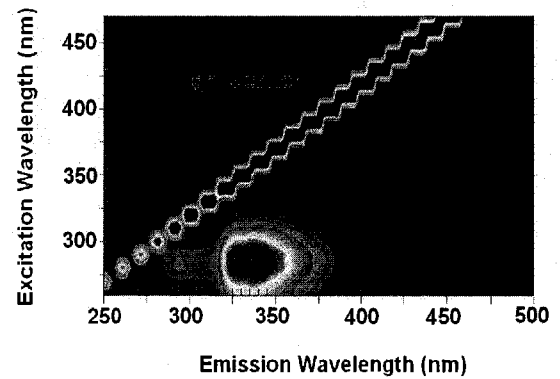


Figure A-10f. Gasoline in Devon silt EEM  
(neat)

0 1 2 3 4 5  $\times 10^3$  (a.u.)

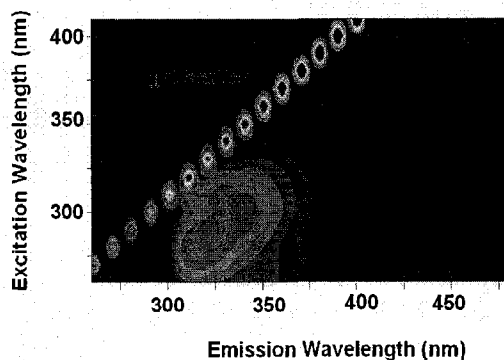


Figure A-11a. Diesel in hexane EEM (1 mL/L)

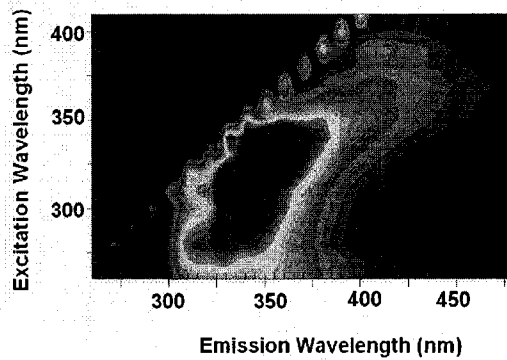


Figure A-11b. Diesel in hexane EEM (10 mL/L)

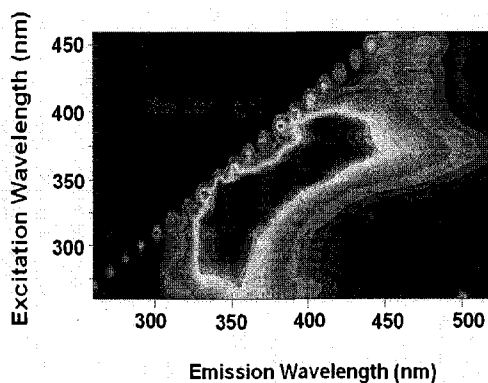


Figure A-11c. Diesel in hexane EEM (50 mL/L)

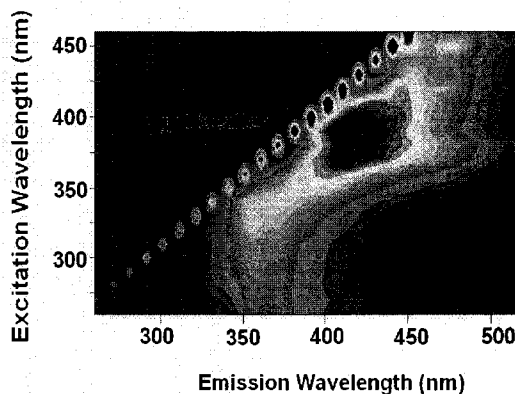


Figure A-11d. Diesel in hexane EEM (200 mL/L)

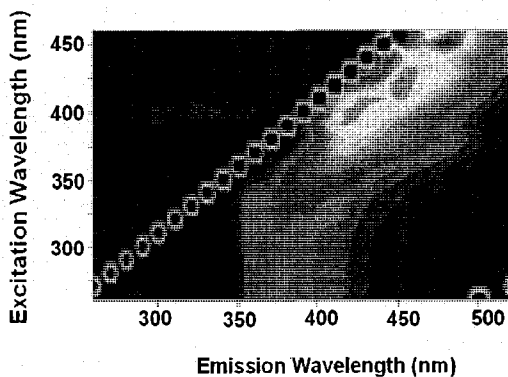


Figure A-11e. Diesel in hexane EEM (800 mL/L)

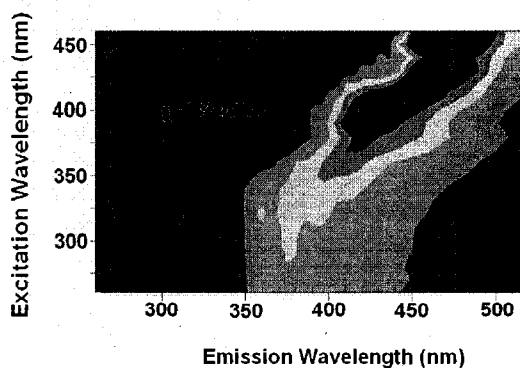


Figure A-11a. Diesel EEM (neat)

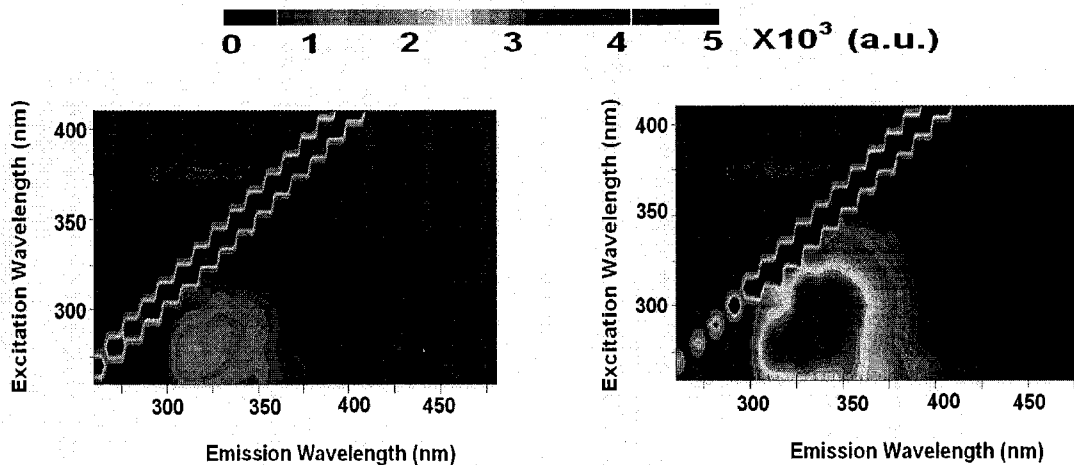


Figure A-12a. Diesel in Ottawa sand EEM  
(1 mL/L)

Figure A-12b. Diesel in Ottawa sand EEM  
(10 mL/L)

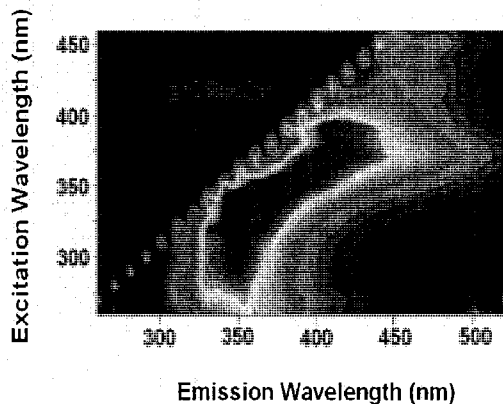


Figure A-12c. Diesel in Ottawa sand EEM  
(50 mL/L)

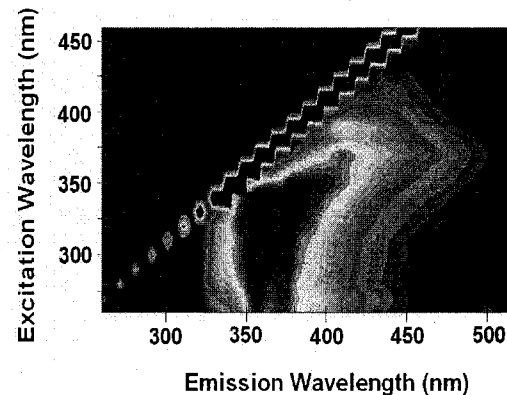


Figure A-12d. Diesel in Ottawa sand EEM  
(200 mL/L)

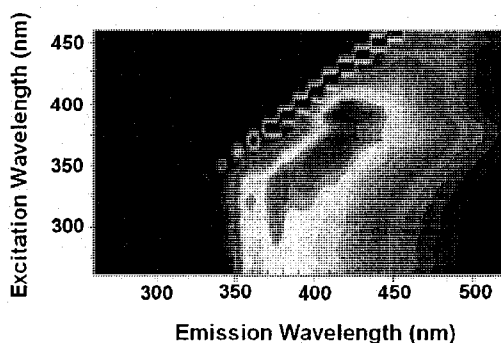


Figure A-12e. Diesel in Ottawa sand EEM  
(800 mL/L)

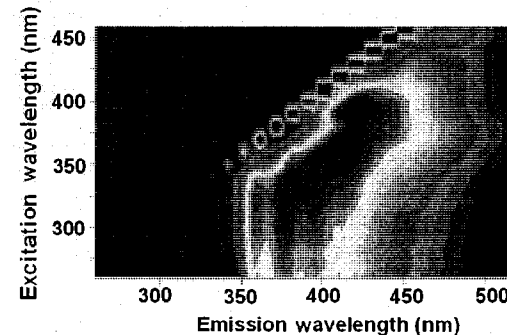


Figure A-12f. Diesel in Ottawa sand EEM  
(neat)

0 1 2 3 4 5  $\times 10^3$  (a.u.)

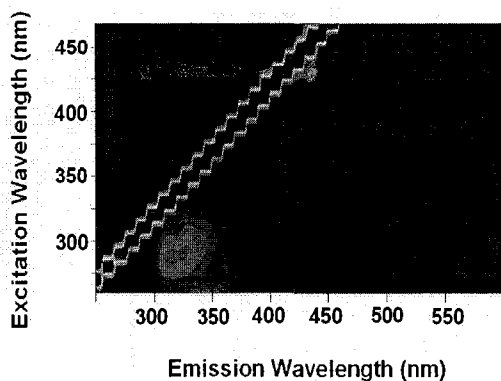


Figure A-13a. Diesel in well graded sand  
EEM (1 mL/L)

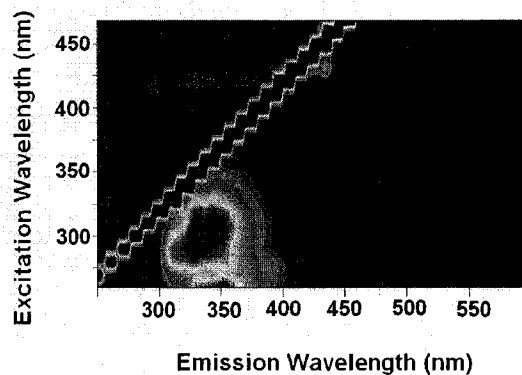


Figure A-13b. Diesel in well graded sand  
EEM (10 mL/L)

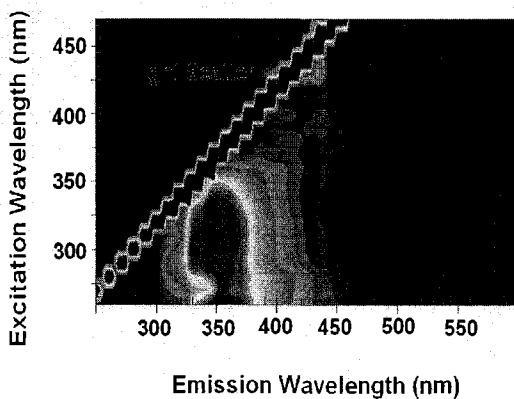


Figure A-13c. Diesel in well graded sand  
EEM (50 mL/L)

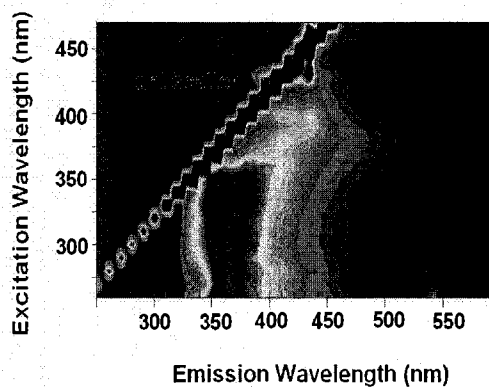


Figure A-13d. Diesel in well graded sand  
EEM (200 mL/L)

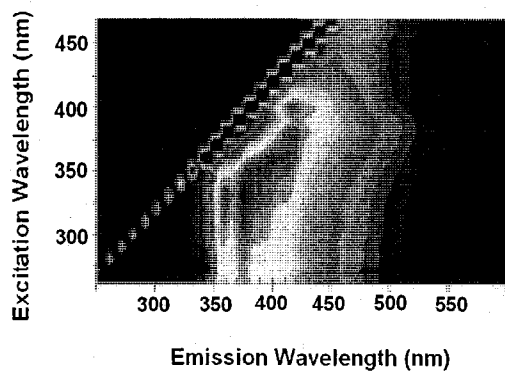


Figure A-13e. Diesel in well graded sand  
EEM (800 mL/L)

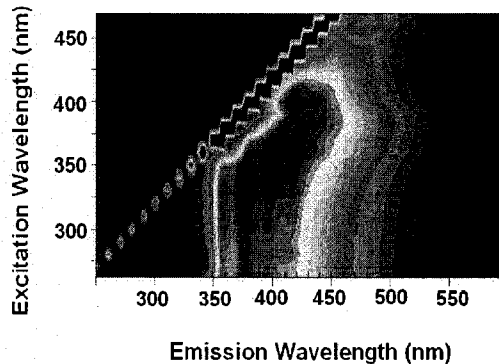


Figure A-13f. Diesel in well graded sand  
EEM (neat)

0 1 2 3 4 5  $\times 10^3$  (a.u.)

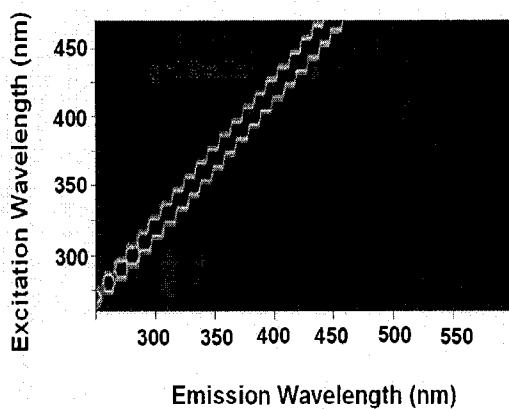


Figure A-14a. Diesel in well graded sand and Devon silt EEM (1 mL/L)

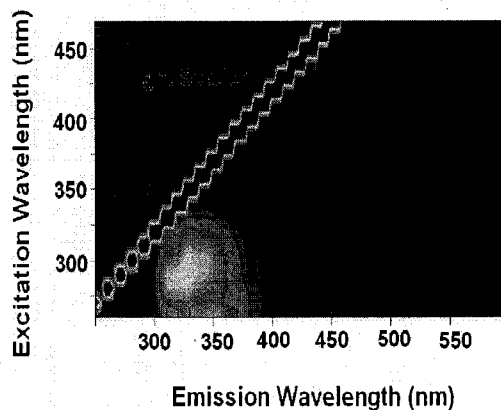


Figure A-14b. Diesel in well graded sand and Devon silt EEM (10 mL/L)

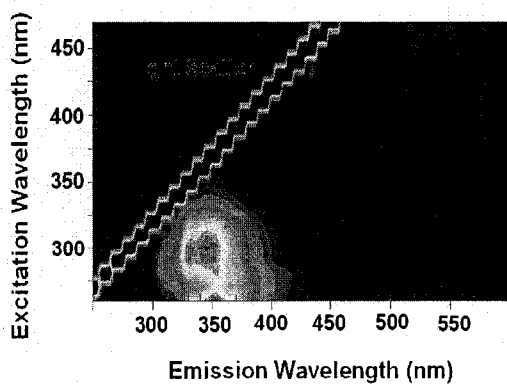


Figure A-14c. Diesel in well graded sand and Devon silt EEM (50 mL/L)

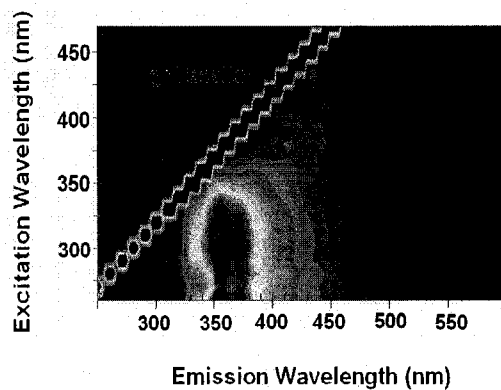


Figure A-14d. Diesel in well graded sand and Devon silt EEM (200 mL/L)

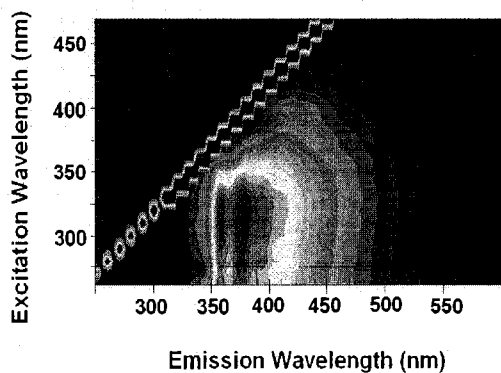


Figure A-14e. Diesel in well graded sand and Devon silt EEM (800 mL/L)

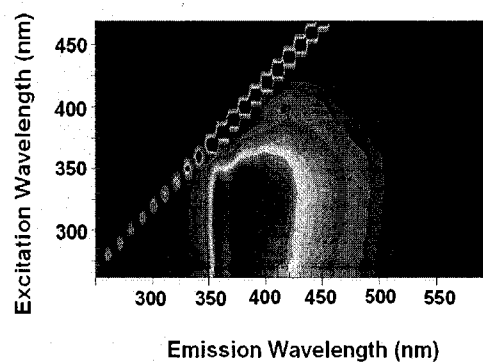


Figure A-14f. Diesel in well graded sand and Devon silt EEM (neat)

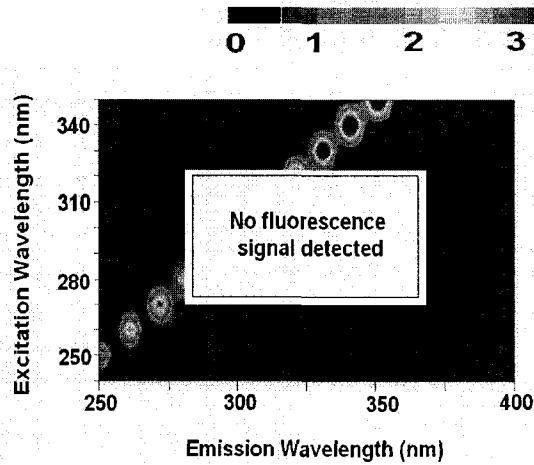


Figure A-15a. Diesel in Devon silt EEM (1 mL/L)

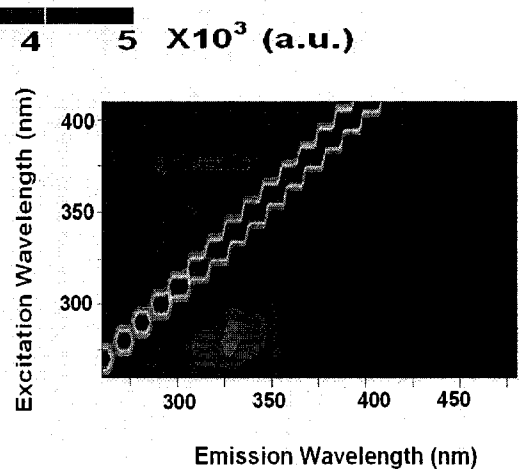


Figure A-15b. Diesel in Devon silt EEM (10 mL/L)

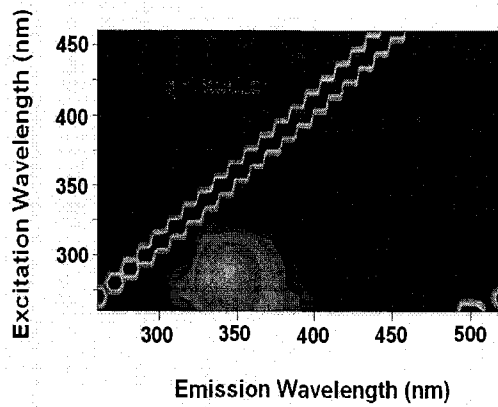


Figure A-15c. Diesel in Devon silt EEM (50 mL/L)

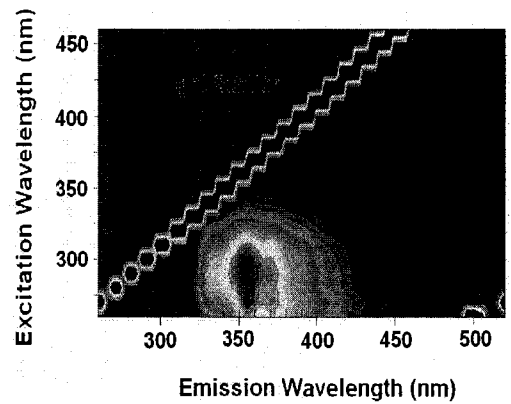


Figure A-15d. Diesel in Devon silt EEM (200 mL/L)

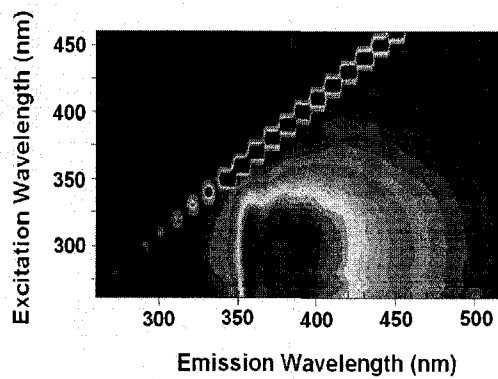


Figure A-15e. Diesel in Devon silt EEM (800 mL/L)

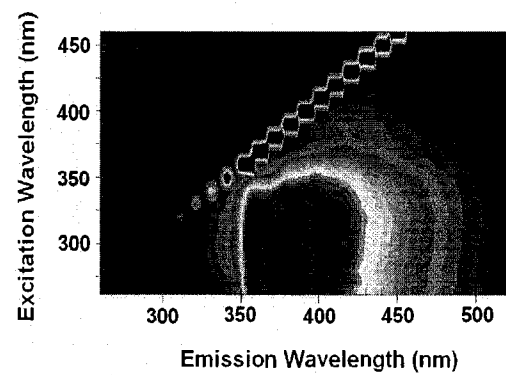


Figure A-15f. Diesel in Devon silt EEM (neat)

0 1 2 3 4 5  $\times 10^3$  (a.u.)

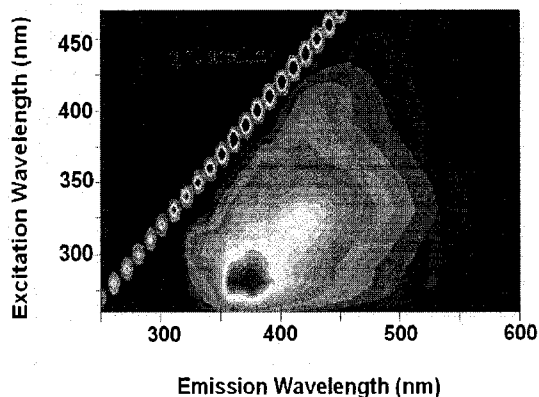


Figure A-16a. Flare pit residue in chloroform EEM (1 mL/L)

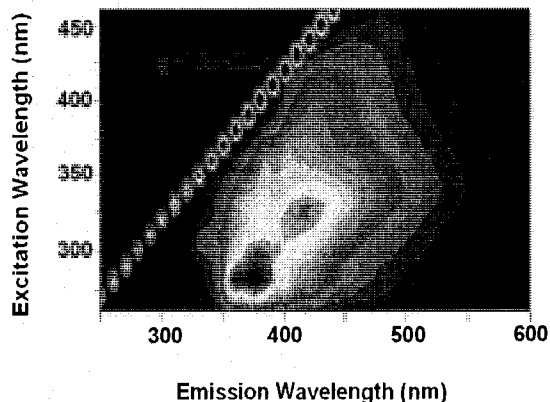


Figure A-16b. Flare pit residue in chloroform EEM (10 mL/L)

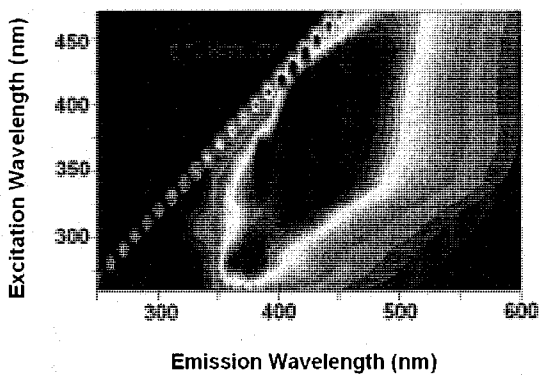


Figure A-16c. Flare pit residue in chloroform EEM (50 mL/L)

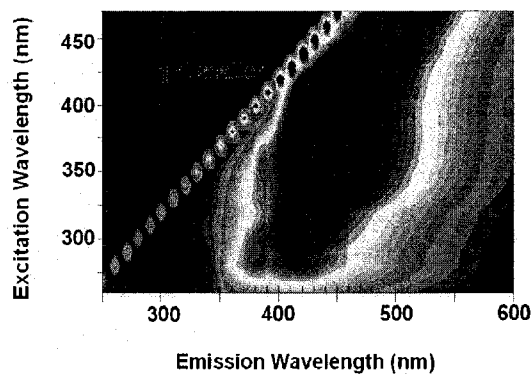


Figure A-16d. Flare pit residue in chloroform EEM (200 mL/L)

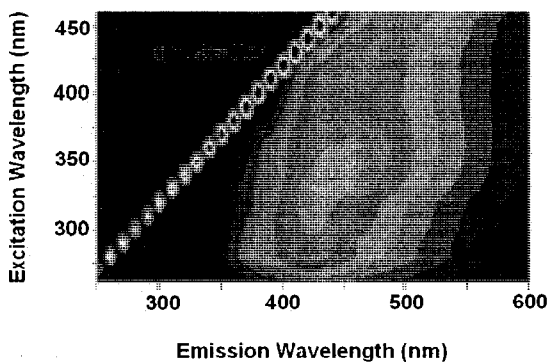


Figure A-16e. Flare pit residue in chloroform EEM (600 mL/L)

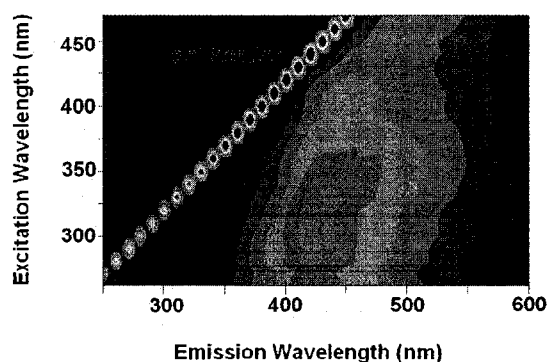


Figure A-16f. Flare pit residue EEM (neat)



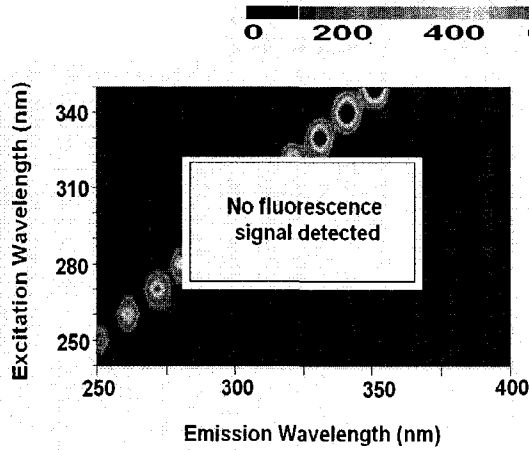


Figure A-17a. Flare pit residue in Ottawa sand EEM (1 mL/L)

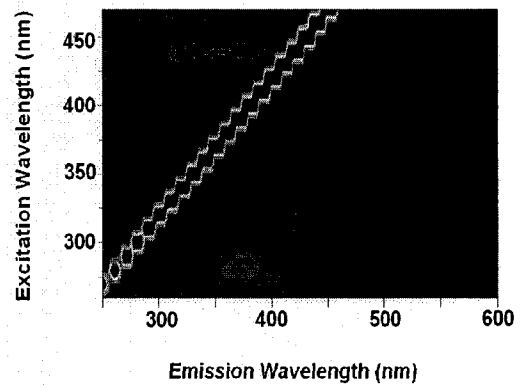


Figure A-17b. Flare pit residue in Ottawa sand EEM (10 mL/L)

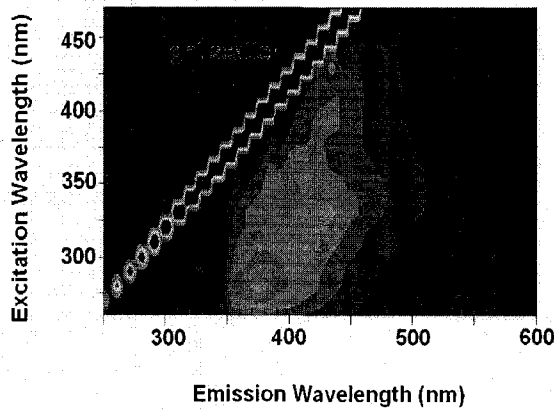


Figure A-17c. Flare pit residue in Ottawa sand EEM (50 mL/L)

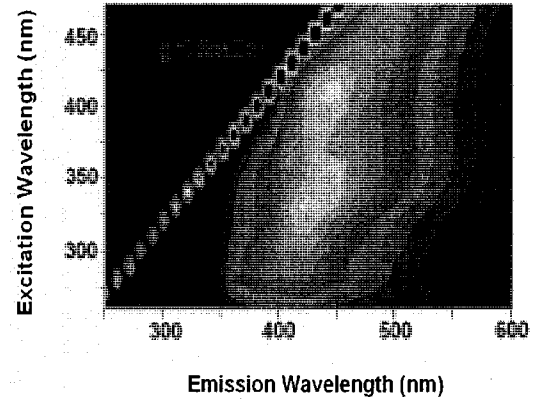


Figure A-17d. Flare pit residue in Ottawa sand EEM (200 mL/L)

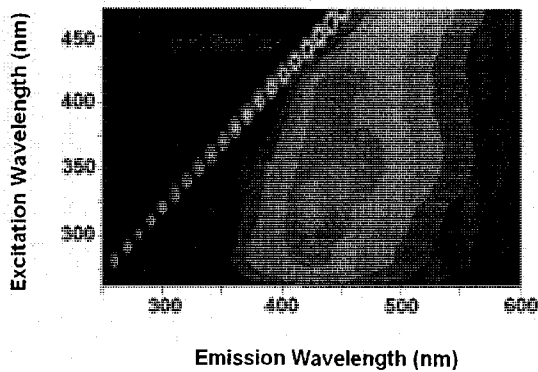


Figure A-17e. Flare pit residue in Ottawa sand EEM (600 mL/L)

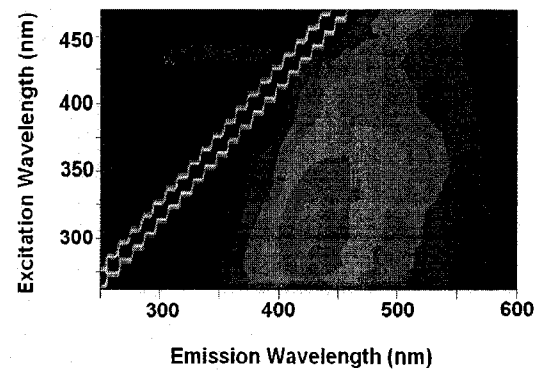


Figure A-17f. Flare pit residue in Ottawa sand EEM (neat)

0 200 400 600 800 1000 (a.u.)

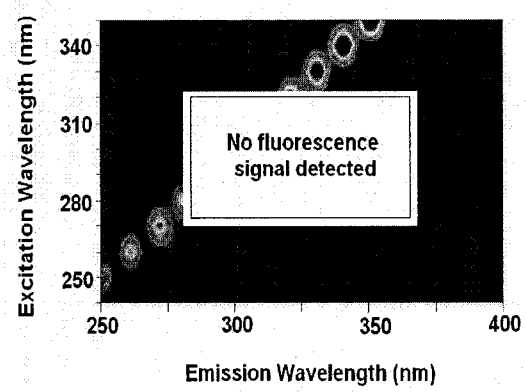


Figure A-18a. Flare pit residue in well graded sand EEM (1 mL/L)

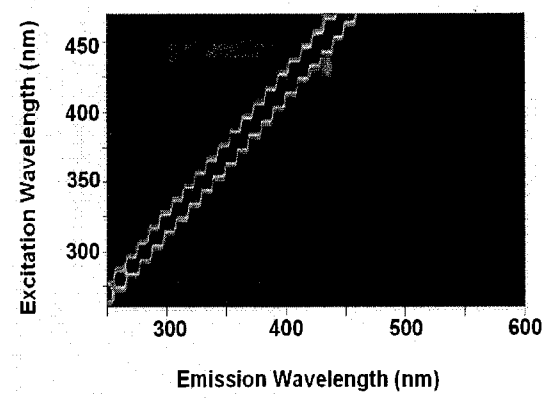


Figure A-18b. Flare pit residue in well graded sand EEM (10 mL/L)

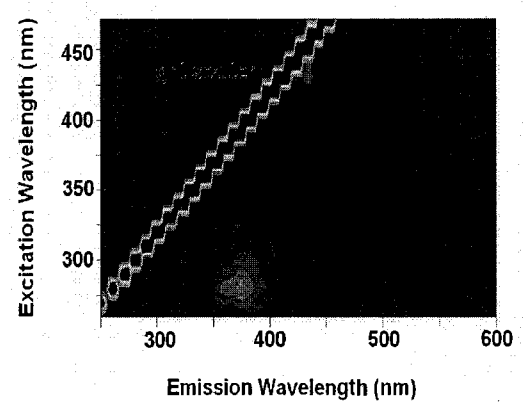


Figure A-18c. Flare pit residue in well graded sand EEM (50 mL/L)

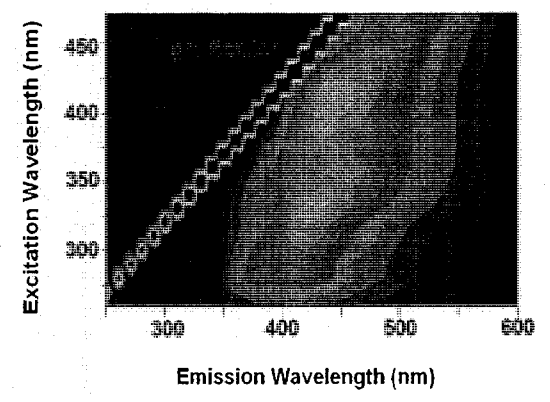


Figure A-18d. Flare pit residue in well graded sand EEM (200 mL/L)

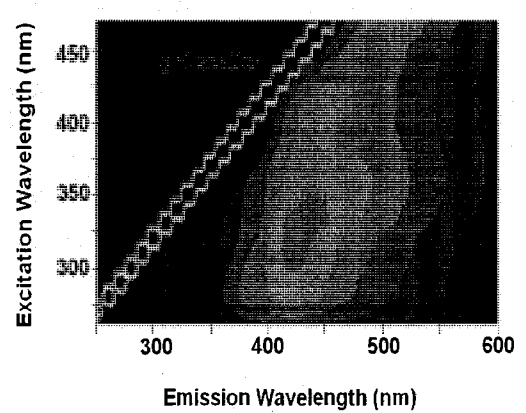


Figure A-18e. Flare pit residue in well graded sand EEM (600 mL/L)

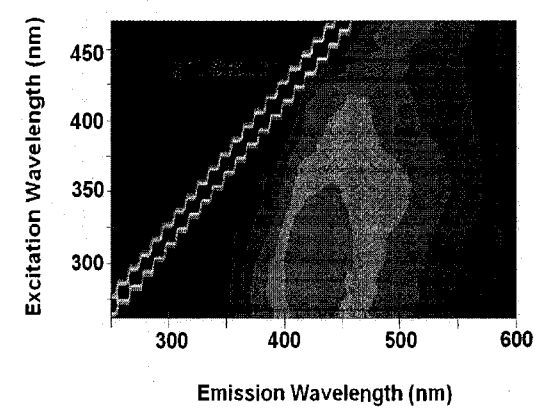


Figure A-18f. Flare pit residue in well graded sand EEM (neat)

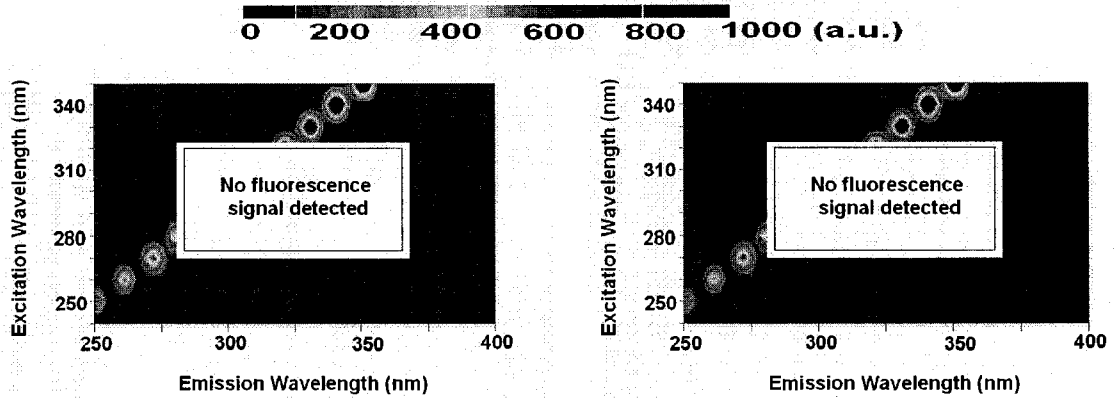


Figure A-19a. Flare pit residue in well graded sand and Devon silt EEM (1 mL/L)

Figure A-19b. Flare pit residue in well graded sand and Devon silt EEM (10 mL/L)

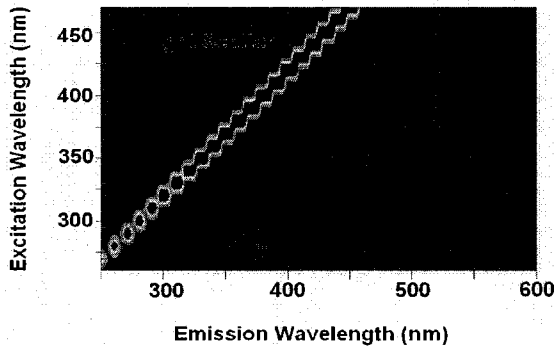


Figure A-19c. Flare pit residue in well graded sand and Devon silt EEM (50 mL/L)

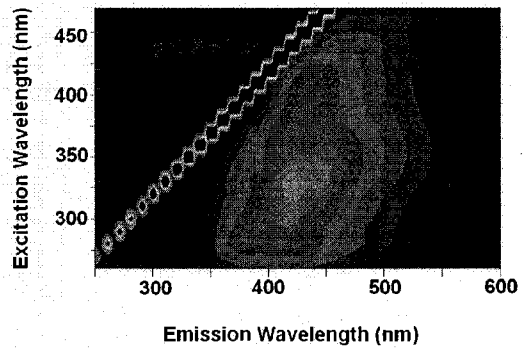


Figure A-19d. Flare pit residue in well graded sand and Devon silt EEM (200 mL/L)

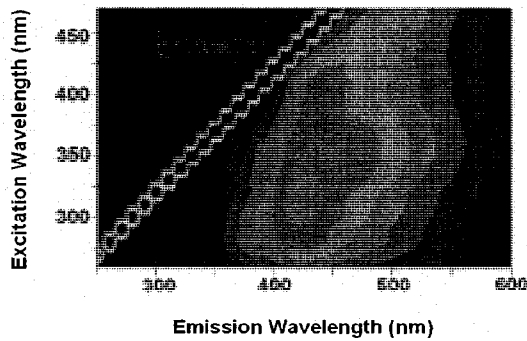


Figure A-19e. Flare pit residue in well graded sand and Devon silt EEM (600 mL/L)

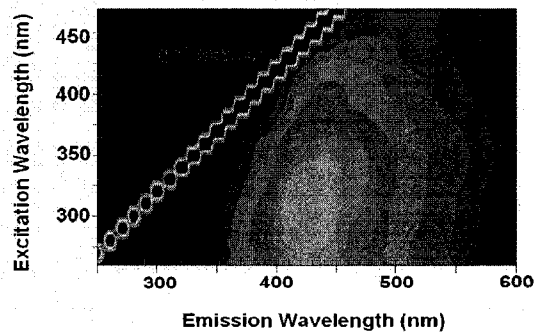


Figure A-19f. Flare pit residue in well graded sand and Devon silt EEM (neat)

0 200 400 600 800 1000 (a.u.)

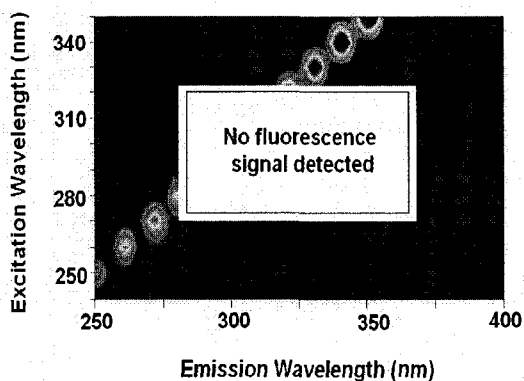


Figure A-20a. Flare pit residue in Devon silt EEM (1 mL/L)

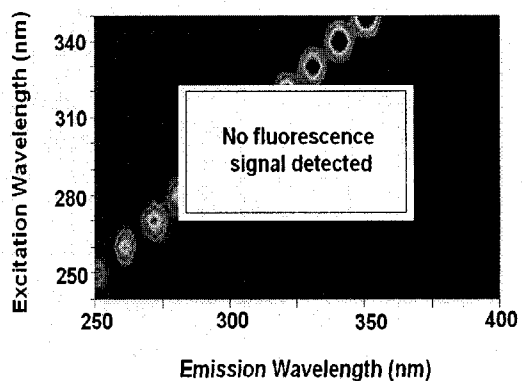


Figure A-20b. Flare pit residue in Devon silt EEM (10 mL/L)

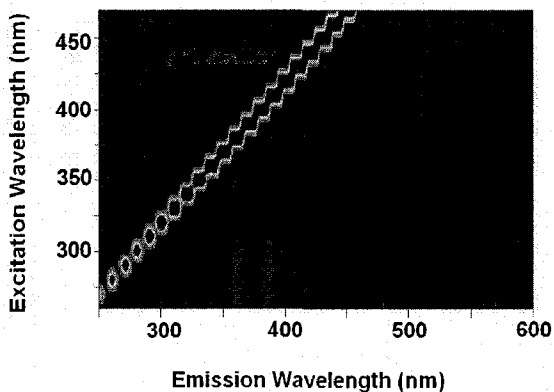


Figure A-20c. Flare pit residue in Devon silt EEM (50 mL/L)

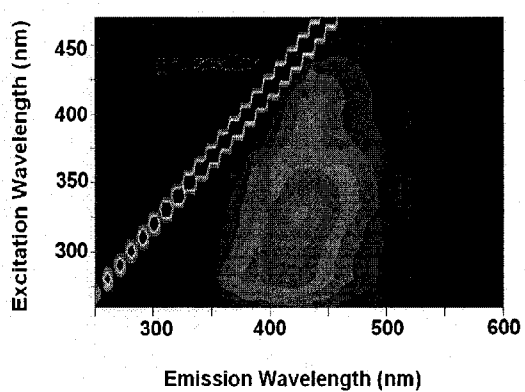


Figure A-20d. Flare pit residue in Devon silt EEM (200 mL/L)

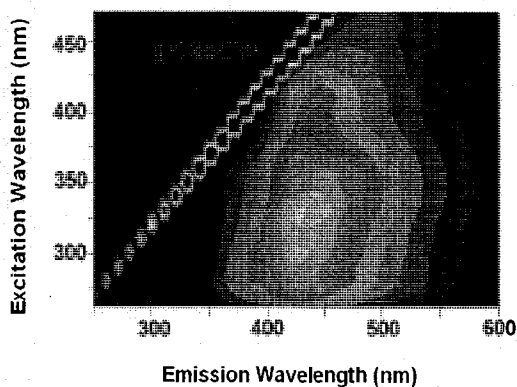


Figure A-20e. Flare pit residue in Devon silt EEM (600 mL/L)

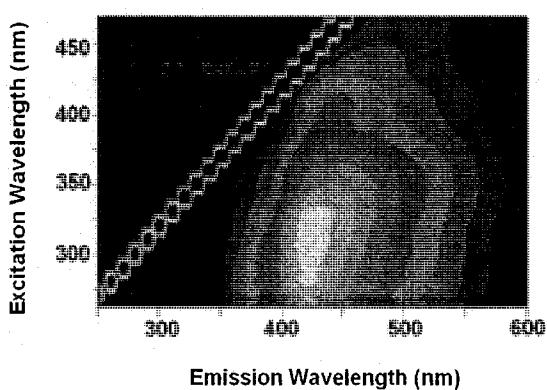


Figure A-20f. Flare pit residue in Devon silt EEM (neat)

0 200 400 600 800 1000 (a.u.)

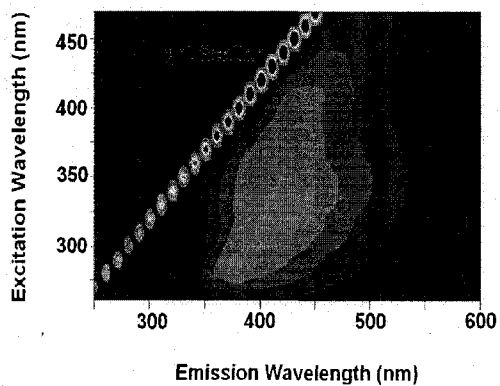


Figure A-21a. Crude oil in chloroform  
EEM (1 mL/L)

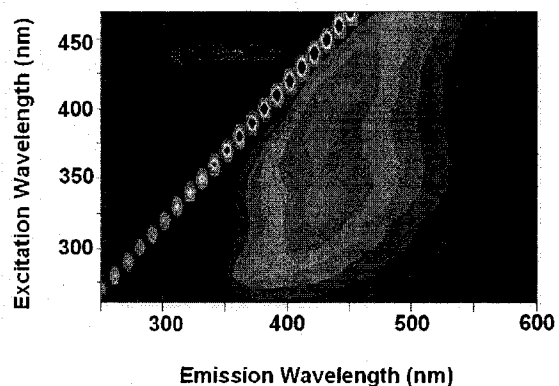


Figure A-21b. Crude oil in chloroform  
EEM (10 mL/L)

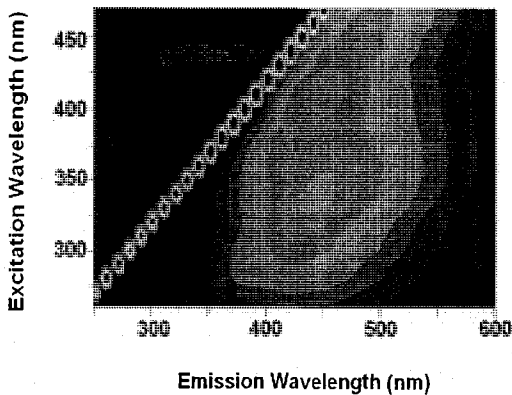


Figure A-21c. Crude oil in chloroform  
EEM (40 mL/L)

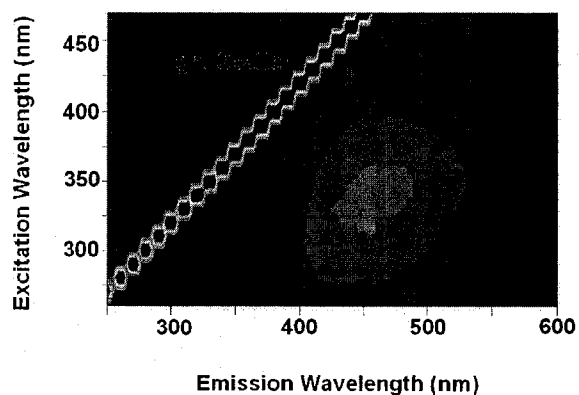


Figure A-21d. Crude oil in chloroform  
EEM (200 mL/L)

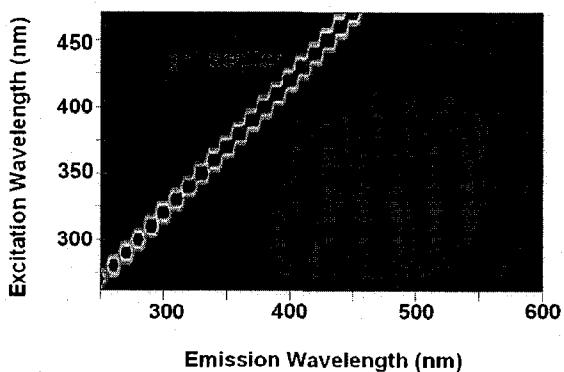


Figure A-21e. Crude oil in chloroform  
EEM (640 mL/L)

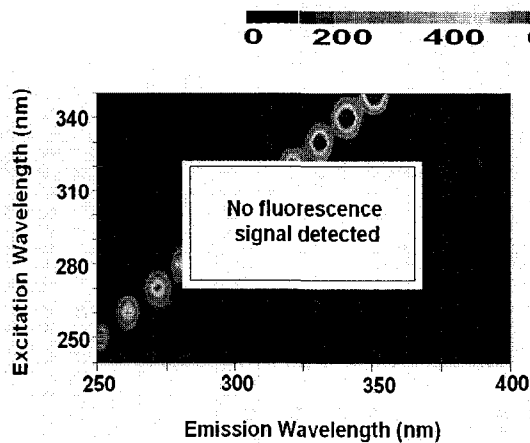


Figure A-22a. Crude oil in Ottawa sand  
EEM (1 mL/L)

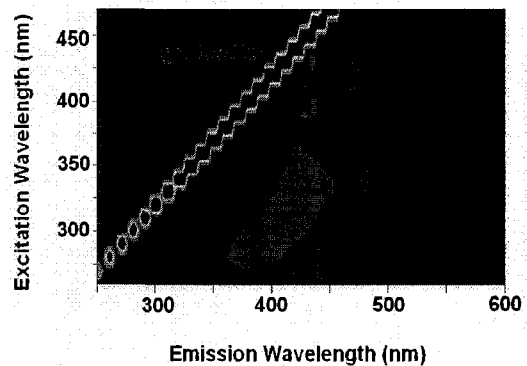


Figure A-22b. Crude oil in Ottawa sand  
EEM (10 mL/L)

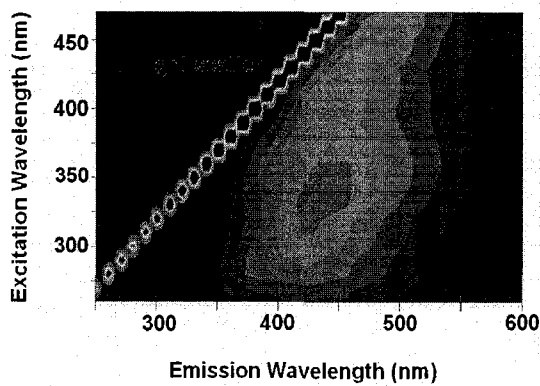


Figure A-22c. Crude oil in Ottawa sand  
EEM (40 mL/L)

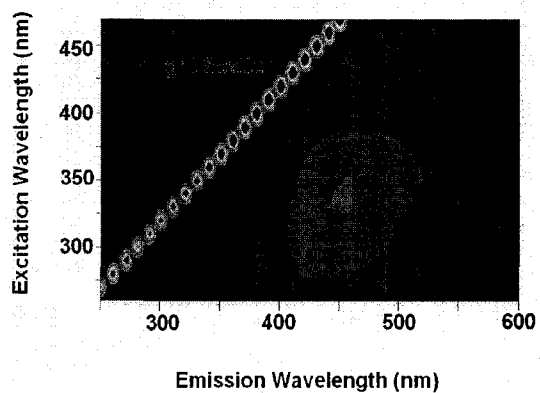


Figure A-22d. Crude oil in Ottawa sand  
EEM (200 mL/L)

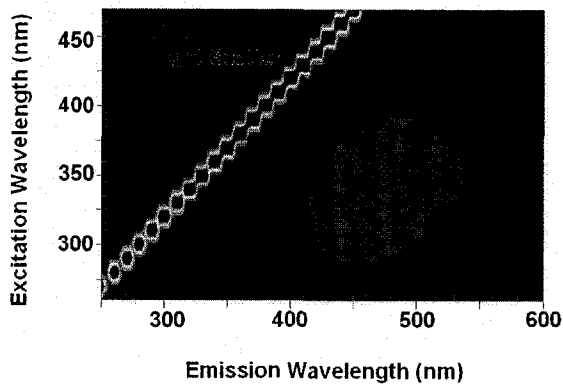


Figure A-22e. Crude oil in Ottawa sand  
EEM (640 mL/L)

0 200 400 600 800 1000 (a.u.)

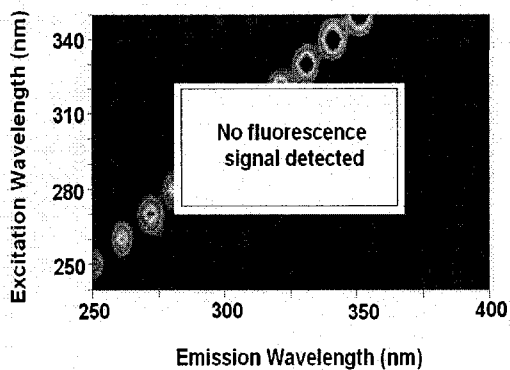


Figure A-23a. Crude oil in well graded sand EEM (1 mL/L)

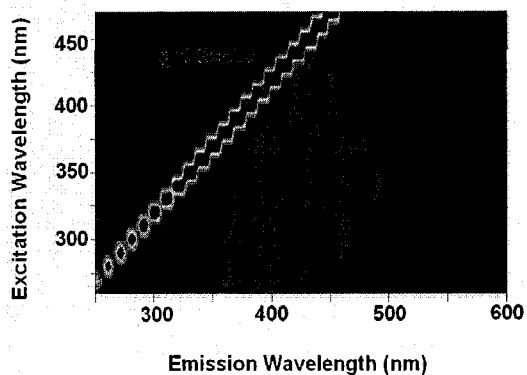


Figure A-23b. Crude oil in well graded sand EEM (10 mL/L)

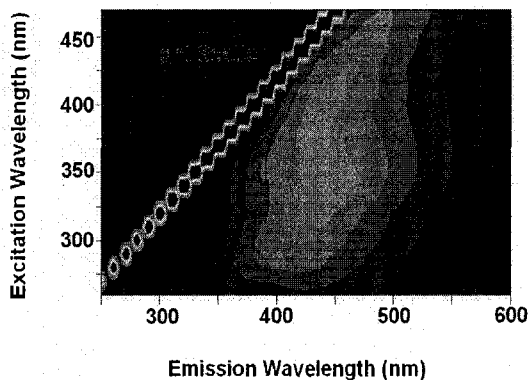


Figure A-23c. Crude oil in well graded sand EEM (40 mL/L)

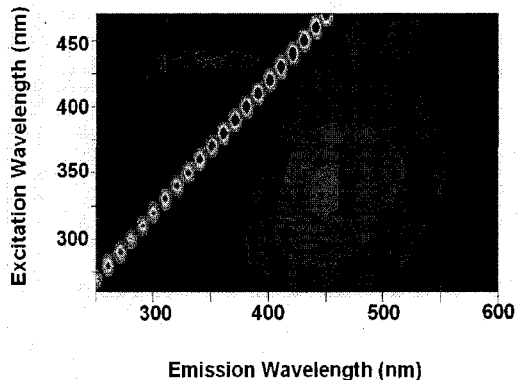


Figure A-23d. Crude oil in well graded sand EEM (200 mL/L)

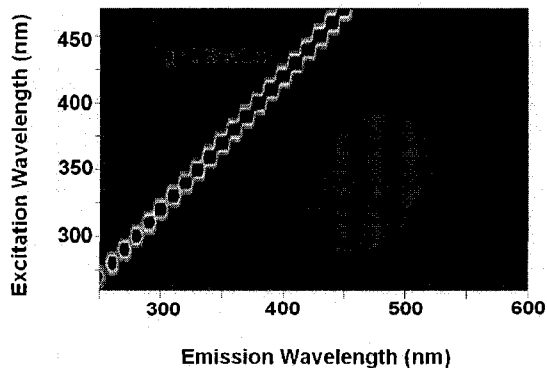


Figure A-23e. Crude oil in well graded sand EEM (640 mL/L)

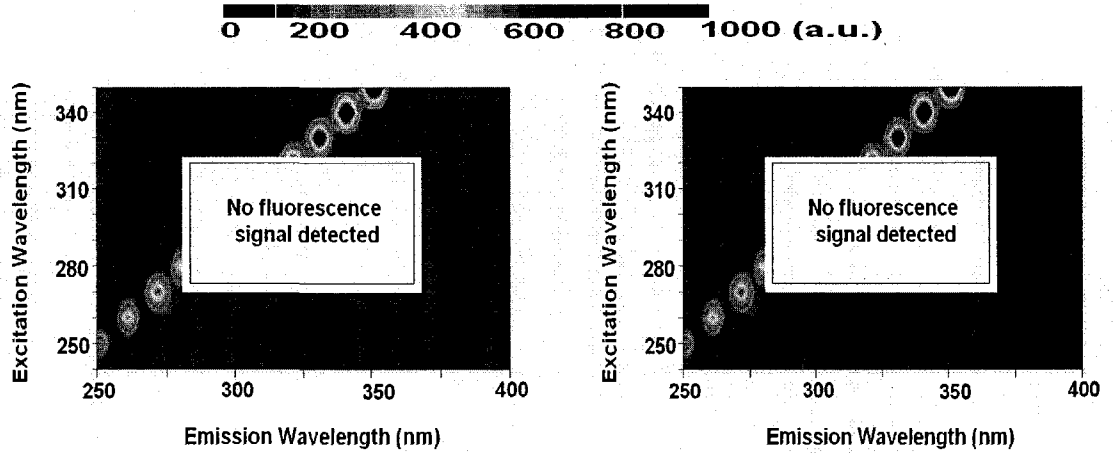


Figure A-24a. Crude oil in well graded sand and Devon silt EEM (1 mL/L)

Figure A-24b. Crude oil in well graded sand and Devon silt EEM (10 mL/L)

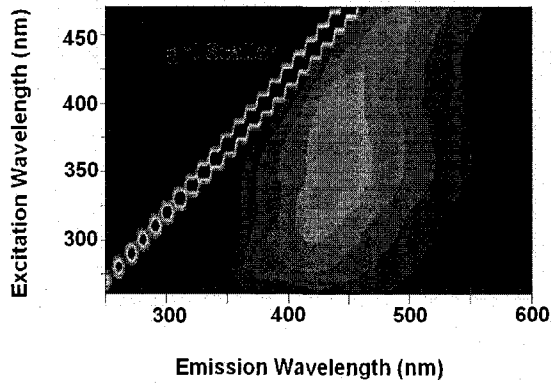


Figure A-24c. Crude oil in well graded sand and Devon silt EEM (40 mL/L)

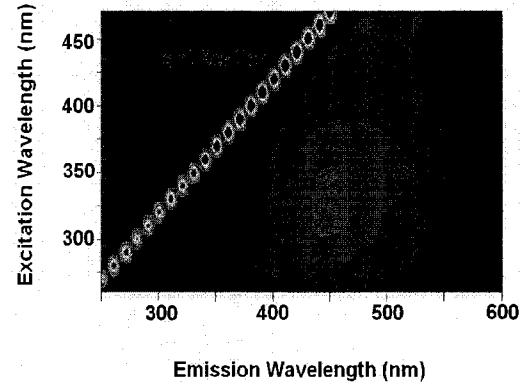


Figure A-24d. Crude oil in well graded sand and Devon silt EEM (200 mL/L)

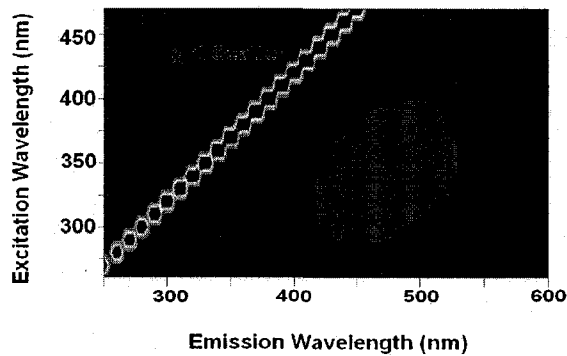


Figure A-24e. Crude oil in well graded sand and Devon silt EEM (640 mL/L)



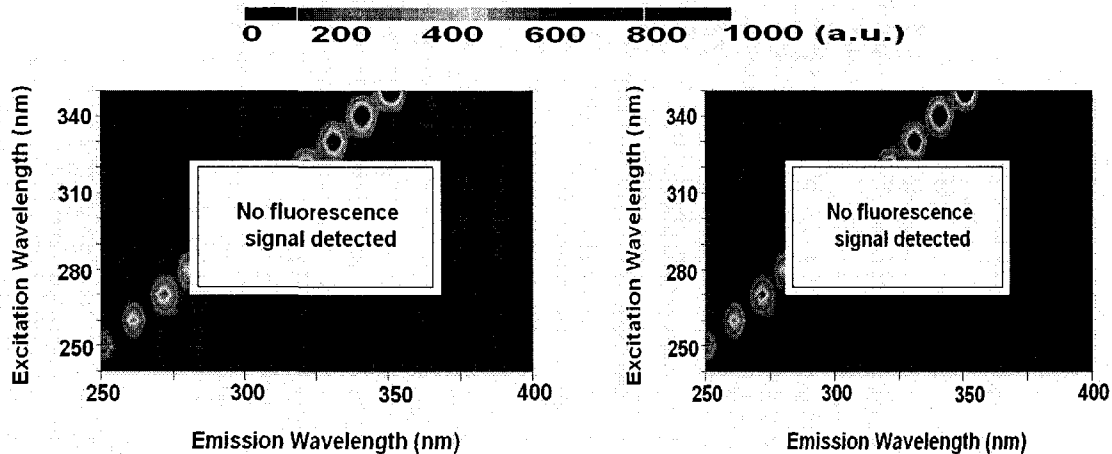


Figure A-25a. Crude oil in Devon silt EEM (1 mL/L)

Figure A-25b. Crude oil in Devon silt EEM (10 mL/L)

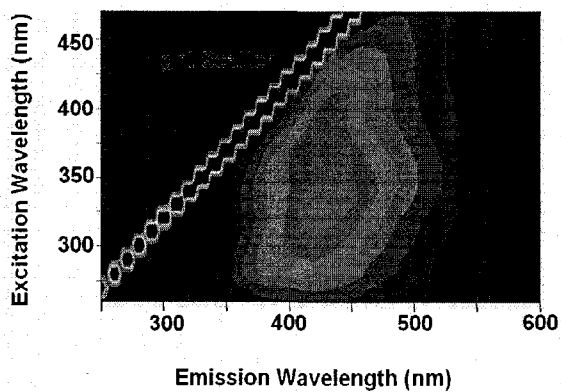


Figure A-25c. Crude oil in Devon silt EEM (40 mL/L)

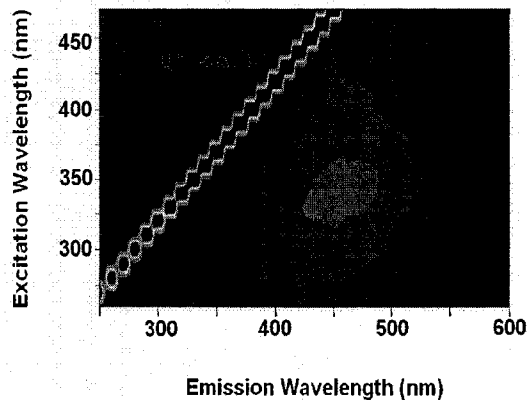


Figure A-25d. Crude oil in Devon silt EEM (200 mL/L)

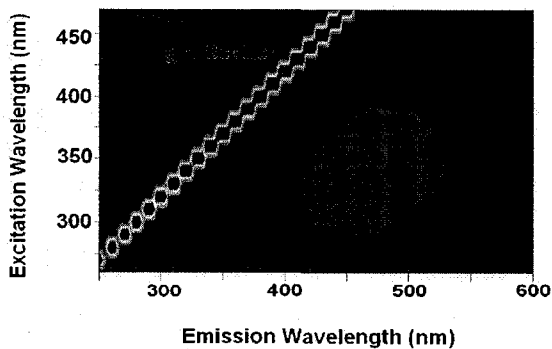


Figure A-25e. Crude oil in Devon silt EEM (640 mL/L)

**Appendix B**  
Fluorescence EEMs  
(*Using Newly Developed UVIF  
sensor*)

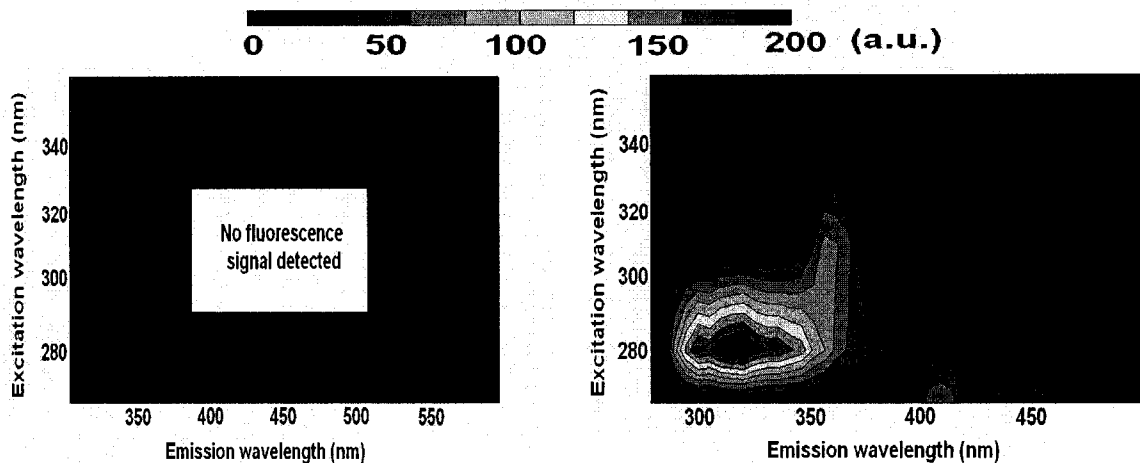


Figure B1-a. Gasoline in hexane EEM (1 mL/L)

Figure B1-b. Gasoline in hexane EEM (10 mL/L)

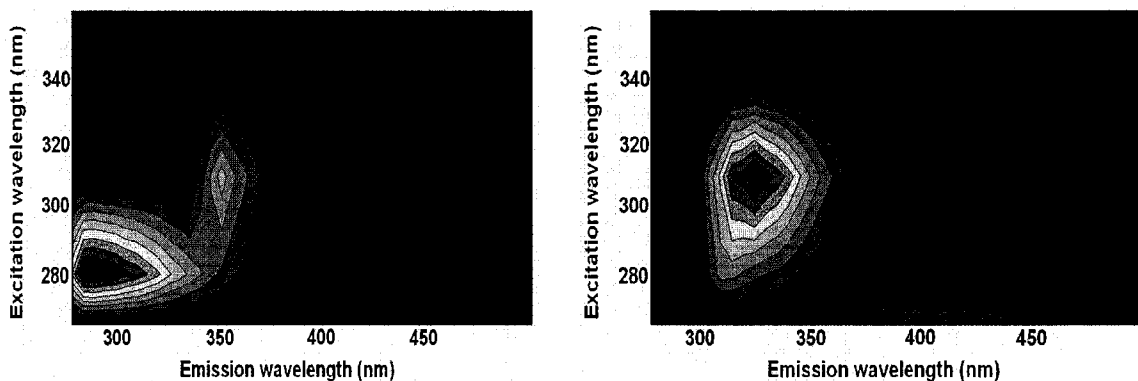


Figure B1-c. Gasoline in hexane EEM (50 mL/L)

Figure B1-d. Gasoline in hexane EEM (200 mL/L)

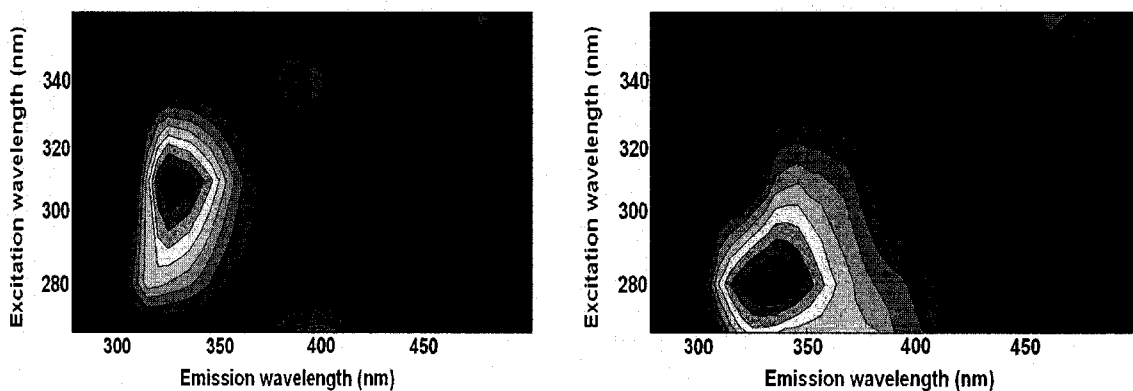


Figure B1-e. Gasoline in hexane EEM (600 mL/L)

Figure B1-f. Gasoline in hexane EEM (neat)

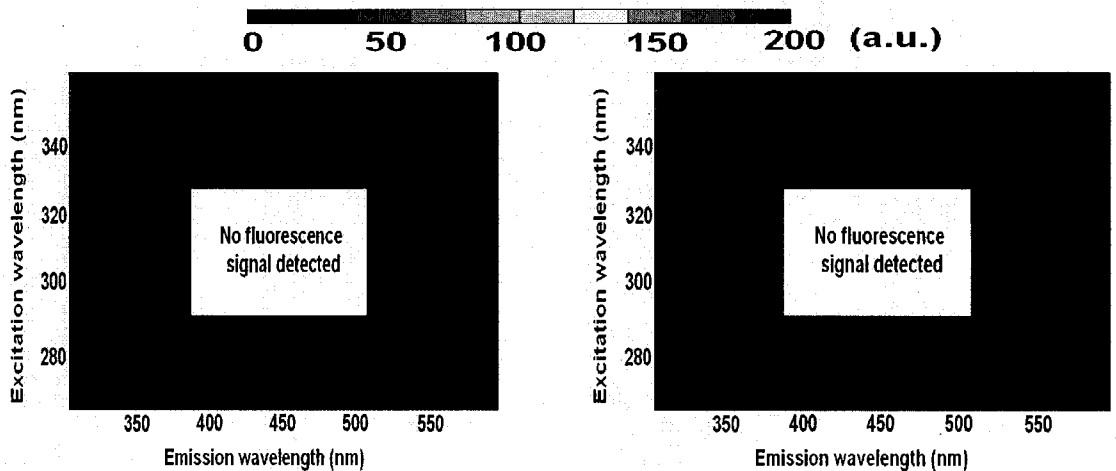


Figure B-2a. Gasoline in Ottawa sand  
EEM (1 mL/L)

Figure B-2b. Gasoline in Ottawa sand EEM  
(10 mL/L)

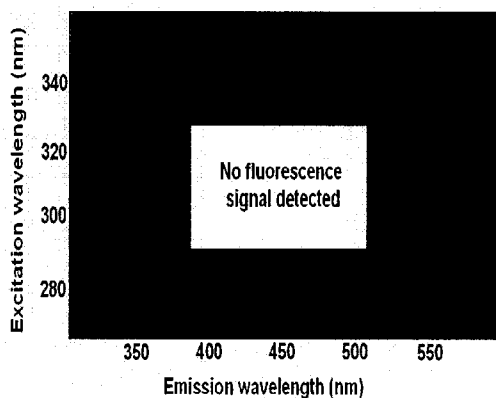


Figure B-2c. Gasoline in Ottawa sand  
EEM (50 mL/L)

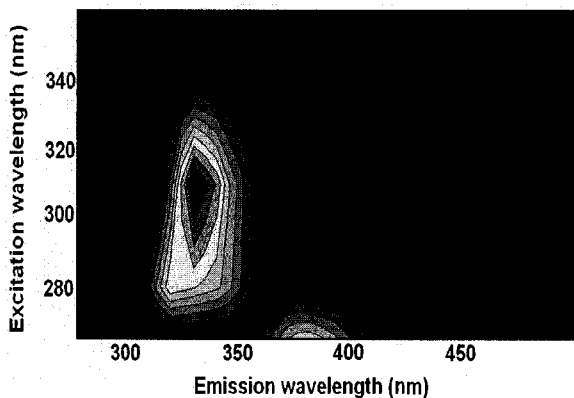


Figure B-2d. Gasoline in Ottawa sand EEM  
(200 mL/L)

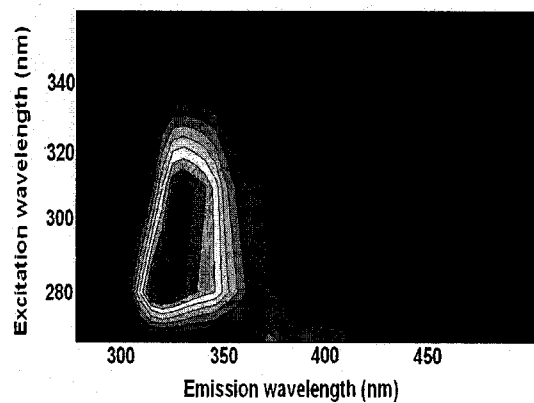


Figure B-2e. Gasoline in Ottawa sand  
EEM (600 mL/L)

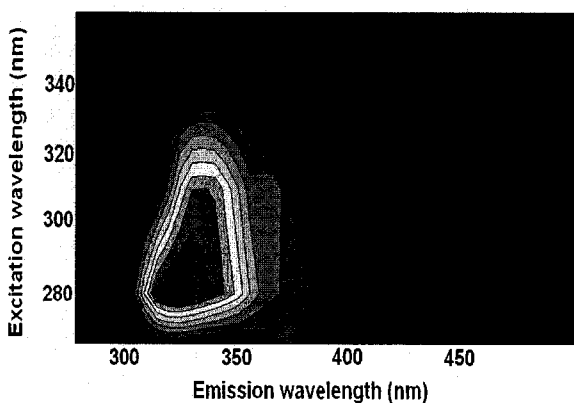


Figure B-2f. Gasoline in Ottawa sand EEM  
(neat)

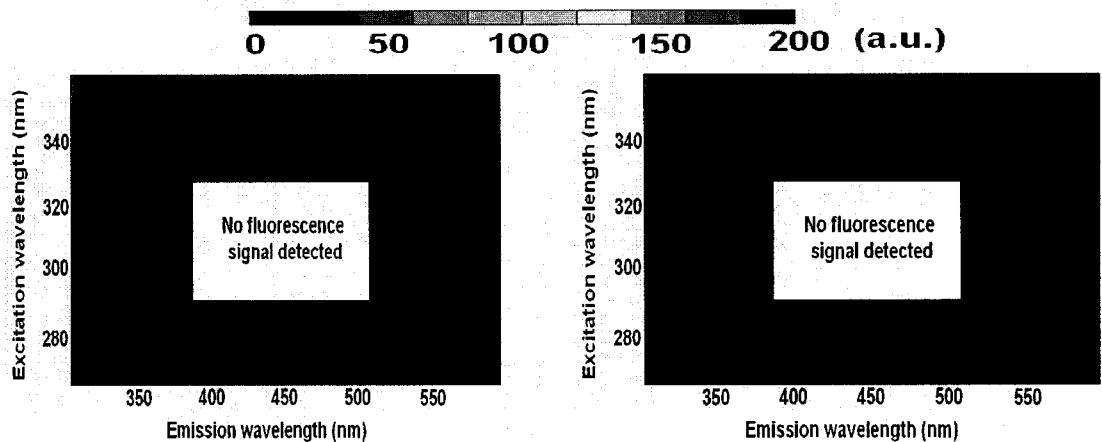


Figure B-3a. Gasoline in well graded sand EEM (1 mL/L)

Figure B-3b. Gasoline in well graded sand EEM (10 mL/L)

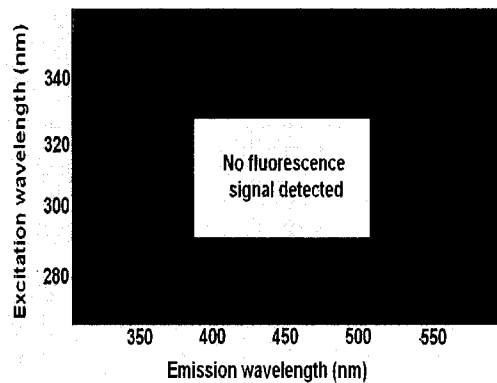


Figure B-3c. Gasoline in well graded sand EEM (50 mL/L)

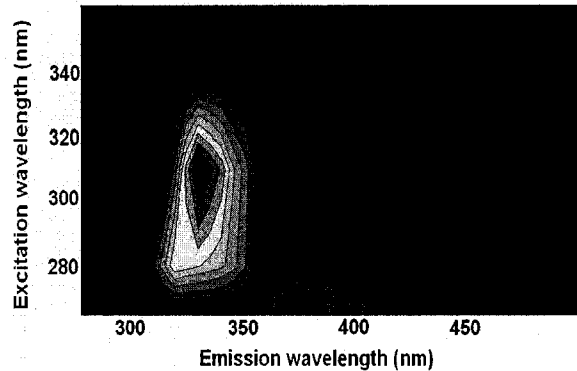


Figure B-3d. Gasoline in well graded sand EEM (200 mL/L)

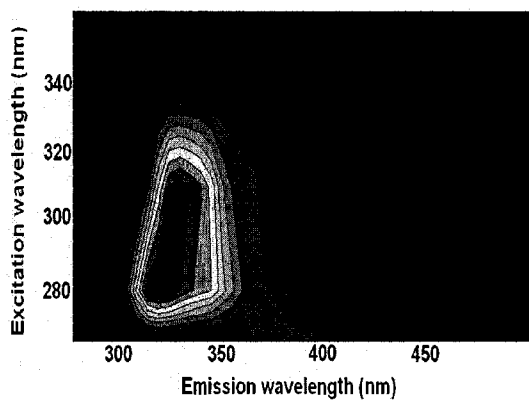


Figure B-3e. Gasoline in well graded sand EEM (600 mL/L)

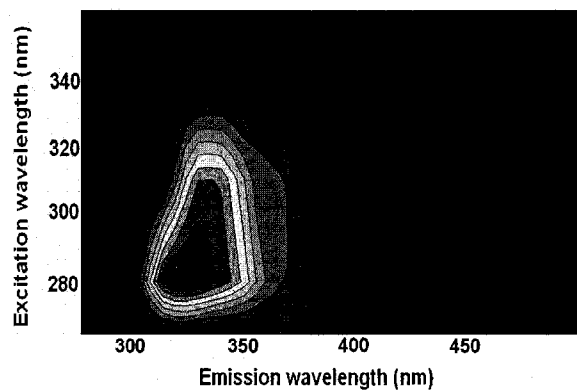


Figure B-3f. Gasoline in well graded sand EEM (neat)

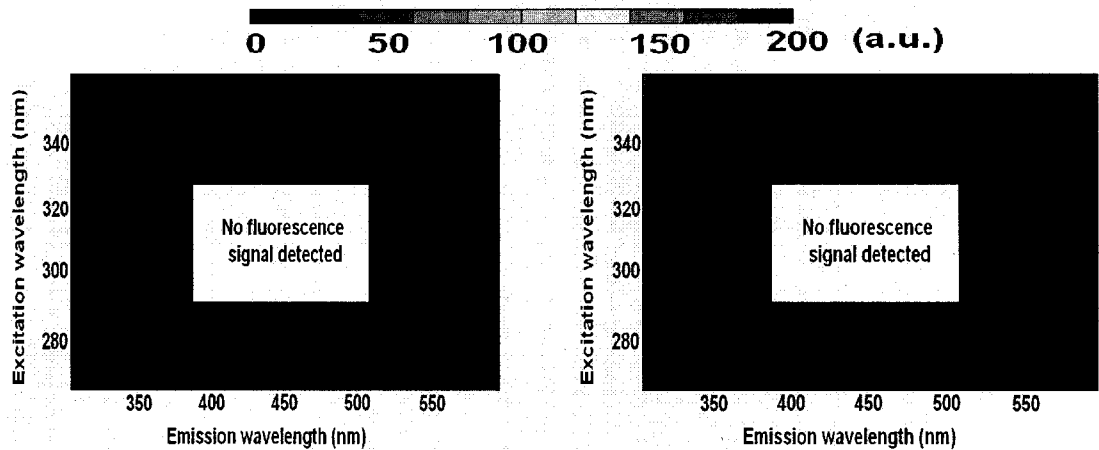


Figure B-4a. Gasoline in well graded sand and Devon silt EEM (1 mL/L)

Figure B-4b. Gasoline in well graded sand and Devon silt EEM (10 mL/L)

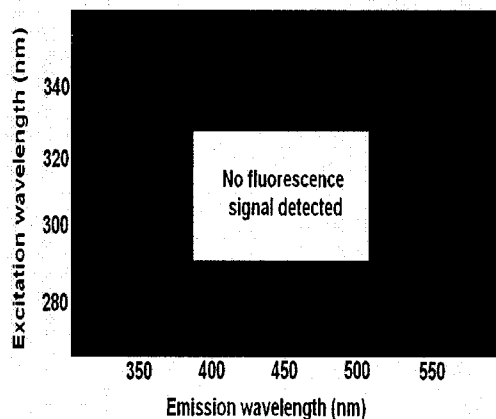


Figure B-4c. Gasoline in well graded sand and Devon silt EEM (50 mL/L)

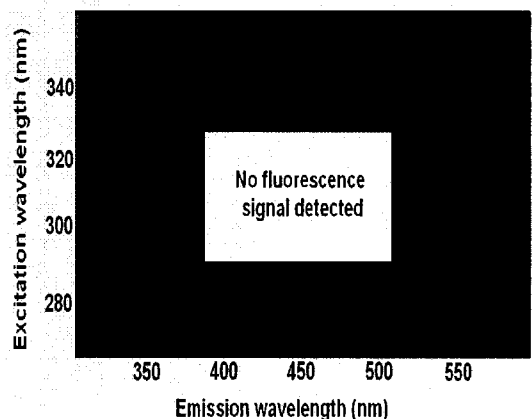


Figure B-4d. Gasoline in well graded sand and Devon silt EEM (600 mL/L)

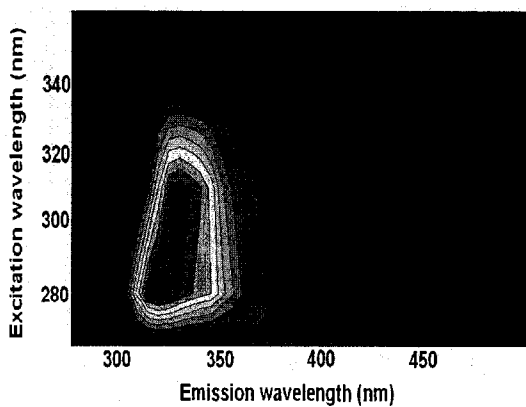


Figure B-4e. Gasoline in well graded sand and Devon silt EEM (600 mL/L)

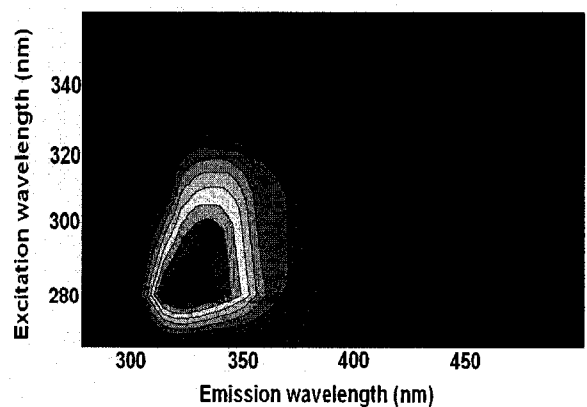


Figure B-4f. Gasoline in well graded sand and Devon silt EEM (neat)

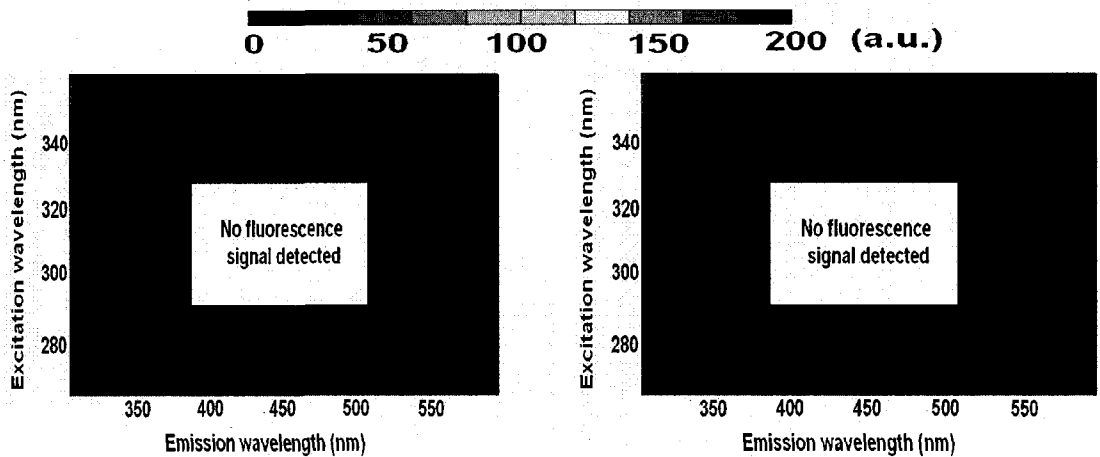


Figure B-5a. Gasoline in Devon silt EEM (1 mL/L)

Figure B-5b. Gasoline in Devon silt EEM (10 mL/L)

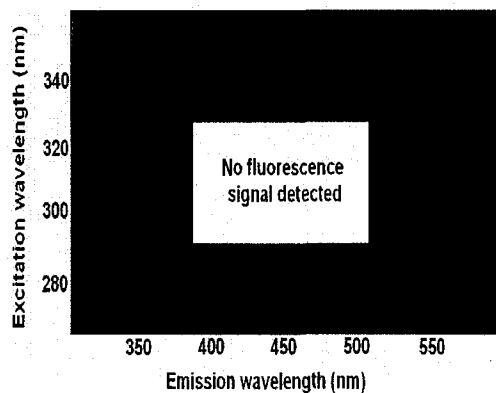


Figure B-5c. Gasoline in Devon silt EEM (50 mL/L)

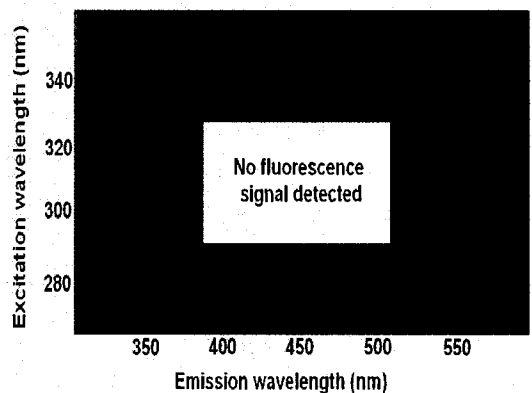


Figure B-5d. Gasoline in Devon silt EEM (200 mL/L)

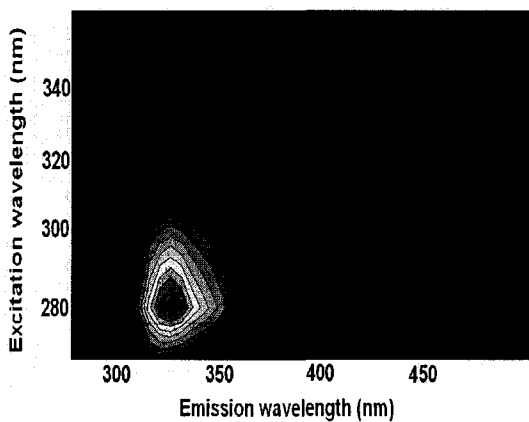


Figure B-5e. Gasoline in Devon silt EEM (600 mL/L)

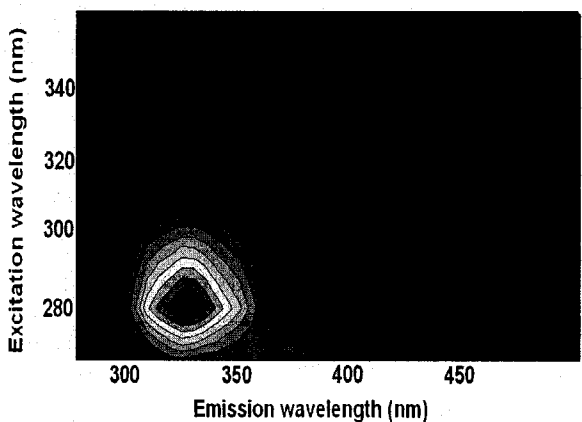


Figure B-5f. Gasoline in Devon silt EEM (neat)

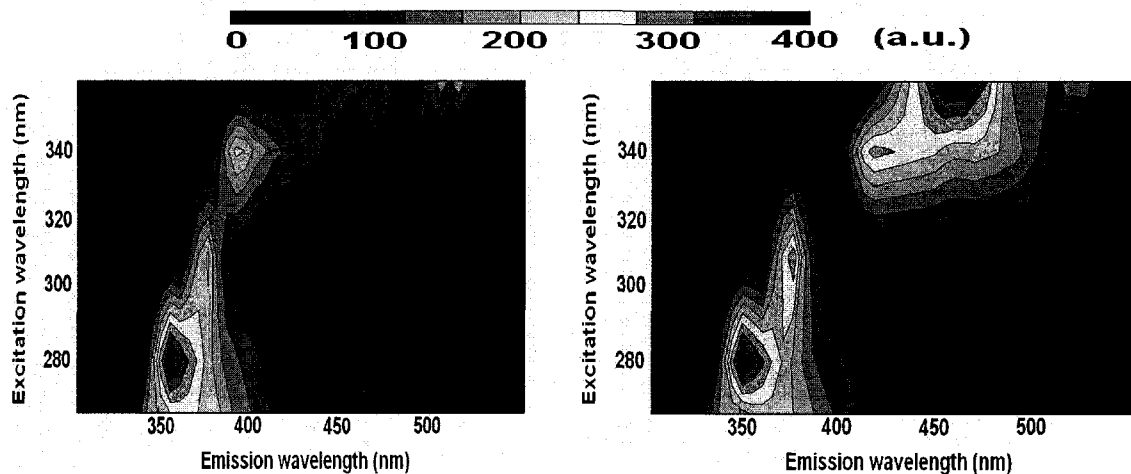


Figure B-6a. Diesel in hexane EEM (1 mL/L)

Figure B-6b. Diesel in hexane EEM (10 mL/L)

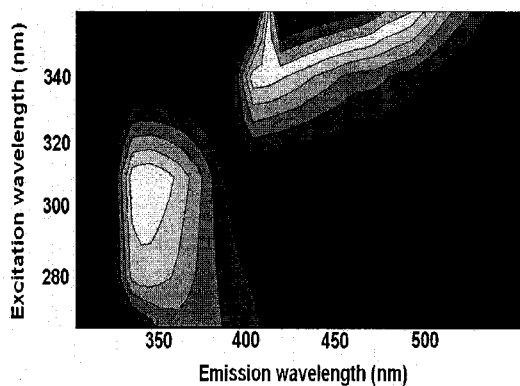


Figure B-6c. Diesel in hexane EEM (50 mL/L)

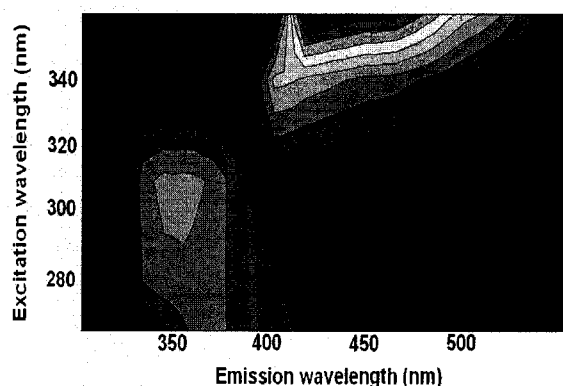


Figure B-6d. Diesel in hexane EEM (200 mL/L)

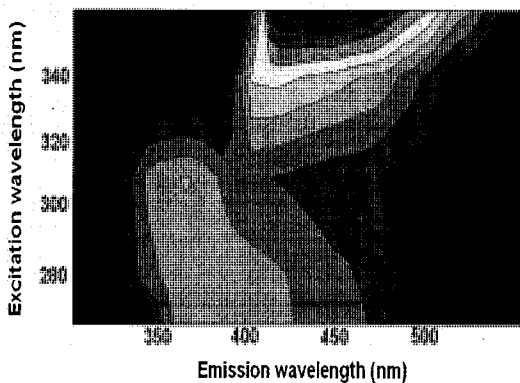


Figure B-6e. Diesel in hexane EEM (800 mL/L)

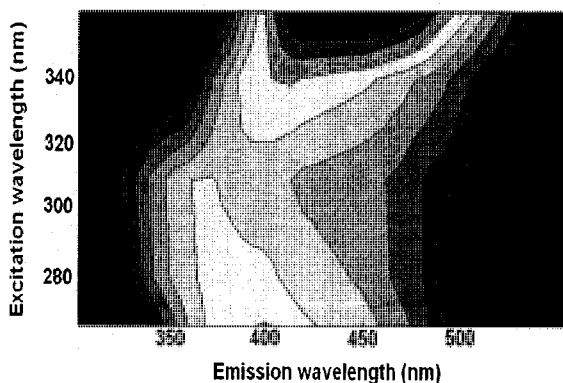


Figure B-6f. Diesel in hexane EEM (neat)



0 100 200 300 400 (a.u.)

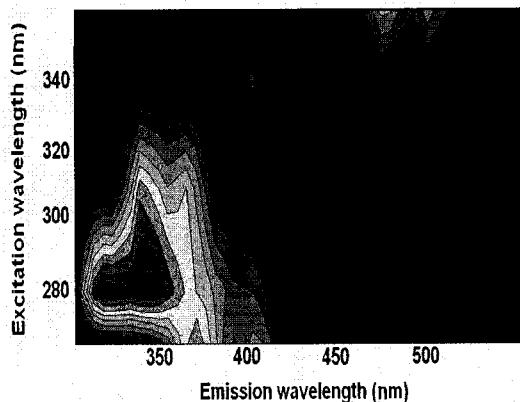


Figure B-7a. Diesel in Ottawa sand EEM (1 mL/L)

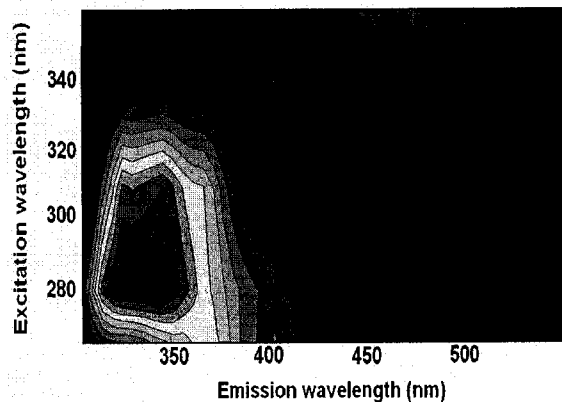


Figure B-7b. Diesel in Ottawa sand EEM (10 mL/L)

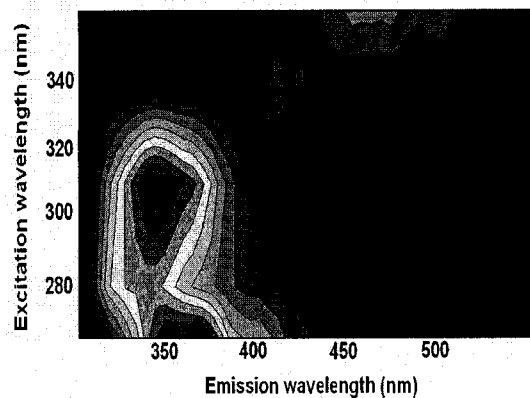


Figure B-7c. Diesel in Ottawa sand EEM (50 mL/L)

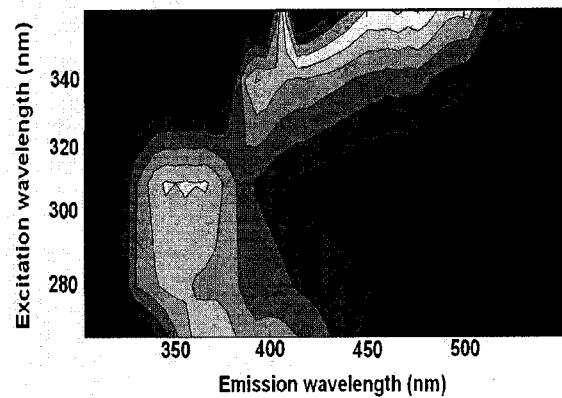


Figure B-7d. Diesel in Ottawa sand EEM (200 mL/L)

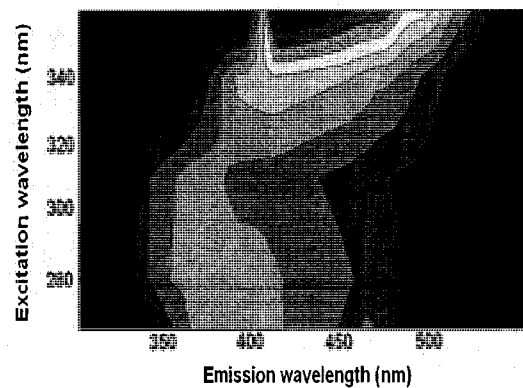


Figure B-7e. Diesel in Ottawa sand EEM (800 mL/L)

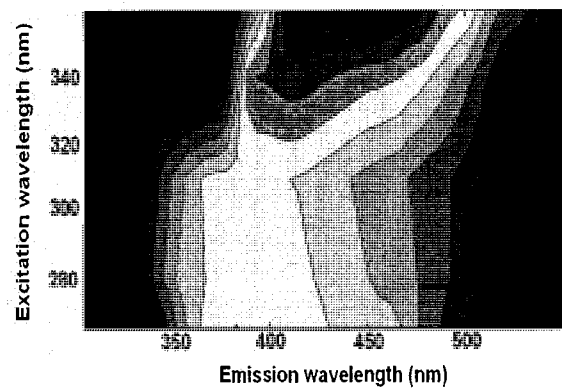


Figure B-7f. Diesel in Ottawa sand EEM (neat)

0 100 200 300 400 (a.u.)

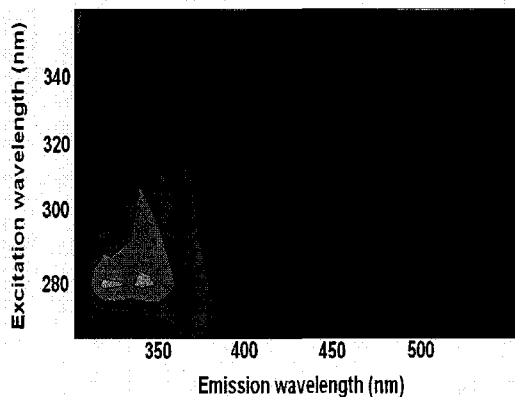


Figure B-8a. Diesel in well graded sand  
EEM (1 mL/L)

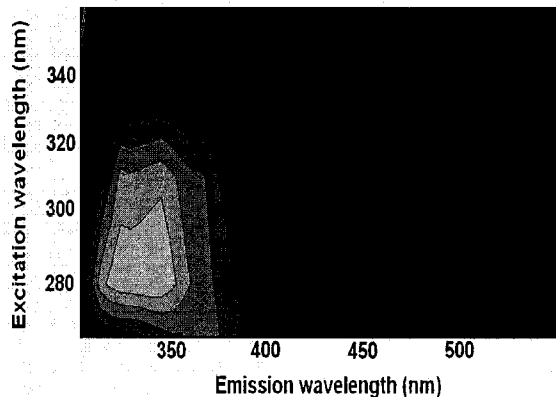


Figure B-8b. Diesel in well graded sand  
EEM (10 mL/L)

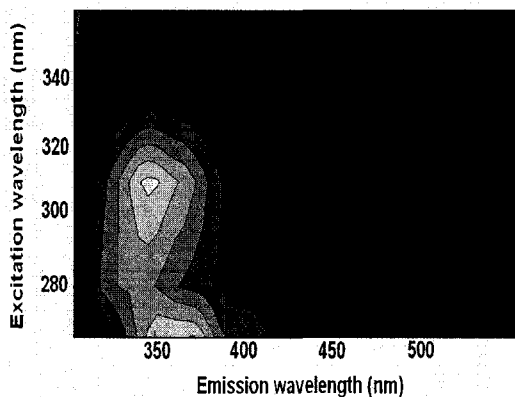


Figure B-8c. Diesel in well graded sand  
EEM (50 mL/L)

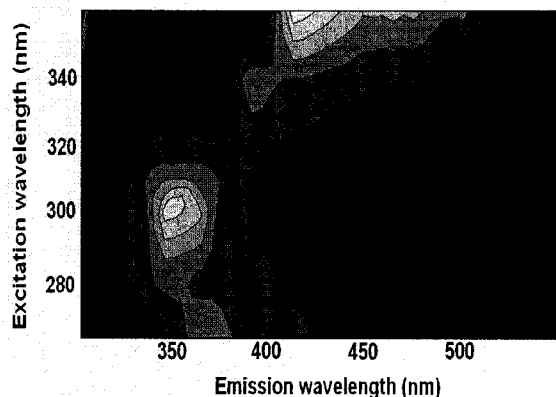


Figure B-8d. Diesel in well graded sand  
EEM (200 mL/L)

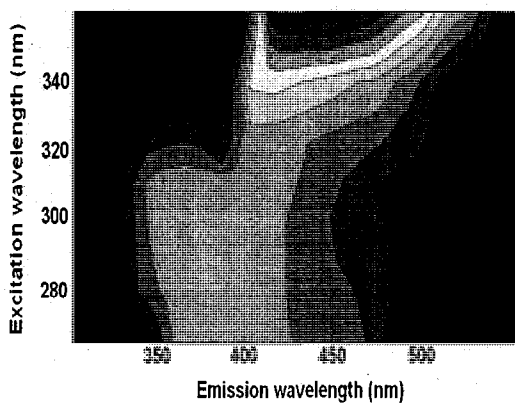


Figure B-8e. Diesel in well graded sand  
EEM (800 mL/L)

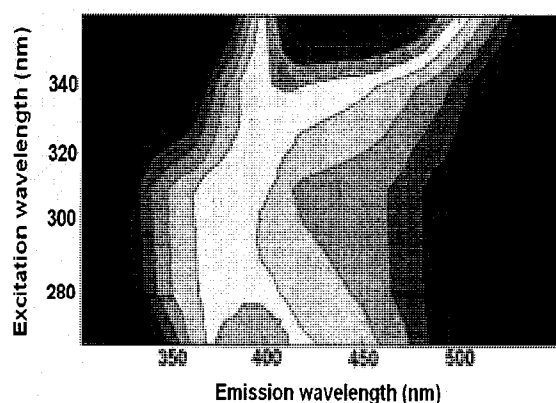


Figure B-8f. Diesel in well graded sand EEM  
(neat)

0 100 200 300 400 (a.u.)

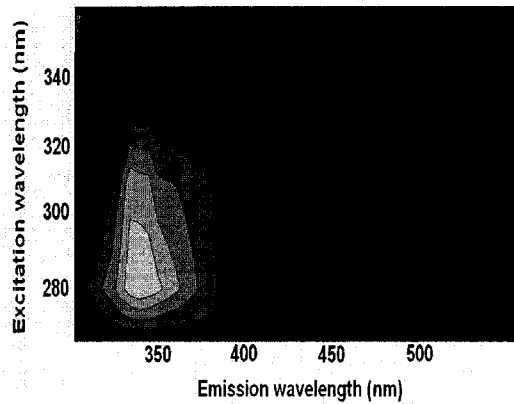


Figure B-9a. Diesel in well graded sand and Devon silt EEM (1 mL/L)

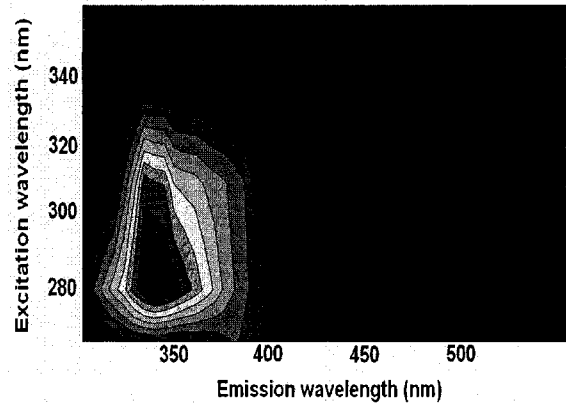


Figure B-9b. Diesel in well graded sand and Devon silt EEM (10 mL/L)

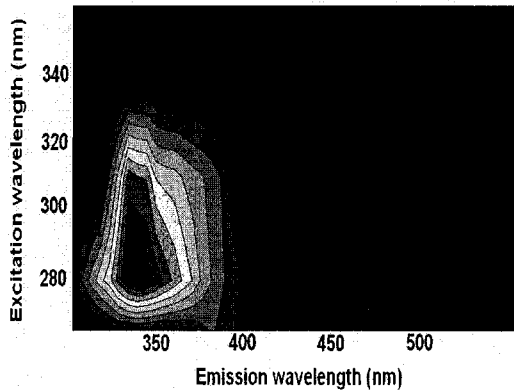


Figure B-9c. Diesel in well graded sand and Devon silt EEM (50 mL/L)

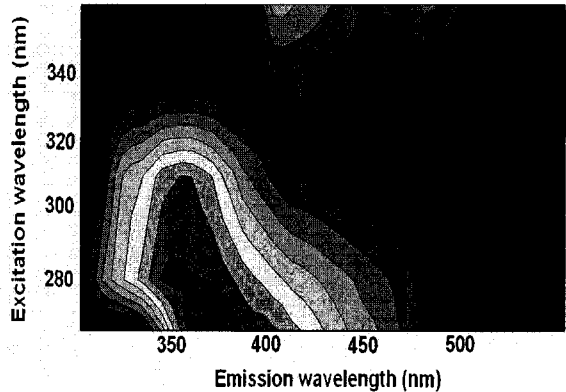


Figure B-9d. Diesel in well graded sand and Devon silt EEM (200 mL/L)

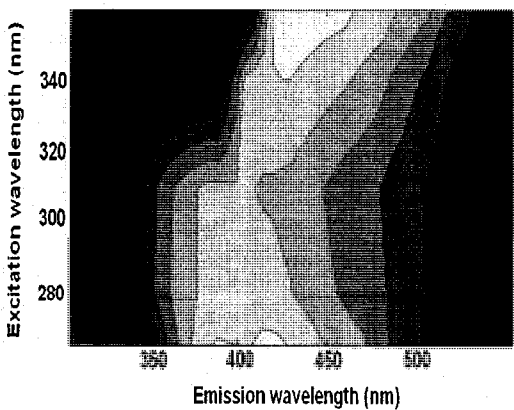


Figure B-9e. Diesel in well graded sand and Devon silt EEM (800 mL/L)

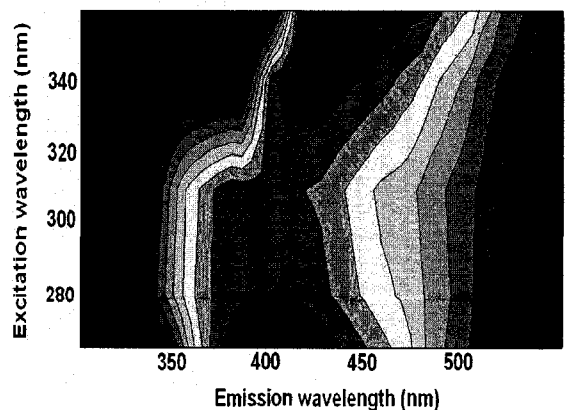


Figure B-9f. Diesel in well graded sand and Devon silt EEM (neat)

0 100 200 300 400 (a.u.)

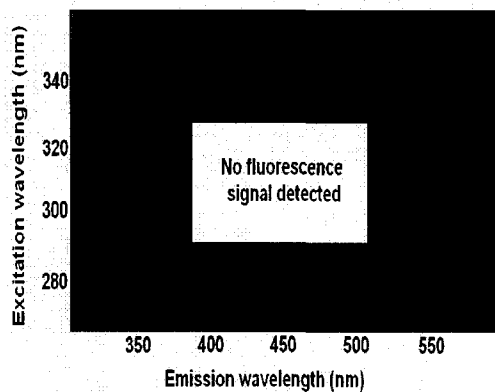


Figure B-10a. Diesel in Devon silt EEM  
(1 mL/L)

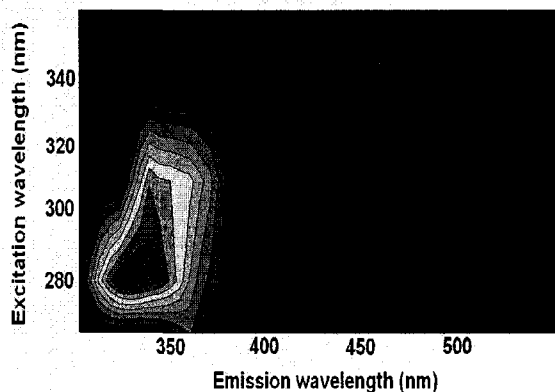


Figure B-10b. Diesel in Devon silt EEM (10  
mL/L)

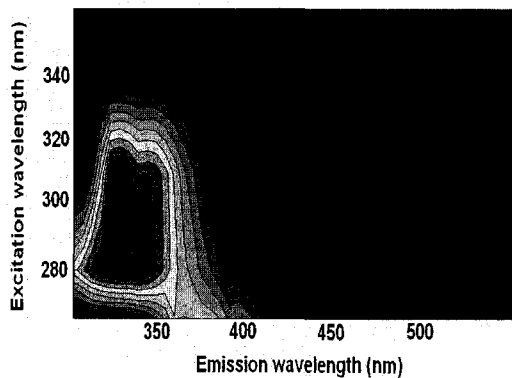


Figure B-10c. Diesel in Devon silt EEM  
(50 mL/L)

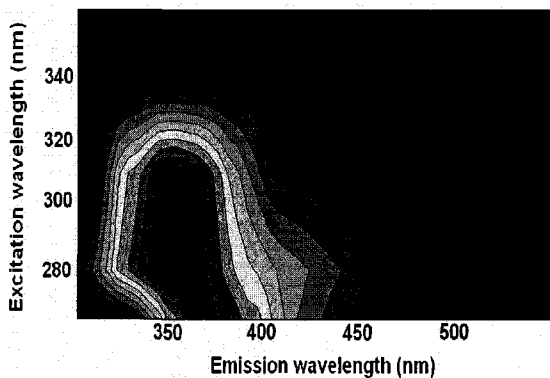


Figure B-10d. Diesel in Devon silt EEM (200  
mL/L)

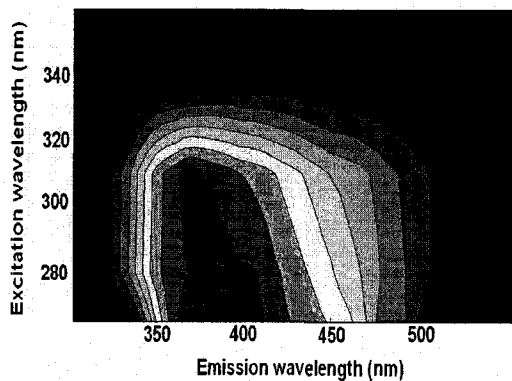


Figure B-10e. Diesel in Devon silt EEM  
(800 mL/L)

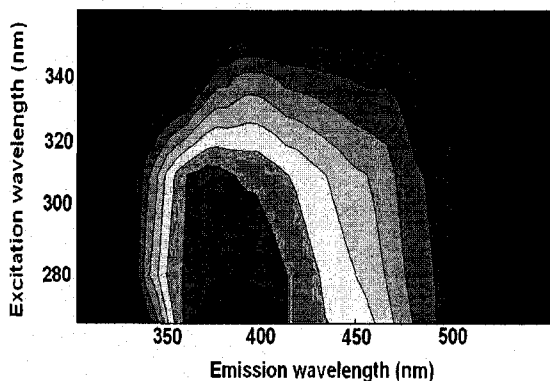


Figure B-10f. Diesel in Devon silt EEM  
(neat)

0 50 100 150 200 (a.u.)

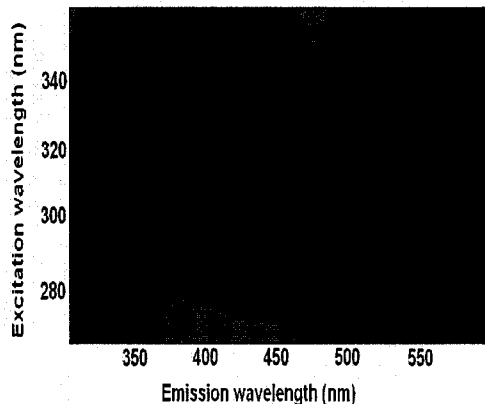


Figure B-11a. Flare pit residue in chloroform EEM (1 mL/L)

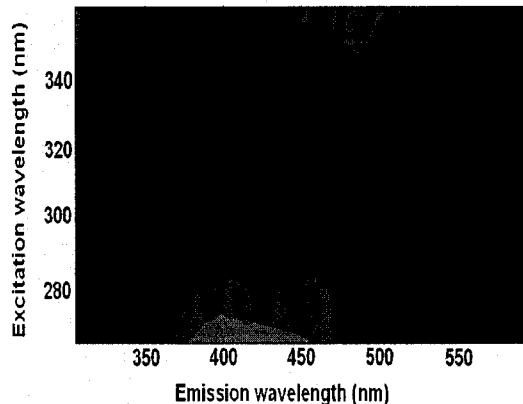


Figure B-11b. Flare pit residue in chloroform EEM (10 mL/L)

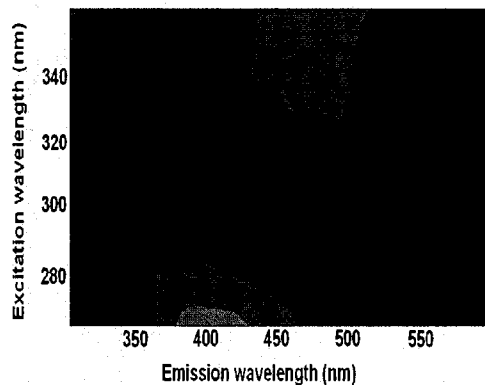


Figure B-11c. Flare pit residue in chloroform EEM (50 mL/L)

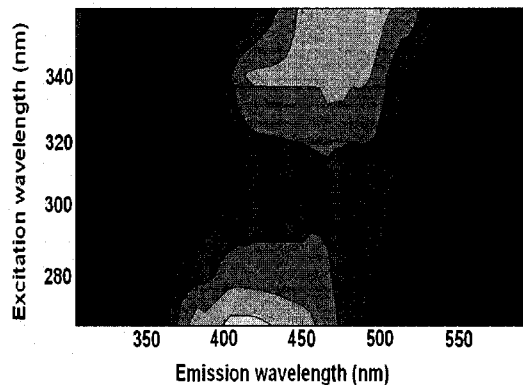


Figure B-11d. Flare pit residue in chloroform EEM (200 mL/L)

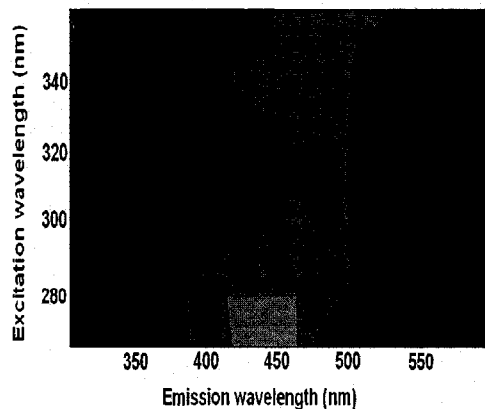


Figure B-11e. Flare pit residue in chloroform EEM (600 mL/L)

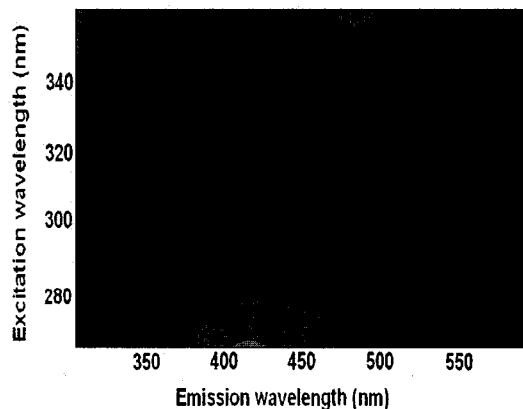


Figure B-11f. Flare pit residue EEM (neat)

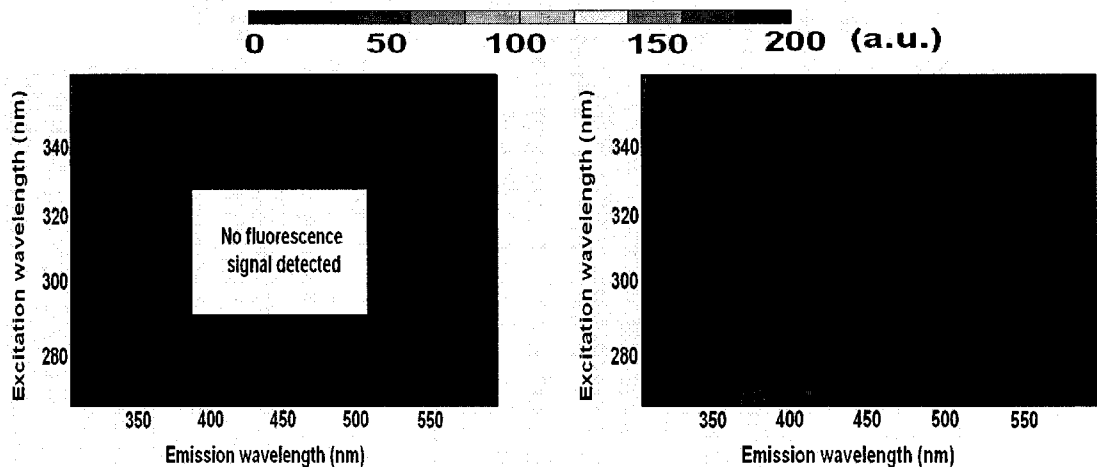


Figure B-12a. Flare pit residue in Ottawa sand EEM (1 mL/L)

Figure B-12b. Flare pit residue in Ottawa sand EEM (10 mL/L)

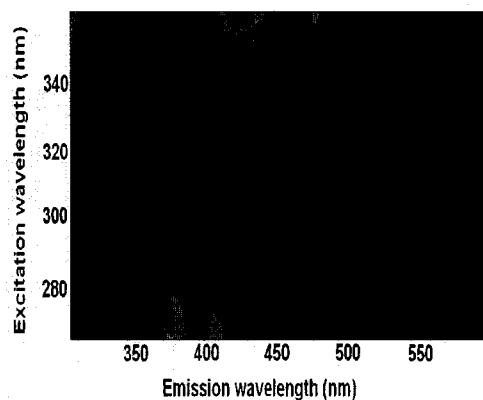


Figure B-12c. Flare pit residue in Ottawa sand EEM (50 mL/L)

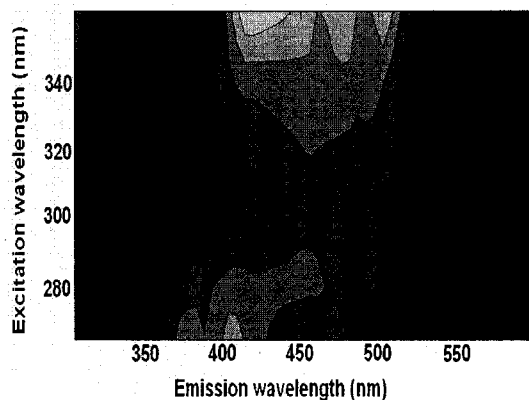


Figure B-12d. Flare pit residue in Ottawa sand EEM (200 mL/L)

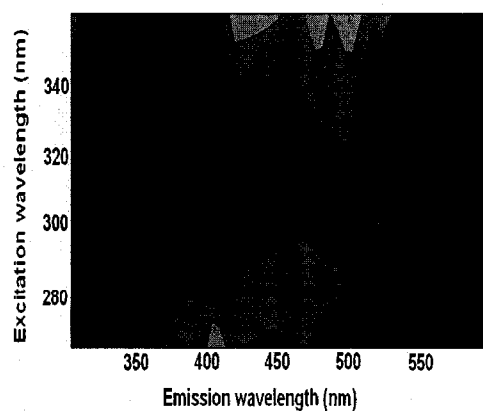


Figure B-12e. Flare pit residue in Ottawa sand EEM (600 mL/L)

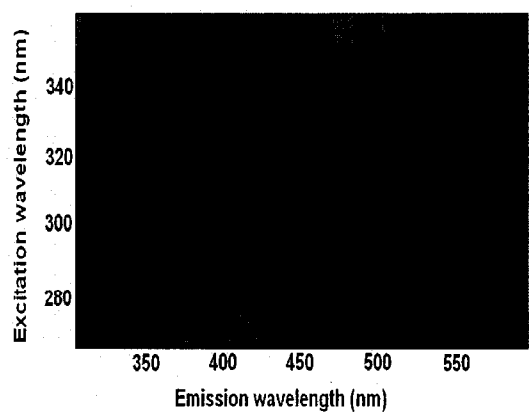


Figure B-12f. Flare pit residue in Ottawa sand EEM (neat)

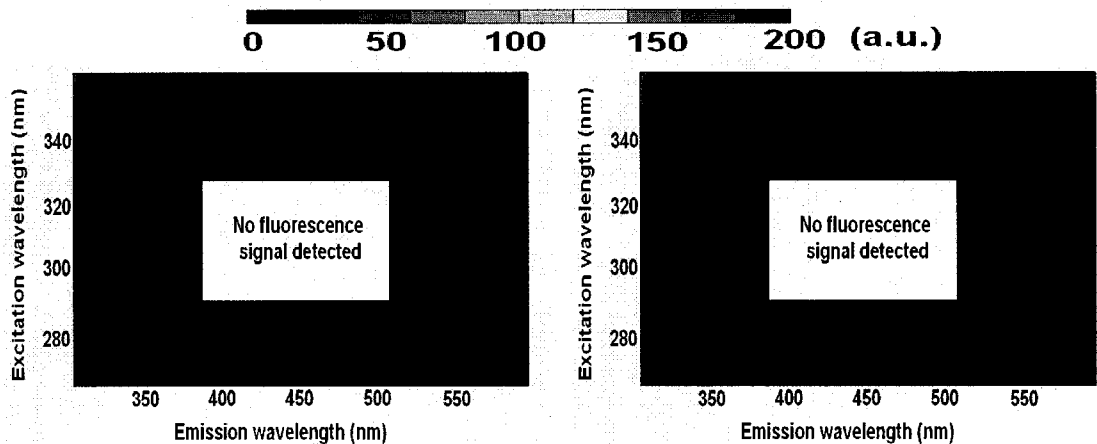


Figure B-13a. Flare pit residue in well graded sand EEM (1 mL/L)

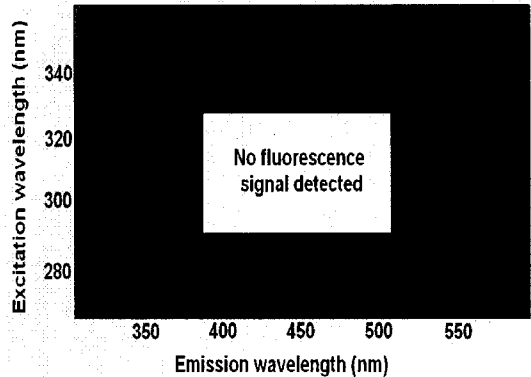


Figure B-13b. Flare pit residue in well graded sand EEM (10 mL/L)

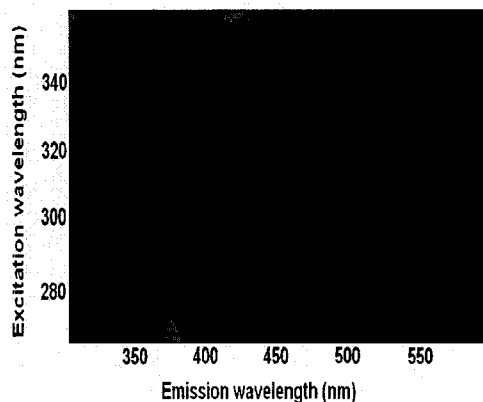


Figure B-13c. Flare pit residue in well graded sand EEM (50 mL/L)

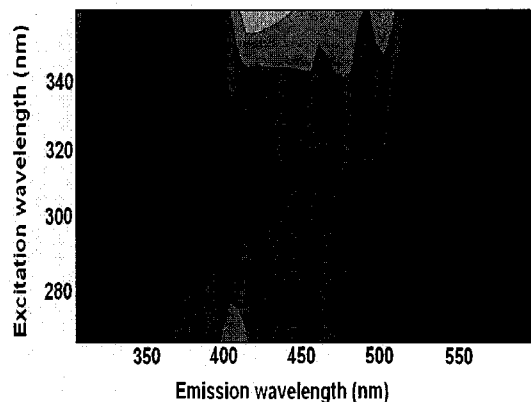


Figure B-13d. Flare pit residue in well graded sand EEM (200 mL/L)

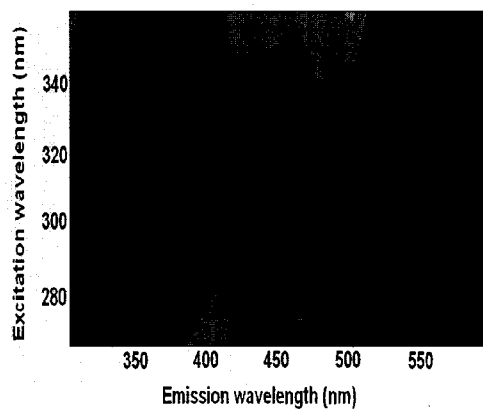


Figure B-13e. Flare pit residue in well graded sand EEM (600 mL/L)

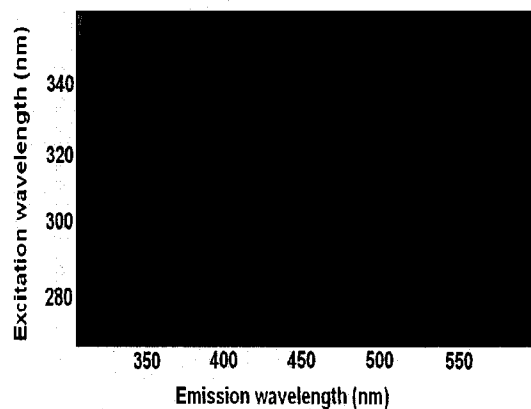


Figure B-13f. Flare pit residue in well graded sand EEM (neat)

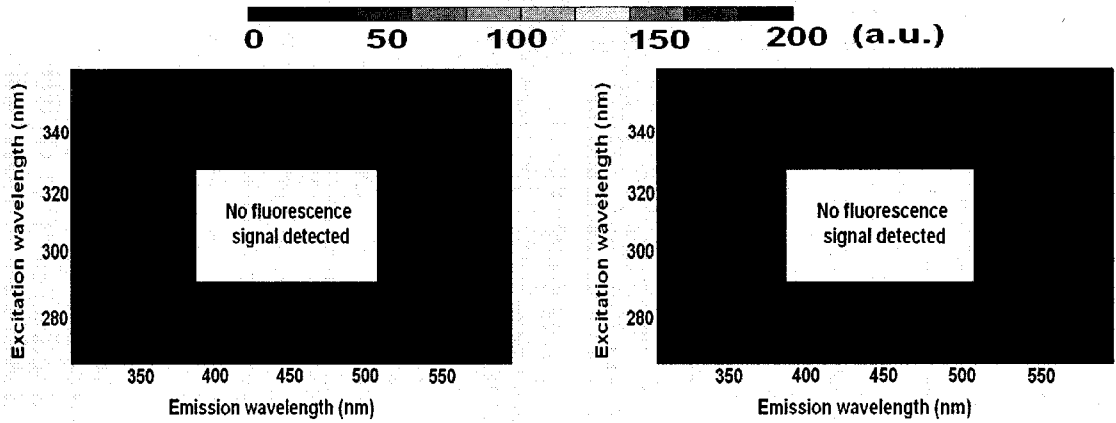


Figure B-14a. Flare pit residue in well graded sand and Devon silt EEM (1 mL/L)

Figure B-14b. Flare pit residue in well graded sand and Devon silt EEM (10 mL/L)

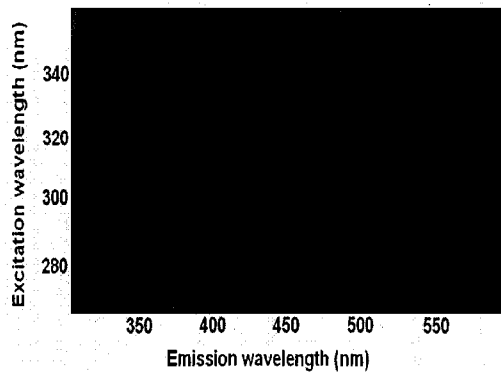


Figure B-14c. Flare pit residue in well graded sand and Devon silt EEM (50 mL/L)

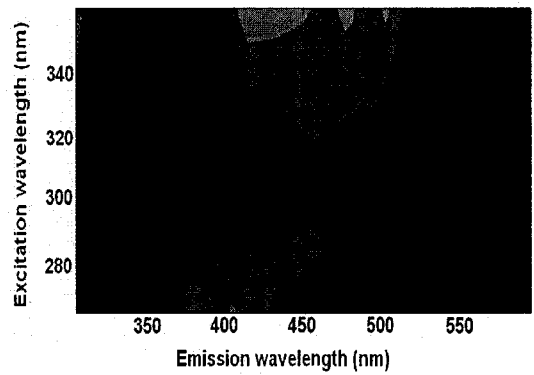


Figure B-14d. Flare pit residue in well graded sand and Devon silt EEM (200 mL/L)

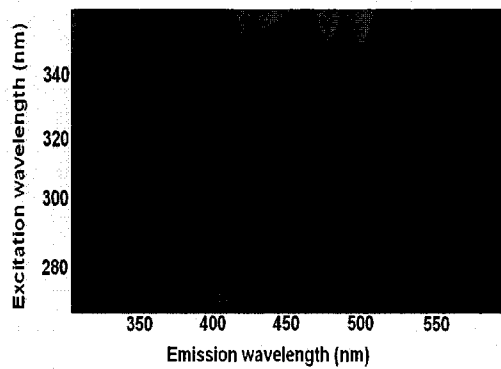


Figure B-14e. Flare pit residue in well graded sand and Devon silt EEM (600 mL/L)

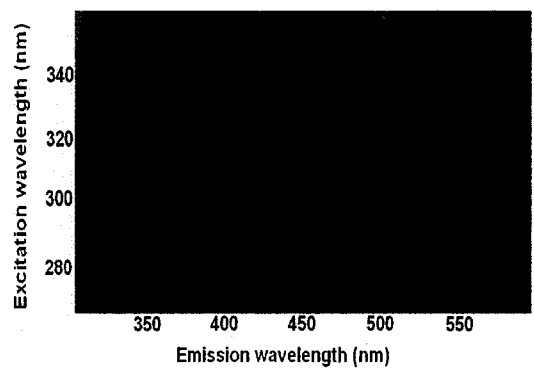


Figure B-14f. Flare pit residue in well graded sand and Devon silt EEM (neat)



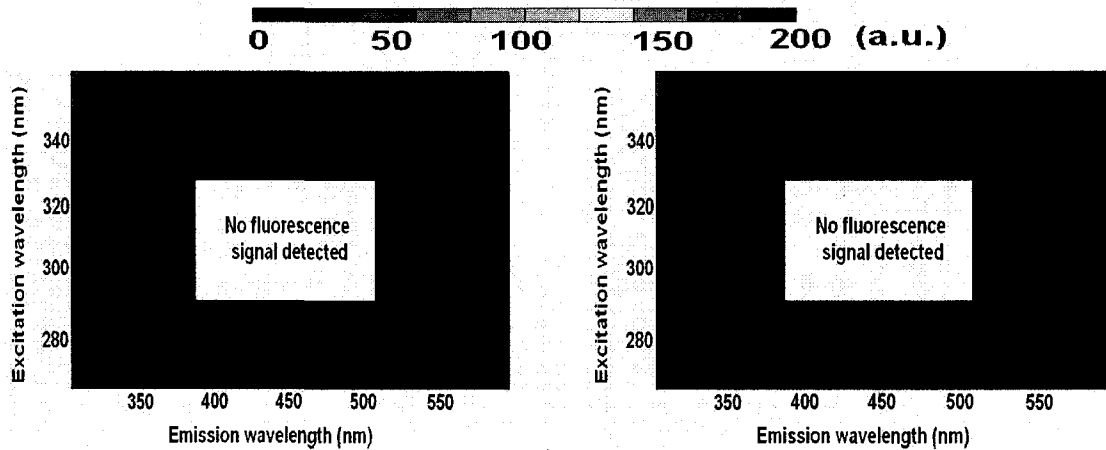


Figure B-15a. Flare pit residue in Devon silt EEM (1 mL/L)

Figure B-15b. Flare pit residue in Devon silt EEM (10 mL/L)

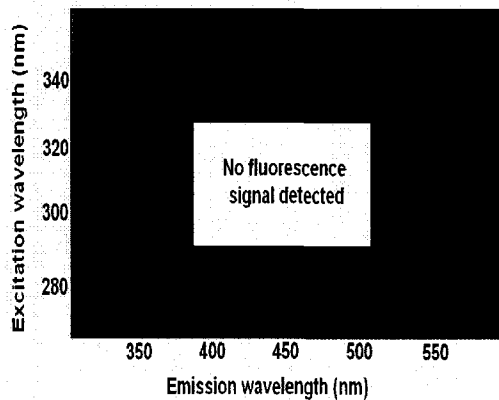


Figure B-15c. Flare pit residue in Devon silt EEM (50 mL/L)

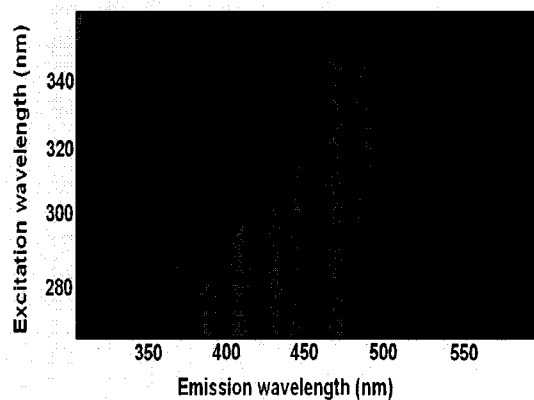


Figure B-15d. Flare pit residue in Devon silt EEM (200 mL/L)

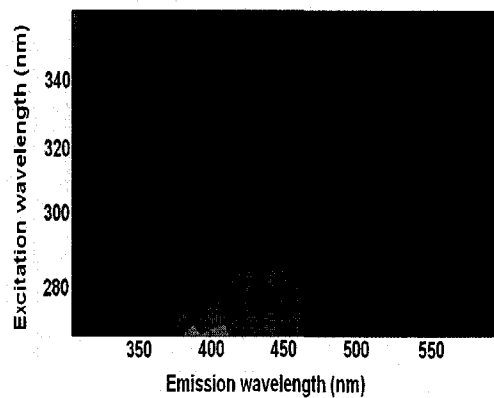


Figure B-15a. Flare pit residue in Devon silt EEM (600 mL/L)

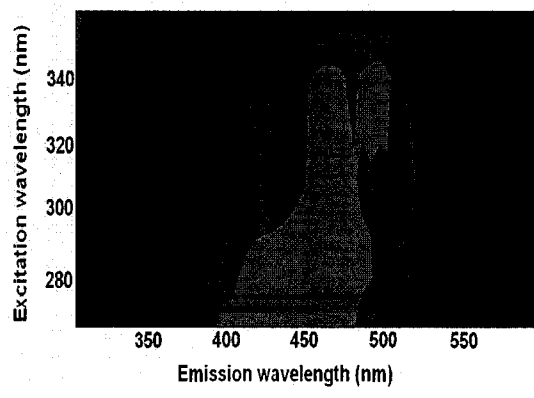


Figure B-15b. Flare pit residue in Devon silt EEM (neat)

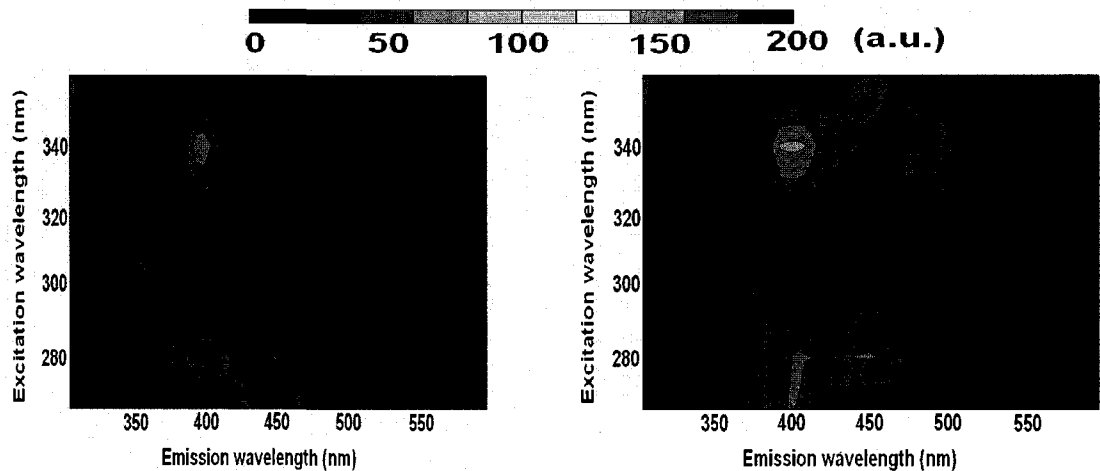


Figure B-16a. Crude oil in chloroform  
EEM (1 mL/L)

Figure B-16b. Crude oil in chloroform EEM  
(10 mL/L)

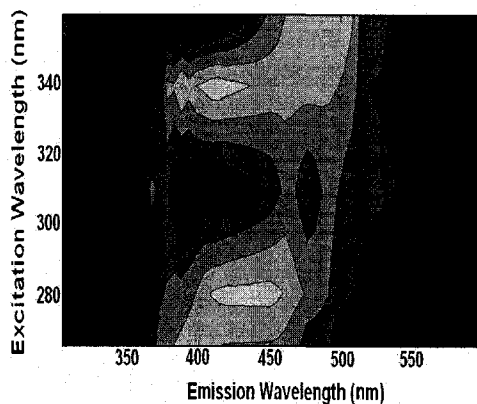


Figure B-16c. Crude oil in chloroform  
EEM (40 mL/L)

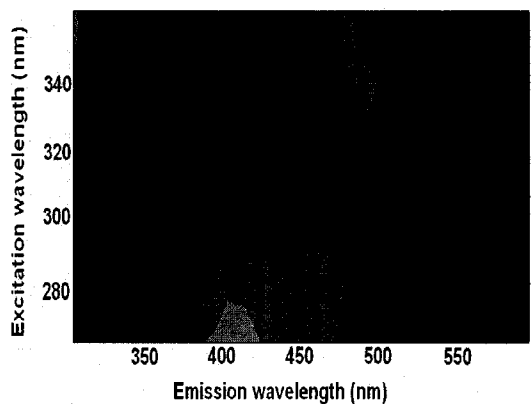


Figure B-16d. Crude oil in chloroform EEM  
(200 mL/L)

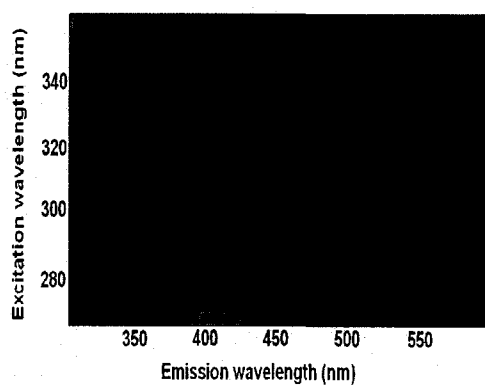


Figure B-16e. Crude oil in chloroform  
EEM (640 mL/L)

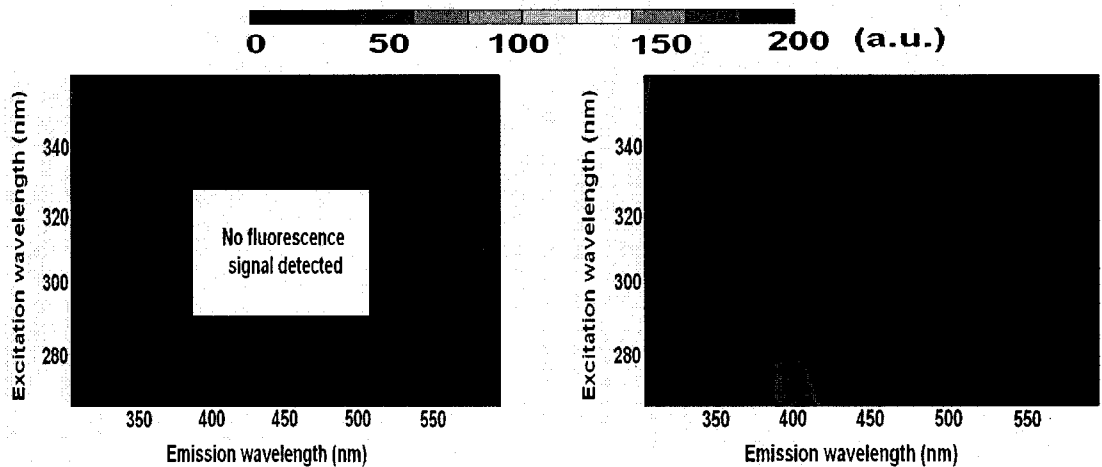


Figure B-17a. Crude oil in Ottawa sand  
EEM (1 mL/L)

Figure B-17b. Crude oil in Ottawa sand EEM  
(10 mL/L)

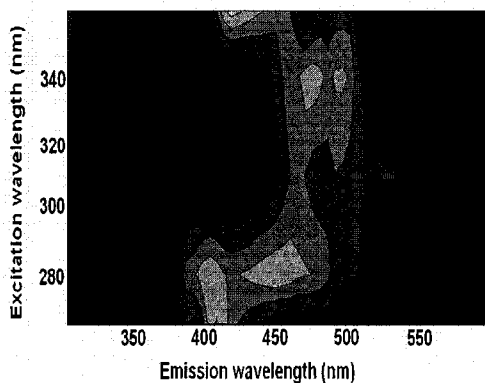


Figure B-17c. Crude oil in Ottawa sand  
EEM (40 mL/L)

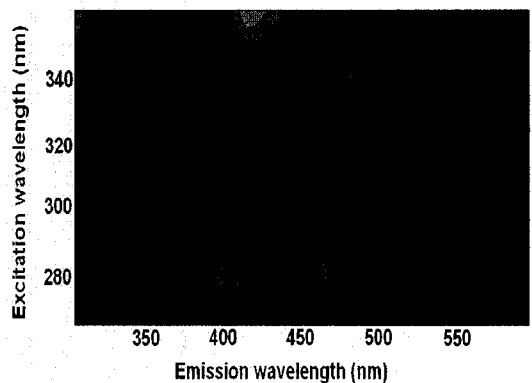


Figure B-17d. Crude oil in Ottawa sand EEM  
(200 mL/L)

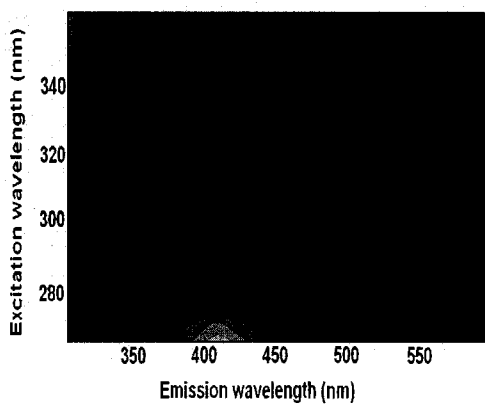


Figure B-17e. Crude oil in Ottawa sand  
EEM (640 mL/L)

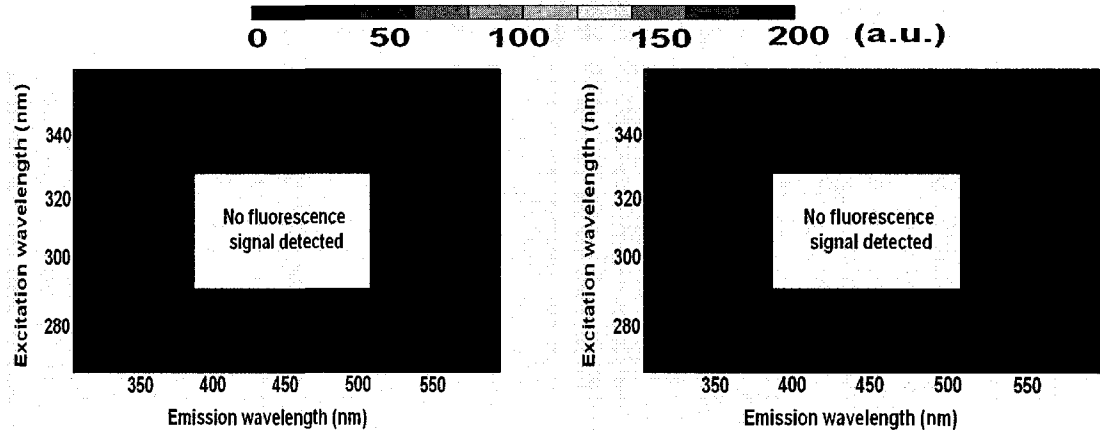


Figure B-18a. Crude oil in well graded sand EEM (1 mL/L)

Figure B-18b. Crude oil in well graded sand EEM (10 mL/L)

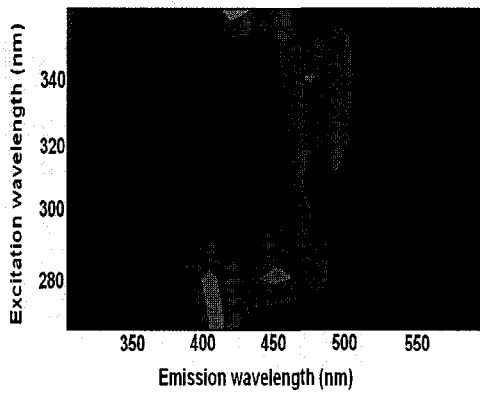


Figure B-18c. Crude oil in well graded sand EEM (40 mL/L)

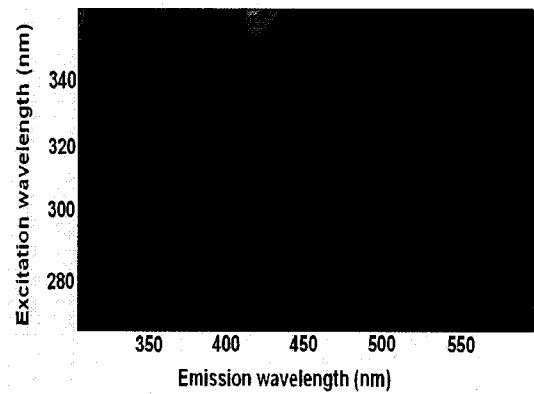


Figure B-18d. Crude oil in well graded sand EEM (200 mL/L)

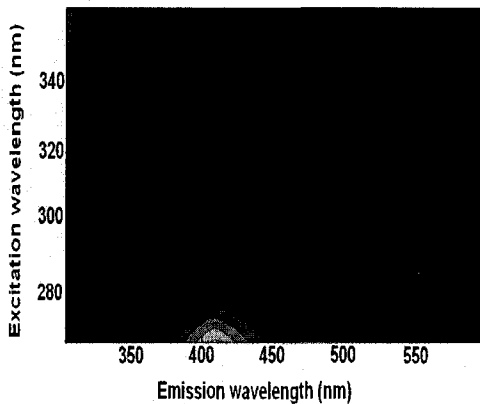


Figure B-18e. Crude oil in well graded sand EEM (640 mL/L)

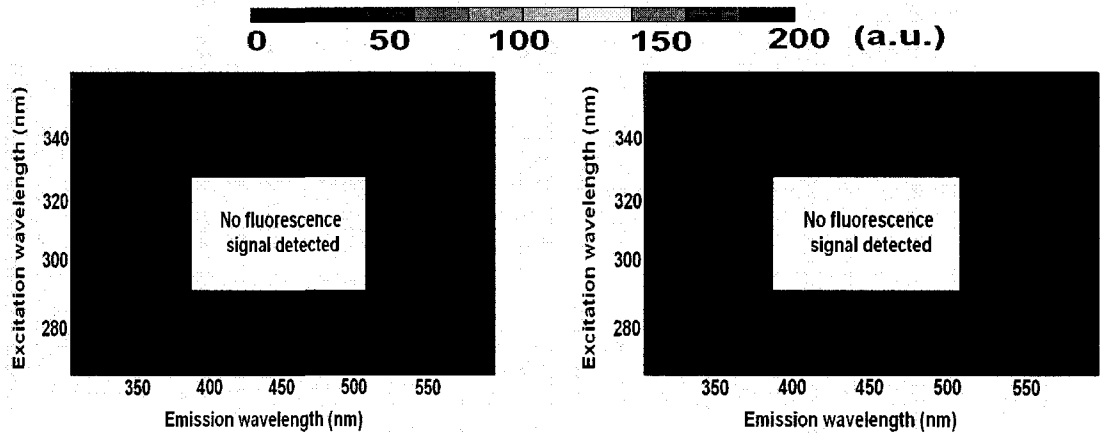


Figure B-19a. Crude oil in well graded sand and Devon silt EEM (1 mL/L)

Figure B-19b. Crude oil in well graded sand and Devon silt EEM (10 mL/L)

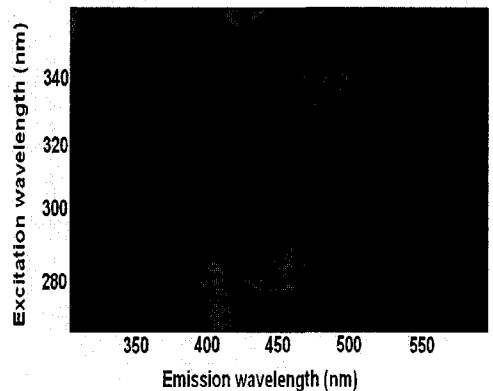


Figure B-19c. Crude oil in well graded sand and Devon silt EEM (40 mL/L)

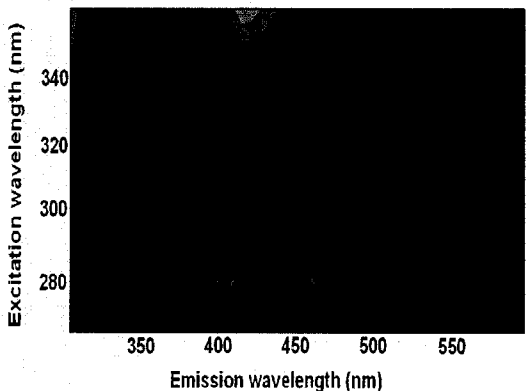


Figure B-19d. Crude oil in well graded sand and Devon silt EEM (200 mL/L)

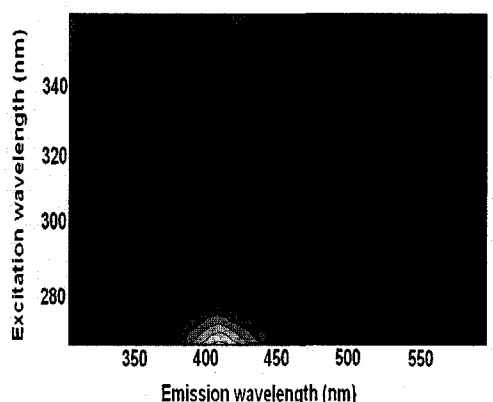


Figure B-19e. Crude oil in well graded sand and Devon silt EEM (640 mL/L)

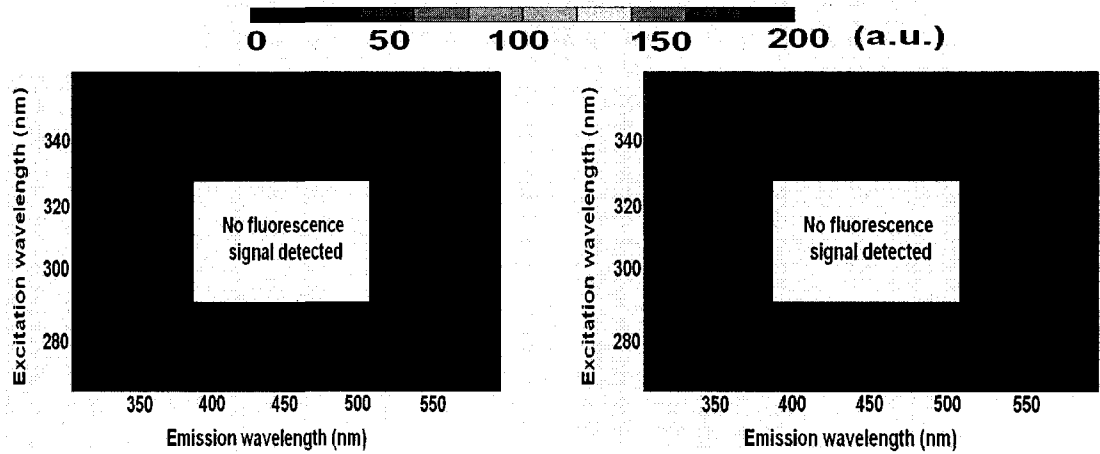


Figure B-20a. Crude oil in Devon silt  
EEM (1 mL/L)

Figure B-20b. Crude oil in Devon silt EEM  
(10 mL/L)

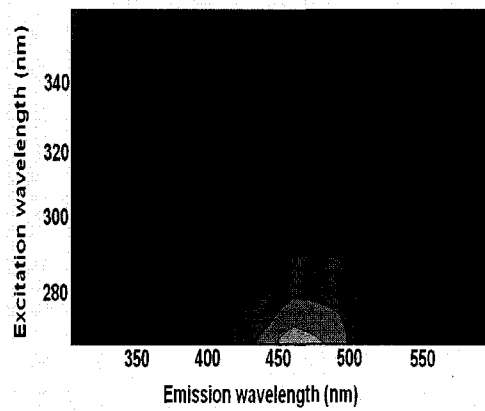


Figure B-20c. Crude oil in Devon silt  
EEM (40 mL/L)

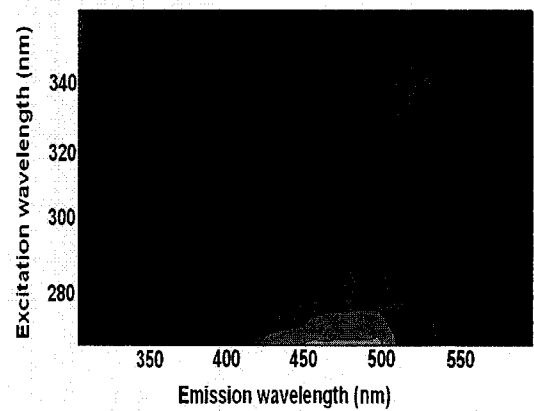


Figure B-20d. Crude oil in Devon silt EEM  
(200 mL/L)

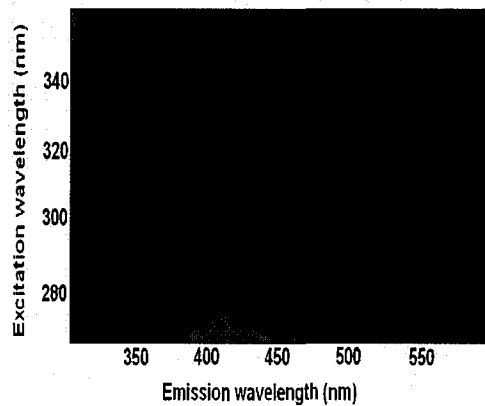


Figure B-20e. Crude oil in Devon silt  
EEM (640 mL/L)

**Appendix C**  
Fluorescence calibration  
curves  
*(Using Varian Eclipse  
Spectrometer)*

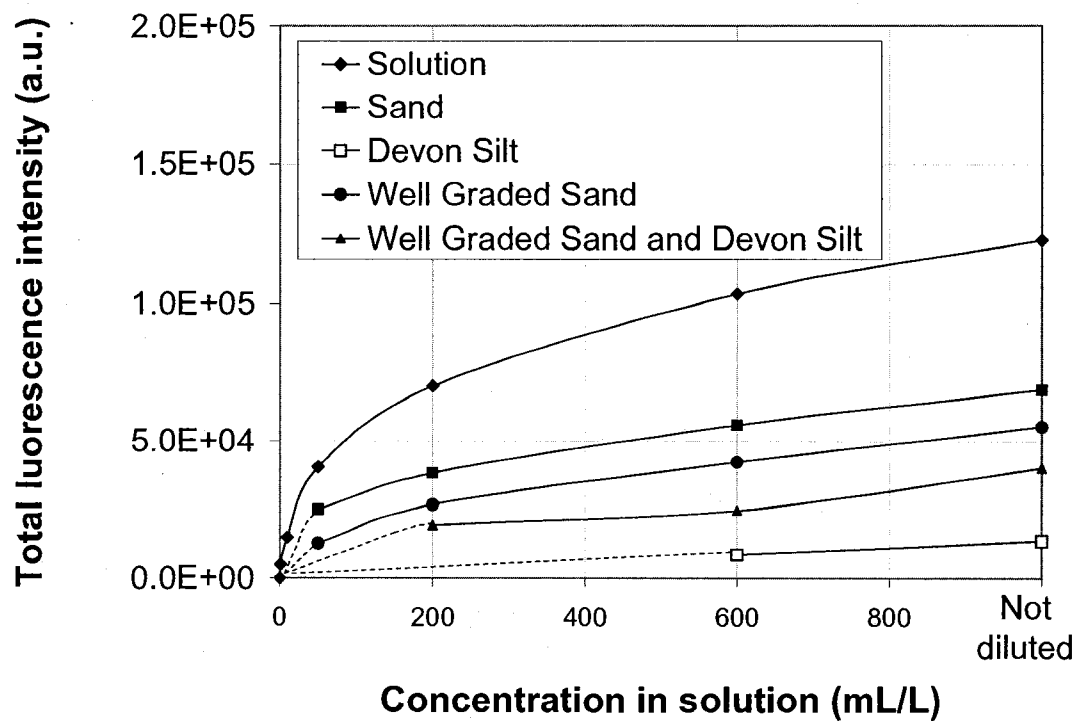


Figure C-1. Gas condensate fluorescence calibration curves in solvent solution and soil



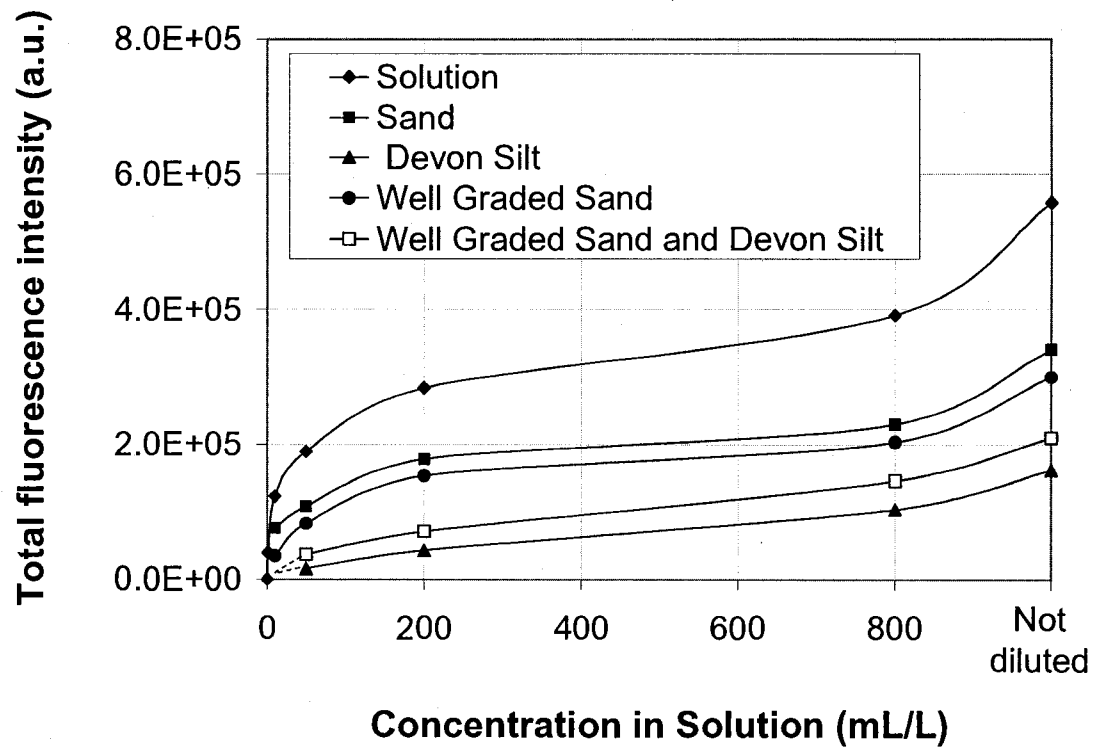


Figure C-2. Gasoline fluorescence calibration curves in solvent solution and soil

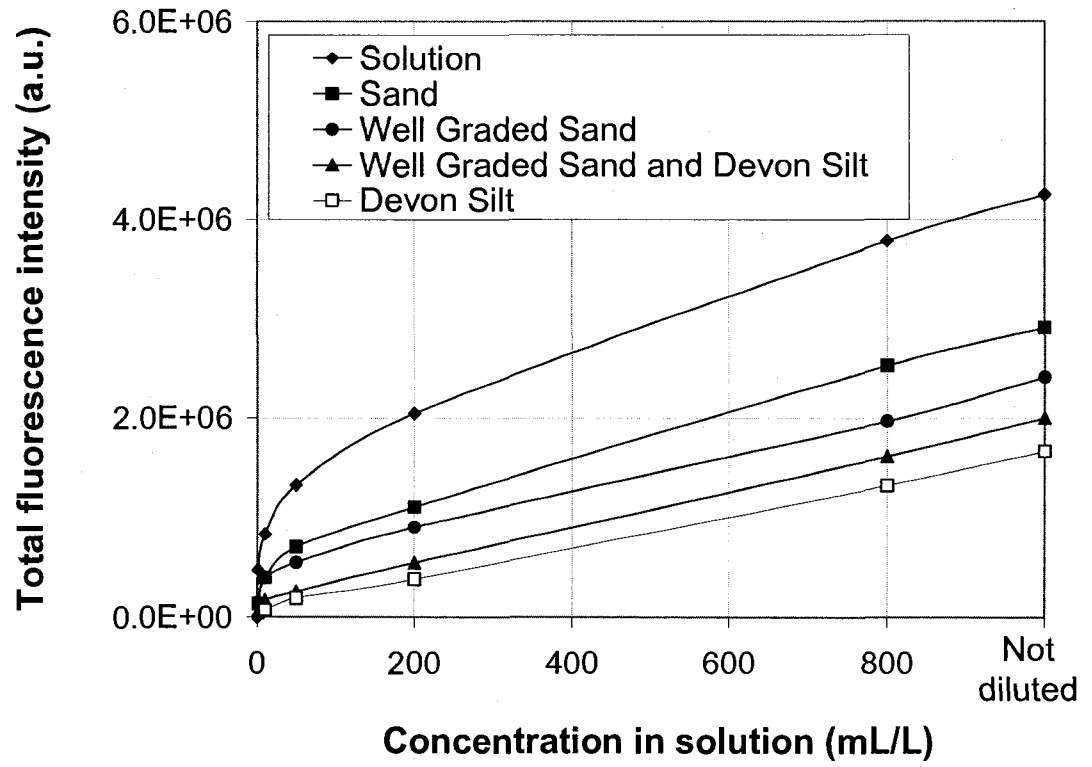


Figure C-3. Diesel fluorescence calibration curves in solvent solution and soil

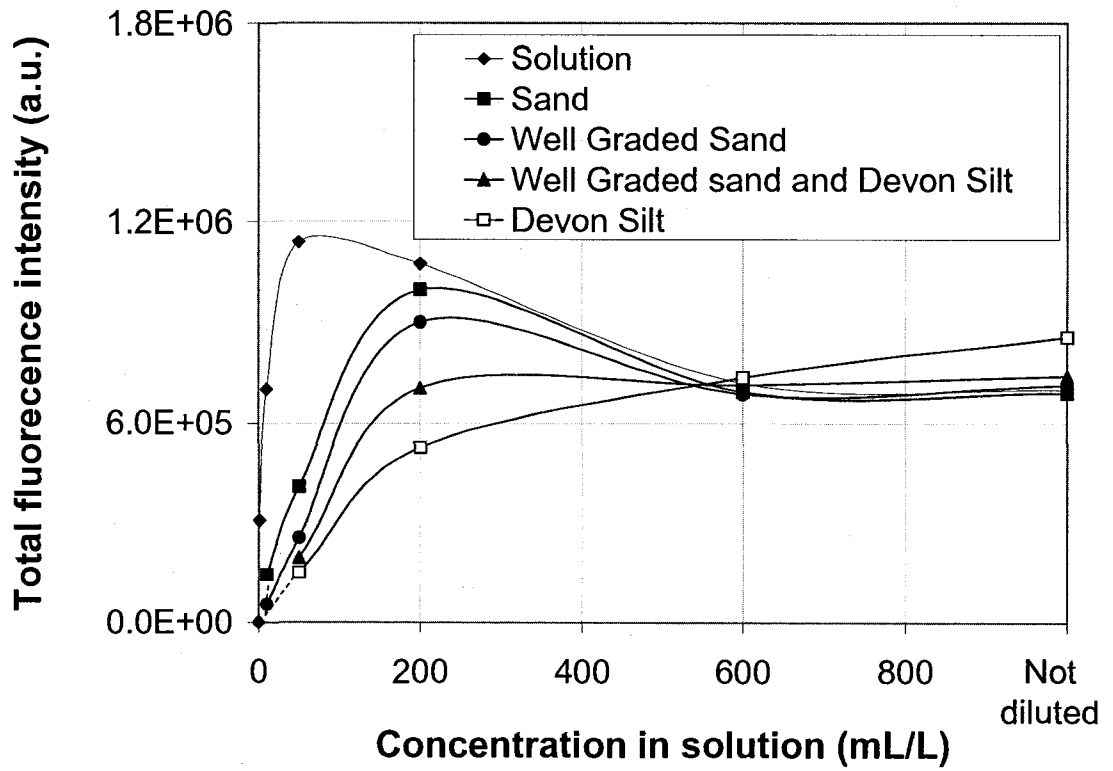


Figure C-4. Flare pit residue fluorescence calibration curves in solvent solution and soil

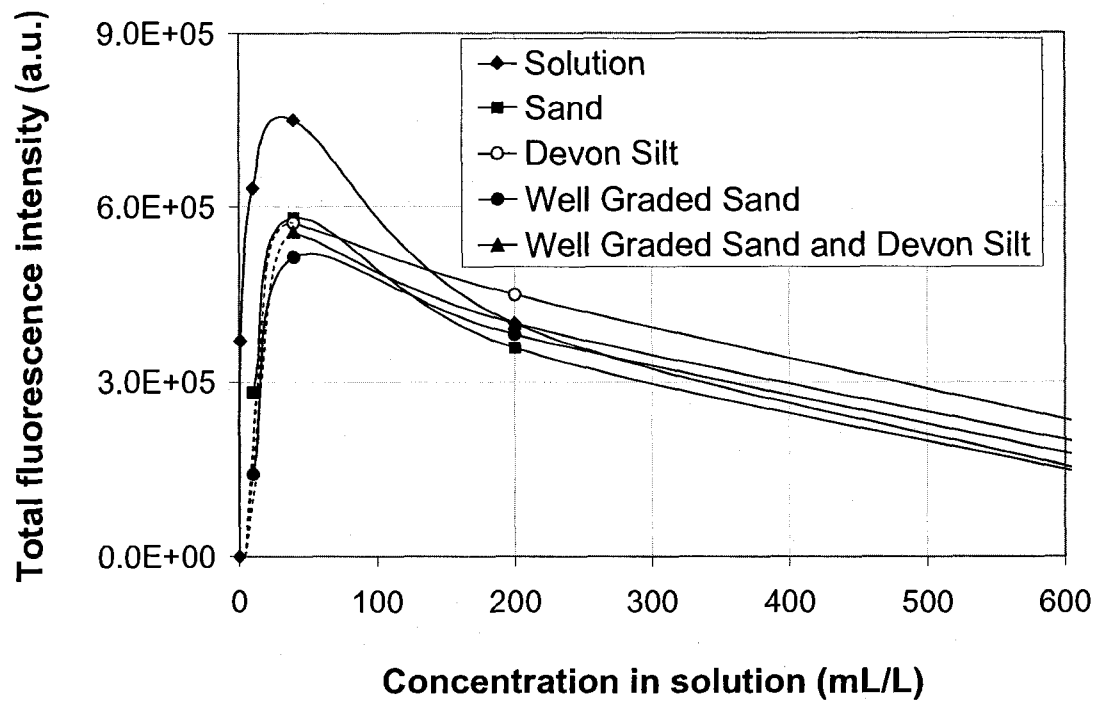


Figure C-5. Crude oil fluorescence calibration curves in solvent solution and soil

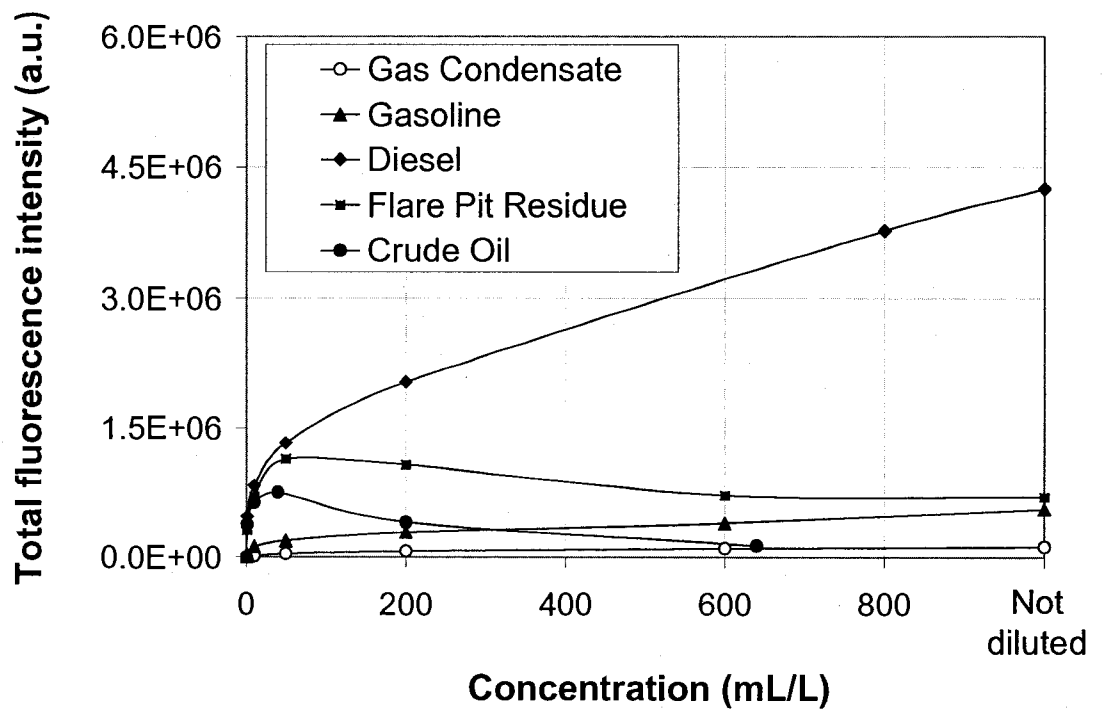


Figure C-6. Tested petroleum products fluorescence calibration curves in solvent solutions

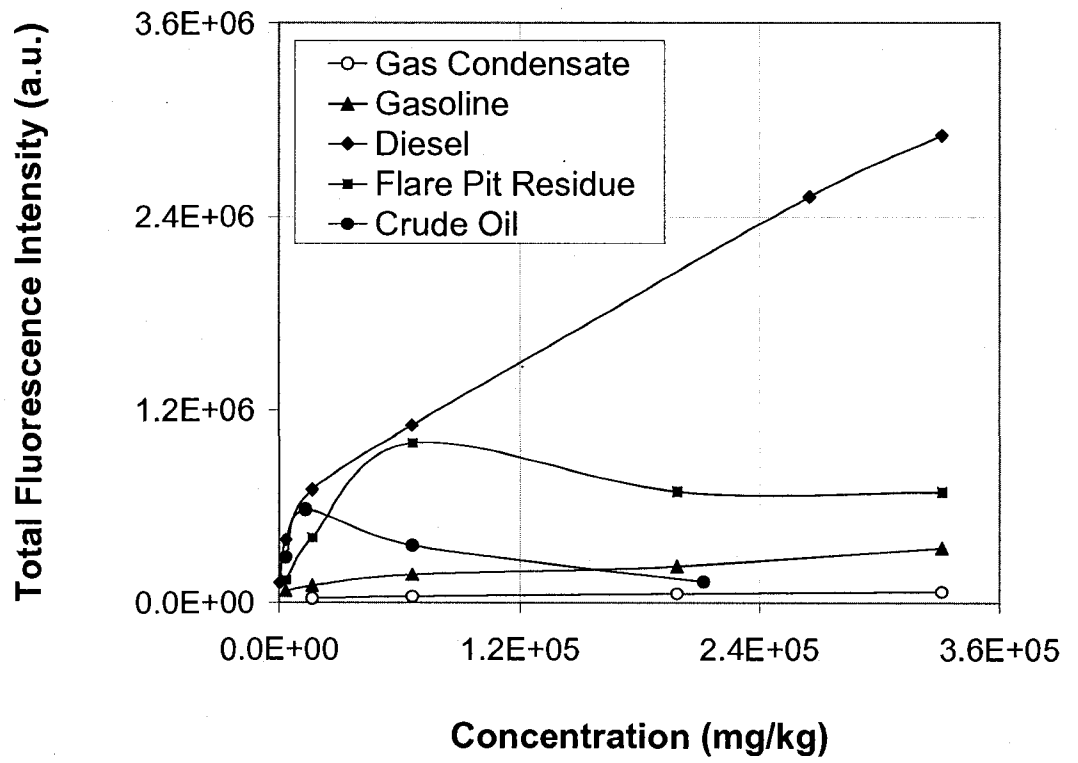


Figure C-7. Tested petroleum products fluorescence calibration curves in Ottawa sand

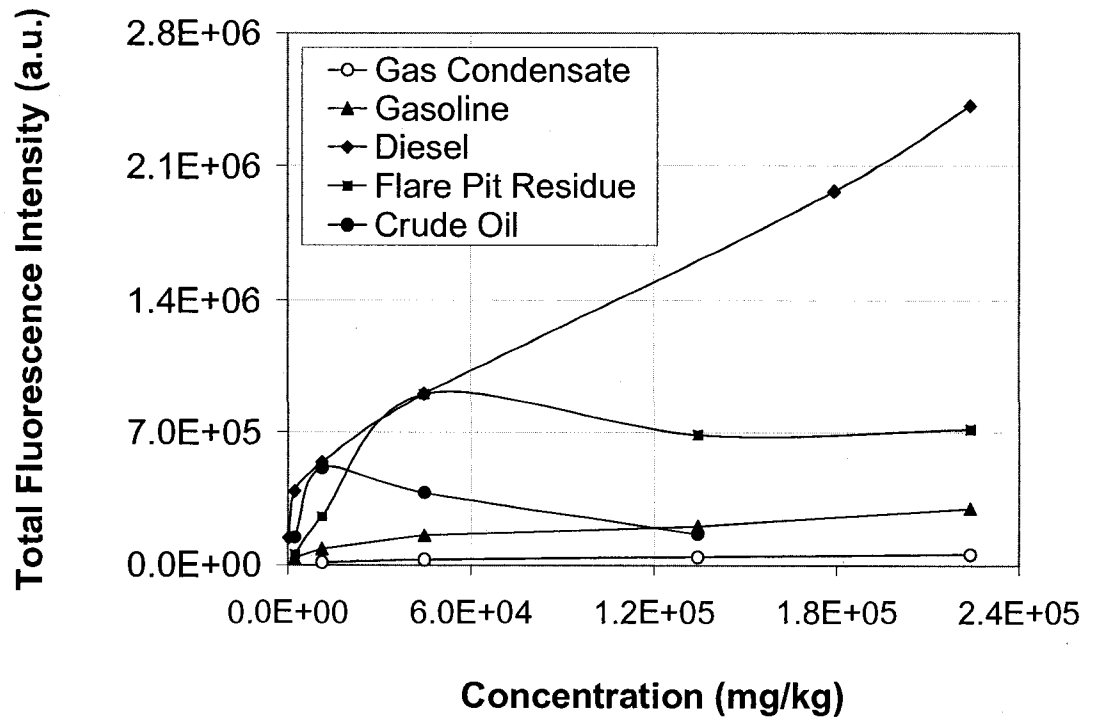


Figure C-8. Tested petroleum products fluorescence calibration curves in well graded sand

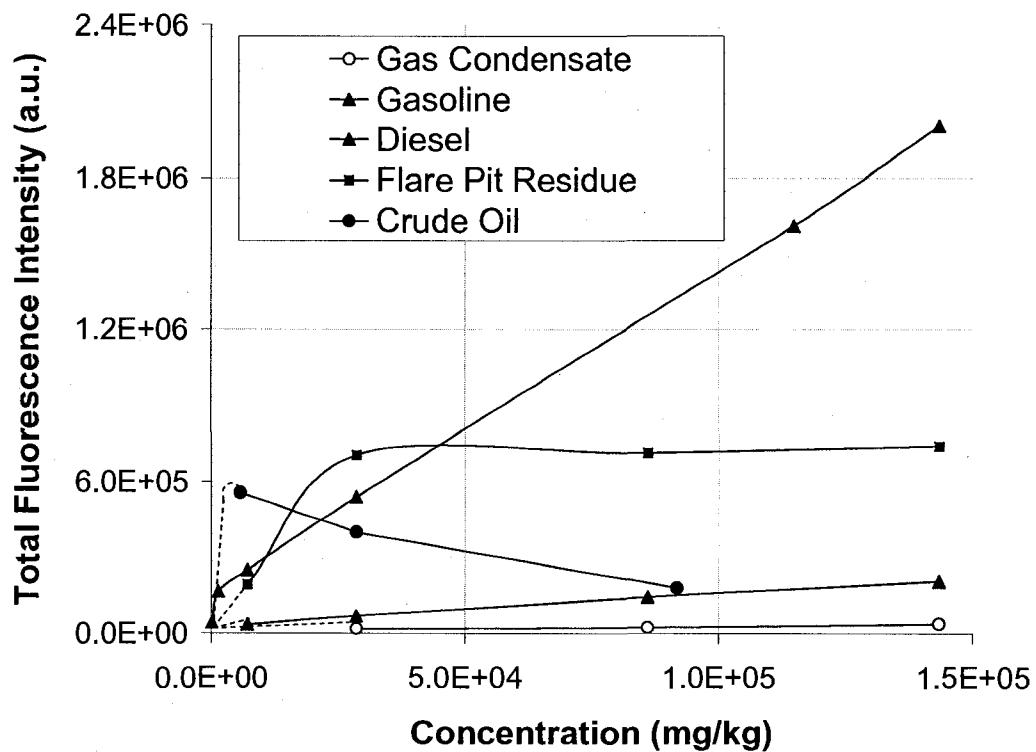


Figure C-9. Tested petroleum products fluorescence calibration curves in well graded sand and Devon silt



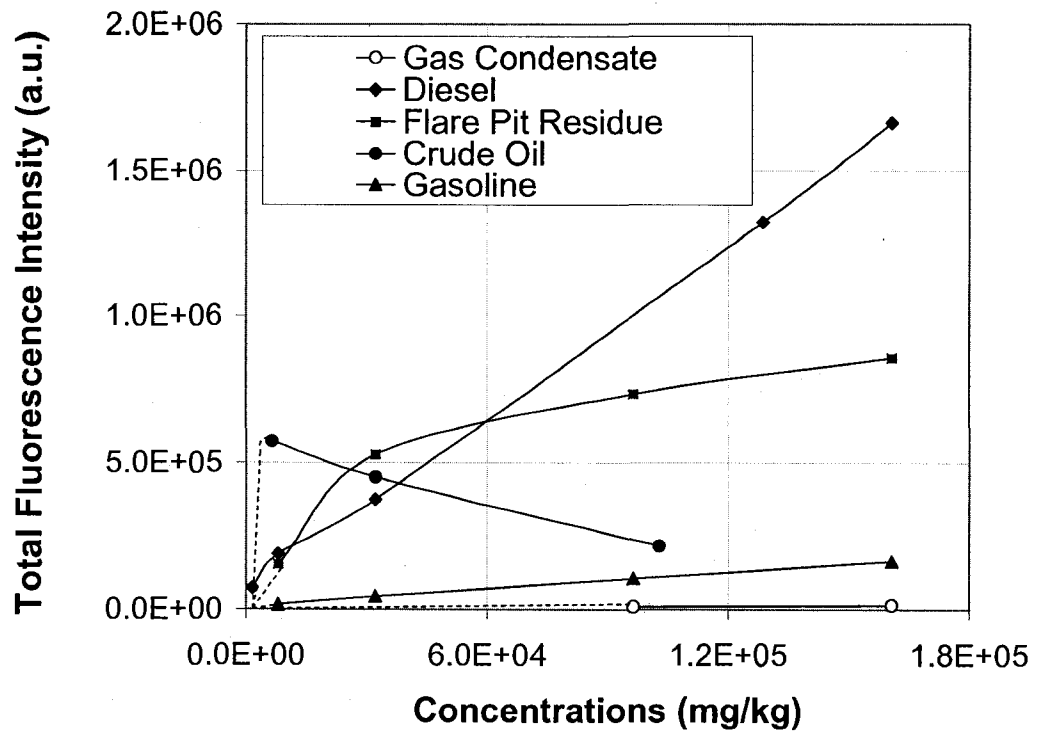


Figure C-10. Tested petroleum products fluorescence calibration curves in Devon silt

**Appendix D**  
Fluorescence and Porosity  
Relationship  
*(Using Varian Eclipse  
Spectrometer)*

# **Porosity Calculations**

## SOIL POROSITY CALCULATIONS

To obtain porosities for tested soils, small and large sample preparation methods were used as follows.

### Small sample preparation and calculation

Three samples of known weight of each soil were mixed with a known volumes of the solvent used in the test program (hexane and chloroform) in the sample container. The samples were set aside for 30 minutes to allow the soil grains to settle and sample containers were tapped on the side until no further changes in soil volume was observed. The final heights of soil and excess solvent on top of soil in the sample containers were then measured through the glass top and the volumes of soil and excess solvent were calculated using average value of measured heights that had variation of less than 3%. The difference between the volume of the solvent that was originally in the sample container and the excess solvent equaled the volume of the voids in each soil matrix. The porosity was then obtained for each soil type using the following relationship:

$$n = V_{\text{voids}} / V_{\text{soil}} \quad [\text{D-1}]$$

Where,  $n$  is the porosity,  $V_{\text{voids}}$  is the non-solid volume (pores) and  $V_{\text{soil}}$  is the total volume of material, including the solid and non-solid parts.

### Ottawa sand

---

Average soil height in the sample container	14.68 mm
Volume occupied by soil in the sample container	4132.52 mm <sup>3</sup>
Average excess solvent height in the sample container	3.31 mm
Volume occupied by excess solvent in the sample container	2117.19 mm <sup>3</sup>
Total solvent volume	3939.39 mm <sup>3</sup>
Voids volume occupied by excess solvent in the soil matrix	1822.20 mm <sup>3</sup>
Soil porosity calculated using equation [D-1]	44.09%

---

### Well graded sand

---

Average soil height in the sample container	13.77 mm
Volume occupied by soil in the sample container	3561.79 mm <sup>3</sup>
Average excess solvent height in the sample container	4.25 mm
Volume occupied by excess solvent in the sample container	2117.19 mm <sup>3</sup>
Total solvent volume	3939.39 mm <sup>3</sup>
Voids volume occupied by excess solvent in the soil matrix	1232.33 mm <sup>3</sup>
Soil porosity calculated using equation [D-1]	34.60%

---

**Well graded sand and Devon silt**

---

Average soil height in the sample container	13.25 mm
Volume occupied by soil in the sample container	3244.06 mm <sup>3</sup>
Average excess solvent height in the sample container	4.73 mm
Volume occupied by excess solvent in the sample container	2999.30 mm <sup>3</sup>
Total solvent volume	3787.88 mm <sup>3</sup>
Voids volume occupied by excess solvent in the soil matrix	788.58 mm <sup>3</sup>
Soil porosity calculated using equation [D-1]	24.31%

---

**Devon silt**

---

Average soil height in the sample container	12.55 mm
Volume occupied by soil in the sample container	2823.12 mm <sup>3</sup>
Average excess solvent height in the sample container	2.31 mm
Volume occupied by excess solvent in the sample container	1423.27 mm <sup>3</sup>
Total solvent volume	1969.70 mm <sup>3</sup>
Voids volume occupied by excess solvent in the soil matrix	546.43 mm <sup>3</sup>
Soil porosity calculated using equation [D1]	19.36%

---

### Large sample preparation and calculation

Three samples of known volume of each soil were mixed with a known volumes of the solvent used in the test program in a graded volumetric beaker. These samples were set aside for a few hours to allow the soil grains to settle. Beakers were sealed to eliminate solvent evaporation and tapped on the side until no further changes in soil volume was observed. The solvent was removed from above the soil surface and the solvent volume was measured. The difference between the volume of the solvent that was originally in the beaker and the solvent that was removed equaled the volume of the voids in each soil matrix. The porosity was then obtained for each soil type using the relationship in equation [D-1].

#### Ottawa sand

---

Average volume occupied by soil	425 ml
Average volume occupied by excess solvent	15 ml
Total solvent volume	200 ml
Voids volume occupied by excess solvent in the soil matrix	185 ml
Soil porosity calculated using equation [D-1]	43.59%

---

#### Well graded sand

---

Average volume occupied by soil	365 ml
Average volume occupied by excess solvent	15 ml
Total solvent volume	140 ml
Voids volume occupied by excess solvent in the soil matrix	125 ml
Soil porosity calculated using equation [D-1]	34.25%

---

**Well graded sand and Devon silt**

---

Average volume occupied by soil	320 ml
Average volume occupied by excess solvent	11 ml
Total solvent volume	90 ml
Voids volume occupied by excess solvent in the soil matrix	79 ml
Soil porosity calculated using equation [D-1]	24.69%

---

**Devon silt**

---

Average volume occupied by soil	380 ml
Average volume occupied by excess solvent	19 ml
Total solvent volume	90 ml
Voids volume occupied by excess solvent in the soil matrix	71 ml
Soil porosity calculated using equation [D-1]	18.68%

---



**Relationship  
between  
fluorescence  
intensity and  
porosity of tested  
samples**

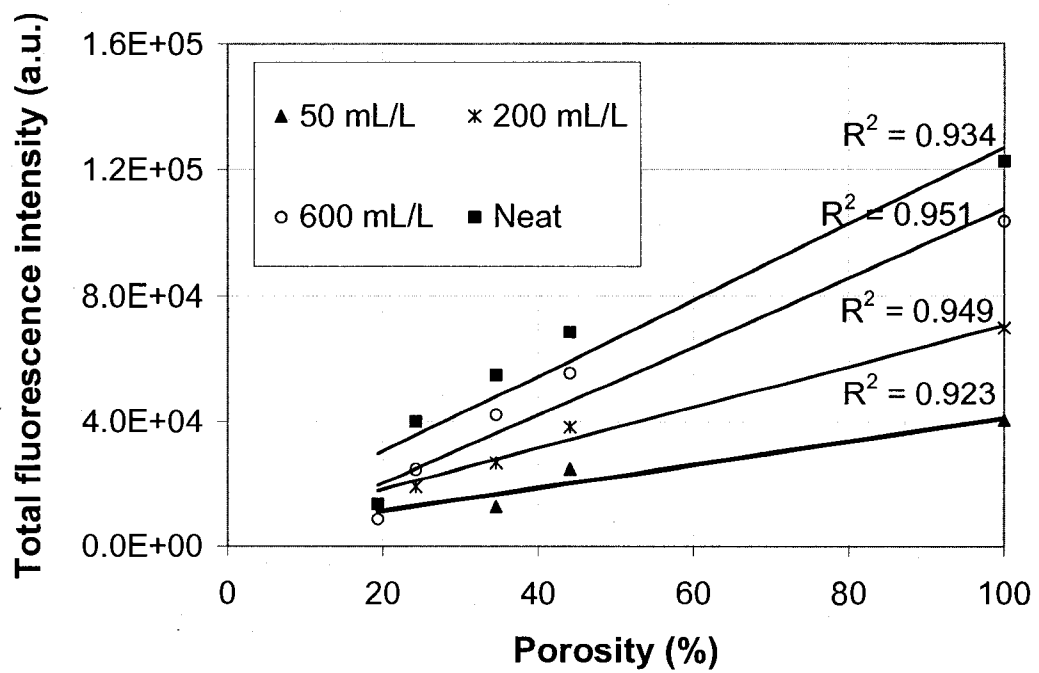


Figure D-1. Gas condensate fluorescence intensity versus soil porosity at different concentrations

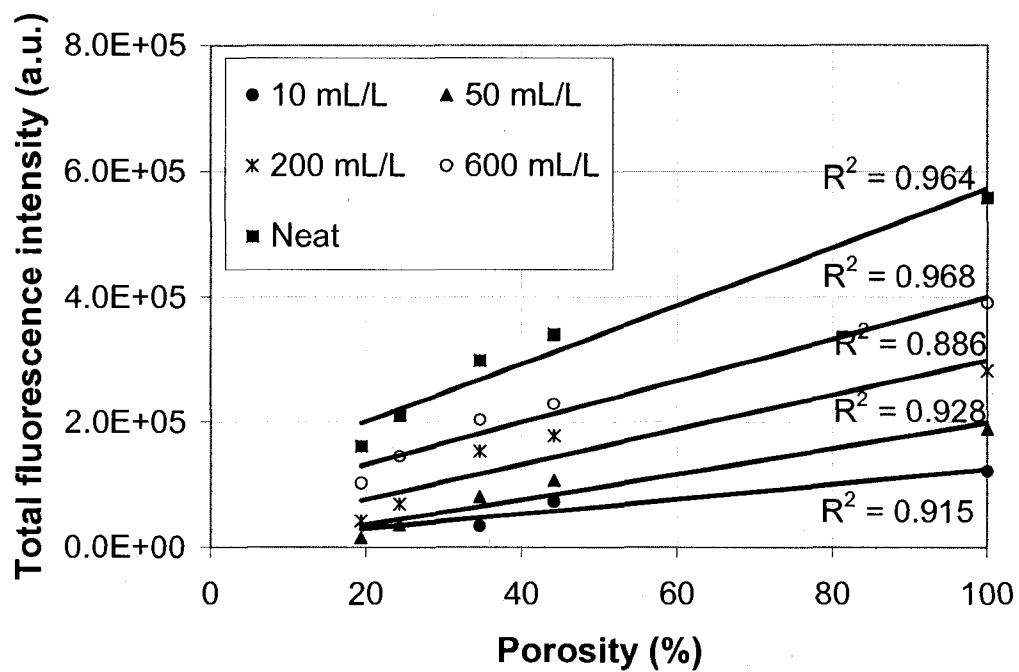


Figure D-2. Gasoline fluorescence intensity versus soil porosity at different concentrations

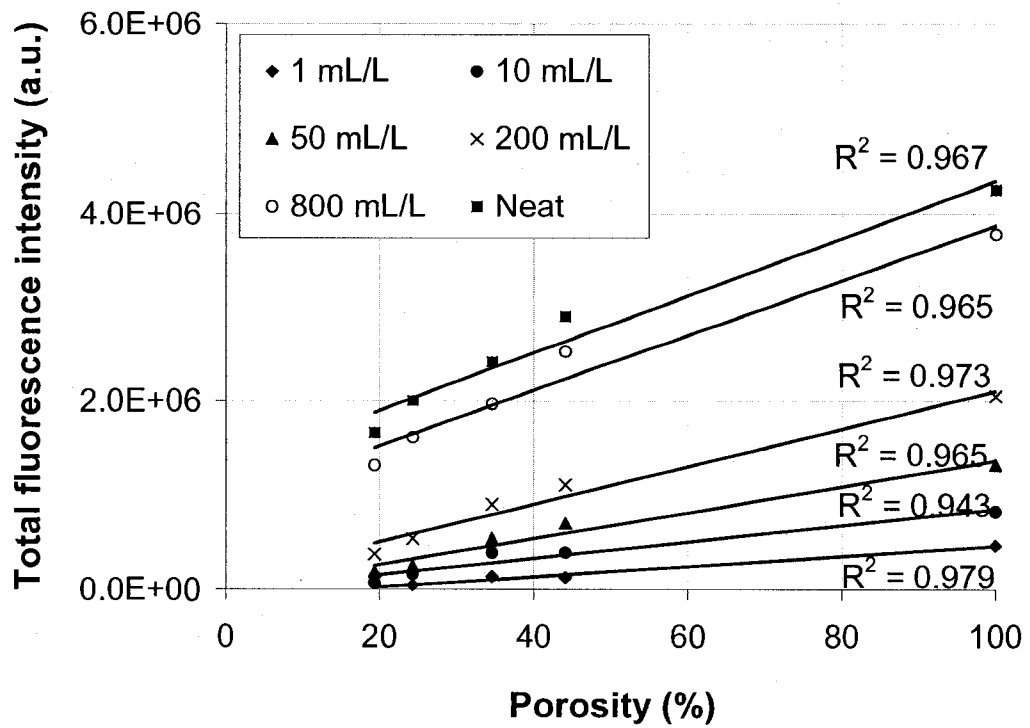


Figure D-3. Diesel fluorescence intensity versus soil porosity at different concentrations

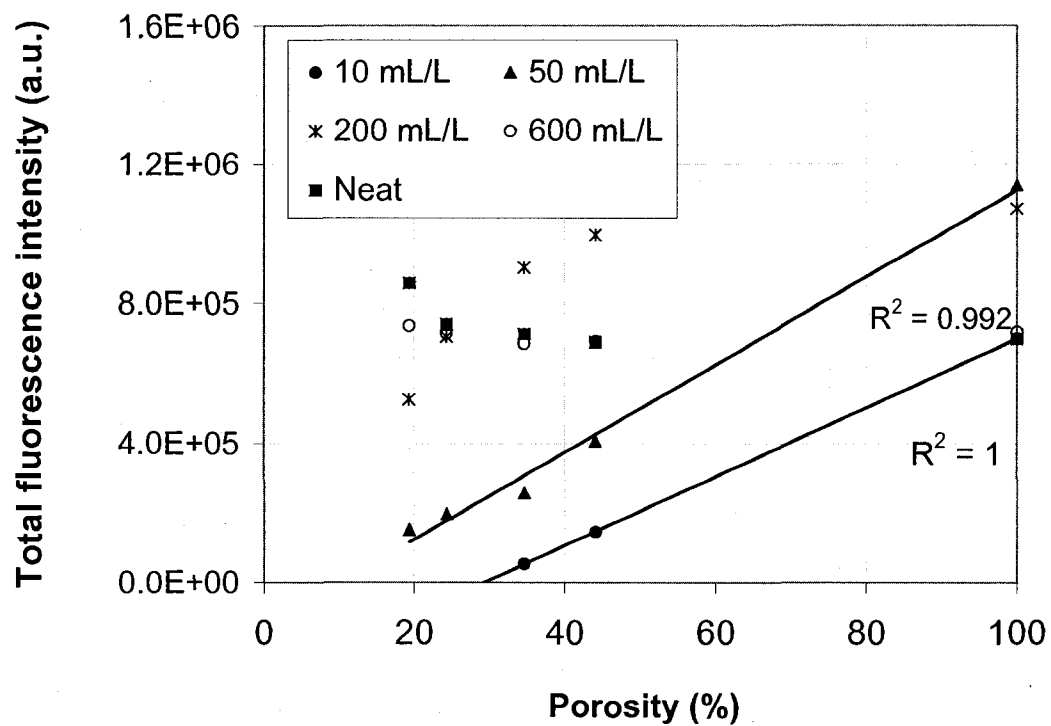


Figure D-4. Flare pit residue fluorescence intensity versus soil porosity at different concentrations

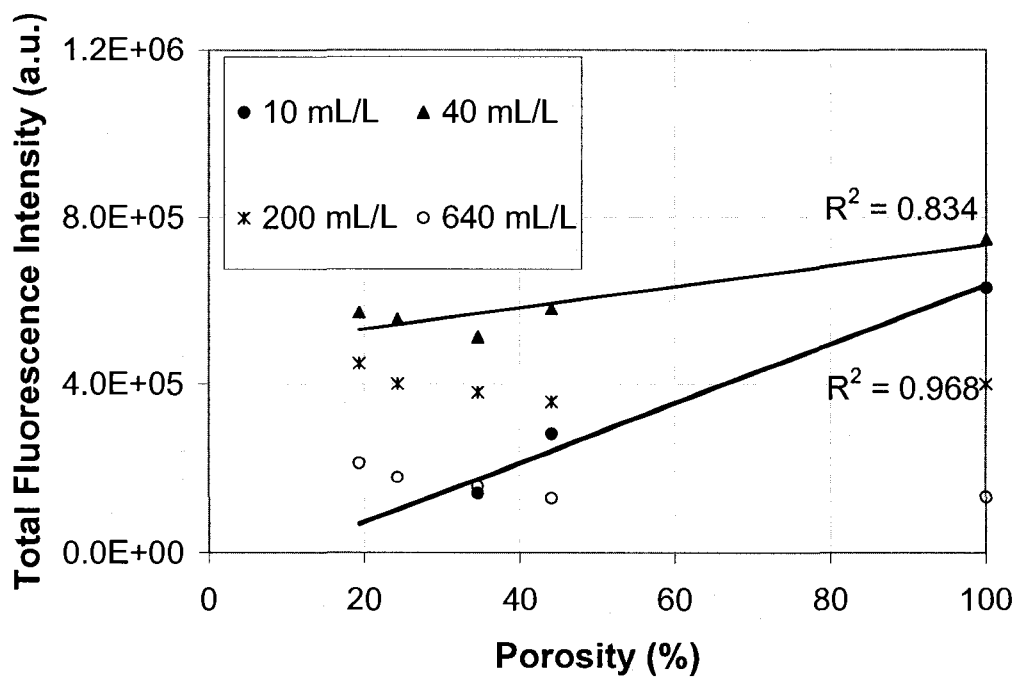


Figure D-5. Crude oil fluorescence intensity versus soil porosity at different concentrations

**Appendix E**  
Fluorescence calibration  
curves  
*(Using newly developed UVIF  
sensor)*

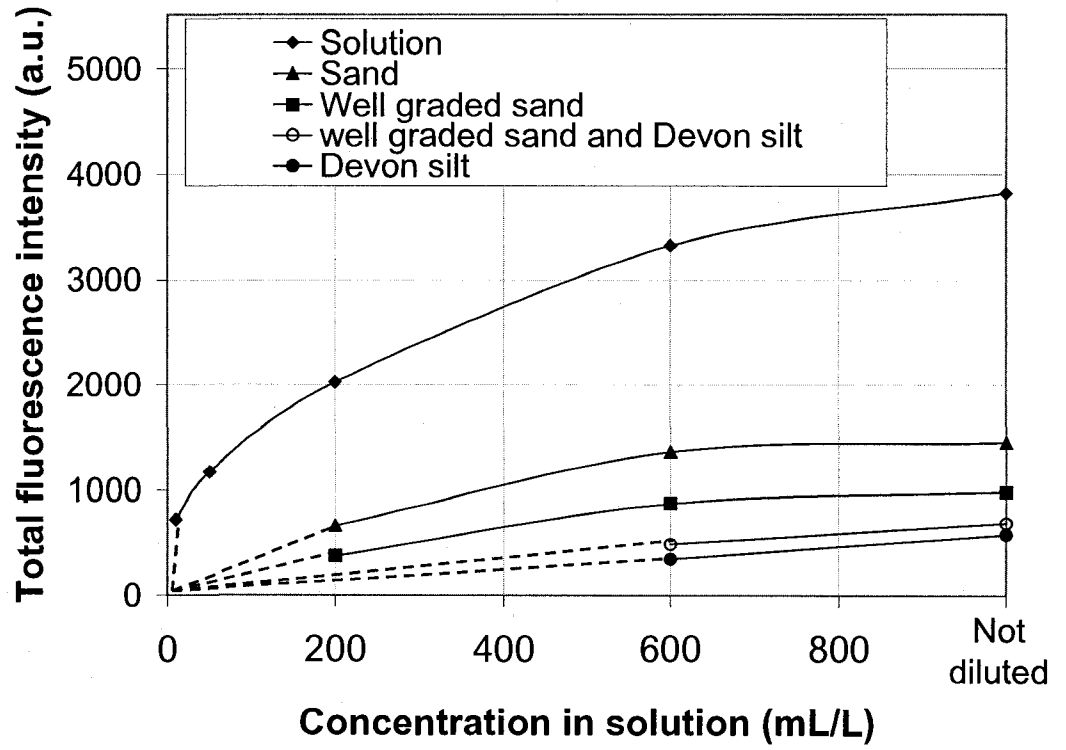


Figure E-1. Gasoline fluorescence calibration curves in solvent solution and soil



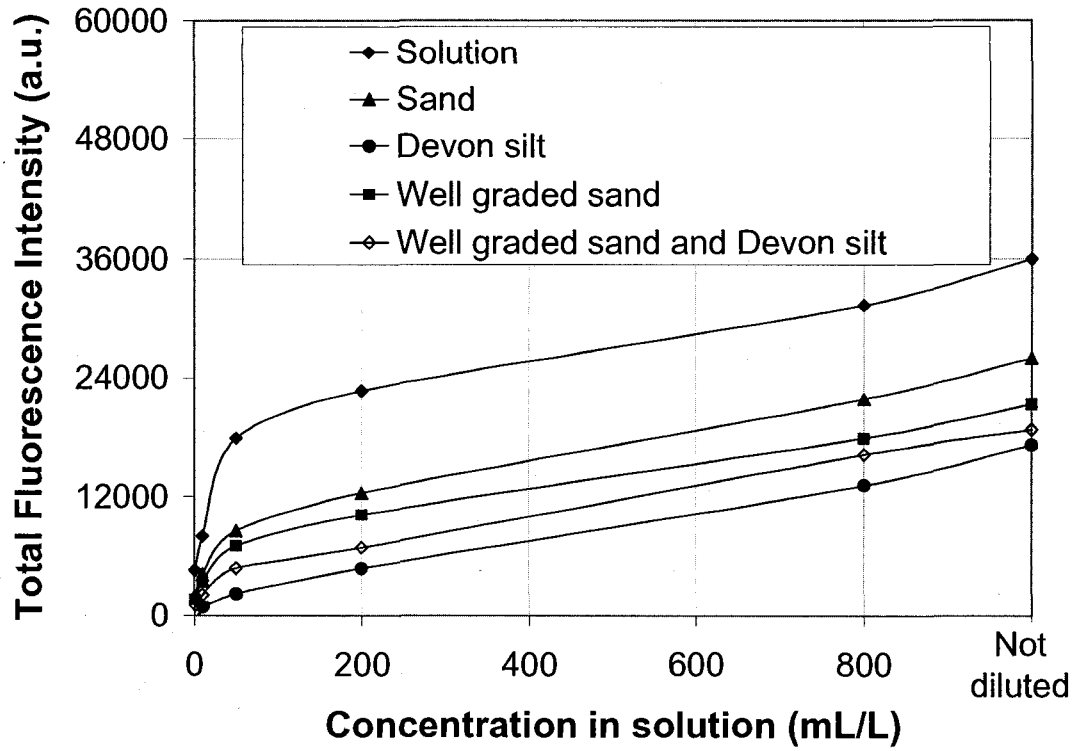


Figure E-2. Diesel fluorescence calibration curves in solvent solution and soil

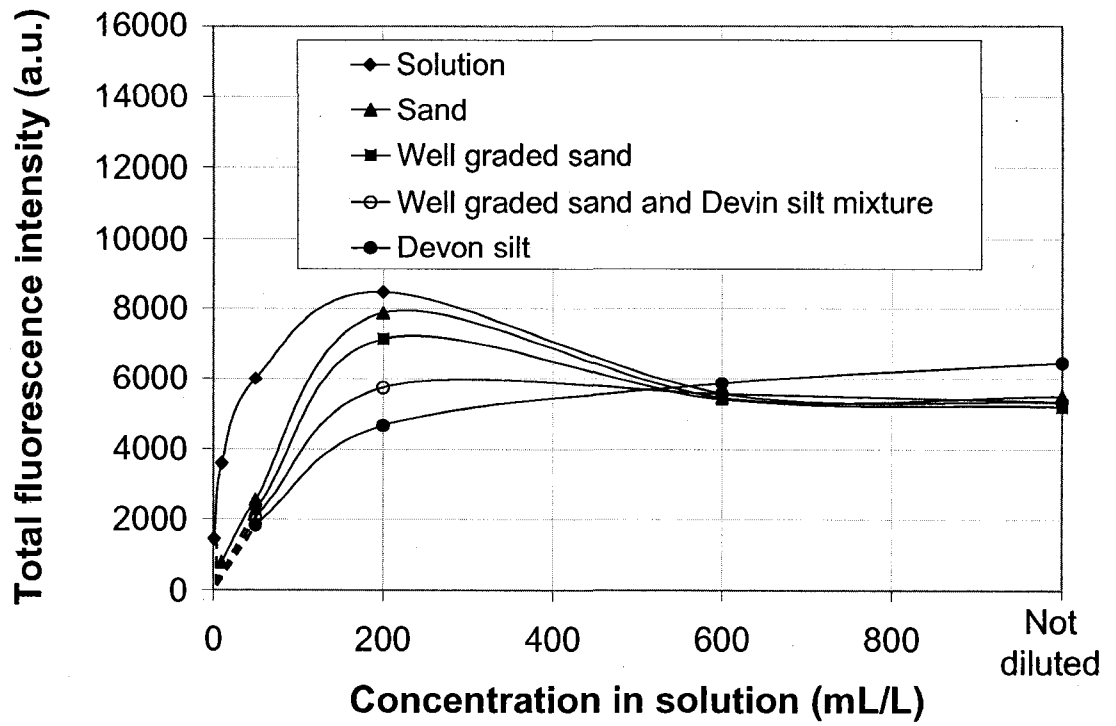


Figure E-3. Flare pit residue fluorescence calibration curves in solvent solution and soil

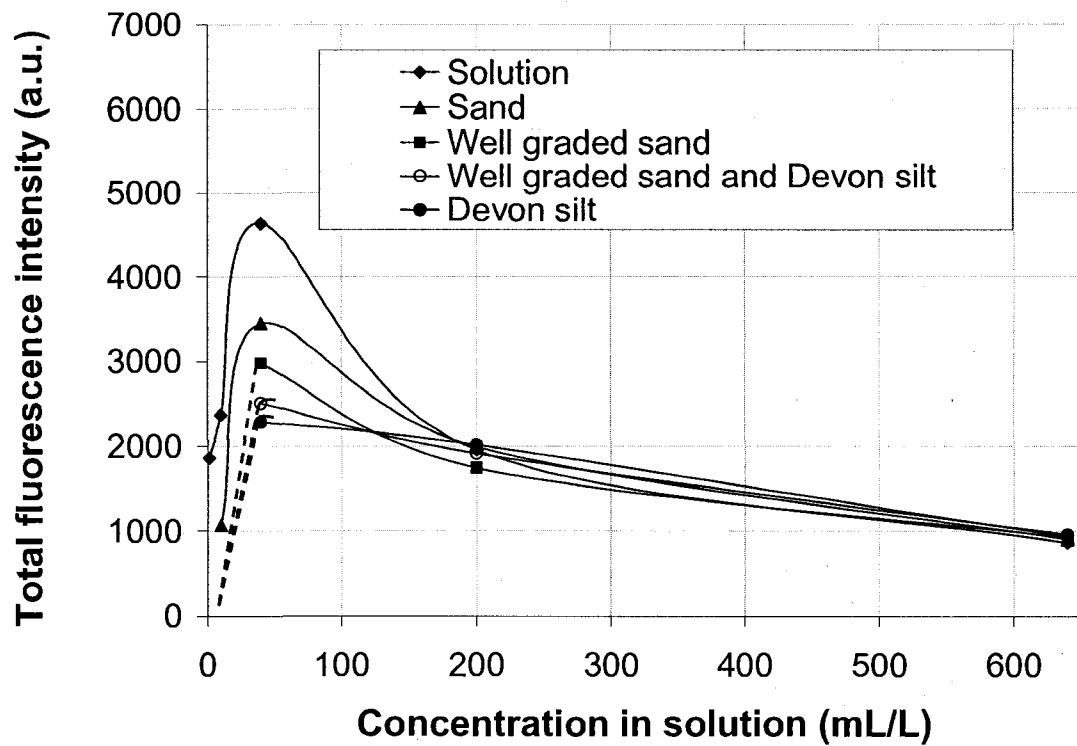


Figure E-4. Crude oil fluorescence calibration curves in solvent solution and soil

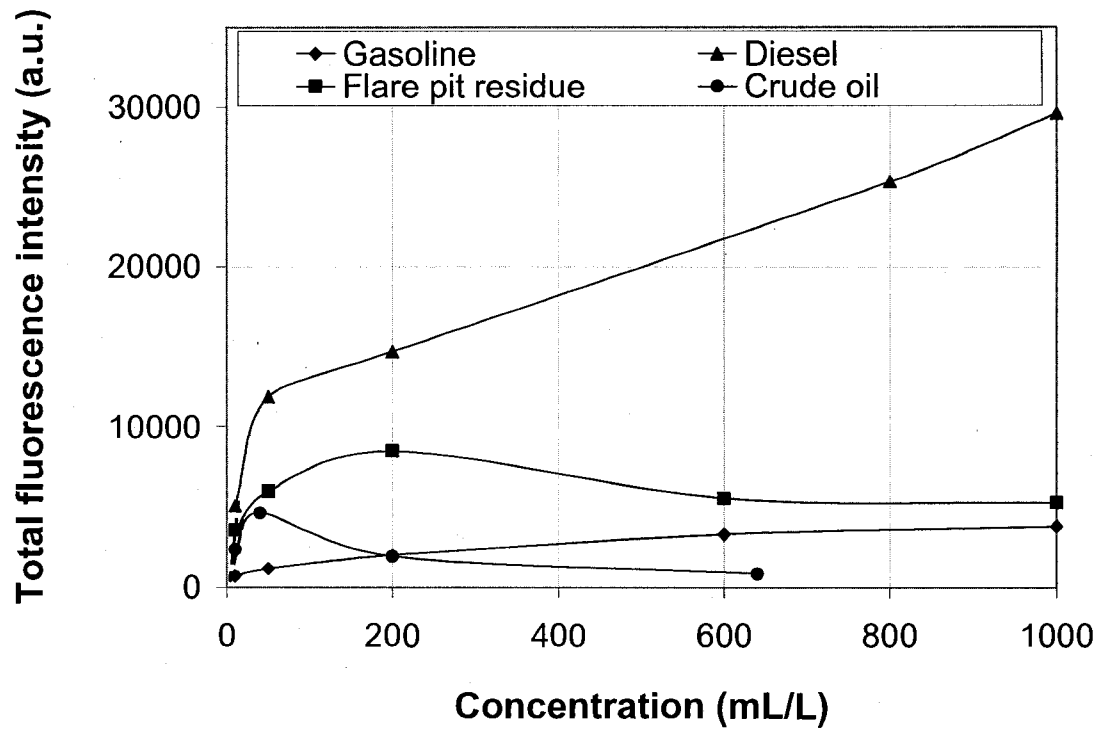


Figure E-5. Tested petroleum products fluorescence calibration curves in solvent solutions

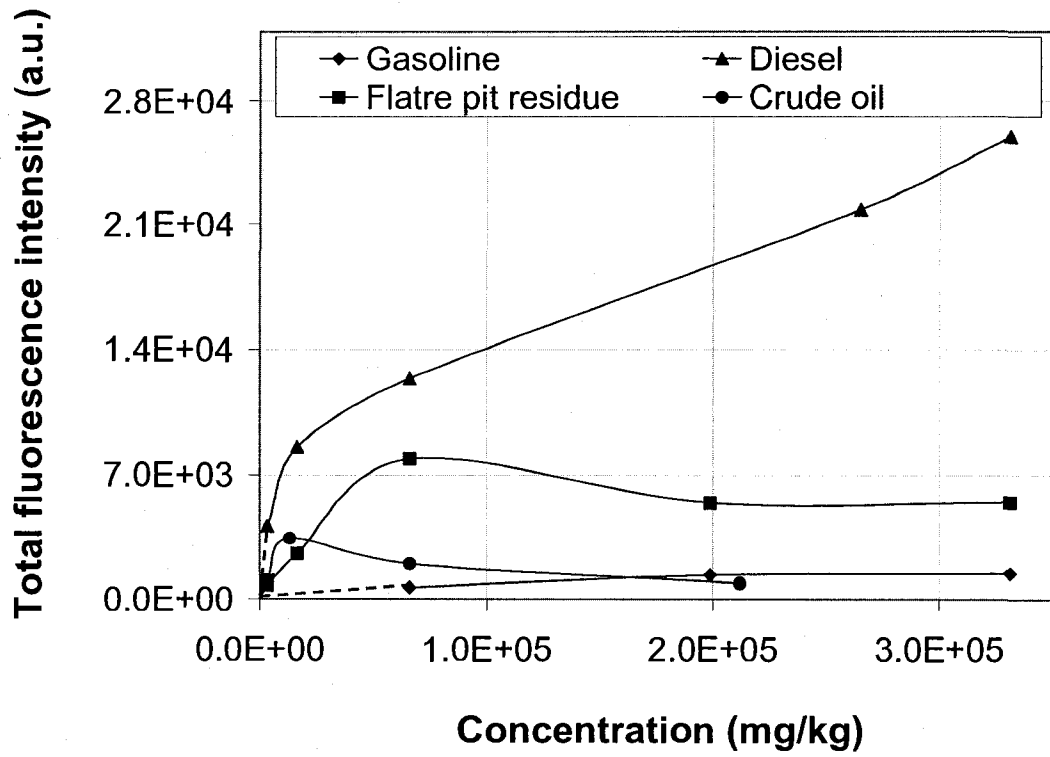


Figure E-6. Tested petroleum products fluorescence calibration curves in Ottawa sand

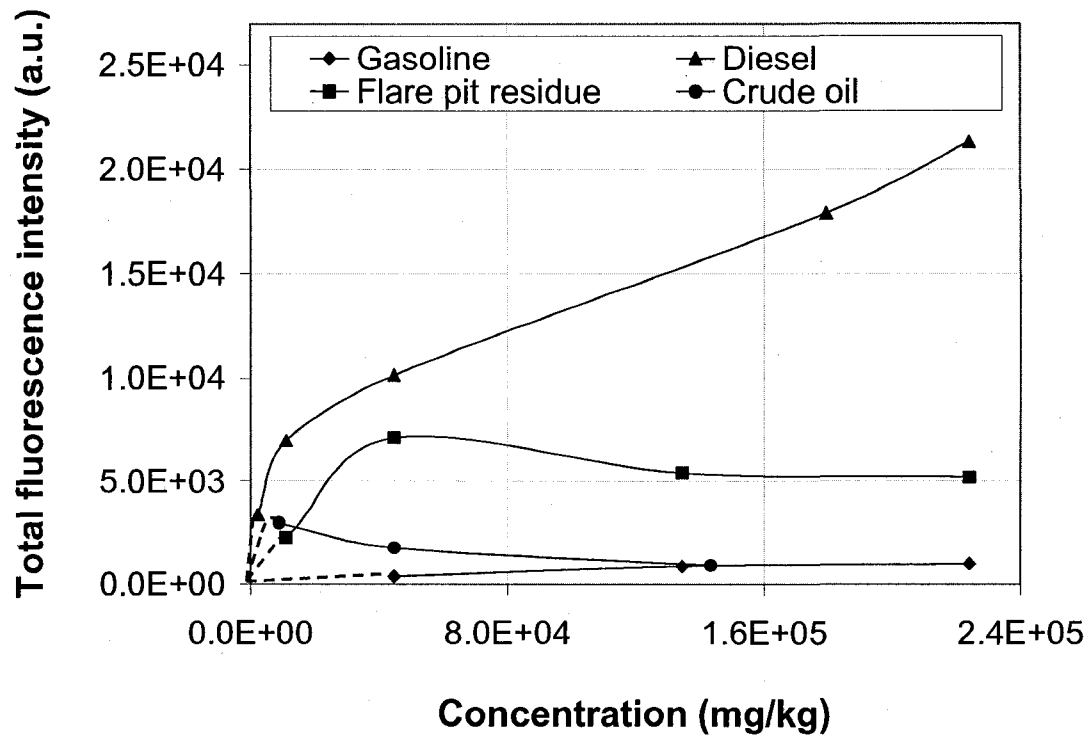


Figure E-7. Tested petroleum products fluorescence calibration curves in well graded sand

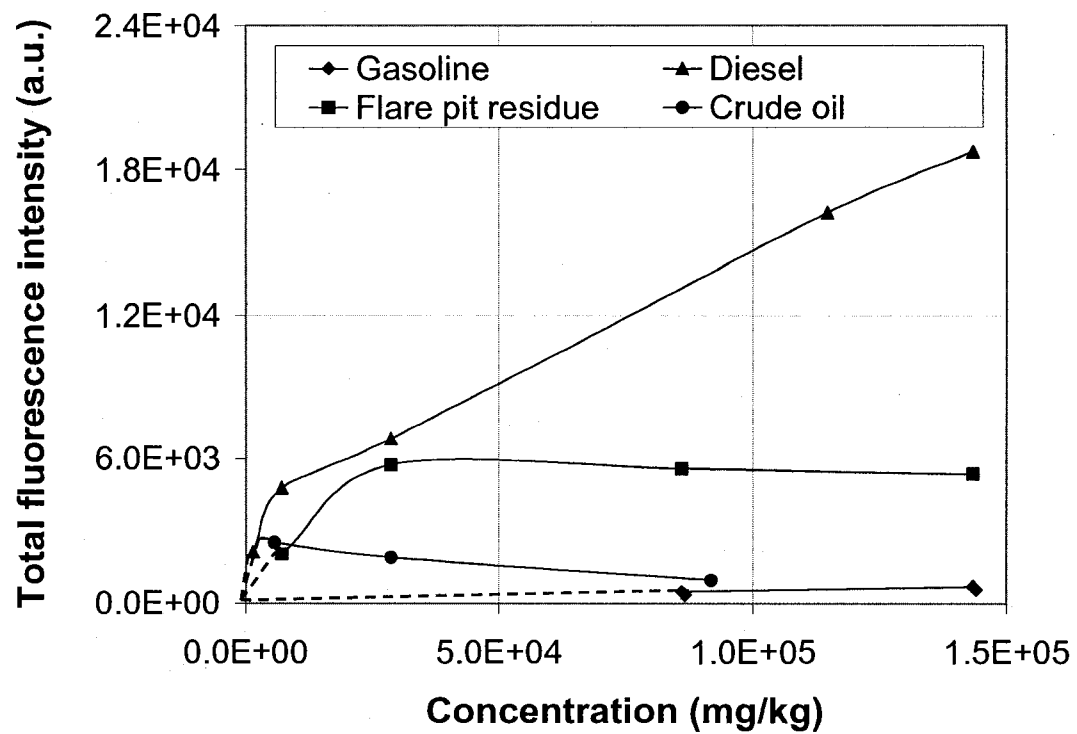


Figure E-8. Tested petroleum products fluorescence calibration curves in well graded sand and Devon silt

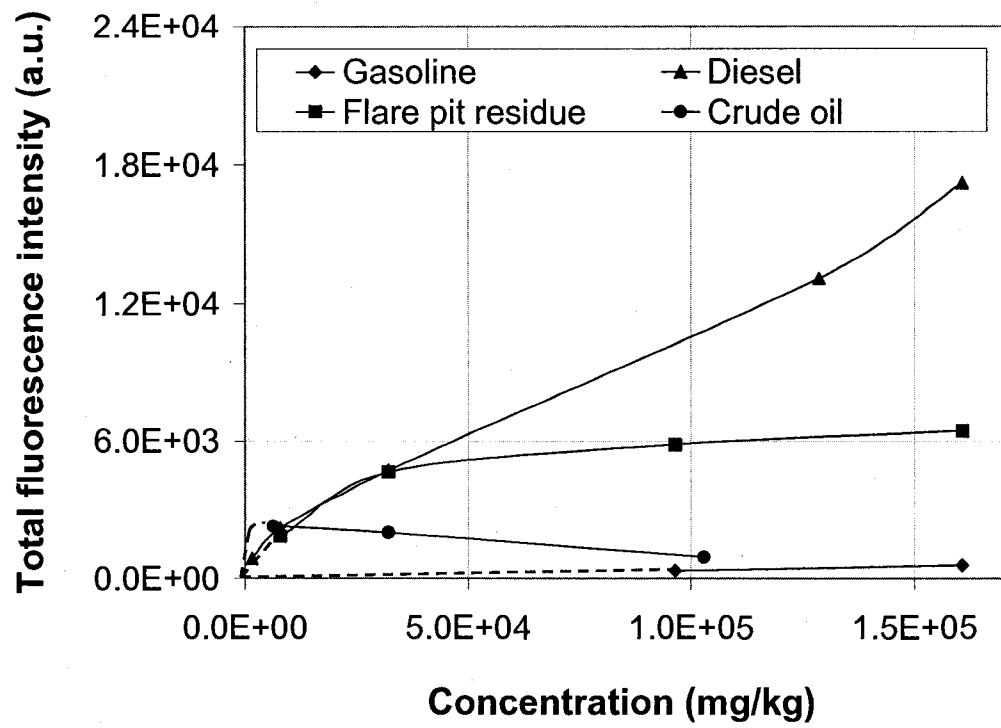


Figure E-9. Tested petroleum products fluorescence calibration curves in Devon silt



**Appendix F**  
Fluorescence and Porosity  
Relationship  
*(Using newly developed UVIF  
sensor)*

Table F-1. Equations of linear relationship between total fluorescence values of tested petroleum products (where F is total fluorescence, m is the slope, n the porosity and b the intercept)

<b>Gasoline</b>		
<b>Concentration (ml/L)</b>	<b>F = m*n + b</b>	<b>R<sup>2</sup></b>
1	-	-
10	-	-
50	-	-
200	$F = 24.90*n - 4.63*10^2$	0.999
600	$F = 37.18*n - 3.77*10^2$	0.997
Neat	$F = 41.12*n - 3.24*10^2$	0.996
<b>Diesel</b>		
<b>Concentration (ml/L)</b>	<b>F = m*n + b</b>	<b>R<sup>2</sup></b>
1	$F = 51.33*n - 4.39*10^2$	0.958
10	$F = 81.51*n + 75.27$	0.961
50	$F = 182.29*n - 28.15$	0.981
200	$F = 212.55*n + 1.90*10^3$	0.979
800	$F = 212.59*n + 1.06*10^4$	0.967
Neat	$F = 229.65*n + 1.36*10^4$	0.972
<b>Flare Pit Residue</b>		
<b>Concentration (ml/L)</b>	<b>F = m*n + b</b>	<b>R<sup>2</sup></b>
1	-	-
10	-	-
50	$F = 52.62*n + 5.87*10^2$	0.978
200	N/A	N/A
600	N/A	N/A
Neat	N/A	N/A
<b>Crude Oil</b>		
<b>Concentration (ml/L)</b>	<b>F = m*n + b</b>	<b>R<sup>2</sup></b>
1	-	-
10	-	-
40	$F = 28.08*n + 1.92*10^3$	0.960
200	N/A	N/A
640	N/A	N/A

*Note: N/A is used to refer to concentration at which linear relationship between total fluorescence values and porosity doesn't exist.*

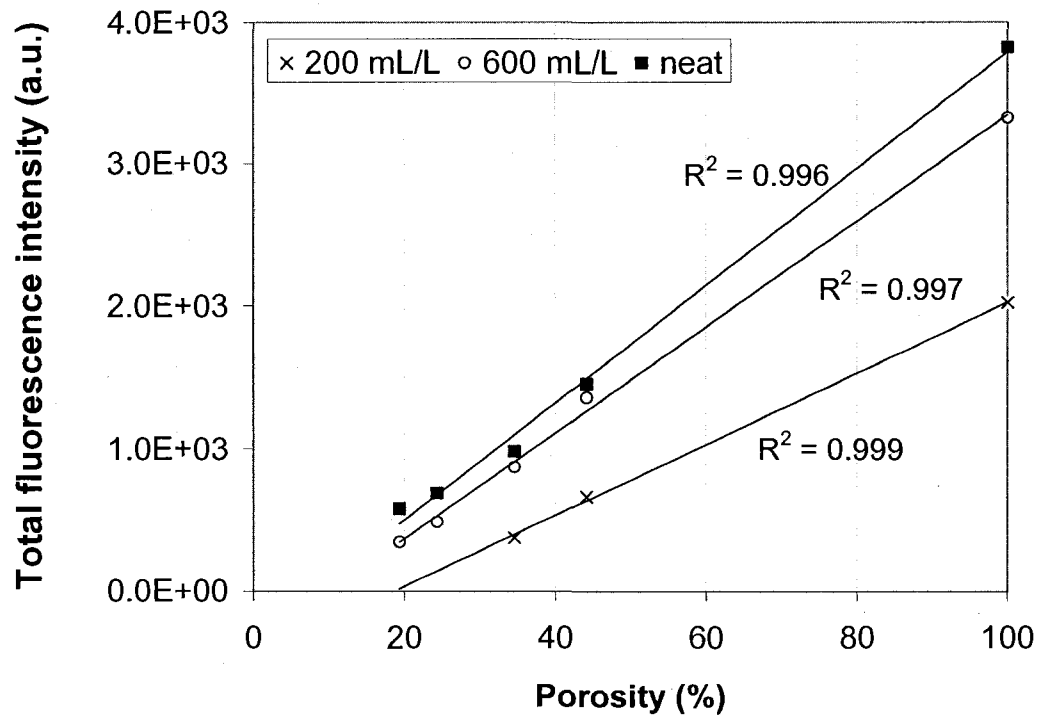


Figure F-1. Gasoline fluorescence intensity versus soil porosity at different concentrations

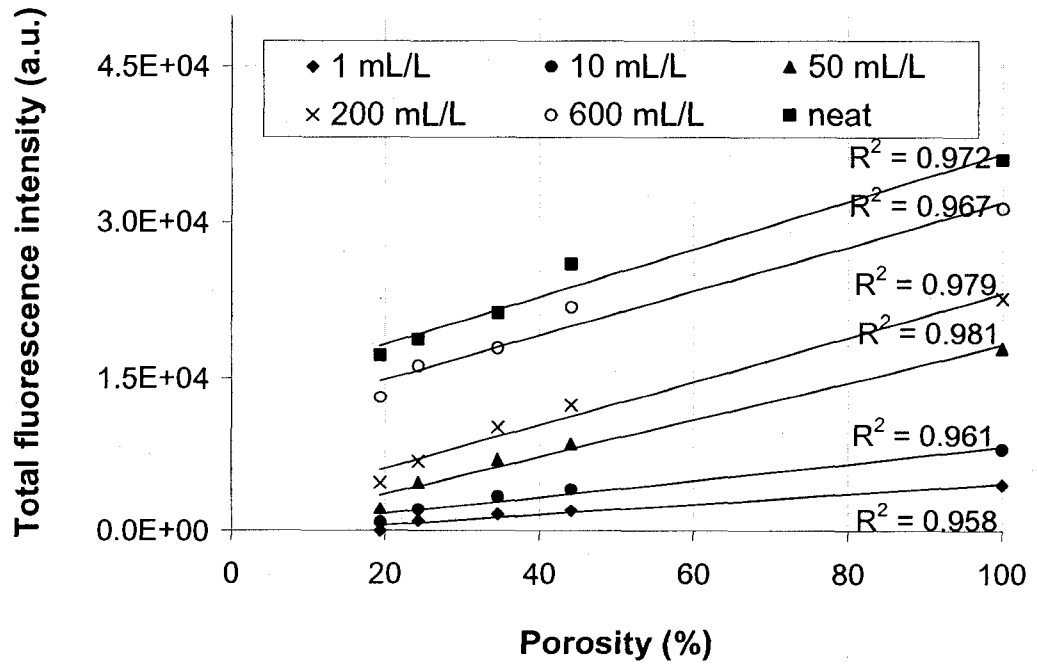


Figure F-2. Diesel fluorescence intensity versus soil porosity at different concentrations

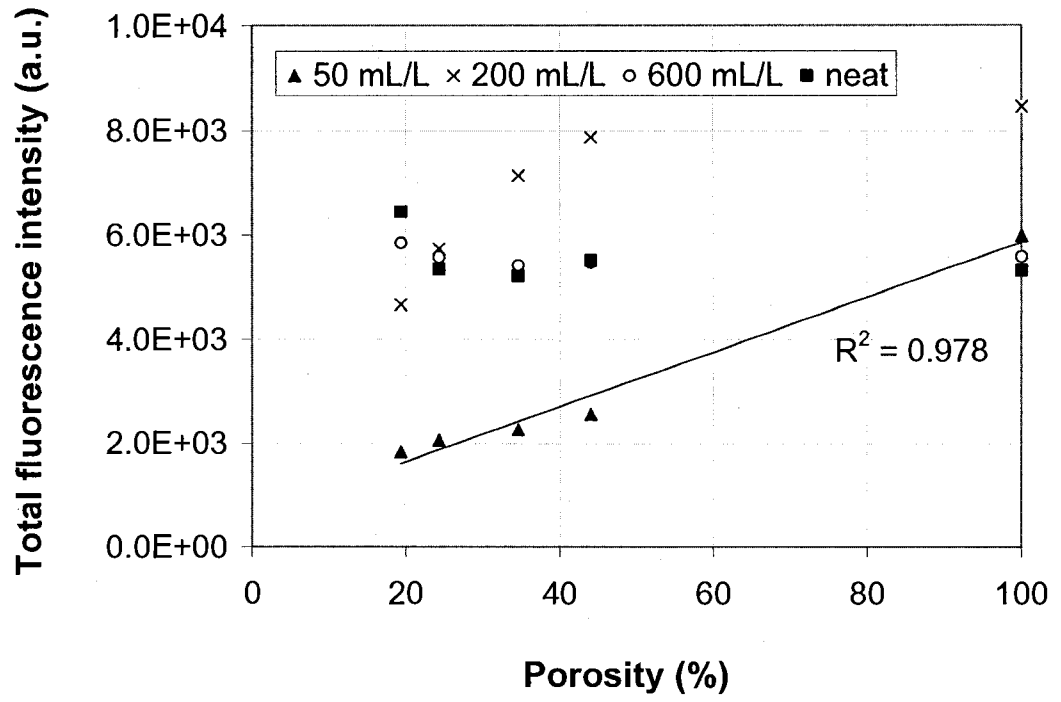


Figure F-3. Flare pit residue fluorescence intensity versus soil porosity at different concentrations

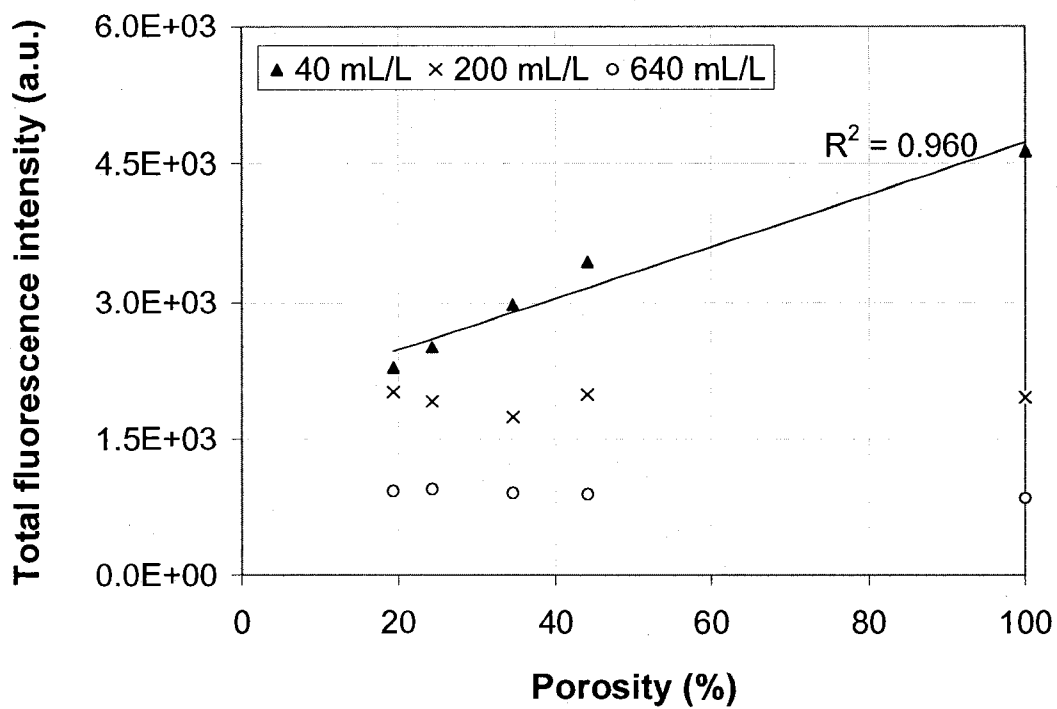


Figure F-4. Crude oil fluorescence intensity versus soil porosity at different concentrations

**Appendix G**  
**PARAFAC and SIMCA**  
**Modeling**

# **PARAFAC Models**



## STEP TO CONSTRUCT PARAFAC MODEL

Constructing the PARAFAC model for a particular petroleum product using related fluorescence EEMs at different concentrations in solution or soil samples is composed of four basic steps:

- 1- Stack EEMs of petroleum product under analysis at all tested concentrations into one data matrix of class “dataset”.
- 2- Set the scatter region to “NaN”
- 3- Set non-negativity constraints on each mode
- 4- Fit a PARAFAC model with varying number of factors using PLS-Toolbox
- 5- Choose appropriate number of factors based selection criteria discussed later in this appendix.

The following is a sample command history used to fit a PARAFAC model to gas condensate (in solution) fluorescence EEMs.

### Command History

```
Condensate_1 = Condensate_1(:,2:2:14);
```

```
Condensate_10 = Condensate_10(:,2:2:14);
```

```
Condensate_10 = data(:,2:2:14);
```

```
Condensate_50 = data(:,2:2:14);
```

```
Condensate_200 = data(:,2:2:14);
```

```
Condensate_600 = data(:,2:2:14);
```

```
Condensate(1,,:) = Condensate_1;
```

```

Condensate(2,,:) = Condensate_10;
Condensate(3,,:) = Condensate_50;
Condensate(4,,:) = Condensate_200;
Condensate(5,,:) = Condensate_600;
Condensate = dataset(Condensate);
options = parafac('options');
for n = 1:5; CondensateSum = Condensate.data(n,:); end
for n = 1:5; CondensateSum = CondensateSum + Condensate.data(n,:); end
map = NaNweight(CondensateSum);
for n = 1:5; CondensateNaN(n,:) = Condensate.data(n,:) .* map; end
CondensateNaN = dataset(CondensateNaN);
model3 = parafac(CondensateNaN,3,[],options);
model4 = parafac(CondensateNaN,4,[],options);
model5 = parafac(CondensateNaN,5,[],options);

```

The same steps were used to produce PARAFAC models for other petroleum products in solution and soil samples. Related details to PARAFAC modelling and dealing with scattered light regions are described in sections 3.4.1.2. and 4.4.2.

Determination of the appropriate number of factors was based on:

1- Number of iterations

The solution to the PARAFAC model can be found by alternating least squares (ALS) by successively assuming the loadings in two modes known

and then estimating the unknown set of parameters of the last mode. A number of iterations are usually required necessary before the relative change in fit between two iterations is below a certain value. Appropriate number of PARAFAC factors can be reliably extracted from fluorescence EEM data sets with relatively low number of iterations (within 500 iterations), which indicates fast convergence of the PARAFAC model. Once the optimal number of PARAFAC components is exceeded, a significant increase in the number of iterations will be noticed (Bro, 1997).

## 2- Core consistency

This criterion has been suggested by Bro and Kiers (2003) for determining the proper number of components for multi-way models. Core consistency plots produced by PLS\_toolbox 3.5 in MATLAB ver.7.1 upon performing PARAFAC analysis show the distribution of actual core elements (red and green) calculated from PARAFAC loadings around a blue line that represents a binary array with zeros in all places except for the super-diagonal which contains only values of one (Figure G-1). The array can be utilized statistically to verify that the trilinear structure of the PARAFAC model is appropriate. The red elements are those that should be ideally non-zero and the green elements are those that should be ideally zero. If the PARAFAC model is valid then red and green elements should follow the blue line. If the data can not approximately be described by a trilinear model or too many components are used then red and green elements, will deviate from the blue target.

### 3- Analysis of residuals

Analysing fluorescence data residuals allow determining the appropriateness of the PARAFAC model and the correct number of components. When suitable PARAFAC component numbers are obtained, residuals will then describe noise instead of systematic variation of fluorescence data (Bro 1997). Residual plots produced by PLS\_toolbox 3.5 in MATLAB ver.7.1 upon performing PARAFAC analysis show the distribution of actual of residuals in all the analyzed samples (Figure G-2). If the PARAFAC model is valid then residuals are related to noise in fluorescence data and should not have systematic variation.

Target, Ideally zero/non-zero core elements

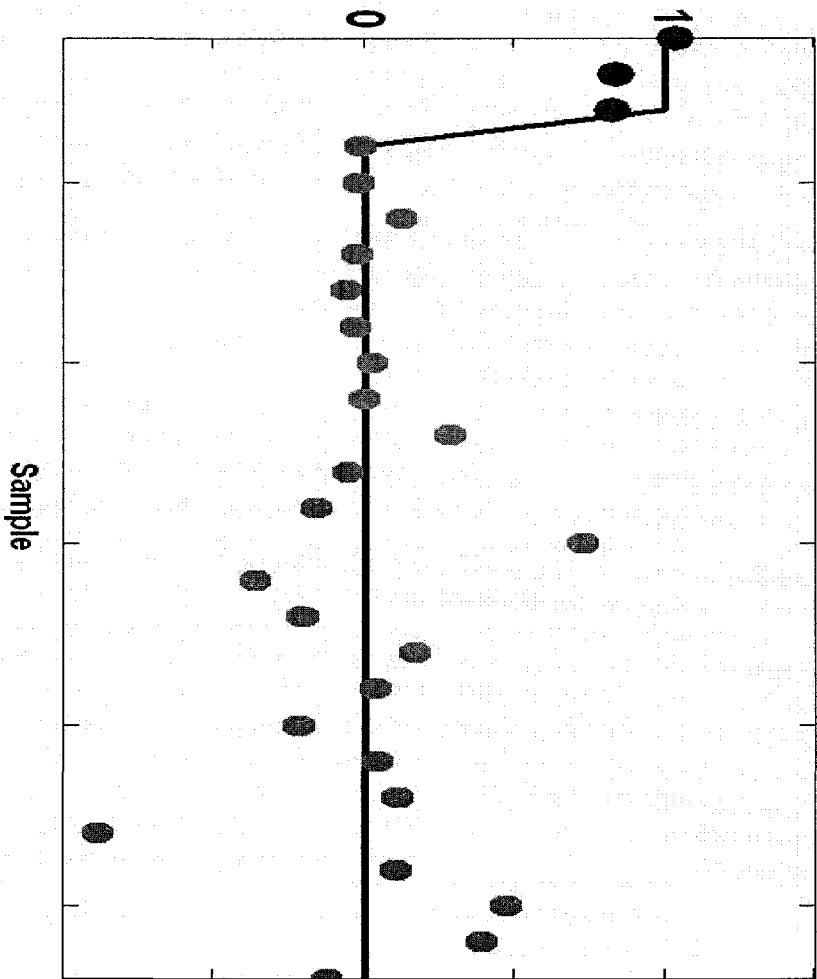


Figure G-1. Core consistency plot

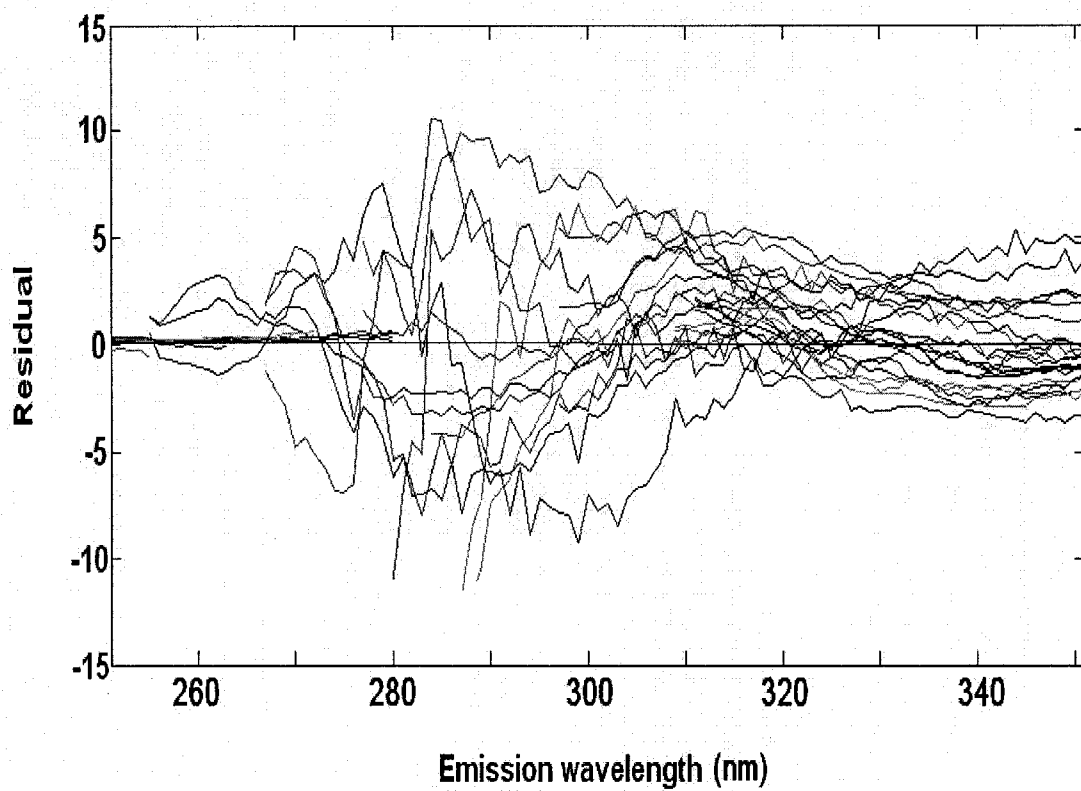


Figure G-2. Residual fluorescence data plot

# **PARAFAC Models for Petroleum Products in Solution Samples**

### Gas condensate PARAFAC model

- Number of fitted PARAFAC components: 1, 2, 3, 4, 5

Optimal number of PARAFAC components: 3

- Number of iterations to model the optimal number of PARAFAC components: 59
- Core consistency analysis: Figure G-3 of core consistency plot of gas condensate PARAFAC model with 3 predicted components (represented by the red dots) indicate that zero and non-zero core elements follow the blue line.

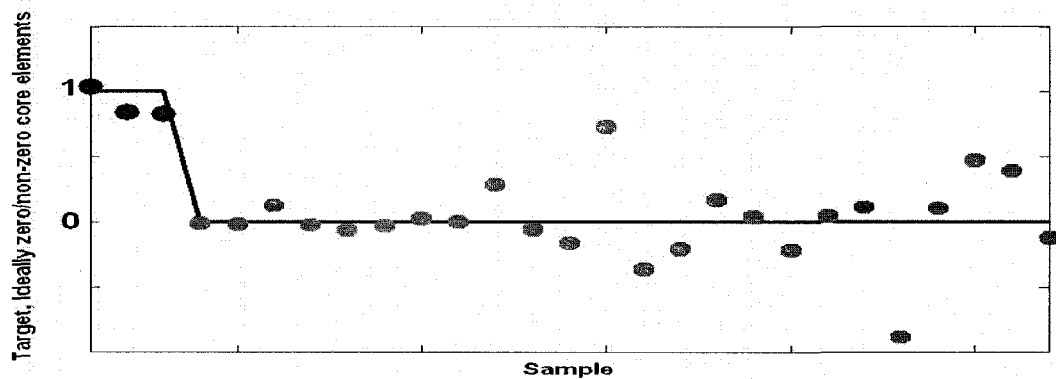


Figure G-3. Core consistency plot of gas condensate PARAFAC model

- Residual analysis: Figure G-4 of fluorescence data residual plot of gas condensate PARAFAC model indicating that residuals don't have systematic variation.

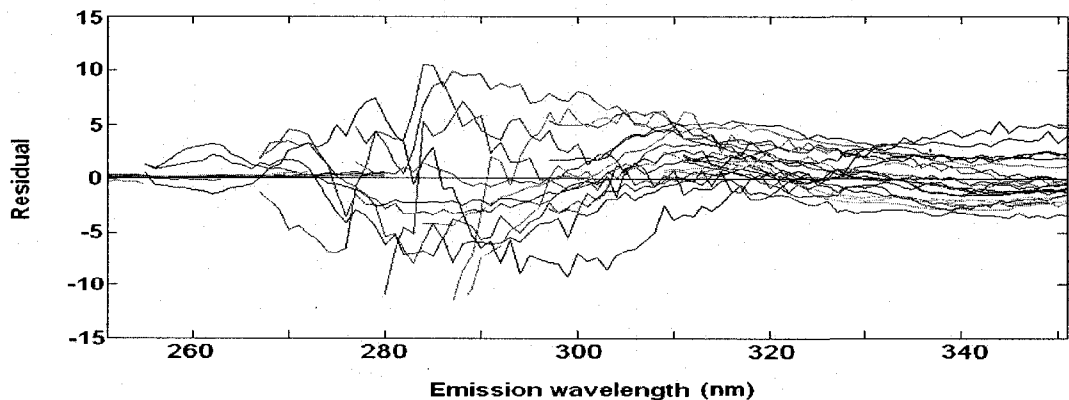


Figure G-4. Fluorescence data residual plot of gas condensate PARAFAC model



## Gasoline PARAFAC model

- Number of fitted PARAFAC components: 1, 2, 3, 4, 5

Optimal number of PARAFAC components: 3

- Number of iterations to model the optimal number of PARAFAC components: 97

- Core consistency analysis: Figure G-5 of core consistency plot of gasoline

PARAFAC model with 3 predicted components (represented by the red dots)

indicate that zero and non-zero core elements follow the blue line.

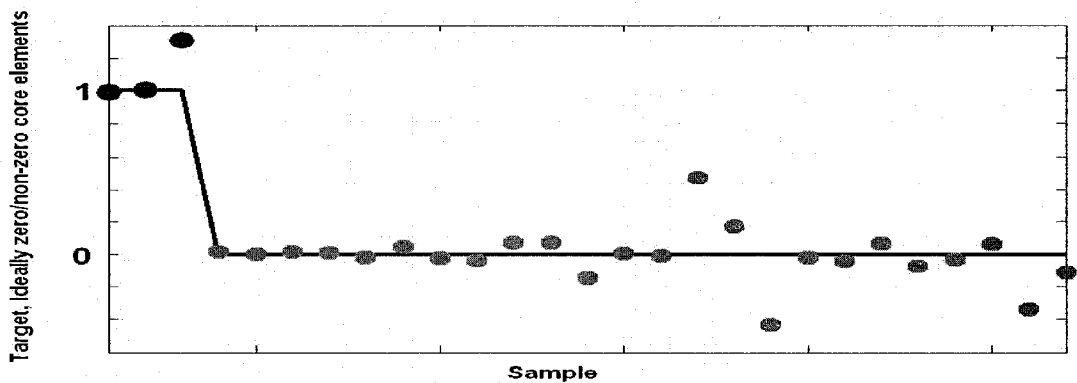


Figure G-5. Core consistency plot of gasoline PARAFAC model

- Residual analysis: Figure G-6 of fluorescence data residual plot of gasoline PARAFAC model indicating that residuals don't have systematic variation.

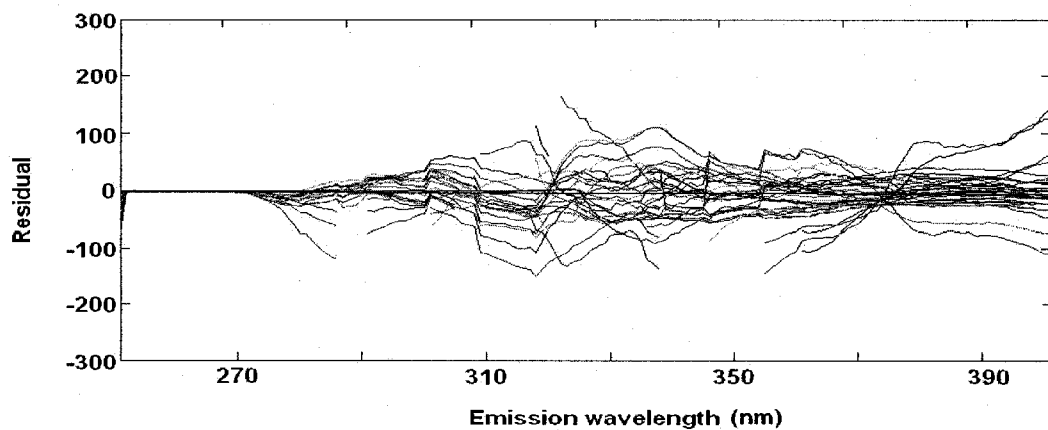


Figure G-6. Fluorescence data residual plot of gasoline PARAFAC model

## Diesel PARAFAC model

- Number of fitted PARAFAC components: 1, 2, 3, 4, 5

Optimal number of PARAFAC components: 4

- Number of iterations to model the optimal number of PARAFAC components: 176
- Core consistency analysis: Figure G-7 of core consistency plot of diesel PARAFAC

model with 4 predicted components (represented by the red dots) indicate that zero and non-zero core elements follow the blue line.

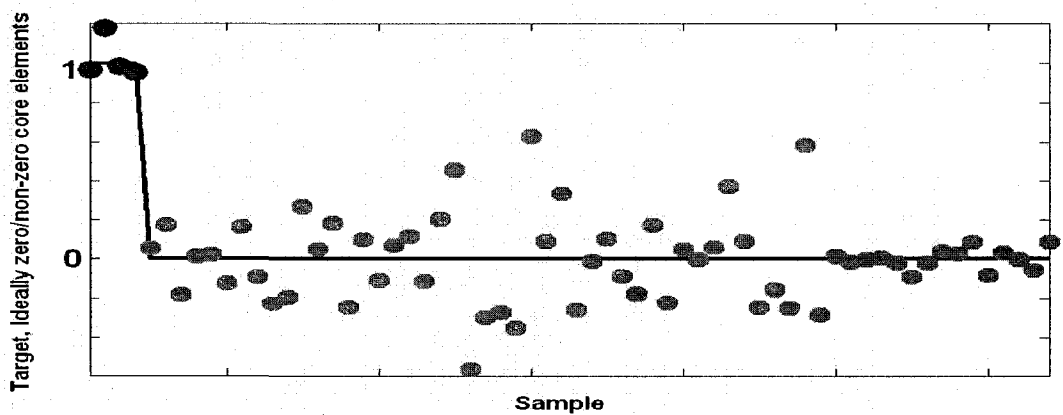


Figure G-7. Core consistency plot of diesel PARAFAC model

- Residual analysis: Figure G-8 of fluorescence data residual plot of diesel PARAFAC model indicating that residuals don't have systematic variation.

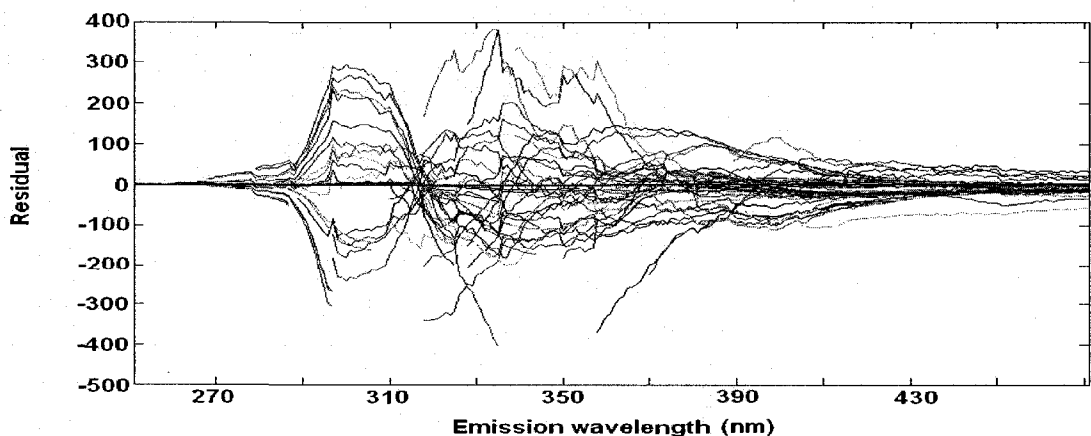


Figure G-8. Fluorescence data residual plot of diesel PARAFAC model

## Flare pit residue PARAFAC model

- Number of fitted PARAFAC components: 1, 2, 3, 4, 5

Optimal number of PARAFAC components: 4

- Number of iterations to model the optimal number of PARAFAC components: 132
- Core consistency analysis: Figure G-9 of core consistency plot of flare pit residue

PARAFAC model with 4 predicted components (represented by the red dots) indicate that zero and non-zero core elements follow the blue line.

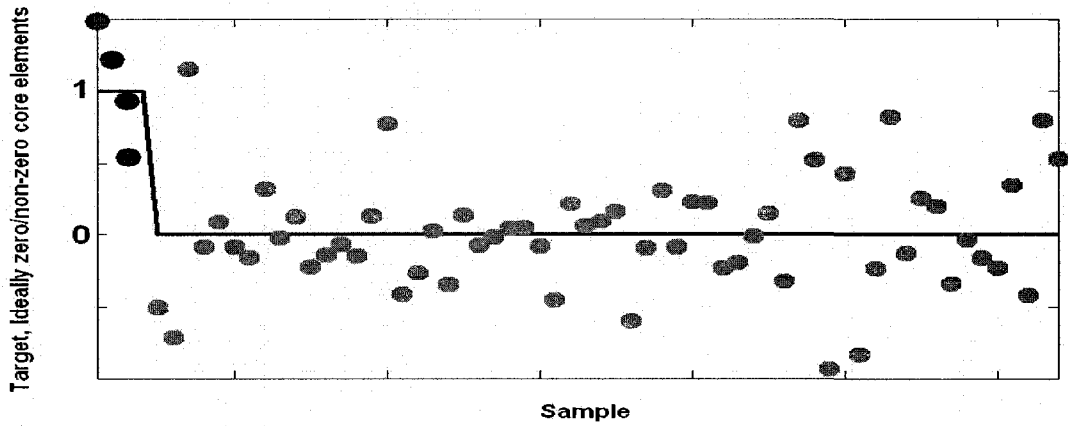


Figure G-9. Core consistency plot of flare pit residue PARAFAC model

- Residual analysis: Figure G-10 of fluorescence data residual plot of flare pit residue PARAFAC model indicating that residuals don't have systematic variation.

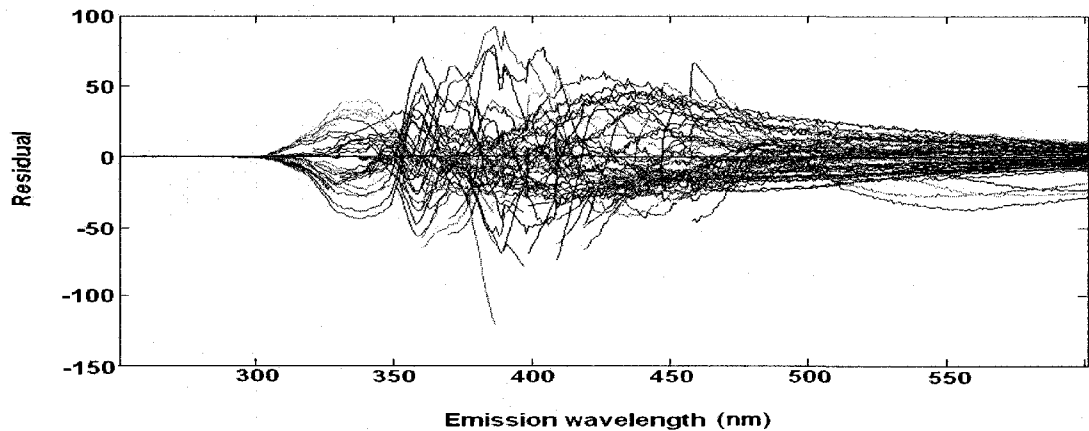


Figure G-10. Fluorescence data residual plot of flare pit residue PARAFAC model

## Crude oil PARAFAC model

- Number of fitted PARAFAC components: 1, 2, 3, 4, 5

Optimal number of PARAFAC components: 3

- Number of iterations to model the optimal number of PARAFAC components: 127
- Core consistency analysis: Figure G-11 of core consistency plot of crude oil

PARAFAC model with 3 predicted components (represented by the red dots)

indicate that

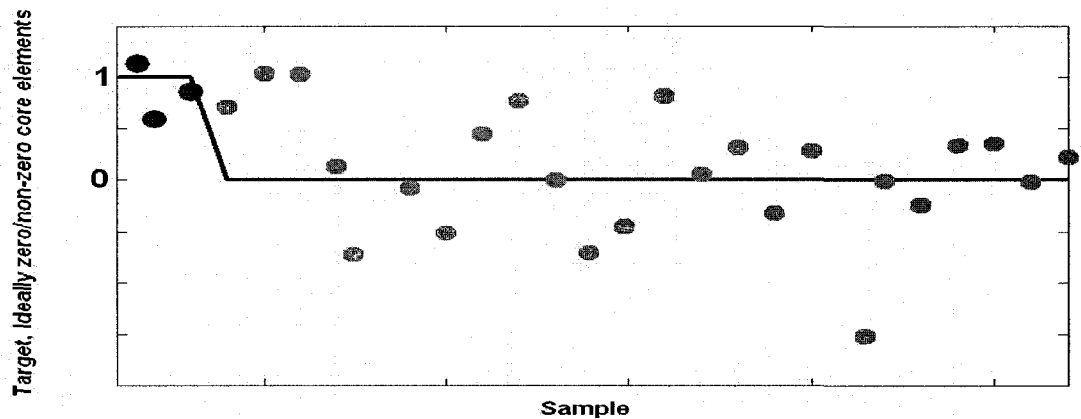


Figure G-11. Core consistency plot of crude oil PARAFAC model

- Residual analysis: Figure G-12 of fluorescence data residual plot of crude oil PARAFAC model indicating that residuals don't have systematic variation.

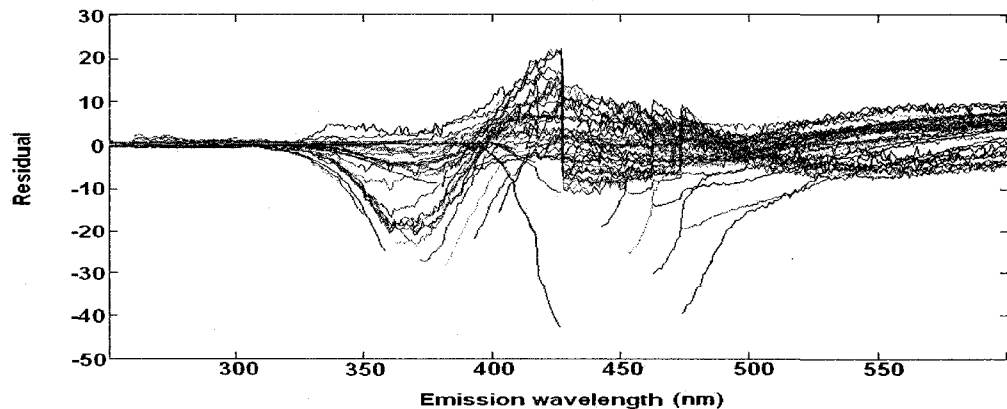


Figure G-12. Fluorescence data residual plot of crude oil PARAFAC model

# **PARAFAC Models for Petroleum Products in Soil Samples**

## Gas condensate in soil PARAFAC model

- Number of fitted PARAFAC components: 1, 2, 3, 4, 5

Optimal number of PARAFAC components: 3

- Number of iterations to model the optimal number of PARAFAC components: 69
- Core consistency analysis: Figure G-13 of core consistency plot of gas condensate (in soil) PARAFAC model with 3 predicted components (represented by the red dots) indicate that zero and non-zero core elements follow the blue line.

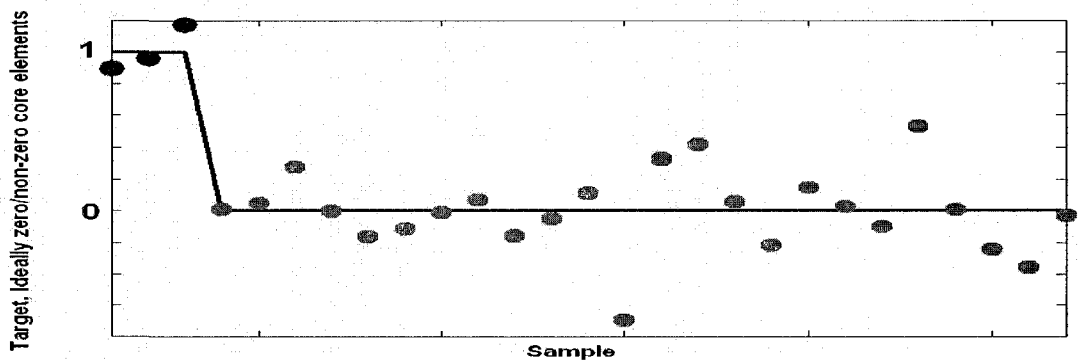


Figure G-13. Core consistency plot of gas condensate PARAFAC model (in soil)\*

- Residual analysis: Figure G-14 of fluorescence data residual plot of gas condensate (in soil) PARAFAC model indicating that residuals don't have systematic variation.

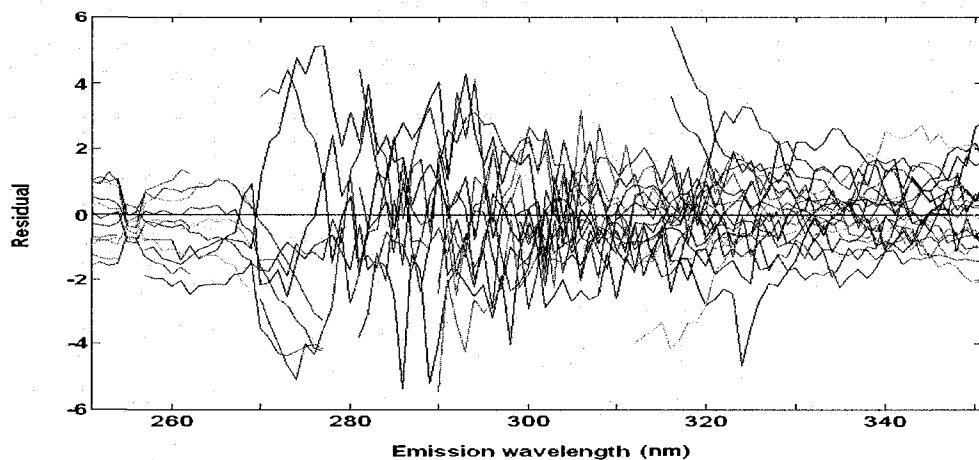


Figure G-14. Fluorescence data residual plot of gas condensate PARAFAC model (in soil)\*

## Gasoline PARAFAC model

- Number of fitted PARAFAC components: 1, 2, 3, 4, 5

Optimal number of PARAFAC components: 3

- Number of iterations to model the optimal number of PARAFAC components: 87
- Core consistency analysis: Figure G-15 of core consistency plot of gasoline (in soil)

PARAFAC model with 3 predicted components (represented by the red dots)

indicate that zero and non-zero core elements follow the blue line.

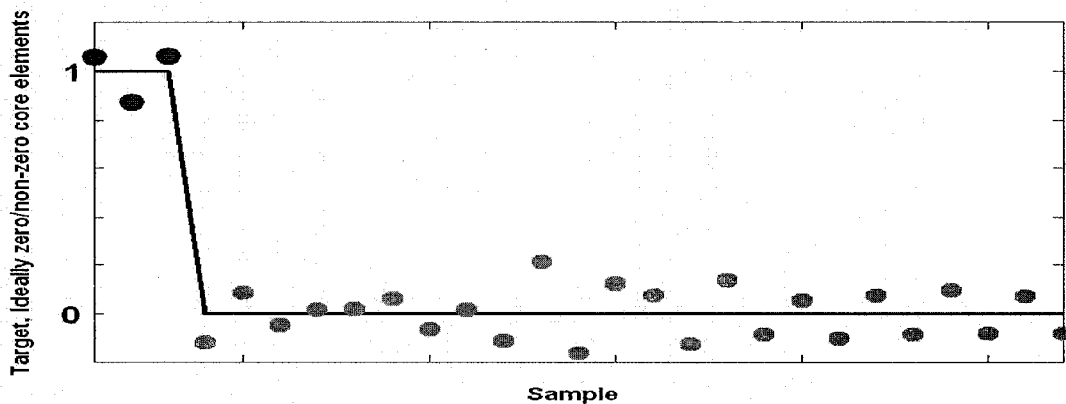


Figure G-15. Core consistency plot of gasoline PARAFAC model (in soil)\*

- Residual analysis: Figure G-16 of fluorescence data residual plot of gasoline (in soil) PARAFAC model indicating that residuals don't have systematic variation.

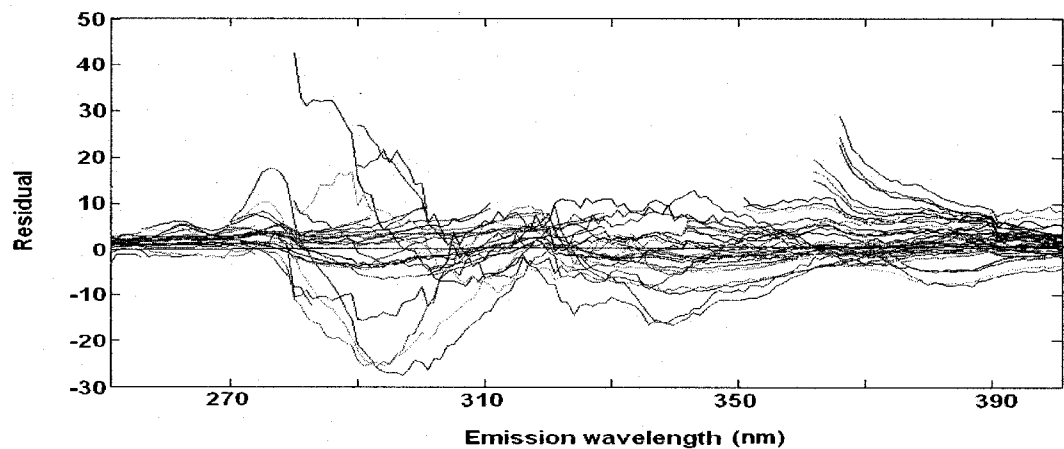


Figure G-16. Fluorescence data residual plot of gasoline PARAFAC model (in soil)\*

## Diesel PARAFAC model

- Number of fitted PARAFAC components: 1, 2, 3, 4, 5

Optimal number of PARAFAC components: 4

- Number of iterations to model the optimal number of PARAFAC components: 204
- Core consistency analysis: Figure G-17 of core consistency plot of diesel (in soil)

PARAFAC model with 4 predicted components (represented by the red dots) indicate that zero and non-zero core elements follow the blue line.

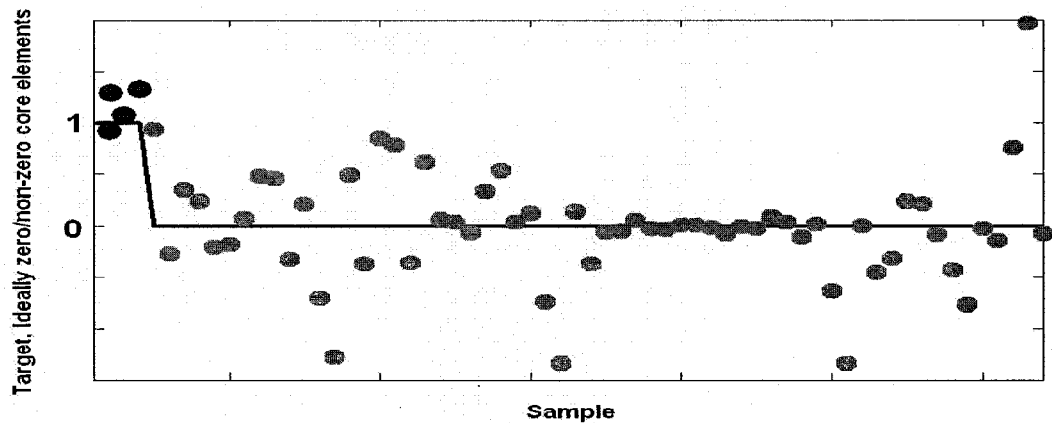


Figure G-17. Core consistency plot of diesel PARAFAC model (in soil)\*

- Residual analysis: Figure G-18 of fluorescence data residual plot of diesel (in soil) PARAFAC model indicating that residuals don't have systematic variation.

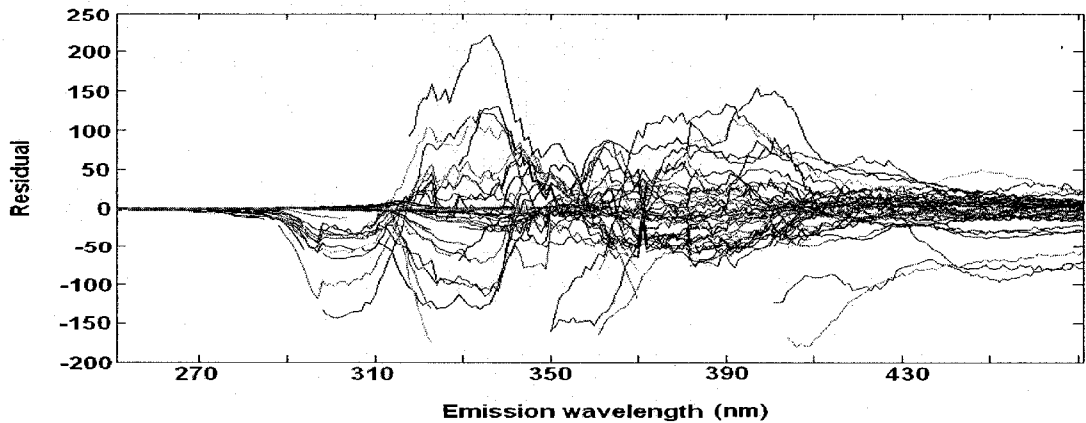


Figure G-18. Fluorescence data residual plot of diesel PARAFAC model (in soil)\*



## Flare pit residue PARAFAC model

- Number of fitted PARAFAC components: 1, 2, 3, 4, 5

Optimal number of PARAFAC components: 4

- Number of iterations to model the optimal number of PARAFAC components: 188
- Core consistency analysis: Figure G-19 of core consistency plot of flare pit residue (in soil) PARAFAC model with 4 predicted components (represented by the red dots) indicate that zero and non-zero core elements follow the blue line.

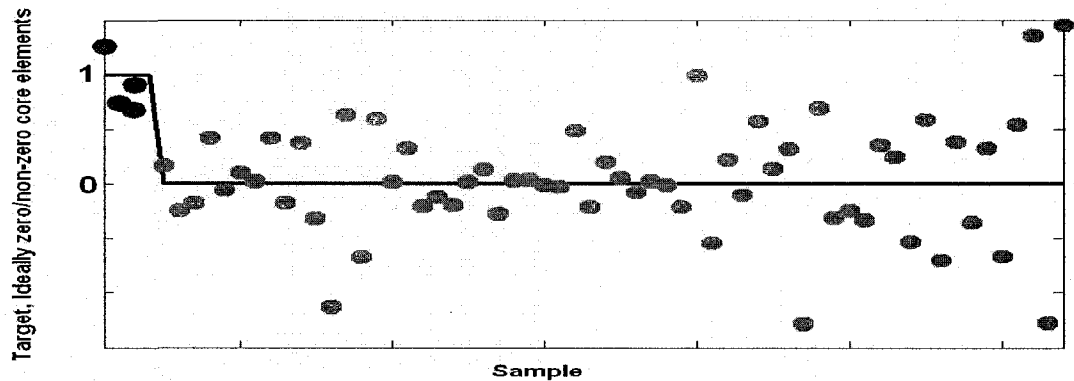


Figure G-19. Core consistency plot of flare pit residue PARAFAC model (in soil)\*

- Residual analysis: Figure G-20 of fluorescence data residual plot of flare pit residue (in soil) PARAFAC model indicating that residuals don't have systematic variation.

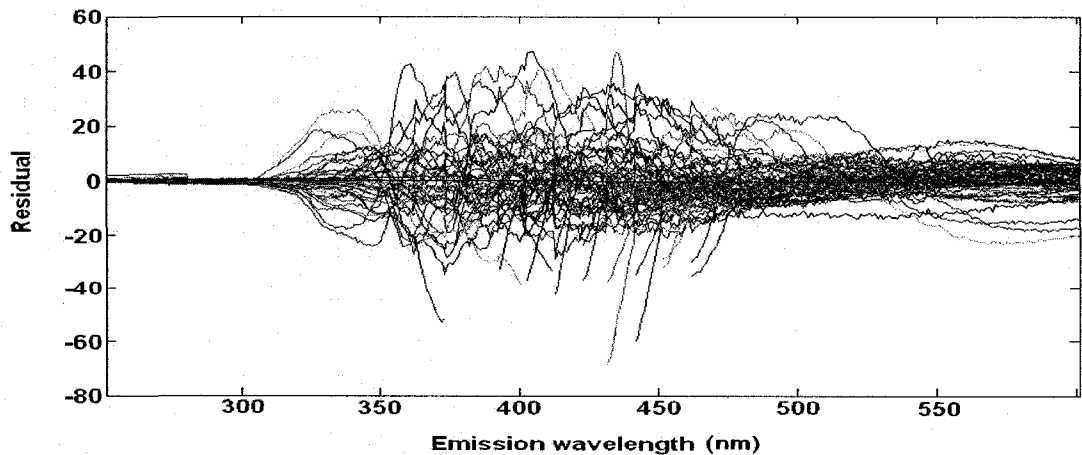


Figure G-20. Fluorescence data residual plot of flare pit residue PARAFAC model (in soil)\*

## Crude oil PARAFAC model

- Number of fitted PARAFAC components: 1, 2, 3, 4, 5

Optimal number of PARAFAC components: 3

- Number of iterations to model the optimal number of PARAFAC components: 163
- Core consistency analysis: Figure G-21 of core consistency plot of crude oil (in soil)

PARAFAC model with 3 predicted components (represented by the red dots)

indicate that zero and non-zero core elements follow the blue line.

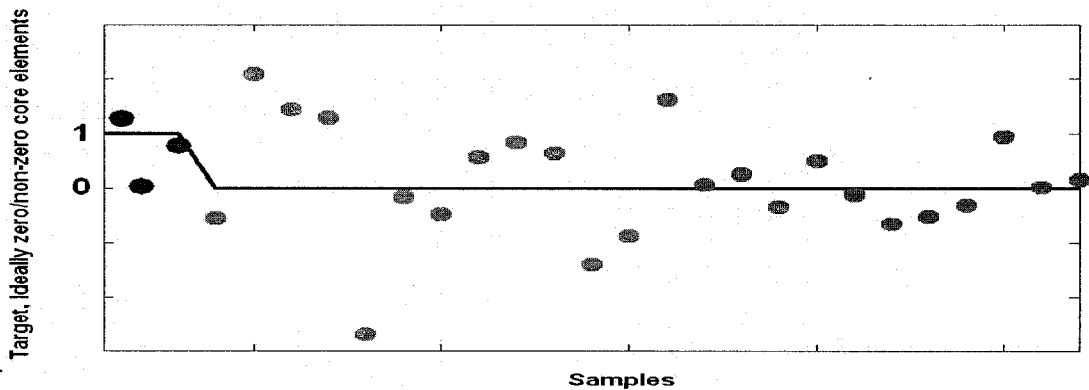


Figure G-21. Core consistency plot of crude oil PARAFAC model (in soil)\*

- Residual analysis: Figure G-22 of fluorescence data residual plot of crude oil (in soil) PARAFAC model indicating that residuals don't have systematic variation.

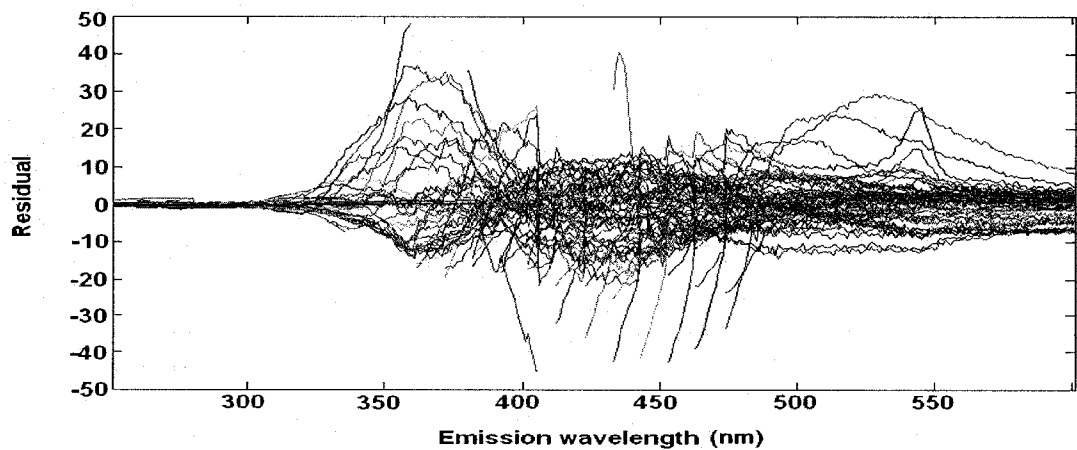


Figure G-22. Fluorescence data residual plot of crude oil PARAFAC model (in soil)\*

# **SIMCA Models**

## **STEP TO CONSTRUCT SIMCA MODEL**

Constructing a SIMCA model for a particular petroleum product using PARAFAC modeled score values of each of the predicted components, consists of four basic steps:

- 1- Normalize PARAFAC scores in matrix A for each of the modeled components.
- 2- Assemble the normalized scores into data matrix of class "dataset".
- 3- Assign a class for each of data set.
- 4- Fit a SIMCA model with varying number of factors using PLS-Toolbox.

# **SIMCA Models for Petroleum Products in Solution Samples**

## INPUT FILES

ALL_SIMCA	(Data set that contains normalized scores of PARAFAC modeled components of gas condensate, gasoline, diesel, flare pit residue and crude oil samples
CONDENSATE_SIMCA	Double matrix that contains normalized scores of PARAFAC modeled components of gas condensate samples.
GASOLINE_SIMCA	Double matrix that contains normalized scores of PARAFAC modeled components of gasoline samples.
DIESEL_SIMCA	Double matrix that contains normalized scores of PARAFAC modeled components of diesel samples.
FLARE_SIMCA	Double matrix that contains normalized scores of PARAFAC modeled components of flare pit residue samples.
CRUDE_SIMCA	Double matrix that contains normalized scores of PARAFAC modeled components of crude oil samples.

## SIMCA MODEL

```
>> model = simca(ALL_SIMCA,3,options);
```

T<sup>2</sup> and Q were set to be 0.95 and 0.95 in the “options”

The following classes were assigned in the model

Petroleum Product	Class ID
Gas Condensate	1
Gasoline	2
Diesel	3
Flare pit residue	4
Crude oil	5

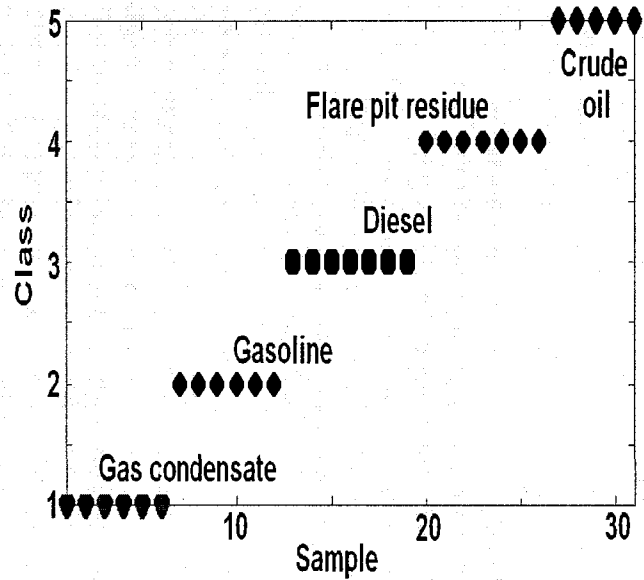


Figure G-23. Classes of analyzed petroleum

## OUTPUT (CLASS DISCRIMINATION)

### *Gas condensate class discrimination*

```
>> pred = simca(CONDENSATE_SIMCA,model,options);
```

Sample 1 belongs to 2 classes  
They are classes 2  
It is nearest the center of class 1

Sample 2 belongs to 2 classes  
They are classes 2  
It is nearest the center of class 1

Sample 3 belongs to 3 classes  
They are classes 3  
It is nearest the center of class 1

Sample 4 belongs to 5 classes  
They are classes 5  
It is nearest the center of class 1

Sample 5 belongs to 2 classes  
They are classes 2  
It is nearest the center of class 1

Sample 6 belongs to 2 classes  
They are classes 2  
It is nearest the center of class 1

*(All samples were classified as gas condensate)*

---

### ***Gasoline class discrimination***

```
>> pred=simca(GASOLINE_SIMCA,model,options);
```

Sample 1 belongs to 2 classes  
They are classes 2  
It is nearest the center of class 2

Sample 2 belongs to 3 classes  
They are classes 3  
It is nearest the center of class 2

Sample 3 belongs to 4 classes  
They are classes 4  
It is nearest the center of class 2

Sample 4 belongs to 5 classes  
They are classes 5  
It is nearest the center of class 1

Sample 5 belongs to 3 classes  
They are classes 3  
It is nearest the center of class 2

Sample 6 belongs to 2 classes  
They are classes 2  
It is nearest the center of class 2

*(5 of 6 samples were classified as gasoline)*

---

### ***Diesel class discrimination***

```
>> pred=simca(DIESEL_SIMCA,model,options);
```

Sample 1 belongs to 5 classes  
They are classes 5  
It is nearest the center of class 3



Sample 2 belongs to 5 classes  
They are classes 5  
It is nearest the center of class 3

Sample 3 belongs to 5 classes  
They are classes 5  
It is nearest the center of class 3

Sample 4 belongs to 5 classes  
They are classes 5  
It is nearest the center of class 3

Sample 5 belongs to 5 classes  
They are classes 5  
It is nearest the center of class 5

Sample 6 belongs to 3 classes  
They are classes 3  
It is nearest the center of class 3

Sample 7 belongs to 3 classes  
They are classes 3  
It is nearest the center of class 1

(5 of 7 samples were classified as Diesel)

---

***Flare pit residue class discrimination***

```
>> pred=simca(FLARE_SIMCA,model,options);
```

Sample 1 belongs to 5 classes  
They are classes 5  
It is nearest the center of class 1

Sample 2 belongs to 5 classes  
They are classes 5  
It is nearest the center of class 5

Sample 3 belongs to 5 classes  
They are classes 5  
It is nearest the center of class 4

Sample 4 belongs to 4 classes  
They are classes 4

It is nearest the center of class 1

Sample 5 belongs to 5 classes

They are classes 5

It is nearest the center of class 5

Sample 6 belongs to 5 classes

They are classes 5

It is nearest the center of class 4

Sample 7 belongs to 4 classes

They are classes 4

It is nearest the center of class 4

(3 of 7 samples were classified as flare pit residue)

---

### ***Crude oil class discrimination***

```
>> pred=simca(CRUDE_SIMCA,model,options);
```

Sample 1 belongs to 5 classes

They are classes 5

It is nearest the center of class 1

Sample 2 belongs to 5 classes

They are classes 5

It is nearest the center of class 5

Sample 3 belongs to 5 classes

They are classes 5

It is nearest the center of class 3

Sample 4 belongs to 4 classes

They are classes 4

It is nearest the center of class 5

Sample 5 belongs to 5 classes

They are classes 5

It is nearest the center of class 4

Sample 6 belongs to 5 classes

They are classes 5

It is nearest the center of class 1

(2 of 6 samples were classified as crude oil)

# **SIMCA Models for Petroleum Products in Soil Samples**

## INPUT FILES

ALL_SOIL_SIMCA	(Data set that contains normalized scores of PARAFAC modeled components of gas condensate, gasoline, diesel, flare pit residue and crude oil in soil samples
CONDENSATE_SOIL_SIMCA	Double matrix that contains normalized scores of PARAFAC modeled components of gas condensate in soil samples.
GASOLINE_SOIL_SIMCA	Double matrix that contains normalized scores of PARAFAC modeled components of gasoline in soil samples.
DIESEL_SOIL_SIMCA	Double matrix that contains normalized scores of PARAFAC modeled components of diesel in soil samples.
FLARE_SOIL_SIMCA	Double matrix that contains normalized scores of PARAFAC modeled components of flare pit residue in soil samples.
CRUDE_SOIL_SIMCA	Double matrix that contains normalized scores of PARAFAC modeled components of crude oil in soil samples.

## SIMCA MODEL

```
>> model = simca(ALL_SOIL_SIMCA,3,options);
```

T<sup>2</sup> and Q were set to be 0.95 and 0.95, respectively, in the “options”

The following classes were assigned in the model

Petroleum product	Class ID
Gas Condensate	1
Gasoline	2
Diesel	3
Flare pit residue	4
Crude oil	5

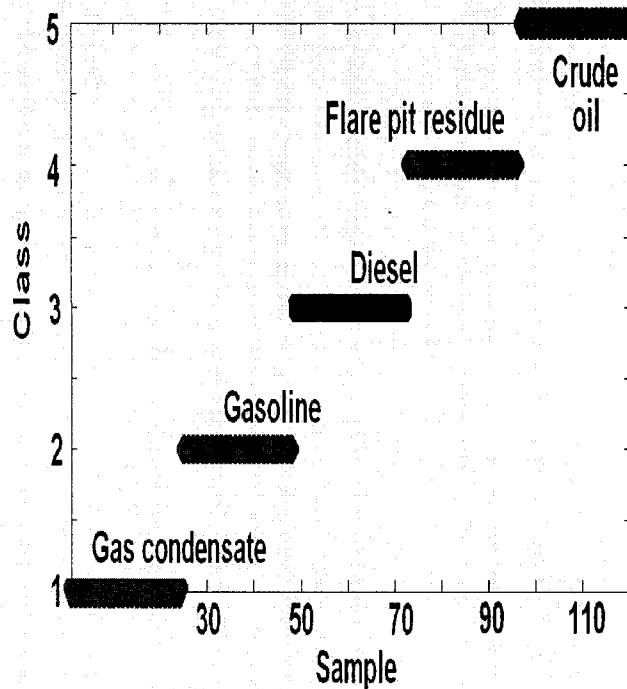


Figure G-24. Classes of analyzed petroleum products in soil samples

## OUTPUT (CLASS DISCRIMINATION)

### *Gas condensate in soil class discrimination*

```
>> pred = simca(CONDENSATE_SOIL_SIMCA,model,options);
```

Sample 1 belongs to 5 classes  
They are classes 5  
It is nearest the center of class 1

Sample 2 belongs to 5 classes  
They are classes 5  
It is nearest the center of class 1

Sample 3 belongs to 3 classes  
They are classes 3  
It is nearest the center of class 1

Sample 4 belongs to class 1

Sample 5 belongs to 2 classes  
They are classes 2  
It is nearest the center of class 1

Sample 6 belongs to class 1

Sample 7 belongs to 3 classes  
They are classes 3  
It is nearest the center of class 1

Sample 8 belongs to 3 classes  
They are classes 3  
It is nearest the center of class 4

Sample 9 belongs to 3 classes  
They are classes 3  
It is nearest the center of class 1

Sample 10 belongs to class 1

Sample 11 belongs to 2 classes  
They are classes 2  
It is nearest the center of class 1

Sample 12 belongs to class 1

Sample 13 belongs to 4 classes  
They are classes 4  
It is nearest the center of class 2

Sample 14 belongs to 2 classes  
They are classes 2  
It is nearest the center of class 3

Sample 15 belongs to 3 classes  
They are classes 3  
It is nearest the center of class 1

Sample 16 belongs to class 1

Sample 17 belongs to 5 classes  
They are classes 5  
It is nearest the center of class 1

Sample 18 belongs to class 1

Sample 19 belongs to 5 classes  
They are classes 5  
It is nearest the center of class 1

Sample 20 belongs to 4 classes  
They are classes 4  
It is nearest the center of class 3

Sample 21 belongs to 3 classes  
They are classes 3  
It is nearest the center of class 1

Sample 22 belongs to class 1

Sample 23 belongs to 2 classes  
They are classes 2  
It is nearest the center of class 1

Sample 24 belongs to class 1

*(20 of 24 samples were classified as gas condensate)*

---

### ***Gasoline in soil class discrimination***

```
>> pred=simca(GASOLINE_SOIL_SIMCA,model,options);
```

Sample 1 belongs to 4 classes  
They are classes 4  
It is nearest the center of class 5

Sample 2 belongs to 4 classes  
They are classes 4  
It is nearest the center of class 3

Sample 3 belongs to 2 classes  
They are classes 2  
It is nearest the center of class 2

Sample 4 belongs to 2 classes  
They are classes 2  
It is nearest the center of class 2

Sample 5 belongs to 2 classes  
They are classes 2  
It is nearest the center of class 2

Sample 6 belongs to class 2

Sample 7 belongs to 3 classes  
They are classes 3  
It is nearest the center of class 2

Sample 8 belongs to 2 classes  
They are classes 2  
It is nearest the center of class 4

Sample 9 belongs to 2 classes  
They are classes 2  
It is nearest the center of class 2

Sample 10 belongs to 2 classes  
They are classes 2  
It is nearest the center of class 2

Sample 11 belongs to class 2

Sample 12 belongs to class 2

Sample 13 belongs to class 2

Sample 14 belongs to 4 classes  
They are classes 4  
It is nearest the center of class 3

Sample 15 belongs to class 2

Sample 16 belongs to 2 classes  
They are classes 2  
It is nearest the center of class 2

Sample 17 belongs to 2 classes  
They are classes 2  
It is nearest the center of class 2

Sample 18 belongs to class 2

Sample 19 belongs to 4 classes  
They are classes 4



It is nearest the center of class 5

Sample 20 belongs to 3 classes  
They are classes 3  
It is nearest the center of class 2

Sample 21 belongs to 2 classes  
They are classes 2  
It is nearest the center of class 2

Sample 22 belongs to 2 classes  
They are classes 2  
It is nearest the center of class 2

Sample 23 belongs to 2 classes  
They are classes 2  
It is nearest the center of class 2

Sample 24 belongs to class 2

(19 of 24 samples were classified as gasoline)

---

***Diesel in soil class discrimination***

```
>> pred=simca(DIESEL_SOIL_SIMCA,model,options);
```

Sample 1 belongs to 5 classes  
They are classes 5  
It is nearest the center of class 3

Sample 2 belongs to 5 classes  
They are classes 5  
It is nearest the center of class 3

Sample 3 belongs to 3 classes  
They are classes 3  
It is nearest the center of class 2

Sample 4 belongs to 4 classes  
They are classes 4  
It is nearest the center of class 3

Sample 5 belongs to 5 classes  
They are classes 5  
It is nearest the center of class 3

Sample 6 belongs to class 3

Sample 7 belongs to 4 classes  
They are classes 4  
It is nearest the center of class 3

Sample 8 belongs to 4 classes  
They are classes 4  
It is nearest the center of class 5

Sample 9 belongs to 4 classes  
They are classes 4  
It is nearest the center of class 3

Sample 10 belongs to 4 classes  
They are classes 4  
It is nearest the center of class 3

Sample 11 belongs to 5 classes  
They are classes 5  
It is nearest the center of class 3

Sample 12 belongs to 5 classes  
They are classes 5  
It is nearest the center of class 3

Sample 13 belongs to 2 classes  
They are classes 2  
It is nearest the center of class 4

Sample 14 belongs to class 3

Sample 15 belongs to 5 classes  
They are classes 5  
It is nearest the center of class 3

Sample 16 belongs to 5 classes  
They are classes 5  
It is nearest the center of class 3

Sample 17 belongs to 3 classes  
They are classes 3  
It is nearest the center of class 2

Sample 14 belongs to class 3

Sample 19 belongs to 5 classes  
They are classes 5  
It is nearest the center of class 3

Sample 20 belongs to class 3

Sample 21 belongs to 4 classes  
They are classes 4  
It is nearest the center of class 3

Sample 22 belongs to class 3

Sample 23 belongs to 2 classes  
They are classes 2  
It is nearest the center of class 3

Sample 24 belongs to 4 classes  
They are classes 4  
It is nearest the center of class 3

(20 of 24 samples were classified as Diesel)

---

***Flare pit residue in soil class discrimination***

```
>> pred=simca(FLARE_SOIL_SIMCA,model,options);
```

Sample 1 belongs to 4 classes  
They are classes 4  
It is nearest the center of class 3

Sample 2 belongs to 4 classes  
They are classes 4  
It is nearest the center of class 4

Sample 3 belongs to 4 classes  
They are classes 4  
It is nearest the center of class 4

Sample 4 belongs to 4 classes  
They are classes 4  
It is nearest the center of class 3

Sample 5 belongs to 2 classes

They are classes 2  
It is nearest the center of class 2

Sample 6 belongs to 5 classes  
They are classes 5  
It is nearest the center of class 4

Sample 7 belongs to 3 classes  
They are classes 3  
It is nearest the center of class 2

Sample 8 belongs to 4 classes  
They are classes 4  
It is nearest the center of class 5

Sample 9 belongs to 4 classes  
They are classes 4  
It is nearest the center of class 4

Sample 10 belongs to 5 classes  
They are classes 5  
It is nearest the center of class 4

Sample 11 belongs to 4 classes  
They are classes 4  
It is nearest the center of class 4

Sample 12 belongs to 2 classes  
They are classes 2  
It is nearest the center of class 2

Sample 13 belongs to 5 classes  
They are classes 5  
It is nearest the center of class 3

Sample 14 belongs to 2 classes  
They are classes 2  
It is nearest the center of class 3

Sample 15 belongs to 4 classes  
They are classes 4  
It is nearest the center of class 4

Sample 16 belongs to 4 classes  
They are classes 4  
It is nearest the center of class 4

Sample 17 belongs to 2 classes  
They are classes 2  
It is nearest the center of class 2

Sample 18 belongs to 2 classes  
They are classes 2  
It is nearest the center of class 4

Sample 19 belongs to 3 classes  
They are classes 3  
It is nearest the center of class 2

Sample 20 belongs to 3 classes  
They are classes 3  
It is nearest the center of class 4

Sample 21 belongs to 4 classes  
They are classes 4  
It is nearest the center of class 4

Sample 22 belongs to 5 classes  
They are classes 5  
It is nearest the center of class 3

Sample 23 belongs to 2 classes  
They are classes 2  
It is nearest the center of class 2

Sample 24 belongs to 3 classes  
They are classes 3  
It is nearest the center of class 2

(11 of 24 samples were classified as flare pit residue)

---

***Crude oil in soil class discrimination***

```
>> pred=simca(CRUDE_SOIL_SIMCA,model,options);
```

Sample 1 belongs to 4 classes  
They are classes 4  
It is nearest the center of class 3

Sample 2 belongs to 4 classes  
They are classes 4

It is nearest the center of class 5

Sample 3 belongs to 4 classes

They are classes 4

It is nearest the center of class 3

Sample 4 belongs to 3 classes

They are classes 3

It is nearest the center of class 5

Sample 5 belongs to 4 classes

They are classes 4

It is nearest the center of class 5

Sample 6 belongs to 5 classes

They are classes 5

It is nearest the center of class 3

Sample 7 belongs to 3 classes

They are classes 3

It is nearest the center of class 5

Sample 8 belongs to 4 classes

They are classes 4

It is nearest the center of class 5

Sample 9 belongs to 4 classes

They are classes 4

It is nearest the center of class 5

Sample 10 belongs to 4 classes

They are classes 4

It is nearest the center of class 3

Sample 11 belongs to 4 classes

They are classes 4

It is nearest the center of class 2

Sample 12 belongs to 3 classes

They are classes 3

It is nearest the center of class 5

Sample 13 belongs to 4 classes

They are classes 4

It is nearest the center of class 4

Sample 14 belongs to 2 classes  
They are classes 2  
It is nearest the center of class 5

Sample 15 belongs to 2 classes  
They are classes 2  
It is nearest the center of class 5

Sample 16 belongs to 3 classes  
They are classes 3  
It is nearest the center of class 3

Sample 17 belongs to 4 classes  
They are classes 4  
It is nearest the center of class 5

Sample 18 belongs to 3 classes  
They are classes 3  
It is nearest the center of class 3

Sample 19 belongs to 4 classes  
They are classes 4  
It is nearest the center of class 5

Sample 20 belongs to 2 classes  
They are classes 2  
It is nearest the center of class 5

Sample 21 belongs to 4 classes  
They are classes 4  
It is nearest the center of class 5

Sample 22 belongs to 2 classes  
They are classes 2  
It is nearest the center of class 3

Sample 23 belongs to 3 classes  
They are classes 3  
It is nearest the center of class 2

Sample 24 belongs to 4 classes  
They are classes 4  
It is nearest the center of class 5

(15 of 24 samples were classified as crude oil)

## REFERENCES

Bro, R. 1997. PARAFAC: Tutorial and Applications. *Journal of Chemometrics*, Vol. 38, pp. 149-71.

Bro, R. and Kiers, H. 2003. A new efficient method for determining the number of components in PARAFAC models. *Journal of Chemometrics*, 17, pp. 274-286.



**Appendix H**  
Standard Aromatic  
Hydrocarbon Fluorescence  
Calibration Curves and  
Estimation Procedure  
*(Using Varian Eclipse  
Spectrometer)*

**Standard Aromatic  
Hydrocarbon  
Fluorescence Calibration  
Curves**

## **AROMATIC HYDROCARBON FLUORESCENCE CALIBRATION CURVES**

Individual standards of aromatic hydrocarbons were prepared including: BTEX compounds (Benzene, Toluene, Ethyl-Benzene and Xylenes), Naphthalene and Methyl-Naphthalene, Phenanthrene, Fluorene, Pyrene, Dibenzothiophene, and Fluoranthene. In total 120 stock solution samples (including duplicates) of standard aromatic hydrocarbon compounds were prepared with concentrations that ranged from 0.08 to 50 mL/L (or in equivalent g/L) using hexane as solvent. A collection of emission scans from 250 to 600 nm with 1 nm increments was obtained at varying excitation wavelengths ranging from 240 to 450 nm with 10 nm increments. The bandwidths (slit width) were 5 nm for both excitation and emission for most scans, but were reduced to 2.5 nm when fluorescence intensity was out of range. The scan rate was 600 nm/min, which gave a scan time of about 20 minutes per sample.

To obtain calibration curves for tested aromatic hydrocarbon compounds, the relationship between total fluorescence intensity and aromatic hydrocarbon compound concentrations in solvent solution was investigated. Total fluorescence values were obtained by integrating the areas under all fluorescence curves (signals) in the related fluorescence EEM. The integration was consistent in all EEMs and limited to excitation and emission wavelengths between 250 nm and 450nm, and 260 nm and 600 nm, respectively. For each aromatic hydrocarbon compound, total fluorescence values were plotted versus related concentrations in solvent solution. Calibration curves are presented in Figures H-1, 2, 3 and 4. In Figure H-4, it appears that pyrene has two calibration curves due to that fact that pyrene fluorescence

spectrum is known to have two different emission peaks (at 384 and 470 nm) at lower and higher concentrations (less or greater than 0.2 g/L) due to formation of excimers,

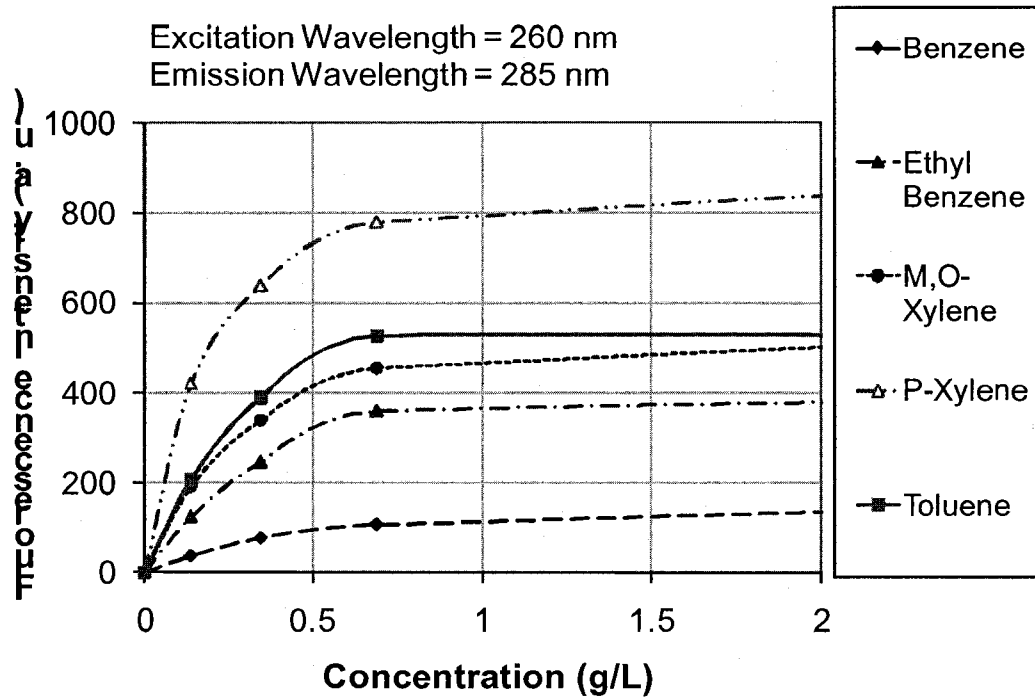


Figure H-1. Fluorescence intensity versus concentration (*aromatic compounds with 1 benzene ring*)

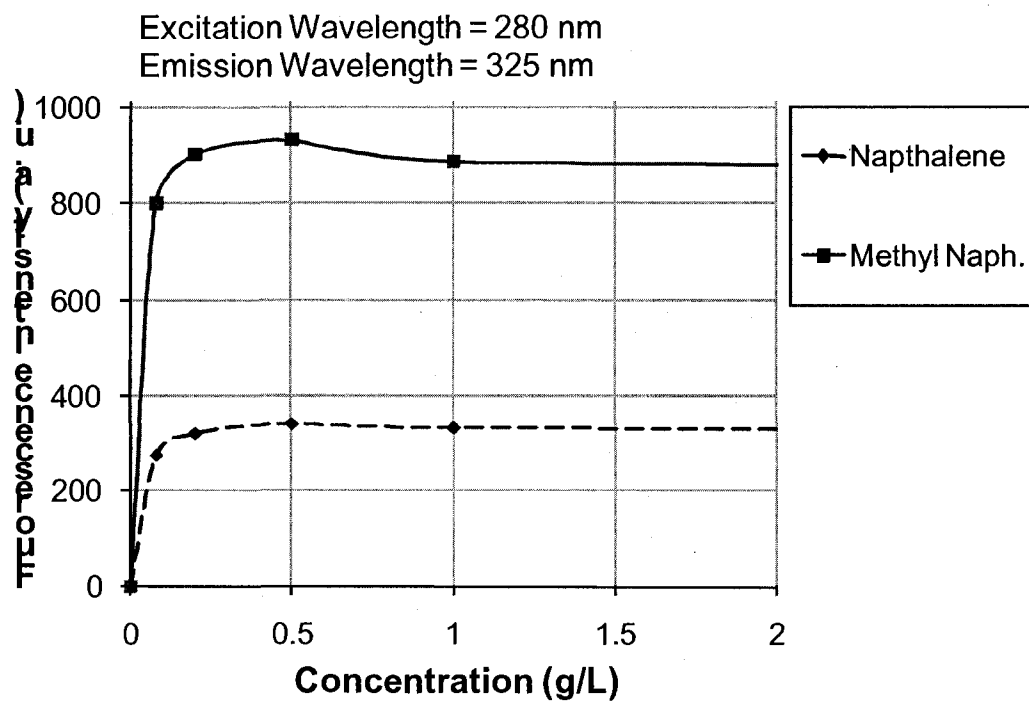


Figure H-2. Fluorescence intensity versus concentration (*aromatic compounds with 2 benzene ring2*)

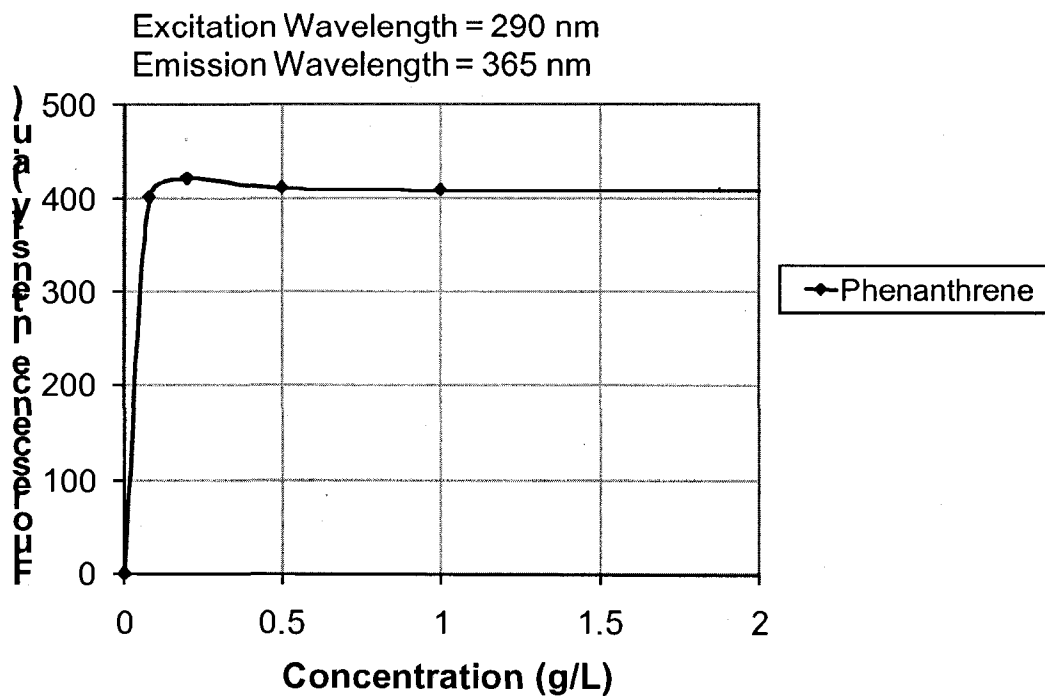


Figure H-3. Fluorescence intensity versus concentration (*aromatic compounds with 3 benzene rings*)

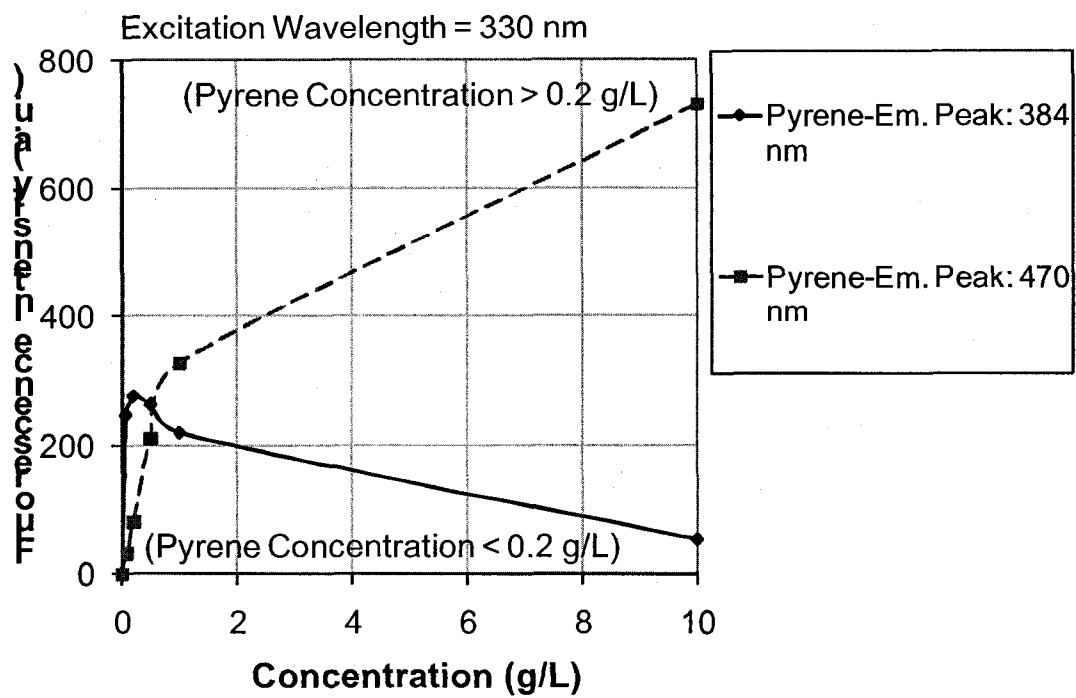


Figure H-4. Fluorescence intensity versus concentration (*aromatic compounds with 4 benzene rings*)

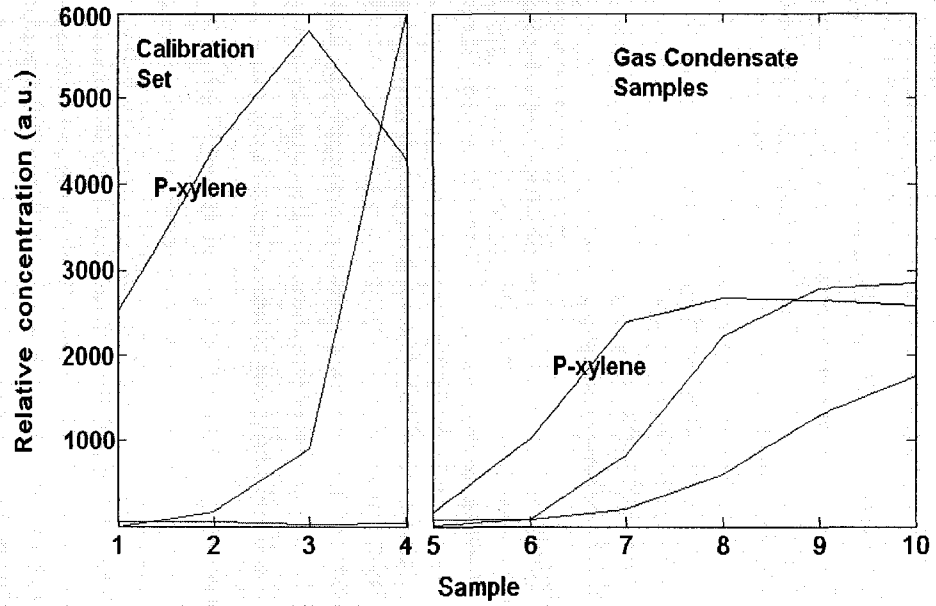


**Estimation of Standard  
Aromatic Hydrocarbon  
Concentrations in Tested  
Petroleum Products Using  
PARAFAC Scores**

## **ESTIMATION OF AROMATIC HYDROCARBON CONCENTRATIONS IN TESTED PETROLEUM PRODUCTS**

Concentrations of the aromatic compounds in petroleum products can be estimated using information produced by PARAFAC analysis in the A matrix (the score matrix) that describe the relative concentration of underlying components derived from the variation of their fluorescence intensity in analyzed solution samples. Details of procedures to obtain equivalent aromatic hydrocarbon concentrations using chemical analysis results and related fluorescence intensity information are described in section 3.4.2.2. The section also explains how to estimate unknown aromatic hydrocarbons concentrations in tested petroleum using PARAFAC scores.

## Estimation of equivalent p-xylene in gas condensate



### P-xylene calibration curve

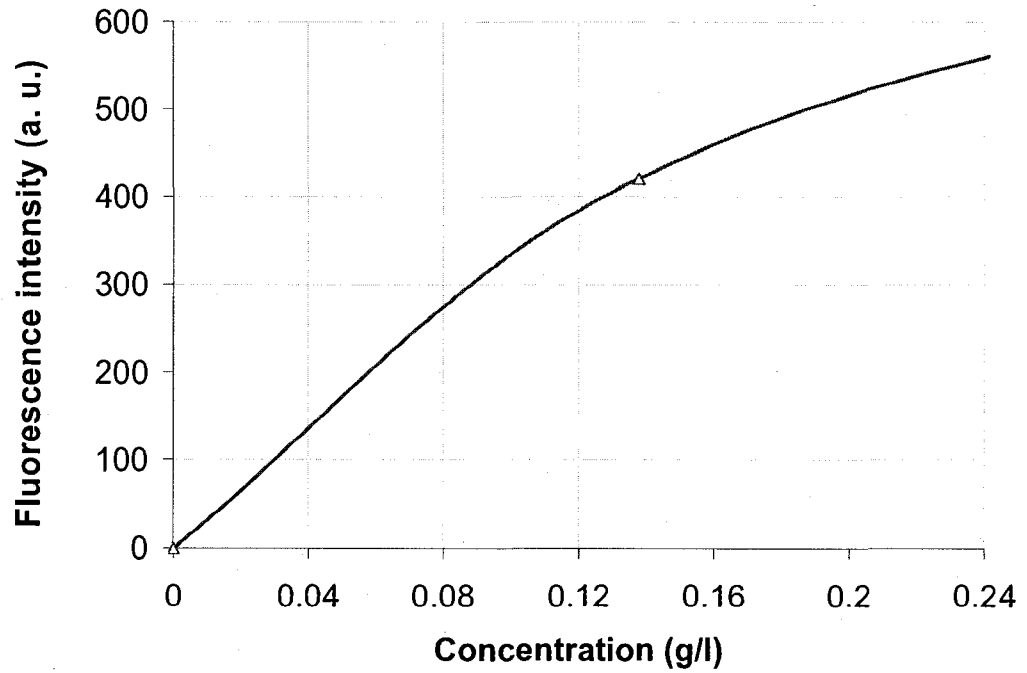


Figure H-5. Gas condensate -PARAFAC score and calibration curve of p-xylene

- P-xylene concentration in sample N° 1 in calibration set = 0.14 g/L
- Relative concentration (fluorescence intensity) of p-xylene in sample N° 1 in PARAFAC score matrix = 2600
- Relative concentration (fluorescence intensity) of p-xylene in sample N° 5 in PARAFAC score matrix = 130
- Relative concentration (fluorescence intensity) ratio = 0.05
- Actual fluorescence intensity of p-xylene concentration equivalent to sample N° 1 in laboratory generated p-xylene calibration curve = 440 a. u.
- Actual fluorescence intensity of p-xylene in sample N° 5 using Relative concentration (fluorescence intensity) ratio = 20 a. u.
- Corresponding concentration of p-xylene in sample N° 5 using laboratory generated p-xylene calibration curve = 0.008 g/L
- Concentration of gas condensate in sample N° 5 (Dilution factor) = 1 mL/L (diluted 1000 times)
- Concentration of p-xylene in neat gas condensate sample = 8 g / L

### **Estimation of equivalent methyl-naphthalene in gas condensate**

Proper PARAFAC model couldn't be generated when methyl-naphthalene calibration set was included in the analysis with gas condensate samples.

### Estimation of equivalent p-xylene in gasoline

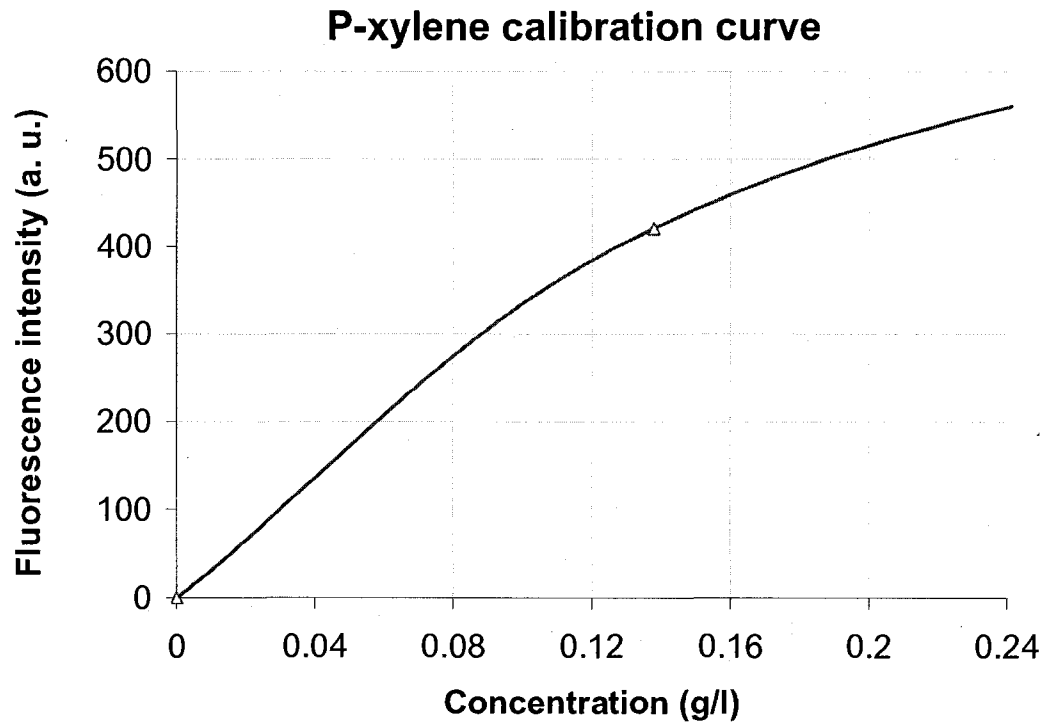
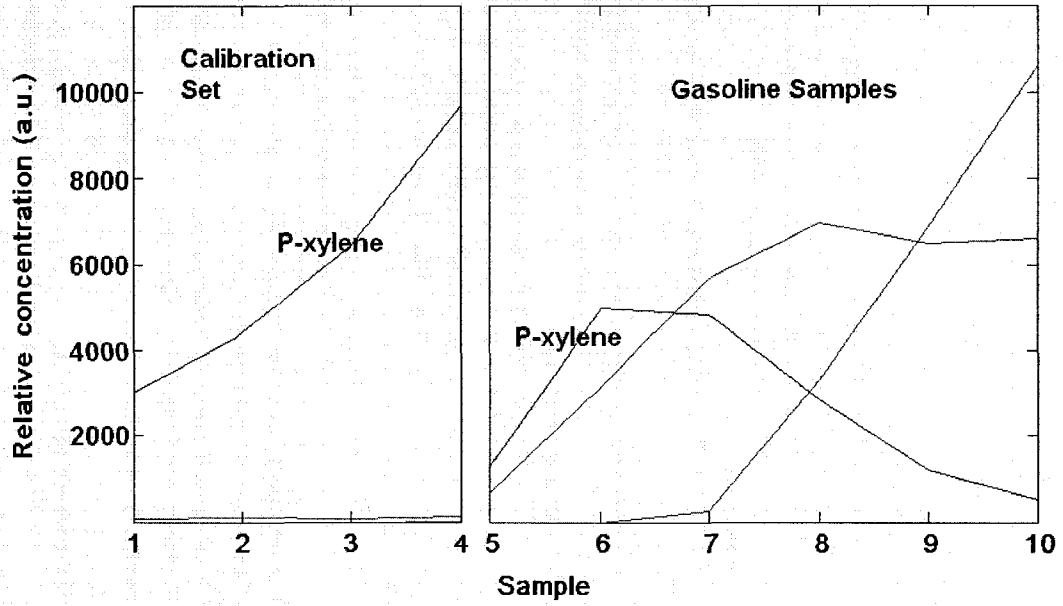
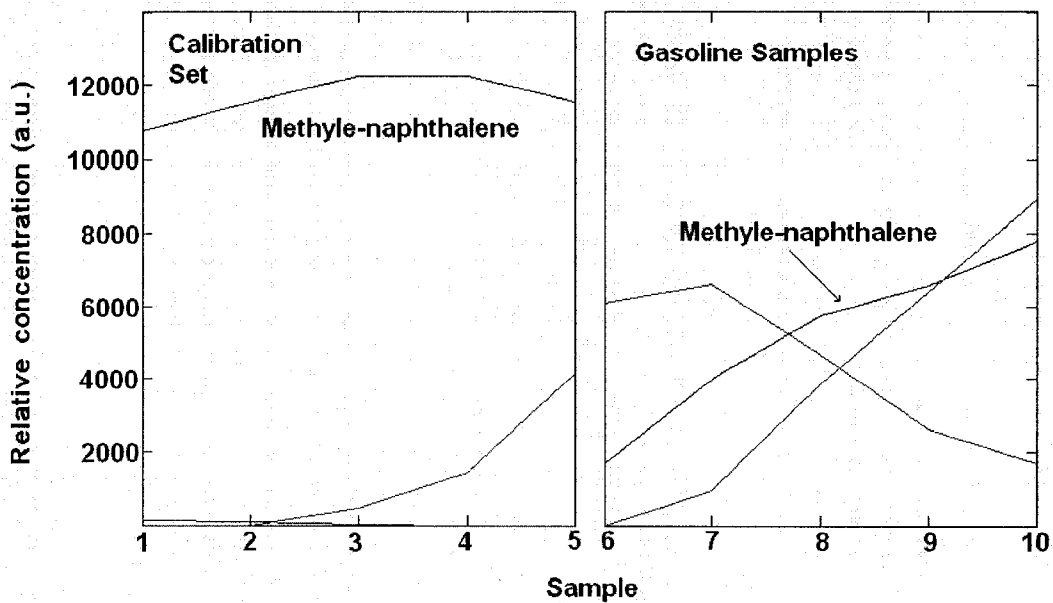


Figure H-6. Gasoline -PARAFAC score and calibration curve of p-xylene

- P-xylene concentration in sample N° 1 in calibration set = 0.14 g/L
- Relative concentration (fluorescence intensity) of p-xylene in sample N° 1 in PARAFAC score matrix = 3000
- Relative concentration (fluorescence intensity) of p-xylene in sample N° 5 in PARAFAC score matrix = 1900
- Relative concentration (fluorescence intensity) ratio = 0.63
- Actual fluorescence intensity of p-xylene concentration equivalent to sample N° 1 in laboratory generated p-xylene calibration curve = 440 a. u.
- Actual fluorescence intensity of p-xylene in sample N° 5 using Relative concentration (fluorescence intensity) ratio = 275 a. u.
- Corresponding concentration of p-xylene in sample N° 5 using laboratory generated p-xylene calibration curve = 0.08 g/L
- Concentration of gasoline in sample N° 5 (Dilution factor) = 1 mL/L (diluted 1000 times)
- Concentration of p-xylene in neat gasoline sample = 80 g / L

## Estimation of equivalent methyl-naphthalene in gasoline



### Methyl-Naphthalene calibration curve

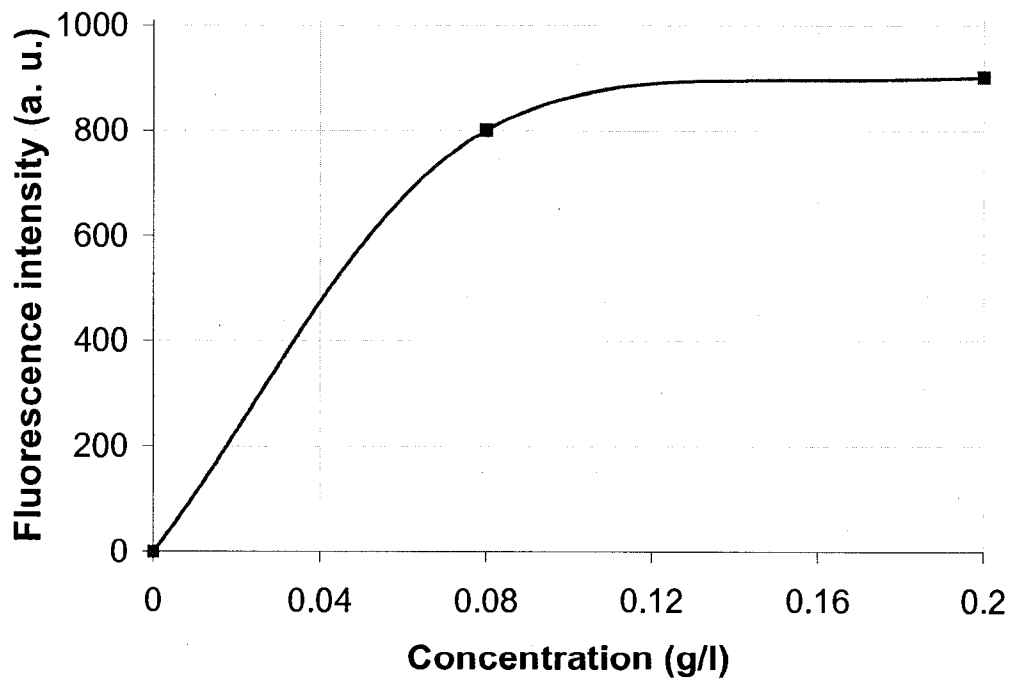


Figure H-7. Gasoline -PARAFAC score and calibration curve of methyl-naphthalene

- Methyl-naphthalene concentration in sample N° 1 in calibration set = 0.08 g/L
- Relative concentration (fluorescence intensity) of methyl-naphthalene in sample N° 1 in PARAFAC score matrix = 10800
- Relative concentration (fluorescence intensity) of methyl-naphthalene in sample N° 6 in PARAFAC score matrix = 1500
- Relative concentration (fluorescence intensity) ratio = 0.14
- Actual fluorescence intensity of methyl-naphthalene concentration equivalent to sample N° 1 in laboratory generated methyl-naphthalene calibration curve = 800 a. u.
- Actual fluorescence intensity of methyl-naphthalene in sample N° 6 using Relative concentration (fluorescence intensity) ratio = 112 a. u.
- Corresponding concentration of methyl-naphthalene in sample N° 6 using laboratory generated methyl-naphthalene calibration curve = 0.015 g/L
- Concentration of gasoline in sample N° 6 (Dilution factor) = 10 mL/L (diluted 100 times)
- Concentration of methyl-naphthalene in neat gasoline sample = 1.5 g / L



## Estimation of equivalent p-xylene in diesel

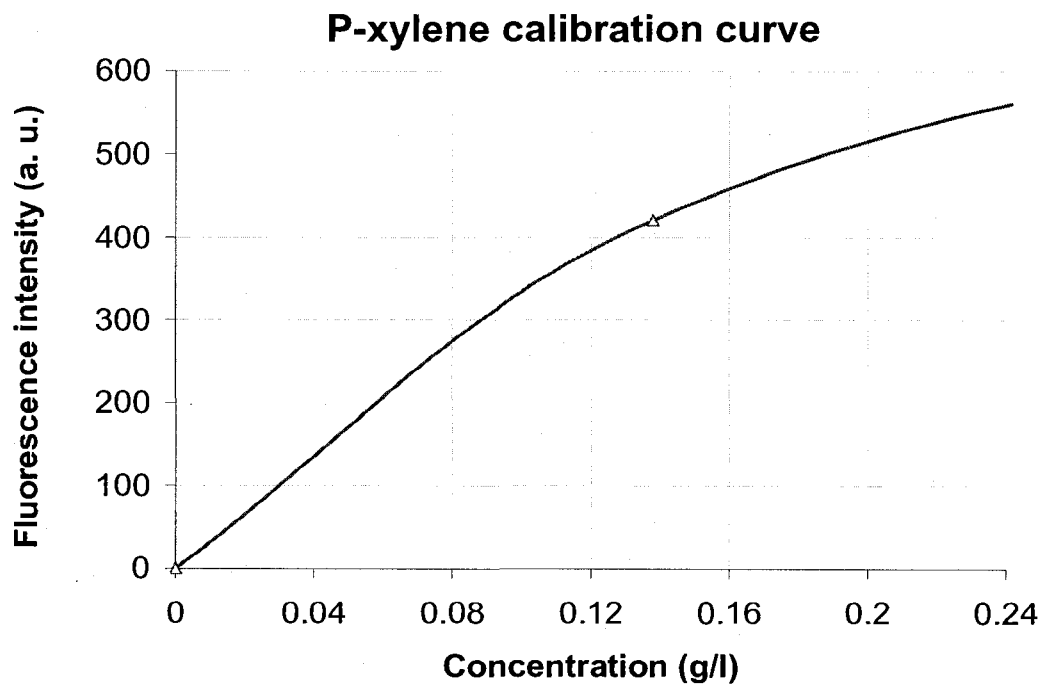
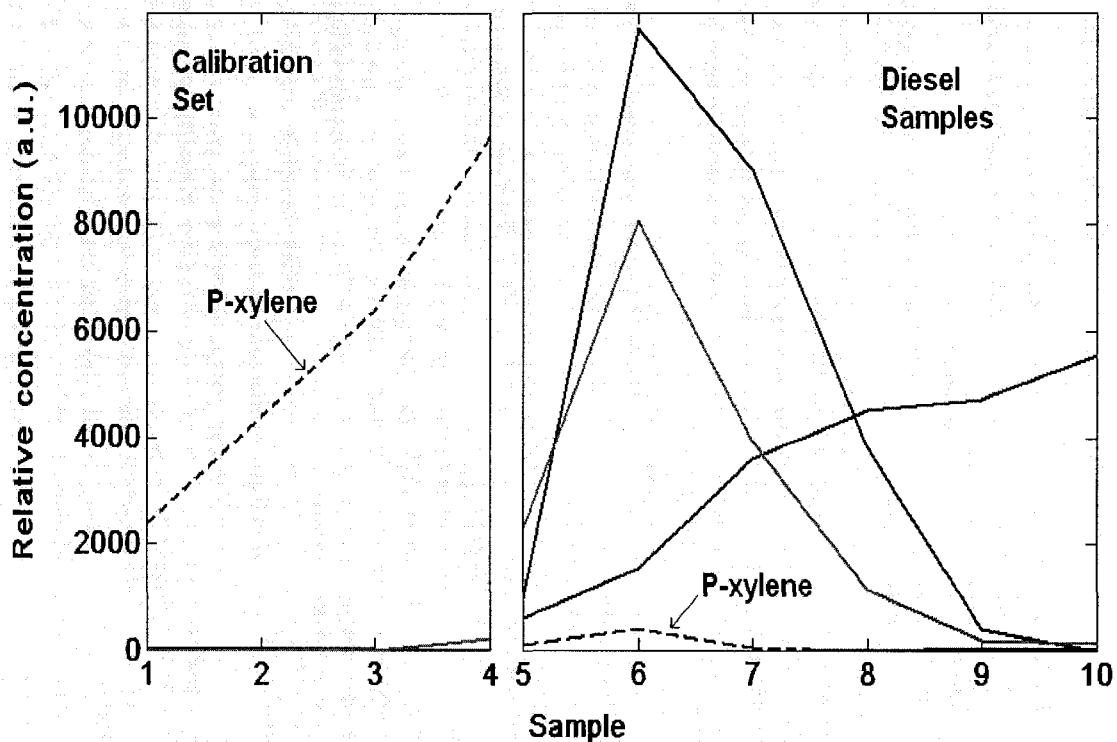
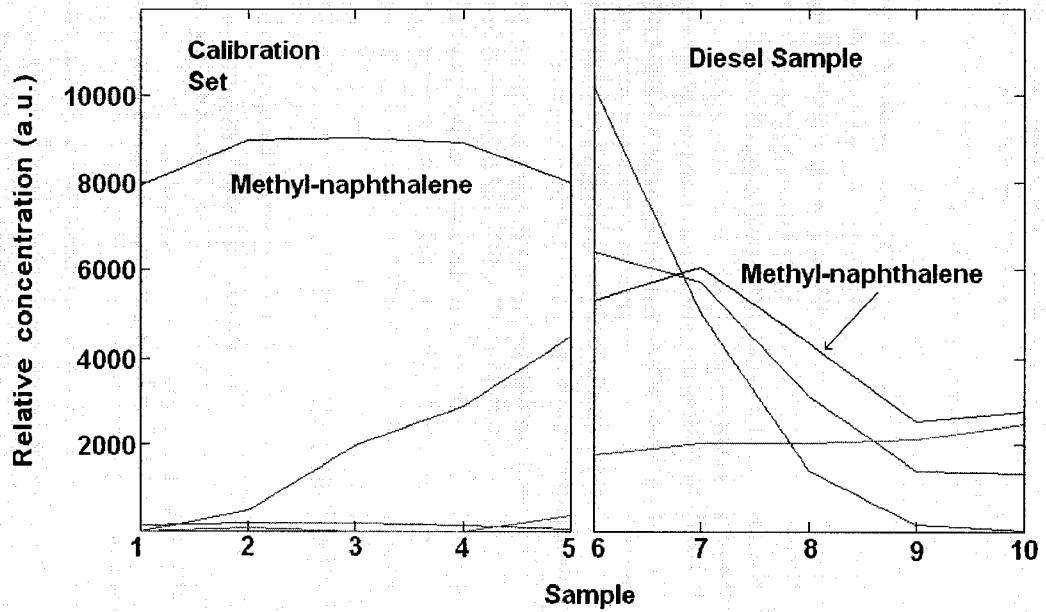


Figure H-8. Diesel -PARAFAC score and calibration curve of p-xylene

- P-xylene concentration in sample N° 1 in calibration set = 0.14 g/L
- Relative concentration (fluorescence intensity) of p-xylene = 2410  
in sample N° 1 in PARAFAC score matrix
- Relative concentration (fluorescence intensity) of p-xylene = 103  
in sample N° 5 in PARAFAC score matrix
- Relative concentration (fluorescence intensity) ratio = 0.04
- Actual fluorescence intensity of p-xylene concentration = 420 a. u.  
equivalent to sample N° 1 in laboratory generated p-xylene  
calibration curve
- Actual fluorescence intensity of p-xylene in sample N° 5 = 18 a. u.  
using Relative concentration (fluorescence intensity) ratio
- Corresponding concentration of p-xylene in sample N° 5 = 0.005 g/L  
using laboratory generated p-xylene calibration curve
- Concentration of diesel in sample N° 5 (Dilution factor) = 1 mL/L (diluted  
1000 times)
- Concentration of diesel in neat gasoline sample = 5 g / L

## Estimation of equivalent methyl-naphthalene in diesel



## Methyl-Naphthalene calibration curve

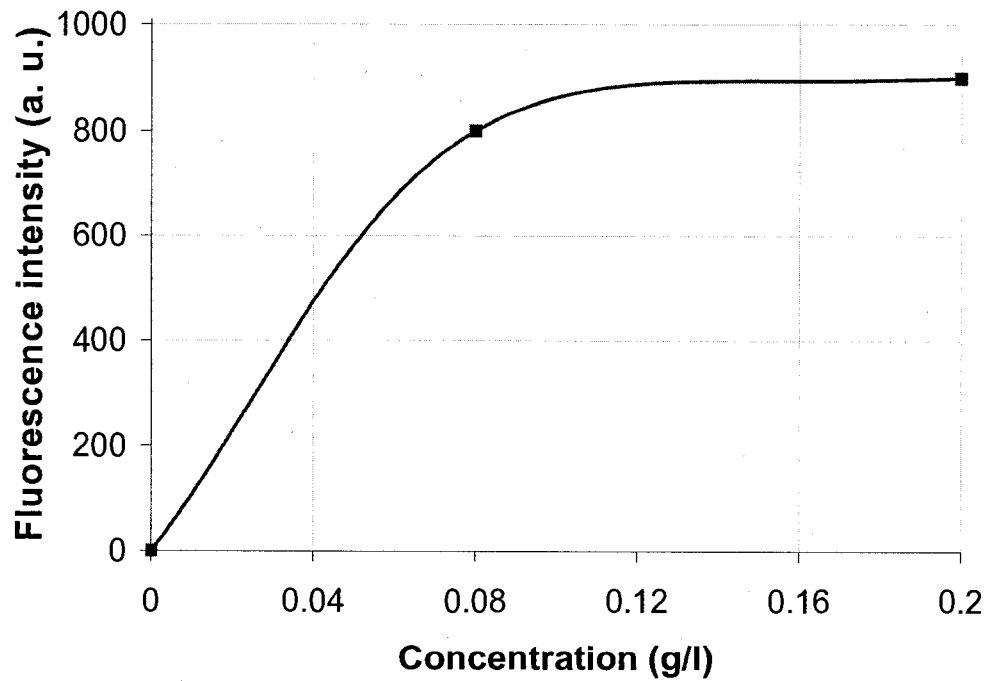
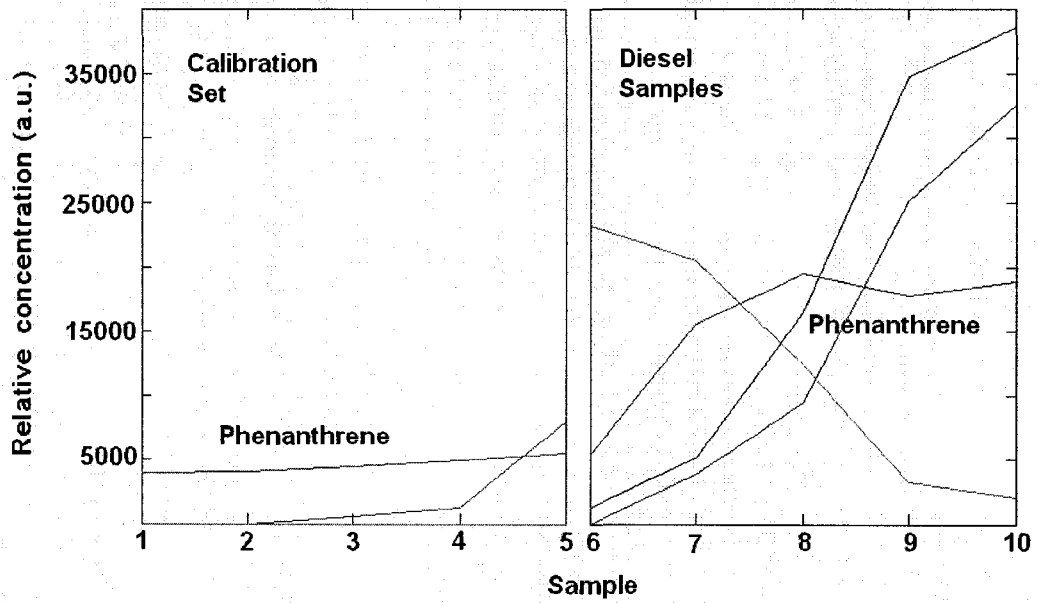


Figure H-9. Diesel -PARAFAC score and calibration curve of methyl-naphthalene

- Methyl-naphthalene concentration in sample N° 1 in calibration set = 0.08 g/L
- Relative concentration (fluorescence intensity) of methyl-naphthalene in sample N° 1 in PARAFAC score matrix = 8000
- Relative concentration (fluorescence intensity) of methyl-naphthalene in sample N° 6 in PARAFAC score matrix = 5000
- Relative concentration (fluorescence intensity) ratio = 0.63
- Actual fluorescence intensity of methyl-naphthalene concentration equivalent to sample N° 1 in laboratory generated methyl-naphthalene calibration curve = 800 a. u.
- Actual fluorescence intensity of methyl-naphthalene in sample N° 6 using Relative concentration (fluorescence intensity) ratio = 500 a. u.
- Corresponding concentration of methyl-naphthalene in sample N° 6 using laboratory generated methyl-naphthalene calibration curve = 0.045 g/L
- Concentration of diesel in sample N° 6 (Dilution factor) = 10 mL/L  
(diluted 100 times)
- Concentration of methyl-naphthalene in neat diesel sample = 4.5 g / L

### Estimation of phenanthrene in diesel



### Phenanthrene calibration curve

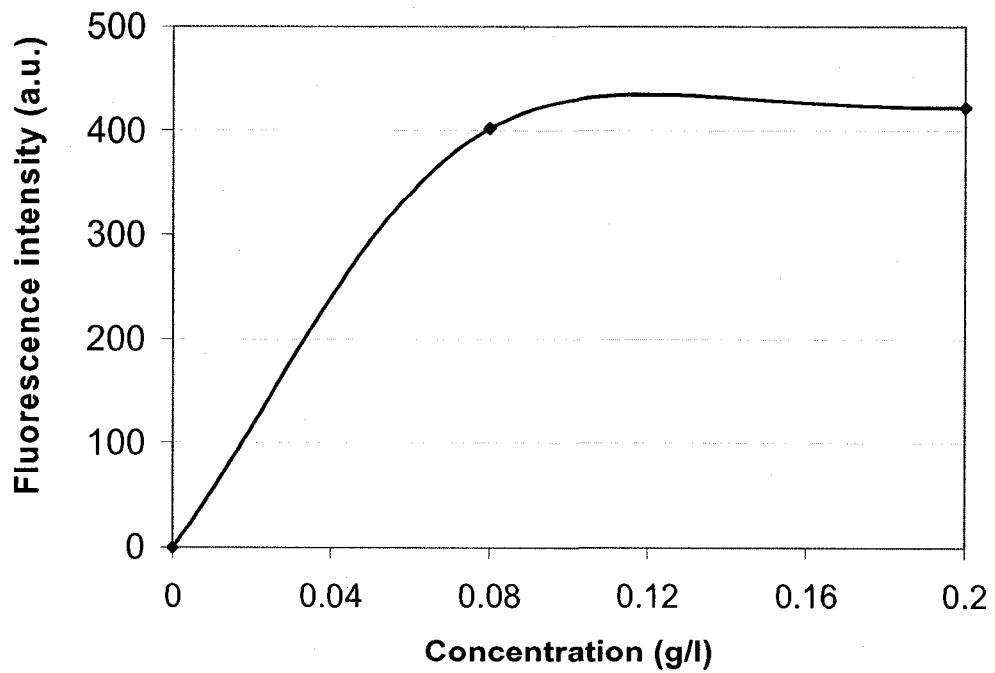


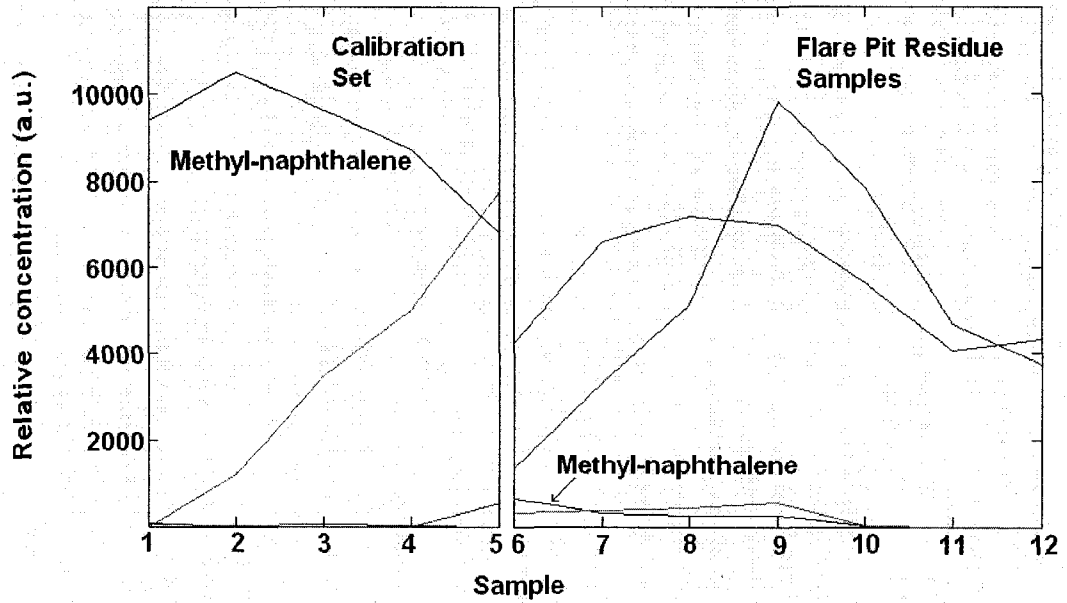
Figure H-10. Diesel -PARAFAC score and calibration curve of phenanthrene

- Phenanthrene concentration in sample N° 1 in calibration set = 0.08 g/L
- Relative concentration (fluorescence intensity) of phenanthrene in sample N° 1 in PARAFAC score matrix = 4000
- Relative concentration (fluorescence intensity) of phenanthrene in sample N° 7 in PARAFAC score matrix = 4000
- Relative concentration (fluorescence intensity) ratio = 1.0
- Actual fluorescence intensity of phenanthrene concentration equivalent to sample N° 1 in laboratory generated phenanthrene calibration curve = 400 a. u.
- Actual fluorescence intensity of phenanthrene in sample N° 7 using Relative concentration (fluorescence intensity) ratio = 400 a. u.
- Corresponding concentration of phenanthrene in sample N° 7 using laboratory generated phenanthrene calibration curve = 0.08 g/L
- Concentration of diesel in sample N° 7 (Dilution factor) = 50 mL/L  
(diluted 20 times)
- Concentration of phenanthrene in neat diesel sample = 1.6 g / L

### **Estimation of pyrene in diesel**

Proper PARAFAC model couldn't be generated when pyrene calibration set was included in the analysis with diesel samples.

## Estimation of equivalent methyl-naphthalene in flare pit residue



### Methyl-Naphthalene calibration curve

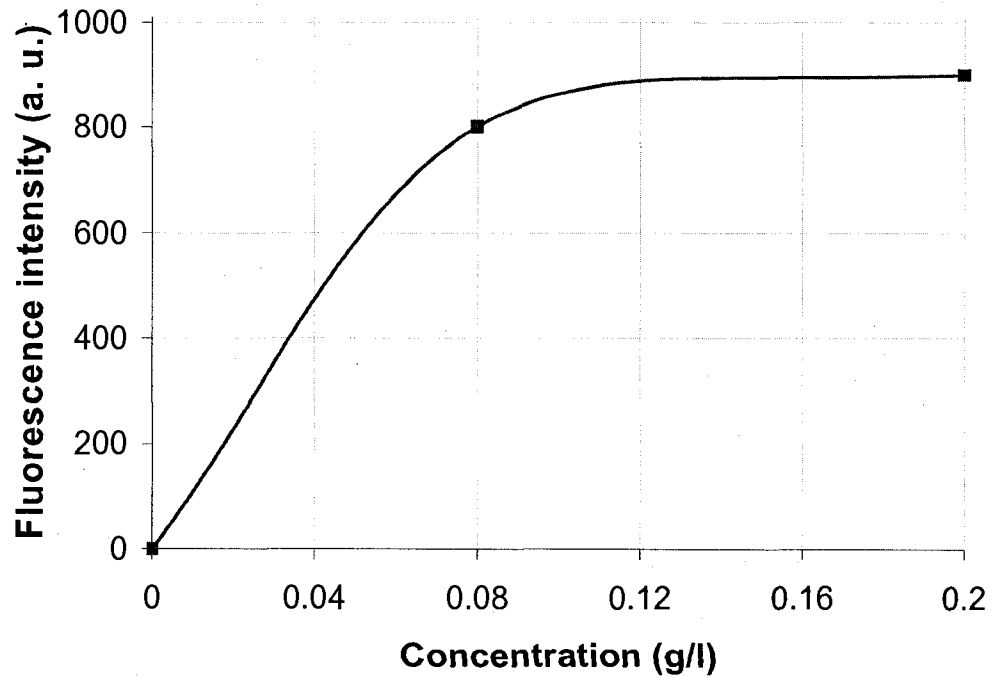


Figure H-11. Flare pit residue -PARAFAC score and calibration curve of methyl-naphthalene

- Methyl-naphthalene concentration in sample N° 1 in calibration set = 0.08 g/L
- Relative concentration (fluorescence intensity) of methyl-naphthalene in sample N° 1 in PARAFAC score matrix = 9500
- Relative concentration (fluorescence intensity) of methyl-naphthalene in sample N° 6 in PARAFAC score matrix = 700
- Relative concentration (fluorescence intensity) ratio = 0.07
- Actual fluorescence intensity of methyl-naphthalene concentration equivalent to sample N° 1 in laboratory generated methyl-naphthalene calibration curve = 800 a. u.
- Actual fluorescence intensity of methyl-naphthalene in sample N° 6 using Relative concentration (fluorescence intensity) ratio = 59 a. u.
- Corresponding concentration of methyl-naphthalene in sample N° 6 using laboratory generated methyl-naphthalene calibration curve = 0.002 g/L
- Concentration of flare pit residue in sample N° 6 (Dilution factor) = 1 mL/L (diluted 1000 times)
- Concentration of methyl-naphthalene in neat flare pit residue sample = 2.5 g / L



## Estimation of phenanthrene in flare pit residue

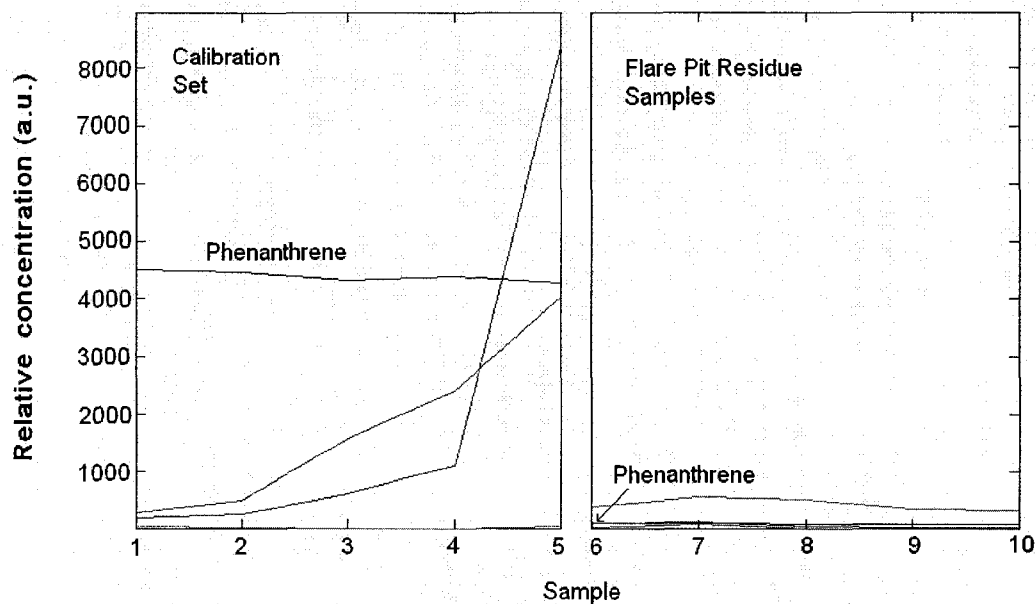


Figure H-12. Flare pit residue -PARAFAC score and calibration curve of phenanthrene

The generated phenanthrene concentrations in score matrix of flare pit residue samples by PARAFAC model were negligible compared to concentrations in calibration set (Figure H-12). Therefore, phenanthrene concentrations could not be estimated in flare pit residue samples.

## Estimation of pyrene in flare pit residue

Proper PARAFAC model couldn't be generated when pyrene calibration set was included in the analysis with flare pit residue samples.

## Estimation of equivalent methyl-naphthalene in crude oil

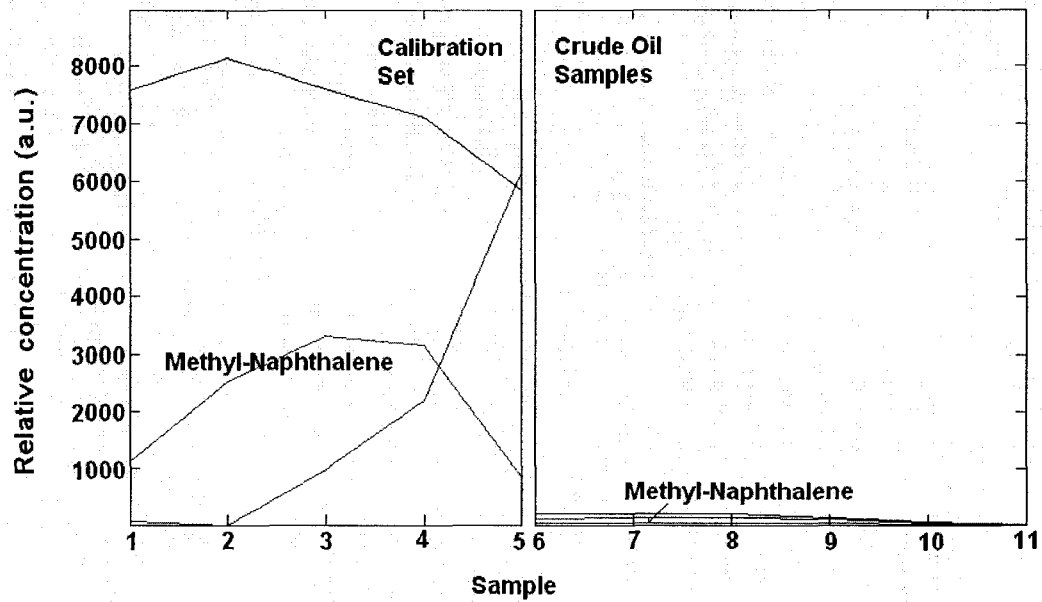


Figure H-13. Crude oil -PARAFAC score and calibration curve of methyl-naphthalene

The generated methyl-naphthalene concentrations in score matrix of crude oil samples by PARAFAC model were negligible compared to concentrations in calibration set (Figure H-13). Therefore, methyl-naphthalene concentrations could not be estimated in crude oil samples.

## Estimation of phenanthrene in crude oil

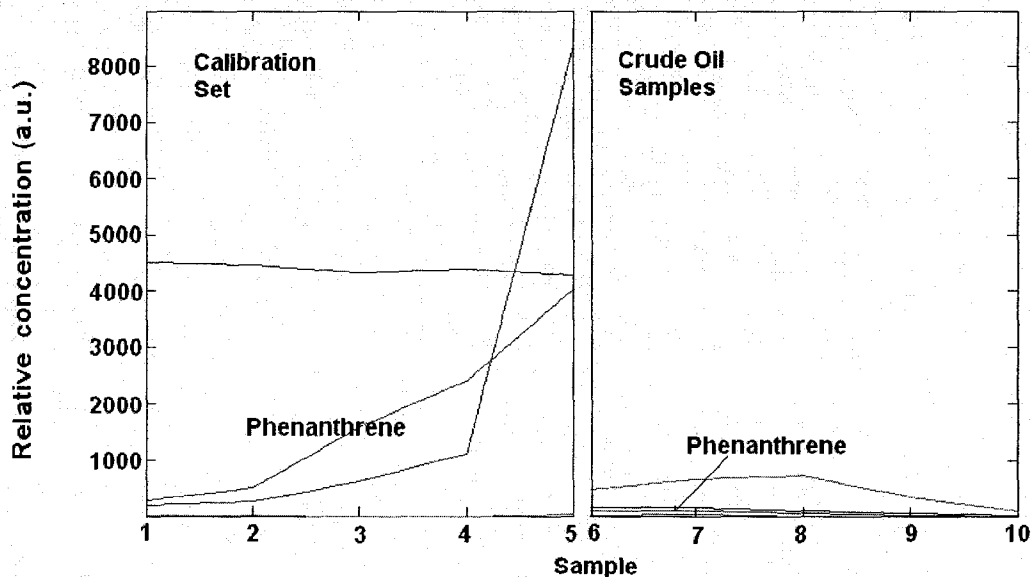


Figure H-14. Crude oil -PARAFAC score and calibration curve of phenanthrene

The generated phenanthrene concentrations in the score matrix of crude oil samples by PARAFAC model were negligible compared to concentrations in the calibration set (Figure H-14). Therefore, phenanthrene concentrations could not be estimated in crude oil samples.

## Estimation of pyrene in crude oil

A proper PARAFAC model could not be generated when the pyrene calibration set was included in the analysis with crude oil samples.

